NEW BIOTECHNOLOGICAL METHODS FOR INTRACELLULAR DELIVERY

Rossella Tarallo

Dottorato in Scienze Biotecnologiche XXV ciclo
Indirizzo Biotecnologie Industriale e Molecolare
Università di Napoli Federico II

Dottorato in Scienze Biotecnologiche XXV ciclo
Indirizzo Biotecnologie Industriale e Molecolare
Università di Napoli Federico II

NEW BIOTECHNOLOGICAL METHODS FOR INTRACELLULAR DELIVERY

Rossella Tarallo

Dottoranda:	Rossella Tarallo
Relatore:	Prof. Stefania Galdiero
Coordinatore:	Prof. Giovanni Sannia

ACKNOWLEDGEMENTS

I would never have been able to conduct my researches and write the present PhD thesis without the guidance, help and support of all the people I share my days with.

I would like to express my deepest and sincere gratitude to my advisor, Prof. Stefania Galdiero, for her guidance, care, motivation, enthusiasm and for providing me with an excellent scientific knowledge that allowed me to perform a working experience in an extraordinary atmosphere.

I would like to thank my colleagues and friends, Dr. Annarita Falanga and Dr. Marco Cantisani, for the continuous support, guidance, encouragement, patience, great suggestions, immense knowledge; particularly, I will never forget their scientific and moral support that guided me during these years and helped me to develop my background.

I also thank the Department of Pharmacy of the University of Naples, and in particular, Prof. Carlo Pedone, Prof. Giancarlo Morelli, Dr. Antonella Accardo, for giving me assistance since the beginning of this PhD. I am grateful to Dr. Luca De Luca for his assistance in using the software necessary for my thesis.

I am most grateful to Prof. Marcus Weck of the Department of Chemistry of the New York University, for giving me the opportunity to work in his research group and allowing the establishment of a strong cooperation between the Italian and the American groups now working on several exciting projects.

I thank my labmates, Dr. Ivan De Paola, Dr. Emiliana Perillo for the stimulating discussions, challenging questions and for all the fun we had in these years.

Last but not the least, I would like to thank my best friend Antonella, Antonio and my family; they have always been supporting me spiritually and encouraging with their best wishes throughout my life.

Rossella Tarallo

RIASSUNTO

NUOVI METODI BIOTECNOLOGICI PER IL TRASPORTO INTRACELLULARE

Le Nanotecnologie si basano sulla comprensione e la conoscenza approfondita delle proprietà della materia su scala nanometrica. I benefici di questa nuova scienza hanno apportato significative innovazioni in diverse aree della ricerca, quali: elettronica, cosmetica, agricoltura e medicina. In particolare l'applicazione delle nanotecnologie in campo biomedico si propone l'obiettivo di realizzare un monitoraggio completo e continuo dell'organismo umano e di contribuire alla tutela della salute, lavorando a livello molecolare per ottenere benefici medici e clinici mediante l'utilizzo di nanodispositivi e nanostrutture; l'ottimizzazione delle tecnologie già esistenti per una più completa applicazione nel settore medico; lo sviluppo di nuovi sistemi multifunzionali per la diagnosi delle malattie e la somministrazione mirata dei farmaci; un aumento delle competenze e delle conoscenze che consenta di produrre materiali sempre più affidabili, specializzati e riproducibili, aumentando l'efficacia e riducendo i costi.

Questo progetto di ricerca si inserisce nell'ambito delle nanotecnologie ed ha come obiettivo l'identificazione, progettazione e caratterizzazione di nuovi nanodispositivi di natura peptidica in grado di mediare il trasporto e il rilascio intracellulare di molecole bioattive utilizzabili sia nel settore diagnostico che terapeutico.

Ora, i sistemi utilizzati per il delivery sono principalmente di tipo virale e non virale. I vettori virali, che derivano da virus a DNA (vettori adenovirali, adenoassociati etc.) e a RNA (Retrovirus), sono utilizzati per il trasporto in cellule eucariotiche di sequenze geniche, per la regolazione di funzioni cellulari o per esprimere proteine terapeutiche. Sebbene le strategie virali siano potenzialmente efficienti, ad esse sono associati diversi svantaggi quali l'elevata immunogenicità e tossicità.

La strategia non virale invece, comprende approcci sia di tipo fisico quali microiniezione ed elettroporazione, che di tipo chimico mediato dall'utilizzo di biomolecole come lipidi, proteine, peptidi, nanoparticelle etc.

Sebbene le metodiche fisiche siano comunemente utilizzate sia per studi *in vitro* sia *in vivo*, esse risultano invasive e potrebbero col tempo danneggiare la membrana plasmatica delle cellule sottoposte a trattamento. Per questo motivo risulta di fondamentale importanza identificare sistemi meno invasivi da utilizzare per il trasporto intracellulare, e l'utilizzo di sequenze peptidiche, costituisce l'alternativa non virale attualmente più promettente.

I Cell Penetrating Peptides (CPPs) sono peptidi carichi in grado di trasportare macromolecole attraverso la membrana plasmatica in modo efficiente ed il loro utilizzo è notevolmente aumentato negli ultimi anni. Il principale problema associato al loro utilizzo è il meccanismo di traslocazione che coinvolge principalmente processi di natura endocitica. Quindi, solo una piccola quantità della molecola cargo è in grado di sfuggire agli endosomi, dove avvengono le comuni reazioni di degradazione intracellulare, e di raggiungere il sito di azione. E' quindi necessario identificare nuovi peptidi ed eventualmente nanosistemi funzionalizzati con peptidi con diverse caratteristiche chimico-fisiche, che utilizzino solo parzialmente il meccanismo endocitico, migliorando così le proprietà farmacocinetiche e farmacodinamiche, la distribuzione e localizzazione intracellulare e di conseguenza l'attività sito-specifica.

A tale scopo il gruppo di ricerca in cui ho condotto il lavoro di ricerca, si è recentemente occupato dello studio delle strategie utilizzate dai virus per infettare la cellula ospite. I virus sono classificati in virus con envelope e virus senza envelope, in

base alla presenza o meno di una membrana a doppio strato fosfolipidico che circonda il capside. Il processo di infezione utilizzato dipende dal tipo di virus; i virus senza envelope utilizzano principalmente meccanismi endocitici e, quelli con envelope utilizzano principalmente meccanismi di fusione. Tale processo è mediato da glicoproteine che durante la penetrazione sottostanno ad un cambio conformazionale che induce l'esposizione in superficie di sequenze idrofobiche, le quali interagendo e destabilizzando la membrana cellulare promuovono la penetrazione del virus attraverso un processo non endocitico ma di tipo passivo.
Per tale motivo, risulta essere particolarmente interessante lo studio di sequenze membranotropiche di derivazione virale.
In particolare il gruppo in cui lavoro ha precedentemente identificato la sequenza gH625-644 che deriva dalla glicoproteina gH presente sull'envelope del virus Herpes simplex di tipo 1. gH625 interagisce con le membrane biologiche ed è coinvolto nel processo di fusione con la membrana della cellula bersaglio. Il peptide contiene residui amminoacidici cruciali per l'interazione e destabilizzazione delle membrane. La sequenza è ricca in residui idrofobici quali glicine, leucine ed alanine, residui aromatici quali triptofano e tirosine. La struttura NMR del peptide mostra la sua natura di elica anfipatica dove tutti i residui idrofobici sono presenti su un lato dell'elica e quelli idrofilici sul lato opposto. La porzione idrofobica della molecola svolge sicuramente un ruolo attivo nel processo di interazione e fusione con le membrane.
L'interazione peptide-lipide è probabilmente mediata, inizialmente, dall'arginina presente all'estremità C-terminale, infatti quando tale residuo è mutato l'attività fusogenica del peptide risulta fortemente alterata. Come già detto, anche il dominio idrofobico è cruciale nella fase di inserzione del peptide infatti le interazioni idrofobiche tra le proteine di fusione e i fosfolipidi di membrana, danno inizio ai processi di perturbazione di membrana tipici dello stadio precoce di infezione virale. L'internalizzazione di gH625 è probabilmente associata alla sua capacità di interagire con i fosfolipidi di membrana e di formare una struttura α-elica transiente che destabilizza temporaneamente la membrana facilitandone la sua inserzione e traslocazione. Studi di internalizzazione condotti mediante tecniche sia quantitative, quali citometria a flusso, che qualitative, quali microscopia confocale, dimostrano che il peptide gH625 attraversa la membrana cellulare utilizzando essenzialmente meccanismi di traslocazione passiva, mostrando solo una parziale colocalizzazione con vescicole endosomiali, infatti, le sue cinetiche non sono alterate quando gli esperimenti sono condotti a 4°C, temperatura a cui tutti i meccanismi attivi sono inibiti. I dati ottenuti confermano che il peptide attraversa il doppio strato lipidico soprattutto attraverso meccanismi energia-indipendenti, risultando quindi, da un punto di vista farmacocinetico, un ottimo candidato per il delivery intracellulare di molecole bioattive.
Sulla base delle analisi chimico-fisiche e biologiche condotte su gH625 lo scopo di questa tesi di dottorato è stato l'identificazione, sintesi e caratterizzazione di un nuovo nanosistema opportunamente funzionalizzato con gH625 da utilizzare come sistema innovativo nel campo del delivery intracellulare. In particolare, mi sono occupata dell'analisi delle cinetiche e del meccanismo di internalizzazione intracellulare del peptide da solo, della coniugazione del peptide a nanostrutture di diversa natura quali Quantum Dots, Liposomi, Dendrimeri e Nanoparticelle di polistirene. L'idea è stata quella di unire i benefici chimici di questi nanosistemi al vantaggio associato all'utilizzo di gH625, e alla sua capacità di superare le barriere cellulari mediante un processo di traslocazione non attivo.

FUNZIONALIZZAZIONE DI QUANTUM DOTs

I QDs sono una nuova classe di fluorofori che differiscono dai convenzionali fluorofori organici, per diverse caratteristiche chimico-fisiche quali: l'elevata luminescenza e fotostabilità, e picchi di emissione che variano in funzione delle loro dimensioni; tali caratteristiche li rendono particolarmente interessanti per le possibili applicazioni nel campo dell'imaging terapeutico. Tuttavia, nonostante essi costituiscono degli ottimi candidati per la progettazione di nuovi sistemi da utilizzare in teranostica, presentano scarsa efficienza di internalizzazione intracellulare.

Alcuni studi *in vivo* dimostrano che, sebbene i QDs presentino una elevata tossicità cellulare, dovuta probabilmente alla loro degradazione intracellulare e successivo rilascio di ioni metallici tossici che producono specie reattive dell'ossigeno, quando passivati sulla loro superficie, la tossicità risulta notevolmente ridotta. Dunque, il legame di trasportatori peptidici sulla superficie dei QDs rappresenta una nuova strategia per migliorarne l'internalizzazione e ridurne la tossicità. Numerosi lavori riportano la funzionalizzazione dei QDs con la sequenza Tat o con altri CPPs carichi positivamente; le analisi dei risultati dimostrano che il meccanismo di internalizzazione adoperato è principalmente quello endocitico. Dunque, risulta di fondamentale importanza l'utilizzo di un peptide con proprietà chimico-fisiche diverse dai convenzionali CPPs, come gH625, che utilizzi meccanismi di internalizzazione alternativi al fine di aumentarne la biodisponibilità intracellulare.

I QDs da soli alla concentrazione di 50nM hanno una bassa affinità per la membrana plasmatica di cellule HeLa. La coniugazione dei QDs con gH625 ne aumenta notevolmente l'internalizzazione intracellulare e da studi di inibizione dei processi endocitici si evince che il sistema QD-gH625 utilizza meccanismi di internalizzazione passivi, a differenza di quello che accade quando si utilizzano QDs funzionalizzati con il Tat nelle stesse condizioni; in quest'ultimo caso la cinetica e l'efficienza di internalizzazione sono notevolmente ridotte e i meccanismi di internalizzazione sono di tipo endocitico. In particolare, è stato precedentemente riportato che Tat quando legato a molecole di piccole dimensione attraversa la membrana plasmatica e raggiunge i compartimento nucleare, mentre quando Tat è complessato ai QDs resta intrappolato in vescicole endosomiali. Questo effetto è probabilmente dovuto alle maggiori dimensioni dei QDs che influenzano il processo con cui Tat è internalizzato. Al contrario, quando i QDs sono funzionalizzati con gH625 entrano nelle cellule con distribuzione extravescicolare. In conclusione peptidi con diverse proprietà biofisiche possono influenzare il processo di internalizzazione della stessa molecola cargo.

FUNZIONALIZZAZIONE CON LIPOSOMI

I liposomi sono vescicole non tossiche, non immunogeniche, biodegradabili e di diametro compreso tra 50-500 nm. La loro struttura si caratterizza per la presenza di uno o più doppi strati fosfolipidici esterni che delimitano all'interno un core. In questo modo, le sostanze idrosolubili contenute all'interno delle microsfere liposomiali possono essere facilmente veicolate all'interno delle cellule, riducendo la tossicità associata ad alcune molecole bioattive come i farmaci antineoplastici. Per questo motivo sono degli ottimi candidati per la veicolazione intracellulare di principi attivi. E' stato dimostrato che la funzionalizzazione della superficie liposomiale, migliora in maniera notevole l'internalizzazione e quindi l'efficacia antitumorale del farmaco trasportato. La strategia sintetica utilizzata per la funzionalizzazione di liposomi con peptidi dipende dalla natura chimico-fisica del peptide; in particolare, l'utilizzo di un peptide idrofobico risulta più complicato a causa della sua bassa solubilità in ambiente acquoso e dalla sua tendenza a distribuirsi preferenzialmente nella regione

idrofobica del doppio strato lipidico piuttosto che in superficie. gH625 è stato legato a liposomi, preformati e caricati con Doxorubicina, utilizzando la click-chemistry; inoltre la sua capacità di attraversare le membrane plasmatiche è stata valutata attraverso esperimenti di microscopia confocale.
Le cellule sono state incubate a 37°C con una soluzione 1μM di Doxorubicina libera, Doxorubicina caricata in liposomi e Doxorubicina caricata in liposomi e funzionalizzati con gH625. I risultati ottenuti dopo 5 ore di incubazione dimostrano che la Doxo e liposomi-Doxo hanno una localizzazione nucleare; al contrario il liposoma con Doxo e peptide ha una localizzazione citoplasmatica. Questa diversa distribuzione intracellulare è probabilmente dovuta alla presenza del peptide che altera il meccanismo di internalizzazione del sistema e il rilascio intracitoplasmatico del farmaco. Sebbene il meccanismo non sia ancora ben definito i risultati ottenuti, risultano utili per la progettazione di sistemi di trasporto e rilascio controllato di Doxorubicina, al fine di ridurne i suoi effetti indesiderati.

FUNZIONALIZZAZIONE CON DENDRIMERI

I dendrimeri sono molecole che contengono una serie di ramificazioni che si estendono da un nucleo centrale. Generalmente presentano diverse copie dello stesso gruppo funzionale al termine delle ramificazioni, hanno una struttura e dimensione ben definita rispetto a polimeri lineari aventi stessa composizione e peso molecolare.
Vi sono essenzialmente due strategie sintetiche che possono essere utilizzate per la preparazione di dendrimeri: l'approccio convergente e l'approccio divergente.
Con l'approccio divergente, il dendrimero è preparato a partire da un nucleo polifunzionale per successive aggiunte di ramificazioni. Con l'approccio convergente, si parte dalle unità funzionali superficiali e si aggiungono progressivamente ramificazioni interne. I dendrimeri hanno avuto un forte impatto nelle bioscienze e in particolare in campo biomedico come potenziali trasportatori di farmaci. Studi di internalizzazione condotti su dendrimeri PAMAM da soli e funzionalizzati con la sequenza Tat dimostrano che il meccanismo utilizzato è prevalentemente di tipo endocitico. I nostri studi, condotti mediante esperimenti di interazione con le membrane, citometria in flusso e microscopia confocale, su dendrimeri poli-amidici funzionalizzati con la sequenza fusogenica gH625, dimostrano invece che il complesso fonde membrane modello, come liposomi, e che attraversa efficientemente le membrane cellulari utilizzando un meccanismo di traslocazione passivo.

FUNZIONALIZZAZIONE CON NANOPARTICELLE DI POLISTIRENE

L'utilizzo di farmaci per le patologie neurologiche attualmente in via di sperimentazione, sono limitate dall'incapacità dell'agente terapeutico di attraversare efficientemente la barriera ematoencefalica (BBB). La BBB è una barriera dinamica e selettiva che protegge il sistema nervoso dall'invasione di sostanze e organismi indesiderati; ma rappresenta anche un notevole ostacolo da un punto di vista terapeutico in quanto limita l'attraversamento e il rilascio dei farmaci nel loro sito di azione. Per questo motivo è fondamentale identificare e sviluppare un sistema che permetta un migliore rilascio del farmaco nei compartimenti del sistema nervoso. La maggior parte delle strategie in fase di sperimentazione che hanno avuto un notevole impatto terapeutico, come la microiniezione diretta, risultano talvolta troppo invasive in quanto danneggiano in maniera irreversibile la BBB.
Particolare interesse attualmente è rivolto allo studio di Nanoparticelle (NPs),

eventualmente funzionalizzate, per utilizzarle come trasportatori di farmaci attraverso la barriera ematoencefalica. Le Nanoparticelle sono costituite da aggregati atomici o molecolari con un diametro compreso approssimativamente fra 2 e 200 nm e si distinguono da gli altri nanosistemi per la loro piccola dimensione, elevata area superficiale, forma, composizione chimica e carica.
Sono stati condotti esperimenti di internalizzazione con NPs di polistirene, di 100nm di diametro, opportunatamente funzionalizzate con la sequenza gH625, su cellule dell'endotelio cerebrale (bEnd3). I risultati ottenuti dimostrano che la presenza, sulla superficie delle NPs, di gH625 ne migliora la loro internalizzazione. Inoltre, il loro movimento intracitoplasmatico risulta di tipo casuale e non direzionale. Questo comportamento è indicativo di un meccanismo passivo di internalizzazione. I dati preliminari dimostrano che il nostro sistema, presenta delle caratteristiche ottimali, per il trasporto di molecole attraverso la barriera ematoencefalica e potrebbe essere utilizzato per la cura delle patologie del Sistema Nervoso Centrale.

CONCLUSIONI

La scelta di un sistema di natura peptidica per il trasporto intracellulare di molecole bioattive da utilizzare nel campo della teranostica, rappresenta attualmente una delle strategie chimiche, non virali e non invasive più promettenti. Il meccanismo di internalizzazione utilizzato da tali costrutti peptidici risulta di fondamentale importanza per il destino della molecola bioattiva eventualmente da loro trasportata. E' stato dimostrato che la maggior parte dei CPPs utilizza processi endocitici che inducono una riduzione della biodisponibilità intracellulare della molecola internalizzata. A tale proposito l'identificazione di una sequenza di derivazione virale, capace quindi di mimare il processo di fusione utilizzato da alcuni virus per infettare la cellula ospite, ha avuto un forte impatto nella progettazione di nanosistemi utilizzabili sia nel campo della diagnostica che della terapia. In conclusione, i risultati ottenuti dalla funzionalizzazione con gH625, convergono tutti nella stessa direzione; non solo gH625 è capace di attraversare la membrana plasmatica in maniera efficiente, attraverso meccanismi di traslocazione passiva, ma è anche in grado di facilitare l'ingresso intracellulare di molecole biologicamente attive.

SUMMARY

Biological membranes represent a critical hindrance for administering active molecules which are often unable to reach their designated intracellular target.
In order to overcome this barrier-like behavior, not easily circumvented by many pharmacologically-active molecules, and to promote cellular uptake, synthetic peptide-based transporters have been exploited. In fact, linking or complexing therapeutic molecules to peptides that can translocate through the cellular membranes could enhance their internal delivery, and consequently, a higher amount of active compound would reach the site of action. Use of Cell Penetrating Peptides (CPPs) is one of the most promising non invasive strategies to efficiently translocate macromolecules through the plasma membrane, and have, recently, attracted a great attention. A new viral traslocator peptide (gH625) is described in this thesis, which is derived from the Herpes simplex virus type 1 (HSV-1) glycoprotein H (gH). gH625 has proved to be a useful delivery vehicle due to its intrinsic properties of inducing membrane perturbation. Quantum dots (QDs), Liposomes, Dendrimers and Polystyrene Nanoparticles (NPs) have been used as powerful platforms for studying the behavior of gH625 as a nano-vehicles.
QDs are a new class of fluorescent probes under intense research and development for broad application in molecular, cellular and *in vivo* imaging. QDs do not significantly traverse the membrane bilayer on their own. On the contrary, when functionalized with gH625, are able to translocate through cellular plasma membranes by a mechanism which seems to be only relatively dependent on the endocytic route of entry.
Liposomal aggregates have been successfully used as *in vivo* carriers of active principles; they display some unique pharmacokinetic properties and can be adapted to a wide range of therapeutic agents. An easy and versatile synthetic strategy, based on click chemistry, has been used to bind, in a controlled way, several copies of gH625 peptide on the external surface of DOPG based liposomes. Liposomes have been also loaded with the cytotoxic doxorubicin drug and their ability to penetrate inside cells has been evaluated by confocal microscopy experiments. Results suggest that liposomes functionalized with gH625 may act as promising intracellular targeting carriers for efficient delivery of drugs, such as chemotherapeutic agents, into tumor cells.
Dendrimers are perfectly hyperbranched macromolecules with a well-defined structure, which exhibit properties very different from linear polymers with the same composition and molecular weight. A poly(amide)-based dendrimer was synthesized and conjugated with gH625. The attachment of the peptide sequences to the termini of a dendrimer allows the conjugate to penetrate into the cellular matrix, whereas the unfunctionalized dendrimer is excluded from translocation. The peptide functionalized dendrimer is rapidly taken into the cells mainly through a non-active translocation mechanism.
The surface of fluorescent aminated polystyrene nanoparticles (NPs) was functionalized with gH625 via a covalent binding procedure, and the NP uptake mechanism and permeation across in vitro Blood Brain Barrier (BBB) models were studied. At early incubation times, the uptake of NPs with gH625 by brain endothelial cells is greater than that of the NPs without the peptide, and their intracellular motion is mainly characterized by a random walk behavior. Most importantly, gH625 peptide decreases NP intracellular accumulation as large aggregates and enhances their BBB crossing. In summary, these results establish that gH625 may represent a good choice for the design of promising carriers to deliver drugs for the treatment of human diseases.

1 INTRODUCTION

1.1 NANOTECHONOLGY FOR ADVANCED DRUG DELIVERY SYSTEMS

Nanotechnology is the branch of science correlated to physics, chemistry, biology and medicine and dedicated to materials with dimensions in the order of 100 nm or less. It is actually receiving great attention with a never-seen-before enthusiasm because of its potentialities which can literally revolutionize any field in which it is applied.

In particular, the main areas in which nanotechnology is bringing significant innovations are electronics, energy, heavy industry, foods and nanofoods, cosmetics, agriculture, medicine etc. The application of nanotechnology in the biomedical field is the objective of achieving a comprehensive and continuous monitoring of the human body and contributes to the protection of health, working at the molecular level to obtain clinical and medical benefits through the use of nanostructures and nanodevices, the optimization of existing technologies for a more complete application in the medical sector, the development of new multifunctional systems for disease diagnosis and targeted drug delivery, raising the skills and knowledge that allows the production of materials more reliable, specialized and reproducible, increasing efficiency and reducing costs.

Nanoparticles are generally defined as clusters of atoms in the range of 1 to 100 nm, which possess defined chemical, optical and mechanical properties and are becoming extremely promising for their activities in many fields; their properties are believed to be linked to their large surface area to volume ratio. To put a nanometre in context: a strand of DNA is 2.5 nm wide, a red blood cell is 7,000 nm and a human hair is 80,000 nm wide. Reducing the particle size of materials has demonstrated to be an efficient and reliable tool for improving their biocompatibility; furthermore, nanomaterials thanks to the possibility of decorating their surface with functional groups can also be modified for better efficiency to facilitate their applications in bioscience and medicine, thus, opening up a whole new world of science and discovery. As their diameter decreases, the available surface area of the particle itself increases dramatically and as a consequence there is an increase over the original properties of their corresponding bulk materials, and this feature makes them superior and indispensable in many areas of human activity and excellent candidates for biomedical applications as a variety of biological processes occur at nanometer level. It suffices to consider that cells are typically of 10 μm across and proteins are usually of 5 nm, which are dimensions comparable with those of the smallest synthetic nanoparticle. The biological interactions are generally multivalent and often involve multiple copies of receptors and ligands that bind in a coordinated manner, resulting in enhanced specificities, efficiencies, and strengths of such interactions that make nanosystems very versatile in that they can be involved in multiple interactions.

These properties allow nanoparticulate systems to overcome current limitations of conventional formulations as they facilitate the intracellular uptake to specific cellular targets. Thus, nanotechnology is having a huge impact in the area of nanomedicine and in particular in several fields such as drug/gene delivery[1], imaging[2] and diagnostics[3], therapy, biomaterials and tissue engineering (Table 1).

Drug delivery	Nanoscale delivery vehicles can (1) enhance the therapeutic efficacy and minimize adversities associated with available drugs; (2) enable new classes of therapeutics; and (3) encourage the re-investigation of pharmaceutically suboptimal but biologically active new molecular entities that were previously considered undevelopable.
In vitro diagnostics	Nanotechnology-based sensors (e.g., nanowires, nanotubes, nanoparticles, cantilevers, and micro/nanoarrays) can enable fast and high throughput detection of disease biomarkers with higher sensitivity and lower sample consumption. Nanotechnology also offers hope for the early detection of viruses, bacteria, and circulating tumor cells, as well as for single cell analysis.
In vivo imaging	Targeted imaging nanoprobes (e.g., magnetic nanoparticles, quantum dots, and carbon nanotubes) could provide a faster, less invasive, and more accurate way to diagnose diseases (e.g., cancer) at their earliest stages and monitor disease progression. Some other possible opportunities include reporting *in vivo* efficacy of therapeutics and tracking nanocarrier biodistribution in the body. In addition, imaging nanoprobes could help surgeons to locate tumors and their margins, identify important adjacent structures, and map sentinel lymph nodes.
Therapy techniques	Certain nanomaterials have unique therapeutic properties that differ from conventional drugs, and can, therefore, be directly used to treat diseases. For example, hafnium oxide- and gold-based nanoparticles can greatly enhance X-ray therapy; gold nanoshells/nanorods, carbon nanotubes, magnetic nanoparticles can induce hypothermia to kill cancer cells; and nanocrystalline silver is being used as an antimicrobial agent.
Biomaterials	Biocompatible nanomaterials that have optimal mechanical properties can be used as medical implants, such as dental restoratives and bone substitutes (also categorized as hard-tissue engineering.). Nanocoatings or nanostructured surfaces can also improve the biocompatibility and adhesion of biomaterials.
Tissue engineering	Nanotechnology can enable the design and fabrication of biocompatible scaffolds at the nanoscale and control the spatiotemporal release of biological factors, resembling native extracellular matrix, to direct cell behaviors, and eventually lead to the creation of implantable tissues.

Table 1. Applications of nanotechnology in medicine.

In drug delivery, nanotechnology is just beginning to make an impact. Many of the current "nano" drug delivery systems, however, are remnants of conventional drug delivery systems that happen to be in the nanometer range, such as liposomes, polymeric micelles, nanoparticles, dendrimers, and nanocrystals. Liposomes and polymer micelles were first prepared in 1960's; nanoparticles and dendrimers in 1970's and colloidal gold particles in nanometer sizes were first prepared by Michael Faraday more than 150 years ago, but were never referred to or associated with nanoparticles or nanotechnology until recently. Subsequently, as illustrated in Figure 1, a variety of other organic and inorganic biomaterials for drug delivery were developed. The first controlled release polymer system for delivery of macromolecules was described in 1976. More complex drug delivery systems capable of responding to changes in pH which trigger drug release, as well as the first example of cell-specific targeting of liposomes[4,5] were first described in 1980. The first long-circulating liposome was described in 1987, and the concept was later named "stealth liposomes"[6]. The use of polyethylene glycol (PEG) was shown to increase circulation times of liposomes[7] and polymeric nanoparticles[8] in 1990 and 1994, respectively, paving the road for the development and subsequent approval of Doxil (doxorubicin liposome) in 1995, for the treatment of AIDS-associated Kaposi's Sarcoma.

A variety of organic/inorganic nanomaterials and devices have been used as delivery vehicles to develop effective therapeutic modalities (Figure 1). So far, there are over two dozen nanotechnology-based therapeutic products approved by Food and Drug Administration (FDA) for clinical use, and more are in clinical trials[9-11]. Of these products, the majority are composed of a non-targeted delivery system (e.g., liposomes and polymers) and a drug, and are therefore considered first generation nano-therapeutics[12].

The importance of nanotechnology in drug delivery is correlated to the possibility of manipulating molecules and supramolecular structures in order to produce devices with programmed functions, allowing to achieve: 1) improved delivery of poorly water-soluble drugs; 2) targeted delivery of drugs in a cell- or tissue-specific manner; 3) transcytosis of drugs across tight epithelial and endothelial barriers; 4) delivery of large macromolecule drugs to intracellular sites of action; 5) co-delivery of two or

more drugs or therapeutic modality for combination therapy; 6) visualization of sites of drug delivery by combining therapeutic agents with imaging modalities; and 7) real-time read on the *in vivo* efficacy of a therapeutic agent[13]. Additionally, the manufacturing complexity of nanotechnological therapeutics may also create a significant hurdle for generic drug companies to develop equivalent therapeutics readily.

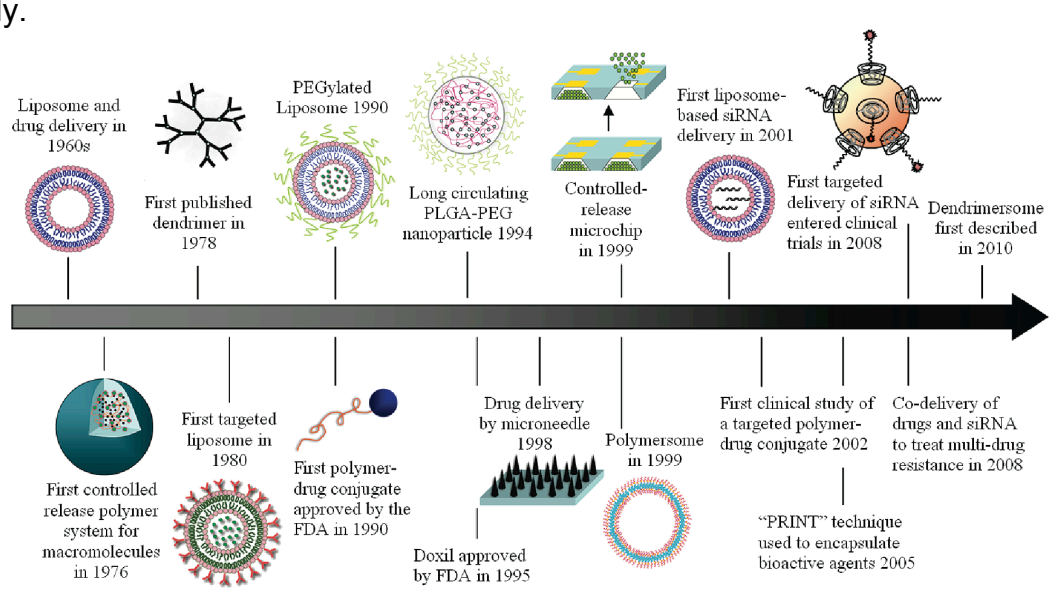

Figure 1. Organic and inorganic nanomaterials and devices.

1.2 VIRAL AND NON VIRAL VECTORS FOR DRUG DELIVERY

Actually, drug delivery is performed using viral and non-viral vectors. Viral vectors are used to deliver genes into eukaryotic cells to regulate cellular functions or to express therapeutically useful proteins. This strategy is still facing major technical hurdles which need to be more efficiently investigated, such as selectivity, tissue tropism, regulation and level of gene expression and immunogenicity; although, several strategies have been developed, their clinical application has often been drawn back by side effect and toxicity problems. Viral vectors can be based either on RNA viruses or DNA viruses.

Nonviral delivery techniques include *physical approaches* (such as microinjection, particle bombardment and electroporation) and *chemical approaches* (such as cationic lipids, diethyl aminoethyl (DEAE)-dextran, calcium phosphate, proteins, peptides, dendrimers, liposomes and controlled-release polymers) that are mostly aimed at depositing DNA into cells.

1.2.1 VIRAL VECTORS

Vectors based on RNA viruses.

Retroviruses were initially chosen as the most promising gene-transfer vehicles and about 60% of all approved clinical protocols utilize them. Retroviruses have minimal risks because they have evolved into relatively non-pathogenic parasites (although there are exceptions, such as the human immunodeficiency viruses (HIV) and human T-cell lymphotropic viruses (HTLV). The vectors themselves have all of the viral genes removed, are fully replication-defective and can accept up to about 8 kilobases (kb) of exogenous DNA.

The problems that investigators face in developing retroviral vectors, that are effective in treating diseases, are of four main types: obtaining efficient delivery, sustaining long-term gene expression, and developing a cost-effective way to manufacture the vector.

Obtaining efficient delivery.
Currently, the cells transduced by retroviral vectors possess a high level of the natural MuLV (amphotropic) receptor and an important target cell is the Hematopoietic Stem Cell (HSC) because gene transfer into these primitive cells would result in gene-engineered cells for the life of the recipient. Unfortunately, HSCs have a low level of amphotropic receptor resulting poorly transducible[14]. The broad range of cell types possessing the amphotropic receptor, known to be a phosphate symport, limits the target-specific utility of these vectors in the *in vivo* approach.
Progress has been made using a second approach to targeting called 'tethering', consisting into the insertion of a ligand that recognizes any extracellular matrix (ECM) components, such as fibronectin and collagen[15,16].

Improving gene expression.
Several factors are involved in maintaining the stable expression of genes after their transfer; first, the regulatory sequences that control gene expression often do not remain active and second, even if the gene stays active within the cell, the cell often dies because the immune system is designed to recognize and eliminate foreign gene products and cells that produce foreign proteins.
Another important factor that could reduce the gene expression stability is that even if regulatory elements are active, they may not function without the proper signals and feedback mechanisms. The goal is to use regulatory sequences that respond to the body's own physiological signals or to drugs that can be used to control the level of gene activity.

Manufacturing the vector.
Retroviral vectors are biological agents: they can only be made by living cells that do not represent the easiest systems in which to carry out good manufacturing practice (GMP) and quality assurance/quality control (QA/QC) procedures mandated by the Food and Drug Administration (FDA).
The possibility that a replication-competent retrovirus (RCR) could arise during the manufacturing process and the ability of retroviral vectors to integrate randomly into host cell DNA, limit considerably their manufacturing. These issues are resolvable, but it will take several years of product development to achieve a cost-effective system that will produce safe, efficient gene-therapy vectors on a sufficient scale to allow worldwide marketing.

Vectors based on DNA viruses
Adenoviral vectors
Adenoviruses are DNA viruses, they have been isolated from a large number of different species, and more than 100 different serotypes have been reported. Adenoviruses are used as vehicles to administer targeted therapy; first-generation adenoviral vectors are replication attenuated by removal of the early region 1 (E1a and E1b). Without the E1A gene, viral genes are not expressed at high enough levels for effective replication and packaging, leaving the recombinant virus as a simple carrier of therapeutic genes. More recently, so-called second-generation vectors

have even more viral genes removed to allow for larger transgene packages and to minimize host immune response to viral gene products.
Adenoviral vectors have several positive features: they are large and can therefore potentially hold large DNA inserts (up to 35 kb); they are human viruses and are able to transduce a large number of different human cell types with very high efficiency (often reaching nearly 100~% in vitro); they can transduce non-dividing cells; and they can be produced at very high titres in culture. Nevertheless adenoviral vectors have certain drawbacks; first generation vectors have to be deleted for several DNA regions in order to render them replication-defective and to create space for the insertion of transgenes and the deletion of more and more viral genes may not always be advantageous because some of these genes may have beneficial attributes, for example suppressing an immune response against the vector.

Adeno-associated viral vectors.

Another DNA virus used in clinical trials is the adeno-associated virus (AAV). This is a non-pathogenic virus that is widespread in the human population (about 80% of humans have antibodies directed against AAV). Interest in this virus has arisen because it is the only known mammalian virus showing preferential integration into a specific region in the genome; consequently its insertion site appears to be a 'safe' region in the genome.
However, there are several disadvantages: some cells require a very high multiplicity of infection (the number of viral particles per cell required to achieve transduction); the AAV genome is small, only allowing room for about 4.8 kb of added DNA; and the production of viral particles is still very labour intensive because efficient packaging cells have not yet been developed.

Other DNA virus-based vectors.

Other DNA viruses are being studied as possible gene-therapy vectors for specific situations. For example, herpes simplex virus (HSV) vectors have a propensity for transducing cells of the nervous system[17,18], as well as several other cell types. A stripped-down version of the HSV may have certain advantages, particularly when combined with components from other viral systems[19]. A number of other DNA virus vectors are under study including poxviruses.

Although viral systems are potentially very efficient, two factors suggest that non-viral gene delivery systems will be the preferred choice in the future: safety, and easy of manufacturing. A totally synthetic gene-delivery system could be engineered to avoid the danger of producing recombinant virus or other toxic effects engendered by biologically active viral particles. Also, manufacturing a synthetic product should be less complex than using tissue culture cells.

1.2.2 NON VIRAL VECTORS

1.2.2.1 Physical approaches:

Multiple physical devices have been used to overcome biological barriers:
Ultrasound devices (sonophoresis, sonoporation and acoustic ablation).
The use of ultrasound to deliver drugs across the skin has a long history dating back to the middle of the 20th century, a phenomenon termed as sonophoresis or phonophoresis. A broad spectrum of ultrasound frequencies (20 kHz–16 MHz) has been used for sonophoresis. However, in early–mid 1990s, low-frequency ultrasound (20–100 kHz) was shown to be more effective compared to high frequencies and was shown to deliver high molecular weight drugs including proteins and nucleotides[20]. Ultrasound induces nano-scale ultrastructural defects in the lipid regions of the stratum corneum, thus increasing its permeability[21]. This opens up the possibility for using ultrasound in the treatment of diabetes by simultaneous continuous monitoring of blood glucose level and delivery of insulin.
Ultrasound-induced disruption of the blood–brain-barrier has been used to enhance drug penetration into to the brain by disrupting the tight junctions between the capillary endothelial[22-24].

Electrical devices (iontophoresis and electroporation).
Application of low amplitude electric currents has been shown to enhance transdermal transport of drugs, especially for charged molecules, a phenomenon referred to as iontophoresis[25]. This phenomenon has been used for transdermal delivery of various low molecular weight drugs including lidocaine[26] and dexamethasone[27] as well as high molecular weight drugs including insulin[28] and luteinizing hormone-releasing hormone[29]. Iontophoretic delivery of lidocaine has been clinically approved for local anesthesia[26] and of pilocarpine for diagnosis of cystic fibrosis[30].

High pressure devices (liquid and powder injections).
Liquid jet injections employ a high-speed jet to puncture the skin and deliver drugs without the use of a needle. The basic design of liquid jet injectors consists of a compressed gas or spring, drug-loaded compartment and a nozzle with orifice sizes typically ranging between 150 and 300 μm.
The key advantages of jet injectors include the ability to use currently approved formulations, ability to work without electronics and power and provision of small portable devices.
Jet injectors have been used for mass immunization programs for diseases including measles, smallpox, cholera, hepatitis B, influenza and polio. They have also been used for delivery of insulin and growth hormones[31].

Microneedles (solid, hollow and degradable microneedles).
Microneedles are arrays of short and thin needles that can penetrate into skin at least up to epidermis and enhance drug penetration into skin. Four different types of microneedle designs have been developed: (i) solid microneedles that pierce the skin and enhance skin permeability, (ii) solid microneedles that are coated with dry powder drugs or vaccines that dissolve in the skin upon piercing, (iii) polymer microneedles that encapsulate drugs and deliver them in the skin similar to implanted polymer devices, and (iv), hollow microneedles that infuse drugs in the skin.

Microneedles have been made from various metals and organic polymers including biodegradable materials.
Numerous studies have been performed that report the ability of microneedles to enhance the penetration of drugs *in vitro*, in animals and in humans. Microneedle application has been shown to enhance skin permeability to a variety of compounds ranging from low molecular weight tracers to proteins, DNA and nanoparticles. Human studies have shown delivery of various drugs including naltrexone, lidocaine and insulin[32].

Thermal and optical devices (lasers and radio-frequency heating).
Several studies have reported on the use of thermal and laser sources for ablation of biological barriers. Thermal ablation of skin that selectively removes stratum corneum without damaging deeper tissues is achieved through careful control of skin surface temperature over a short duration of time. Rapid heating of skin restricts the ablation to stratum corneum while leaving deeper viable tissue cooler and structurally intact[33]
Lasers have also been used to enhance drug delivery into various tissues including skin. In case of skin, lasers are used to ablate the stratum corneum of the skin by deposition of optical energy, which induces instant evaporation of water leading to the formation of microchannels in the skin. The depth of the channels can be controlled through exposure time and other parameters and is often controlled to less than 200 μm so as to avoid pain and bleeding.

Although these methodologies are commonly used for both *in vitro* and *in vivo* studies, they appear invasive and over time they could damage cellular membrane; for this reason, the identification of a non invasive system, useful for intracellular delivery of a bioactive molecule, results indispensable.

1.2.2.2 Chemical approaches

Peptide vectors for intracellular delivery.
Cell penetrating peptides (CPP) are among the most promising non-viral strategies. Although defining CPPs is rather difficult in view of the fact that new CPPs are continuously discovered; they can generally be considered as short peptides of less than 30 amino acids either derived from proteins or from chimeric sequences which are very promising for cellular uptake and membrane interaction studies. While individual CPPs differ in length and sequence, they share some common features, which include their amphipathic nature, net positive charge, hydrophobicity and helical moment, the ability to interact with lipidic membranes, and to adopt a distinct secondary structure upon association with lipids[34-36]. CPPs can be subdivided into two main classes; the first requiring chemical linkage with the cargo and the second involving the formation of stable, noncovalent complexes[36,37]. CPPs from both classes have been described to efficiently deliver a large number of cargos (plasmid DNA, oligonucleotide, siRNA, PNA, protein, peptide, liposome, nanoparticle, etc.) into a wide variety of cell types and *in vivo* models[35]. The idea of molecular transporters came about 20 years ago based on the observation that some proteins; mainly transcription factors; could move within cells and from one cell to another. The first protein able to translocate across cell membranes and to reach intracellular access was described in 1988. This was the human immunodeficiency virus (HIV) transactivator of transcription protein called Tat[38]. This key discovery was soon after followed by the identification of Antennapedia (Antp), a transcription factor of *Drosophila melanogaster* that was shown to be internalized by neuronal cells[39].

These works laid the foundation for the discovery that selected portions of proteins could translocate inside cells. The first of these domains which was named Protein Transduction Domain (PTD), was a 16-mer peptide derived from the third helix of the homeodomain of Antennapedia named Penetratin. The first use of a PTD as a vector was described when penetratin was employed for the delivery of a small exogenous peptide in 1994[40]. In 1997, Vives *et al.* reported the identification of the minimal sequence of Tat required for cellular uptake[41] and the first application of PTDs *in vivo* was reported by Schwarze *et al.* for the delivery of a biologically active beta-galactosidase protein into the mouse[42]. The concept of cell penetrating peptide (CPP) was introduced in 1998; with the design of the first synthetic peptide carrier, the Transportan, which is a 27 amino acid long peptide containing 12 functional amino acids from the amino terminus of the neuropeptide galanin and mastoparan (a wasp venom peptide) at the carboxyl terminy[43]. Nowadays the definitions PTD and CPP are overlapping.

Since the early discoveries, the list of available CPPs has impressively grown and their number continues to increase (Table 2).

Actually, CPPs constitute one of the most promising tool for the non-invasive intracellular transport of cargos and have been successfully applied for the delivery of therapeutic molecules varying from small chemical molecules, nucleic acids, proteins, peptides, liposomes to particles.

Novel classes and applications of CPPs are being constantly discovered and have been reported through the study of proteins of the most various organisms. They differ significantly in their sequence, hydrophobicity, and polarity. Mainly, CPPs can be divided into three classes: a) protein derived peptides represented by short stretches of a protein domain that are the primary responsible for their translocation ability (examples: TAT, penetratin or pANTP, transportan, HSV-1 VP22); b) amphipathic peptides resulting from the sequential assembly of hydrophobic and hydrophilic domains (examples: MAP, MPG, Pep-1); c) synthetic or cationic peptides such as poliarginines (Arg9). Examples of known CPPs are reported.

Penetratin

The Antennapedia motif is derived from a family of Drosophila homeoproteins; a class of trans-activating factors involved in the developmental process. These proteins recognise and bind DNA through a 60 amino acid carboxy-terminal region arranged in three α-helical sequences; called the homeodomain. The third helix of the homeodomain, comprising just 16 amino acids, also possesses this unusual property, enabling small molecules to be taken up into live cells [44]. Today, this peptide is commonly referred to as penetratin. The two residues of tryptophan present in penetratin are considered a necessary requirement for traslocation; their replacement with hydrophobic amino acids strongly decreases the internalization. The high arginine and lysine content of penetratin gives it a positive charge at physiological pH. Penetratin shows high propensity to adopt an helical conformation in membrane mimetic conditions; but in presence of phospholipids vesicles it adopts a β-sheet structure with a residual α-helical content at low concentrations[45,46].

Transportan

Trasportan is a synthetic analogue of the peptide galanin synthesized by Poogie *et al.* and described in their study in 1998[43]. It is a 27 amino acids long peptide and contains 12 functional amino acids taken from the neuropeptide galanin followed by a lysine connection and the remaining is made by mastoparan, a wasp venom peptide toxin. Transportan can, in contrast to the galanin and mastoparan peptides alone, translocate through biological membranes and carry large hydrophilic molecules into

the cell without destroying the membrane[47] After entering the cell, the peptide can be detected in the nuclear membrane and subsequently in the nucleus. Circular dichroism studies of transportan revealed a random coil secondary structure in water which could reach 60% helical conformation in SDS mimetic conditions. Further studies by Nuclear Magnetic Resonance (NMR) in lipidic bicelles showed a well-defined α-helix in the C-terminal mastoparan part of the peptide and a weaker tendency to form an α-helix in the N- terminal domain[48].

Model Amphipathic Peptides (MAP)

Model amphipathic peptides (MAP) are derived from the α-helical amphipathic model peptide KLALKLALKALKAALKLA, designed by Steiner ***et al.***[49] in 1991. Lysine is the main positive charge contributor and is distributed on one face of the α-helix, while the opposite face is rich in alanine residues.

This peptide has been shown to internalize by multiple, non-specific, energy-dependent and -independent processes into several types of cells[50].

Arg9

Arg9 is the prototype of the so-called polyarginine–based peptides, that simply derive from the observation that positive charged residues are crucial for translocation through biological membranes. Several studies using different cationic peptides showed the higher efficiency of polyarginines compared to the use of other residues such as histidines or lysine. As a result, homoarginine sequences have been investigated as drug delivery vehicles[51].

Other major viral-derived CPPs

Peptides derived from viral proteins seem very interesting as intracellular transporters also in consideration that the first protein showing the ability to cross membranes was the HIV-1 Tat protein. Some examples of viral derived peptide investigated and included in the CPPs family are briefly described below.

Tat 48-60 Peptide

Tat is a transcription activating factor of 101 amino acids derived from HIV-1, necessary for the replication of the virus, which has the ability to cross the plasma membrane of neighbouring cells. In particular, a short basic sequence from amino acid 48 to 60 is required for the binding of Tat to its activator RNA, which has been shown to adopt an extended structure[52]. Several peptides carrying mutations within the cationic domain of the original peptide were useful in clarifying that the translocating activity of the Tat protein is controlled by this cationic cluster of amino acids and that deletion of arginine led to non-translocating peptide.

MPG

An amphipathic peptide whose primary sequence is composed of a motif mainly constituted of hydrophobic amino acids derived from the fusion sequence of the HIV-1 protein gp41 (GALFLGFLGAAGSTMGA) associated to an hydrophilic domain with positively charged residues derived from the Nuclear Localization Sequence (NLS) of Simian virus 40 (SV40) large T antigen (PKKKRKV). These hydrophilic and hydrophobic segments are separated by a three amino-acid spacer (WSQ)[53]. It represents an interesting synthetic peptide that utilize the known properties of the glycine-rich region of viral gp41 essential for membrane fusion activity and structural stabilization in addition to the NLS of the SV40 large T antigen able to improve the nuclear targeting[54].

Pep-1

It is at least partially derived from MPG; in fact, it conserves an identical C-terminal hydrophilic domain (the NLS of SV40 large T antigen) and spacer motif, while the hydrophobic region of Pep-1 corresponds to a tryptophan-rich segment

(KETWWETWWTE) derived from the HIV-1 reverse transcriptase[55]. Pep-1 has been shown to be able to efficiently deliver a variety of peptides and proteins into several cell lines in a fully biologically active form.

Herpes Simplex Virus Type 1 (HSV-1) Protein VP22

VP22, the product of the UL49 gene of herpes simplex virus, is a major component of the tegument, a structure residing between the capsid and envelope of herpes virus particles and has been reported to traffic between cells[56]. The C-terminal 40 amino acids region of the 301 residues VP22 protein is principally responsible for the transduction property of the whole protein and can mediate the delivery of DNA and RNA oligonucleotides into cells. Sciortino *et al.*[57] Have shown that VP22 can deliver a complete mRNA that is translated within the recipient cell.

Hepatitis-B Virus (HBV) PreS2 Domain

The property of cell permeability was observed in the PreS2- domain (PLSSIFSRIGDP; subtype ayw) of the hepatitis-B virus surface antigens. PreS2 has been shown to present an amphipathic α-helix between amino acids 41 and 52. This domain is involved in PreS2 dimerization and the mutagenesis of amino acid residues within the amphipathic α-helix resulted in a loss of the α-helical structure and led to β-sheet conformation[58]. These mutations also led to a reduced oligomerization tendency and no significant cell permeability.

Name	Origin	Sequence	AA	Net Charge	Structure Water/lipid	Mean Hydro-phobicity
Protein Transduction domains						
penetratin	Antennapedia Droso-phila melanogaster	RQIKIWFQNRRMKWKK	16	+6	Random/β- sheet	-2.33
Tat 48-60	Hiv-1 Transactivator (Tat)	GRKKRRQRRRPPQ	13	+8	Random/ Random	-7.27
Chimeric CPPs						
Pep1	NLS from Simian Virus 40 large antigenti and reverse transcriptase of HIV	KETWWETWWTEWSQPKKKRKV	21	+2	Random/ β- sheet or α-helix	-2.55
Transportan	Galanin and mastoparan	GWTLNSAGYLLGKINLKALAALA KKIL	27	+4	Random/α- helix	0.84
Syntheic CPPs						
Arg9	Oligoarginine	RRRRRRRRR	9	+9	Random/ Random	-10.0
MAP	Model amphipatic pep-tides	KLALKLALKALKAALKLA	18	+5	Random/α- helix	0.65
Viral membranotropic peptides						
gH625	Glycoprotein gH of HSV typeI	HGLASTLTRWAHYNALIRAF	20	+2	Random/α- helix	0.32
MPG	A hydrofobic domain from the fusion se-quence of HIV gp41 and NLS of SV40 T-antigen	GALFLGFLGAAGSTMGAWSQPKK KRKV	27	+5	Random/β- sheet	-0.63
INF	Influenza HA2	GLFEAIEGFIENGWEGMIDGWYGC	24	-5	Random/α- helix	0.66
CADY	PPTG1 peptide	GLWRALWRLLRSLWRLLWRA	20	+5	Random/α- helix	2.39

Table 2. Examples of commonly used CPPs and some of their properties related to interaction with membranes.

1.3 BIOMOLECULES PASSAGE ACROSS THE CELL MEMBRANE

Once a drug has been administered by any route it must be absorbed into the bloodstream from the site of administration. The drug then is distributed into various body fluids and tissues to attain an effective, yet safe, concentration for a sufficient period of time at the site of action. Subsequently, the drug is inactivated or eliminated from the body, generally by metabolism (usually lipid-soluble drugs) and excretion

(mainly renal and biliary routes). The effectiveness of these processes with respect to time (pharmacokinetics) varies with the particular drug and species of animal. Within species, it is further influenced by physiologic states (age, gender, pregnancy) and disease. Finally, combinations of drugs may lead to drug interactions that can alter both drug response and disposition.

A drug usually must cross a number of cell or basement membranes before it reaches its site of action. Membrane barriers may be composed of several layers of cells (skin, vagina, cornea, placenta) or a single layer of cells (enterocytes, renal tubular epithelial cells), or they may consist only of a boundary less than 1 cell in thickness (hepatic sinusoids, mitochondrion, nucleus).

A common feature of all cell membranes is the phospholipid bilayer, about 10 nm thick, arranged with the hydrophilic heads on the outside and the lipophilic chains facing inwards. This gives a sandwich effect, with two hydrophilic layers surrounding the central hydrophobic one. Spanning this bilayer or attached to the outer or inner leaflets are glycoproteins, which may act as ion channels, receptors, intermediate messengers (G-proteins) or enzymes.

Nevertheless, the general cell membrane structure is modified in certain tissues to allow more specialized functions. Capillary endothelial cells have fenestrae, which are regions of the endothelial cell where the outer and inner membranes are fused together, with no intervening cytosol; these make the endothelium of the capillary relatively permeable; fluid in particular can pass rapidly through the cell by this route. In the case of the renal glomerular endothelium, gaps or clefts exist between cells to allow the passage of larger molecules as part of filtration. Tight junctions exist between endothelial cells of brain blood vessels, forming the blood brain barrier (BBB), intestinal mucosa and renal tubules. These limit the passage of polar molecules and also prevent the lateral movement of glycoproteins within the cell membrane, which may help to keep specialized glycoproteins at their site of action (e.g. transport glycoproteins on the luminal surface of intestinal mucosa).

Therefore, an important function of a biological membrane is to serve as a barrier against the outside world. However, membranes are not impenetrable walls, obviously, nutrients must enter the cell and waste products have to leave in order for the cell to survive; for example, the movement of ions across membranes is important in regulating vital cell features such as cellular pH and osmotic pressure.

For this and many other reasons, it is crucial that membranes are selectively permeable; membrane high selectivity and controlled permeability are indeed key determinant in the effectiveness of drug absorption, distribution, and elimination. Accordingly, approaches to knock down these barriers have received significant attention in the last few decades.

The efficacy of a biomolecule, which should be used as a therapeutic and/or diagnostic agent in biomedical research and in the pharmaceutical industry, is subject to its pharmacodistribution properties. Thus, cell compartmentalization and impermeability of membranes represent the major obstacle for delivery of therapeutic molecules; in fact, many bioactive molecules are incapable of overcoming the membrane permeability barrier and this represents the major impediment for gene and drug targeting in theranostics. Although a wide variety of biodrugs, including peptides and proteins, are now produced on a commercial scale, one challenging task for pharmaceutical researchers is devise ways to deliver these drugs effectively and safely via non-invasive, patient-friendly routes.

In particular, many pharmaceutical agents should be delivered intracellularly to exert their therapeutic action inside the cytoplasm or onto individual organelles, such as

nuclei (target for gene and antisense therapy), lysosomes (target for the delivery of deficient lysosomal enzymes), and mitochondria (target for pro-apoptotic anticancer drugs). Thus, intracellular delivery of therapeutic molecules is one of the key problems in drug delivery[59].

1.3.1 Factors influencing the rate of diffusion

The drug rate of diffusion and consequently its intracellular bioavailability depend on several parameters relative to drug and membrane physicochemical properties, in particular: molecular size, concentration gradient, ionization, lipid solubility.

Molecular size.

The rate of passive diffusion is inversely proportional to the square root of molecular size (Graham's law). In general, small molecules will diffuse much more readily than large ones.

Concentration gradient.

Fick's law states that the rate of transfer across a membrane is proportional to the concentration gradient across the membrane. Thus, increasing the plasma concentration of the unbound fraction of drug will increase its rate of transfer across the membrane and will accelerate the onset of its pharmacological effect.

Ionization.

The lipophilic nature of the cell membrane only permits the passage of the uncharged fraction of any drug. The degree to which a drug is ionized in a solution depends on the molecular structure of the drug and the pH of the solution in which it is dissolved and is given by the Henderson–Hasselbalch equation.

Lipid solubility.

The lipid solubility of a drug reflects its ability to pass through the cell membrane; this property is independent of the pKa of the drug. However, high lipid solubility alone does not necessarily result in a rapid onset of action.

1.3.2 Cell membranes crossing mechanisms

The efficacy of a macromolecule to be internalized into the cytoplasm and to exercise its intracellular action also depends on the mechanism used to cross the plasmatic membrane.

Several basic cellular mechanisms can be exploited for the intracellular delivery of a compound across the plasma membrane (Figure 2). There are active mechanisms, such as endocytosis, and passive mechanisms, such as translocation across the lipid bilayer; alternatively, there are highly invasive procedures, such as microinjection and/or electroporation, which could cause transient damage to membranes.

The internalization processes are mainly classified in three types and a brief description is reported below.

Passive diffusion

This is the commonest method for crossing the cell membrane. Drug molecules move down a concentration gradient, from an area of high concentration to one of low concentration, and the process requires no energy to proceed. Many drugs are weak acids or weak bases and can exist in either the unionized or ionized form, depending on the pH. The unionized form of a drug is lipid-soluble and diffuses easily by dissolution in the lipid bilayer. Thus the rate at which transfer occurs depends on the pKa of the drug in question.

In addition, there are specialized ion channels in the membrane that allow intermittent passive movement of selected ions down a concentration gradient.

Ion channels may have their permeability altered by endogenous compounds or by

drugs.

Facilitated diffusion

Facilitated diffusion refers to the process where molecules combine with membrane-bound carrier proteins to cross the membrane. The rate of diffusion of the molecule–protein complex is still down a concentration gradient but is faster than would be expected by diffusion alone. Examples of this process include the absorption of steroids and amino acids from the gut lumen. The absorption of glucose, a very polar molecule, would be relatively slow if it occurred by diffusion alone and requires facilitated diffusion to cross membranes (including the BBB) rapidly.

Active transport

It is an energy-requiring process, like the endocytosis. The molecule is transported against its concentration gradient by a molecular pump, which requires energy to function. Energy can be supplied either directly to the ion pump, or indirectly by coupling pump-action to an ionic gradient that is actively maintained.

Pinocytosis

Pinocytosis is the process by which an area of the cell membrane invaginates around the (usually large) target molecule and moves it into the cell. The molecule may then be released into the cell or may remain in the created vacuole, until the reverse process occurs on the opposite side of the cell.

The process is usually used for molecules that are too large to traverse the membrane easily via another mechanism.

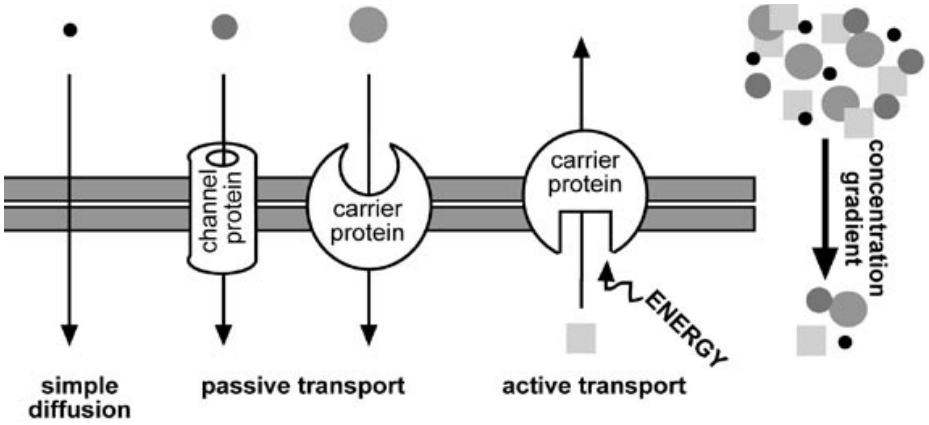

Figure 2. Cell membranes crossing mechanisms.

1.3.3 CPPs cell entry

The entry mechanism of CPPs into cells is still a matter of debate. Historically, two hypotheses were put forward to explain how these peptides could cross the plasmatic membrane and possibly deliver various kinds of molecules into the cell[60] It was first proposed that CPPs, especially Tat and Antennapedia, but also others such as poly-Arg[61], Transportan[62], MPG[53] or Pep-1[55], could pass through the plasma membrane via an energy-independent pathway. This hypothesis of a direct translocation through the plasma membrane became less popular when the entry mechanism for the Tat and the poly-arginine CPPs had to be re-evaluated following evidences of fixation artifacts during the preparation of samples for microscopic observation[63]. Indeed, fixation has been described to interfere with the sub-cellular localization of constructs with a high content of cationic residues, such as histones and the VP22 protein[64].

As a consequence, the majority of the new microscopic studies on CPPs localization have been conducted on living cells and the conclusions that can be drawn from these very elegant works could be that CPPs mainly follow a cellular endocytosis-mediated uptake[65-67].

According to this mechanism, CPPs, particularly those with a high content in cationic residues, are first simply adsorbed at the cell surface thanks to the numerous anionic moieties, such as heparan sulfate, sialic or phospholipidic acid[68-70], then CPP-mediated transport proceeds through different endocytosis routes[63]: caveolae[71], macropinocytosis[72,73], clathrin-dependent pathway[74], cholesterol-dependent clathrin-mediated pathways[75] or the trans-Golgi network[76].

Moreover, the way of entry into the cell is also influenced by the nature of the cargo (eventually transported), the type of CPP, the cell line and the conditions of incubation.

Since the endosomial pathway is mainly involved in the cellular delivery of CPPs and CPPs-conjugated molecules independent from initial route, a strong enzymatic degradation within this compartment and consequently a poor cytoplasmic release of intact molecules are expected, leading to a global weak drug transfer into the cytoplasm. In conclusion, the endosomal entrapment may limit the utility of CPPs.

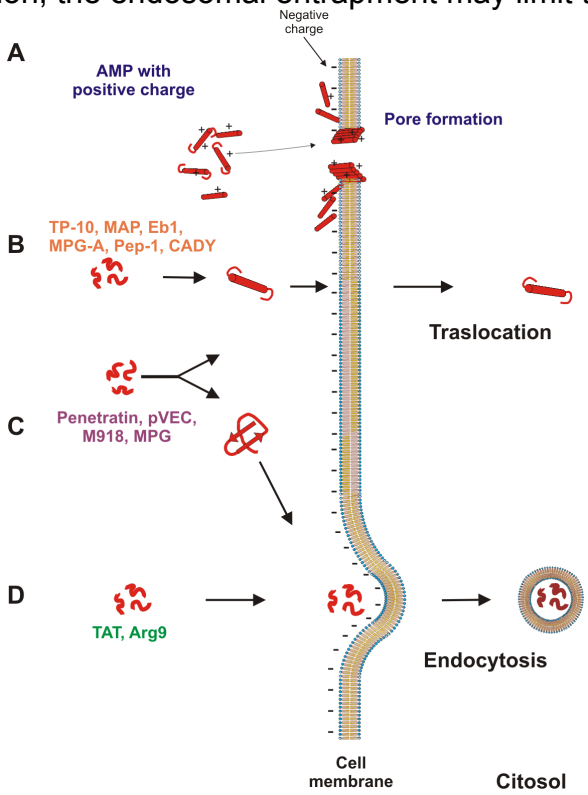

Figure 3. Proposed mechanisms of cellular internalization pathways of different CPPs. For simplicity; the pathways described have been indicated for specific peptides; none of the pathways proposed is mutually exclusive.

Toxicity of cationic CPPs.

Several groups work on the determination of *in vitro* and *in vivo* cellular toxicity of CPPs. When the minimal membrane-translocating Tat domain was discovered, no toxicity was found in very extreme conditions on HeLa cells (24 h incubation at 100 micromolar concentration), this absence of toxicity was also shown in other studies for example, Toro *et al.* confirmed that the short Tat peptide was not toxic for lymphocytes at dose up to 300 μM[77] and no toxicity was observed in HeLa or Jurkat

cells up to 20-30 μM concentrations of Antp, Rev and VP22[78]. Nevertheless, because of their highly cationic nature, some CPPs could be as toxic as other cationic polymers such as poly-L-Lysine or poly-ethylene imine (PEI)[79].
Finally, the internalization mechanism used by CPPs, as well as their supposed toxicity, seems to reduce considerably their applications in the planning of novel useful drug delivery systems (Figure 3).
Although the uptake mechanism of CPPs is largely debated it seems to involve mainly the endocytic pathway, trapping the conjugated cargo (eventually transported) in endosomes lastly ending in lysosomes where common enzymatic degradation processes take place decreasing its intracellular bioavailability.
Therefore, it is of paramount importance to identify novel peptides and peptide-based drug delivery tools, with different physicochemical properties and which use alternative internalization routes in order to optimize the uptake kinetic/rate and the intracytoplasmatic distribution improving thus their target-specific bioactivity.

1.4 VIRAL INFECTION STRATEGIES

Viruses can be classified as enveloped and non-enveloped viruses according to the presence or absence of a membrane bilayer surrounding the capsid. The mechanisms of genome release are widely different between enveloped and non-enveloped viruses. In fact, enveloped viruses fuse with the plasma or endosome membranes, thereby exposing the genome or capsid to the cytosol; whereas non-enveloped viruses partially disrupt membranes to release viral nucleic acids[80-82].
But, in any case, the transfer of the genome through the barrier of a cellular membrane into the cytosol is imperative for viral infections to occur.
Non-enveloped viruses
Non-enveloped viruses can seize the cytoplasm of the host cell by direct penetration through the plasma membrane or by a variety of endocytotic mechanisms that collectively lead to the penetration of internal membranes. In such way they do not differ much from what enveloped viruses do while invading cells; that is taking control of common cellular pathways. The main difference with enveloped viruses is posed by the absence of a membrane surrounding the proteinaceous capsid; therefore fusion events cannot happen; but capsid-dependent mechanisms for penetrating the cell membrane or, alternatively, for lysing the endosome are likely to be required.
The process of non-enveloped viruses entry is generally started by an interaction with a cellular stimulus (e.g.; receptors, low pH, proteases) at the penetration site which drives a conformational change that in some instances triggers the release of viral components with membrane lytic activity. This is followed by the binding of the hydrophobic component or lytic factor to the cell membrane.
Therefore, membrane penetration seems to be mediated by short, membrane interacting, amphipathic or hydrophobic sequences contained in proteins which have undergone a conformation transition, allowing the exposure of such sequences and consequently their interaction with membranes[83].
Enveloped Viruses
All enveloped viruses use two main routes to enter cells, either by the endocytic or non-endocytic routes, and share common steps. Clathrin coated vesicles, but non-clathrin-coated pits; macropinocytosis or caveolae are all pathways exploited by viruses preferring the endocytic route; while the non-endocytic path involves direct crossing of the plasma membrane at neutral pH.
Essentially the basic mode of entry by enveloped viruses is through membrane

fusion; an essential and ubiquitous mechanism in most cellular events. Virally-induced fusion is mediated by viral membrane proteins which undergo remarkable conformational modifications as a consequence of a trigger that is represented either by low endosomal pH or receptor binding. These conformational changes lead to the exposure of hydrophobic peptides, loops or patches (the so called fusion peptides), which then interact with and destabilize one or both of the opposing membranes.
Three different classes of viral fusion proteins have been identified to date based on their common post-fusion structural motifs[80,84]. These are: (i) class I fusion proteins, characterized by trimers of hairpins containing a central α-helical coiled-coil structure; (ii) class II fusion proteins, characterized by trimers of hairpins composed of β-structures; (iii) class III fusion proteins, that show features of both classes.
Viruses, like all obligate intracellular pathogens, must overcome numerous barriers in the host cell to deliver their nucleic acid into the cytosol or nucleus. This is the key to initiating their infectious cycle and involves a number of distinct and subsequent steps like binding to one or more cellular receptors and entry, capsid destabilization and genome uncoating, ending in the release of viral nucleic acids at the proper site of replication. The most critical barrier is represented by the complex membranous system surrounding the host cell.
Since viruses may enter cells either through a endosomal pathway or via direct fusion on the plasma membrane through the activity of membranotropic peptides; great attention has been devoted to the study of hydrophobic peptides that efficiently traverse biological membranes, promoting lipid-membrane reorganizing processes, such as fusion or pore formation and involving temporary membrane destabilization and subsequent reorganization[85,86], which may be able to circumvent the endosomal entrapment either favouring the escape from the endosome or by translocating a cargo through the plasma membrane directly into the cytosol. Delivery across cellular membranes involves several mechanisms such as direct transfer through cell surface membrane by lipid membrane fusion or transient permeabilization of the cell membrane. Alternatively, following endocytosis, transfer across vesicular membranes by lipid disruption, pore formation or fusion may take place. Several of these membrane reorganization steps are also involved in the cell entry of viruses and other microorganisms, as well as being triggered by protein toxins and defence peptides[87]. Several related processes, such as intracellular vesicle budding, cell to cell fusion[86], sperm-egg fusion or the immune response share common features to the mechanism of viral-induced membrane fusion.
Therefore, it is of paramount importance to discover new methodologies to reproduce enveloped viruses non endocytic-behaviour assumed during the host cells infection phase.
Recently, great attention has been devoted to the study of virus derived hydrophobic peptides that efficiently traverse biological membranes, promoting membrane-reorganizing processes, like fusion or pore formation for the design of novel delivering tools.

1.4.1 Herpes simplex virus type 1 fusion machinery

Herpes simplex virus (HSV), the prototype of the alpha herpes viruses, is a human pathogen that infects epithelial cells before spreading to the peripheral nervous system to establish a life-long latent infection. HSV-1 infection, similarly to other enveloped viruses, is achieved through fusion of the lipid bilayer of the viral envelope with a host cell membrane. The core fusion machinery of herpesviruses is well

conserved and consists of the envelope glycoprotein B (gB) and the heterodimeric complex of gH/gL[88]. Although numerous studies have indicated that both gB and gH/gL exhibit varying degrees of fusogenic properties, the complete fusion is only achieved when the three proteins act together[89]. Because both glycoproteins (gB and gH) are conserved in all herpesvirus subfamilies, it is likely that they perform a common function in all members of this virus family; they appear to be triggered by the action of glycoprotein gD, which binds cellular receptors, *e.g.* nectin1, and either bridges gB and gH/gL into a larger complex or interacts with gB/gH/gL-preformed complexes[90]. Notwithstanding how the active complex is assembled, the quartet of envelope glycoproteins promotes fusion of the virion envelope with cellular membranes, and both gB and gH appear to be directly involved in membrane fusion, *i.e.* in mixing of lipids.

Structural knowledge of the proteins participating in herpes-virus fusion is essential for understanding the molecular mechanism of the entry process. The recently solved crystal structure of the HSV-1 gB ectodomain revealed an unexpected structural homology with the fusogenic protein G of vesicular stomatitis virus[91].

The fusogenic properties of gB are now well established[92] and its structural details suggested that it belongs to a third class of fusion proteins where the fusion peptide is represented by a bipartite loop domain. HSV-1 gH is an 838-residue glycoprotein, the ectodomain contains 7 N-glycosylation sites and 8 cysteine residues forming at least 2 disulfide bonds between cysteines 5 and 6 (residue 554 and 589) and cysteines 7 and 8 (residues 652 and 706)[93]. Several domains likely to be important for membrane fusion have been identified in the C-terminal region of gH. For example, mutations in the pretransmembrane domain[94], transmembrane region, and cytoplasmic tail[95] affect fusion. Furthermore, peptides matching a number of regions of the gH ectodomain have been shown to interact with membranes and proposed to play a role in the fusion process.

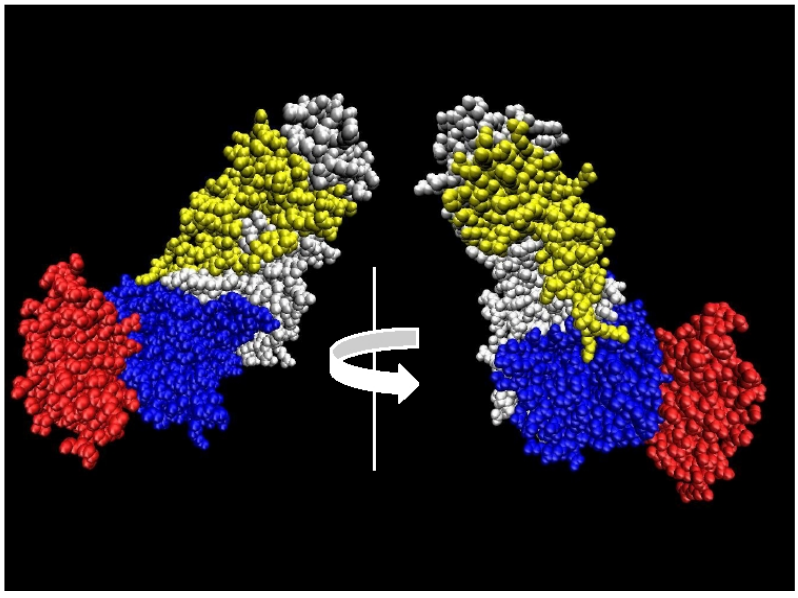

Figure 4 Crystal structure of gH-gL complex. White: H1 Domain; Blue: H2 Domain and Red: H3 Domain of gH. Yellow: gL interacting with H1of gH.

Moreover, peptides spanning the heptad-repeat region of gH inhibit the entry of both human cytomegalovirus[96] and HSV-1, while others have the ability to bind and disrupt

model membranes. The recently solved crystal structure of the gH-gL complex (Figure 4) showed that gH has no structural homology with any known fusion protein supporting the hypothesis that gH may act as a regulator of fusion through interactions with gB, while the crystal structure of the gH-gL complex of EBV presents considerable differences in the structural arrangements of domains supporting the view that the complex can undergo dynamic rearrangements.

1.4.2 Identification of a membranotropic peptide: gH625

To determine the best sequence able to induce HSV fusion, several gH and gB derived peptides were synthesized and modified; these studies brought to the identification of gH-625.
The nineteen residues peptide gH625 (from aa 625 to aa 644), is a membrane-perturbing domain derived from the gH fusion glycoprotein of Herpes simplex virus type 1[88,97]. gH625 interacts with biological membranes and is implicated in the merging of the viral envelope and the cellular membrane[98,99]. The peptide gH625 contains particular residues that are crucial for the capacity of the peptide to interact and destabilize target lipid membranes. It is rich in hydrophobic residues including glycines, leucines, alanines, and aromatic residues such as tryptophan and tyrosines, which are known to be located preferentially at the membrane interface. An amphipathic α-helix is believed to be an important feature of fusion peptides playing a crucial role in mediating lipid-protein interactions during the binding of proteins to membranes and once bound, the hydrophobic face of the amphipathic peptide would then allow the peptide to enter the membrane interior, thereby triggering local fusion of the membrane leaflets, pore formation, cracks and membrane fusion. gH625 has been shown to strongly interact and to spontaneously penetrate the lipid-phase and insert into membranes[100]. The peptide–lipid interactions are initiated by the arginine residue located at the C-terminus, in fact, when the arginine is mutated the fusogenic activity of the peptide is strongly impaired. The hydrophobic domain is also crucial for insertion of the peptide into the membrane and corroborates the notion that hydrophobic interactions between fusion proteins and cell-membrane phospholipids initiate membrane perturbation in the early stages of viral fusion. gH625 cellular uptake is thus associated with its ability to interact with membrane lipids and to form a transient helical structure that temporarily affects membrane organization, thereby facilitating insertion into the membrane and translocation[59]. Compared to Tat peptide which mainly exploits the endocytic pathway, the viral membranotropic peptide gH625 crosses membrane bilayers mainly through a translocation mechanism. A one aminoacid shorter version of this fusogenic peptide from HSV-1 gH (missing the histidine at position 625) was also found to improve the endosomal release of DNA/Lipofectamine lipoplexes and transgene expression up to 30-fold in human cell lines[101].

AIM OF WORK

This project targets major advances in the design and realization of a new nanotechnological system for theranostics. A fundamental limitation of current diagnostics and therapeutics is the lack of a single delivery system that has the potential to deliver therapeutics not only to the disease site of interest with high fidelity, i.e. target delivery, but also allows for diagnostics and cell delivery, i.e. cell penetration and uptake. The goal of this research project was to overcome this limitation and to create a toolbox that allows an efficient intracellular delivery of bioactive molecules. As a first step toward this goal, the objective was to engineer novel peptide based scaffolds with controlled architecture groups to enhance cellular uptake and present a drug, and group(s) for imaging. This goal was addressed with a multidisciplinary approach involving peptide design and synthesis, organic synthesis and cellular biology knowledges. The overall objective of the project of this thesis has been accomplished following two specific aims:

1. *Identification and characterization of a novel viral derived peptide able to efficiently enter into the cells;*
2. *Synthesis and physicochemical characterization of several viral peptide based nano-vehicles useful in theranostic.*

Over the past years, my research team has worked extensively on antiviral peptides derived from HSV-1 glycoproteins B and H and they have identified the gH-625 membranotropic sequence, derived from gH, as a potential intracellular transporter.

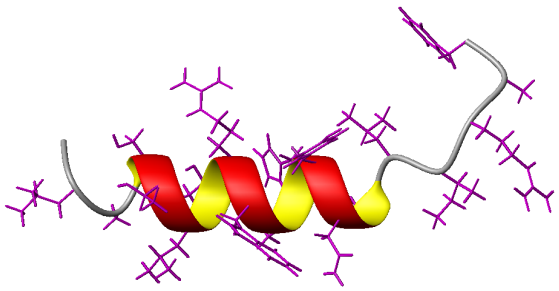

Figure 5. Three-dimensional NMR structure of gH625-644.

While the complete fusion mechanism is not completely understood, they showed that gH625 interacts with biological membranes, i.e. lipid bilayers, and is implicated in the merging of the viral envelope and the cellular membrane.

Peptide gH625 cellular uptake is thus associated with its ability to interact with membrane lipids and to form a transient helical structure that temporarily affects membrane organization, thereby facilitating insertion into the membrane and translocation. Compared to the commonly used cell penetrating peptide (CPP) Tat (RKKRRQRRR, derived from HIV-1), which mainly exploits the endocytic pathway, the viral membranotropic peptide gH625 crosses membrane bilayers mainly through a translocation mechanism. While poly(cationic) species like the Tat peptide have been known to produce cytotoxic effects, my research team has shown that gH625 is non-toxic to cells up to a concentration of 400 μM, and is at all times less toxic than the Tat peptide.

This PhD thesis research project started from the working hypothesis that gH625 could be exploited to develop a novel nanosystem for theranostics. In particular, we proposed to explore its ability to cross the lipidic bilayer and to transport, inside different cell lines, a cargo which could be drug-loaded, and could be used for the study and care of human diseases.

The rate of diffusion across the cellular barrier, that may depend on the internalization mechanism adopted, represents one of the most important factors that

a new pharmacological system has to increase in order to explicate, efficiently, its intracellular functions. Thus, the project objective focused on the identification, synthesis and characterization, through different kinds of physicochemical and biological analysis, of gH625 based nanosystems applicable in the drug delivery field. In particular, several nanosystems (Quantum Dots, Liposomes, Dendrimers and Nanoparticles, described in detail below) with different composition, shape and size, were complexed to gH625 and characterized.
The specific goal was to combine the benefits of the chemistry of these molecules with a cell-internalization unit that can overcome the cell membrane mainly via a non-active translocation mechanism.

Quantum Dots (QDs)
Quantum dots are inorganic nanoparticles that have emerged a few years ago as drug and gene delivery systems, imaging agents and diagnostic biosensors[102,103]. Magnetic drug targeting (such as the use of iron) is characterized by conjugating a magnetic material under the action of the external magnetic field, which can accumulate in target tissue areas under the action of the external magnetic field[104]. They are a new type of fluorescence probe with high luminescence efficiency and with their emission peak tunable depending on their size. In addition, the excellent photostability of QDs gives them great potential in cellular labeling and bioimaging, and a number of works have shown these characteristics in different kinds of biological systems. QDs are advantageous due to their nanometer size, broad excitation, narrow emission, bright photoluminescence and high photostability. However, wide application of QDs to intracellular and molecular imaging has been hampered by their insufficient ability to traverse cell membranes. Thus, to use QDs as biological probes for intracellular applications, their delivery has to be improved significantly. Several authors recently reported on the functionalization of QDs with the Tat peptide or other positively charged CPPs as enhancer of cell penetration and reported on the endosomal uptake of QDs and escape from the endosomal system. Similar delivery methods may enable the implementation of the next generation of QDs capable of long-term intracellular monitoring.

Liposomes
Liposomes are phospholipid based vehicles composed of a bilayer membrane that can be divided into small unilamellar vesicles (or SUV from 20 nm to 100 nm), large unilamellar vesicles (LUV from 100 to 500 nm) and multilamellar vesicles (MVL exceeding 500 nm)[105]. These systems have the ability to encapsulate both lipophilic drugs within their membrane and hydrophilic drugs inside or outside the aqueous core and the membrane of these carriers can be altered and tuned[106]. Liposomes, which are most commonly produced with phosphatidylcholine, show great compatibility, ease of preparation, wide range of drug compatibilities, increased solubility of drugs (e.g. cycloporin A)[107], tuned pharmacokinetic profile and improved oral absorption. Commonly, they present difficulties when orally delivered due to the poor stability of the vesicles under the physiological conditions typically found in the GI tract.
Liposomal aggregates have attracted great attention due to their success as *in vivo* carriers of active principles. Liposomes display some unique pharmacokinetic properties and can be adapted to a wide range of therapeutic agents; in particular, they are non-toxic, biodegradable and non-immunogenic. Benefits associated with liposomal drugs can arise from protection of encapsulated drugs from chemical or

metabolic degradation after injection; reduced toxicity through decreased exposure of antineoplastics to susceptible healthy tissues and increased antitumor activity resulting from a relatively long systemic circulation time, an extended exposure and tumor selective accumulation in sites of tumor growth. Moreover, liposomes exhibit preferential extravasation and accumulation at the site of solid tumors due to increased endothelial permeability and reduced lymphatic drainage in these tissues, which has been defined as enhanced permeability and retention effect. Thus, associating a drug with liposomes markedly changes its pharmacokinetic and pharmacodynamic properties and lowers systemic toxicity; furthermore, the drug is prevented from early degradation and/or inactivation[108,109].

Dendrimers

Dendrimers are perfectly branched macromolecules with well-defined structures[110]. They exhibit different properties compared to linear polymers with the same composition and molecular weight[111]. The high concentration of terminal functional groups on a dendrimers surface will generally dictate the solubility of the entire compound; dendrimers have been used as unimolecular micelles, that is, hydrophobic dendrimers, that are water soluble due to peripheral hydrophilic groups or vice versa[112]. Traditional dendrimers are synthesized from monomers with the structure AB_n[113-115]. Addition of another generation of monomers causes the dendrimer to grow radially with an exponential increase in both mass and number of free termini compared to the previous generation, but only a minimal increase in the physical size of the structure. This causes the termini to become more closely packed.

Unlike many other scaffolds, dendrimers have the benefit of a highly controlled synthesis as well as yielding a single monodisperse compound, giving perfect control over the size, weight, and terminal functionalities of the resulting structure. Moreover, highly branched structures generally exhibit longer blood circulation times due to their inability to reptate through renal pores[116]. Dendrimers have been shown to have extended lifetimes *in vivo*[117] whereas lipid complexes are usually rapidly cleared from circulation by splenic and hepatic phagocytes[118]. Dendrimers represent a very promising tool for drug delivery, combining the advantageous features of nanoparticles (ideal size as *in vivo* carriers, multivalency), polymeric materials (low cost, tunable proper- ties, biocompatibility) and small molecules (monodispersity and detailed control of their properties)[119]. Little information is available on the mechanism of dendrimer uptake and intracellular trafficking. Studies performed on PAMAM dendrimers[120] and PAMAM dendrimers functionalized with the Tat[121] indicate that endocytosis mechanisms contribute to the internalization and intracellular trafficking. Some reports show that the cellular internalization mechanism of PAMAM dendrimers can be tuned by altering surface charges or hydrophobicity, but these uptake mechanisms are still mainly endocytic[122]. Other reports show that dendrimers can successfully deliver cargoes when terminated by guanidinyl units; however, in one case, it was shown that adding the Tat peptide failed to enhance delivery efficiency over the native PAMAM dendrimer. Studies using cationic PAMAM dendrimers, showed that they tend to insert into the lipid bilayer, which has the potential of weakening or forming holes in the membrane[123].

Nanoparticles (NPs)

Particles with at least one dimension smaller than 1 micron and potentially as small as atomic and molecular length scales (~0.2 nm). Many authors limit the size of

nanomaterials to 50 nm or 100 nm[124], the choice of this upper limit being justified by the fact that some physical properties of nanoparticles approach those of bulk when their size reaches these and they can therefore be classified as either nanoparticles NP (any dimension smaller than 1 micron) or microparticles MP (all dimensions larger than one micron). Generally, the sizes of nanomaterials are comparable to those of viruses, DNA and proteins, while microparticles are comparable to cells, organelles, and larger physiological structures (Figure 6).
Nanoparticles are generally classified based on their dimensionality, morphology, composition, uniformity, and agglomeration.

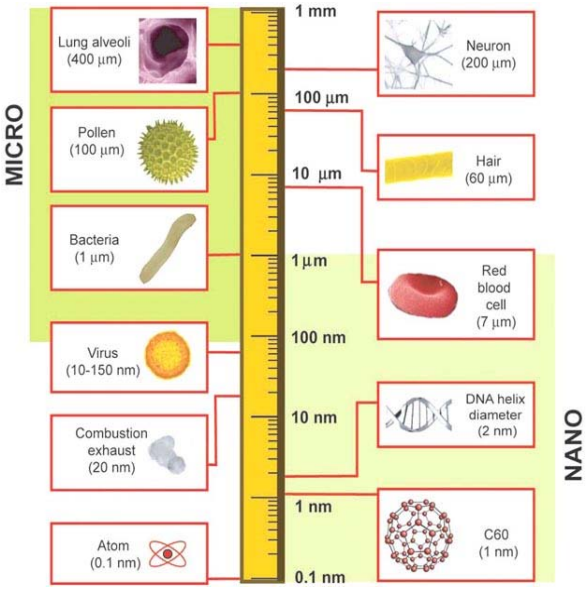

Figure 6. Nano and micro material sizes

Dimensionality

1D nanomaterials. Materials with one dimension in the nanometer scale are typically thin films or surface coatings, and include the circuitry of computer chips and the antireflection and hard coatings on eyeglasses. Thin films have been developed and used for decades in various fields, such as electronics, chemistry, and engineering

2D nanomaterials. These include 2D nanostructured films, with nanostructures firmly attached to a substrate, or nanopore filters used for small particle separation and filtration. Free particles with a large aspect ratio, with dimensions in the nanoscale range, are also considered 2D nanomaterials. Asbestos fibers are an example of 2D nanoparticles.

3D nanomaterials. Materials that are nanoscaled in all three dimensions are considered 3D nanomaterials. These include thin films deposited under conditions that generate atomic-scale porosity, colloids, and free nanoparticles with various morphologies.

Morphology

Morphological characteristics to be taken into account are: flatness, sphericity, and aspect ratio. A general classification exists between high and low aspect ratio particles. High aspect ratio nanoparticles include nanotubes and nanowires, with various shapes, such as helices, zigzags, belts, or perhaps nanowires with diameter that varies with length. Small-aspect ratio morphologies include spherical, oval, cubic, prism, helical, or pillar. Collections of many particles exist as powders, suspension, or colloids.

Composition

Nanoparticles can be composed of a single constituent material or be a composite of several materials. The nanoparticles found in nature are often agglomerations of materials with various compositions, while pure single-composition materials can be easily synthesized today by a variety of methods.

Uniformity and agglomeration

Based on their chemistry and electromagnetic properties, nanoparticles can exist as dispersed aerosols, as suspensions/colloids, or in an agglomerate state. For example, magnetic nanoparticles tend to cluster, forming an agglomerate state,

unless their surfaces are coated with a non-magnetic material. In an agglomerate state, nanoparticles may behave as larger particles, depending on the size of the agglomerate. Hence, it is evident that nanoparticle agglomeration, size and surface reactivity, along with shape and size, must be taken into account when deciding, considering health and environmental regulation of new materials.
Currently materials composed by NPs are being used in a wide variety of applications such as engineering, food industry, cosmetics and medicine[125,126]. In medicine there are major expectations for the use of nanoparticles to facilitate targeted drug delivery[127]. Due to the novelty of these applications and to ensure their success, a precise characterization of the interactions between NPs and cells is essential.
Polystyrene (PS) NPs are widely used as a model to study interactions between NPs and cells due to various practical reasons including their commercial availability, high quality and wide variety of size and surface chemistry. These NPs have been reported to enter different cell types including hepatocytes[128] macrophages[129] and lung[130]. One general conclusion is that particles smaller than 100 nm are able to enter mammalian cells. The specific uptake pathways of these NPs, as well as the uptake rates, have been shown to be cell type[131] NP size[132] and shape-dependent[133] but are also related to the surface chemistry of the NP and its hydrophobicity[134].
The nanoparticles toxicity is widely discussed in literature; the total number of papers on toxicity, however, remains low compared to the total number of publications on nanomaterials, with only around 500 publications in the year *2013*.
Thus, it is very important to recognize that not all nanoparticles are toxic; toxicity depends on at least chemical composition and shape in addition to simply size and particle ageing. In fact, many types of nanoparticles seem to be non-toxic[135], others can be rendered non-toxic while others appear to have beneficial health effects[136].

RESEARCH MANAGEMENT
The internalization of bioactive molecules is one of the most critical problems to overcome in theranostics. In order to improve pharmacokinetic and pharmacodynamic properties, synthetic transporters were widely investigated. A new nanotechnological transporter, gH625, based on a viral peptide sequence derived from the Herpes simplex virus type 1 glycoprotein H (gH) has proved to be a useful delivery vehicle, due to its intrinsic properties of inducing membrane perturbation. The peptide functionalization with several kinds of nanoparticles like quantum dots, dendrimers, and liposomes could be of particular interest in biomedical applications to improve drug release within cells, to increase site-specific action, and eventually to reduce related cytotoxicity.
This PhD project is inherently multidisciplinary. The overall project has been organized and coordinated by my group (Prof. Stefania Galdiero) from the Department of Pharmacy at the University of Naples and was also partially performed at the Molecular Design Institute & Department of Chemistry at New York University (Prof. Marcus Weck). The research team of NYU brought the following expertise to the project: functionalized monomer synthesis, dendrimer synthesis, dendrimer multifunctionalization, self-assembly, polymer characterization and fabrication, while the “Federico II” research team was involved in the planning and organization of the project, in the identification of the peptides for the delivery and in the establishment of the best synthetic strategy for the coupling of the peptide to the nanomaterial; moreover the structural characterization was performed in Naples and partially in New York.

2 MATERIAL AND METHODS

2.1 MATERIALS

Peptides were synthesized by standard solid-phase techniques on a Syro I MultiSynThec GmbH automatic synthesizer. Protected Fmoc-amino acid derivatives, coupling reagents and Rink amide *p*-methylbenzhydrylamine (MBHA) resin were purchased from Calbiochem-Novabiochem (Laufelfingen, Switzerland), Wang resin was purchased from Fluka. The Fmoc-8-amino-3,6-dioxaoctanoic acid (Fmoc-AdOO-OH) and Fmoc-L-propargylglycine (Fmoc-Pra-OH) were purchased from Neosystem (Strasbourg, France). Fmoc-l-propargylglycine (Fmoc-Pra-OH) was purchased from Neosystem. 1,2-Dioleoyl-*sn*-Glycero-3-Phosphocholine (DOPG) was purchased by Avanti Polar Lipids (Alabaster, AL). Fmoc-TOAC-OH ((2,2,6,6-tetramethylpiperidine-N-oxide-4-(9-fluorenylmethyloxycarbonyl-amino)-4-carboxylic acid) spin-label was kindly provided by Prof. C. Toniolo of the University of Padua (Italy). 4-Chloro-7-nitrobenzofurazan (NBD-Cl), Doxorubicin Hydrochloride (Dox) and the other chemicals were purchased from Sigma-Aldrich, Fluka (Buchs, Switzerland) or LabScan (Stillorgan, Dublin, Ireland) and were used as received, unless otherwise stated.

Dendron **1** was synthesized as previously reported[137,138] from starting materials purchased from Frontier Scientific. 3-Azidopropylamine[139] and 7-nitro-4-(prop-2-ynylamino) benzofurazan (NBD-CCH)[140] were synthesized as previously reported.

Orange fluorescent amine-modified polystyrene, 100 nm, (NP-NH2) were purchased by Sigma-Aldrich. Amine-functionalized eFluor Nanocrystals composed of CdSe were purchased by eBioscience.

Dialysis membranes (SpectraPor 6) were purchased from Spectrum Labs and used after rinsing the membrane in water for 30 min.

LCMS data were recorded on an Agilent LCMSD Trap XCT spectrometer using electrospray ionization (ESI) and methanol as eluent.

NMR Spectra were recorded using a Bruker AV-400 spectrometer (^{1}H: 400.1 MHz; ^{13}C: 100.6 MHz). Deuterated solvents were purchased from Cambridge Isotope Laboratories.

IR spectra were recorded with a Magna 550 FTIR on poly(ethylene) cards. Circular dichroism spectra were recorded on an Aviv model 202SF stopped flow circular dichroism spectrometer. Scanning transmission electron microscopy was performed on a Zeiss Merlin FESEM. Peptide purification was performed on LC_8 Shimadzu HPLC with a Phenomenex C_{18} column (300Å, 250x21.20 mm, 5µ) and a UV lambda-Max model 481 detector. Peptide purity was analyzed by a Finnigan Surveyor MSQ single quadrupole ESI LC-MS with a Phenomenex C_{18} column and the same eluent system.

Size-exclusion chromatography was performed using a 1 x 18 cm Sephadex G-50 column.

Cell media (Phosphate buffered saline [PBS, pH 7.4], Fetal bovine serum [FBS], 0.25% trypsin in EDTA, Eagle's minimum essential medium [EMEM], and penicillin/streptomycin solution) were purchased from Invitrogen.

Cell microscopy was done by a Nikon Eclipse Ti inverted microscope equipped with a FITC filter set for fluorescence imaging. Dynamic light scattering (DLS) was performed at 25°C on a DynaPro Protein Solutions DLS in aqueous solution.

2.2 SOLID-PHASE PEPTIDE SYNTHESIS.

Peptides (Table 1) were synthesized using standard solid-phase-9-fluorenylmethoxycarbonyl (Fmoc) procedures using a Syro I MultiSynThec GmbH (Wullener, Germany) automatic synthesizer. The Rink-amide MBHA resin (substitution 0.51 mmol/g) was used as the solid-phase support, and syntheses were performed on a scale of 20 μmol. Fmoc-amino acids, 4 equivalents relative to resin loading, were coupled according to the PyBop/HOBt/DIPEA (benzotriazol-1-yl-oxytris(pyrrolidino)phosphonium / N-hydroxybenzotriazole / Di-iso-propylethylamine) method: 1 equivalent of Fmoc-amino acid, 1 equivalent of PyBOP, 1 equivalent of HOBt (0.5 mM HOBt in DMF) and 2 equivalents of DIPEA (2 mM DIPEA in DMF). The Fmoc protecting group was removed with 30% piperidine in DMF (v/v). All couplings were performed twice for 35 minutes.

NBD labeling of peptides was performed on resin-bound peptides as previously reported by Rapaport & Shai[141] . Briefly, 30-70 mg of resin-bound peptide (10-25 μmol) was treated with piperidine in DMF in order to remove the Fmoc protecting group of the N-terminal amino-acid of the linked peptide. The resin-bound peptide was then reacted with 4-chloro-7-nitrobenz-2-oxa-1,3-diazole (NBD-Cl) in DIPEA 2 M (3-4 equiv.) in DMF. After 24 h, the resin-bound peptides were washed thoroughly with methylene chloride, and the peptides were cleaved from the resin and purified.

When necessary peptides-Pra were synthesized coupling Fmoc-Pra-OH once for 45 min with 2 equivalents of PyBop/HOBt and 2 equivalents of DIPEA.

Peptides labeled with TOAC (A628K(TOAC)-gH625-Pra, A635K(TOAC)-gH625-Pra, A639K(TOAC)-gH625-Pra and A643K(TOAC)-gH625-Pra) were synthesized introducing the spin label directly in solid phase. For the incorporation of the TOAC moiety, peptides containing Lys(Mtt) in substitution of Ala residues were first synthetized: A628K(Mtt)-gH625-Pra, A635K(Mtt)-gH625-Pra, A639K(Mtt)-gH625-Pra and A643K(Mtt)-gH625-Pra. The Mtt (4-Methyltrityl) from the side chain of the lysine residue was cleaved by treatment with 1% TFA, 5% TIS (triisopropylsilane), 94% DCM, 10 times for 1 min. The TOAC residue was doubly coupled for 3h using 2-fold Fmoc-TOAC-OH molar excess (40 μmol) and HATU (40 mmol) as activating agent in presence of DIPEA (1:1:2). The Fmoc protecting group was removed with 30% piperidine in DMF (v/v).

Fully-synthesized peptides were deprotected from the resin with trifluoroacetic acid (TFA) with 2.5% (v/v) water, 2.0% (v/v) anisole, 2.0% (v/v) thioanisole as scavengers, at room temperature, and then precipitated in ice-cold ethyl ether, filtered, dissolved in water and lyophilized. After TFA cleavage and HPLC purification, TOAC containing peptides were submitted to alkaline treatment with aqueous ammonia (pH 9.5) for 6 h at room temperature to regenerate the chemical integrity of the nitroxide moiety [142].

The crude peptides were purified by RP-HPLC on a LC_8 Shimadzu HPLC system (Shimadzu Corporation, Kyoto, Japan) equipped with a UV lambda-Max Model 481 detector using a Phenomenex (Torrance, CA) C_{18} (300 Å, 250x21.20 mm, 5 μm) column eluted with an H_2O/0.1% TFA (A) and CH_3CN/0.1% TFA (B) from 20% to 80% over 20 minutes at 20 mL/min flow rate. Purity and identity were assessed by analytical LC–MS Analysis by using Finnigan Surveyor MSQ single quadrupole electrospray ionization (Finnigan/Thermo Electron Corporation San Jose, CA), column: C_{18}-Phenomenex eluted with H_2O/0.1% TFA (A) and CH_3CN/0.1% TFA *(B)* from 20% to 80% over 10 minutes at 0.8 mL/min flow rate. The final yields of purified peptides ranged between 20 and 40%.

PEPTIDES	SEQUENCES	MW
gH625	NH_2-HGLASTLTRWAHYNALIRAF-$CONH_2$	2297.1
Tat	NH_2-GRKKRRQRRR-$CONH_2$	1395.6
NBD-gH625	NBD-HGLASTLTRWAHYNALIRAF-$CONH_2$	2461,1
NBD-Tat	NBD-GRKKRRQRRR-$CONH_2$	1559,6
Ac-gH625-GGG	Ac-HGLASTLTRWAHYNALIRAF-GGG-COOH	2512.8
Ac-Tat-GGG	Ac-GRKKRRQRRR-GGG-COOH	1610,8
gH625-Pra	NH_2-HGLASTLTRWAHYNALIRAF-Pra-$CONH_2$	2391.3
NBD-gH625-Pra	NBD-HGLASTLTRWAHYNALIRAF-Pra-$CONH_2$	2537.9
NBD-Pra	NBD-Pra-$CONH_2$	258.9
A643K(TOAC)-gH625-	NH_2-HGLASTLTRWAHYNALIRK(TOAC)F-Pra-$CONH_2$	2644.6
A639K(TOAC)-gH625-	NH_2-HGLASTLTRWAHYNK(TOAC)LIRAF-Pra-$CONH_2$	2644.6
A635K(TOAC)-gH625-	NH_2-HGLASTLTRWK(TOAC)HYNALIRAF-Pra-$CONH_2$	2644.6
A628K(TOAC)-gH625-	NH_2-HGLK(TOAC)STLTRWAHYNALIRAF-Pra-$CONH_2$	2644.6

Table 1. Peptide sequences and their molecular weights.

2.3 PREPARATION OF TRIFLYL AZIDE (TFN_3)

Sodium azide (650 mg, 10 mmol) was dissolved in distilled water (1.5 mL) and then dichloromethane (DCM, 2.4 mL) was added. The mixture was cooled on ice bath for 20 min. Triflyl anhydride (336 µL, 2 mmol) was added slowly over 5 min and the mixture was stirred for 2 h. The mixture was extracted with DCM two times. The organic portions, containing the trifyl azide, were pooled, washed once with saturated Na_2CO_3, and evaporated to dryness.

2.4 SYNTHESIS OF AZIDE-ADOO-LYS(C(O)CH2CH2C(O)N-(C18H37)2)-AMIDE ((C18)2L-N3)

$(C_{18})_2L$-N_3 monomer was synthesized in solid phase under standard conditions using Fmoc/tBu strategy. Rink-amide MBHA resin (0.51 mmol/g, 0.1 mmol scale, 0.196 g) was used as polymeric support. The Fmoc protecting group on the resin was removed by a DMF/Piperidine (70/30) mixture. Fmoc-Lys(Mtt)-OH residue (0.125 g, 0.2 mmol) was activated by 1 equiv of PyBop and HOBt and 2 equiv of DIPEA in DMF and coupled on the resin stirring the suspension for 1 h. The N^{α} amine function of the lysine residue was deprotected from Fmoc group, and two equivalents of Fmoc-AdOO-OH were coupled under standard condition in DMF for 1h. After Fmoc removal from linker, peptidyl-resin was washed three times with DMF and three times with MeOH, and treated by 1 mL of solution containing K_2CO_3 (0.04 mmol) $CuSO_4 \cdot 5H_2O$ (0.01 mol) and TFN_3 (2 mmol). The resin was stirred at room temperature overnight. The solution was filtered and the resin was washed 4 times with DCM; the Mtt-protecting group on the N_{ε} amino function of lysine was removed by treatment with the DCM/TIS/TFA (94:5:1) mixture. The peptide resin was stirred with 5.0 mL of this solution for 2 min. This procedure was repeated several times until the solution became colorless. The resin was washed 3 times by DCM and 3 times by DMF. Then, N,N-dioctadecylsuccinamic acid (0.249 g, 0.4 mmol) was coupled twice for 1 h in the NMP (N-methylpyrrolidone)/DCM (1/1) mixture. N,N-dioctadecylsuccinamic acid was synthesized according to published procedure.The lipophilic moiety was activated in situ by the standard HOBt/PyBop/DIPEA procedure.

The coupling was monitored by the qualitative Kaiser test. The resin was washed 3 times by DMF, 3 times by DCM, and 3 times by ethyl ether. $(C_{18})_2$L-N_3 was removed from the resin by treatment with TFA containing TIS (2.5%) dithiothreitol (DTT, 2.5%) and water (2.5%) under vortexing for 2 hours. The crude product was slowly precipitated at 0 °C by adding water drop-wise, washed several time with small portions of water, and lyophilized in order to remove the solvent. The white solid was recrystallized from MeOH/H_2O and recovered with high yields (>85%). The product was identified by MS (ESI+) and NMR spectra. ^{1}H NMR and ^{13}C-NMR spectra were recorded on a Varian 400 MHz spectrometer (Palo Alto, CA).
$(C18)_2$L-N_3: MS (ESI+): m/z (%): 915 (100) [M-H+]= 916.64
^{1}H-NMR ($CDCl_3$/CD_3OD 50/50) (chemical shifts in δ, $CHCl_3$ as internal standard 7.26) = 4.3 (m, 1H, C*H* Lys α), 4.04 (m, 2H, OCH_2CONH), 3.70 (s, 4H, OCH_2CH_2O), 3.42 (t, 2H, $N_3CH_2CH_2O$), 3.25-3.20 (m, 4H, N-CH_2), 3.23 (t, 2H, CH_2 Lys ε), 3.20 (t, 2H, $N_3CH_2CH_2O$), 2.64-2.49 (m, 4H, NHCOCH_2CH_2CO), 1.74 (m, 2H, CH_2 Lys β), 1.55 (m, 2H, CH_2 Lys δ), 1.45 (m, 2H, CH_2 Lys γ), 1.40 (m, 4H, RC$H_2$$CH_3$), 1.25 (m, 60 C$H_2$ aliphatic), 0.88 (t, 6H, CH_3).
^{13}C-NMR ($CDCl_3$/CD_3OD 50/50) (chemical shifts in δ, $CDCl_3$ as internal standard 77.00) = 173.98 (*C*ONH_2), 173.27 (*C*ONH), 171.94 ($CH_3(CH_2)_{17}NCO$), 170.55 (*C*ONH), 72.3 ($COCH_2O$), 70.0 (CH_2N_3), 69.4(OCH_2CH_2O), 52.4 ($NH(CH_2)_4CH$), 51.05 ($NHCH_2(CH_2)_3CH$), 48.6 ($CH_3(CH_2)_{16}CH_2N$), 46.8 ($CH_3(CH_2)_{15}CH_2CH_2N$), 39.3 ($NH(CH_2)_3CH_2CH$), 32.4-32.0 ($NHCH_2(CH_2)_2CH_2CH$), 29.2 ($NCOCH_2CH_2CONH$), 30.2-27.5 ($CH_3CH_2(CH_2)_{14}CH_2CH_2N$), 23.17 ($CH_3CH_2(CH_2)_{16}$), 14.60 ($CH_3CH_2(CH_2)_{16}$).

2.5 SYNTHESIS OF AZIDE-TERMINATED DENDRIMER

2.5.1 Synthesis of Dendron 3

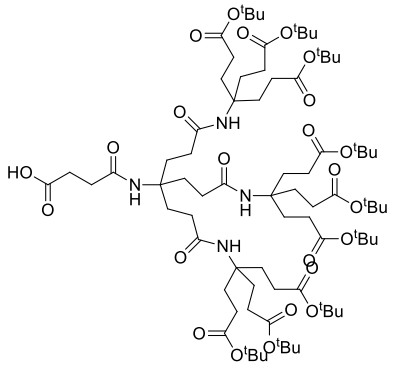

Chemical Formula: $C_{80}H_{138}N_4O_{24}$
Exact Mass: 1538.970
Molecular Weight: 1539.964

Second generation dendron **2** (1.003 g, 694.50 μmol) and succinic anhydride (0.222 mg, 2.22 mmol) were placed in a schlenk flask and the atmosphere was replaced with nitrogen. Anhydrous pyridine (30 mL) was added and the reaction was left to stir at room temperature for 15 h, after which the solvent was removed under vacuum. To the remaining oil, water was added. The mixture was agitated for 1 hour, after which the white residue was separated with ether. The organic phase was dried over sodium sulfate and concentrated to give pure **3** as a white foam (0.916 g, 85%) and compared exactly to a reference standard[143]. ^{1}H NMR (MeOD, 400 MHz, δ_{ppm} vs. *Me*OH): 2.66 (br t, *J* = 5.6 Hz, 2H, CH_2COOH); 2.40 (br t, *J* = 5.6 Hz, 2H, C$H_2$$CH_2$COOH); 2.25-2.17 (m, 24H, CH_2COO); 2.01-1.91 (m, 24H, $C_qCH_2CH_2$); 1.44

(s, 81H, C(CH_3)$_3$). MS-ESI (M-H)$^-$ *m/z* calcd for $C_{80}H_{137}N_4O_{24}$: 1537.962, found 1538.1.

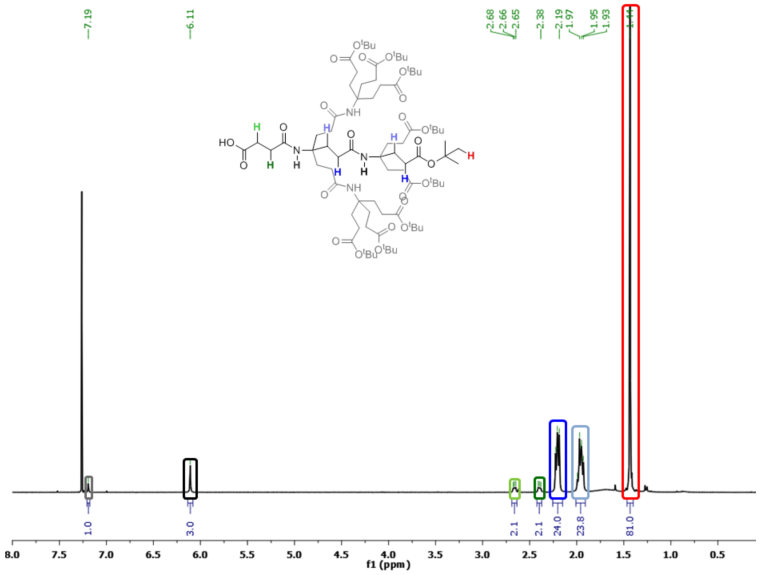

^{1}H NMR spectra of Dendron 3

2.5.2 Synthesis of Dendrimer 4

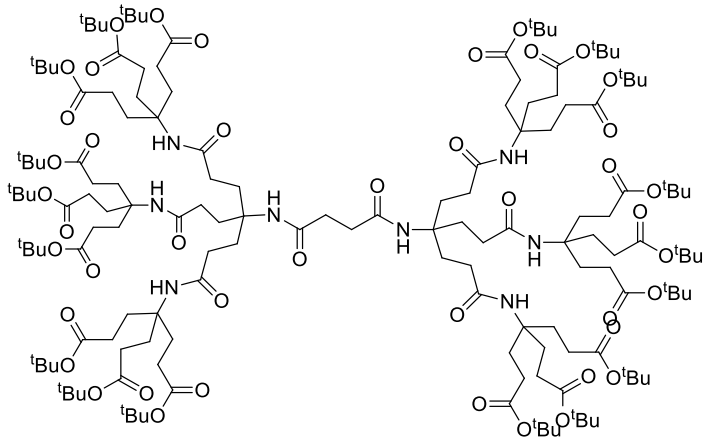

Chemical Formula: $C_{156}H_{270}N_8O_{44}$
Exact Mass: 2959.914
Molecular Weight: 2961.840

Dendron **3** (0.916 g, 594.82 µmol) and dendron **2** (0.946 g, 656.99 µmol) were placed in a schlenk flask with HATU (0.306 g, 804.78 µmol) and the atmosphere was replaced with nitrogen. Anhydrous DMF (30 mL) was added, and then DIPEA (0.3 mL, 1.72 mmol). The reaction was left to stir at room temperature for 2 d. After concentration, the product was dry-packed onto a basic alumina plug and purified by silica column chromatography (hexane → 1:1 hexane:EtOAc → 2:3). Concentration afforded **4** as a white foam (1.383 g, 79%). ^{1}H NMR ($CDCl_3$, 400 MHz, δ_{ppm} vs. TMS): 7.35 (s, 2H, N*H*COCH$_2$CH$_2$CON*H*); 6.32 (s, 6H, CON*H*); 2.41 (s, 4H, COC*H*$_2$C*H*$_2$CO); 2.25-2.12 (m, 48H, C*H*$_2$CO); 2.00-1.91 (m, 48H, C$_q$C*H*$_2$); 1.43 (s, 81H, C(C*H*$_3$)$_3$). ^{13}C NMR ($CDCl_3$, 400 MHz, δ_{ppm} vs. TMS): 172.9 (C$_q$CH$_2$CH$_2$*C*ONHC$_q$); 172.8 (*C*OOC(CH$_3$)$_3$); 171.9 (*C*OCH$_2$CH$_2$*C*O); 80.4 (*C*(CH$_3$)$_3$); 57.8 (COCH$_2$CH$_2$CONC$_q$); 57.4 (CONC$_q$); 31.5 (*C*H$_2$*C*H$_2$CONH); 31.4 (*C*H$_2$CONC$_q$); 29.9 (*C*H$_2$CH$_2$CONH); 29.8

($CH_2COOC(CH_3)_3$); 28.2 ($C(CH_3)_3$); 28.1 (CH_2CH_2COOH). MS-ESI $(M+2Na)^{2+}$ *m/z* calcd for $C_{156}H_{270}N_8O_{44}Na_2$: 1502.947, found 1503.7. MALDI-TOF/TOF *m/z* calcd for $C_{156}H_{270}N_8O_{44}Na$: 2982.903, found 2983.216.

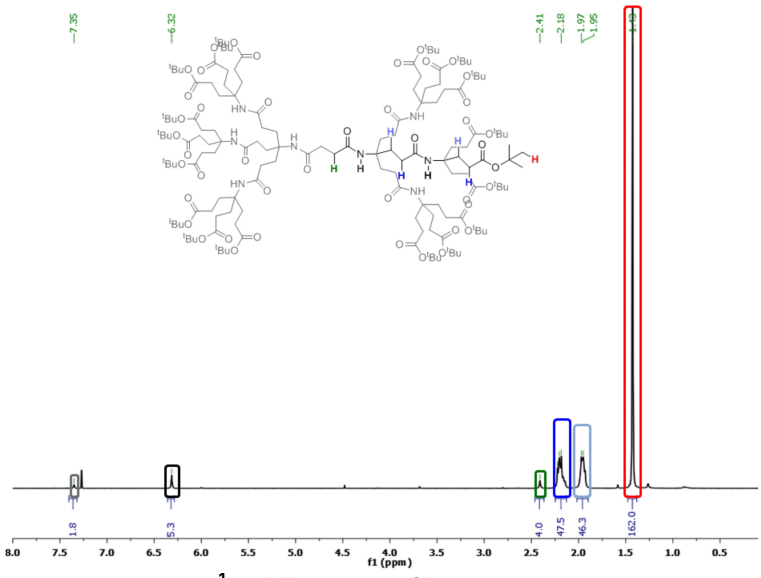

^{1}H NMR spectra of Dendrimer 4

2.5.3 Synthesis of Dendrimer 5

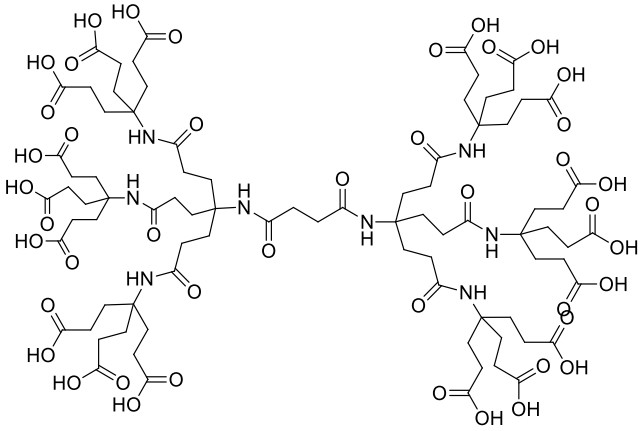

Chemical Formula: $C_{84}H_{126}N_8O_{44}$
Exact Mass: 1950.787
Molecular Weight: 1951.926

Dendrimer **4** (0.328 g, 110.74 µmol) was dissolved in formic acid (25 mL) and water (2.5 mL). This was left to stir for 1 day. After concentration, the residue was dissolved in a minimal amount of methanol and precipitated from ether. After centrifugation, decantation, and drying, dendrimer **5** was obtained as a white powder (0.197 g, 91%). ^{1}H NMR (MeOD, 400 MHz, δ_{ppm} vs. *Me*OH): 2.47 (s, 4H, $COCH_2CH_2CO$); 2.36-2.14 (m, 48H, CH_2CO); 2.09-1.87 (m, 48H, C_qCH_2). ^{13}C NMR (MeOD, 400 MHz, δ_{ppm} vs. *Me*OH): 177.3 (*C*OOH); 175.8 ($C_qCH_2CH_2CONHC_q$); 174.6 ($COCH_2CH_2CO$); 59.1 ($COCH_2CH_2CONC_q$); 58.7 ($CONC_q$); 33.5 (CH_2CH_2CONH); 32.0 (CH_2CONC_q); 31.9 (CH_2CH_2CONH); 30.6 (CH_2COOH); 29.4

(CH_2CH_2COOH). MS-ESI $(M-H)^-$ *m/z* calcd for $C_{84}H_{125}N_8O_{44}$: 1949.779, found 1950.0. MALDI-TOF/TOF *m/z* calcd for $C_{84}H_{125}N_8O_{44}Na$: 1973.777, found 1973.902.

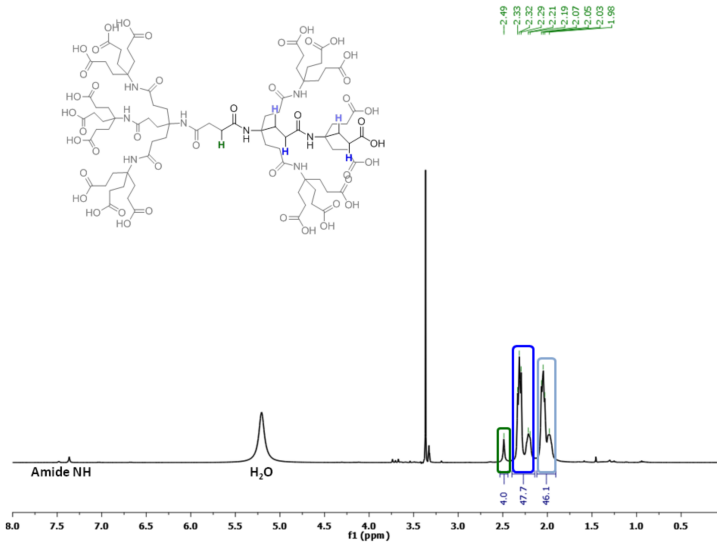

^{1}H NMR spectra of Dendrimer 5

2.5.4 Synthesis of Dendrimer 6

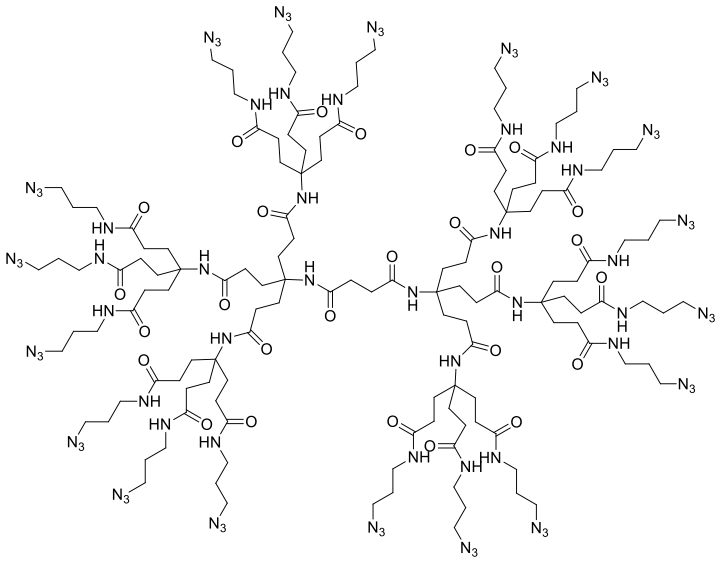

Chemical Formula: $C_{138}H_{234}N_{80}O_{26}$
Exact Mass: 3427.945
Molecular Weight: 3429.855

Dendrimer **5** (31 mg, 15.88 µmol) and HATU (383.98 µmol) were introduced into a schlenk flask and placed under nitrogen. Anhydrous DMF (2 mL) was added, then DIPEA (0.11 mL, 631.52 µmol), and finally 3-azidopropylamine (125 mg, 1.25 mmol). The reaction was left to stir for 2 d. The solvent was then removed and the resulting oil was purified by dialysis against methanol (1000 MWCO) to afford a dendrimer **6** as a colorless film (34.78mg, 64%). ^{1}H NMR (MeOD, 400 MHz, δ_{ppm} vs. *Me*OH): 3.37 (t, *J* = 6.7 Hz, 36H, NHCH_2CH$_2$CH$_2$N$_3$); 3.25 (t, *J* = 6.8 Hz, 36H, CH_2N$_3$); 2.46 (s, 4H, COCH_2CH_2CO); 2.27-2.15 (m, 48H, CH_2CO); 2.05-1.91 (m, 48H, C$_q$CH_2); 1.76 (p, *J* = 6.8 Hz, 36H, CH$_2$CH_2CH$_2$N$_3$). ^{13}C NMR (MeOD, 400 MHz, δ_{ppm} vs. *Me*OH): 175.8

(*C*ONHCH$_2$CH$_2$CH$_2$N$_3$); 175.6 (C$_q$CH$_2$CH$_2$*C*ONHC$_q$); 175.3 (*C*OCH$_2$CH$_2$*C*ONH); 59.3 (CH$_2$CH$_2$CONC$_q$); 59.1 (CONC$_q$); 50.3 (*C*H$_2$CH$_2$CH$_2$N$_3$); 38.0 (*C*H$_2$N$_3$); 32.2 (*C*H$_2$CH$_2$CONH); 32.0 (*C*H$_2$CONC$_q$); 31.8 (*C*H$_2$CONCH$_2$); 31.4 (*C*H$_2$CH$_2$CONH); 29.9 (CH$_2$*C*H$_2$CH$_2$N$_3$). MS-ESI (M+2H)$^{2+}$ *m/z* calcd for C$_{138}$H$_{236}$N$_{80}$O$_{26}$: 1714.980, found 1715.0. MALDI-TOF/TOF *m/z* calcd for C$_{138}$H$_{234}$N$_{80}$O$_{26}$Na: 3450.935, found 3450.853. IR 2098.5 cm^{-1} (azide stretch).

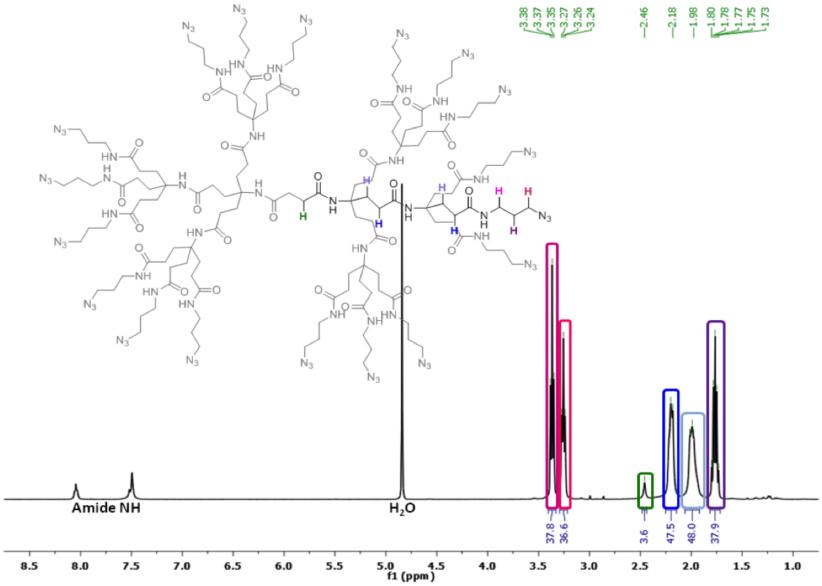

^{1}H NMR spectra of Azide-terminated dendrimer

2.6 LIPOSOME PREPARATION

Large unilamellar vesicles (LUVs) consisting of PC/Chol (1:1 molar ratios), when necessary containing also Rho-PE and NBD-PE, and DOPG/(C18)$_2$L-N$_3$ (90:10 molar ratios) were prepared, according to the extrusion method of Hope *et al*. [144]. The compounds were dissolved and mixed in a small amount of chloroform, and subsequently evaporating the solvent by slowly rotating the tube containing the solution under a stream of nitrogen, and lyophilized overnight. In this way a thin film of amphiphiles was obtained.
Dry lipid film was suspended in 10 mM HEPES buffer, when required in 5 mM HEPES, 100 mM NaCl, at pH 7.4 by vortexing; then the lipid suspension was freeze-thawed 10 times and extruded 20 times thought a polycarbonate membrane with 100 nm pore size, using a *Mini-extruder* purchased from Avanti Polar Lipids (Usa, Canada). Lipid concentrations were determined by phosphate analysis[145].

2.7 DOXORUBICIN LOADING

Doxorubicin was remote-loaded in DOPG/(C$_{18}$)$_2$L-N$_3$ liposomes via an ammonium sulfate gradient method and the free Dox was removed by gel filtration. Briefly, 1 mM liposomal solution was prepared as above reported in 250 mM ammonium sulfate at pH 5.5. Next, liposomes were passed on Sephadex G-50 column pre-equilibrated with 10 mM HEPES buffer at pH 7.4 and 27 µL of 2.54×10^{-3} M Dox solution in water were added to 500 µL of liposomal solution. This suspension was stirred for 30 min at 60°C and subsequently unloaded doxorubicin was removed by Sephadex G50

column. The Dox concentration was determined by spectroscopic measurements (UV and fluorescence) using calibration curves obtained by measuring absorbance at 480 nm or fluorescence emission at 590 nm. Emission spectra were recorded at room temperature. The Dox loading content (DLC, defined as the weight ratio of encapsulated Dox versus the amphiphilic moieties) was quantified by subtraction of the amount of Dox removed from the total amount of Dox loaded. Finally, Dox pre-loaded liposomes were modified with gH625 peptides using the click reaction procedure, as above reported for empty liposomes.

2.8 PEPTIDES CONJUGATION TO QUANTUM DOTS

Solution of peptides, EDC (1-Ethyl-3(3-dimethylamino-propyl)-carbodiimide, hydrochloride) and NHS (N-Hydroxysuccinimide) was prepared in PBS buffer at pH7.2 in molar ratio of 4:4:1. QDs were conjugated with the preactivated-peptides in a molar ratio of 1:200, in MES buffer at pH 5.5 for 3 hours. The fluorescence spectra of peptide-QDs and un-conjugated QDs were measured in a Cary Eclipse Varian fluorescence spectrophotometer in the same condition. In all the reported confocal experiments we used the same peptide concentration and thus the QDs concentration was 200 times lower.

2.9 PEPTIDES CONJUGATION TO LIPOSOMES

Click-reaction was carried out on DOPG/$(C18)_2$L-N_3 liposomes at $1 \cdot 10^{-3}$ M concentration in 10 mM HEPES buffer at pH 7.4. The reaction was carried out by adding 4.4 equivalents of $CuSO_4 \cdot 5H_2O$, 6.7 equivalents of ascorbic acid and 1 equivalent of peptide derivative with respect to the azido moiety. In particular, solutions containing 40 mM $CuSO_4 \cdot 5H_2O$ (solution A), 57 mM ascorbic acid (solution B), and 0.8 mM of alkyne modified peptide (solution C) were freshly prepared in water. 43.6µL of solution A, 48 µL of solution B and 408.4 µL of solution C were added to 500 µL of a suspension of azido functionalized liposomes in HEPES. Concentration of solution C was determined by absorbance on a UV-vis Jasco V-5505 spectrophotometer.
The reaction mixture was stirred at 40°C for 30 minutes and successively left overnight at room temperature. After the conjugation step, liposomes were purified by exclusion chromatography on a 1 × 18 cm Sephadex G-50 (Amersham Biosciences) column pre-equilibrated in HEPES buffer.
The number of functional groups present on the external surface of the liposomes and the number of molecules of gH625 that were effectively linked to the liposome were determined by using NBD-labeled Pra and NBD-labeled gH625-Pra. The amount of NBD-Pra or NBD-gH625-Pra grafted to the liposome surface were estimated by fluorescence spectroscopy using calibration curves obtained by measuring fluorescence emission at 530 nm. Fluorescence spectra were recorded at room temperature on a Jasco Model FP-750 spectrofluorophotometer in 1.0 cm path length quartz cell. Equal excitation and emission bandwidths were used throughout experiments, with a recording speed of 125 nm/min and automatic selection of the time constant. The percentage of functionalization was calculated as the ratio of bound NBD-Pra or NBD-gH625-Pra to their total amount.

2.10 PEPTIDES CONJUGATION TO DENDRIMER

A methanol/water (1:1) solution of peptide gH625–Pra (660 µL, 30.33 equiv), an aqueous solution of $CuSO_4 \cdot 5\ H_2O$ (10 µL, 1.46 mmol, 1 equiv), and an aqueous solution of sodium ascorbate (50 µL, 1.17 mmol, 4 equiv) were added to dendrimer 6 (50 mg, 0.0146 mmol) in a 1:1 water/methanol solution (280 µL). The mixture was stirred, overnight. Then, the mixture was concentrated and purified by size-exclusion chromatography. Peptides 1 and 1–NBD were obtained in quantitative yield. IR (cast on polyethylene)): $\tilde{\nu}$ =3295, 1658, 1545, 1471, 1203 cm^{-1}. No peak at 2098 cm^{-1} was observed. CD: 208 nm; UV/Vis (water): λ_{max} = 193, 273 nm. Synthesis of dendrimer 7, due to its poor solubility, was performed in a 1:1 mixture of THF/H2O as solvent, and purification was carried out by dialysis (1000 MWCO) against 1:1water/methanol. Yield: approximately 20 %; UV/Vis (MeOH): λ_{max} = 452 nm.

2.11 PEPTIDES CONJUGATION TO NPS

A solution of the peptide, EDC (1-ethyl-3(3-dimethylamino-propyl)-carbodiimide, hydrochloride) and NHS (N-Hydroxysuccinimide) in molar ratio of 4:4:1 was prepared in PBS buffer at pH 7.4, at room temperature under stirring for 30 min. NPs were conjugated with the preactivated-peptide, in MES 0.1 M buffer at pH 5.5 for 3 h at room temperature in presence of Tween 20 and the yield of the reaction was higher than 90%. The peptide-NPs were purified from the unconjugated-NPs by exclusion chromatography on a 1 × 18 cm Sephadex G-50 (Amersham Biosciences) column pre-equilibrated in PBS buffer at pH7.4. The fluorescence spectra of peptide-NPs and unconjugated NPs were measured in a Cary Eclipse Varian fluorescence spectrophotometer in the same condition. Peptide-NPs were prepared with several degrees of functionalization: 25%, 35% and 50%.

2.12 MEMBRANES INTERACTION EXPERIMENTS OF PEPTIDES AND CONIUGATED-PEPTIDES

Large unilamellar vesicles (LUVs) consisting of PC/Chol (55:45) and, when necessary, containing Rho-PE and NBD-PE, were prepared according to the extrusion method of Hope *et al.* [146] in 5 mM HEPES containing 100 mM NaCl at pH 7.4.

Peptide and conjugated-peptides ability to induce the fusion of model membranes, like liposomes, was evaluated by the *Lipid Mixing Assays.* Membrane lipid mixing was monitored using the resonance energy transfer assay reported by Struck *et al.* [147]. The assay is based on the dilution of the NBD-PE (donor) and rhodamine-PE (acceptor). Dilution because of membrane mixing results in an increase in NBD-PE fluorescence. Thus, we monitored the change in donor emission as aliquots of peptides were added to vesicles. Vesicles containing 0.6 mol % of each probe were mixed with unlabeled vesicles at a 1:4 ratio (final lipid concentration, 0.1 mM). Small volumes of peptides in dimethyl sulfoxide (DMSO) were added; the final concentration of DMSO in the peptide solution was no higher than 2%. The NBD emission at 530 nm was followed with the excitation wavelength set at 465 nm. A cutoff filter at 515 nm was used between the sample and the emission monochromator to avoid scattering interferences. The fluorescence scale was calibrated such that the zero level corresponded to the initial residual fluorescence of

the labeled vesicles, and the 100% value corresponding to complete mixing of all lipids in the system was set by the fluorescence intensity of vesicles upon the addition of Triton X-100 (0.05% v/v) at the same total lipid concentrations of the fusion assay. All fluorescence measurements were conducted in PC/Chol (1:1) LUVs and at 37°C.

Peptides and conjugated peptides induced phospholipid-mixing of the *inner monolayer* was measured by a modification of the phospholipid-mixing measurement as reported elsewhere. The concentration of each of the fluorescent probes within the liposome membrane was 0.6% mol. LUVs were treated with sodium dithionite to completely reduce the NBD-labelled phospholipid located at the outer monolayer of the membrane. The final concentration of sodium dithionite was 100 mM (from a stock solution of 1 M dithionite in 1 M TRIS, pH 10.0) and it was incubated for approximately 1 h on ice in the dark. Sodium dithionite was then removed by size exclusion chromatography through a Sephadex G-75 filtration column (Pharmacia, Uppsala, Sweden) eluted with buffer containing 10 mM TRIS, 100 mM NaCl, and 1 mM EDTA, pH 7.4. The NBD emission at 530 nm was followed with the excitation wavelength set at 465 nm. A cut off filter at 515 nm was used between the sample and the emission monochromator to avoid scattering interferences. The fluorescence scale was calibrated such that the zero level corresponded to the initial residual fluorescence of the labelled vesicles and the 100% value corresponding to complete mixing of all lipids upon the addition of Triton X-100 (0.05% v/v). All fluorescence measurements were conducted in PC/Chol (1:1) LUVs, were repeated at least three times and results were averaged. All the experiments were performed at 37°C.

The ANTS/DPX assay was used to measure the ability of the peptides and conjugated peptides to induce leakage of ANTS/DPX pre-encapsulated in liposomes. Details of this assay can be found elsewhere[148]. To initiate a leakage experiment, the compounds, in a stock solution at pH 7.4 containing 5 mM HEPES and 100 mM NaCl, were added to the stirred vesicle suspension (0.1 mM lipid).

Data points were recorded at 0.5-s intervals over a 10-min period after which vesicles were lysed with the detergent Triton X-100 to obtain the maximal fluorescence value, which was set to 100% leakage. Fluorescence from intact vesicles in buffer was set to 0% leakage, and results were normalized according to this scale.

2.13 FLOW CYTOMETRY OF CELL ASSOCIATION OF PEPTIDES AND CONIUGATED-PEPTIDES

HeLa cells were cultured in RPMI medium supplemented with 10% fetal bovine serum. Cells were diluted at 3 x 10^5 cells mL^{-1} 1 day before the experiment. Cell association was measured by flow cytometry using a FACScan (Becton Dickinson). NBD-labelled peptides, NBD-dendrimer and NBD-peptidodendrimer (1, 5, 10, 20 μM) were incubated with HeLa cells (5 x 10^5 cells mL^{-1}) in Opti-MEM medium at 37°C for various periods of time (10, 30, 60 min) in a final volume of 0.5 mL. Thereafter, the cells were washed twice and then resuspended in 0.5 mL of ice-cold NaCl/Pi for flow cytometric analysis. Cell-associated fluorophores were excited at 465 nm and fluorescence was measured at 530 nm. A histogram of fluorescence intensity per cell (1 x 10^4) was obtained and the calculated mean of this distribution was considered as representative of the amount of cell associated peptide. A stock solution of dithionite was freshly prepared in 1 M Tris solution (pH 10). Following flow cytometric analysis, 5 μL of dithionite stock solution was added to cells maintained at 4°C and the fluorescence of internalized peptides was measured after 5 min.

To further study the mechanism of internalization, experiments were performed at low temperature. In particular, cells were preincubated for 30 min at 4°C before being incubated with the compound solution.

2.14 FLUORESCENCE AND CONFOCAL MICROSCOPY STUDIES ON PEPTIDES AND CONIUGATED-PEPTIDES

Cellular uptake experiments. NBD labelled peptides and conjugated-peptides were diluted in cell culture medium; in particular the final concentration of NBD conjugated to the peptides was 1, 10 and 20 μM; while the final concentration of QDs conjugated to the peptide was 5, 50 and 100 nM. 70% confluent HeLa cells, seeded on 12 mm-diameter glass coverslips, were incubated with 200 μl of peptide conjugated to the NBD or to QDs at 37°C for 1 h and at 4°C for 10 min. For localization of peptides in lysosome organelles, LysoTracker reagent (Molecular Probes, Invitrogen) was added to cell culture medium containing peptides and incubated with cells for 1 h at 37°C according to manufacturer's procedure. After incubation, cells were rinsed twice with PBS to remove non internalised peptides and fixed with 4% paraformaldehyde for 20 min.
For peptides and conjugated-peptides uptake kinetics experiments on non-fixed living cells, HeLa cells were incubated with 10 μM of NBD-peptide solutions and with 50 nM QD-peptide solutions, with liposomes functionalized with gH625 and pre-loaded with Dox with a concentration of Dox of 1 μM at 37°C for 1, 5 and 17 hours and with NBD-peptidodendrimer and NBD-Dendrimer (10 or 20 μM relative to peptides, 0.56 or 1.11 μM dendrimer) at 37°C for either 1 or 2 h. After incubation, cells were rinsed twice with PBS and fresh cell culture medium without phenol red was added.
To inhibit the endocytosis pathway sodium azide and low-temperature experiments were conducted: 40 μM sodium azide was added to the cell culture medium for 30 min followed by 1h incubation with peptides, 20 μM of peptides and conjugated peptides solution were incubated for only 10 minutes at 4°C before imaging.
All the samples were observed by a confocal laser scanning microscope (CLSM)(LSM510, Zeiss) equipped with a He-Ne and an Argon laser lines at the wavelengths of 543 nm and 488 nm, respectively, with a 63x objective and by a Nykon Eclipse Ti inverted microscope equipped with a FITC filter set for fluorescence imaging.
Colocalization with Lysosomes and Caveolae. For indirect immunofluorescence, after NPs incubation, cells were firstly rinsed twice with PBS to remove non internalized NPs and fixed with paraformaldehyde 4% for 20 min. Then, cells were incubated with Triton 100 X 0.1% in PBS for 10 min and with PBS-BSA 0.5% for 15 min at room temperature (RT). Caveolae were localized by incubating samples first with rabbit anti-caveolin 1 (Abcam) primary antibodies. After primary antibodies incubation, Alexa-fluor 568 goat anti-rabbit secondary antibodies (Molecular Probes, Invitrogen) were used. Afterward, samples were rinsed three times with PBS. For lysosomes localization, LysoTracker Red DND-99 (Molecular Probes, Invitrogen) was used following manufacturer's procedure on non-fixed cells. Immunofluorescence analyses were performed by means of confocal laser scanning microscope (CLSM)(LSM510, Zeiss), equipped with an argon laser, at a wavelength of 488 nm, and a He–Ne laser, at a wavelength of 543 nm, and 63x objective. Images were acquired with a resolution of 1024 × 1024 pixels. Colocalization was estimated by an ImageJ software plugin.
Cytochalasin D Treatment: to disassemble actin microfilaments, cells were treated

with 30 μM cytochalasin D in cell culture medium for 30 min at 37°C before NP incubation. After cytochalasin D treatment, cells were incubated with a NP suspension for 15 min. Then, cells were rinsed with PBS to remove non-internalized NPs, fixed with paraformaldehyde 4% for 20 min and observed by CLSM. Quantification of NP uptake was performed as described above.
Quantification of NP Aggregates: to measure the size of NP aggregates within cell cytoplasm, bEnd3 cells were incubated with NP suspension for 30, 90, 1440 minutes at 37°C. After incubation, cells were rinsed twice with PBS, fixed with paraformaldehyde 4% for 20 min and observed by confocal microscope (Leica). Images were analyzed by an ImageJ software plugin. About 50 cells per each sample were analyzed. The size distribution of NP aggregates was split in four intervals (0.01÷0.03 μm^2; 0.04÷0.10 μm^2; 0.11÷0.30 μm_2; >0.31 ìm2) and data reported as percentage of NP aggregates respect to the total number of NP aggregates per cell.

2.15 STRUCTURAL STUDIES OF PEPTIDES AND CONIUGATED-PEPTIDES

Circular Dichroism Measurements Far-UV CD spectra were recorded from 260 to 195 nm on a Jasco J-810 spectropolarimeter equipped with a NesLab RTE111 thermal controller unit using a 1.0 , 0.1 cm or 0.1 mm quartz cell at 25 °C. CD spectra of gH625-Pra and of its analogs in which each Ala residues were replaced by Lys(TOAC) residues were recorded at $8 \cdot 10^{-4}$ M concentration in HEPES buffer in presence and in absence of 20% TFE (trifluoroethanol). Moreover peptidodendrimer spectra were recorded at 8 μM solution in HEPES buffer containing various percentages of trifluoroethanol, and NPs spectra were conducted at different percentages (25-50%) of functionalization with gH625 peptide. Other experimental settings were: scan speed, 10 nm/min; sensitivity, 50 mdeg; time constant, 16 s; bandwidth, 1 nm. Each spectrum was obtained averaging three scans, subtracting contributions from other species in solution, and converting the signal to mean residue ellipticity.
Size and Z-potential. For Dynamic light scattering characterizations self-assembled liposomes in isotonic HEPES solution were prepared at the final concentration of $1x10^{-4}$ M. Samples were centrifuged at room temperature at 13,000 rpm for 5 min. gH625 NPs and blank-NPs measurements were conducted at 25 °C using a 3.6×10^{10} NP/ml suspension at pH 4, 7, 8 and 9.
The measurements were performed with a setup composed of a Photocor compact goniometer, a SMD 6000 Laser Quantum 50 mW light source operating at 5325 Å and a PMT and correlator obtained from Correlator.com. All the measurements were performed at (25.00 ± 0.05)°C with use of a thermostat bath, other measurements were conducted on a Zetasizer Nano-ZS (Malvern Instruments, Worcestershire, UK).
For Z-potential analysis gH625 NPs and blank-NPs were made with a Zetasizer Nano-ZS (Malvern Instruments, Worcestershire, UK). The measurements were conducted at 25 °C using a 3.6×10^{10} NP/ml suspension at pH 4, 7, 8 and 9. All measurements were performed in triplicate for each sample.
EPR Measurements. EPR spectra of spin-labeled peptides chemically linked to the liposome surface were recorded on an Elexys E-500 EPR spectrometer from Bruker (Rheinstetten, Germany) operating in the X band. As references, spectra of the “free” spin-labeled peptides in aqueous buffer and in the presence of liposomes were also registered. Flame-sealed capillaries containing the samples were placed in a standard 4 mm quartz sample tube. The temperature of the sample was regulated

and maintained constant during the measurement by blowing thermo stated nitrogen gas through a quartz Dewar. The samples were investigated at 25 °C. The instrumental settings were as follows: sweep width, 120 G; resolution, 1024 points; modulation frequency, 100 kHz; modulation amplitude, 1.0 G; time constant, 20.5 ms; sweep time, 42 s; incident power, 5.0 mW. For samples subjected to the click chemistry reaction up to 128 scans were accumulated to improve the signal-to-noise ratio[149]. For all the other samples, 8 scans were accumulated.
InfraRed measurements- Infrared data for dendrimers was performed by dropping a methanol solution of the compound on poly(ethylene) IR cards at room temperature.

2.16 SPECTROFLUORIMETRIC STUDIES ON PEPTIDES AND CONIUGATED-PEPTIDES

Quantification of Nanoparticle Uptake Kinetics: To evaluate cell uptake of NPs as a function of NP surface functionalization with gH625 peptide, about 5×10^4 cells were seeded in a 96-well. Blank-NPs and gH625-NPs were dispersed in cell culture medium at the final concentration of 3.6×10^{10} NP/mL. Cells were incubated with NP suspensions for 0, 10, 60, 180, and 300 min. After incubation, cells were rinsed with PBS and lysed with 1% Triton ×100 in PBS. Cell lysates were analyzed by a spectrofluorometer (Wallac 1420 Victor2, Perkin–Elmer, USA) to measure the amount of internalized NPs.
Permeability Experiments. Cells were seeded at a density of 5×10^4 cells/cm^2 on Transwell permeable inserts (6.5 mm in diameter, 3 μm pores size; Corning Incorporated, Corning, NY). Transendothelial electrical resistance (TEER) was measured by using Millicell1-ERS voltohmmeter (Millipore, Billerica, MA) to assess the growth of cells on inserts. Permeability experiments were performed on the monolayer 7 days after cell seeding, allowing sufficient time for the cells to develop the junctions between cells. On the day of experiment, Transwell insert filter was washed with PBS, and then the media of the donor chamber was filled with 150 ìL cell culture medium w/o phenol red containing 0.5 mg/ mL rhodaminated BSA and 3.6×10^{10} NPs/mL while the acceptor chamber was filled with 400 ìL cell culture medium without phenol red. The samples of 100 μL were drawn every 10 min for 90 min from the acceptor chamber and were then replaced with the same amount of fresh medium. The fluorescence tracer concentration in the samples was determined by a spectrofluorometer (Victor, Wallac, PerkinElmer), and the excitation and emission wavelengths were set to 540 and 615 nm and 485 and 535 nm, respectively, for BSA and NPs. The solute permeability P of the monolayer was calculated according to the following equation:

$$P = \frac{\Delta C_A / \Delta t \times V_A}{C_D \times S}$$

Where $\Delta C_A / \Delta t$ is the increase in fluorescence concentration in the acceptor chamber during the time interval Δt, C_D is fluorescence concentration in the donor chamber (assumed to be constant during the experiment), V_A is the volume of the acceptor chamber, and S is the surface area of the filter. The experiments were performed in triplicate.

2.17 MULTIPLE PARTICLE TRACKING

Images of NPs internalized in End3 cells were collected in real time for about 100 s with a time resolution of ~1 s by using Olympus Cell-R system equipped with 60× oil immersion objective. Tracking algorithm has been described in detailed elsewhere [150]. From the NP trajectories the mean square displacement (MSD) was derived. Indicated with $\langle r^2 \rangle$, MSD was related to the NPs diffusion coefficient *D* by the Equation

$$\langle r^2 \rangle = nDt^{\alpha} + \upsilon^2 t^2$$

where *D* is the diffusion coefficient, υ the NP rate and a represents the time dependence. The first term of the equation is related to the random diffusion of the nanoparticles, whereas the second one reflects the active motion along the filaments due to the action of molecular motors (for NPs that undergo to Brownian motion such term becomes negligible). By fitting the MSD curve of each tracked bead using the equation, informations concerning the nature of particle motion into the cells were gained. In particular, nanoparticles, exhibiting MSD curve that undergo a power law with exponent minor or equal to unity, were classified as Brownian (α = 1) or sub-diffusive (α < 1). Particles presenting MSD, whose dependence on time was well described by the power law with α> 1, were indicated as super-diffusive. During the experiments the MSD of 226 (NPs-NH_2), 105 (NPs-gH625 25%), 38 (NPs-gH625 35%) and 574 (NPs-gH625 50%) distinct objects was evaluated. For each degree of peptide functionalization, at least, 3 cells were analyzed.

2.18 SCANNING ELECTRON MICROSCOPY (SEM)

Dendrimer Sem microscopy was performed by drop-casting a 5 nM solution in water (20% TFE v/v) of dendrimer on a Cu grid and drying at room temperature. The sample was stained by placing it in a closed container containing a solution of RuO_4. NPs SEM microscopy was performed incubating the cells for 10 min with blank NPs and gH625-NPs, then the cells were rinsed with PBS, fixed with 2.5% glutaraldehyde for 2 h at 4 °C and dehydrated in increasing ethanol series (70%, 80%, 95%, and 100%) and by critical point. The samples were gold-sputtered and analyzed by ESEM Quanta 200 (FEI Company) at 25 kV and 6.8 mm working distance.

2.19 TRANSMISSION ELECTRON MICROSCOPY (TEM)

TEM was performed to precisely localize the intracellular nanoparticles. After 24 h incubation with blank NPs and gH625-NPs, cells were rinsed with PBS and fixed with 2% paraformaldehyde + 0.2% glutaraldehyde for 2 h at room temperature. Afterwards, cells were scraped, harvested in centrifuge tubes, embedded in 12% gelatine solution in PBS and infused in 2.3 M sucrose at 4 °C. Sections were cut with a Leica Cryo-ultramicrotome and examined with Leica EM FC7.

2.20 STATISTICAL ANALYSES

Quantitative data were reported as mean ± standard deviation (SD). Statistical analyses were performed using a one-way analysis of variance (ANOVA). Results

repeats were compared by analysis of variance (ANOVA), and a p value < 0.05 was considered statistically significant.

2.21 PEPTIDES AND CONIUGATED-PEPTIDES CITOTOXICITY

*MTT assay for cell viability***.** Methylthiazolyldiphenyl-tetrazolium (MTT) bromide reduction was used to examine the metabolic activity of the cells. The MTT assay is based on the reduction of the yellowish MTT to the insoluble and dark blue formazan by viable and metabolically active cells [151]. HeLa cells were subcultured in 96-well plates at a seeding density of 2 x 10^4 cells/well. For assessing the cytotoxic effect of gH625 and Tat peptides, HeLa cells were incubated with different concentration of peptides (10, 50, 100, 200, 400 μM) for 24 h. For assessing the cytotoxicity of dendrimer and peptidodendrimer, Vero cells were incubated with different concentrations (1.1, 2.8, 5.5 μM) for 3 and 24 h. Then, the medium was gently aspirated and MTT solution (5 mg/mL) was added to each well and cells were incubated for a further 3 h at 37°C. The medium with MTT solution was removed, and the formazan crystals were dissolved with DMSO. The absorption values were measured at 570 nm using a Bio-Rad Microplate Reader (Bio-Rad Laboratories, Inc.). The viability of HeLa cells in each well was presented as a percentage of control cells.

*Lactate dehydrogenase (LDH) assay***.** LDH released into the culture medium was measured by monitoring fluorometrically the production of NAD^+ from NADH during the conversion of pyruvate to lactate [152]. For assessing the plasma membrane integration upon the exposure to gH625 and Tat peptides, HeLa cells were subcultured in 96-well plates at a seeding density of 2 x 10^4 cells/well. Twenty-four hours later cells were incubated with different concentration of peptides (10, 50, 100, 200, 400 μM) for 24 h. The cell supernatant (100 μl) was incubated with 0.18 mM NADPH and 0.60 mM pyruvate in 50 mM phosphate buffer (pH 7.4). The rate of NAD^+ formation was monitored for 1 min by reading the fluorescence in a fluorescence reader with the excitation filter set at 360 nm and the emission filter set at 460 nm. LDH leakage was expressed as a percentage of untreated or control cells which was designated as 100%.

3 RESULTS AND DISCUSSION

3.1 gH625 MEMBRANE INTERACTION AND INTRACELLULAR INTERNALIZATION

3.1.1 NBD-peptides synthesis

Peptides were synthesized, using standard solid-phase-Fmoc method, with 4-chloro-7-nitrobenz-2-oxa-1,3-diazole (NBD) at the N terminus (*gH625: NBD-HGLASTLTRWAHYNALRAF-COOH, Tat: NBD-GRKKRRQRRRGGG-COOH*). All purified peptides were obtained with good yields (30-40%).

3.1.2 NBD-Peptide interaction with liposomes (LUVs)

To support the hypothesis that the peptide is able to diffuse inside lipidic vesicles without involving pore formation, we performed the fusion, inner monolayer, and leakage experiments as indicators of the interaction and perturbation of the lipid membrane caused by the peptide.
Membrane disturbance upon peptide insertion was evaluated by vesicle fusion experiment in liposomes composed of different lipids. The best fusogenic activity was obtained using PC/Chol lipids and Figure 1A shows that 20-30% of fusion is already reached at 0.01 peptide/lipid ratio.

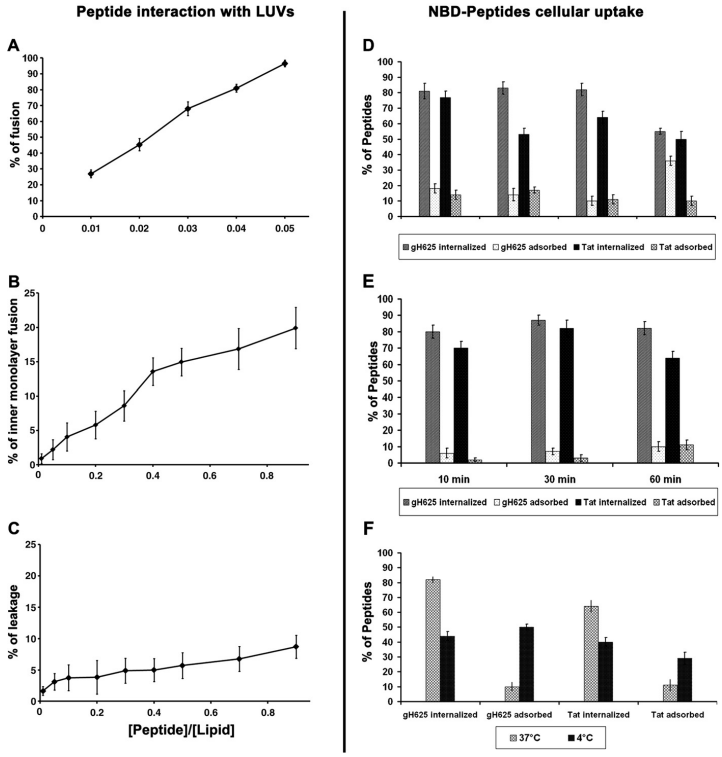

Figure 1. Peptide interaction with PC/Chol LUVs (A,B,C), the dose dependence is reported and each trace represents an average of 3 independent experiments. (A) Lipid mixing; (B) Inner monolayer assay. (C) Leakage of ANTS/DPX. NBD-peptide cellular uptake (D-E-F), the percentage of internalized and bound peptides are reported. HeLa cells were incubated with (D) increasing concentrations of NBD-peptides (1, 5, 10, 20 μM) for 60 min. (E) 10 μM NBD-peptides for 10, 30 and 60 min. (F) NBD-peptides at 37° and 4°C.

In the inner monolayer, the fluorescence from the vesicle membranes' outer monolayer is eliminated by the addition of an aqueous reducing agent, and this experiment reveals the extent of lipid mixing between the inner monolayers of vesicles in solution. Figure 1B shows that a small fusion of the inner monolayer is observed only at a peptide lipid ratio of approximately 0.8. This assay clearly indicates that the peptide gH625 induces only hemifusion at peptide-to-lipid ratios between 0 and 0.1. A contents-mixing assay was employed to monitor any mixing of internal vesicle components as a consequence of vesicle exposure to gH625. Release of ANTS and DPX from vesicles is commonly used as a measure of bilayer perturbation and interpreted as “transient pore formation”. Contents mixing is manifested by a decrease in fluorescence intensity if vesicles encapsulating a fluorescent cargo (e.g., ANTS) merge contents with those containing a quencher (e.g., DPX).
Figure 1C shows that no contents mixing occurs over the same P/L range where substantial outer monolayer lipid mixing occurs, corroborating the presence of vesicle hemifusion in our system. The agreement of contents mixing assays and inner monolayer lipid-mixing assays gives full confidence in the finding of peptide-induced hemifusion for gH625. These results can be used as qualitative indicators of peptide translocation or bilayer perturbation with relevance for the direct-penetration mode of cell entry, or for the steps of endosomal membrane translocation or endosomal escape. We have not detected any significant pore formation; vesicle fusion events not accompanied by leakage of the aqueous contents of the vesicle were also reported for other peptides in a study published by Thoren *et al*.[153].

3.1.3 NBD-peptides cellular uptake by flow cytometry analysis (FACS)

The fraction of NBD-labeled peptide taken up into HeLa cells was determined by flow cytometry. The experiment is based on a method previously introduced by McIntyre and Sleight[148] to measure the transbilayer distribution of NBD phospholipid analogues. The distribution is determined by comparing the fluorescence intensity before and after addition of sodium dithionite, an essentially membrane-impermeant molecule, which suppresses irreversibly the fluorescence of the accessible NBD-moiety localized on the external cell surface.
We incubated gH625-NBD with HeLa cells at 37°C at different concentrations (1, 5, 10, 20 μM). After 1 hour of incubation, we measured the quenching of the peptide by dithionite treatment. The dithionite reaction was performed at low temperature (4°C) because the dithionite crossing of biological membranes is strongly reduced in comparison with high temperatures. Upon stabilization of the initial fluorescence, dithionite was added to initiate quenching. Before the addition of dithionite we observed that approximately 90% of gH625-NBD was not washed away and thus was internalized or bound to the membrane bilayer; after the addition of dithionite the internalized peptide was 80% (Figure 1D). We performed the same experiment on Tat-NBD as a reference; and before the addition of dithionite we observed that approximately 70% of the peptide was internalized or bound to the membrane bilayer; after the addition of dithionite, the internalized peptide was approximately 60% (Figure 1D). Increasing dithionite concentration did not result in a modification of the extent of quenching, indicating that the entire accessible NBD label was quenched by 1 M dithionite (data not shown). These results show that the use of dithionite allows efficient measurement of the fraction of internalized peptide inside the cells. To exclude the possibility that the fluorescence signal could have been due

to the internalization of the fluorochrome itself, the NBD moiety was used in the same *in vitro* assay conditions, and no cellular fluorescence was observed at concentrations up to 20 µM (data not shown).To measure the kinetics of import of gH625-NBD into cells, we incubated the peptide with cells at 37°C for various times (10, 30, and 60 minutes) and then determined the remaining fluorescence following treatment with dithionite. Figure 1E shows the fraction of peptide taken up by cells. The uptake is very rapid and seems to reach a plateau after 1 hour of incubation. The influence of temperature on the intracellular accumulation was studied to see whether the uptake depended on a translocation mechanism or a cellular process. We incubated the peptide with HeLa cells at both 37°C and 4°C; the amount of internalized gH625-NBD at low temperature (Figure 1F) is reduced for both peptides, with an increase in the quantity bound to the membrane and a substantial decrease of the quantity of internalized peptide. The reduction of internalized or bound peptide was more significant for Tat peptide.

3.1.4 NBD-peptides intracellular delivery by confocal microscopy

To confirm the peptide internalization, we examined its uptake and intracellular localization by confocal microscopy. We used concentrations of 1 and 10 µM and a time of 60 minutes as selected by the flow cytometry experiments. Both peptides are efficiently internalized and we observe a significant colocalization with the LysoTracker, indicating a partial confinement within the endosomal compartments (Figure 2).

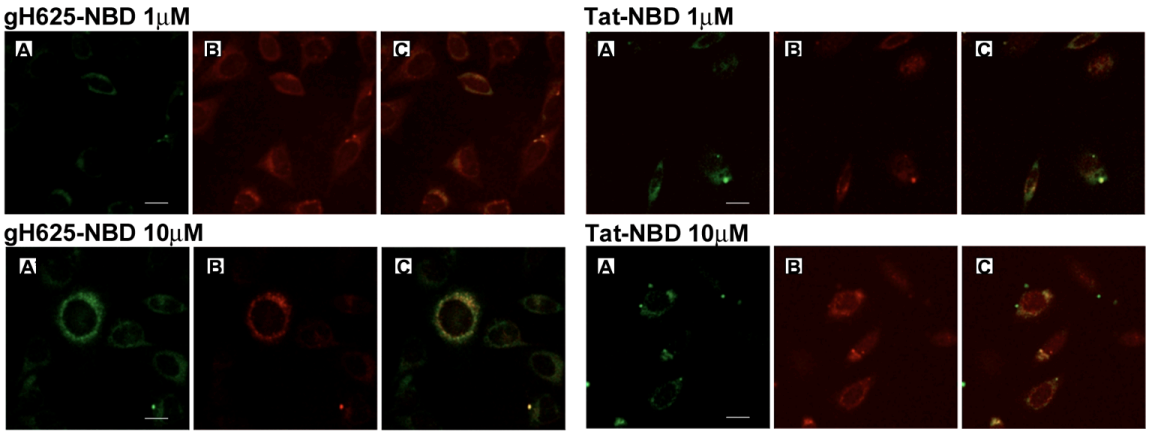

Figure 2. Fluorescence images of NBD-peptides, at 1 and 10 µM. Panel A shows the peptide in green; Panel B shows the LysoTracker in red and Panel C shows the merge of the two images. Bar = 10 µm.

Recently, it has been reported that cell-fixation protocols induce the apparent translocation and nuclear localization of positively charged peptides and this has been previously proved for the Tat peptide. We have examined the possibility that the translocation observed for gH625 could be the result of such an effect. As shown in Figure 3, although the penetration of the Tat-NBD in living cells is lower than with fixed cells, indicating that a portion of surface-bound peptide diffuses into the cytoplasm during the fixation step, the penetration of gH625-NBD is not affected by fixing protocols. The NBD alone at a concentration of 10 µM is almost unable to penetrate inside cells (Figure 3).

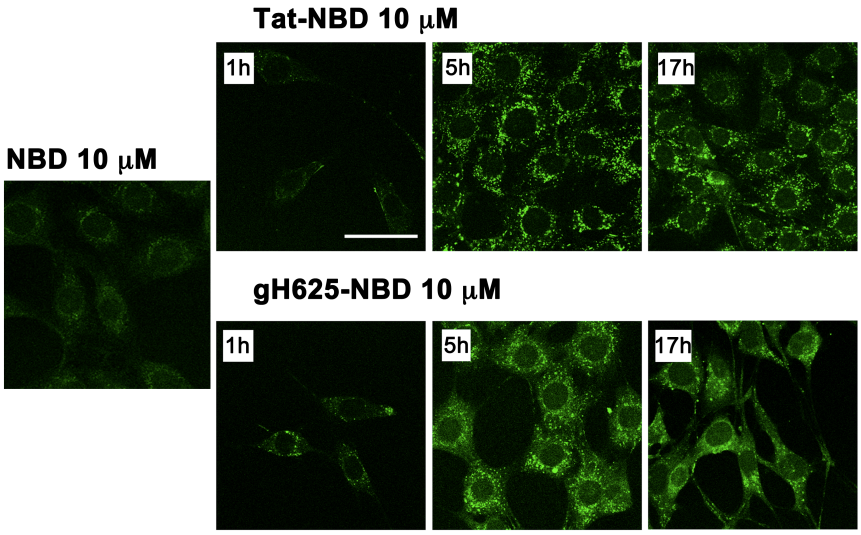

Figure 3. Uptake kinetics of NBD-peptides (10 μM) in HeLa cells after 1, 5 and 17 h of incubation at 37°C. Bar = 50 μm.

3.1.5 Inhibition of active intracellular internalization of NBD-peptides

The influence of metabolic inhibitors on the intracellular penetration of NBD-peptides was studied to see whether the uptake depended on a translocation mechanism or a cellular process. The analysis of the results indicates that the endocytosis is more significant for Tat than for gH625. Sodium azide is an oxidative phosphorylation inhibitor commonly used to abolish ATP production within the cell membrane.

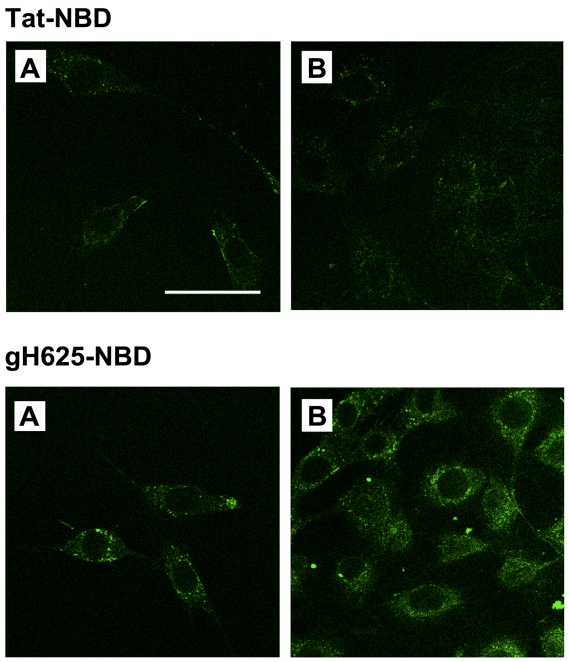

Figure 4. Endocytosis inhibition experiments of HeLa cells incubated for 1 h with 10 μM NBD peptides. (A) Non treated cells and (B) 40 μM NaN3 treated cells; bar = 50 μm.

As shown in Figure 4A, B, a marked decrease of Tat internalization was observed when conjugated to NBD indicating that endocytosis is the main process involved in Tat penetration. On the contrary, gH625 penetration is not influenced significantly by the treatment with sodium azide, indicating that endocytosis does not affect gH625 transduction.

3.1.6 gH625 and TAT toxicity

The cell viability was measured using MTT and LDH assays. LDH is of great value as an in vitro marker for cellular toxicity. Figure 5A shows the results obtained with the MTT assay, and Figure 5B shows the results of the LDH assay. To evaluate the cell toxicity of both gH625 and Tat peptides, increasing doses of the peptides were applied to HeLa cells. The addition of Tat or gH625 did not affect HeLa cell viability up to 200 µM. A low level of toxicity was observed when the peptides' concentration reached 400 µM. In the conditions used, different sensitivity was observed for the 2 assays, with the MTT assay being slightly more sensitive in detecting cytotoxic events in comparison with the LDH leakage assay. In conclusion, both peptides were not toxic at concentrations lower than 400 µM, and at this concentration, Tat was slightly more toxic than gH625.

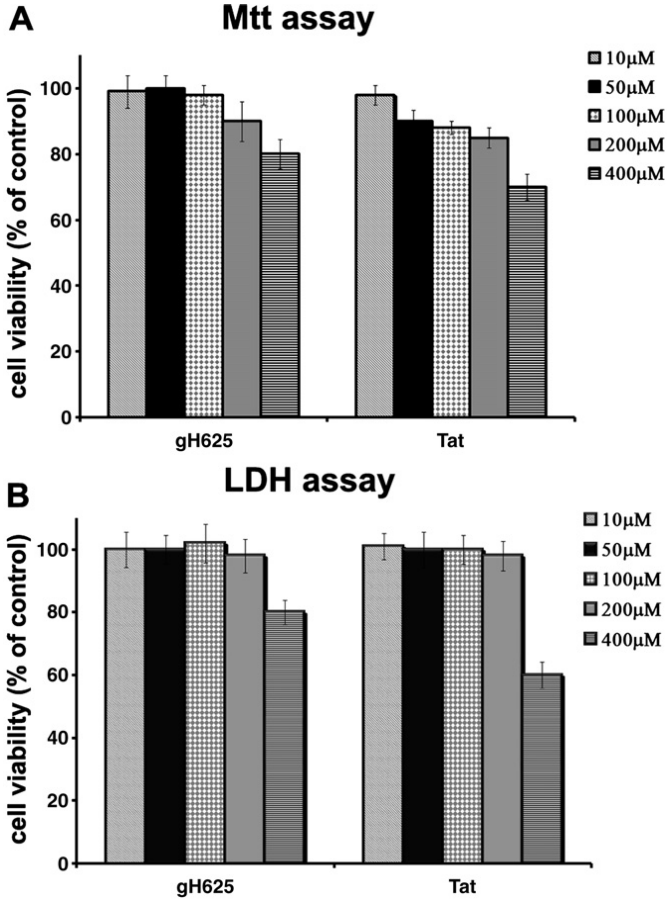

Figure 5. Effect of peptides on the viability of HeLa cells. Cytotoxic effect of gH625 and Tat peptides determined by the MTT (panel A) assay and by measuring the efflux of lactate dehydrogenase (LDH) into the culture medium (panel B). HeLa cells were treated with the indicated concentrations of peptides for 24 h. The values shown are the percentages of viable cells and LDH release relative to control cells.

3.2 gH625 FUNCTIONALIZED QUANTUM DOTS (QDS)

3.2.1 gH625 synthesis and functionalization of QDs

The gH625 peptide sequence was synthesized with an acetyl protecting group at the N terminus by solid-phase methods according to standard SPPS protocols with Fmoc/tBu chemistry *(Ac-HGLASTLTRWAHYNALIRAF-COOH)*. The purified peptide was obtained with good yields (30-40%). Functionalization of QDs was performed in PBS buffer and the functionalization degree was confirmed by determining the amount of peptide attached by UV analysis (ε_{gH625} = 7000 M^{-1} cm^{-1} at λ = 280 nm) and corresponded at 100%.

3.2.2 QDs-peptides intracellular delivery by confocal microscopy

To confirm the QDs-gH625 internalization, we examined its uptake and intracellular localization by confocal microscopy using QDs-Tat as reference. We used concentrations of 5 and 50 nM and a time of 60 minutes as selected by the flow cytometry experiments. Both QDs-peptides are efficiently internalized and we observe a significant colocalization with the LysoTracker, indicating a partial confinement within the endosomal compartment (Figure 6).

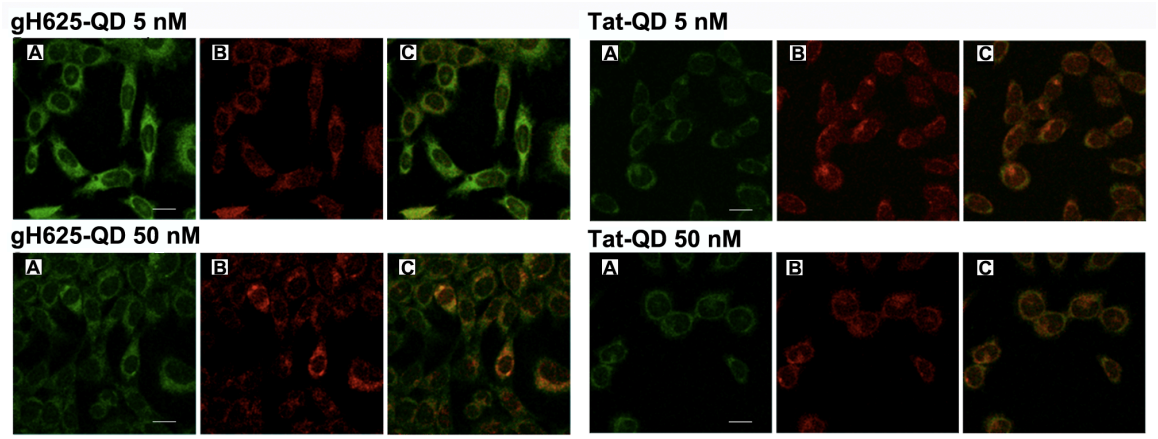

Figure 6. Fluorescence images of QD-peptides at 5 and 50 nM Panel A shows the peptide in green; Panel B shows the LysoTracker in red and Panel C shows the merge of the two images. Bar = 10 µm.

Intracellular uptake experiments on living cells were performed in order to avoid not real results due to the use of cell-fixation protocols, as previously described for NBD-peptides. Delivery of QDs to living cells consists of 2 phases: QDs are initially bound to plasma membrane of cells, and then are gradually internalized by cells. QDs alone have a poor affinity for the plasma membrane of HeLa cells at the concentration of 50 nM (Figure 7). The peptide conjugation to QDs enhanced their membrane bound ability providing a favorable condition for the cellular internalization. Figure 7 clearly shows their intracellular distribution in HeLa cells at concentrations of 5 and 50 nM.

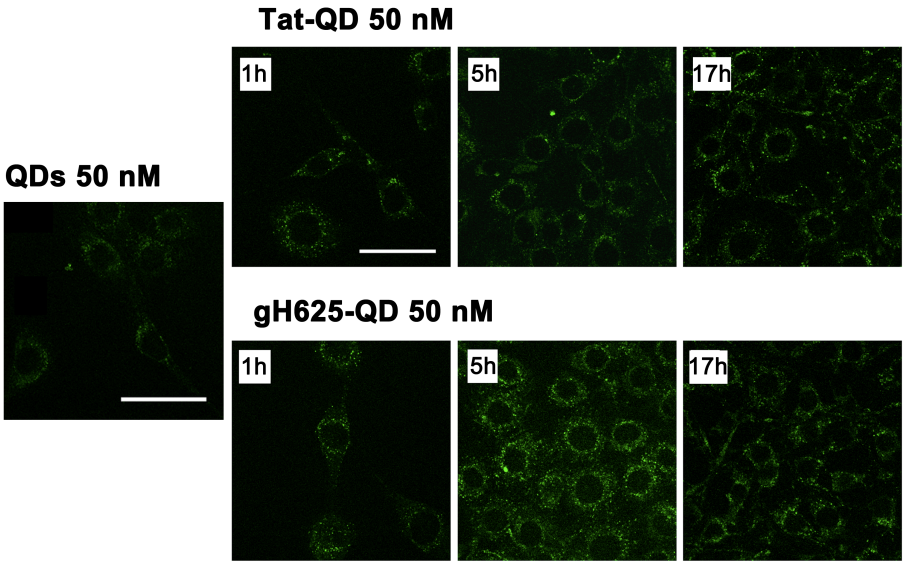

Figure 7. Uptake kinetics of QD-peptides (50 nM) in HeLa cells after 1, 5 and 17 h of incubation at 37°C. Bar = 50 µm.

3.2.3 Inhibition of active intracellular internalization of QDs-peptides

The influence of metabolic inhibitors on the intracellular penetration of QDs-peptides was studied to see whether the uptake depended on a translocation mechanism or a cellular process. The analysis of the results indicates that the endocytosis is more significant for Tat than for gH625.

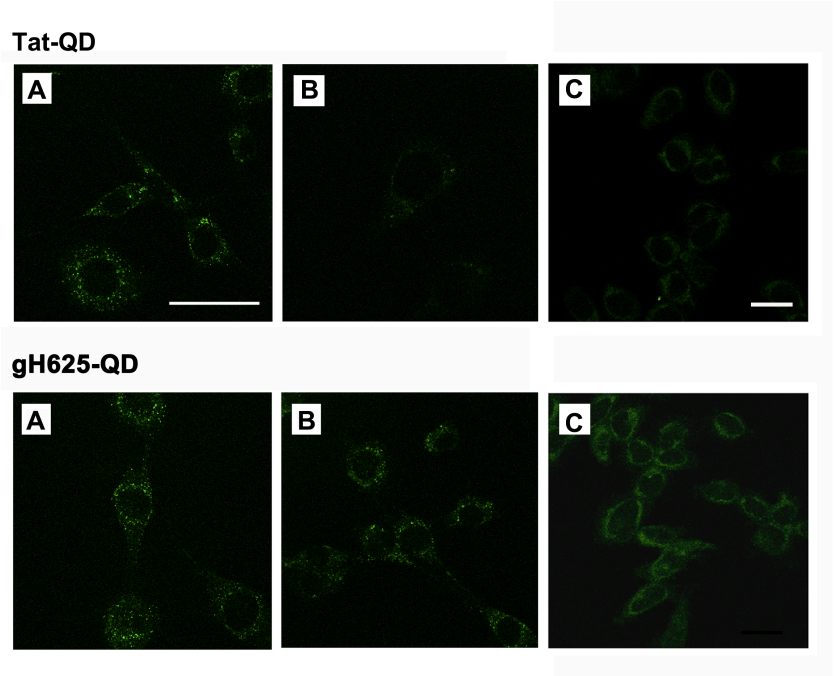

Figure 8. Endocytosis inhibition experiments of HeLa cells incubated for 1 h with 50 nM QD peptides. (A) Non treated cells and (B) 40 µM NaN3 treated cells; bar = 50 µm. Panel C reports the fluorescence images of gH625 QD and TAT QD at 100 nM incubated with HeLa cells at 4°C; bar = 10 µm.

As shown in Figure 8 A, B, a marked decrease of QDs-Tat internalization was observed indicating that endocytosis is the main process involved in Tat penetration.

On the contrary, QDs-gH625 penetration is not influenced significantly by the treatment with sodium azide, indicating that endocytosis does not affect gH625 membrane crossing.

3.3 gH625 FUNCTIONALIZED LIPOSOMES

3.3.1 Peptides synthesis and functionalization of liposomes

The coupling of a bioactive ligand on the surface of liposomes can be obtained according to several synthetic approaches. The choice of the strategy depends on whether it is necessary to perform the coupling before or after the liposome assembly. The coupling before the assembly of liposomes is, in principle, chemically less complicate, but has the disadvantage that a fraction of the ligand remains entrapped in the liposome inner region and is not available to play its biological function. This strategy is the preferred choice for amphiphilic peptides, anyway it remains unsuitable for poorly hydrophilic or mainly hydrophobic peptides. In these cases the coupling of the ligand can be performed after the assembly of the liposomes using activated functional groups introduced onto the external side of unilamellar liposomes. Activated functional groups must be compatible with liposome preparation and they should remain available on the surface for an efficient chemical ligation of the ligand.
gH625 is a hydrophobic peptide (see in Table 1 the amino acid sequence of gH625 peptide and of the gH625 derivatives used in this study) with high tendency to locate in the hydrophobic portion of liposomes; thus, for the preparation of liposomes decorated by gH625 a post-aggregation pathway based on click chemistry methods was chosen.

PEPTIDES	SEQUENCES	M.W
gH625	NH_2-HGLASTLTRWAHYNALIRAF-$CONH_2$	2297.1
gH625-Pra	NH_2-HGLASTLTRWAHYNALIRAF-Pra-$CONH_2$	2391.3
A643K(TOAC)-gH625-Pra	NH_2-HGLASTLTRWAHYNALIRK(TOAC)F-Pra-$CONH_2$	2644.6
A639K(TOAC)-gH625-Pra	NH_2-HGLASTLTRWAHYNK(TOAC)LIRAF-Pra-$CONH_2$	2644.6
A635K(TOAC)-gH625-Pra	NH_2-HGLASTLTRWK(TOAC)HYNALIRAF-Pra-$CONH_2$	2644.6
A628K(TOAC)-gH625-Pra	NH_2-HGLK(TOAC)STLTRWAHYNALIRAF-Pra-$CONH_2$	2644.6
NBD-gH625-Pra	NBD-HGLASTLTRWAHYNALIRAF-Pra-$CONH_2$	2537.9
NBD-Pra	NBD-Pra-$CONH_2$	258.9

Table 1. Peptide sequences and their molecular weight.

This procedure involves a copper(I)-catalyzed Huisgen 1,3-dipolar cyclo-addition reaction of azides and alkynes yielding 1,4-disubstituted1,2,3-triazole linked conjugates. The unreactive nature of both azides and alkynes towards any other functional group present in the biomolecules, as well as the thermal and hydrolytical stability of their cycloaddition product make this reaction particularly appealing for liposome functionalization with peptides.
Click-reaction was performed between DOPG/$(C18)_2$L-N_3 liposomes (90/10 molar ratio), obtained according to classical procedures for the preparation of mixed liposomes, and the peptide gH625 bearing a propargylglycine moiety (gH625-Pra).

The click- reaction, performed in an aqueous solvent system, was catalyzed by Cu(I) generated, in situ, by reduction of CuSO4 with ascorbic acid (Figure 9C).

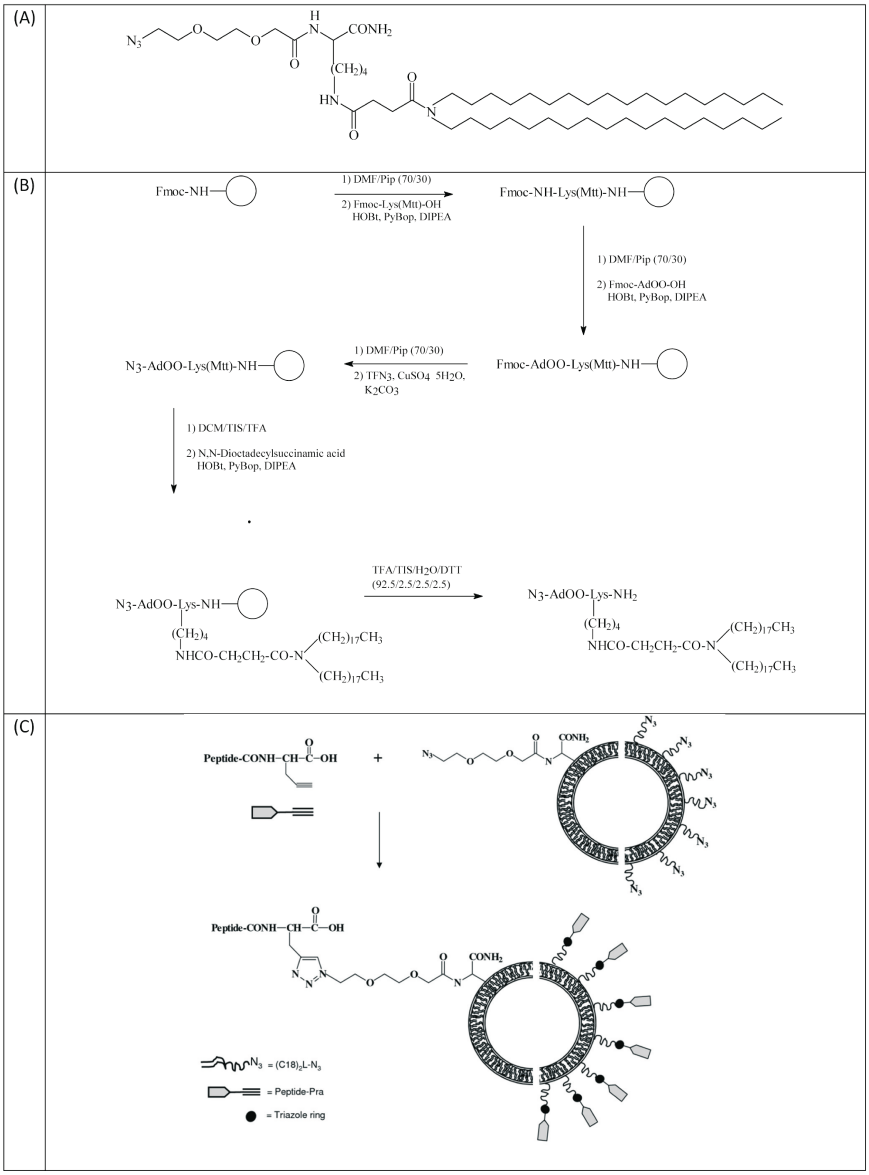

Figure 9. (A) Schematic representation of $(C18)_2L\text{-}N_3$ synthetic monomer; (B) Scheme for the solid-phase synthesis of the $(C18)_2L\text{-}N_3$ monomer. Rink-amide Resin is schematically represented as an empty circle; (C) Coupling of the gH625-Pra peptide to azide functionalized liposomes by click-chemistry reaction.

The click chemistry reactants gH625-Pra peptide and the liposome component $(C18)_2L\text{-}N_3$ were synthesized by solid-phase methods according to standard SPPS protocols with Fmoc/tBu chemistry. In the case of gH625-Pra peptide (see Table 1), the alkyne moiety was introduced in the peptide sequence in the C-terminal position as L- propargylglycine (Pra). $(C18)_2L\text{-}N_3$ (Figure 9A) was synthetized on solid phase following a modified protocol of the classical Fmoc/tBu strategy, as indicated in Figure 9B. The Fmoc-Lys(Mtt)-OH was anchored to the Rink amide resin. After removing of the Fmoc protecting group, an ethoxylic linker was introduced, and its NH2 function was converted in azide by diazo transfer using a sulfonyl azide, as previously reported in the literature. After removal of the Mtt group from the Nε lysine amino function, the lipid chains were added. As expected, no reductive side reaction

of azide functionalized derivative was observed during the cleavage step of the lysine derivative from the resin (data not shown)[148]. Both gH625-Pra and $(C18)_2$L-N_3 were collected in good yields (20÷40% and 85%, respectively) after HPLC-RP purification, and analyzed by mass spectrometry (Maldi-Tof), ^{1}H and ^{13}C-NMR (for $(C18)_2$L-N_3) and HPLC to confirm compound identity and purity.
In order to determine the number of functional groups present on the external surface of the liposomes and the number of molecules of gH625 that were effectively linked to the liposome NBD-labeled Pra and NBD-labeled gH625-Pra fluorescent derivatives were used. NBD fluorescence emission at 530 nm was measured, after click reaction, on both the liposome and the NBD-Pra containing fractions, and the percentage of functionalization was calculated as the ratio of bound NBD-Pra to its total amount. The results confirm that about 50% of the total of azido functions is located on the external leaflet of the liposome. When starting with an equimolar mixture of NBD-gH625-Pra and azido functions on the liposome surface, the expected gH625 functionalized liposomes were obtained with a yield higher than 90% after 12h at room temperature. In the absence of copper catalyst no reaction was observed.
gH625-Pra analogues, labeled with the TOAC radical group through a site- directed spin-labeling approach, were synthesized for EPR studies. Since the spin label is relatively hydrophobic[154], it was introduced in the peptide sequence at the Ala positions. Being the four Ala almost equally spaced along the peptide sequence (in position 628, 635, 639 and 643, the numbering being that of the entire gH protein), we obtained four labeled peptides (A628K(TOAC)-gH625-Pra, A635K(TOAC)-gH625-Pra, A639K(TOAC)-gH625-Pra and A643K(TOAC)-gH625-Pra) bearing the reporter moiety in positions regularly distributed from the N- to the C-termini. For the synthesis of the four TOAC labeled peptide derivatives, the four alanine residues were replaced one by one by Lys(Mtt). After removal of the Mtt moiety from the side chain of the lysine, the coupling of the TOAC residue was performed using HATU as activating agent [155]. The TOAC containing Pra-peptides have been purified by HPLC using standard TFA-containing eluents and gradients; treatment of the peptide in aqueous ammonia (pH 9.0) for 6h at room temperature is required in order to restore the chemical integrity of the nitroxide moiety after HPLC elution. Liposomes derivatized with TOAC containing Pra-peptides were obtained by using click chemistry procedures, as above reported in the case of gH625-Pra peptide derivative.

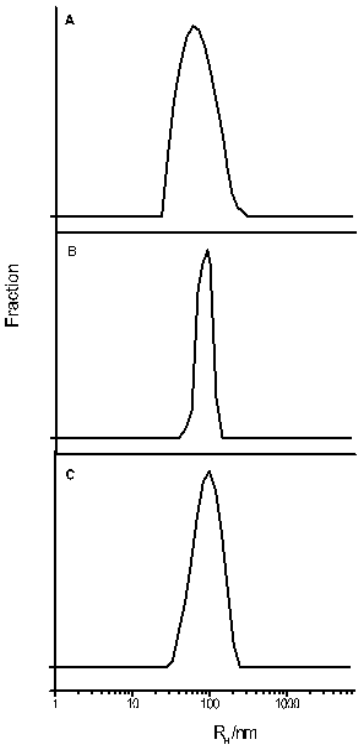

Figure 10. DLS spectra at 25°C with a liposome concentration of $1 \cdot 10^{-4}$ M. (A) DOPG/$(C_{18})_2$L-N_3 (90/10 molar ratio) liposomes; (B) DOPG/(C18)2L-gH625 liposomes obtained after click reaction; (C) DOPG/$(C_{18})_2$L-A635K(TOAC)-gH625

3.3.2 Dynamic Light Scattering (DLS) of liposome-peptides.

DLS measurements were performed at q =90° on liposomes composed of DOPG/$(C18)_2$L-N_3 at 90/10 molar ratio and on liposomes functionalized with gH625 as well as liposomes functionalized with TOAC peptide derivatives. Inspection of Figure 2 shows that all liposome solutions present a monomodal distribution due

to a translational diffusion process, which could be attributed to liposome aggregates. The Stokes-Einstein equation (1) $R_H = \frac{K_B T}{6\pi\eta D_0}$ is used to evaluate the hydrodynamic radius, R_H, at infinite dilution where D_0 is the translational diffusion coefficient at infinite dilution, K_B is the Boltzmann constant, T is the absolute temperature, and η is the solvent viscosity. Due to the high solution dilution (C = $1 \cdot 10^{-4}$ M) of the studied systems, we have approximately $D \sim D^0$, and equation (2) can be reasonably used to estimate the hydrodynamic radius of the aggregates. Diffusion coefficients, together with hydrodynamic radius values obtained through Eq. (2) (see experimental section), are reported in Table 2. The hydrodynamic radius of DOPG/$(C18)_2$L-N_3 liposome (90/10 molar ratio) is 69.43 ± 23.36 nm. As expected the introduction of a small amount of (C18)2L-N3 synthetic monomer does not influence the size of DOPG liposomes[156]. Figure 2B and 2C display the structural evolution of liposomes obtained after click reaction of gH625-Pra and four TOAC labeled Pra-peptides. In all cases liposome decorated by peptides show an increase of about 30% in diameter (see Table 2). From a structural point of view, this increase in size is in good agreement with the other targeted liposomal systems reported in literature[157,158] moreover, the TOAC moieties do not cause additional significant structural variations in the size of the aggregates.

Systems	**$D*10^{-12}/m^2s^{-1}$**	**R_H /nm**
DOPG/$(C18)_2$L-N_3	2.9 ± 0.7	69.43 ± 23.36
DOPG/$(C18)_2$L-gH625	2.2 ± 0.3	90.38 ± 13.50
DOPG/$(C18)_2$L-A643K(TOAC)-gH625	2.1 ± 0.5	95.40 ± 23.80
DOPG/$(C18)_2$L-A639K(TOAC)-gH625	2.1 ± 0.5	92.32 ± 25.22
DOPG/$(C18)_2$L-A635K(TOAC)-gH625	2.0 ± 0.5	97.60 ± 25.01
DOPG/$(C18)_2$L-A628K(TOAC)-gH625	2.2 ± 0.5	91.32 ± 24.45

Table 2. Diffusion coefficients and hydrodynamic radius R_H obtained from Dynamic Light Scattering measurements for the studied systems.

3.3.3 Circular Dichroism of gH625 and analogues with TOAC

The secondary structures of gH625 and of all the analogues with Lys(TOAC) in substitution of alanine residues were determined by CD spectroscopy (Figure 11). As gH625 assumes a random conformation in aqueous buffer while it assumes a α-helical structure in membrane mimetic environments. gH625 and the Lys(TOAC) derivatives, in water solution containing 20% TFE, show a helical structure with a slightly increase in ellipticity for the peptides where the modification are localized in the center of the peptide, as clearly evident from the spectra of the gH625 native peptide and of the Lys(TOAC) peptide derivatives. These data clearly show that the introduction of the TOAC moiety does not modify the gH625 peptide conformation, and Lys(TOAC) gH625 derivatives could be used in EPR studies to define peptide positioning.

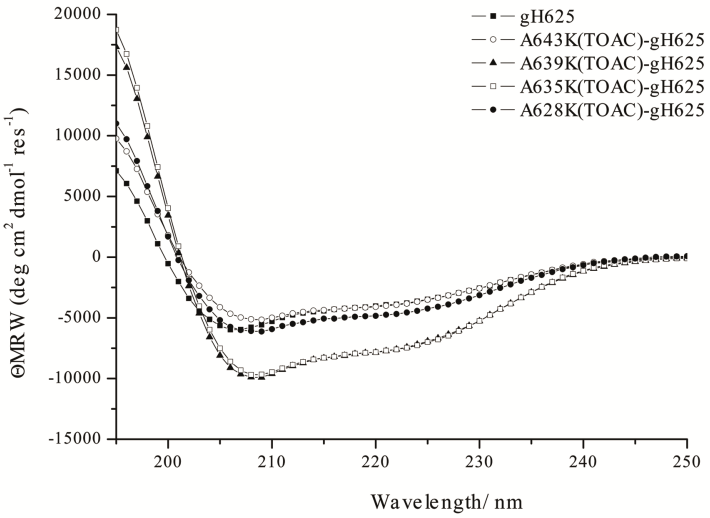

Figure 11. Circular dichroism spectra of gH625 peptides and of analogues with Lys(TOAC) in substitution of alanine residues, obtained in HEPES buffer at 20% TFE.

3.3.4 Determination of the position of gH625 on liposomes by EPR spectroscopy.

The peptide positioning relative to the liposome surface was investigated by EPR spectroscopy. To this aim gH625-Pra analogues, labeled with the TOAC radical group through a site- directed spin-labeling approach, were used. The EPR spectra of the free labeled peptides dissolved in 10 mM HEPES buffer consist of three narrow lines (see Figure 12A for an example), typical of an unstructured peptide with few constraints on the motion of the reporter group and consistent with the observed random coil CD spectrum. Subsequently, the labeled peptides were chemically linked to the DOPG/$(C18)_2$L-N_3 liposomes by following the same procedure used for the parent unlabeled peptide, obtaining four suspensions of functionalized liposomes. The analysis of their EPR spectra, reported in Figure 4A, gives information on the positioning of the gH625 relative to the surface of the liposome to which it is linked. In all cases a clearly defined axially anisotropic line shape is observed, indicating that the reporter group, wherever positioned along the peptide sequence, assumes a well defined orientation relative to the bilayer. This behavior indicates that the peptide does not protrude in the aqueous medium surrounding the liposome, in which the label would have assumed a much higher mobility freedom, but rather interacts with the surface of the lipid bilayer. Analysis of the figure shows that the spectrum anisotropy increases in going from A628K(TOAK)-gH625 to A643K(TOAC)-gH625, indicating that the peptide segments closer to the C-terminus, which is chemically linked to the lipid, are more strictly oriented relative to the bilayer. This evidence can be easily quantified by measuring the outer hyperfine splitting, 2Amax, which is a reliable and easy to perform estimate of the segmental chain mobility. 2Amax is defined as separation, expressed in gauss, between the low-field maximum and the high-field-minimum of the spectrum, and tends to increase with increasing the restriction in the label mobility. Figure 12B shows that, as the label position is moved from position 628 to 643, 2Amax increases. This evidence suggests that the peptide does not insert in the bilayer hydrophobic core, but rather remains adsorbed on its surface remaining exposed to aqueous environment. This result confirms the possibility of using our synthetic strategy to bind a hydrophobic peptide on the liposome external surface; the use of a short linker may also provide steric

restrictions for the peptide insertion inside the liposome.

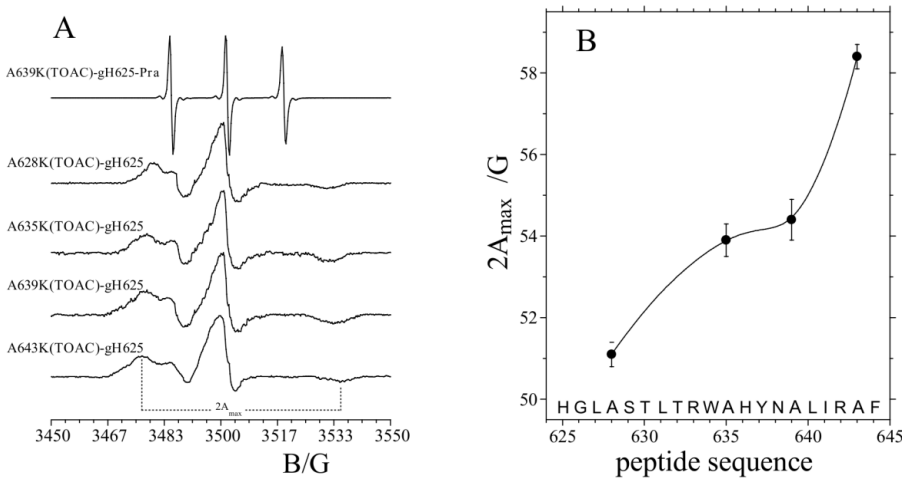

Figure 12. (A) EPR spectra of TOAC peptides linked to DOPG/$(C18)_2$L-N_3 liposomes. An EPR spectrum of the free peptide A639K(TOAC)-gH625-Pra in aqueous buffer is also shown. (B) Dependence on spin-label position along the peptide sequence of the outer hyperfine splitting, 2Amax, of TOAC peptides linked DOPG/$(C18)_2$L-N_3 liposomes.

3.3.5 Liposomes Doxorubicin loading.

Cytotoxic doxorubicin was loaded into DOPG/$(C18)_2$L-N_3 liposomes using the well-assessed procedures based on ammonium sulfate gradient[159 160] in particular, doxorubicin solution was incubated under stirring for 30 min at 60°C. Subsequently, unloaded doxorubicin was removed by Sephadex G50 column pre-equilibrated with 10 mM HEPES buffer at pH 7.4. The drug/lipid weight ratio chosen for the loading experiments was 0.1.
The doxorubicin loading content (DLC) was calculated by UV-Vis measurements at 480 nm and was above 95% of the total. The resulting Dox-loaded liposomes were then efficiently modified with gH625-Pra peptide according the click chemistry procedure used in the case of empty liposomes.

3.3.6 Liposome- gH625 cellular uptake by confocal microscopy.

To study the cellular internalization of doxorubicin loaded liposomes functionalized with gH625 peptide, we examined their uptake and intracellular localization in living HeLa cells by confocal microscopy. Cells were incubated with 1 μM of Dox free and encapsulated in liposomes for 1, 5, 17 hours at 37 °C. The results obtained after 5 hours of incubation are reported in Figure 5. As expected, after 5 hours free Dox is able to enter the cell and translocate into the nucleus as indicated by the green fluorescence in the center of the cell body (Figure 13 A-C). Also in the case of DOPG/$(C18)_2$L-N_3/Dox liposomes, cell nuclei appear fluorescent due to Dox accumulation in DNA and a slight diffuse fluorescence in the cytoplasm is observed suggesting a Dox release from the liposomes (Figure 13 D-F). Conversely, gH625 functionalized liposomes encapsulating Dox accumulate in the cytoplasm, without entering into the nucleus (Figure 13 G-I). Indeed, cell nuclei are dark and only green fluorescent spots, distributed in the cytoplasm, are visible. These results suggest that

the functionalization of liposomes with gH625 peptide could affect uptake mechanism of liposomes and, thus, their intracellular distribution and Dox release. This evidence could be useful in the design of carriers for a controlled delivery and release of Dox in order to avoid side effects associated to Dox itself.

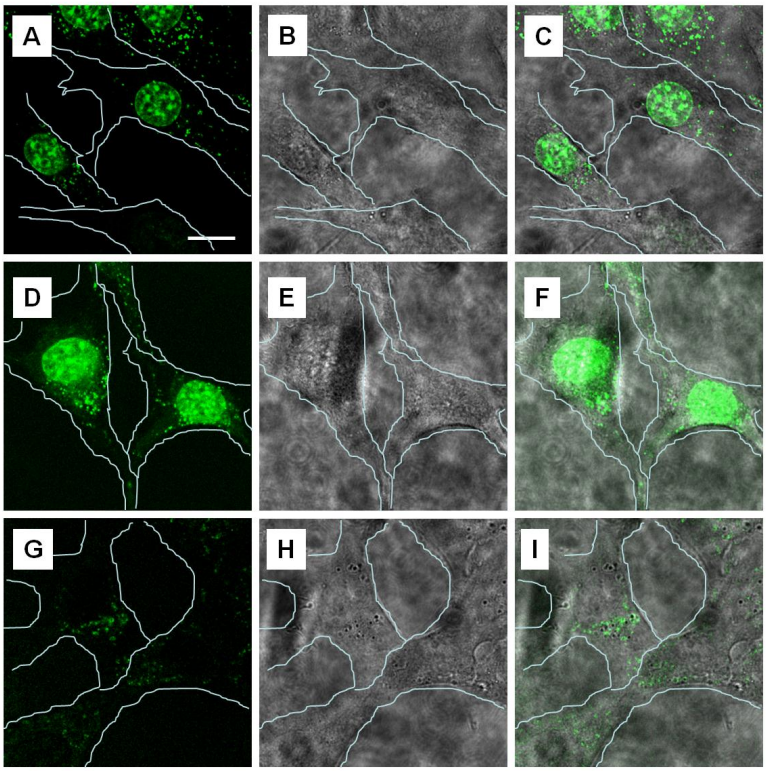

Figure 13. Confocal microscopy images of HeLa cells after 5 h incubation with 1μM of A, D, G fluorescence images of Dox accumulation within the cells; B, E, H transmission line indicates the cell boundaries. Bar 20 μm.

3.4 FUNCTIONALIZED DENDRIMERS

3.4.1 Synthesis of the octadecaazide dendrimer

The second generation Newkome-style dendron 2 was first functionalized at the amine terminus with succinic anhydride to afford the hemisuccinate dendron 3. Coupling dendrons 2 and 3 by using 2-[7-aza-1H-benzotriazol-1-yl]-1,1,3,3-tetramethyluronium hexafluorophosphate (HATU) as coupling agent afforded the symmetrical dendrimer 4. Acidic deprotection of the terminal tert-butyl esters resulted in the formation of the octadecaacid dendrimer 5. Reaction between the terminal carboxylic acid groups and an azido-terminated amine linker afforded the octadecaazide dendrimer 6 (Scheme 1).

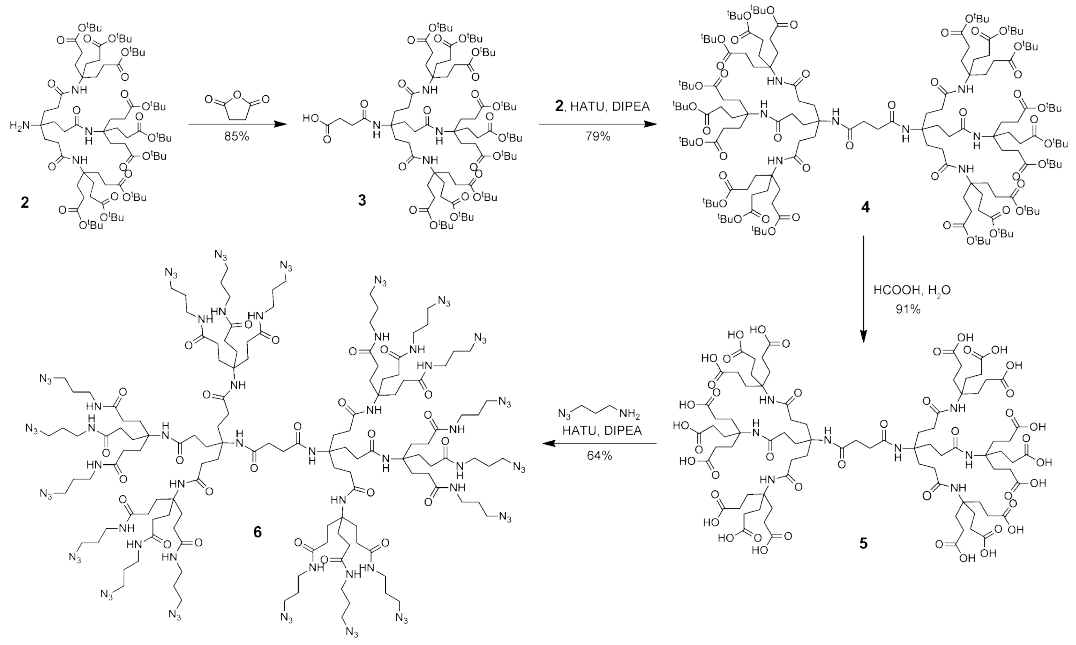

Scheme 1. Synthesis of the azide-terminated dendrimer used in this study.

3.4.2 gH625 synthesis and functionalization of the dendrimers

The gH625 peptide sequence was synthesized with a propargylglycine residue (Pra) at the C terminus to provide a handle for the CuAAC reaction. Functionalization of 6 was performed in a water/ methanol solution (1:1 v/v) by using CuSO4·5H2O as catalyst and sodium ascorbate as reducing agent (Scheme 2). The complete functionalization of peptidodendrimer 1 was confirmed by determining the amount of peptide attached by UV analysis (ε_{gH625} = 7000 M^{-1} cm^{-1} at λ = 280 nm[88] and comparing this to the amount of dendrimer initially used for reaction (18 mol peptide per mol dendrimer). IR analysis showed the disappearance of the azide stretch at 2098 cm^{-1} confirming that within the instrumental error range, all azides were consumed, thus suggesting complete functionalization of the dendrimer with peptides was obtained. The functionalization was also performed by using the same peptide containing a nitrobenzo-furazan fluorescent tag (1–NBD) and an alkynyl fluorophore[41,161]. All sequences used for functionalization are shown in Table 3. Functionalization of dendrimer 7 was also confirmed by UV/Vis spectroscopy (ε_{NBD} = 1696 M^{-1} cm^{-1} at λ = 452 nm).

Name	Sequence[a]	Compound
gH625	NH_2-HGLASTLTRWAHYNALIRAFX-$CONH_2$	1
gH625-NBD	NBD-HGLASTLTRWAHYNALIRAFX-$CONH_2$	1-NBD
NBD-CCH	NBD-$CH_2C{\equiv}CH$	7

Table 3. Sequences used to functionalize dendrimer X = propargylglycine, NBD = (7-nitrobenzofurazanyl)amino)

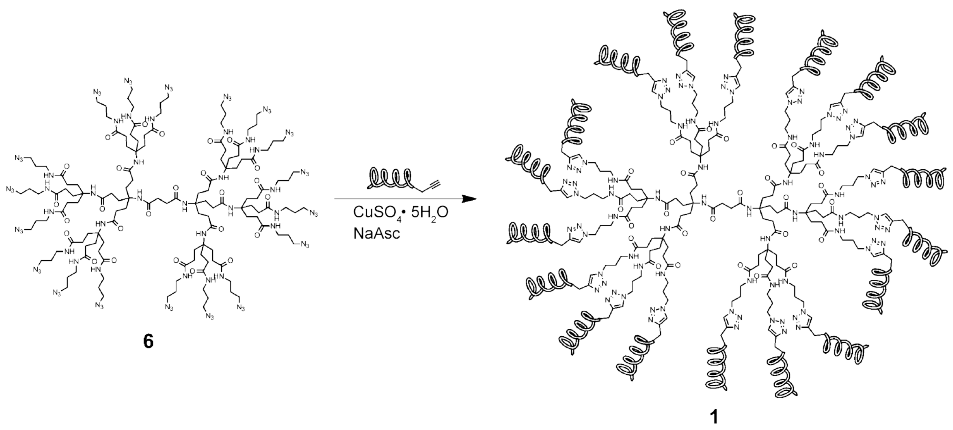

Scheme 2. Functionalization of dendrimer 6 by CuAAC reaction. Shown is the functionalization with gH625 to synthesize 1.

3.4.3 Structure of the peptidodendrimer

As previously reported[88], the gH625 peptide adopts a random coil in aqueous media, but forms a helix in membrane-mimetic environments. Circular dichroism (CD) spectra in several percentages of trifluoroethanol (TFE, allowing the solution to mimic the environment of the membrane) show that gH625 at a concentration of 8μM adopts a a-helix (Figure 14A). The CD spectra of the peptidodendrimer at a peptide concentration of 8 mM (18 peptides per dendrimer; concentration of dendrimer=0.4 mM) exhibited a shape indicative of a α-helix, suggesting that the secondary structure of the peptide was not disturbed by attachment to a dendrimer (Figure 14 B).

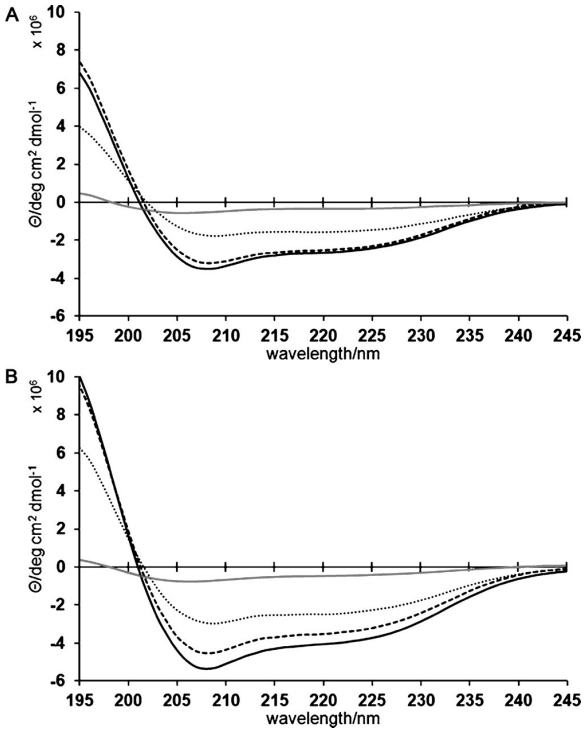

Figure 14. CD spectra of: A) peptide gH625, and B) peptidodendrimer 1 at 8 μM (8 μM peptide corresponds to a dendrimer concentration of 0.4 μM) in aqueous solution with varying amounts of TFE: 0% (c), 20% (g), 40% (a).

The size of peptidodendrimer 1 increased greatly upon the addition of the peptide sequences. Dendrimer 6 is too small to be accurately resolved by most techniques,

but the increase in size after the addition of the peptides makes it resolvable by light scattering and non-optical microscopy techniques. Dynamic light scattering (DLS) measurements were complicated by significant aggregation, most likely due to the dendrimers relatively hydrophobic terminal peptides in aqueous solution. At low concentrations, a signal was observed corresponding to a hydrodynamic radius of 5.6nm**.** This was confirmed by scanning transmission electron microscopy (STEM), which gave an average particle diameter of 12.66nm.

3.4.4 Fusogenic properties of the peptidodendrimer

In order to understand the membrane interacting behavior of the peptide when linked to the dendrimer, we performed lipid mixing, inner-monolayer fusion, and leakage experiments as indicators of the interaction and perturbation of the lipid membrane caused by the peptidodendrimer (Figure 15).
We carried out lipid-mixing experiments (Figure 15 A); for these studies, a population of 55:45 phosphatidylcholine/cholesterol with nitrobenzoxadiazole and (PC/Chol) LUVs labeled rhodamine-phosphatidylethanolamine (NBD-PE and Rho-PE) was mixed with a population of unlabeled LUVs, and increasing amounts of gH625, dendrimer 6, or peptidodendrimer 1 were added. Dilution of the fluorescently labeled vesicles by membrane fusion induced a reduction in the fluorescence energy transfer efficiency, hence dequenching of the donor fluorescence. In order to compare data, the percentage of lipid mixing as a function of the peptide to lipid molar ratio was calculated. The peptide and dendrimer 6 induced low levels of fusion at the concentration at which peptidodendrimer 1 induced high levels of fusion. In particular, we observed a significant increase of activity with the peptidodendrimer system. This shows that the peptidodendrimer is even more effective than the native peptide at interacting with and fusing lipid membranes, showing its efficacy as a membrane-perturbing agent.
In the inner-monolayer fusion assay, the fluorescence from the vesicle membranes outer monolayer is eliminated by the addition of an aqueous reducing agent, and this experiment reveals the extent of lipid mixing between the inner monolayers of vesicles in solution. Figure 15 B shows that gH625, dendrimer, and peptidodendrimer show only slightly lower inner-monolayer fusion than the total fusion observed from the lipid- mixing experiment. This indicates that under these experimental conditions, all three compounds were able to induce fusion significantly to both the inner and outer lipid monolayers; thus, we can confirm that the peptide, dendrimer, and peptidodendrimer are all able to interact strongly with and penetrate inside the lipid bilayer.
A contents-mixing assay was employed to monitor any mixing of internal vesicle components as a result of vesicle exposure to the peptide or the peptidodendrimer 1. Release of ANTS (1-aminonaphthalene-3,6,8-trisulfonate) and DPX (p-xylene-bispyridinium bromide) from the vesicle is commonly used as a measure of bilayer perturbation and is interpreted as “transient pore formation”[162,163]. Contents-mixing is manifested by a decrease in fluorescence intensity if vesicles encapsulating the fluorescent cargo (e.g., ANTS) merge contents with those containing quenchers (e.g., DPX). No content-mixing occurs under the same conditions and peptide/lipid ratio range at which substantial outer monolayer lipid-mixing was observed (data not shown); this corroborates the presence of vesicle hemifusion within our system not only for the peptide alone but also for the peptide–dendrimer system.

The present results can be used as qualitative indicators of the peptidodendrimer translocation or bilayer perturbation, with relevance for the direct penetration mode of cell entry, or for the steps of endosomal membrane translocation or endosomal escape. Using peptidodendrimer 1, we have not detected any significant pore formation; vesicle fusion events were not accompanied by leakage of the aqueous contents of the vesicle as was previously reported for gH625 and for other peptides[59,153].

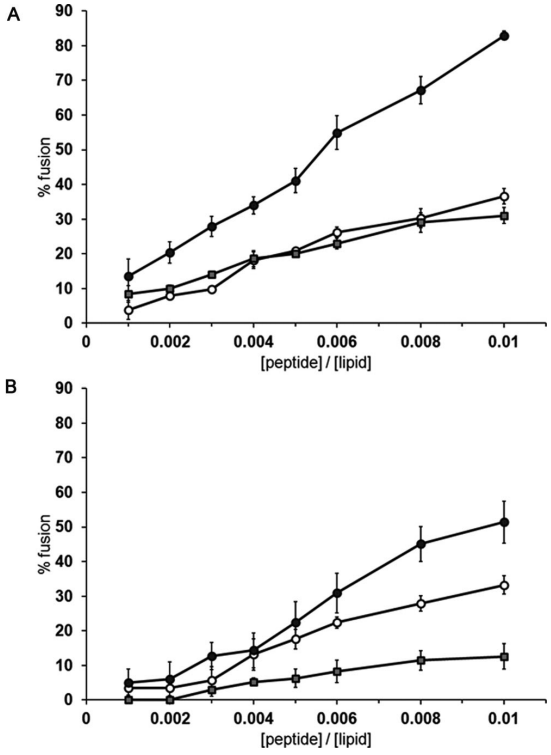

Figure 15. Interaction of peptide gH625 (filled squares), dendrimers (open circles), and peptidodendrimer 1 (filled circles) with PC/Chol LUVs; the dose dependence is reported according to the concentration of the peptides (18 peptides per dendrimer) and each trace represents an average of three independent experiments. A) Lipid-mixing, B) inner- monolayer assays.

3.4.5 Peptidodendrimer uptake by Flow cytometry

We have determined the fraction of the labeled peptide gH625–NBD and labeled peptidodendrimer 1–NBD taken up by HeLa cells using flow cytometry based on a method previously described.

We incubated the peptide and the peptidodendrimer with HeLa cells at 37°C at different concentrations (1, 5, 10, and 20 μM in peptide). After 1 h incubation, we measured the quenching of the NBD by dithionite treatment. The dithionite reaction was performed at low temperature (4°C) because the dithionite crossing of biological membranes is strongly reduced compared to high temperatures [164]. Before the addition of dithionite, we observed that approximately 90% of peptide gH625–NBD or 1–NBD was not washed away, suggesting they were internalized or bound to the membrane bilayer. After the addition of dithionite, the fluorescence of the internalized peptide and 1–NBD were slightly reduced (Figure 16A). Increasing the dithionite concentration did not result in a modification of the extent of quenching, indicating

that the entire accessible NBD label was quenched by 1M dithionite (data not shown). To exclude the possibility that the fluorescence signal could have been due to the internalization of the fluorochrome itself, the NBD moiety was used in the same in vitro assay conditions; no cellular fluorescence was observed at concentrations up to 20 μM.

To measure the kinetics of import into cells, we incubated gH625–NBD and 1–NBD with cells at 37°C for 10, 30, and 60 min, and then determined the remaining fluorescence following treatment with dithionite. Figure 16B shows the fraction of molecules taken up by cells. The uptake is very rapid and seems to reach a plateau after 1 h incubation.

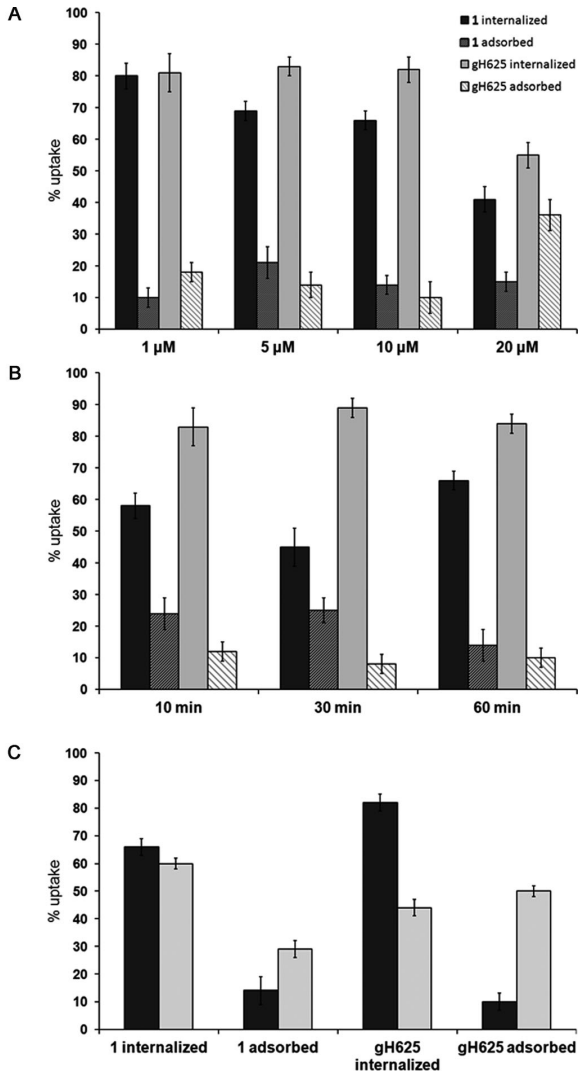

Figure 16. Percentage uptake graphs of peptidodendrimer 1–NBD versus gH625–NBD in HeLa cells under various conditions: A) 1 h incubation with various concentrations of peptide; B) incubation at 10 μM (in peptide) for various times; C) incubation at 10 μM (in peptide) for 15 min at various temperatures: 37°C (black bar); 4°C (grey bar).

The influence of temperature on the intracellular accumulation was studied to investigate whether the uptake depended on a passive translocation mechanism or an active process. We incubated gH625–NBD and 1–NBD with HeLa cells at both 37°C and 4°C; the amounts of internalized peptide and 1 at low temperature (Figure

16C) are reduced for both molecules with an increase in the amount bound to the membrane and a decrease of the internalized quantity. The reduction of internalized or bound molecule was less significant for 1, indicating a minor involvement of active mechanisms of internalization.

3.4.6 Peptidodendrimer intracellular delivery by confocal microscopy

The cellular uptake ability of 1 was explored by incubating an aqueous solution of 1 with live cells (Figure 17). HeLa cells were incubated for 2 h with a 20 μM solution of the fluorescently labeled 1–NBD (concentration relative to peptides; concentration of dendrimer=1.1μM). After incubation, excess fluorophore was washed away and the cells were imaged. The cells exhibited fluorescence even after being washed, suggesting that the NBD-labeled dendrimer was interacting with the cellular membranes. Control experiments against dendrimer 7, containing the fluorophore but no peptide, showed extremely little fluorescence in the cells, suggesting the peptides were required for efficient membrane interaction.

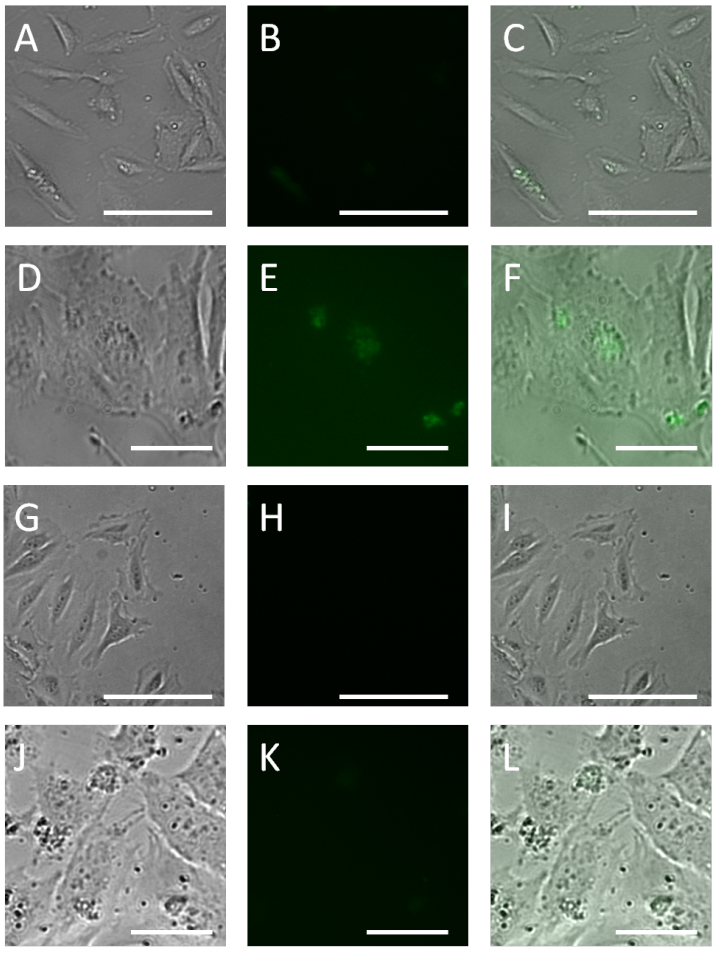

Figure 17. Fluorescence microscopy images from the cellular uptake study. A)–C) Incubation at 37°C with peptidodendrimer 1 (20 μM) for 2 h; D)– F) incubation at 37°C with dendrimer 7 (20 μM) for 2 h; G)–I) incubation at 4°C with peptidodendrimer 1 (20 μM) for 15 min; J)–L) same as (A– C), but after preincubating the cells with NaN3 (40 μM) for 30 min. A), D), G), J) Transmission images; B), E), H), K) fluorescence images; C), F), I), L) overlay; scale bars: 20 μM.

In order to explore the mechanism of interaction, the cellular uptake studies were

also performed under conditions that inhibit active translocation mechanisms. First, incubation was carried out with the 20 μM (in peptide) peptidodendrimer solution for 15 min at 4°C. At 4°C, the cells are almost unable to take up the dendrimers endocytically. The fluorescence intensity of the cells was decreased but still observed, suggesting that the compound is able to enter into cells without undergoing an active translocation mechanism (Figure 17G). The cells were also incubated with 1 after preincubating with sodium azide (40 mm), which is a known inhibitor of oxidative phosphorylation[165]. After this preincubating, the cells were unable to produce ATP in the membrane and to perform endocytosis. Again, the cells were able to fluoresce after this preincubating, suggesting that 1 can enter the cells through a non-active mechanism (Figure 17 J).
We also incubated the cells with the 20 μM (in peptide) solution of 1–NBD for different lengths of time to observe the uptake kinetics. As we showed with the flow cytometry measurements, the cells exhibited fluorescence as early as 30 min after addition, showing the rapid uptake of the peptidodendrimer (Figure 18).

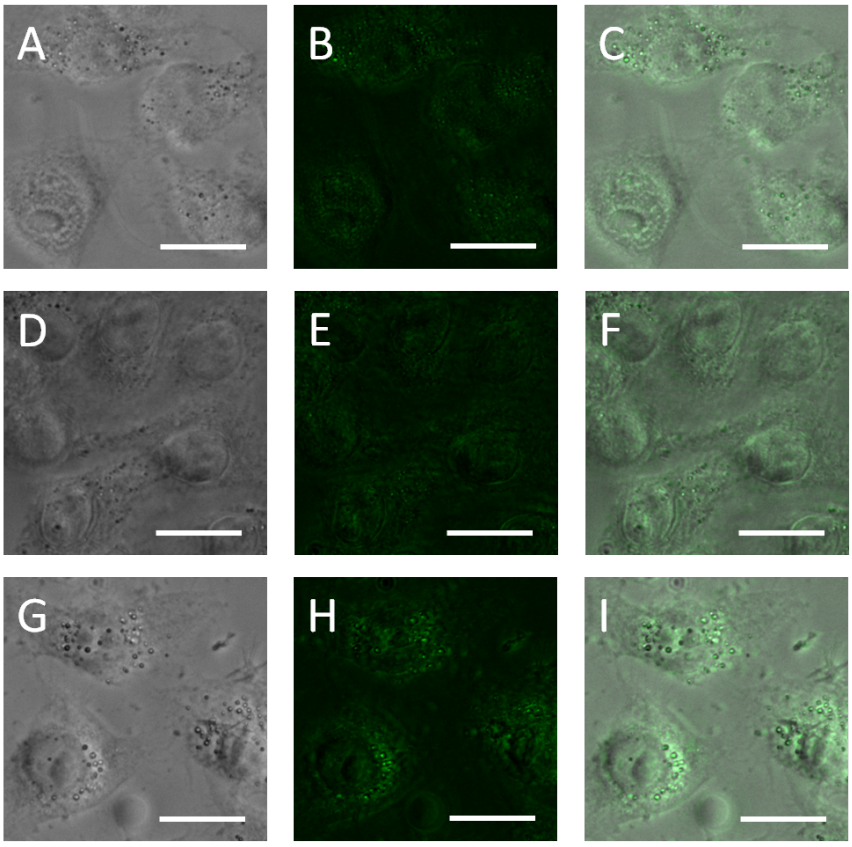

Figure 18. Fluorescence microscopy images from the cellular uptake kinetic study, incubating with dendrimer 1–NBD (20 μM) at 37°C for various times : A)–C) 30 min ; D)–F) 1 h ; G)–I) 2 h ; A), D), G) transmission images ; B), E), H) fluorescence images ; C), F), I) overlay ; scale bars : 20 μm.

3.4.7 Peptidodendrimer toxicity

To confirm that dendrimer and gH625 functionalized dendrimer do not exert toxic effects on cells, monolayers of Vero cells were exposed to different concentrations (0.28, 0.55, 1.1, 2.8, 5.5 μM) of each compound for 3 and 24 hours, and cell viability was quantified by the MTT assay. No statistical difference was observed between the

viability of control (untreated) cells and that of cells exposed to the peptidodendrimer (Figure 19) up to the concentration used in antiviral testing. Minimal toxicity was observed for the dendrimer without the peptides linked to its termini, but only at concentrations that were considerably higher than those required for antiviral activity.

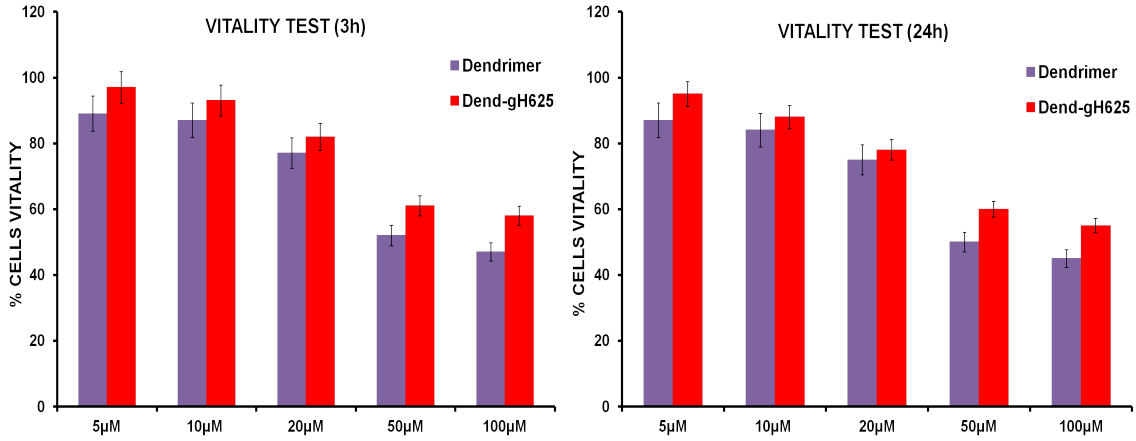

Figure 19. Cell viability measured by the MTT assay for 3 and 24 hours for the dendrimer (1) and peptidodendrimer (2).

3.5 gH625 FUNCTIONALIZED NANOPARTICLES (NPS)

3.5.1 gH625 synthesis and functionalization of Nanoparticles

The gH625 peptide sequence was synthesized with an acetyl protecting group at the N terminus and with 3 glycines at the C terminus in order to increase the space between the peptides and the nanoparticle *(Ac-HGLASTLTRWAHYNALIRAFGGG-COOH)*. The peptide synthesis was performed using solid-phase methods according to standard SPPS protocols with Fmoc/tBu chemistry. The purified peptide was obtained with good yields (30-40%). Functionalization of NPs was conducted in Mes buffer. Peptide-nanoparticles were prepared at several functionalization degrees (25-35 and 50 %), confirmed by determining the amount of peptide attached by UV analysis (ε_{gH625} = 7000 M^{-1} cm^{-1} at λ = 280 nm).

3.5.2 Circular Dichroism of gH625-Nanoparticles

To verify the secondary structure of the peptide bound to the nanoparticles we performed circular dichroism (CD) experiments. CD data confirmed that gH625 retains its structure (helical) when bound to the nanoparticle surface as previously reported also for other peptides[166]. The spectra obtained at different percentages of functionalization indicate a helical structure in all conditions (Figure 20A, B).

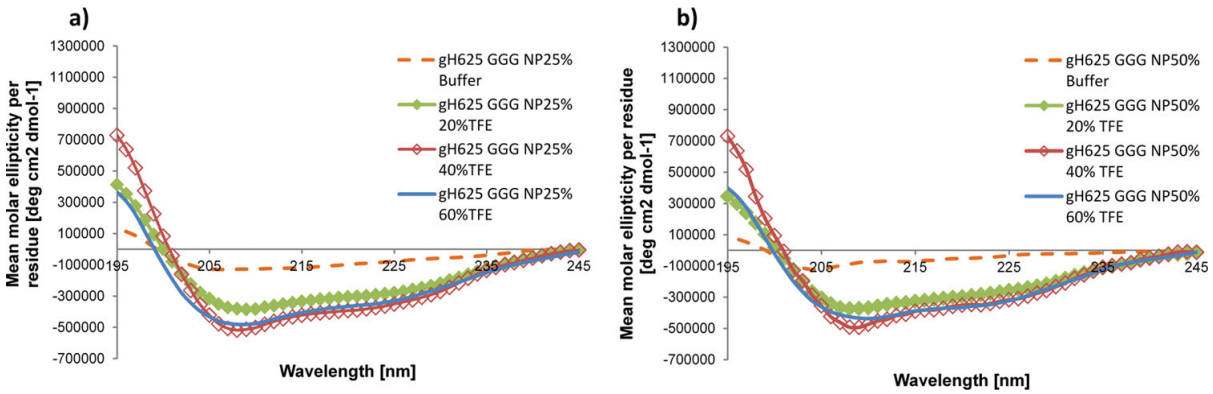

Figure 20. Circular dichroism spectra of polystyrene NPs at 25% (a) and 50% (b) degrees of functionalization with gH625 peptide.

3.5.3 Dynamic Light Scattering (DLS) and zeta potential of gH625-Nanoparticles

To further investigate the effect of the peptide functionalization (25, 35, and 50%) on the size of nanoparticles, we performed dynamic light scattering (DLS) measurements. After functionalization, the hydrodynamic size of nanoparticles with 25, 35, and 50% of gH625 in aqueous medium at pH 7 was found to be respectively 96.68 ± 0.43 nm, 95.64 ± 0.19 nm and 96.76 ± 0.07 nm, with polydispersity values of ca. 0.08, indicating a narrow distribution of the particle size at the pH used for all the experiments (Table 4). To elucidate the colloidal stability of functionalized nanoparticles at different pH values, which is a crucial parameter correlated to their functionalization, measurements of the zeta potential and of the hydrodynamic radius (DH) were carried out (Table 4). For NPs alone, the colloidal stability is strongly pH-dependent because it is mainly due to electrostatic repulsion between particles. It is widely accepted that at high values of z-potential (over 30 mV, positive or negative) the electrostatic interactions between particles are strong enough for electrostatic stability, while at intermediate values of z-potential, near their isoelectric point, particles can flocculate. Table 4 shows both z-potential and mean hydrodynamic diameter of blank NPs and NPs at different degrees of functionalization as a function of pH. In presence of peptide, the DH of the functionalized NPs remained nearly constant over the entire pH range, with no sign of aggregation in spite of the lower values of the zeta potential observed at pH 8. Such a behavior highlights that their stabilization is via steric hindrance rather than electrostatic repulsion. In particular, by increasing the percentage of functionalization NPs zeta potential increases from about +30 mV to +35 mV at pH 7. At these zeta potential values, NPs DH remains nearly about 100 nm. Only at pH 8, we observed a lower zeta potential for 25% functionalized NPs, indicating that in this condition the functionalized nanoparticles are still partially aggregated and their behavior is similar to non-functionalized NPs.
These data indicate that the peptide bound to the NPs is able to retain its helical structure in all the conditions tested and is able to completely prevent NPs aggregation at 35 and 50% of functionalization.

		pH 4	pH 7	pH 8	pH 9
NP	ζ potential (mV) [a]	44.9 ± 5.26	51.6 ± 1.08	-11.1 ± 0.60	-32 ± 1.22
	Size (d.nm) [a]	106.5 ± 2.52	137 ± 1.19	848.4 ± 48.33	473.6 ± 1.81
	PDI	0.18	0.31	0.25	0.30
NP-gH625 25%	ζ potential (mV) [a]	33.13 ± 1.11	30.77 ± 2.40	10.93 ± 0.76	-33.33 ± 1.36
	Size (d.nm) [a]	242.3 ± 1.39	96.58 ± 0.43	103.37 ± 1.14	231.77 ± 6.67
	PDI	0.25	0.08	0.13	0.28
NP-gH625 35%	ζ potential (mV) [a]	34.13 ± 2.42	30.9 ± 0.79	18.43 ± 0.91	-33.17 ± 1.07
	Size (d.nm) [a]	114.93 ± 1.40	95.64 ± 1.09	96.27 ± 0.67	99.92 ± 0.50
	PDI	0.14	0.08	0.08	0.10
NP-gH625 50%	ζ potential (mV) [a]	33.83 ± 1.98	35.1 ± 2.43	17.77 ± 0.76	-28.03 ± 1.82
	Size (d.nm) [a]	102.1 ± 0.36	96.76 ± 0.07	97.53 ± 0.20	99.65 ± 0.70
	PDI	0.12	0.09	0.09	0.10

Table 4. Zeta potential and size measurements of NP and NP at different degrees of functionalization as a function of pH. ([a](mean value ±SD,n=3).

3.5.4 Multiple Particle Tracking (MPT) of gH625-Nanoparticles

We previously demonstrated that the conjugation of the peptide gH625 enhances cellular uptake of quantum dots[59], liposomes[167] and dendrimers[168] in HeLa cells in vitro. However, no evidences of the effect of gH625 on nanoparticle uptake in brain endothelial cells have been previously reported. Moreover, the exact mechanism used by gH625 to facilitate cargos transport through cell membranes has not yet been understood in details. Therefore, in this work we studied the effect of gH625 on polystyrene NP uptake mechanisms on mouse brain endothelial bEnd3 cells.
We first tested the cytotoxicity of blank NP and gH625-NP on bEnd3 cell line by Alamar Blue Assay and we verified that blank NPs and gH625-NPs at 50% functionalization did not affect cell viability in the experimental conditions used for the assay compared to non-treated control cells (data not shown).
Once internalized, NPs can follow different fates: i.e., particle degradation inside lysosomal compartments, accumulation in other organelles, recycling to the plasma membrane or transcytosis to the basal surface of endothelium. Furthermore, the routes of NP intracellular trafficking might give some indications not only about the fate of NP, but also about the mechanisms driving cellular uptake[150,169]. To address this issue, multiple particle tracking (MPT) gives a strong contribution compared to traditional techniques (spectroscopy, microscopy, etc.)[170]. In particular, MPT technique can provide quantitative (diffusivity and velocity) and qualitative (transport mode and directionality) information of internalized NPs, by evaluating the time-resolved trajectories of tens of NPs. Therefore, in order to study the effect of NP surface functionalization with gH625 on NP internalization mechanism, we followed and analyzed their intracellular motion. Figure 21 shows a snapshot of the detected trajectories generated by MPT routines. By shape, trajectories can already be split in two different types: i) Brownian-like trajectories, suggesting NPs random movement between cytosolic structures, and ii) pearls-on-a-string trajectories, derived by a combination of random and linear walk, indicative of motor protein facilitated transport, mediated by endocytic vesicles and motor proteins[171]. Evaluating the time dependence of mean square displacement (MSD) of each tracked NP we classified the particles transport mechanisms into diffusive and super-diffusive motion. In particular, to perform NPs diffusive mode classification we evaluated the exponent of each fitting MSD curve by the equation described in the Methods section.
Particle trajectories revealed a substantial heterogeneity in particle intracellular dynamics, both for blank NPs and gH625-NPs. However, for blank NPs, most

trajectories resulted in a combination of random and linear walk with a pearls-on-a-string trajectory, indicative of motor protein facilitated transport, mediated by endocytic vesicles (Figure 21). Whereas, only a lower percentage of blank NPs appeared to follow a purely diffusive behavior (random walk), suggesting no particular interaction between NPs and cytosolic structures (Figure 21).
Conversely, in presence of peptide functionalization, we observed that most trajectories showed a random walk behavior while a lower percentage resulted in a pearls-on-a- string trajectory. In particular, this behavior is more evident at lower percentages of functionalization with an optimum at 35% peptide functionalization degree.
These data suggest that the effect of the peptide could depend on its concentration/density on the NP surface. In fact, we theoretically estimated the surface density of peptide of about 3, 4, and 6 peptides/nm^2 for 25%, 35% and 50% functionalized NPs, respectively. We hypothesized that a lower peptide surface density (3 and 4 peptides/nm^2) could promote the correct peptide orientation and interaction with membrane lipids. Conversely, a higher peptide surface density (6 peptides/nm^2) hinders the correct orientation of peptide aminoacidic residues and their interaction with cell membrane. Indeed, recently, we structurally characterized gH625 peptide in a membrane-mimicking DPC micellar environment to gain insight into how gH fuses with the cell membrane [172]. We reported a model of gH625 peptide structure and orientation indicating that both electrostatic and hydrophobic interactions work in concert to mediate membrane penetration. In particular, the function of the aromatic residues is to cause the peptide insertion into the membrane interface while the basic residues stabilize this interaction by linking the negatively charged headgroups as shown in other systems using both NMR[173,174] and EPR[175]. Since we observed that the 35% functionalized NPs showed a good stability in aqueous suspension and the ability to penetrate cells using a random walk behavior, we performed all the other experiments at this percentage of functionalization.

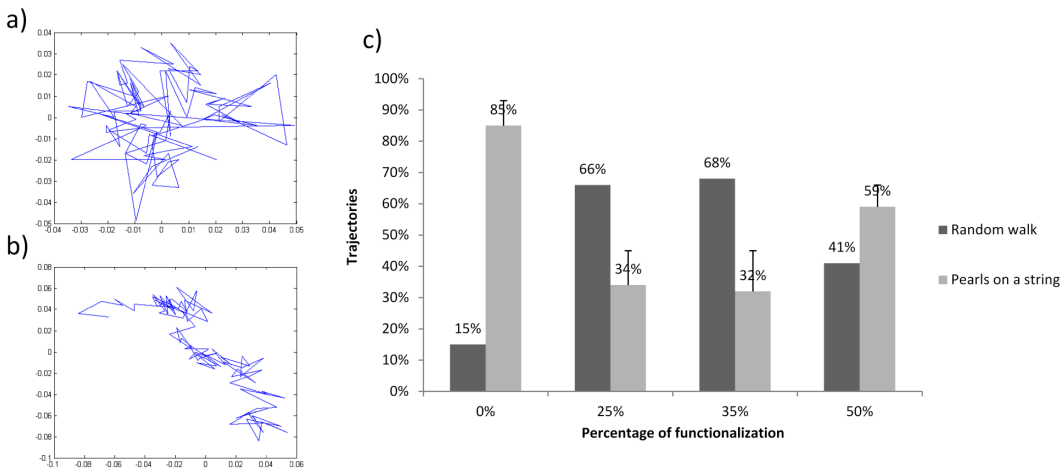

Figure21. MPT analysis of blank and gH625-NPs. Examples of "random walk" (a) and "pearls on a string" (b) trajectories. c) Percentage of "random walk" and "pearls on a string" trajectories as a function of functionalization degree.

3.5.5 gH625-Nanoparticles Uptake Kinetics

To study the effect of surface functionalization with gH625 on NPs internalization, we

performed NP uptake experiments. Figure 22A shows that after 10 minutes of incubation, both functionalized and blank NPs were internalized by bEnd3 cells and the number of internalized nanoparticles increases as a function of incubation time. However, the amount of internalized gH625-NPs is higher than blank NPs and this effect is more evident at early time of NP uptake kinetic. While after longer incubation time the amount of internalized NPs is quite similar, probably due to the saturation of the uptake mechanism mediated by the gH625 peptide.
bEnd3 cells are able to form a confluent monolayer that mimics permeability properties of primary culture models of early passages [176] [177]. We tested the ability of gH625 peptide to enhance NPs crossing of a bEnd3 confluent monolayer. Data reported in Figure 3B show that gH625-NPs cross more efficiently the endothelial layer than blank NPs. More precisely, the permeability (P) of the monolayer was $(0.43 \pm 0.02) \times 10^{-6}$ cm/s for gH625-NPs, almost two fold higher than P value reported for blank-NPs ($(0.24 \pm 0.02) \times 10^{-6}$ cm/s). These data are in agreement with cell uptake kinetic results. In fact, by focusing at early incubation time, also the uptake rate of peptide-conjugated NPs was approximately double compared to blank NPs (see the insert in Figure 22A). Moreover, no changes in BSA-TRITC permeability were observed after exposure to both blank and gH625-NPs, indicating that these NPs did not perturb the integrity of the cell monolayer in the experimental conditions used for the assay (data not shown).

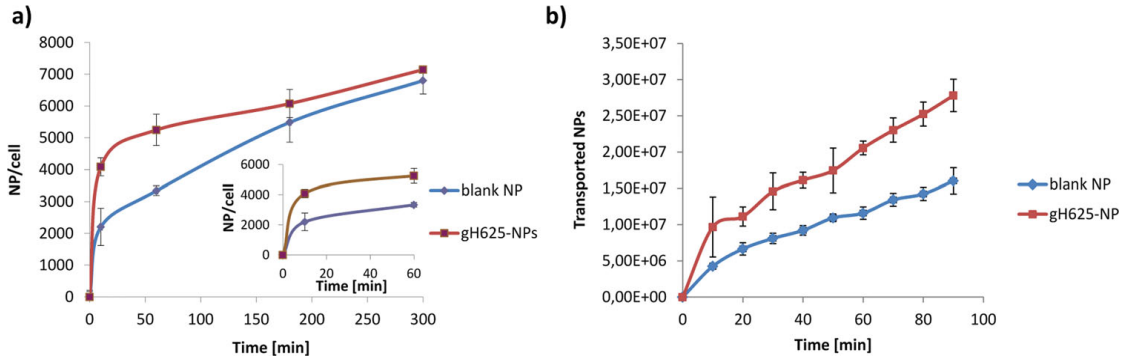

Figure 22. Uptake kinetics of blank and 35% functionalized gH625-NPs in bEnd3 cells (a). Effect of peptide functionalization in NP crossing of a confluent bEnd3 cell monolayer (b).

3.5.6 gH625-Nanoparticles Uptake Mechanisms

Nanoparticles usually enter the cells using a cell-mediated mechanism, called endocytosis. After endocytosis, endosomes can fuse with lysosomes or can deliver their cargo across the cell by transcytosis processes. Several works reported that caveolae are involved in the endocytosis and transcytosis processes in brain endothelial cells[178]. Thus, in order to study if the nanoparticle functionalization with gH625 could affect the mechanisms of NP internalization, we performed confocal microscope analyses to investigate the colocalization of NPs with lysosomes and caveolae in absence of peptide and with 35% of peptide functionalization. Figure 23 shows that both blank and gH625-NPs partially colocalized with lysosomes. However, the percentage of colocalization was about 4.68% for blank and 62% for gH625-NPs.

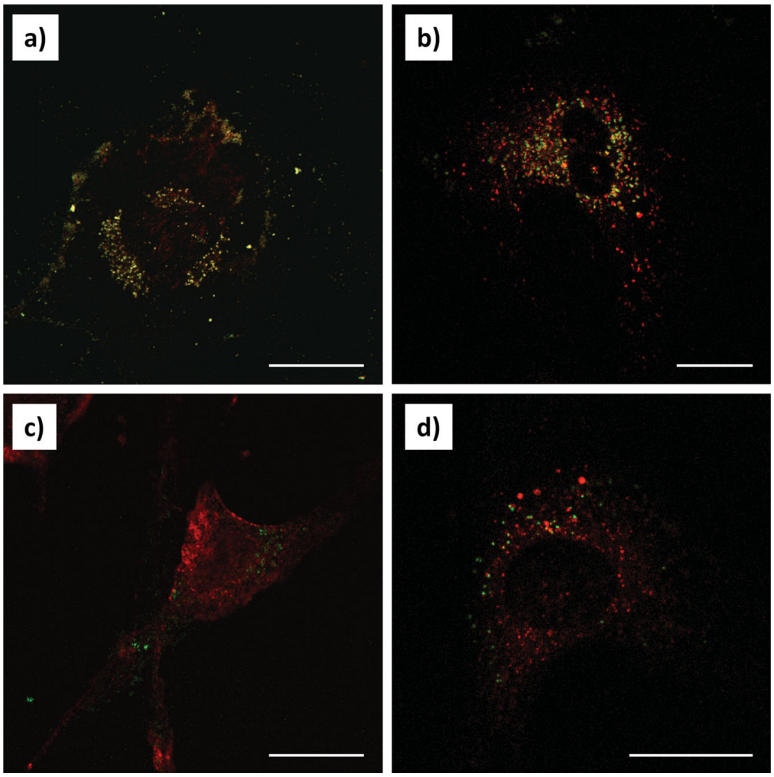

Figure 23. Colocalization of non-functionalized (a, b) and gH625-functionalized (c, d) NPs with caveolae (a, c) and lysosomes (b, d) after 24h incubation in bEnd3 cells. Green: NPs; red: caveolin1 and lysotracker. Magnification bar: 20 μm..

On the other hand, concerning caveolin1, a molecular marker for caveolar structures, no colocalization of gH625-NPs was observed, while blank NPs showed 0.74% of colocalization. These data indicate that the peptide could change the mechanism of nanoparticle uptake by inducing an alternative penetration pathway. To further investigate this issue, we treated cells with cytochalasin D that inhibits macropinocytosis by disrupting microfilaments. Results demonstrate that the uptake of blank NPs was drastically reduced after cytochalasin D treatment (Figure 24A–F). On the other hand, gH625-NPs uptake was almost not affected by microfilament depolymerization (Figure 24G–L). Indeed, confocal microscope z-sectioning analysis demonstrate that the most part of gH625-NPs were inside the cells and only a small amount (less than 30%) was just adsorbed on cell membrane (Figure 24M). Moreover, quantitative analysis of NP uptake showed a decrease of about 85% and 15% for blank-NP and gH625-NP uptake, respectively, after cytochalasin D treatment (Figure 24N). Taken all together these data indicate that blank NPs might enter the cells mainly by macropinocytosis. Conversely, gH625-NPs could use a different mechanism to cross cell membrane.

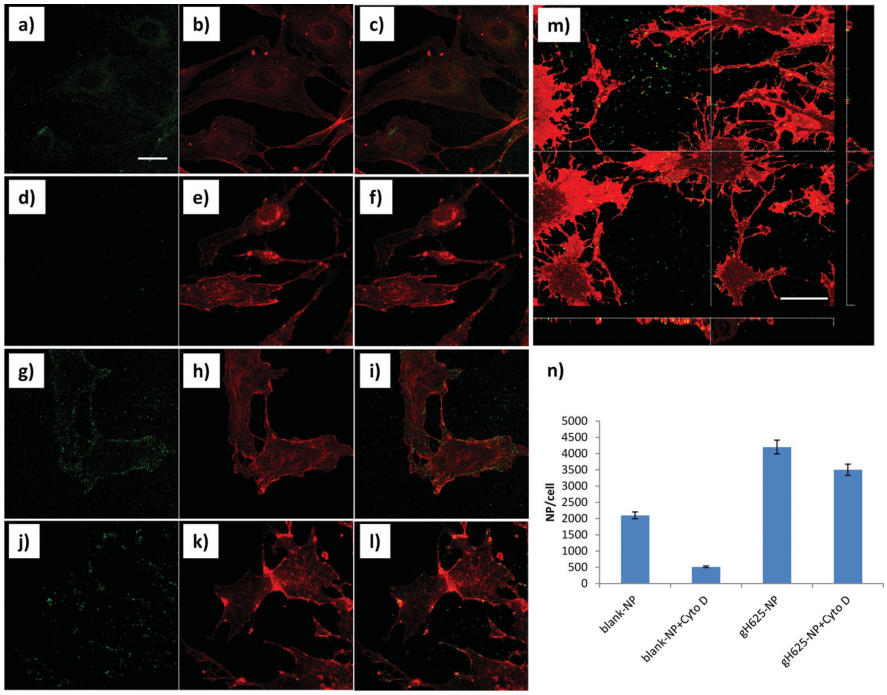

Figure 24. Cytochalasin D treated bEnd3 cells incubated with blank NPs (d–f) and gH625-NPs (j–m) for 10 min at 37°C. Non-treated control cells incubated with blank NPs (a–c) and gH625-NPs (g–i) for 10 min at 37°C. Nanoparticles (a, d, g, j); phalloidin stained microfilaments (b, e, h, k); merge (c, f, i, l). Green fluorescent nanoparticles and red fluorescent WGA stained cell membrane confocal z-sectioning (m). Section thickness: 0.2 µm. . Z-stack size: 10 µm. Magnification bar: 20 µm..

Previous works demonstrated that gH625 peptide shows a particular tropism for lipidic membranes, which is strongly dependent on its amphipathic nature [179 99 180]. Thus, we hypothesized that the presence of the peptide on the NP surface could enhance its interaction with the cell membrane and promote NPs passage through cell membranes. To verify this hypothesis, scanning electron microscopy (SEM) analyses were performed. SEM micrographs showed that, after 5 min of incubation, a high number of gH625-NPs was visible on the cell surface (Figure 25A, B). Conversely, very few blank NPs were present on the cell surface and some of these formed small aggregates (Figure 25C, D). SEM results suggest a different interaction of gH625-NPs with cell membrane compared to blank-NPs. Moreover, accordingly to cell uptake kinetics (Figure 22), these observations indicate a better and more rapid adsorption of gH625-NPs on cell membrane, compared to blank-NPs after 10 min incubation, probably due to the membrane tropism of the peptide and, thus, an enhancement of gH625-NP internalization.

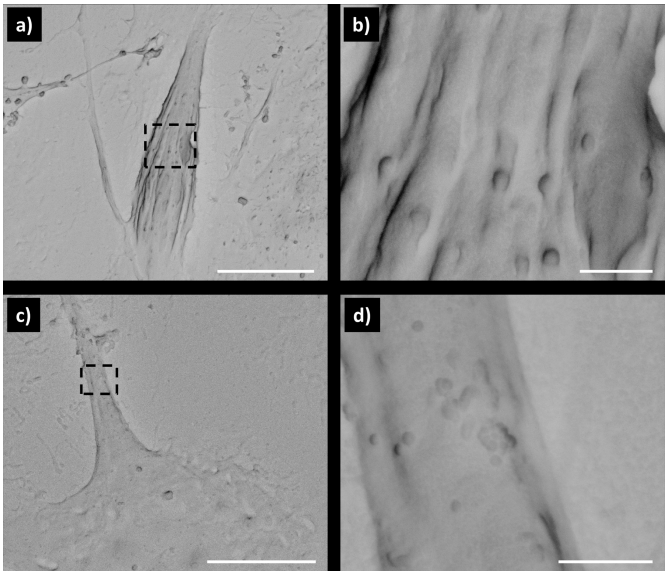

Figure 25. SEM micrographs of bEnd3 cells incubated with gH625-NPs (a, b) and blank NPs (c, d) for 5 min at 37 °C. Dashed squares in panels (a, c) indicate the zoomed areas shown in panels (b, d). Magnification bar: 10 μm (a, c) and 1 μm (b, d).

In order to understand if the different behavior of gH625-NPs implied a different intracellular fate of NPs, we performed transmission electron microscopy (TEM) analyses. Figure 26 shows TEM micrographs of gH625-NPs and blank NPs after 24 h incubation with bEnd3 cells. Inside the cells, gH625-NPs were organized in very small aggregates of 3-4 particles within the cytoplasm, mainly localized in vesicular structures, probably early endosomes (Figure 26A) and multi-vesicular bodies (MVBs) (Figure 26C). On the other hand, for blank-NPs, many and larger aggregates associated to vesicular structures within the cytoplasm were observed (Figure 26B–D). Furthermore, no gH625- or blank-NPs were localized in the nucleus.

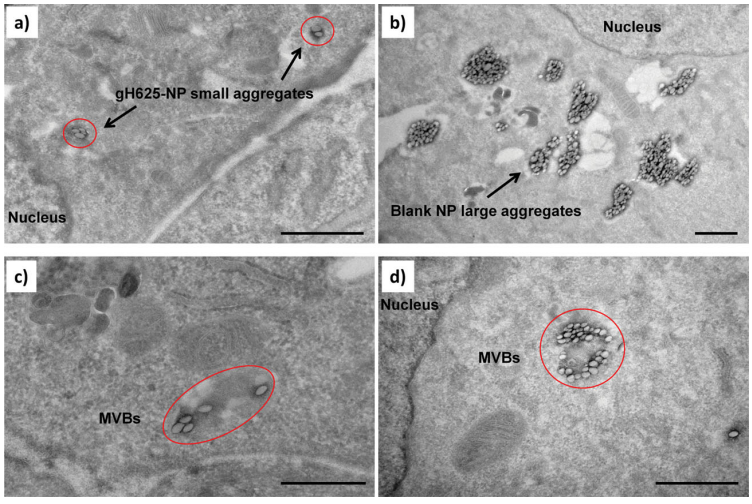

Figure 26. TEM micrographs of bEnd3 cells incubated 24 h with gH625-NPs (a, c) and blank NPs (b, d) at 37 °C. Magnification bar: 1 μm..

For obtaining deeper details on the intracellular distribution of gH625-NPs, we followed the formation and the growth of gH625- or blank-NP aggregates with time by a confocal microscope image analysis. Figure 27 shows gH625- and blank-NP aggregates within bEnd3 cell cytoplasm after 10 min and 24 h incubation. At early

times, gH625-NPs formed a huge number of small aggregates (Figure 27A, E). Moreover, increasing the incubation time, the average size of the aggregates remained almost unchanged (Figure 27B, E). Conversely, for blank NPs, at early times, the average size of aggregates increased with time indicating that these NPs tend to accumulate in the cell (Figure 27C, D, F).
Taken altogether, these observations demonstrate a different behavior between gH625- and blank-NPs. In particular, NP conjugation with gH625 peptide changes NP destination by reducing their accumulation and promoting NP escape/exit from the cell. However, further investigations are needed to better understand which intracellular compartments gH625-NPs are localized in and what the intracellular pathways are followed by these functionalized NPs that dictate their fate.

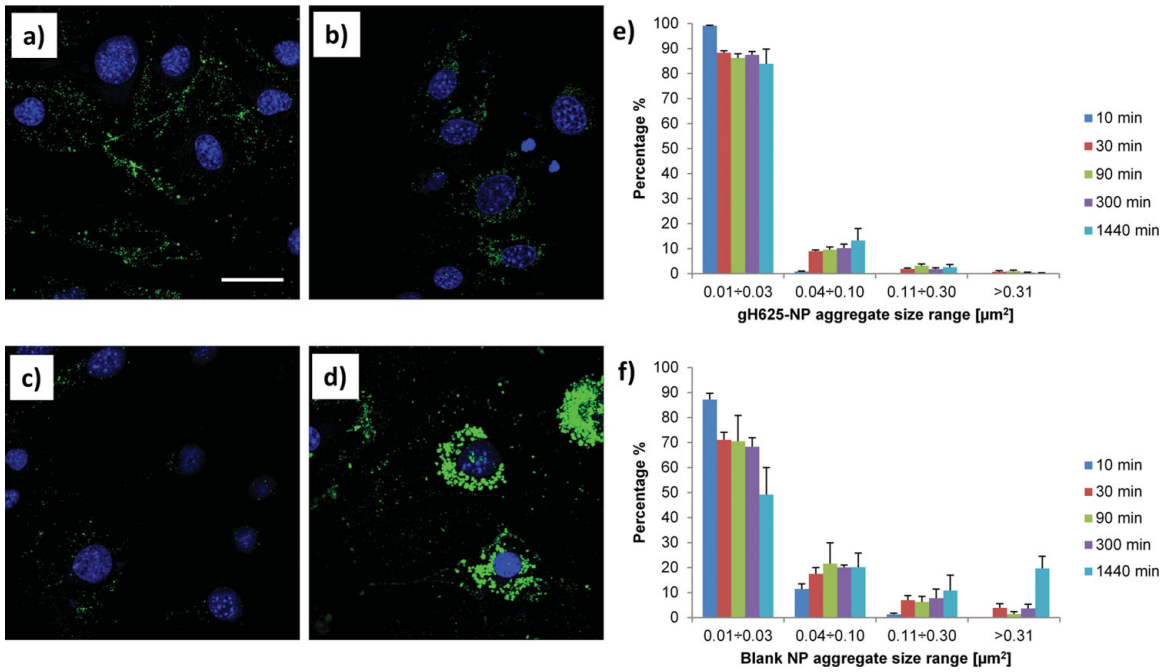

Figure 27. Confocal microscope images of bEnd3 cells incubated with gH625-NPs for 10 min (a) and 1440 min (b) and blank-NPs for 10 min (c) and 1440 min (d). Blue: nuclei; Green: NPs; Magnification bar: 20 µm; . gH625- (e) and blank-NP (f) aggregate analysis. Charts show the size distribution of NP aggregates at different observation time (10, 30, 90, 300, and 1440 min). NP aggregate sizes were split in four intervals: 0.01÷ 0.03 ìm2; 0.04÷ 0.10 µm^2; 0.11÷ 0.30 µm^2; >0.31 µm^2.

4 CONCLUSION

The main objective of this study was to identify innovative peptide based systems with a higher impact in the pharmacodynamics and pharmacokinetic fields compared to the conventional systems used in drug delivery.
In particular, this thesis describes a new molecule, classified as a new CPPs, that could be used for effective intracellular delivery. The ability of gH625, a peptide derived from glycoprotein gH of Herpes simplex virus type 1, to be internalized was analysed both in presence and absence of cargoes for a better understanding of the mechanism of uptake of this membranotropic domain and to verify the possibility to use it for delivering bioactive macromolecules into cells.
Cell penetrating peptides are considerably important for the purpose of delivering cargoes to the inside of cells and hundreds of sequences fall within CPP classification. The process by which membrane translocation is achieved has received great attention with the aim of gaining higher efficiency of penetration. Most CPP are able to cross the membrane bilayer and to deliver a cargo across the membrane although their mechanism of uptake involves essentially endocytic pathways. The discovery of novel systems which use non-canonical mechanisms for internalization may lead to greater efficiency both from a therapeutical and a diagnostic point of view. In fact, most drugs are actually internalized by endocytosis mechanisms with consequently a set of limitations in biodistribution, bioactivity, specificity and toxicity; on the contrary, novel delivery tools able to cross biological membranes using completely or at least partially a different mechanism of internalization may open up new avenues for the administration of drugs with a lower impact on the health of patients.
This thesis focuses on recent data obtained on the viral membranotropic peptide gH625 and its use as well as its advantages compared to other CPPs as a drug delivery tool.
This thesis, firstly, describes the ability of gH625 alone to cross efficiently the plasma membranes and then few examples of applications of gH625 to the delivery of several kinds of cargos into the cells.
Labelling the peptide with the NBD group allowed the comparison of cellular uptake and phospholipid binding and analysis of the physico-chemical properties required for translocation. To measure cellular uptake of NBD-labelled peptide we have used the dithionite method, which allows the estimation of the peptide fraction localized inside the cell. We determined by flow cytometry that after 1 h of incubation with HeLa cells at 37°C and 4°C, most of gH625-NBD was localized intracellularly; our results show that the peptide internalization in HeLa cells can occur at 37°C and to a slightly lesser extent at 4°C, supporting the view that the internalization mechanism does not involve entirely endocytosis.
The kinetic of internalization of gH625-NBD is rapid and reaches a plateau after 1 h. We confirmed by confocal microscopy that indeed the NBD-peptide is inside the cell and its penetration is not induced by cell fixation protocols as previously found for the Tat peptide[181].
The amount of cell-associated peptide represents the sum of internalized peptide and of peptide remaining on the cell surface after cell wash. Furthermore, the membrane interaction experiments showed that the peptide stably inserts into the PC/Chol membranes but it is unable to form pores; and it is unable to fuse the inner

monolayer as well as to induce leakage of vesicles; further supporting the view that the mechanism of lipid/peptide association plays a key role in the translocation activity. gH625 cellular uptake is associated with its ability to interact with membrane lipids and to form a transient helical structure that temporarily affects membrane organization, thereby facilitating insertion into the membrane and translocation.
gH625 showed very low toxicity in *in vitro* studies when used at concentrations up to 400 μM, therefore it seems suitable for being used as a delivery system.
The first application of our peptide for the delivery of a cargo was the uptake of Quantum Dots (QDs). Quantum dots are a new class of fluorescent probes under intense research and development for broad applications in molecular, cellular and *in vivo* imaging. QDs have unique functional and structural properties, such as size and composition tunable fluorescence emission, large absorption cross sections and exceptional brightness and photostability compared with organic dyes and fluorescent proteins. Although considerable success has been achieved in using QDs for labelling fixed cells and for imaging cell membrane proteins, only limited progress has been made for molecular imaging inside living cells. A major problem is the lack of efficient methods for delivering single QDs into the cytoplasm of living cells.
The results obtained from the gH625 functionalization with QDs clearly indicate that the nanosystem is efficiently internalized, more effectively than Tat-QDs, and its internalization only partially involves the endocytic pathway.
In particular, when conjugated with QDs, gH625 translocates through cellular plasma membranes with a mechanism only relatively dependent on the endocytic route of entry. It has been previously reported that Tat peptide conjugated with small molecules enters cytoplasm and eventually the cell nuclei, while Tat-QDs remain trapped in vesicles. This difference in the intracellular fate of Tat peptide-conjugated molecules and Tat-QDs is likely caused by differences in the sizes of the cargos. QDs are much larger than standard molecules and are thus more difficult to escape from vesicles. On the contrary, gH625-QDs are present in the cytoplasm in a more punctuated form compared to Tat-QDs. Therefore, we can hypothesise a different mechanism of entry between Tat-QDs and gH625-QDs, and this is of particular interest since peptides with different biophysical characteristics are able to condition the entry pathway of the same macromolecular cargo. These results make gH625-QDs an interesting compound for recognising specific targets in the cytoplasm resulting thus potentially applicable to the diagnosis and therapy of human diseases.
The second application was the study of the uptake of liposomes loaded with anticancer drugs such as doxorubicin.
Liposomes, composed of a phospholipid bilayer which entirely surrounds an internal aqueous core used for drug encapsulation, have been shown to be optimal for the delivery of chemotherapeutic agents to tumor cells. Being larger than micelles they have the ability to deliver greater amounts of the chemotherapeutic agent to the tumor site while minimizing the risks associated with premature leakage. In addition, liposomes also have the ability to accommodate both hydrophilic as well as hydrophobic drugs either in the internal aqueous core or in the lipid bilayer. When compared with conventional drugs, liposomal treatment has been shown to dramatically reduce some of the traditional side effects associated with chemotherapy, such as nausea and vomiting [182].
This nanosystem is characterized by the conjugation of the gH625 peptide on the surface of liposomes. Being the peptide hydrophobic, click chemistry appeared to be very useful for the decoration of the external surface of DOPG based liposomes. According to this synthetic procedure, azide modified DOPG based liposomes react, under mild conditions, with Pra modified gH625 peptides giving stable and well

defined peptide modified liposomes. The click chemistry procedure described appears of general utility for liposome functionalization; in fact, azide modified liposomes could constitute a stable and ready-to-use suspension of reactive liposomes that could be functionalized with different Pra modified peptides. In this case, an increase of liposome diameter of approximately 30% after peptide introduction is observed by DLS measurement. Moreover, the peptide positioning relative to the liposome surface has been investigated by EPR spectroscopy; the data obtained indicated that the peptide does not insert in the bilayer hydrophobic core, but rather remains exposed to the aqueous environment and, thus, able to perform its biological function.

In order for a chemotherapeutic agent to be effective, it has to be active against cancer cells while having minimal toxic effects on healthy cells, tissues and organs. Thus, once carriers loaded with chemotherapeutic agents are systemically introduced, their uptake by the reticuloendothelial system (RES) must be minimized, allowing prolonged circulation of the carriers in the blood. The longer the drug circulates in the blood, the more likely it encounters the tumor as a result of the enhanced permeability of leaky tumor blood vessels. The enhanced permeability and retention effect is considered the primary mechanism of preferential accumulation of long-circulating nanoparticulates in solid tumors. Polymeric drug carrier systems that use various approaches to address these challenges have been intensively developed; while adding a targeting moiety, such as a peptide or an antibody, helps the cellular uptake and reduces systemic clearance of anticancer drug. The exact mechanism of doxorubicin antitumor activity still remains unclear; it is known that it intercalates into DNA, which results in the blocking of topoisomerase II activity, preventing DNA replication and cell division. For encapsulated Dox, the reduced toxicity is associated to the presence of the carrier that hinders the intercalation of Dox into DNA. Confocal microscopy revealed differences between the uptake mechanism of free Dox and encapsulated Dox. The nuclear accumulation of free Dox can be attributed to diffusion. In contrast, encapsulated Dox remain mostly in the cytoplasm with negligible nuclear accumulation.

The conducted experiments provided proof of principle for efficient gH625 peptide mediated delivery of DOPG based liposomes into cells. gH625 attached to the liposome surface needs to be non-shielded and accessible for cell membrane experiments and it was showed that coupling the peptide on the pre-assembled liposomes allows the obtainment of liposomes decorated on their surface with the peptide.

The third application was the preparation of a peptidodendrimeric scaffold, that has the potential to be used as a cellular delivery platform. The dendrimer cellular uptake is significantly enhanced thanks to the attachment of the gH625 peptide at the termini. The peptide does not rely on heavily positively charged residues (Arg, Lys) for translocation. Previously Kang *et al.*[121] reported the failure of Tat to enhance the intracellular delivery of PAMAM dendrimers, which they attributed to the highly positive charges of both the dendrimer and the peptide[121]. Our dendrimer is made in a facile and scalable synthesis, and can be functionalized efficiently. We showed that the peptidodendrimer is able to fully fuse lipidic vesicles, even more significantly than the peptide alone; moreover, it is able to do so without inducing leakage of vesicles.

These data further support the view that the mechanism of lipid–peptide association plays a key role in the translocation activity. The gH625 cellular uptake is associated with its ability to interact with membrane lipids and to form a transient helical structure that temporarily affects membrane organization, thereby facilitating insertion into the

membrane and translocation. The cellular uptake of the peptidodendrimer was measured by flow cytometry and fluorescence microscopy. After 1 h of incubation with HeLa cells at 37 °C and 4 °C, most of the gH625 functionalized dendrimer was localized intracellularly. The internalization in HeLa cells can occur at 37°C, and to a lesser extent at 4°C, supporting the view that the internalization mechanism does not involve entirely endocytosis. The kinetics of internalization is rapid and reaches a plateau after 1 h. It was confirmed, by fluorescence microscopy, that indeed the peptidodendrimer is inside the cells. Our studies have shown that dendrimer functionalized with the gH625 peptide sequence is not only an effective vehicle for intracellular delivery but it can do so via a passive translocation mechanism. This allows the cargo to be released directly into the intracellular milieu as opposed to being entrapped in endosomes, from which the cargo might not be able to escape before lysosomal degradation.

The last application of our peptide was the delivery of polystyrene nanoparticles and we further investigated its ability to translocate through the BBB in an in vitro model. The functionalized nanoparticles were thoroughly characterized using a variety of complementary techniques to gain a better understanding of their properties and showed that gH625-NPs only slightly modified the particle sizes with a z-potential indicative of colloidal stability at pH 7. gH625-NPs translocated efficiently across cell membranes and cell internalization does not seem to exclusively involve classical endocytosis mechanisms. In fact, conjugation with gH625 facilitated the delivery of nanoparticles across the BBB, leading to significant higher cell uptake and crossing. To the best of our knowledge, gH625 represents the first cell translocation motif reported for the crossing of the BBB and further studies could allow the application to the design of a drug delivery system specific for the brain. Therefore, it might be regarded as a promising strategy to design delivery systems for administration of therapeutical compounds to the brain, deserving further investigations to more precisely characterize the mechanism by which gH625 crosses the BBB and to address the cell specificity issue by linking to the nanosystem also molecules specifically recognized by the brain endothelium.

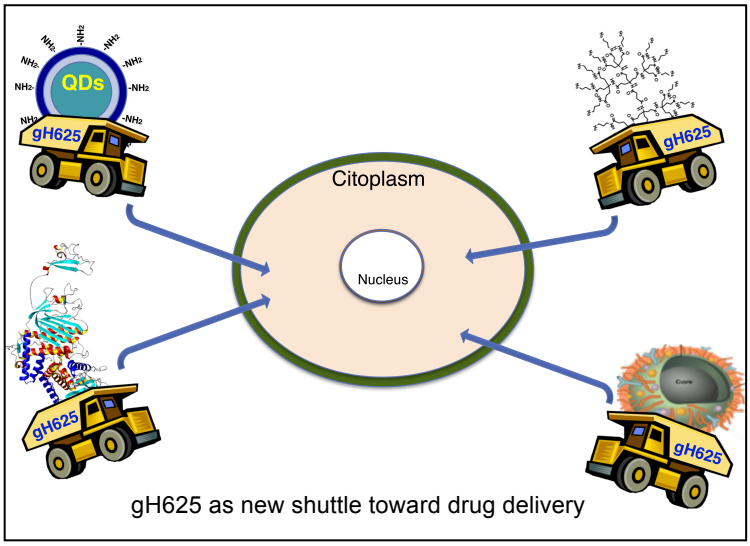

gH625 as new shuttle toward drug delivery

In conclusion, the data described in this thesis suggest that membranotropic sequences represent a new valuable tool for intracellular delivery for applications in theranostics. The opportunity to use a delivery tool with a different internalization mechanism may represent the possibility of reducing the doses and thus increase the results of therapies, contemporary reducing toxicity.

Although the internalization mechanism og gH625 functionalized nanosystems still remains to be fully established, our results seem to support the hypothesis that the peptide allows a better penetration of QDs, liposomes, Dendrimers and Nanoparticles. Thus, the approaches described may have important application for

drug and DNA delivery into the cell cytoplasm in different protocols for drug administration or *ex vivo* treatments.

REFERENCES

1. Geldenhuys, W,Mbimba, T,Bui, T,Harrison, K,Sutariya, V. Brain-targeted delivery of paclitaxel using glutathione-coated nanoparticles for brain cancers. *J Drug Target* 2011**;** *19 (9):* 837.
2. Taratula, O,Garbuzenko, OB,Kirkpatrick, P,Pandya, I,Savla, R,Pozharov, VP,He, H,Minko, T. Surface-engineered targeted PPI dendrimer for efficient intracellular and intratumoral siRNA delivery. *J Control Release* 2009**;** *140 (3):* 284.
3. Brambilla, D,Le Droumaguet, B,Nicolas, J,Hashemi, SH,Wu, LP,Moghimi, SM,Couvreur, P,Andrieux, K. Nanotechnologies for Alzheimer's disease: diagnosis, therapy, and safety issues. *Nanomedicine* 2011**;** *7 (5):* 521.
4. Leserman, LD,Barbet, J,Kourilsky, F,Weinstein, JN. Targeting to cells of fluorescent liposomes covalently coupled with monoclonal antibody or protein A. *Nature* 1980**;** *288 (5791):* 602.
5. Heath, TD,Fraley, RT,Papahdjopoulos, D. Antibody targeting of liposomes: cell specificity obtained by conjugation of F(ab')2 to vesicle surface. *Science* 1980**;** *210 (4469):* 539.
6. Allen, TM,Chonn, A. Large unilamellar liposomes with low uptake into the reticuloendothelial system. *FEBS Lett* 1987**;** *223 (1):* 42.
7. Klibanov, AL,Maruyama, K,Torchilin, VP,Huang, L. Amphipathic polyethyleneglycols effectively prolong the circulation time of liposomes. *FEBS Lett* 1990**;** *268 (1):* 235.
8. Gref, R,Minamitake, Y,Peracchia, MT,Trubetskoy, V,Torchilin, V,Langer, R. Biodegradable long-circulating polymeric nanospheres. *Science* 1994**;** *263 (5153):* 1600.
9. Wagner, V,Dullaart, A,Bock, AK,Zweck, A. The emerging nanomedicine landscape. *Nat Biotechnol* 2006**;** *24 (10):* 1211.
10. Zhang, L,Gu, FX,Chan, JM,Wang, AZ,Langer, RS,Farokhzad, OC. Nanoparticles in medicine: therapeutic applications and developments. *Clin Pharmacol Ther* 2008**;** *83 (5):* 761.
11. Davis, ME,Chen, ZG,Shin, DM. Nanoparticle therapeutics: an emerging treatment modality for cancer. *Nat Rev Drug Discov* 2008**;** *7 (9):* 771.
12. Riehemann, K,Schneider, SW,Luger, TA,Godin, B,Ferrari, M,Fuchs, H. Nanomedicine--challenge and perspectives. *Angew Chem Int Ed Engl* 2009**;** *48 (5):* 872.
13. Ferrari, M. Cancer nanotechnology: opportunities and challenges. *Nat Rev Cancer* 2005**;** *5 (3):* 161.
14. Orlic, D,Girard, LJ,Jordan, CT,Anderson, SM,Cline, AP,Bodine, DM. The level of mRNA encoding the amphotropic retrovirus receptor in mouse and human hematopoietic stem cells is low and correlates with the efficiency of retrovirus transduction. *Proc Natl Acad Sci U S A* 1996**;** *93 (20):* 11097.
15. Hanenberg, H,Xiao, XL,Dilloo, D,Hashino, K,Kato, I,Williams, DA. Colocalization of retrovirus and target cells on specific fibronectin fragments increases genetic transduction of mammalian cells. *Nat Med* 1996**;** *2 (8):* 876.
16. Hall, FL,Gordon, EM,Wu, L,Zhu, NL,Skotzko, MJ,Starnes, VA,Anderson, WF. Targeting retroviral vectors to vascular lesions by genetic engineering of the MoMLV gp70 envelope protein. *Hum Gene Ther* 1997**;** *8 (18):* 2183.
17. Breakefield, XO,DeLuca, NA. Herpes simplex virus for gene delivery to neurons. *New Biol* 1991**;** *3 (3):* 203.
18. Fink, DJ,Glorioso, JC. Engineering herpes simplex virus vectors for gene transfer to neurons. *Nat Med* 1997**;** *3 (3):* 357.
19. Jacoby, DR,Fraefel, C,Breakefield, XO. Hybrid vectors: a new generation of virus-based vectors designed to control the cellular fate of delivered genes. *Gene Ther* 1997**;** *4 (12):* 1281.
20. Mitragotri, S,Blankschtein, D,Langer, R. Ultrasound-mediated transdermal protein delivery. *Science* 1995**;** *269 (5225):* 850.
21. Paliwal, S,Menon, GK,Mitragotri, S. Low-frequency sonophoresis: ultrastructural basis for stratum corneum permeability assessed using quantum dots. *J Invest Dermatol* 2006**;** *126 (5):* 1095.
22. Vykhodtseva, NI,Gavrilov, LR,Mering, TA,Iamshchikova, NG. [Use of focused ultrasound for local destruction of different brain structures]. *Zh Nevropatol Psikhiatr Im S S Korsakova* 1976**;** *76 (12):* 1810.
23. Hynynen, K,McDannold, N,Vykhodtseva, N,Jolesz, FA. Noninvasive MR imaging-guided focal opening of the blood-brain barrier in rabbits. *Radiology* 2001**;** *220 (3):* 640.
24. Mesiwala, AH,Farrell, L,Wenzel, HJ,Silbergeld, DL,Crum, LA,Winn, HR,Mourad, PD. High-intensity focused ultrasound selectively disrupts the blood-brain barrier in vivo. *Ultrasound Med Biol* 2002**;** *28 (3):* 389.
25. Kalia, YN,Naik, A,Garrison, J,Guy, RH. Iontophoretic drug delivery. *Adv Drug Deliv Rev* 2004**;** *56 (5):* 619.

26. Spierings, EL,Brevard, JA,Katz, NP. Two-minute skin anesthesia through ultrasound pretreatment and iontophoretic delivery of a topical anesthetic: a feasibility study. *Pain Med* 2008**;** *9 (1):* 55.
27. Lark, MR,Gangarosa, LP, Sr. Iontophoresis: an effective modality for the treatment of inflammatory disorders of the temporomandibular joint and myofascial pain. *Cranio* 1990**;** *8 (2):* 108.
28. Langkjaer, L,Brange, J,Grodsky, GM,Guy, RH. Iontophoresis of monomeric insulin analogues in vitro: effects of insulin charge and skin pretreatment. *J Control Release* 1998**;** *51 (1):* 47.
29. Raiman, J,Koljonen, M,Huikko, K,Kostiainen, R,Hirvonen, J. Delivery and stability of LHRH and Nafarelin in human skin: the effect of constant/pulsed iontophoresis. *Eur J Pharm Sci* 2004**;** *21 (2-3):* 371.
30. Coury, AJ,Fogt, EJ,Norenberg, MS,Untereker, DF. Development of a screening system for cystic fibrosis. *Clin Chem* 1983**;** *29 (9):* 1593.
31. Baxter, J,Mitragotri, S. Needle-free liquid jet injections: mechanisms and applications. *Expert Rev Med Devices* 2006**;** *3 (5):* 565.
32. Gupta, J,Felner, EI,Prausnitz, MR. Rapid pharmacokinetics of intradermal insulin administered using microneedles in type 1 diabetes subjects. *Diabetes Technol Ther* 2011**;** *13 (4):* 451.
33. Bramson, J,Dayball, K,Evelegh, C,Wan, YH,Page, D,Smith, A. Enabling topical immunization via microporation: a novel method for pain-free and needle-free delivery of adenovirus-based vaccines. *Gene Ther* 2003**;** *10 (3):* 251.
34. Deshayes, S,Morris, MC,Divita, G,Heitz, F. Cell-penetrating peptides: tools for intracellular delivery of therapeutics. *Cell Mol Life Sci* 2005**;** *62 (16):* 1839.
35. Heitz, F,Morris, MC,Divita, G. Twenty years of cell-penetrating peptides: from molecular mechanisms to therapeutics. *Br J Pharmacol* 2009**;** *157 (2):* 195.
36. Deshayes, S,Morris, M,Heitz, F,Divita, G. Delivery of proteins and nucleic acids using a non-covalent peptide-based strategy. *Adv Drug Deliv Rev* 2008**;** *60 (4-5):* 537.
37. Eguchi, A,Dowdy, SF. siRNA delivery using peptide transduction domains. *Trends Pharmacol Sci* 2009**;** *30 (7):* 341.
38. Frankel, AD,Pabo, CO. Cellular uptake of the tat protein from human immunodeficiency virus. *Cell* 1988**;** *55 (6):* 1189.
39. Joliot, A,Pernelle, C,Deagostini-Bazin, H,Prochiantz, A. Antennapedia homeobox peptide regulates neural morphogenesis. *Proc Natl Acad Sci U S A* 1991**;** *88 (5):* 1864.
40. Derossi, D,Joliot, AH,Chassaing, G,Prochiantz, A. The third helix of the Antennapedia homeodomain translocates through biological membranes. *J Biol Chem* 1994**;** *269 (14):* 10444.
41. Vives, E,Brodin, P,Lebleu, B. A truncated HIV-1 Tat protein basic domain rapidly translocates through the plasma membrane and accumulates in the cell nucleus. *J Biol Chem* 1997**;** *272 (25):* 16010.
42. Schwarze, SR,Ho, A,Vocero-Akbani, A,Dowdy, SF. In vivo protein transduction: delivery of a biologically active protein into the mouse. *Science* 1999**;** *285 (5433):* 1569.
43. Pooga, M,Hallbrink, M,Zorko, M,Langel, U. Cell penetration by transportan. *FASEB J* 1998**;** *12 (1):* 67.
44. Gehring, WJ,Affolter, M,Burglin, T. Homeodomain proteins. *Annu Rev Biochem* 1994**;** *63:* 487.
45. Bellet-Amalric, E,Blaudez, D,Desbat, B,Graner, F,Gauthier, F,Renault, A. Interaction of the third helix of Antennapedia homeodomain and a phospholipid monolayer, studied by ellipsometry and PM-IRRAS at the air-water interface. *Biochim Biophys Acta* 2000**;** *1467 (1):* 131.
46. Magzoub, M,Kilk, K,Eriksson, LE,Langel, U,Graslund, A. Interaction and structure induction of cell-penetrating peptides in the presence of phospholipid vesicles. *Biochim Biophys Acta* 2001**;** *1512 (1):* 77.
47. Lindgren, M,Gallet, X,Soomets, U,Hallbrink, M,Brakenhielm, E,Pooga, M,Brasseur, R,Langel, U. Translocation properties of novel cell penetrating transportan and penetratin analogues. *Bioconjug Chem* 2000**;** *11 (5):* 619.
48. Barany-Wallje, E,Andersson, A,Graslund, A,Maler, L. NMR solution structure and position of transportan in neutral phospholipid bicelles. *FEBS Lett* 2004**;** *567 (2-3):* 265.
49. Steiner, V,Schar, M,Bornsen, KO,Mutter, M. Retention behaviour of a template-assembled synthetic protein and its amphiphilic building blocks on reversed-phase columns. *J Chromatogr* 1991**;** *586 (1):* 43.
50. Oehlke, J,Scheller, A,Wiesner, B,Krause, E,Beyermann, M,Klauschenz, E,Melzig, M,Bienert, M. Cellular uptake of an alpha-helical amphipathic model peptide with the potential to deliver polar compounds into the cell interior non-endocytically. *Biochim Biophys Acta* 1998**;** *1414 (1-2):* 127.

51. Futaki, S,Suzuki, T,Ohashi, W,Yagami, T,Tanaka, S,Ueda, K,Sugiura, Y. Arginine-rich peptides. An abundant source of membrane-permeable peptides having potential as carriers for intracellular protein delivery. *J Biol Chem* 2001**;** *276 (8):* 5836.
52. Loret, EP,Vives, E,Ho, PS,Rochat, H,Van Rietschoten, J,Johnson, WC, Jr. Activating region of HIV-1 Tat protein: vacuum UV circular dichroism and energy minimization. *Biochemistry* 1991**;** *30 (24):* 6013.
53. Morris, MC,Vidal, P,Chaloin, L,Heitz, F,Divita, G. A new peptide vector for efficient delivery of oligonucleotides into mammalian cells. *Nucleic Acids Res* 1997**;** *25 (14):* 2730.
54. Gallaher, WR. Detection of a fusion peptide sequence in the transmembrane protein of human immunodeficiency virus. *Cell* 1987**;** *50 (3):* 327.
55. Morris, MC,Depollier, J,Mery, J,Heitz, F,Divita, G. A peptide carrier for the delivery of biologically active proteins into mammalian cells. *Nat Biotechnol* 2001**;** *19 (12):* 1173.
56. Sciortino, MT,Suzuki, M,Taddeo, B,Roizman, B. RNAs extracted from herpes simplex virus 1 virions: apparent selectivity of viral but not cellular RNAs packaged in virions. *J Virol* 2001**;** *75 (17):* 8105.
57. Sciortino, MT,Taddeo, B,Poon, AP,Mastino, A,Roizman, B. Of the three tegument proteins that package mRNA in herpes simplex virions, one (VP22) transports the mRNA to uninfected cells for expression prior to viral infection. *Proc Natl Acad Sci U S A* 2002**;** *99 (12):* 8318.
58. Hildt, E,Urban, S,Hofschneider, PH. Characterization of essential domains for the functionality of the MHBst transcriptional activator and identification of a minimal MHBst activator. *Oncogene* 1995**;** *11 (10):* 2055.
59. Falanga, A,Vitiello, MT,Cantisani, M,Tarallo, R,Guarnieri, D,Mignogna, E,Netti, P,Pedone, C,Galdiero, M,Galdiero, S. A peptide derived from herpes simplex virus type 1 glycoprotein H: membrane translocation and applications to the delivery of quantum dots. *Nanomedicine* 2011**;** *7 (6):* 925.
60. Dietz, GP,Bahr, M. Delivery of bioactive molecules into the cell: the Trojan horse approach. *Mol Cell Neurosci* 2004**;** *27 (2):* 85.
61. Futaki, S. Arginine-rich peptides: potential for intracellular delivery of macromolecules and the mystery of the translocation mechanisms. *Int J Pharm* 2002**;** *245 (1-2):* 1.
62. Pooga, M,Soomets, U,Hallbrink, M,Valkna, A,Saar, K,Rezaei, K,Kahl, U,Hao, JX,Xu, XJ,Wiesenfeld, HZ,Hokfelt, T,Bartfai, T,Langel, U. Cell penetrating PNA constructs regulate galanin receptor levels and modify pain transmission in vivo. *Nat Biotechnol* 1998**;** *16 (9):* 857.
63. Richard, JP,Melikov, K,Vives, E,Ramos, C,Verbeure, B,Gait, MJ,Chernomordik, LV,Lebleu, B. Cell-penetrating peptides. A reevaluation of the mechanism of cellular uptake. *J Biol Chem* 2003**;** *278 (1):* 585.
64. Lundberg, M,Johansson, M. Positively charged DNA-binding proteins cause apparent cell membrane translocation. *Biochem Biophys Res Commun* 2002**;** *291 (2):* 367.
65. Futaki, S. Membrane-permeable arginine-rich peptides and the translocation mechanisms. *Adv Drug Deliv Rev* 2005**;** *57 (4):* 547.
66. Jones, SW,Christison, R,Bundell, K,Voyce, CJ,Brockbank, SM,Newham, P,Lindsay, MA. Characterisation of cell-penetrating peptide-mediated peptide delivery. *Br J Pharmacol* 2005**;** *145 (8):* 1093.
67. Duchardt, F,Fotin-Mleczek, M,Schwarz, H,Fischer, R,Brock, R. A comprehensive model for the cellular uptake of cationic cell-penetrating peptides. *Traffic* 2007**;** *8 (7):* 848.
68. Vives, E,Richard, JP,Rispal, C,Lebleu, B. TAT Peptide Internalization: Seeking the Mechanism of Entry. *Curr Protein Pept Sci* 2003**;** *4 (2):* 125.
69. Brooks, H,Lebleu, B,Vives, E. Tat peptide-mediated cellular delivery: back to basics. *Adv Drug Deliv Rev* 2005**;** *57 (4):* 559.
70. Nakase, I,Tadokoro, A,Kawabata, N,Takeuchi, T,Katoh, H,Hiramoto, K,Negishi, M,Nomizu, M,Sugiura, Y,Futaki, S. Interaction of arginine-rich peptides with membrane-associated proteoglycans is crucial for induction of actin organization and macropinocytosis. *Biochemistry* 2007**;** *46 (2):* 492.
71. Fittipaldi, A,Ferrari, A,Zoppe, M,Arcangeli, C,Pellegrini, V,Beltram, F,Giacca, M. Cell membrane lipid rafts mediate caveolar endocytosis of HIV-1 tat fusion proteins. *J Biol Chem* 2003*(278:):* 34141
72. Kaplan, IM,Wadia, JS,Dowdy, SF. Cationic TAT peptide transduction domain enters cells by macropinocytosis. *J Control Release* 2005**;** *102 (1):* 247.
73. Nakase, I,Niwa, M,Takeuchi, T,Sonomura, K,Kawabata, N,Koike, Y,Takehashi, M,Tanaka, S,Ueda, K,Simpson, JC,Jones, AT,Sugiura, Y,Futaki, S. Cellular uptake of arginine-rich peptides: roles for macropinocytosis and actin rearrangement. *Mol Ther* 2004**;** *10 (6):* 1011.

74. Richard, JP,Melikov, K,Brooks, H,Prevot, P,Lebleu, B,Chernomordik, LV. Cellular uptake of unconjugated TAT peptide involves clathrin-dependent endocytosis and heparan sulfate receptors. *J Biol Chem* 2005**;** *280 (15):* 15300.
75. Vandenbroucke, RE,De Smedt, SC,Demeester, J,Sanders, NN. Cellular entry pathway and gene transfer capacity of TAT-modified lipoplexes. *Biochim Biophys Acta* 2007**;** *1768 (3):* 571.
76. Fischer, R,Kohler, K,Fotin-Mleczek, M,Brock, R. A Stepwise Dissection of the Intracellular Fate of Cationic Cell-penetrating Peptides. *J Biol Chem* 2004**;** *279 (13):* 12625.
77. Toro, A,Paiva, M,Ackerley, C,Grunebaum, E. Intracellular delivery of purine nucleoside phosphorylase (PNP) fused to protein transduction domain corrects PNP deficiency in vitro. *Cell Immunol* 2006**;** *240 (2):* 107.
78. Sugita, T,Yoshikawa, T,Mukai, Y,Yamanada, N,Imai, S,Nagano, K,Yoshida, Y,Shibata, H,Yoshioka, Y,Nakagawa, S,Kamada, H,Tsunoda, SI,Tsutsumi, Y. Comparative study on transduction and toxicity of protein transduction domains. *Br J Pharmacol* 2008.
79. El-Aneed, A. An overview of current delivery systems in cancer gene therapy. *J Control Release* 2004**;** *94 (1):* 1.
80. White, JM,Delos, SE,Brecher, M,Schornberg, K. Structures and mechanisms of viral membrane fusion proteins: multiple variations on a common theme. *Crit Rev Biochem Mol Biol* 2008**;** *43 (3):* 189.
81. Tsai, B. Penetration of nonenveloped viruses into the cytoplasm. *Annu Rev Cell Dev Biol* 2007**;** *23:* 23.
82. Zlotnick, A,Reddy, VS,Dasgupta, R,Schneemann, A,Ray, WJ, Jr.,Rueckert, RR,Johnson, JE. Capsid assembly in a family of animal viruses primes an autoproteolytic maturation that depends on a single aspartic acid residue. *J Biol Chem* 1994**;** *269 (18):* 13680.
83. Banerjee, M,Johnson, JE. Activation, exposure and penetration of virally encoded, membrane-active polypeptides during non-enveloped virus entry. *Curr Protein Pept Sci* 2008**;** *9 (1):* 16.
84. Lamb, RA,Paterson, RG,Jardetzky, TS. Paramyxovirus membrane fusion: lessons from the F and HN atomic structures. *Virology* 2006**;** *344 (1):* 30.
85. Galdiero, S,Vitiello, M,Falanga, A,Cantisani, M,Incoronato, N,Galdiero, M. Intracellular delivery: exploiting viral membranotropic peptides. *Curr Drug Metab* 2012**;** *13 (1):* 93.
86. Falanga, A,Cantisani, M,Pedone, C,Galdiero, S. Membrane fusion and fission: enveloped viruses. *Protein Pept Lett* 2009**;** *16 (7):* 751.
87. Galdiero, S,Galdiero, M,Pedone, C. beta-Barrel membrane bacterial proteins: structure, function, assembly and interaction with lipids. *Curr Protein Pept Sci* 2007**;** *8 (1):* 63.
88. Galdiero, S,Falanga, A,Vitiello, M,Browne, H,Pedone, C,Galdiero, M. Fusogenic domains in herpes simplex virus type 1 glycoprotein H. *J Biol Chem* 2005**;** *280 (31):* 28632.
89. Cai, WH,Gu, B,Person, S. Role of glycoprotein B of herpes simplex virus type 1 in viral entry and cell fusion. *J Virol* 1988**;** *62 (8):* 2596.
90. Avitabile, E,Forghieri, C,Campadelli-Fiume, G. Cross talk among the glycoproteins involved in herpes simplex virus entry and fusion: the interaction between gB and gH/gL does not necessarily require gD. *J Virol* 2009**;** *83 (20):* 10752.
91. Heldwein, EE,Lou, H,Bender, FC,Cohen, GH,Eisenberg, RJ,Harrison, SC. Crystal structure of glycoprotein B from herpes simplex virus 1. *Science* 2006**;** *313 (5784):* 217.
92. Gage, PJ,Levine, M,Glorioso, JC. Syncytium-inducing mutations localize to two discrete regions within the cytoplasmic domain of herpes simplex virus type 1 glycoprotein B. *J Virol* 1993**;** *67 (4):* 2191.
93. Cairns, TM,Landsburg, DJ,Whitbeck, JC,Eisenberg, RJ,Cohen, GH. Contribution of cysteine residues to the structure and function of herpes simplex virus gH/gL. *Virology* 2005**;** *332 (2):* 550.
94. Galdiero, M,Whiteley, A,Bruun, B,Bell, S,Minson, T,Browne, H. Site-directed and linker insertion mutagenesis of herpes simplex virus type 1 glycoprotein H. *J Virol* 1997**;** *71 (3):* 2163.
95. Harman, A,Browne, H,Minson, T. The transmembrane domain and cytoplasmic tail of herpes simplex virus type 1 glycoprotein H play a role in membrane fusion. *J Virol* 2002**;** *76 (21):* 10708.
96. Lopper, M,Compton, T. Coiled-coil domains in glycoproteins B and H are involved in human cytomegalovirus membrane fusion. *J Virol* 2004**;** *78 (15):* 8333.
97. Galdiero, S,Falanga, A,Vitiello, M,D'Isanto, M,Cantisani, M,Kampanaraki, A,Benedetti, E,Browne, H,Galdiero, M. Peptides containing membrane-interacting motifs inhibit herpes simplex virus type 1 infectivity. *Peptides* 2008**;** *29 (9):* 1461.
98. Galdiero, S,Vitiello, M,D'Isanto, M,Falanga, A,Cantisani, M,Browne, H,Pedone, C,Galdiero, M. The identification and characterization of fusogenic domains in herpes virus glycoprotein B molecules. *Chembiochem* 2008**;** *9 (5):* 758.

99. Galdiero, S,Falanga, A,Vitiello, M,Raiola, L,Russo, L,Pedone, C,Isernia, C,Galdiero, M. The presence of a single N-terminal histidine residue enhances the fusogenic properties of a Membranotropic peptide derived from herpes simplex virus type 1 glycoprotein H. *J Biol Chem* 2010**;** *285 (22):* 17123.
100. Galdiero, S,Falanga, A,Vitiello, G,Vitiello, M,Pedone, C,D'Errico, G,Galdiero, M. Role of membranotropic sequences from herpes simplex virus type I glycoproteins B and H in the fusion process. *Biochim Biophys Acta* 2010**;** *1798 (3):* 579.
101. Tu, Y,Kim, JS. A fusogenic segment of glycoprotein H from herpes simplex virus enhances transfection efficiency of cationic liposomes. *J Gene Med* 2008**;** *10 (6):* 646.
102. Mody, VV,Siwale, R,Singh, A,Mody, HR. Introduction to metallic nanoparticles. *J Pharm Bioallied Sci* 2010**;** *2 (4):* 282.
103. Arvizo, RR,Miranda, OR,Moyano, DF,Walden, CA,Giri, K,Bhattacharya, R,Robertson, JD,Rotello, VM,Reid, JM,Mukherjee, P. Modulating pharmacokinetics, tumor uptake and biodistribution by engineered nanoparticles. *PLoS One* 2011**;** *6 (9):* e24374.
104. Arias, JL. Novel strategies to improve the anticancer action of 5-fluorouracil by using drug delivery systems. *Molecules* 2008**;** *13 (10):* 2340.
105. Korting, HC,Schafer-Korting, M. Carriers in the topical treatment of skin disease. *Handb Exp Pharmacol* 2010*(197):* 435.
106. Lattin, JR,Belnap, DM,Pitt, WG. Formation of eLiposomes as a drug delivery vehicle. *Colloids Surf B Biointerfaces* 2012**;** *89:* 93.
107. Fricker, G,Kromp, T,Wendel, A,Blume, A,Zirkel, J,Rebmann, H,Setzer, C,Quinkert, RO,Martin, F,Muller-Goymann, C. Phospholipids and lipid-based formulations in oral drug delivery. *Pharm Res* 2010**;** *27 (8):* 1469.
108. Bally, MB,Nayar, R,Masin, D,Hope, MJ,Cullis, PR,Mayer, LD. Liposomes with entrapped doxorubicin exhibit extended blood residence times. *Biochim Biophys Acta* 1990**;** *1023 (1):* 133.
109. Coukell, AJ,Spencer, CM. Polyethylene glycol-liposomal doxorubicin. A review of its pharmacodynamic and pharmacokinetic properties, and therapeutic efficacy in the management of AIDS-related Kaposi's sarcoma. *Drugs* 1997**;** *53 (3):* 520.
110. Newkome, GR,Moorefield, CN,Vögtle, F *Dendrimers and Dendrons: Concepts, Synthesis Applications* Weinheim2001; Vol. 2nd Edition.
111. Lee, CC,MacKay, JA,Fréchet, JMJ,Szoka, FC. Designing dendrimers for biological applications. *Nature Biotech.* 2005**;** *23 (12):* 1517.
112. Liu, M,Kono, K,Fréchet, JMJ. Water-soluble dendritic unimolecular micelles: Their potential as drug delivery agents. *J. Control. Release* 2000**;** *65 (1-2):* 121.
113. Hawker, C,Fréchet, JMJ. A New Convergent Approach to Monodisperse Dendritic Macromolecules. *J. Chem. Soc. Chem. Commun.* 1990*:* 1010.
114. Newkome, GR,Shreiner, CD. Poly(amidoamine), polypropylenimine, and related dendrimers and dendrons possessing different 1 → 2 branching motifs: An overview of the divergent procedures. *Polymer* 2008**;** *49 (1):* 1.
115. Ornelas, C,Weck, M. Construction of well-defined multifunctional dendrimers using a trifunctional core. *Chem Commun (Camb)* 2009*(38):* 5710.
116. Fox, ME,Szoka, FC,Frechet, JM. Soluble polymer carriers for the treatment of cancer: the importance of molecular architecture. *Acc Chem Res* 2009**;** *42 (8):* 1141.
117. Kobayashi, H,Brechbiel, MW. Dendrimer-based nanosized MRI contrast agents. *Curr Pharm Biotechnol* 2004**;** *5 (6):* 539.
118. Zhang, JS,Liu, F,Huang, L. Implications of pharmacokinetic behavior of lipoplex for its inflammatory toxicity. *Adv Drug Deliv Rev* 2005**;** *57 (5):* 689.
119. Gillies, ER,Frechet, JM. Dendrimers and dendritic polymers in drug delivery. *Drug Discov Today* 2005**;** *10 (1):* 35.
120. Seib, FP,Jones, AT,Duncan, R. Comparison of the endocytic properties of linear and branched PEIs, and cationic PAMAM dendrimers in B16f10 melanoma cells. *J Control Release* 2007**;** *117 (3):* 291.
121. Kang, H,DeLong, R,Fisher, MH,Juliano, RL. Tat-conjugated PAMAM dendrimers as delivery agents for antisense and siRNA oligonucleotides. *Pharm Res* 2005**;** *22 (12):* 2099.
122. Albertazzi, L,Serresi, M,Albanese, A,Beltram, F. Dendrimer internalization and intracellular trafficking in living cells. *Mol Pharm* 2010**;** *7 (3):* 680.
123. Smith, PE,Brender, JR,Durr, UH,Xu, J,Mullen, DG,Banaszak Holl, MM,Ramamoorthy, A. Solid-state NMR reveals the hydrophobic-core location of poly(amidoamine) dendrimers in biomembranes. *J Am Chem Soc* 2010**;** *132 (23):* 8087.

124. Borm, PJ,Robbins, D,Haubold, S,Kuhlbusch, T,Fissan, H,Donaldson, K,Schins, R,Stone, V,Kreyling, W,Lademann, J,Krutmann, J,Warheit, D,Oberdorster, E. The potential risks of nanomaterials: a review carried out for ECETOC. *Part Fibre Toxicol* 2006**;** *3:* 11.
125. Dekkers, S,Krystek, P,Peters, RJ,Lankveld, DP,Bokkers, BG,van Hoeven-Arentzen, PH,Bouwmeester, H,Oomen, AG. Presence and risks of nanosilica in food products. *Nanotoxicology* 2011**;** *5 (3):* 393.
126. Osmond, MJ,McCall, MJ. Zinc oxide nanoparticles in modern sunscreens: an analysis of potential exposure and hazard. *Nanotoxicology* 2010**;** *4 (1):* 15.
127. Farokhzad, OC,Langer, R. Impact of nanotechnology on drug delivery. *ACS Nano* 2009**;** *3 (1):* 16.
128. Johnston, HJ,Semmler-Behnke, M,Brown, DM,Kreyling, W,Tran, L,Stone, V. Evaluating the uptake and intracellular fate of polystyrene nanoparticles by primary and hepatocyte cell lines in vitro. *Toxicol Appl Pharmacol* 2010**;** *242 (1):* 66.
129. Xia, T,Kovochich, M,Liong, M,Zink, JI,Nel, AE. Cationic polystyrene nanosphere toxicity depends on cell-specific endocytic and mitochondrial injury pathways. *ACS Nano* 2008**;** *2 (1):* 85.
130. Geys, J,Coenegrachts, L,Vercammen, J,Engelborghs, Y,Nemmar, A,Nemery, B,Hoet, PH. In vitro study of the pulmonary translocation of nanoparticles: a preliminary study. *Toxicol Lett* 2006**;** *160 (3):* 218.
131. Foster, KA,Yazdanian, M,Audus, KL. Microparticulate uptake mechanisms of in-vitro cell culture models of the respiratory epithelium. *J Pharm Pharmacol* 2001**;** *53 (1):* 57.
132. Gaumet, M,Gurny, R,Delie, F. Localization and quantification of biodegradable particles in an intestinal cell model: the influence of particle size. *Eur J Pharm Sci* 2009**;** *36 (4-5):* 465.
133. Gratton, SE,Ropp, PA,Pohlhaus, PD,Luft, JC,Madden, VJ,Napier, ME,DeSimone, JM. The effect of particle design on cellular internalization pathways. *Proc Natl Acad Sci U S A* 2008**;** *105 (33):* 11613.
134. Lorenz, S,Hauser, CP,Autenrieth, B,Weiss, CK,Landfester, K,Mailander, V. The softer and more hydrophobic the better: influence of the side chain of polymethacrylate nanoparticles for cellular uptake. *Macromol Biosci* 2010**;** *10 (9):* 1034.
135. Connor, EE,Mwamuka, J,Gole, A,Murphy, CJ,Wyatt, MD. Gold nanoparticles are taken up by human cells but do not cause acute cytotoxicity. *SMALL* 2005**;** *1 (3):* 325.
136. Bosi, S,Da Ros, T,Spalluto, G,Prato, M. Fullerene derivatives: an attractive tool for biological applications. *Eur J Med Chem* 2003**;** *38 (11-12):* 913.
137. Newkome, GR,Behera, RK,Moorefield, CN,Baker, GR. Cascade Polymers: Syntheses and Characterization of One-Directional Arborols Based on Adamantane. *J. Org. Chem.* 1991**;** *56 (25):* 7162.
138. Brettreich, M,Hirsch, A. Convergent Synthesis of 1 → 3 C-Branched Polyamide Dendrons. *Synlett* 1998*:* 1396.
139. Vercillo, OE,Andrade, CKZ,Wessjohan, LA. Design and Synthesis of Cyclic RGD-Pentapeptoids by Consecutive Ugi Reactions. *Org. Lett.* 2008**;** *10:* 205.
140. McGill, NW,Williams, SJ. 2,6-Disubstituted Benzoates As Neighboring Groups for Enhanced Diastereoselectivity in β-Galactosylation Reactions: Synthesis of β-1,3-Linked Oligogalactosides Related to Arabinogalactan Proteins. *J. Org. Chem.* 2009**;** *74 (24):* 9388.
141. Rapaport, D,Shai, Y. Interaction of fluorescently labeled pardaxin and its analogues with lipid bilayers. *J Biol Chem* 1991**;** *266 (35):* 23769.
142. Nakaie, CR,Schreier, S,Paiva, AC. Synthesis and properties of spin-labeled angiotensin derivatives. *Biochim Biophys Acta* 1983**;** *742 (1):* 63.
143. Goyal, P,Yoon, K,Weck, M. Multifunctionalization of dendrimers through orthogonal transformations. *Chemistry* 2007**;** *13 (31):* 8801.
144. Deshayes, S,Gerbal-Chaloin, S,Morris, MC,Aldrian-Herrada, G,Charnet, P,Divita, G,Heitz, F. On the mechanism of non-endosomial peptide-mediated cellular delivery of nucleic acids. *Biochim Biophys Acta* 2004**;** *1667 (2):* 141.
145. Deshayes, S,Heitz, A,Morris, MC,Charnet, P,Divita, G,Heitz, F. Insight into the mechanism of internalization of the cell-penetrating carrier peptide Pep-1 through conformational analysis. *Biochemistry* 2004**;** *43 (6):* 1449.
146. Hope, MJ,Bally, MB,Webb, G,Cullis, PR. Production of large unilamellar vesicles by a rapid extrusion procedure. Characterization of size distribution, trapped volume and ability to maintain a membrane potential. *Biochimica et Biophysica Acta (BBA) - Biomembranes* 1985**;** *812 (1):* 55.
147. Hoekstra, D. Role of lipid phase separations and membrane hydration in phospholipid vesicle fusion. *Biochemistry* 1982**;** *21 (12):* 2833.

148. McIntyre, JC,Sleight, RG. Fluorescence assay for phospholipid membrane asymmetry. *Biochemistry* 1991**;** *30 (51):* 11819.
149. Kveder, M,Pifat, G,Pecar, S,Schara, M,Ramos, P,Esterbauer, H. Nitroxide reduction with ascorbic acid in spin labeled human plasma LDL and VLDL. *Chem Phys Lipids* 1997**;** *85 (1):* 1.
150. Guarnieri, DG, A.; Fusco, S.; Netti, P.A. Effect of serum proteins on polystyrene nanoparticle uptake and intracellular trafficking in endothelial cells. . *Journal of Nanoparticle Research* 2011**;** *13 (9):* 15.
151. Imahashi, D. Quantitation of LDH isoenzymes by the fluorimetric and colorimetric methods. *Can J Med Technol* 1968**;** *30 (6):* 235.
152. Matsuzaki, K,Murase, O,Fujii, N,Miyajima, K. Translocation of a channel-forming antimicrobial peptide, magainin 2, across lipid bilayers by forming a pore. *Biochemistry* 1995**;** *34 (19):* 6521.
153. Thoren, PE,Persson, D,Lincoln, P,Norden, B. Membrane destabilizing properties of cell-penetrating peptides. *Biophys Chem* 2005**;** *114 (2-3):* 169.
154. Yu, YG,Thorgeirsson, TE,Shin, YK. Topology of an amphiphilic mitochondrial signal sequence in the membrane-inserted state: a spin labeling study. *Biochemistry* 1994**;** *33 (47):* 14221.
155. Peggion, C,Jost, M,Baldini, C,Formaggio, F,Toniolo, C. Total syntheses in solution of TOAC-labelled alamethicin F50/5 analogues. *Chem Biodivers* 2007**;** *4 (6):* 1183.
156. Ertel, A,Marangoni, AG,Marsh, J,Hallett, FR,Wood, JM. Mechanical properties of vesicles. I. Coordinated analysis of osmotic swelling and lysis. *Biophys J* 1993**;** *64 (2):* 426.
157. Said Hassane, F,Frisch, B,Schuber, F. Targeted liposomes: convenient coupling of ligands to preformed vesicles using "click chemistry". *Bioconjug Chem* 2006**;** *17 (3):* 849.
158. Cavalli, S,Tipton, AR,Overhand, M,Kros, A. The chemical modification of liposome surfaces via a copper-mediated [3 + 2] azide-alkyne cycloaddition monitored by a colorimetric assay. *Chem Commun (Camb)* 2006*(30):* 3193.
159. Tardi, PG,Boman, NL,Cullis, PR. Liposomal doxorubicin. *J Drug Target* 1996**;** *4 (3):* 129.
160. Fritze, A,Hens, F,Kimpfler, A,Schubert, R,Peschka-Suss, R. Remote loading of doxorubicin into liposomes driven by a transmembrane phosphate gradient. *Biochim Biophys Acta* 2006**;** *1758 (10):* 1633.
161. Angeles-Boza, AM,Erazo-Oliveras, A,Lee, Y-J,Pellois, J-P. Generation of Endosomolytic Reagents by Branching of Cell-Penetrating Peptides. *Bioconjugate Chem.* 2010**;** *21 (12):* 2164.
162. Ellens, H,Bentz, J,Szoka, FC. pH-induced destabilization of phosphatidylethanolamine-containing liposomes: role of bilayer contact. *Biochemistry* 1984**;** *23 (7):* 1532.
163. Parente, RA,Nir, S,Szoka, FC, Jr. Mechanism of leakage of phospholipid vesicle contents induced by the peptide GALA. *Biochemistry* 1990**;** *29 (37):* 8720.
164. Angeletti, C,Nichols, JW. Dithionite quenching rate measurement of the inside-outside membrane bilayer distribution of 7-nitrobenz-2-oxa-1,3-diazol-4-yl-labeled phospholipids. *Biochemistry* 1998**;** *37 (43):* 15114.
165. Drin, G,Cottin, S,Blanc, E,Rees, AR,Temsamani, J. Studies on the internalization mechanism of cationic cell-penetrating peptides. *J Biol Chem* 2003**;** *278 (33):* 31192.
166. Nygren, P,Lundqvist, M,Broo, K,Jonsson, BH. Fundamental design principles that guide induction of helix upon formation of stable peptide-nanoparticle complexes. *Nano Lett* 2008**;** *8 (7):* 1844.
167. Tarallo, R,Accardo, A,Falanga, A,Guarnieri, D,Vitiello, G,Netti, P,D'Errico, G,Morelli, G,Galdiero, S. Clickable functionalization of liposomes with the gH625 peptide from Herpes simplex virus type I for intracellular drug delivery. *Chemistry* 2011**;** *17 (45):* 12659.
168. Carberry, TP,Tarallo, R,Falanga, A,Finamore, E,Galdiero, M,Weck, M,Galdiero, S. Dendrimer functionalization with a membrane-interacting domain of herpes simplex virus type 1: towards intracellular delivery. *Chemistry* 2012**;** *18 (43):* 13678.
169. Jin, H,Heller, DA,Strano, MS. Single-particle tracking of endocytosis and exocytosis of single-walled carbon nanotubes in NIH-3T3 cells. *Nano Lett* 2008**;** *8 (6):* 1577.
170. Ewers, H,Smith, AE,Sbalzarini, IF,Lilie, H,Koumoutsakos, P,Helenius, A. Single-particle tracking of murine polyoma virus-like particles on live cells and artificial membranes. *Proc Natl Acad Sci U S A* 2005**;** *102 (42):* 15110.
171. Blocker, A,Severin, FF,Burkhardt, JK,Bingham, JB,Yu, H,Olivo, JC,Schroer, TA,Hyman, AA,Griffiths, G. Molecular requirements for bi-directional movement of phagosomes along microtubules. *J Cell Biol* 1997**;** *137 (1):* 113.
172. Galdiero, S,Russo, L,Falanga, A,Cantisani, M,Vitiello, M,Fattorusso, R,Malgieri, G,Galdiero, M,Isernia, C. Structure and orientation of the gH625-644 membrane interacting region of herpes simplex virus type 1 in a membrane mimetic system. *Biochemistry* 2012**;** *51 (14):* 3121.

173. Zhang, W,Crocker, E,McLaughlin, S,Smith, SO. Binding of peptides with basic and aromatic residues to bilayer membranes: phenylalanine in the myristoylated alanine-rich C kinase substrate effector domain penetrates into the hydrophobic core of the bilayer. *J Biol Chem* 2003**;** *278 (24):* 21459.
174. Jing, W,Hunter, HN,Hagel, J,Vogel, HJ. The structure of the antimicrobial peptide Ac-RRWWRF-NH2 bound to micelles and its interactions with phospholipid bilayers. *J Pept Res* 2003**;** *61 (5):* 219.
175. Rauch, ME,Ferguson, CG,Prestwich, GD,Cafiso, DS. Myristoylated alanine-rich C kinase substrate (MARCKS) sequesters spin-labeled phosphatidylinositol 4,5-bisphosphate in lipid bilayers. *J Biol Chem* 2002**;** *277 (16):* 14068.
176. Brown, RC,Morris, AP,O'Neil, RG. Tight junction protein expression and barrier properties of immortalized mouse brain microvessel endothelial cells. *Brain Res* 2007**;** *1130 (1):* 17.
177. Omidi, Y,Campbell, L,Barar, J,Connell, D,Akhtar, S,Gumbleton, M. Evaluation of the immortalised mouse brain capillary endothelial cell line, b.End3, as an in vitro blood-brain barrier model for drug uptake and transport studies. *Brain Res* 2003**;** *990 (1-2):* 95.
178. Nag, S. Morphology and properties of brain endothelial cells. *Methods Mol Biol* 2011**;** *686:* 3.
179. Vitiello, G,Falanga, A,Galdiero, M,Marsh, D,Galdiero, S,D'Errico, G. Lipid composition modulates the interaction of peptides deriving from herpes simplex virus type I glycoproteins B and H with biomembranes. *Biochim Biophys Acta* 2011**;** *1808 (10):* 2517.
180. Galdiero, S,Falanga, A,Vitiello, M,Raiola, L,Fattorusso, R,Browne, H,Pedone, C,Isernia, C,Galdiero, M. Analysis of a membrane interacting region of herpes simplex virus type 1 glycoprotein H. *J Biol Chem* 2008**;** *283 (44):* 29993.
181. Suzuki, T,Futaki, S,Niwa, M,Tanaka, S,Ueda, K,Sugiura, Y. Possible existence of common internalization mechanisms among arginine-rich peptides. *J Biol Chem* 2002**;** *277 (4):* 2437.
182. Lasic, DD. Novel applications of liposomes. *Trends Biotechnol* 1998**;** *16 (7):* 307.

Pubblications[1-10]

1) Tarallo, R.; Carberry, T. P.; Falanga, A.; Vitiello, M.; Galdiero, S.; Galdiero, M.; Weck, M. Int J Nanomedicine 2013, 8, 521.
2) Galdiero, S.; Falanga, A.; Tarallo, R.; Russo, L.; Galdiero, E.; Cantisani, M.; Morelli, G.; Galdiero, M. J Pept Sci 2013, 19, 148.
3) Falanga, A.; Tarallo, R.; Galdiero, E.; Cantisani, M.; Galdiero, M.; Galdiero, S. Journal of Nanophotonics 2013, 7, 071599.
4) Guarnieri, D. F., A.; Muscetti, O.; Tarallo, R.; Fusco, S.; Galdiero, M.; Galdiero, S.; Netti, P.A. SMALL 2012.
5) Falanga, A.; Tarallo, R.; Vitiello, G.; Vitiello, M.; Perillo, E.; Cantisani, M.; D'Errico, G.; Galdiero, M.; Galdiero, S. PLoS One 2012, 7, e32186.
6) Carberry, T. P.; Tarallo, R.; Falanga, A.; Finamore, E.; Galdiero, M.; Weck, M.; Galdiero, S. Chemistry 2012, 18, 13678.
7) Galdiero, S.; Falanga, A.; Cantisani, M.; Tarallo, R.; Della Pepa, M. E.; D'Oriano, V.; Galdiero, M. Curr Protein Pept Sci 2012, 13, 843.
8) Galdiero, M.; Cantisani, M.; Tarallo, R.; Falanga, A.; Galdiero, S. "Severe Sepsis and Septic Shock" 2012, 21.
9) Tarallo, R.; Accardo, A.; Falanga, A.; Guarnieri, D.; Vitiello, G.; Netti, P.; D'Errico, G.; Morelli, G.; Galdiero, S. Chemistry 2011, 17, 12659.

Book Chapter

10) Falanga, A.; Vitiello, M. T.; Cantisani, M.; Tarallo, R.; Guarnieri, D.; Mignogna, E.; Netti, P.; Pedone, C.; Galdiero, M.; Galdiero, S. Nanomedicine 2011, 7, 925.

Oral presentation at international meetings

13th Naples Workshop on Bioactive Peptides. “Peptides in nanotechnology and nanomedicine”. Title of the presentation:”*Functionalization of a Dendrimer with a Membrane-Interacting-Domain of Herpes simplex Virus Type I: Application toward intracellular delivery*”. June 2012.

Abstracts

1) S. Galdiero, A. Falanga, G. Vitiello, M. Cantisani, M. Vitiello, **R. Tarallo**, G. D’Errico, C. Pedone, M. Galdiero. “Role of membranotropic and antiviral sequences from Herpes Simplex virus type I glycoproteins B and H in the fusion process” 12th Naples Workshop on Bioactive Peptides and 2nd Italy-Korea Symposium on Antimicrobial Peptides, June 2010.
2) A. Falanga, **R. Tarallo**, M. Cantisani, M. Vitiello, D. Guarnieri, E. Mignogna, P. Netti, C. Pedone, M. Galdiero**,** S. Galdiero”A peptide derived from Herpes Simplex Virus type 1 glycoprotein H: membrane translocation and applications to the delivery of quantum dots”. 10th workshop on pharmacobiometallics. Pozzuoli 2010.
3) A. Falanga, **R. Tarallo**, A. Accardo, D. Guarnieri, P. Netti, G. D’Errico, C. Pedone, G. Morelli, S. Galdiero Clickable functionalization of liposomes with gH625 peptide from Herpes simplex virus type I for intracellular delivery. XXIV Congresso Nazionale della Società Chimica Italiana, Lecce 11-16 Settembre 2011.
4) S. Galdiero, A. Falanga, M. Vitiello, M. Cantisani, **R. Tarallo**, D. Guarnieri, E. Mignogna, P Netti, C. Pedone, M. Galdiero. A peptide derived from Herpes Simplex Virus type 1 glycoprotein H: membrane translocation and applications to the delivery of quantum dots. XXIV Congresso Nazionale della Società Chimica Italiana, Lecce 11-16 Settembre 2011.
5) A. Falanga, D. Guarnieri , **R. Tarallo**, O. Muscetti, S. Fusco, M. Cantisani, M. Galdiero, P. Netti, S. Galdiero. gH625 modified polystyrene nanoparticle: uptake and permeation across blood brain endothelium. Workshop on Bioactive Peptides Giugno, Napoli 7 10 Giugno2012
6) M. Cantisani, A. Falanga, **R. Tarallo**, E. Perillo,G. Vitiello, M. Vitiello, G. D’Errico, M. Galdiero, S. Galdiero. Biophysical characterization and membrane interaction of the two fusion loops of glycoprotein B from herpes simplex virus type I. Workshop on Bioactive Peptides Giugno, Napoli 7 - 10 Giugno 2012
7) **R. Tarallo**, A. Falanga, T. P. Carberry, E. Finamore, M. Galdiero, M. Weck, S. Galdiero. Functionalization of a Dendrimer with a Membrane-Interacting Domain of Herpes Simplex Virus Type

1: Applications toward Intracellular Delivery. Workshop on Bioactive Peptides Giugno, Napoli 7 - 10 Giugno 2012.
8) Cantisani M., Falanga A., **Tarallo R**., Vitiello M., Finamore E., Galdiero M., Galdiero S**.**. "Peptides complementary to the active loop of porin P2 from Haemophilus influenzae modulate its activity" Divisione di Chimica dei Sistemi Biologici DSCB, Convegno di Napoli 24-25 Settembre 2012.
9) A. Falanga, D. Guarnieri , **R. Tarallo**, O. Muscetti, S. Fusco, M. Cantisani, M. Galdiero, P. Netti, S. Galdiero "A novel system for delivery" Divisione di Chimica dei Sistemi Biologici DSCB, Convegno di Napoli 24-25 Settembre 2012.
10) G. Morelli, A. Falanga, **R. Tarallo**, A. Accardo, D. Guarnieri, P. Netti, G. D'Errico, C. Pedone, S. Galdiero **"**Peptide shuttles for intracellular delivery of CdSe Quantum Dots" Biomet12 CIRC MSB, Padova 26-28 Ottobre 2012.

Foreign educational experience and future employment

July 2011- January 2012, permanence at the Molecular Design Institute & Department of Chemistry of New York University, head of the group Prof. Marcus Weck.
May 2013 – on Position for research activity at the Molecular Design Institute & Department of Chemistry of New York University, head of the group Prof. Marcus Weck.

Journal of Nanophotonics

SPIEDigitalLibrary.org/jnp

Review of a viral peptide nanosystem for intracellular delivery

Annarita Falanga
Rossella Tarallo
Emilia Galdiero
Marco Cantisani
Massimiliano Galdiero
Stefania Galdiero

SPIE

Review of a viral peptide nanosystem for intracellular delivery

Annarita Falanga,[a] Rossella Tarallo,[a] Emilia Galdiero,[b] Marco Cantisani,[a] Massimiliano Galdiero,[c] and Stefania Galdiero[a]

[a]University of Naples Federico II, Department of Biological Sciences, Division of Biostructures and Centro Interuniversitario di Ricerca sui Peptidi Bioattivi, Via Mezzocannone 16, 80134, Napoli, Italy
sgaldier@unina.it

[b]University of Naples Federico II, Department of Structural and Functional Biology, Viale Cinzia, Monte Sant'Angelo, Napoli, Italy

[c]II University of Naples, Department of Experimental Medicine, Via De Crecchio 7, 80138, Napoli, Italy

Abstract. The internalization of bioactive molecules is one of the most critical problems to overcome in theranostics. In order to improve pharmacokinetic and pharmacodynamic properties, synthetic transporters are widely investigated. A new nanotechnological transporter, gH625, is based on a viral peptide sequence derived from the herpes simplex virus type 1 glycoprotein H (gH) that has proved to be a useful delivery vehicle, due to its intrinsic properties of inducing membrane perturbation. The peptide functionalization with several kinds of nanoparticles like quantum dots, dendrimers, and liposomes could be of particular interest in biomedical applications to improve drug release within cells, to increase site-specific action, and eventually to reduce related cytotoxicity. [DOI: 10.1117/1.JNP.7.071599]

Keywords: quantum dots; peptide; virus; delivery; dendrimer; liposomes.

Paper 12136V received Oct. 3, 2012; revised manuscript received Dec. 13, 2012; accepted for publication Dec. 14, 2012; published online Jan. 16, 2013.

1 Introduction

The membrane bilayer is a semipermeable barrier defining the interior (or cytoplasm) of an individual cell. The existence of this finely tuned barrier confers to cells their potential to survive and function properly. Nevertheless, crossing the cellular membranes remains a major obstacle for the delivery of therapeutics.[1,2] The lipophilic nature of biological membranes restricts the direct intracellular delivery of most compounds, and whereas small molecules and ions can diffuse across the barrier, large molecules (more than 1kD) are generally excluded from simple diffusion into the cell. The differing hydrophobicity/hydrophilicity of the lipid membrane can make transfer across this barrier extremely difficult, due to differences in solubility.

Novel compounds with therapeutic potential are strictly dependent on their pharmacodistribution properties to reach the stage of pharmaceutical preparations and stimulate industrial interest. In particular, many pharmaceutical agents should be delivered intracellularly to exert their therapeutic action inside the cytoplasm or on individual organelles, such as nuclei (targets for gene and antisense therapy), lysosomes (targets for the delivery of deficient lysosomal enzymes) and mitochondria (targets for pro-apoptotic anticancer drugs).

Several basic cellular mechanisms can be exploited for the intracellular delivery of a compound across the plasma membrane. There are active mechanisms, such as endocytosis, and passive mechanisms, such as translocation across the lipid bilayer; alternatively, there are highly invasive procedures, such as microinjection and/or electroporation, which could cause transient damage to membranes. The use of viral particles as delivery tools, which seemed very promising for gene therapies, presents several problems in terms of side effects and toxicity.[3]

Recently, cell-penetrating peptides (CPPs) have been used extensively, due to their capability to transport several kinds of macromolecules across the bilayer *in vitro* and *in vivo*.[4–6]

CPPs are short and usually basic amino acid rich peptides that can cross biological barriers. Although the mechanism of cellular uptake is still unknown, CPPs are able to deliver various entities into cells, including small molecules, peptides, proteins, DNA/RNA, liposomes, and other supramolecular aggregates. They are usually divided into three classes: protein derived peptides (such as TAT, penetratin or pANTP, transportan, and HSV-1 VP22), amphipathic peptides resulting from the sequential assembly of hydrophobic and hydrophilic domains (such as MAP, MPG, and Pep-1), and synthetic or cationic peptides such as poliarginines (such as Arg9).[7]

The uptake mechanism of CPPs is still debated and is believed to involve mainly the endocytic pathway, trapping the conjugated cargo in endosomes and eventually ending in lysosomes, where common enzymatic degradation mechanisms take place, decreasing its intracellular bioavailability. In order to avoid the endocytic pathway completely or partially, it is paramount to discover new molecules with different mechanism of uptake.

Recently, great attention has been devoted to viruses; in fact, many viruses have evolved quite efficient systems for endosomal release.[8] Therefore, the discovery of new methodologies to reproduce their behavior represents a key objective. Since viruses may enter cells either through a endosomal pathway or via direct fusion on the plasma membrane through the activity of membranotropic peptides, great attention has been devoted to the study of hydrophobic peptides that traverse biological membranes efficiently, promoting lipid-membrane reorganizing processes such as fusion or pore formation and involving temporary membrane destabilization and subsequent reorganization,[7,9] which may be able to circumvent the endosomal entrapment by favoring the escape from the endosome or by translocating a cargo through the plasma membrane directly into the cytosol. Delivery across cellular membranes involves several mechanisms, such as direct transfer through the cell surface membrane by lipid membrane fusion or transient permeabilization of the cell membrane. Alternatively, following endocytosis, transfer across vesicular membranes by lipid disruption, pore formation, or fusion may take place. Several of these membrane reorganization steps are also involved in the cell entry of viruses and other microorganisms, as well as being triggered by protein toxins and defense peptides.[10] Several related processes, such as intracellular vesicle budding, cell-to-cell fusion,[9] sperm-egg fusion, and the immune response, share common features with the mechanism of viral-induced membrane fusion.

The 19-residue peptide gH625 (from aa 625 to aa 644) is a membrane-perturbing domain derived from the gH fusion glycoprotein of herpes simplex virus type I.[11,12] It interacts with biological membranes and is implicated in the merging of the viral envelope and the cellular membrane.[13,14] The peptide contains particular residues that are crucial for its capacity to interact with and destabilize target lipid membranes. It is rich in hydrophobic residues, including glycines, leucines, alanines, and aromatic residues such as tryptophan and tyrosines, which are known to be located preferentially at the membrane interface. This hydrophobic domain is also crucial for insertion of the peptide into the membrane.

An amphipathic α-helix is believed to be an important feature of fusion peptides, playing a crucial role in mediating lipid-protein interactions during the binding of proteins to membranes. Once bound, the hydrophobic face of the amphipathic peptide would allow the peptide to enter the membrane interior with an oblique orientation, thereby triggering local fusion of the membrane leaflets, pore formation, cracks, and membrane fusion.

The viral membranotropic peptide gH625 has been shown to interact strongly with and penetrate the lipid-phase spontaneously and insert into membranes.[15] The peptide-lipid interactions are initiated by the arginine residue located at the C-terminus; in fact, when the arginine is mutated, the fusogenic activity of the peptide is strongly impaired.[16] Compared with the TAT peptide, which mainly exploits the endocytic pathway, gH625 crosses membrane bilayers mainly through a translocation mechanism. A version of this fusogenic peptide one amino acid shorter than HSV-1 gH (missing the histidine at position 625) was also found to improve the endosomal release of DNA/Lipofectamine lipoplexes and transgene expression up to 30-fold in human cell lines.[17] It has been recently demonstrated that gH625 can traverse the membrane bilayer and transport into the cytosol several compounds, such as quantum dots (QDs),[16] liposomes,[18] NPs,[19] and dendrimers.[20]

This review focuses on different delivery applications of gH625.

2 Functionalization of Quantum Dots

QDs are a new class of fluorescent probes under intense research and development for broad applications in molecular, cellular, and *in vivo* imaging; compared with organic dyes and fluorescent proteins, they have unique functional and structural properties, such as size and composition-tunable fluorescence emission, large absorption cross sections, and exceptional brightness and photostability.[21] Furthermore, QDs are a well-characterized family of engineered nanostructures that provide an excellent model system to test toxicity. Many *in vitro* studies have suggested that nanomaterials almost always induce toxic responses, which is essentially correlated to the particle breakdown and subsequent release of toxic metal ions[22,23] and the production of reactive oxygen species.[24] However, properly coated and passivated QDs do not exhibit acute toxicity *in vivo*.[25,26] Thus, the coating of QDs with peptide delivery molecules represents a novel strategy to enhance delivery and reduce toxicity.

In addition, the excellent photostability of QDs gives them great potential in cellular labeling and bioimaging, which have been exploited in different kinds of biological systems.[21] Although considerable success has been achieved in using QDs for labeling fixed cells and for imaging cell membrane proteins, only limited progress has been made for molecular imaging inside living cells. Thus, wide application of QDs to intracellular and molecular imaging has been hampered by their insufficient ability to traverse cell membranes. Therefore, in order to use QDs as biological probes for intracellular applications, their delivery needs to be significantly improved, and the methods actually used are still inefficient. Several authors have recently reported on the functionalization of QDs with the TAT peptide or other positively charged CPPs as an enhancer of cell penetration, and they have established that the main route of entrance is via endosomal uptake; therefore, escape from the endosomal system is paramount.[27–29] There is thus a great need to identify novel molecules that use different internalization mechanisms and may prove useful in the delivery of QDs.[11]

In order to assess the ability of gH625 to deliver a cargo inside the cell, QDs were used as a model. QDs alone have a poor affinity for the plasma membrane of HeLa cells at the concentration of 50 nM. The peptide conjugation of QDs enhanced their membrane-bound ability, providing a favorable condition for cellular internalization. Moreover, the gH625-QDs are internalized more effectively than TAT-QDs, and their internalization only partially involves the endocytic pathway. Furthermore, gH625 showed very low toxicity during *in vitro* studies when used at concentrations of up to 400 μM. Therefore, QDs conjugated with gH625 may represent a novel and useful delivery tool.

It is important that, when conjugated with QDs, gH625 exerts an action of translocation through cellular plasma membranes, which seems to be only relatively dependent on the endocytic route of entry. It has been previously reported that TAT peptides conjugated with small molecules enter cytoplasm and eventually the cell nuclei, while TAT QDs remain trapped in vesicles. This difference in the intracellular fate of TAT peptide-conjugated molecules and TAT QDs is likely to be a consequence of the difference in the size of the cargo. QDs have a diameter of about 1 to 10 nm and cannot escape efficiently from vesicles. On the contrary, gH625-QDs are present in the cytoplasm in a more punctuated form in comparison with TAT QDs.[16] Therefore, a difference in mechanism of entry between TAT-QDs and gH625-QDs has been hypothesized, and this is of particular interest because peptides with different biophysical characteristics can condition the entry pathway of the same macromolecular cargo. These results provide new insights into the mechanism of gH625-mediated delivery and for the development of nanoparticle probes for intracellular targeting and imaging (Fig. 1). Similar delivery methods may enable the implementation of the next generation of QDs capable of long-term intracellular monitoring.

3 Functionalization of Lipid-Based Nanocarriers

Liposomal aggregates have been successfully used as *in vivo* carriers of active principles;[30] they display some unique pharmacokinetic properties and can be adapted to a wide range of therapeutic agents. Liposomes are nontoxic, biodegradable, and non-immunogenic, and their size ranges in mean diameter from 50 to 300 nm. The use of liposomal drugs could help in protecting the encapsulated drugs from chemical or metabolic degradation after injection, in reducing

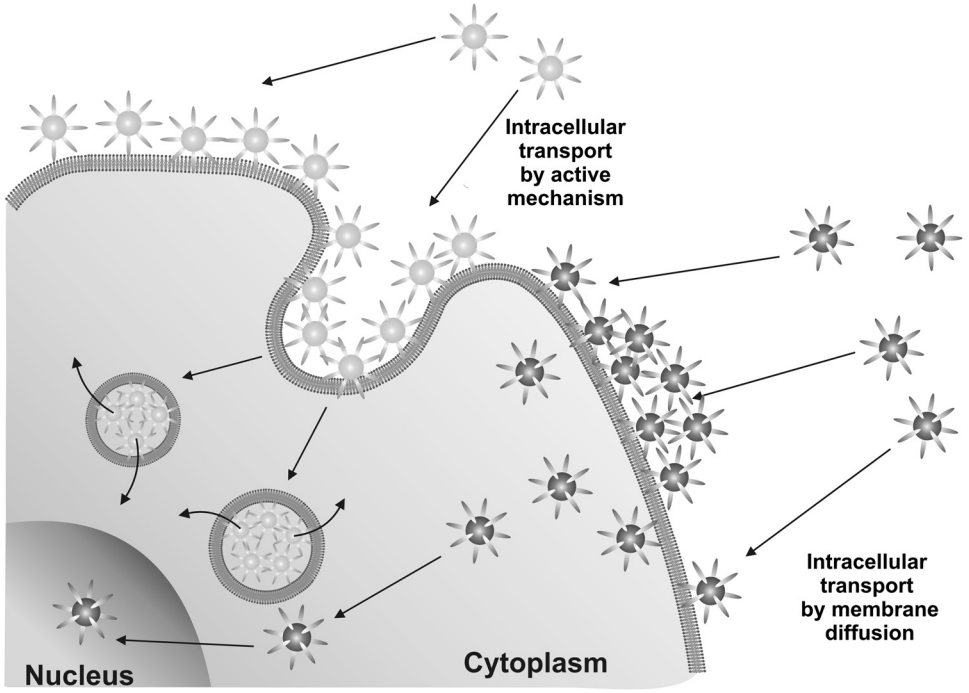

Fig. 1 Intracellular delivery: endocytic mechanisms compared to translocation.

toxicity through decreased exposure of anti-neoplastics to susceptible healthy tissues, and in enhancing antitumor activity resulting from a relatively long systemic circulation time, an extended exposure, and tumor-selective accumulation at specific sites of tumor growth. In particular, liposomes exhibit preferential extravasation and accumulation at the site of solid tumors, due to increased endothelial permeability and reduced lymphatic drainage in these tissues, which has been defined as enhanced permeability and retention effect.[31] A drug encapsulated in liposomes shows marked changes in its pharmacokinetic and pharmacodynamic properties and lower systemic toxicity, while being also protected from early degradation and/or inactivation.[32]

To enhance the antitumor efficacy of liposomal drugs, many research groups are working toward the improvement of their cellular internalization through the addition of surface ligands.

Several peptides, such as penetratin and TAT, have been successfully used for the intracellular delivery of liposomes.[33] Liposomes decorated with gH625 and loaded with doxorubicin can be prepared by different synthetic procedures which involve the coupling of the peptide to the lipid moiety before or after the assembly of the liposome. The ideal strategy depends strongly on the peptide and on the drug. The coupling of a hydrophobic peptide is complicated by the low solubility of the compound and by the higher tendency of the peptide to locate in the hydrophobic region of the bilayer, rather than on the external surface. Thus, the preferable way to obtain liposomes functionalized on the surface with a hydrophobic peptide consists of the coupling of peptide derivatives on pre-assembled liposomes. gH625-modified liposomes were prepared by using a post-aggregation strategy according to click-chemistry procedures.[18] The ability of gH625-functionalized liposomes loaded with doxorubicin to penetrate inside cells was evaluated by confocal microscopy experiments.

Cells were incubated with a 1-μm solution of free Dox, of Dox-loaded liposomes, and of gH625-functionalized liposomes at 37°C. The results obtained after five hours of incubation show that, as expected, free Dox can enter the cell and translocate into the nucleus. Dox-loaded liposomes also enter cell nuclei, where fluorescence due to Dox accumulation in DNA can be observed together with a slight diffuse fluorescence in the cytoplasm suggestive of Dox release from the liposomes. Conversely, gH625-functionalized liposomes encapsulating Dox accumulate in the cytoplasm without entering the nucleus. These results suggest that the functionalization of liposomes with gH625 could affect the uptake mechanism of liposomes, escaping the lysosome accumulation, allowing a more homogeneous intracytoplasmic distribution, and modulating the Dox release. Although the mechanism still remains to be established, the

obtained results could be useful in the design of carriers for a controlled delivery and release of Dox in order to avoid side effects associated with Dox itself.

4 Functionalization of Polymeric Nanocarriers

Dendrimers are perfectly branched macromolecules with a well-defined structure[34] that exhibit properties very different from linear polymers with the same composition and molecular weight.[35] The high concentration of terminal functional groups on a dendrimer's surface determines the solubility of the entire compound—dendrimers have been used as unimolecular micelles, i.e., hydrophobic dendrimers that are water soluble due to peripheral hydrophilic groups or *vice versa*.[36,37] Traditional dendrimers are synthesized from monomers with the structure AB_n;[38–40] from one generation to the following, the dendrimers grow radially with an exponential increase in both mass and number of free termini but only a minimal increase in the physical size of the structure. This causes the termini to become more closely packed. Unlike many other scaffolds, however, dendrimers have the benefit of a highly controlled synthesis, as well as yielding a single monodisperse compound, giving perfect control over the size, weight, and terminal functionalities of the resulting structure. Moreover, highly branched structures generally exhibit longer blood circulation times, due to their inability to pass through renal pores.[41] Dendrimers have been shown to have extended lifetimes *in vivo*,[42] whereas lipid complexes are usually cleared from circulation rapidly by splenic and hepatic phagocytes.[43]

Dendrimers are now considered a very promising tool for drug delivery, thus combining the advantageous features of nanoparticles (such as ideal size as *in vivo* carriers and multivalency) of polymeric materials (such as low cost, tunable properties, and biocompatibility) and of small molecules (such as monodispersity and detailed control of their properties).[35,44] The mechanism of dendrimer uptake and intracellular trafficking is yet to be established.[45] PAMAM dendrimers[46] and PAMAM dendrimers functionalized with the TAT peptide[47] have been proved to involve essentially endocytosis mechanisms for internalization and intracellular trafficking, indicating that the addition of TAT failed to enhance delivery efficiency. Other studies using cationic PAMAM dendrimers showed that the dendrimers can insert themselves into the lipid bilayer, thanks to their potential to weaken the membrane bilayer or form holes.[48]

The combination of the benefits of dendrimers and peptide chemistry may prove useful for the development of a selective carrier that could cross the membrane and be efficiently targeted inside the cell. Targeted dendrimeric systems offer several advantages in their delivery, and their surface modification by means of conjugation or adsorption of a biospecific ligand may allow their delivery to specific sites and the modulation of drug release, minimizing toxic effects and increasing intracellular bioavability.[49]

The binding of gH625 to the dendrimer combines the benefits of dendrimer chemistry with those of a cell internalization unit that can cross the cell membrane mainly via a non-active translocation mechanism. The synthesis of a poly(amide)-based dendrimer containing terminal peptide chains and their cell uptake *in vitro* has been reported recently. The chosen dendrimers had been previously shown to exhibit high biocompatibility, due to their peptide-like backbone.[50,51] The structure of peptidodendrimer, the poly(amide) dendrimer terminated by gH625 peptides, is shown in Fig. 2. The peptidodendrimer can fuse model membranes like liposomes even more significantly than the peptide alone. Moreover, it is unable to fuse the inner monolayer or induce leakage of vesicles. The peptidodendrimer's ability to enter the cells was confirmed by using both qualitative and quantitative methods, and evidence showed that the peptidodendrimer is able to enter cells through a passive translocation mechanism, allowing the cargo to be released directly into the cytoplasm, as opposed to entrapment in endosomes, from which the cargo may not be able to escape before lysosomal degradation. Thus, the dendrimeric scaffolds may be a promising tool for an efficient drug delivery engine.[20]

5 Functionalization of Polystyrene Nanoparticles

Therapies for neurological disorders actually are limited by the inability of the therapeutic agents to cross the blood-brain barrier (BBB) efficiently.[52] The BBB is a selective and dynamic barrier

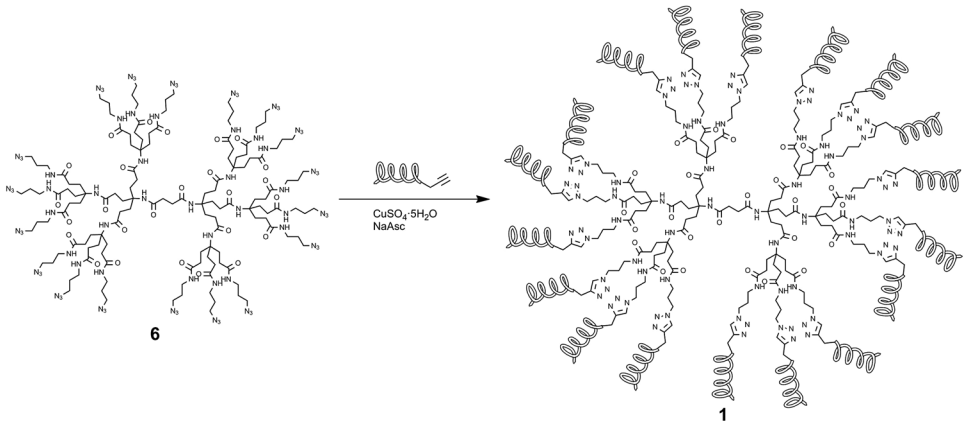

Fig. 2 Structure of peptidodendrimer. The helices represent the gH625 peptide sequence.

protecting the brain against invading organisms and unwanted substances; it also represents a formidable obstacle to the effective delivery of drugs to the central nervous system (CNS). For this reason, it is fundamental to identify and develop more effective strategies to enhance drug delivery to the brain for the therapy and diagnosis of neurological pathologies.

It is now well known that there are several invasive or non-invasive transport routes by which drugs enter the brain. The invasive approaches mainly consist of a temporary disruption of the BBB, allowing the entry of a drug into the CNS, or of direct injection by means of intraventricular or intracerebral administration,[53] while the non-invasive ones involve the systemic application of colloidal drug carriers undergoing a receptor or adsorptive mediated transcytosis mechanism[54] or the passing of the BBB via intranasal delivery.[55]

To overcome this problem, fluorescent polystyrene nanoparticles could be functionalized with the membranotropic peptide gH625. Nanomaterials, such as nanoparticles, differ from other materials, due to a number of special characteristics, including small particle size, large surface area, shape, chemical composition, and charge. Together these characteristics give nanoparticles numerous advantages over other delivery systems, and the targeted delivery of drugs using nanocarriers for the treatment of diseases is a major focus of interest.[56]

The effect of gH625 on the penetration of 100-nm polystyrene nanoparticles (NPs) was analyzed using an *in vitro* BBB model based on bEnd3, an immortalized mouse cerebral endothelial cell line. The intracellular uptake of NPs with gH625 by brain endothelial cells was greater than that of the unfunctionalized NPs, and their intracytoplasmatic motion was mainly characterized by a random-walk behavior indicative of a passive mechanism of internalization. Most importantly, the gH625 peptide decreased NP intracellular accumulation as large aggregates and enhanced the NPs' crossing of the BBB.

This system represents a cell translocation motif never reported before in a BBB *in vitro* analysis and could be applied to the design of a drug delivery system homing to the brain and bypassing the endocytosis entrapment. Therefore, these novel nanoshuttles could be regarded as a promising strategy for engine delivery systems for the administration of therapeutical compounds to the brain.[19]

6 Conclusions

Cell-penetrating peptides are considerably important for the purpose of delivering cargoes to the insides of cells, and hundreds of sequences fall within CPP classification. The process by which membrane translocation is achieved has received great attention with the aim of raising the efficiency of penetration. Most well-studied peptides are able to deliver themselves as well as a cargo across the plasma membrane, although there is strong support for the involvement of endocytic pathways. The discovery of novel systems that use non-canonical mechanisms for internalization may lead to greater efficiency, both from a therapeutic and a diagnostic point of view. Most drugs are internalized by endocytosis mechanisms with a consequential set of limitations in biodistribution, specificity, and toxicity. On the contrary, novel delivery tools that are able to

cross biological membranes using a completely or at least partially different mechanism of internalization may open up new avenues for the administration of drugs with a lower impact on the health of patients. This review focuses on recent data obtained on a viral membranotropic peptide gH625 derived from herpes simplex type 1 and its use, as well as the advantages over other CPPs as a drug delivery tool. The data summarized in this review suggest that membranotropic sequences represent a new and valuable tool for intracellular delivery for applications in theranostics. The opportunity to use a delivery tool with a different internalization mechanism may represent the possibility of reducing the dosages and thus increasing the results of therapies, contemporaneously reducing toxicity.

In conclusion, nanothechnology is developing rapidly and is addressing the safety issue correlated with the use of nanosystems as drug delivery systems, especially for long-term applications. The use of QDs is also particularly important, as they represent a versatile platform which combines unique physical, chemical, and optical properties that may facilitate in-depth studies of interactions of nanosystems with biological systems through real-time monitoring of biodistribution, intracellular uptake, drug release, and long-term fate. QDs offer a powerful platform for studying the behavior of a diverse set of nanovehicles, leading to the design of novel systems for drug delivery.

Acknowledgments

We thank MIUR for financial support (RBAP114AMK/005). We thank A. F. and M. C. for studies on QDs, R. T. for studies on dendrimers, and E. G. and M. G. for *in vitro* studies.

References

1. V. P. Torchilin, "Multifunctional nanocarriers," *Adv. Drug Deliv. Rev.* **58**(14), 1532–1555 (2006), http://dx.doi.org/10.1016/j.addr.2006.09.009.
2. L. M. Bareford and P. W. Swaan, "Endocytic mechanisms for targeted drug delivery," *Adv. Drug Deliv. Rev.* **59**(8), 748–758 (2007), http://dx.doi.org/10.1016/j.addr.2007.06.008.
3. J. K. Raty et al., "Improving safety of gene therapy," *Curr. Drug Saf.* **3**(1), 46–53 (2008), http://dx.doi.org/10.2174/157488608783333925.
4. F. Heitz, M. C. Morris, and G. Divita, "Twenty years of cell-penetrating peptides: from molecular mechanisms to therapeutics," *Br. J. Pharmacol.* **157**(2), 195–206 (2009), http://dx.doi.org/10.1111/j.1476-5381.2009.00057.x.
5. E. Vivès, P. Brodin, and B. Lebleu, "Truncated HIV-1 Tat protein basic domain rapidly translocates through the plasma membrane," *J. Biol. Chem.* **272**(25), 16010–16017 (1997), http://dx.doi.org/10.1074/jbc.272.25.16010.
6. A. M. Angeles-Boza et al., "Generation of endosomolytic reagents by branching of cell-penetrating peptides," *Bioconjugate Chem.* **21**(12), 2164–2167 (2010), http://dx.doi.org/10.1021/bc100130r.
7. S. Galdiero et al., "Intracellular delivery: exploiting viral membranotropic peptides," *Curr. Drug Metab.* **13**(1), 93–104 (2012), http://dx.doi.org/10.2174/138920012798356961.
8. P. L. Leopold et al., "Fluorescent virions: dynamic tracking of the pathway of adenoviral gene transfer vectors in living cells," *Hum. Gene Ther.* **9**(3), 367–378 (1998), http://dx.doi.org/10.1089/hum.1998.9.3-367.
9. A. Falanga et al., "Membrane fusion and fission: enveloped viruses," *Protein Pept. Lett.* **16**(7), 751–759 (2009), http://dx.doi.org/10.2174/092986609788681760.
10. S. Galdiero, M. Galdiero, and C. Pedone, "beta-Barrel membrane bacterial proteins: structure, function, assembly and interaction with lipids," *Curr. Protein Pept. Sci.* **8**(1), 63–82 (2007), http://dx.doi.org/10.2174/138920307779941541.
11. S. Galdiero et al., "Fusogenic domains in herpes simplex virus type 1 glycoprotein H," *J. Biol. Chem.* **280**(31), 28632–28643 (2005), http://dx.doi.org/10.1074/jbc.M505196200.
12. S. Galdiero et al., "Peptides containing membrane-interacting motifs inhibit herpes simplex virus type 1 infectivity," *Peptides* **29**(9), 1461–1471 (2008), http://dx.doi.org/10.1016/j.peptides.2008.04.022.

13. S. Galdiero et al., "The identification and characterization of fusogenic domains in herpes virus glycoprotein B molecules," *Chembiochem* **9**(5), 758–767 (2008), http://dx.doi.org/10.1002/(ISSN)1439-7633.
14. S. Galdiero et al., "The presence of a single N-terminal histidine residue enhances the fusogenic properties of a membranotropic peptide derived from herpes simplex virus type 1 glycoprotein H," *J. Biol. Chem.* **285**(22), 17123–17136 (2010), http://dx.doi.org/10.1074/jbc.M110.114819.
15. S. Galdiero et al., "Role of membranotropic sequences from herpes simplex virus type I glycoproteins B and H in the fusion process," *Biochim. Biophys. Acta* **1798**(3), 579–591 (2010), http://dx.doi.org/10.1016/j.bbamem.2010.01.006.
16. A. Falanga et al., "A peptide derived from herpes simplex virus type 1 glycoprotein H: membrane translocation and applications to the delivery of quantum dots," *Nanomedicine* **7**(6), 925–934 (2011), http://dx.doi.org/10.1016/j.nano.2011.04.009.
17. Y. Tu and J. S. Kim, "A fusogenic segment of glycoprotein H from herpes simplex virus enhances transfection efficiency of cationic liposomes," *J. Gene Med.* **10**(6), 646–654 (2008), http://dx.doi.org/10.1002/(ISSN)1521-2254.
18. R. Tarallo et al., "Clickable functionalization of liposomes with the gH625 peptide from Herpes simplex virus type I for intracellular drug delivery," *Chemistry* **17**(45), 12659–12668 (2011), http://dx.doi.org/10.1002/chem.201101425.
19. D. Guarnieri et al., "Shuttle-mediated nanoparticle delivery to the blood brain barrier," *Small* (2012), http://dx.doi.org/10.1002/smll.201201870; PMID:23135878.
20. T. P. Carberry et al., "Dendrimer functionalization with a membrane-interacting domain of herpes simplex virus type 1: towards intracellular delivery," *Chemistry* **18**(43), 13678–13685 (2012), http://dx.doi.org/10.1002/chem.201202358.
21. F. Pinaud et al., "Probing cellular events, one quantum dot at a time," *Nat. Methods* **7**(4), 275–285 (2010), http://dx.doi.org/10.1038/nmeth.1444.
22. C. Kirchner et al., "Cytotoxicity of colloidal CdSe and CdSe/ZnS nanoparticles," *Nano Lett.* **5**(2), 331–338 (2005), http://dx.doi.org/10.1021/nl047996m.
23. L. O. Cinteza, "Quantum dots in biochemical applications: advances and challenges," *J. Nanophoton.* **4**(1), 42503–42505 (2010), http://dx.doi.org/10.1117/1.3500388.
24. J. Lovric et al., "Unmodified cadmium telluride quantum dots induce reactive oxygen species formation leading to multiple organelle damage and cell death," *Chem. Biol.* **12**(11), 1227–1234 (2005), http://dx.doi.org/10.1016/j.chembiol.2005.09.008.
25. T. S. Hauck et al., "*In vivo* quantum-dot toxicity assessment," *Small* **6**(1), 138–144 (2010), http://dx.doi.org/10.1002/smll.v6:1.
26. L. Ye et al., "A pilot study in non-human primates shows no adverse response to intravenous injection of quantum dots," *Nat. Nanotechnol.* **7**(7), 453–458 (2012), http://dx.doi.org/10.1038/nnano.2012.74.
27. H. Lee, I. K. Kim, and T. G. Park, "Intracellular trafficking and unpacking of siRNA/quantum dot-PEI complexes modified with and without cell penetrating peptide: confocal and flow cytometric FRET analysis," *Bioconjug. Chem.* **21**(2), 289–295 (2010), http://dx.doi.org/10.1021/bc900342p.
28. I. L. Medintz et al., "Intracellular delivery of quantum dot-protein cargos mediated by cell penetrating peptides," *Bioconjug. Chem.* **19**(9), 1785–1795 (2008), http://dx.doi.org/10.1021/bc800089r.
29. J. B. Delehanty et al., "Spatiotemporal multicolor labeling of individual cells using peptide-functionalized quantum dots and mixed delivery techniques," *J. Am. Chem. Soc.* **133**(27), 10482–10489 (2011), http://dx.doi.org/10.1021/ja200555z.
30. E. Cukierman and D. R. Khan, "The benefits and challenges associated with the use of drug delivery systems in cancer therapy," *Biochem.Pharmacol.* **80**(5), 762–770 (2010), http://dx.doi.org/10.1016/j.bcp.2010.04.020.
31. H. Maeda et al., "Tumor vascular permeability and the EPR effect in macromolecular therapeutics: a review," *J. Contr. Release* **65**(1-2), 271–284 (2000), http://dx.doi.org/10.1016/S0168-3659(99)00248-5.

32. M. B. Bally et al., "Liposomes with entrapped doxorubicin exhibit extended blood residence times," *Biochim. Biophys. Acta* **1023**(1), 133–139 (1990), http://dx.doi.org/10.1016/0005-2736(90)90018-J.
33. S. Albrizio et al., "Driving forces in the delivery of penetratin conjugated G protein fragment," *J. Med. Chem.* **50**(7), 1458–1464 (2007), http://dx.doi.org/10.1021/jm060935b.
34. G. R.Newkome and F. Vögtle, Eds., *Dendrimers and Dendrons: Concepts, Synthesis Applications*, Wiley-VCH, Weinheim (2001).
35. C. C. Lee et al., "Designing dendrimers for biological applications," *Nat. Botechnol.* **23**(12), 1517–1526 (2005), http://dx.doi.org/10.1038/nbt1171.
36. S. Stevelmans et al., "Synthesis, characterization, and guest-host properties of inverted unimolecular dendritic micelles," *J. Am. Chem. Soc.* **118**(31), 7398–7399 (1996), http://dx.doi.org/10.1021/ja954207h.
37. M. Liu, K. Kono, and J. M. J. Fréchet, "Water-soluble dendritic unimolecular micelles: their potential as drug delivery agents," *J. Control. Release* **65**(1-2), 121–131 (2000), http://dx.doi.org/10.1016/S0168-3659(99)00245-X.
38. C. Hawker and J. M. J. Fréchet, "A new convergent approach to monodisperse dendritic macromolecules," *J. Chem. Soc. Chem. Commun.* (15), 1010–1013 (1990), http://dx.doi.org/10.1039/c39900001010.
39. G. R. Newkome and C. D. Shreiner, "Poly(amidoamine), polypropylenimine, and related dendrimers and dendrons possessing different 1 → 2 branching motifs: an overview of the divergent procedures," *Polymer* **49**(1), 1–173 (2008), http://dx.doi.org/10.1016/j.polymer.2007.10.021.
40. C. Ornelas and M. Weck, "Construction of well-defined multifunctional dendrimers using a trifunctional core," *Chem. Commun.* (38), 5710–5712 (2009), http://dx.doi.org/10.1039/b913139f.
41. M. E. Fox, F. C. Szoka, and J. M. Frechet, "Soluble polymer carriers for the treatment of cancer: the importance of molecular architecture," *Acc. Chem. Res.* **42**(8), 1141–1151 (2009), http://dx.doi.org/10.1021/ar900035f.
42. H. Kobayashi and M. W. Brechbiel, "Dendrimer-based nanosized MRI contrast agents," *Curr. Pharm. Biotechnol.* **5**(6), 539–549 (2004), http://dx.doi.org/10.2174/1389201043376571.
43. J.-S. Zhang, F. Liu, and L. Huang, "Implications of pharmacokinetic behavior of lipoplex for its inflammatory toxicity," *Adv. Drug Deliv. Rev.* **57**(5), 689–698 (2005), http://dx.doi.org/10.1016/j.addr.2004.12.004.
44. E. R. Gillies and J. M. Frechet, "Dendrimers and dendritic polymers in drug delivery," *Drug Discov. Today* **10**(1), 35–43 (2005), http://dx.doi.org/10.1016/S1359-6446(04)03276-3.
45. M. Najlah and A. D'Emanuele, "Crossing cellular barriers using dendrimer nanotechnologies," *Curr. Opin. Pharmacol.* **6**(5), 522–527 (2006), http://dx.doi.org/10.1016/j.coph.2006.05.004.
46. F. P. Seib, A. T. Jones, and R. Duncan, "Comparison of the endocytic properties of linear and branched PEIs, and cationic PAMAM dendrimers in B16f10 melanoma cells," *J. Contr. Release* **117**(3), 291–300 (2007), http://dx.doi.org/10.1016/j.jconrel.2006.10.020.
47. H. Kang et al., "Tat-conjugated PAMAM dendrimers as delivery agents for antisense and siRNA oligonucleotides," *Pharm. Res.* **22**(12), 2099–2106 (2005), http://dx.doi.org/10.1007/s11095-005-8330-5.
48. P. E. S. Smith et al., "Solid-state NMR reveals the hydrophobic-core location of poly(amidoamine) dendrimers in biomembranes," *J. Am. Chem. Soc.* **132**(23), 8087–8097 (2010), http://dx.doi.org/10.1021/ja101524z.
49. S. Gunaseelan et al., "Surface modifications of nanocarriers for effective intracellular delivery of anti-HIV drugs," *Adv. Drug Deliv. Rev.* **62**(4-5) 518–531 (2010), http://dx.doi.org/10.1016/j.addr.2009.11.021.
50. J. C. Roberts, M. K. Bhalgat, and R. T. Zera, "Preliminary biological evaluation of polyamidoamine (PAMAM) Starburst dendrimers," *J. Biomed. Mater. Res.* **30**(1), 53–65 (1996), http://dx.doi.org/10.1002/(ISSN)1097-4636.
51. C. Ornelas et al., "Construction of a well-defined multifunctional dendrimer for theranostics," *Org. Lett.* **13**(5), 976–979 (2011), http://dx.doi.org/10.1021/ol103019z.

52. E. Neuwelt et al., "Strategies to advance translational research into brain barriers," *Lancet Neurol.* **7**(1), 84–96 (2008), http://dx.doi.org/10.1016/S1474-4422(07)70326-5.
53. G. Tosi et al., "Targeting the central nervous system: *in vivo* experiments with peptide-derivatized nanoparticles loaded with Loperamide and Rhodamine-123," *J. Contr. Release* **122**(1), 1–9 (2007), http://dx.doi.org/10.1016/j.jconrel.2007.05.022.
54. J. Kreuter, "Mechanism of polymeric nanoparticle-based drug transport across the blood-brain barrier (BBB)," *J. Microencapsul.* **30**(1), 49–54 (2013), http://dx.doi.org/10.3109/02652048.2012.692491.
55. S. V. Dhuria, L. R. Hanson, and W. H. Frey II, "Intranasal delivery to the central nervous system: mechanisms and experimental considerations," *J. Pharm. Sci.* **99**(4), 1654–1673 (2010), http://dx.doi.org/10.1002/jps.21924.
56. S. Azarmi, W. H. Roa, and R. Lobenberg, "Targeted delivery of nanoparticles for the treatment of lung diseases," *Adv. Drug Deliv. Rev.* **60**(8), 863–875 (2008), http://dx.doi.org/10.1016/j.addr.2007.11.006.

Annarita Falanga received her degree in food science and technology at the University of Naples Federico II in 2004. From 2004 to 2007, she took the PhD course in microbiological science and was involved in the synthesis and characterization of fusogenic domains derived from membrane glycoproteins of herpes symplex virus type I. From 2007 to 2012, she earned several research contracts at Consiglio Nazionale delle Ricerche, continuing her studies on peptides with antimicrobial activity. Her current research interests are in the development of stable formulation for radiopharmaceutical molecules.

Rossella Tarallo received her degree in biotechnological science at the University of Naples Federico II in 2006. In 2009, she received a master's degree in medical biotechnology with a thesis on nanoparticle's internalization mechanisms. In 2010, she started the PhD course in industrial and molecular biotechnology. In 2011, she worked in the Department of Chemistry at New York University, USA, where she worked on the synthesis and characterization of peptidodendrimers as advanced nanosystems for biomedical applications. Her research projects concern the synthesis and characterization of novel biotechnological peptide systems for intracellular delivery of biomolecules such as liposomes, nanoparticles, and dendrimers functionalized with drugs for cancer therapy.

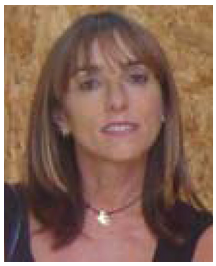

Emilia Galdiero obtained her MD degree from the University of Naples Federico II in 1988. She earned her specialization degree in hygiene and prevention medicine in 1992. She worked as a visiting scholar of infectious disease at the Istituto Superiore di Sanità in 1989. She was appointed a graduate technician in 1990 and worked until 1994 at the Microbiology Institute, Faculty of Pharmacy, University La Sapienza, Rome, and from 1995 to 2000 at the Department of General and Environmental Physiology, Hygiene, and Microbiology Section, University of Naples, Federico II. Since 2001, she has been faculty member in the Department of Structural and Functional Biology, University of Naples Federico II.

Marco Cantisani received his degree in chemistry at the University of Naples Federico II in 2001. From 2002 to 2005, he attended the PhD course in ambiental science at the University of Molise, Italy. During that time, he worked on antimicrobial peptides, in particular human beta-defensins. In 2009, he earned a researcher contract, and since then he has worked at the Centro Interdipartimentale di Ricerca sui Peptidi Bioattivi (CirpeB) in collaboration with CEINGE Scarl on antimicrobial peptide identification, synthesis, characterization, and biomedical applications for the treatment of high-social-impact diseases.

Massimiliano Galdiero obtained his MD degree from the University of Naples Federico II in 1992. He earned his PhD in virology from the University of Cambridge, UK, in 1998. He was appointed a lecturer in microbiology in 1994 at the Department of Animal Health of the Faculty of Veterinary Medicine, University of Naples Federico II. He moved to the Faculty of Medicine of the Second University of Naples, where he was appointed associate professor and then full professor of microbiology in 2004. His more recent research interests are focused on the study of host-microbial interactions and antimicrobial development.

Stefania Galdiero completed her doctorate in chemistry in the field of peptide chemistry at the University of Naples Federico II in 1998. She carried out research activities at Columbia University, New York, from 1996 to 1997, working on the structure of alpha-hemolysin from *S. aureus* and phospholipid interactions. In 1999, she earned the position of lecturer in inorganic chemistry at the University of Naples, and since 2012, she has been adjunct professor at Loyola University, Chicago. She is a member of the Biostructures and Bioimages Institute of the National Research Council of Italy. Her recent research activities focus on the biological activity of bacterial porins and mechanisms of drug intracellular delivery.

Review

Journal of PeptideScience

Received: 28 September 2012 Revised: 7 January 2013 Accepted: 8 January 2013 Published online in Wiley Online Library: 7 February 2013

(wileyonlinelibrary.com) DOI 10.1002/psc.2489

Peptide inhibitors against herpes simplex virus infections

Stefania Galdiero,[a,b,c]* Annarita Falanga,[a,c] Rossella Tarallo,[a,c] Luigi Russo,[e] Emilia Galdiero,[d] Marco Cantisani,[a,b,c] Giancarlo Morelli[a,b,c] and Massimiliano Galdiero[b,e]*

Herpes simplex virus (HSV) is a significant human pathogen causing mucocutaneous lesions primarily in the oral or genital mucosa. Although acyclovir (ACV) and related nucleoside analogs provide successful treatment, HSV remains highly prevalent worldwide and is a major cofactor for the spread of human immunodeficiency virus. Encephalitis, meningitis, and blinding keratitis are among the most severe diseases caused by HSV. ACV resistance poses an important problem for immunocompromised patients and highlights the need for new safe and effective agents; therefore, the development of novel strategies to eradicate HSV is a global public health priority. Despite the continued global epidemic of HSV and extensive research, there have been few major breakthroughs in the treatment or prevention of the virus since the introduction of ACV in the 1980s. A therapeutic strategy at the moment not fully addressed is the use of small peptide molecules. These can be either modeled on viral proteins or derived from antimicrobial peptides. Any peptide that interrupts protein–protein or viral protein–host cell membrane interactions is potentially a novel antiviral drug and may be a useful tool for elucidating the mechanisms of viral entry. This review summarizes current knowledge and strategies in the development of synthetic and natural peptides to inhibit HSV infectivity.

Keywords: herpesvirus; antiviral; peptide; antimicrobial peptide

HSV Infections

Human herpesviruses (Herpesviridae family) consist of large, enveloped, double-stranded DNA viruses that produce a pleteora of infections ranging from skin ulcers to chickenpox to devastating diseases such as encephalitis. There are eight members of the family that infect humans and are divided into three subfamilies, α, β, and γ. Such division is based on biological and genomic similarities, and herpes simplex virus types 1 and 2 (HSV-1 and HSV-2) and varicella-zoster virus belong to the α subfamily, whereas cytomegalovirus and human herpesvirus types 6 and 7 belong to the β subfamily, and Epstein–Barr virus and human herpesvirus type 8 are in the γ subfamily. In addition, there is a further α herpesvirus called herpes B virus, a simian herpesvirus that can occasionally infect humans [1]. HSV infections are among the most common diseases in humans, with an estimated 60–95% of the adult population being infected by at least one of them.

All herpesviruses share the same structural characteristics that render them undistinguishable at the mere observation under the electron microscope. There is an electron-dense central core containing the linear double-stranded DNA genome, which is surrounded by an icosahedral capsid and a proteinaceous tegument layer. This is further enclosed in a lipid envelope presenting spike structures corresponding to virally encoded glycoproteins.

Herpes simplex virus infections have a worldwide distribution and have been described in the medical literature for centuries. The spectrum of disease caused by both HSV-1 and HSV-2 is impacted by the portal of entry, the host's immune response, and whether the infection is the result of primary infection or viral reactivation. In particular, HSV-1 is more frequently associated with oral disease, whereas HSV-2 is more frequently associated with genital disease.

Following a primary infection of mucosal surfaces, HSV is transported by retrograde axonal transport from the infected mucosal area to ganglia of sensory neurons and then establishes a latent infection. The viral DNA is maintained in neuronal nuclei in the absence of any viral production, where the virus persists for the whole lifetime of the host. Because latent infection does not appear to require synthesis of viral polypeptides, antiviral drugs are not able to eliminate the virus in the latent state.

* *Correspondence to: Stefania Galdiero, Department of Pharmacy, University of Naples 'Federico II', Via Mezzocannone 16, 80134, Napoli, Italy. E-mail: stefania.galdiero@unina.it*
Massimiliano Galdiero, Department of Experimental Medicine, II University of Naples, Via De Crecchio 7, 80138, Napoli, Italy. E-mail: massimiliano.galdiero@unina2.it

a *Department of Pharmacy, University of Naples 'Federico II', Via Mezzocannone 16, 80134, Napoli, Italy*

b *Centro Interuniversitario di Ricerca sui Peptidi Bioattivi, University of Naples 'Federico II', Via Mezzocannone 16, 80134, Napoli, Italy*

c *Istituto di Biostrutture e Bioimmagini – CNR, Via Mezzocannone 16, 80134, Napoli, Italy*

d *Department of Biostructural and Fisiological Science, University of Naples 'Federico II', Via Cinzia, Monte Sant'Angelo, Napoli, Italy*

e *Department of Experimental Medicine, II University of Naples, Via De Crecchio 7, 80138, Napoli, Italy*

Journal of PeptideScience

Biography

Dr Stefania Galdiero obtained her doctorate in Chemistry in the field of peptide's chemistry at the University of Naples 'Federico II' in 1998. She carried out research activities at the Columbia University of New York in 1996-1997. In 1999 she earned the position of lecturer in Inorganic Chemistry at the University of Naples and since 2012 she is Adjunct Professor at Loyola University Chicago. She is member of the Biostructures and Bioimages Institute of the National Research Council of Italy. Recent research activities focus on antimicrobial peptides and mechanisms of drug intracellular delivery.

Despite the development of an immune response, reactivations able to cause symptomatic or asymptomatic recurrent infection are triggered by various internal or external stimuli, such as emotional stress, trauma, fever, UV-light exposure, and immunosuppression.

From a clinical standpoint, HSV can cause diseases ranging from mild conditions to lethal infections, especially in neonates and immunocompromised patients. Primary infections and reactivations are often subclinical. Asymptomatic shedding of HSV, prompted by subclinical reactivations, occurs frequently in infected individuals. HSV causes mucocutaneous lesions present as vesicles or ulcerations on various parts of the body. Oropharyngeal infection often results in gingivostomatitis, which is the most common form of symptomatic, primary HSV infection of the oropharynx. The acute illness usually lasts 5–12 days and may be complicated by auto-inoculation at other sites such as fingers, nose, eyes, and genital area. After this initial infection, HSV may become latent within the sensory nerve root ganglia of the trigeminal nerve, and recurrent infections, defined 'herpes labialis', may occur, generally signaled by premonitory tingling or burning in the area, and last for about 7 days. Reactivation may happen without apparent mucosal lesions, but virus excretion is present in the saliva.

Herpes simplex virus type 1 is involved in ocular infections and may cause keratitis followed by the characteristic dendritic ulcer. With recurrence of disease, there may be deeper involvement with corneal scarring that can result in loss of vision; in fact, in developing countries, ocular HSV infection is the prominent cause of corneal blindness.

Genital HSV infection is often more severe and associated with symptoms such as pain. Each episode lasts longer in primary infection compared with reactivation. Genital herpes may be complicated by aseptic meningitis. Both HSV-1 and HSV-2 can cause genital disease, and symptoms and signs of acute infection are similar for both viruses. The main difference, however, can be considered the rare association with reactivations of HSV-1, whereas HSV-2 may be associated with several reactivations per year.

Neonatal herpes is a serious infection predominantly caused by HSV-2 as a result of the transmission of the virus during delivery through infected genital secretions. HSV-1 can also be responsible, as transmission may occur with a primary HSV-1 genital infection or via oral herpes from the mother or other infected individuals that may have close contacts with the newborn. The disease may be localized to skin, eye, and/or mouth infections, or may be associated with neurological symptoms, or even as a disseminated disease with or without internal organ involvement. In the absence of antiviral therapy, the mortality rates can reach 80% in the case of disseminated disease.

Another serious form of HSV infection is encephalitis, which is confined to the frontotemporal and parietal areas of the brain and may progress rapidly to coma and death. HSV encephalitis is a concern for all age groups, in both men and women. Most cases are caused by HSV-1 and occur in adults with high levels of anti-HSV-1 antibodies, suggesting that encephalitis generally results from a reactivation of latent virus. In untreated patients, mortality rates reach 70%, and only 2.5% of surviving patients have no neurological sequelae.

Less common skin infections, due to auto-inoculation or skin-to-skin contact, include 'herpetic whitlow', 'eczema herpeticum', and 'herpes gladiatorum'.

Herpes simplex virus may be particularly severe in immunocompromised patients, especially those with depressed cell-mediated immunity. These patients present frequent reactivation episodes that may be associated with prolonged viral shedding and persistence of lesions [2].

HSV Replication Cycle

Over the past decades, scientific advances have heightened the understanding of the life cycle and pathogenesis of HSV, providing the framework for the development of novel treatment compounds. At the start of infection, the virus attaches to, and enters, the host cell. Although initial studies indicated that HSVs enter cells by direct fusion with the plasma membrane at neutral pH, further analyses revealed that HSV may also exploit endocytosis for its penetration [3,4]. The reason why endocytosis is required in some cell types is unclear, but it is possible that multiple pathways may facilitate productive infection according to different conditions encountered.

Attachment and entry are mediated by a subset of viral envelope glycoproteins present on the herpesvirus envelope (Figure 1); thus, the entry of herpesviruses is a complex process in which multiple glycoproteins are required, and whereas some of them are imperatively needed, others simply enhance entry. The first cellular receptor for HSV is heparan sulfate glycosaminoglycans that have a strong affinity for gC, but this interaction is

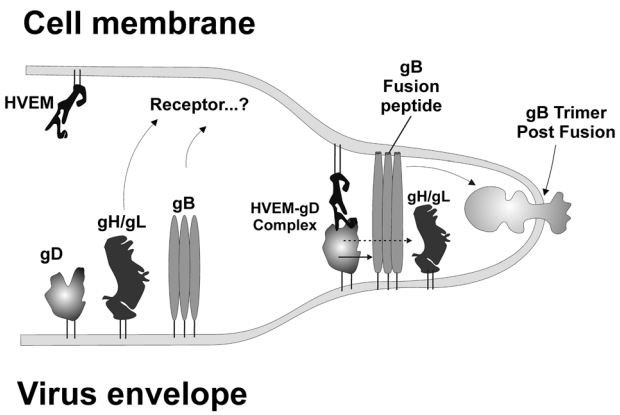

Figure 1. Schematic representation of HSV-1 membrane fusion mechanism. The figure shows (starting from the left) the three fundamental steps including herpesvirus entry mediator (HVEM)/gD complex formation, the exposure of the gB fusion peptides with the formation of the trimer, and the accomplishment of fusion.

not essential for entry *per se* nor does it trigger downstream fusion events. Following this large spectrum of interactions, the main HSV receptor-binding protein is gD that binds three classes of receptors: (i) herpesvirus entry mediator, a member of the tumor necrosis factor receptor family, (ii) nectin 1 and nectin 2, which are cell adhesion molecules of the immunoglobulin superfamily, and (iii) 3-*O*-sulfated heparan sulfate [5–7].

Soluble forms of gD are able to trigger fusion; therefore, the gD–receptor interaction is not only needed to tether the viruses to the cell [8–10]; in fact, the C-terminal region of gD (the so-called 'pro-fusion domain') is required to trigger fusion [8]. Once gD is bound to one of its receptors, its C terminus undergoes a side movement necessary for triggering the fusion [11]. Besides binding heparan sulfate, gB can bind to paired immunoglobulin-like type 2 receptor-α, an immune system regulator [12]. This gB binding can also trigger fusion in the presence of gD, but the *in vivo* significance of the gB–paired immunoglobulin-like type 2 receptor-α interaction is waiting to be investigated. A receptor-binding role for gH–gL has also been reported, but it has not been shown to be necessary for triggering for HSV entry, at least in the available systems. The gH of HSVs contains an RGD motif, which is thought to mediate attachment to integrins [13]. A soluble form of gH–gL binds to $\alpha v\beta 3$ integrin-expressing cells in an RGD motif-specific manner [14], and the engagement of $\alpha v\beta 3$ integrin by gH–gL in the virion may direct the route of entry of HSV-1 [15].

After binding to one or multiple receptors and engaging a series of protein–protein interactions, the virion fuses its envelope with the host cell membrane. The envelope glycoproteins gH/gL, gB, and gD are all essential for the entry process [16], and the expression of this quartet of glycoproteins induces the fusion of cellular membranes in the absence of virus infection [17]. Recently, it was shown that gB and gH/gL interact with each other concomitantly with fusion and that this interaction is triggered by the binding of gD to its cellular receptor [18,19].

The recently solved crystal structures of the gH/gL ectodomains showed that the gH/gL complex has no structural homology with any known fusion protein [20–22]. Furthermore, in recent findings, gH/gL was shown unable to induce hemifusion [23], and cells transfected with varicella-zoster virus gH/gL in a vaccinia virus-free model needed gB to accomplish fusion [24]. Thus, structural and indirect data support the current model where gH/gL is mainly a regulator of fusion through its interactions with gB. Nevertheless, several studies suggest that gH/gL has intrinsic fusogenic capability, which may be utilized by the virus under circumstances different from the actually analyzed models of viral entry. In fact, peptides derived from the gH ectodomain block virus entry [25,26], whereas others have the ability to bind and disrupt model membranes [27–35]. Moreover, gH/gL from HSV-1 was shown to promote fusion of the virion envelope with the outer nuclear membrane during viral egress [36]. On the other hand, the structures of gB from HSV-1 [37] and Epstein-Barr virus [38] demonstrated that gB has structural homology to other viral fusion proteins such as the vesicular stomatitis virus G protein [39] and the baculovirus protein gp64 [40], and it is a key fusion protein of the HSV envelope. Moreover, several synthetic gB peptides induced the fusion of large unilamellar vesicles and inhibited herpes virus infection [41,42].

The described fusion process delivers the viral nucleocapsids into the cytoplasm, where they latch onto microtubules, and are transported to the nuclear envelope. There, they bind to nuclear pores, and the viral DNA is released into the nucleus where replication ensues.

Anti-Herpetic Drugs: Identification and Development of Peptide Inhibitors

Herpes simplex virus remains a major global health problem, and diverse treatments are available for primary and recurrent diseases. However, being many infections asymptomatic, the diffusion of the virus is constantly increasing. Despite the fact that evaluation of vaccination strategies against HSV has been extensively pursued in the past, the virus resulted elusive at the point that an HSV vaccine is still not available.

However, over the past 40 years, antiviral agents for the treatment of infections due to HSV have been developed, and currently, three classes of drugs are licensed for the treatment of HSV infections, and all target the viral DNA replication. These are the following: (i) the nucleoside analogs [acyclovir (ACV), famciclovir, and valaciclovir], (ii) the acyclic nucleotide analog cidofovir, and (iii) the pyrophosphate analog foscarnet [43].

Despite the efforts, ACV remains the reference treatment for HSV infections and the prototypic antiviral agent. The success of ACV is due to the notably safety profile of the compound that needs to be activated by the virally encoded thymidine kinase, therefore enabling the drug to overcome the main safety problems encountered by previous antiviral drugs and separating interference with viral replication from the killing of the host cell.

Resistance of HSV to ACV has become an important clinical problem, especially among immunocompromised patients undergoing long-term therapy [44]. Viral resistance to ACV usually arise from mutations in the viral thymidine kinase gene, although mutations in the viral DNA polymerase gene may rarely occur. Resistant isolates can cause severe, progressive, debilitating mucosal disease, and, rarely, visceral dissemination [45,46].

The other two drugs used in the therapy of HSV infections are cidofovir, which is an acyclic nucleotide phosphonate, and foscarnet, a pyrophosphate. Both are independent of phosphorylation by viral enzymes and, therefore, not susceptible to thymidine kinase mutations. However, being both nephrotoxic, they are reserved for confirmed cases of ACV resistance [47–49]. Although these agents have proven to be efficacious in the treatment of HSV infections, the risk of adverse effects and the frequent development of drug-resistant strains of HSV make it imperative to discover new antiviral agents with lower toxicity, more convenient regimens, and less susceptible to resistance emergence. Several viral and cellular products have been investigated in recent years to find different targets with different mechanisms of action, and literature has been filled by scientific reports of the *in vitro* anti-herpetic activity of a wide variety of natural products and synthetic compounds [50–54].

Besides the numerous strategies being pursued for the development of traditional molecules with enhanced efficacy, the antiviral research is now exploring new avenues, such as antiviral peptides. These peptides may prevent viral attachment to host cell receptors (such as heparan sulfate) or inhibit the replication complex by interfering with protein–protein interactions, dissociating the complex and/or inhibiting its formation [25–31,41,55]. In recent years, a further promising strategy to develop anti-HSV compounds is the use of the so-called antimicrobial peptides (AMP) (Table 1) [56].

Peptides have several advantages over traditional chemical compounds. In fact, they can be highly specific and effective, they can be biodegraded by peptidases limiting their accumulation in tissues and resulting in lower toxicity, and, most importantly, they can exert a broad activity on different microorganisms. Potential

Table 1. Selected examples of HSV antiviral AMPs

Peptide	Structure	Number of° amino acid	Source	Primary amino acid sequence	Mechanism of action	References
Magainin	α-Helix	23	*Xenopus laevis*	GIGKFLHSAKKFGKAFVGEIMNS	Virucidal	[80–82]
Dermaseptin	α-Helix	27	*Phyllomedusa sauvagii*	ALWMTLLKKVLKAAAKALNAVLVGANA	Interference virus-cell surface interactions	[83,84]
Melittin	α-Helix	26	*Apis mellifera*	GIGAVLKVLTTGLPALISWIKRKRQQ	Interaction with cell membrane	[76,78,79]
Defensin (hBD-1)	β-Sheet	36	*Homo sapiens*	DHYNCVSSGGQCLYSACPIFTKIQGTCYRGKAKCCK	Virucidal, interaction with viral glycoproteins, and cell membrane	[70,71]
Lactoferricin	β-Turn	25	*Bos taurus*	FKCRRWQWRMKKLGAPSITCVRRAF	Interference virus–cell surface interactions	[92–98]
Tachyplesin	β-Sheet	17	*Tachyplesus tridentatus*	KWCFRVCYRGICYRRCR	Virucidal	[72,73]
Mytilin-A	β-Sheet	34	*Mytilus galloprovincialis*	GCASRCKAKCAGRRCKGWASAFRGRCYCKCFRC	Competition with the viral attachment/entry sites for binding to cell surface	[74]
Cathelicidin (LL-37)	α-Helix	37	*Homo sapiens*	LLGDFFRKSKEKIGKEFKRIVQRIKDFLRNLVPRTES	Virucidal	[85–89]
Brevinin-1	Mixed	24	*Rana brevipoda porsa*	FLPVLAGIAAKVVPALFCKITKKC	Virucidal	[73–91]
Indolicidin	Mixed	13	*Bos Taurus*	ILPWKWPWWPWRR	Virucidal on progeny virions	[73–90]
Cecropin	α-Helix	37	*Hyalophora cecropia*	KWKLFKKIEKVGQNIRDGIIKAGPAVAVVGQATQIAK	Interference virus–cell surface interactions	[76]
Penaeidin-3a	Mixed	62	*Litopenaeus vannamei*	QVYKGGYTRPIPRPPPFVRPLPGGPIGPYNGCPVSS CRGISFSQARSCCSRLGRCCHVGKGYS	Interference virus–cell surface interaction	[74,75]

Journal of PeptideScience

drawbacks of the use of peptides are their limited ability to cross membrane barriers (at least for some of them), a short half-life (rapid blood clearance) and potential immunogenicity [57], complex modes of action, high production costs, and poor oral absorption, thus often necessitating intravenous administration [58,59]. Nevertheless, it is possible to overcome these limitations through the use of new technologies for modifying these molecules and their stability/delivery properties. Various attempts have been made to improve peptide's characteristics toward the optimization of physicochemical parameters through the introduction of D-amino acid or fluorinated amino acids, by constraining their conformations and by modification with polymers. These methodologies are useful for improving resistance to natural proteases and thus half-life in serum and oral administration. Furthermore, lipidization and glycosylation may enhance cell adhesion of the peptides and transmembrane delivery [60]. Synthetic analogs are also useful for disclosing the structural requirements for peptide antiviral activity, which are often correlated to both high cationic and amphiphilic character as well as to the spatial positioning of the charged residues. Moreover, it has also been demonstrated that peptide analogs with arginine residues have a higher affinity to heparin sulfate than analogs substituted with lysines [61]. The challenge in the near future will be to overcome the current limitations of antimicrobial peptides and develop them, at a reasonable cost, into therapeutics with powerful antiviral activity.

Antiviral Activity of Antimicrobial Peptides

Antimicrobial peptides are a class of peptides with a broad spectrum of antimicrobial activity, which have been isolated from vertebrates and invertebrates [62]. A huge number of host defense peptides has been described to date, and most of them are present in databases for eukaryotic host defense peptides (http://www.bbcm.units.it/~tossi/pag1.htm; http://cnbi2.ca/cgi-bin/amp.pl) [63].

Antimicrobial peptides are widely distributed in nature and appear to play important roles in innate host defenses against bacteria and fungi [64]. These peptides usually display a broad-range activity as they act on bacteria, fungi, metazoans and other parasites, viruses, and even cancer cells. The most common classes of cationic peptides comprise the following: β-sheet peptides stabilized by disulfide bridges and unstructured peptides that fold into amphipathic α-helices upon contact with membranes. Less common are unstructured peptides with a predominance of one or two amino acids such as histidine, glycine, proline, or tryptophan. Most AMPs carry a positive net charge and adopt an amphipathic structure.

Although antibacterial activity of cationic peptides has been extensively studied, little is known about their ability to act as antiviral agents. In particular, the lack of sequence homology among the different peptides makes it difficult to predict their antiviral and cytotoxic activities; moreover, their mechanism of action is still poorly understood. However, the mechanism of antiviral activity may be related to the viral adsorption and entry process [65] or to a direct effect on the viral envelope [66], indicating that the amphiphilic conformation assumed upon membrane interaction plays a key role.

Among the selected examples of HSV antiviral AMPs reported in Table 1, the most noteworthy mammalian AMPs are defensins. These are characterized by a triple-stranded β-hairpin structure, six conserved cysteine residues forming three disulfide bonds, and a positive net charge. On the basis of the pattern of disulfide bonds, two main subfamilies are distinguished: the α-defensins and the α-defensins. Six α-defensins (human neutrophil peptides 1–4 and human defensins 5 and 6) and four β-defensins (hBD-1 to hBD-4) have been identified in humans. The α-defensins and β-defensins show broad antibacterial activity and have antifungal and antiviral properties. α-Defensins and θ-defensin (retrocyclin 2) target viral glycoproteins involved in membrane fusion. In particular, it has been demonstrated that θ-defensin directly binds HSV-2 glycoprotein B with high affinity, thus protecting cells from HSV-2 infections [67]. The antiviral activity of human β-defensins against enveloped viruses such as HSV-1 and HSV-2, immunodeficiency virus type 1 (HIV-1), vesicular stomatitis virus, influenza virus, and cytomegalovirus has been ascribed to the direct inactivation of viral particles [68]. The antimicrobial activity of hBDs 1, 2, and 4, but not hBD3, is impaired by high salt levels. Novel hBD analogs, constituted by different domains of hBD1 (which is constitutively expressed in humans) and of hBD3 (which is induced by microorganisms and inflammatory factors in humans), have been engineered to maintain their antimicrobial activities and be salt-resistant. Antiviral activity against HSV was enhanced by the hybrid chimera constituted by the hBD1 internal region and the hBD3 C-terminal region [69,70].

Tachyplesin I (TP) is a disulfide-linked 17-residue antimicrobial peptide produced from the hemocytes of the horseshoe crab *Tachyplesus tridentatus* [69]. It causes calcein leakage in phosphatidylglycerol-containing lipid vesicles and forms anion-selective pores. In a process that is concomitant with pore formation, TP translocates across the membrane. It adopts a β-hairpin conformation with straight strands, suggesting that TP is immersed in the glycerol backbone region of the membrane and is oriented roughly parallel to the plane of the membrane. This depth of insertion and orientation differs from those of the analogous β-sheet antimicrobial peptide protegrin-1 and suggests the importance of structural amphiphilicity in determining the location and orientation of membrane peptides in lipid bilayers. TP has been found to exhibit antiviral activity against HSV but with a more pronounced ability to inactivate HSV-2 [71].

Mytilin is a 34-residue antibacterial peptide from the mussel *Mytilus galloprovincialis* and possesses significant *in vitro* antiviral activity. The three-dimensional solution structure of the synthetic mytilin consists of the common cysteine-stabilized $\alpha\beta$ motif close to the one observed in the mussel defensin MGD-1. Mytilin is active against HSV-1 and presents a low percentage of inhibition in an assay where peptides and viruses were added simultaneously to the cells, but a complete inhibition of viral replication in a cell pretreatment assay. Therefore, it is possible that it exerts its antiviral activity through a competition with the viral attachment/entry sites for binding to cell surface [72].

Penaeidins are a family of antimicrobial peptides of 47–62 residues isolated from several species of shrimp [73]. These peptides display a proline-rich domain (N-terminal part) and a cysteine-rich domain (C-terminal part) stabilized by three conserved disulfide bonds. Penaeidin-3 of *Litopenaeus vannamei* is a 63-residue peptide; the proline-rich domain, spanning residues 1–28, is unconstrained, whereas the cysteine-rich domain, spanning residues 29–58, displays a well-defined structure, which consists of an amphipathic helix (residues 41–50) linked to the upstream and downstream unstructured sequences by two disulfide bonds (Cys32–Cys47 and Cys48–Cys55). These two unstructured portions are in turn linked together by the third disulfide bond (Cys36–Cys54). Such a disulfide bond packing

gives rise to the amphipathic character required for antimicrobial peptides. Penaeidin-3 exhibited a significant activity against HSV-1 in an assay where peptides and viruses were added simultaneously; at 100-μM concentration, it inhibited over 85% of the viral replication [72].

It has been reported that α-helical peptides can act as virucidal agents or as inhibitors of virus multiplication. α-Helical peptides have been isolated from diverse organisms. Two major types of α-helical peptides have been isolated from insects: melittin, a 26-amino-acid peptide that is the major component of bee venom, and cecropins, a family of antibacterial peptides, 35–39 amino acid residues in length[74]. Whereas melittin, at high concentrations, is lytic for blood red cells, cecropins appear to be nontoxic for mammalian cells [75]. The antiviral activity of melittin against several enveloped viruses has been attributed to the direct lysis of viral membranes; however, at lower non-virolytic concentrations, melittin exhibits inhibitory action against HSV-1, HSV-2, and HIV-1 [76,77]. Even though the mechanism of action of melittin has not been completely elucidated, its broad spectrum of antiviral action might be related to the ability of this peptide to affect ion gradients across the cell membrane. However, this compound is too toxic to consider it as a valuable antiviral agent. Among cecropins, it has been demonstrated that cecropin A inhibits HIV-1 multiplication in acutely and chronically infected cells.

Magainins I and II are 23-residue α-helical peptides isolated from the skin of the frog *Xenopus laevis*, which differ by substitutions in positions 10 and 22 [78,79]. Magainins I and II were found to be active against HSV-1 and HSV-2. The antiviral activity of several synthetic derivatives of magainin against HSV-1 has been attributed to their virucidal action [80], and similarly, also synthetic analogs of magainins display virucidal action toward HSV-1 [80].

Among microbicidal peptides, a family of five linear, lysine-rich peptides designated dermaseptins S1–S5 were isolated from the skin of a tree-dwelling, South American frog (*Pyllomedusa sauvagei*) [81]. They are 28–34 membered peptides with high levels of sequence homology (94% amino acid positional identity). These peptides can adopt an amphipathic α-helical conformation that appears to play an essential role in selective membrane recognition. In this respect, they are similar to other families of amphipathic helical peptides, such as bombinins and magainins, isolated from other frog species [78]. Even structurally unrelated antimicrobial peptides from distant species such as insects and mammalians tend to be amphipathic. The marked cationic character of vertebrate peptides and their ability to form amphipathic structures in the presence of biological membranes allow these peptides to be inserted into phospholipid bilayers and to disturb their organization, thus resulting in membrane permeation and lysis of target cells. Dermaseptin S4 has been shown to inhibit HSV-1 multiplication in Hep-2 cells, probably through interference with virus–cell surface interactions [65]. The other four dermaseptins, despite their high degree of sequence homology to dermaseptin S4, were less effective. This suggests the importance of specific parameters such as charge distribution and hydrophobicity in the polar site for the expression of the antiviral activity.

Cathelicidins are a major family of mammalian proteins that play various roles in host defense and inflammation [82]. Cathelicidins are characterized by a conserved N-terminal domain that is proteolytically cleaved to generate the mature, active peptides contained within the C-terminus. The prosequence is highly homologous to cathelin, an inhibitor of the cysteine protease cathepsin L. The C-terminal domain consists of α-helical or β-hairpin portions or contains unusual amino acids [83]. In some mammals, multiple cathelicidins are found, whereas in humans, only one cathelicidin is present, representing an α-helix-type AMP called LL-37. Considering its small size and relatively simple structure, it is remarkable that LL-37 contains all of the necessary information to perform its diverse functions, including antimicrobial activity, chemotactic effects that contribute to immune responses, release of inflammatory mediators, transcriptional responses, and wound healing as well as antiviral activity against herpes virus. LL-37 is water soluble, but it spontaneously binds to bacterial LPS and lipid bilayers and permeabilizes microbial membranes, leading to rapid cell death. LL-37 binds to lipid bilayers in an α-helical conformation with the helical axis lying parallel to the plane of bilayer [84]. Bovine myeloid antimicrobial peptide, BMAP-28, also belongs to the cathelicidin family. BMAP-28 structure is characterized by an N-terminal region that forms an α-helical conformation in membrane-mimicking environments and a non-helical, hydrophobic C-terminal region. It kills Gram-negative and Gram-positive bacterial and fungal species at micromolar concentrations. It retains strong and broad-spectrum antimicrobial activity in the presence of physiologic salt concentrations [85], and it exhibits antiviral activity against HSV [86].

A further bovine cathelicidin with broad-spectrum activity is indolicidin. Indolicidin, a 13-amino-acid peptide with unordered structure and a high content of tryptophan, isolated from bovine neutrophils showed direct viral inactivation against HIV-1[66]; it also showed a strong virucidal action against HSV-1 and HSV-2. The reduction of HSV yields caused by indolicidin can be ascribed to a direct inactivation of progeny viruses released from indolicidin-treated cells. However, an inhibitory effect of indolicidin on HSV multiplication cannot be excluded.

Brevinin I was first isolated from an extract of the skin of the Japanese pond frog *Rana brevipoda porsa* [87], but subsequent work has shown that orthologous peptides are synthesized in the skins of a wide range of Eurasian and North American species belonging to the family Ranidae.

Brevinin and indolicidin also showed that peptide-mediated inactivation of HSVs is not simply a manifestation of indiscriminate damage to target cell membranes. Although both peptides were potently antiviral, they showed little (indolicidin) or none ((carboxamidomethylated) CAM -brevinin) hemolytic activity, and they caused minimal cytotoxicity[71]. Antiviral compounds are considered to have promise when there is a tenfold difference between the ID50 for antiviral potency and the EC50 for cytotoxicity using a range of drug doses. By this criteria, both CAM-brevinin and indolicidin show great potential as antiviral agents against HSVs.

The milk protein lactoferrin (LF) is a multifunctional glycoprotein, which plays an important role in immune regulation and defense mechanisms against bacteria, fungi, and viruses [88,89]. Upon peptic digestion of LF, a peptide called lactoferricin (Lfcin) is generated. Lfcin corresponds to the N-terminal part of the protein [90]. Lfcin peptides have also shown anti-HSV activity [88,89,91]. It was recently reported [92] that Lfcin can block genital herpes infections in mice and perhaps also be used for post-infection treatments. In the LF molecule, the Lfcin sequence forms an amphipathic α-helical sequence [93,94], but after pepsin cleavage, the peptide changes into a distorted β-sheet [95].

Alloferon is a tridecapeptide isolated from the bacteria-challenged larvae of the blow fly *Calliphora vicina* [96]. It is interesting that not only its primary structure is similar to some functionally relevant proteins, such as influenza virus B hemagglutinin, bovine prion protein I and II, and *Sarcophaga peregrina* antifungal protein, but also that it has antiviral activity against HSV.

Antiviral Activity of Peptides Derived from HSV-1 Envelope Glycoproteins

Infection of a target cell by enveloped viruses requires a virally mediated mechanism to promote membrane fusion [97,98]. This mechanism seems surprisingly conserved across several diverse viral families, which makes the fusion process a potentially attractive target for antiviral drugs [99,100]. Enveloped viruses use transmembrane viral proteins to mediate fusion with host cell membranes [101–103]. These glycoproteins undergo several conformational rearrangements during the fusion process, and several domains that are buried in the prefusion structure may be exposed in the fusogenic structure. As reported earlier, the fusion mechanism of HSV is still unknown, and several domains of fusion glycoproteins have shown antiviral activity. Recent evidences suggest that helical domains as well as surface loops may play an important role in the viral fusion process and represent possible targets for therapeutic interference. In particular, helical sequences derived from gH [25] and gB [25] have shown the ability to inhibit HSV-1 infection of susceptible cells. Moreover, sequences showing fusogenic ability were also demonstrated to exhibit inhibitory activity [25–31,41,42,104,105]. Several laboratories reported that peptides homologous to heptad repeat (HR) regions of gB and gH of HSV-1, bovine herpes virus type 1, and human cytomegalovirus and thus with high probability of forming coiled coils are able to inhibit infection, thus indicating that these regions of the proteins are functionally significant [25,35,106,107]. These studies were fostered by the appreciable results obtained analyzing the counterpart regions of HIV-1. Assuming that viral–cell fusion progresses by formation of an intermediate, a 'prehairpin' conformation, this structure places the N-terminal fusion peptide near or in the target cell membrane, exposing the HR1 and HR2 regions [97]. In this intermediate, both HR regions can bind synthetic peptides, which can thus inhibit viral infection by preventing formation of the fusogenic trimer-of-hairpins. Indeed, HR2 peptides analogs (among which is Enfuvirtide) are potent inhibitors of HIV-1, active at low nanomolar concentration [108,109]. A competitive interaction with the HR1 domain and prevention of the six-helix bundle conformation has been proposed as the mechanism of inhibition [110].

In HSV-1, two helical regions in gH and two in gB were identified, and peptides of different lengths that correspond to the predicted coiled-coil regions were produced and tested in inhibition assays [25,34,35]. gH-Derived peptides were more effective than gB-derived peptides in inhibiting virus infectivity especially when added to virus before or during inoculation onto cells. The mechanism of action of HSV-derived peptides must differ from the 'canonical' dominant-negative refolding inhibition of the HIV HR-fusion inhibitors. The probable existence of interactions between gB and gH during fusion, also involving unknown domains of these glycoproteins, represents an explanation for the inhibitory effect on virus infectivity exerted by peptides that may disrupt protein–protein interactions essential for the fusion process.

Those studies clearly indicated that peptide-based approaches can be useful in identifying functionally important regions of herpesvirus glycoproteins and, therefore, potential inhibitors. Furthermore, analogs of the orthomyxovirus, paramyxovirus, and HIV fusion peptides [111–113] block viral infection, presumably by forming inactive heteroaggregates. Development of peptide fusion inhibitors based on non-HR regions of the viral fusion protein has also been performed. It is by using a physicochemical algorithm, the Wimley–White interfacial hydrophobicity scale in combination with other structural details, that different regions of gH and gB were predicted to be involved in membrane interactions during the entry and fusion process [27]. Because of the nature of the membrane fusion process, functional regions in these viral glycoproteins need to be accessible (surface exposed), hydrophilic, and flexible, because these properties have been found to be important for the protein–protein interactions, necessary for the activation of the fusion event. Therefore, these regions could be used for the design of antiviral peptides. Two recent studies analyze with bioinformatic tools, through improvements of existing algorithms, the druggable regions in viral fusion proteins to optimize peptide hits as potential inhibitors capable of disrupting the protein–protein interactions in membrane fusion events mediated by viral fusion proteins [114,115].

Five peptides (gH220–262, gH381–420, gH493–537, gH493– 512, and gH626–644), corresponding to the domains with high scores of the Wimley and White hydrophobicity, which are able to interact with biological membranes[27], have been screened for their ability to inhibit plaque formation in a dose-dependent inhibition assay of HSV entry[26]. Two of them, peptides gH493–537 and gH626–644 were able to inhibit HSV entry by approximately 50–60% at 250 μM and 60–70% at 500 μM. The shorter peptide gH493–512, corresponding only to the N-terminal part of gH493–537, was able to inhibit HSV entry even more effectively, resulting in approximately 60% inhibition at 250 μM and 90% at 500 μM. Their inhibitory effect appears conditioned by their ability to partition into membranes and aggregate within them. Because the peptides self-associate in aqueous and lipidic solutions, it is possible that they bind to their counterparts in the HSV-1 gH fusion protein, thus suggesting that the inhibition of viral entry may occur via peptides association with their counterpart on wild-type gH. Further studies are required to define the exact inhibitory mechanism, but it is conceivable that gH493–512 and gH626–644 may sterically hinder their relative domain either in a pre-fusogenic or in an intermediate conformation, preventing a complete and functional interaction between gH and the membrane to fuse.

The pre-transmembrane domain of HIV-1 gp41 has been found able to inhibit fusion in a dose-dependent manner [116]. This suggested the possibility of using peptides derived from such domains for the development of fusion inhibitors. Synthetic peptides derived from amino acid residues 761–810 (the pre-transmembrane region of HSV-1 gH) have been proved capable of inhibiting HSV-1 entry [28]. This region might undergo sequential conformational transitions, from an extended arrangement to a helical structure capable of intimately interacting with the viral membrane and concomitantly with the cell membrane. Thereby, isolated peptides modeled on the pre-transmembrane region of gH may interfere with completion of the fusion step during viral entry.

Also, the amino acid sequence of gB has been screened for regions of highly interfacial hydrophobicity, applying the hydrophobicity-at-interface scale proposed by Wimley and White [117], and synthetic peptides corresponding to such regions have been tested for their ability to inhibit virus infection. Peptides HB168–186, HB491–514, and HB632–650 showed dose-dependent inhibition of HSV infectivity when present on the cell monolayers together with the virus inoculum for a 45-min period prior to low pH treatment. The most active peptides were HB632–650 and HB491–514 with approximately 90% inhibition at peptide concentrations of 250 μM. These results have been confirmed in an independent study [118] where a library of 138 overlapping 15-mer peptides encompassing the ectodomain of gB was tested in search of peptides able to inhibit HSV infection. Seven of the 138 peptides tested

Journal of PeptideScience

positive by reducing infection by 50% or more at a presumed concentration of 100 μM in the initial high-throughput screen. When highly purified peptides were retested, three of the seven peptides (gB94, gB122, and gB131) had (half maximal effective concentration) EC_{50} values of less than 20 μM. These peptides, especially gB94 and gB 122 that partially overlap with HB491–514 and HB632–650[41], represent useful lead compounds to be further developed as inhibitors of HSV-1 infection.

In response to the increasing need for improved antiviral drugs, dendrimer-based molecules have a large number of potential therapeutic applications [119,120]. Dendrimers are highly branched macromolecules that are built up in layers (generations) from a reactive core group by the use of branched building blocks and represent a very promising tool for drug delivery[121] and cellular inhibition combining the advantageous features of nanoparticles (ideal size as *in vivo* carriers and multivalency), of polymeric materials (low cost, tunable properties, and biocompatibility), and of small molecules (monodispersity and detailed control of their properties) [104,122–124].

Their hyperbranched structures allow the exposure of a given molecular motif in a highly multivalent fashion, thus offering the opportunity to present multiple ligands, or sites of contact, on a single molecule [119]. This feature provides an array of options for interfering with the infectivity of a virus particle and/or with the multivalent binding interactions between a virus and its target cell. In fact, most of the antiviral dendrimers identified to date have been found to inhibit infection by blocking attachment of the virus to its target cell following their binding to either the virus or the cell surface [125,126]. Thus, the ability of dendrimers to prevent virus–cell binding has prompted the idea that they might also be used as topical microbicides for reducing the spread of sexually transmitted infections [126]. Proof of this concept has been provided from the development of polyanionic dendrimers, such as SPL7013, a lysine-based dendrimer with naphthalene disulfonic acid surface groups, currently undergoing the expanded safety/phase II stage of clinical development as a vaginal microbicide (known as ViVagel) for the prevention of the transmission of sexually transmitted viral diseases [127–130].

The functionalization of a perfectly symmetrical dendrimer with the peptide sequence, gH(625–644), derived from viral fusion proteins of HSV-I allowed the obtainment of a significant inhibition of HSV-1 (Figure 2), indicating that the dendrimer can inhibit the interactions used by viruses to infect cells physically blocking or otherwise interfering with the fusion mechanism between the virus and the cell [131].

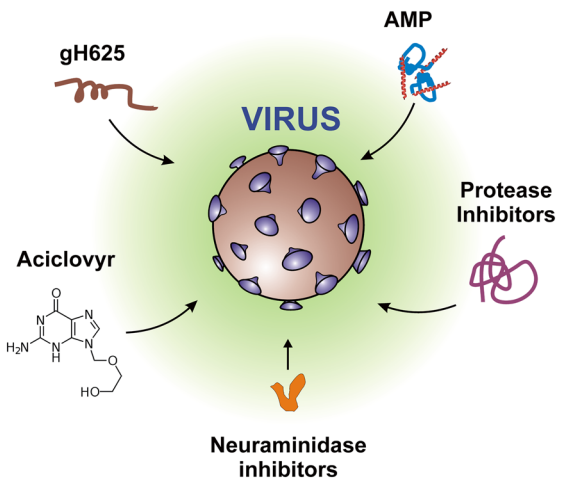

Figure 2. Structure of the poly(amide)-based dendrimer functionalized with the viral peptide gH625.

Conclusion

Despite the extensive research efforts in the battle against the continuous increasing epidemic of HSV, there has been limited advancement in the treatment of HSV infections since the introduction of ACV. Mainly, the use of ACV and related drugs has been optimized with respect to the different clinical necessities, but options for patients who develop drug-resistant variants are still tremendously limited. Therefore, it is time to pursue alternative approaches, and AMPs offer much promise for the future as a complement to the limited number of actual antiviral therapies. The idea of small peptide molecules displaying antibacterial activity has been well established in the past few decades, but the possibility of exploiting their bioactivity against viruses is more recent.

A wide variety of organisms produce AMPs as part of their first defense. Indeed, AMPs have been isolated from single-cell microorganisms, insects, and other invertebrates, plants, amphibians, birds, fish, and mammals, including humans. In addition, a huge number of synthetic peptides have been constructed and among them are the so-called fusion inhibitors that have been designed from a scaffold directly derived by the viral fusogenic glycoprotein ectodomains.

Despite the huge diversity of source of origin, amino acidic sequence as well as secondary structures, they share similar general physical and membranotropic properties. They target various steps in the viral cycle from receptor binding to replication and may be virucidal. In addition, some AMPs can also be translocated into the cell cytoplasm and interact with intracellular targets, interfering with nucleic acid or protein synthesis and with enzymatic activity. Although most of these peptides are in the initial stages of scientific study, the field of antiviral peptides is impressively growing. Therefore, it is of chief importance to understand the mechanisms underlying the antiviral action of AMPs in order to consider this type of compounds as potential useful antiviral agents against HSV and other viruses. The use of viral peptides that could interfere in one of the many steps of membrane fusion is also very attractive and may represent another alternative to existing strategies against herpesviruses.

The actual understanding has provided indications that the strategy of developing antiviral peptides may be particularly useful in this family of viruses, but the use of peptide drugs for antiviral treatment is still in its infancy and needs novel efforts and implementation of new technologies to make a substantial contribution to the never-ending fight against viral infections. In summary, for antiviral peptides to effectively treat an infection, some level of physical (structural), chemical, or composition modifications is probably required to improve its overall pharmacokinetic properties. A therapeutic peptide will be likely to be more effective *in vivo* if used in conjunction with an appropriate delivery system that can extend longevity of the therapeutic action or improve its targeting to the site of infection. Therefore, the application of nanomedicine to the issue of drug delivery makes it possible that therapeutic antiviral peptides will expand to include a wide range of viral infections.

References

1 Pellet P, Roizman B. *The Family Herpesviridae: A Brief Introduction*,Knipe PHDM, Griffin DE, Lamb RA, Martin MA, Roizman B, Straus SE (eds). Lippincott-Williams and Wilkins: New York, N.Y, 2007; 2479–2499.

2 Roizman B, Knipe DM, Whitley RJ. *The Replication of Herpes Simplex Viruses*, Knipe PHDM, Griffin DE, Lamb RA, Martin MA, Roizman B, Straus SE (eds). Lippincott-Williams and Wilkins: New York, N.Y, 2007; 2501–2601.

3 Milne RS, Nicola AV, Whitbeck JC, Eisenberg RJ,Cohen GH. Glycoprotein D receptor-dependent, low-pH-independent endocytic entry of herpes simplex virus type 1. *J. Virol.* 2005; **79**: 6655–6663.

4 Nicola AV, McEvoy AM,Straus SE. Roles for endocytosis and low pH in herpes simplex virus entry into HeLa and Chinese hamster ovary cells. *J. Virol.* 2003; **77**: 5324–5332.

5 Montgomery RI, Warner MS, Lum BJ,Spear PG. Herpes simplex virus-1 entry into cells mediated by a novel member of the TNF/NGF receptor family. *Cell* 1996; **87**: 427–436.

6 Geraghty RJ, Krummenacher C, Cohen GH, Eisenberg RJ,Spear PG. Entry of alphaherpesviruses mediated by poliovirus receptor-related protein 1 and poliovirus receptor. *Science* 1998; **280**: 1618–1620.

7 Shukla D, Liu J, Blaiklock P, Shworak NW, Bai X, Esko JD, Cohen GH, Eisenberg RJ, Rosenberg RD,Spear PG. A novel role for 3-*O*-sulfated heparan sulfate in herpes simplex virus 1 entry. *Cell* 1999; **99**: 13–22.

8 Cocchi F, Fusco D, Menotti L, Gianni T, Eisenberg RJ, Cohen GH, Campadelli-Fiume G. The soluble ectodomain of herpes simplex virus gD contains a membrane-proximal pro-fusion domain and suffices to mediate virus entry. *Proc. Natl. Acad. Sci. U.S.A.* 2004; **101**: 7445–7450.

9 Kwon H, Bai Q, Baek HJ, Felmet K, Burton EA, Goins WF, Cohen JB, Glorioso JC. Soluble V domain of Nectin-1/HveC enables entry of herpes simplex virus type 1 (HSV-1) into HSV-resistant cells by binding to viral glycoprotein D. *J. Virol.* 2006; **80**: 138–148.

10 Tsvitov M, Frampton AR, Jr., Shah WA, Wendell SK, Ozuer A, Kapacee Z, Goins WF, Cohen JB,Glorioso JC. Characterization of soluble glycoprotein D-mediated herpes simplex virus type 1 infection. *Virology* 2007; **360**: 477–491.

11 Lazear E, Carfi A, Whitbeck JC, Cairns TM, Krummenacher C, Cohen GH,Eisenberg RJ. Engineered disulfide bonds in herpes simplex virus type 1 gD separate receptor binding from fusion initiation and viral entry. *J. Virol.* 2008; **82**: 700–709.

12 Satoh T, Arii J, Suenaga T, Wang J, Kogure A, Uehori J, Arase N, Shiratori I, Tanaka S, Kawaguchi Y, Spear PG, Lanier LL,Arase H. PILRalpha is a herpes simplex virus-1 entry coreceptor that associates with glycoprotein B. *Cell* 2008; **132**: 935–944.

13 Galdiero M, Whiteley A, Bruun B, Bell S, Minson T,Browne H. Site-directed and linker insertion mutagenesis of herpes simplex virus type 1 glycoprotein H. *J. Virol.* 1997; **71**: 2163–2170.

14 Parry C, Bell S, Minson T,Browne H. Herpes simplex virus type 1 glycoprotein H binds to alphavbeta3 integrins. *J. Gen. Virol.* 2005; **86**: 7–10.

15 Gianni T, Gatta V, Campadelli-Fiume G. {Alpha}V{beta}3-integrin routes herpes simplex virus to an entry pathway dependent on cholesterol-rich lipid rafts and dynamin2. *Proc. Natl. Acad. Sci. U.S.A.* 2010; **107**: 22260–22265.

16 Connolly SA, Jackson JO, Jardetzky TS,Longnecker R. Fusing structure and function: a structural view of the herpesvirus entry machinery. *Nat. Rev. Microbiol.* 2011; **9**: 369–381.

17 Turner A, Bruun B, Minson T, Browne H. Glycoproteins gB, gD, and gHgL of herpes simplex virus type 1 are necessary and sufficient to mediate membrane fusion in a Cos cell transfection system. *J. Virol.* 1998; **72**: 873–875.

18 Avitabile E, Forghieri C,Campadelli-Fiume G. Complexes between herpes simplex virus glycoproteins gD, gB, and gH detected in cells by complementation of split enhanced green fluorescent protein. *J. Virol.* 2007; **81**: 11532–11537

19 Atanasiu D, Whitbeck JC, Cairns TM, Reilly B, Cohen GH,Eisenberg RJ. Bimolecular complementation reveals that glycoproteins gB and gH/gL of herpes simplex virus interact with each other during cell fusion. *Proc. Natl. Acad. Sci. U.S.A.* 2007; **104**: 18718–18723.

20 Matsuura H, Kirschner AN, Longnecker R,Jardetzky TS. Crystal structure of the Epstein-Barr virus (EBV) glycoprotein H/glycoprotein L (gH/gL) complex. *Proc. Natl. Acad. Sci. U.S.A.* 2010; **107**: 22641–22646.

21 Backovic M, DuBois RM, Cockburn JJ, Sharff AJ, Vaney MC, Granzow H, Klupp BG, Bricogne G, Mettenleiter TC,Rey FA. Structure of a core fragment of glycoprotein H from pseudorabies virus in complex with antibody. *Proc. Natl. Acad. Sci. U.S.A.* 2010; **107**: 22635–22640.

22 Chowdary TK, Cairns TM, Atanasiu D, Cohen GH, Eisenberg RJ, Heldwein EE. Crystal structure of the conserved herpesvirus fusion regulator complex gH-gL. *Nat. Struct. Mol. Biol.* 2010; **17**: 882–888.

23 Jackson JO, Longnecker R. Reevaluating herpes simplex virus hemifusion. *J. Virol.* 2010; **84**: 11814–11821.

24 Suenaga T, Satoh T, Somboonthum P, Kawaguchi Y, Mori Y,Arase H. Myelin-associated glycoprotein mediates membrane fusion and entry of neurotropic herpesviruses. *Proc. Natl. Acad. Sci. U.S.A.* 2010; **107**: 866–871.

25 Galdiero S, Vitiello M, D'Isanto M, Falanga A, Collins C, Raieta K, Pedone C, Browne H,Galdiero M. Analysis of synthetic peptides from heptad-repeat domains of herpes simplex virus type 1 glycoproteins H and B. *J. Gen. Virol.* 2006; **87**: 1085–1097.

26 Galdiero S, Falanga A, Vitiello M, D'Isanto M, Cantisani M, Kampanaraki A, Benedetti E, Browne H,Galdiero M. Peptides containing membrane-interacting motifs inhibit herpes simplex virus type 1 infectivity. *Peptides* 2008; **29**: 1461–1471.

27 Galdiero S, Falanga A, Vitiello M, Browne H, Pedone C,Galdiero M. Fusogenic domains in herpes simplex virus type 1 glycoprotein H. *J. Biol. Chem.* 2005; **280**: 28632–28643.

28 Galdiero S, Falanga A, Vitiello M, D'Isanto M, Collins C, Orrei V, Browne H, Pedone C,Galdiero M. Evidence for a role of the membrane-proximal region of herpes simplex virus type 1 glycoprotein H in membrane fusion and virus inhibition. *Chembiochem* 2007; **8**: 885–895.

29 Galdiero S, Falanga A, Vitiello M, Raiola L, Fattorusso R, Browne H, Pedone C, Isernia C,Galdiero M. Analysis of a membrane interacting region of herpes simplex virus type 1 glycoprotein H. *J. Biol. Chem.* 2008; **283**: 29993–30009.

30 Galdiero S, Falanga A, Vitiello G, Vitiello M, Pedone C, D'Errico G, Galdiero M. Role of membranotropic sequences from herpes simplex virus type I glycoproteins B and H in the fusion process. *Biochim. Biophys. Acta* 2010; **1798**: 579–591.

31 Galdiero S, Falanga A, Vitiello M, Raiola L, Russo L, Pedone C, Isernia C,Galdiero M. The presence of a single N-terminal histidine residue enhances the fusogenic properties of a membranotropic peptide derived from herpes simplex virus type I glycoprotein H. *J. Biol. Chem.* 2010; **285**: 17123–17136.

32 Gianni T, Fato R, Bergamini C, Lenaz G,Campadelli-Fiume G. Hydrophobic alpha-helices 1 and 2 of herpes simplex virus gH interact with lipids, and their mimetic peptides enhance virus infection and fusion. *J. Virol.* 2006; **80**: 8190-8198.

33 Gianni T, Martelli PL, Casadio R. Campadelli-Fiume G The ectodomain of herpes simplex virus glycoprotein H contains a membrane alpha-helix with attributes of an internal fusion peptide, positionally conserved in the herpesviridae family. *J. Virol.* 2005; **79**: 2931–2940

34 Gianni T, Menotti L,Campadelli-Fiume G. A heptad repeat in herpes simplex virus 1 gH, located downstream of the alpha-helix with attributes of a fusion peptide, is critical for virus entry and fusion. *J. Virol.* 2005; **79**: 7042–7049.

35 Gianni T, Piccoli A, Bertucci C,Campadelli-Fiume G. Heptad repeat 2 in herpes simplex virus 1 gH interacts with heptad repeat 1 and is critical for virus entry and fusion. *J. Virol.* 2006; **80**: 2216–2224.

36 Farnsworth A, Wisner TW, Webb M, Roller R, Cohen G, Eisenberg R, Johnson DC. Herpes simplex virus glycoproteins gB and gH function in fusion between the virion envelope and the outer nuclear membrane. *Proc. Natl. Acad. Sci. U.S.A.* 2007; **104**: 10187–10192.

37 Heldwein EE, Lou H, Bender FC, Cohen GH, Eisenberg RJ,Harrison SC. Crystal structure of glycoprotein B from herpes simplex virus 1. *Science* 2006; **313**: 217–220.

38 Backovic M, Longnecker R.Jardetzky TS. Structure of a trimeric variant of the Epstein-Barr virus glycoprotein B. *Proc. Natl. Acad. Sci. U.S.A.* 2009; **106**: 2880–2885.

39 Roche S, Bressanelli S, Rey FA,Gaudin Y Crystal structure of the low-pH form of the vesicular stomatitis virus glycoprotein G. *Science* 2006; **313**: 187–191.

40 Kadlec J, Loureiro S, Abrescia NG, Stuart DI,Jones IM. The postfusion structure of baculovirus gp64 supports a unified view of viral fusion machines. *Nat. Struct. Mol. Biol.* 2008; **15**: 1024–1030.

41 Galdiero S, Vitiello M, D'Isanto M, Falanga A, Cantisani M, Browne H, Pedone C,Galdiero M. The identification and characterization of fusogenic domains in herpes virus glycoprotein B molecules. *Chembiochem* 2008; **9**: 758–767.

42 Falanga A, Tarallo R, Vitiello G, Vitiello M, Perillo E, Cantisani M, D'Errico G, Galdiero M, Galdiero S. Biophysical characterization and membrane interaction of the two fusion loops of glycoprotein B from herpes simplex type I virus. *PLoS One* 2012; **7**: e32186.
43 Kimberlin DW, Whitley RJ. *Antiviral Therapy of HSV-1 and -2*, Arvin A, Campadelli-Fiume G, Mocarski E, Moore PS, Roizman B, Whitley R, Yamanishi K (eds). Cambridge University Press 2007: Cambridge, 2007.
44 Englund JA, Zimmerman ME, Swierkosz EM, Goodman JL, Scholl DR, Balfour HH, Jr.. Herpes simplex virus resistant to acyclovir. A study in a tertiary care center. *Ann. Intern. Med.* 1990; **112**: 416–422
45 Field AK,Biron KK. 'The end of innocence' revisited: resistance of herpesviruses to antiviral drugs. *Clin. Microbiol. Rev.* 1994; **7**: 1–13.
46 Morfin F, Thouvenot D. Herpes simplex virus resistance to antiviral drugs. *J. Clin. Virol.* 2003; **26**: 29–37.
47 Wagstaff AJ, Faulds D,Goa KL. Aciclovir. A reappraisal of its antiviral activity, pharmacokinetic properties and therapeutic efficacy *Drugs* 1994; **47**: 153–205.
48 Lalezari JP, Drew WL, Glutzer E, James C, Miner D, Flaherty J, Fisher PE, Cundy K, Hannigan J, Martin JC,et al. (*S*)-1-[3-hydroxy-2-(phosphonylmethoxy)propyl]cytosine (cidofovir): results of a phase I/II study of a novel antiviral nucleotide analogue. *J. Infect. Dis.* 1995; **171**: 788–796.
49 Safrin S, Cherrington J,Jaffe HS. Cidofovir. Review of current and potential clinical uses. *Adv. Exp. Med. Biol.* 1999; **458**: 111–120.
50 Witvrouw M, De Clercq E. Sulfated polysaccharides extracted from sea algae as potential antiviral drugs. *Gen. Pharmacol.* 1997; **29**: 497–511.
51 Liu YQ, Liu ZL, Tian X, Yang L. Anti-HSV activity of camptothecin analogues. *Nat. Prod. Res.* 2010; **24**: 509–514.
52 Sagar S, Kaur M, Minneman KP. Antiviral lead compounds from marine sponges. *Mar. Drugs* 2010; **8**: 2619–2638.
53 Khan MT, Ather A, Thompson KD, Gambari R. Extracts and molecules from medicinal plants against herpes simplex viruses. *Antiviral Res.* 2005; **67**: 107–119.
54 Dalla Bona A, Formaggio F, Peggion C, Kaptein B, Broxterman QB, Galdiero S, Galdiero M, Vitiello M, Benedetti E, Toniolo C. Synthesis, conformation, and bioactivity of novel analogues of the antiviral lipopeptide halovir A. *J. Pept. Sci.* 2006; **12**: 748–757.
55 Galdiero S, Vitiello M, D'Isanto M, Di Niola E, Peluso L, Raieta K, Pedone C, Galdiero M,Benedetti E. Induction of signaling pathways by herpes simplex virus type 1 through glycoprotein H peptides. *Biopolymers* 2004; **76**: 494–502.
56 Jenssen H. Therapeutic approaches using host defence peptides to tackle herpes virus infections. *Viruses* 2009; **1**: 939–964.
57 Xie D, Yao C, Wang L, Min W, Xu J, Xiao J, Huang M, Chen B, Liu B, Li X, Jiang H. An albumin-conjugated peptide exhibits potent anti-HIV activity and long in vivo half-life. *Antimicrob. Agents Chemother.* 2010; **54**: 191–196.
58 Edwards CM, Cohen MA, Bloom SR. Peptides as drugs. *QJM* 1999; **92**: 1–4.
59 Groner B. *Peptide as Drugs: Discovery and Development*, Groner B (ed.). Wiley-VCH Verlag GmbH & Co. KGaA Weinheim: Germany, 2009; 1–8.
60 Matsuzaki K. Control of cell selectivity of antimicrobial peptides. *Biochim. Biophys. Acta* 2009; **1788**: 1687–1692.
61 Jenssen H, Andersen JH, Mantzilas D,Gutteberg TJ A wide range of medium-sized, highly cationic, alpha-helical peptides show antiviral activity against herpes simplex virus. *Antiviral Res.* 2004; **64**: 119–126.
62 Hancock RE, Chapple DS. Peptide antibiotics. *Antimicrob. Agents Chemother.* 1999; **43**: 1317–1323.
63 Fjell CD, Hancock RE, Cherkasov A. AMPer: a database and an automated discovery tool for antimicrobial peptides. *Bioinformatics* 2007; **23**: 1148–1155.
64 Zasloff M. Antimicrobial peptides of multicellular organisms. *Nature* 2002; **415**: 389–395.
65 Belaid A, Aouni M, Khelifa R, Trabelsi A, Jemmali M,Hani K. In vitro antiviral activity of dermaseptins against herpes simplex virus type 1. *J. Med. Virol.* 2002; **66**: 229–234.
66 Robinson WE, Jr., McDougall B, Tran D,Selsted ME. Anti-HIV-1 activity of indolicidin, an antimicrobial peptide from neutrophils. *J. Leukoc. Biol.* 1998; **63**: 94–100.
67 Yasin B, Wang W, Pang M, Cheshenko N, Hong T, Waring AJ, Herold BC, Wagar EA, Lehrer RI. Theta defensins protect cells from infection by herpes simplex virus by inhibiting viral adhesion and entry. *J Virol* 2004; **78**: 5147–5156.
68 Daher KA, Selsted ME, Lehrer RI. Direct inactivation of viruses by human granulocyte defensins. *J. Virol.* 1986; **60**: 1068–1074
69 Nakamura T, Furunaka H, Miyata T, Tokunaga F, Muta T, Iwanaga S, Niwa M, Takao T,Shimonishi Y. Tachyplesin, a class of antimicrobial peptide from the hemocytes of the horseshoe crab (*Tachypleus tridentatus*). Isolation and chemical structure. *J. Biol. Chem.* 1988; **263**: 16709–16713.
70 Scudiero O, Galdiero S, Cantisani M, Di Noto R, Vitiello M, Galdiero M, Naclerio G, Cassiman JJ, Pedone C, Castaldo G,Salvatore F. Novel synthetic, salt-resistant analogs of human beta-defensins 1 and 3 endowed with enhanced antimicrobial activity. *Antimicrob. Agents Chemother.* 2010; **54**: 2312–2322.
71 Yasin B, Pang M, Turner JS, Cho Y, Dinh NN, Waring AJ, Lehrer RI, Wagar EA. Evaluation of the inactivation of infectious herpes simplex virus by host-defense peptides. *Eur. J. Clin. Microbiol. Infect. Dis.* 2000; **19**: 187–194.
72 Carriel-Gomes MC, Kratz JM, Barracco MA, Bachere E, Barardi CR, Simoes CM. In vitro antiviral activity of antimicrobial peptides against herpes simplex virus 1, adenovirus, and rotavirus. *Mem. Inst. Oswaldo Cruz* 2007; **102**: 469–472.
73 Yang Y, Poncet J, Garnier J, Zatylny C, Bachere E,Aumelas A. Solution structure of the recombinant penaeidin-3, a shrimp antimicrobial peptide. *J. Biol. Chem.* 2003; **278**: 36859–36867.
74 Hancock RE, Diamond G. The role of cationic antimicrobial peptides in innate host defences. *Trends Microbiol.* 2000; **8**: 402–410.
75 Wachinger M, Kleinschmidt A, Winder D, von Pechmann N, Ludvigsen A, Neumann M, Holle R, Salmons B, Erfle V,Brack-Werner R. Antimicrobial peptides melittin and cecropin inhibit replication of human immunodeficiency virus 1 by suppressing viral gene expression. *J. Gen. Virol.* 1998; **79** (Pt 4): 731–740.
76 Wachinger M, Saermark T,Erfle V. Influence of amphipathic peptides on the HIV-1 production in persistently infected T lymphoma cells. *FEBS Lett.* 1992; **309**: 235–241.
77 Baghian A, Kousoulas KG. Role of the Na+,K+pump in herpes simplex type 1-induced cell fusion: melittin causes specific reversion of syncytial mutants with the syn1 mutation to Syn+(wild-type) phenotype. *Virology* 1993; **196**: 548–556.
78 Nicolas P, Mor A. Peptides as weapons against microorganisms in the chemical defense system of vertebrates. *Annu. Rev. Microbiol.* 1995; **49**: 277–304.
79 Nissen-Meyer J,Nes IF. Ribosomally synthesized antimicrobial peptides: their function, structure, biogenesis, and mechanism of action. *Arch. Microbiol.* 1997; **167**: 67–77.
80 Egal M, Conrad M, MacDonald DL, Maloy WL, Motley M, Genco CA. Antiviral effects of synthetic membrane-active peptides on herpes simplex virus, type 1. *Int. J. Antimicrob. Agents* 1999; **13**: 57–60.
81 Mor A, Nguyen VH, Delfour A, Migliore-Samour D, Nicolas P. Isolation, amino acid sequence, and synthesis of dermaseptin, a novel antimicrobial peptide of amphibian skin. *Biochemistry* 1991; **30**: 8824–8830.
82 Zanetti M. Cathelicidins, multifunctional peptides of the innate immunity. *J. Leukoc. Biol.* 2004; **75**: 39–48.
83 Jenssen H, Hamill P, Hancock RE. Peptide antimicrobial agents. *Clin. Microbiol. Rev.* 2006; **19**: 491–511.
84 Porcelli F, Verardi R, Shi L, Henzler-Wildman KA, Ramamoorthy A, Veglia G. NMR structure of the cathelicidin-derived human antimicrobial peptide LL-37 in dodecylphosphocholine micelles. *Biochemistry* 2008; **47**: 5565–5572.
85 Skerlavaj B, Gennaro R, Bagella L, Merluzzi L, Risso A, Zanetti M. Biological characterization of two novel cathelicidin-derived peptides and identification of structural requirements for their antimicrobial and cell lytic activities. *J. Biol. Chem.* 1996; **271**: 28375–28381.
86 Benincasa M, Skerlavaj B, Gennaro R, Pellegrini A, Zanetti M. In vitro and in vivo antimicrobial activity of two alpha-helical cathelicidin peptides and of their synthetic analogs. *Peptides* 2003; **24**: 1723–1731.
87 Morikawa N, Hagiwara K,Nakajima T. Brevinin-1 and -2, unique antimicrobial peptides from the skin of the frog, *Rana brevipoda porsa*. *Biochem. Biophys. Res. Commun.* 1992; **189**: 184–190.
88 Jenssen H, Andersen JH, Uhlin-Hansen L, Gutteberg TJ, Rekdal O. Anti-HSV activity of lactoferricin analogues is only partly related to their affinity for heparan sulfate. *Antiviral Res.* 2004; **61**: 101–109.

89 Andersen JH, Osbakk SA, Vorland LH, Traavik T, Gutteberg TJ. Lactoferrin and cyclic lactoferricin inhibit the entry of human cytomegalovirus into human fibroblasts. *Antiviral Res.* 2001; **51**: 141–149.
90 Tomita M, Bellamy W, Takase M, Yamauchi K, Wakabayashi H, Kawase K. Potent antibacterial peptides generated by pepsin digestion of bovine lactoferrin. *J. Dairy Sci.* 1991; **74**: 4137–4142.
91 van der Strate BW, Beljaars L, Molema G, Harmsen MC, Meijer DK. Antiviral activities of lactoferrin. *Antiviral Res.* 2001; **52**: 225–239.
92 Shestakov A, Jenssen H, Nordstrom I,Eriksson K. Lactoferricin but not lactoferrin inhibit herpes simplex virus type 2 infection in mice *Antiviral Res.* 2012; **93**: 340–345.
93 Baker EN, Anderson BF, Baker HM, Day CL, Haridas M, Norris GE, Rumball SV, Smith CA, Thomas DH. Three-dimensional structure of lactoferrin in various functional states. *Adv. Exp. Med. Biol.* 1994; **357**: 1–12.
94 Haridas M, Anderson BF, Baker HM, Norris GE,Baker EN. X-ray structural analysis of bovine lactoferrin at 2.5 A resolution. *Adv. Exp. Med. Biol.* 1994; **357**: 235–238.
95 Hwang PM, Zhou N, Shan X, Arrowsmith CH, Vogel HJ. Three-dimensional solution structure of lactoferricin B, an antimicrobial peptide derived from bovine lactoferrin. *Biochemistry* 1998; **37**: 4288–4298.
96 Kuczer M, Dziubasik K, Midak-Siewirska A, Zahorska R, Luczak M, Konopinska D. Studies of insect peptides alloferon, Any-GS and their analogues. Synthesis and antiherpes activity. *J. Pept. Sci.* 2010; **16**: 186–189.
97 Eckert DM, Kim PS. Mechanisms of viral membrane fusion and its inhibition. *Annu. Rev. Biochem.* 2001; **70**: 777–810.
98 Earp LJ, Delos SE, Park HE, White JM. The many mechanisms of viral membrane fusion proteins. *Curr. Top. Microbiol. Immunol.* 2005; **285**: 25–66.
99 Dimitrov DS. Virus entry: molecular mechanisms and biomedical applications. *Nat. Rev. Microbiol.* 2004; **2**: 109–122.
100 Dimitrov DS. Therapeutic proteins. *Methods Mol. Biol.* 2012; **899**: 1–26.
101 Belouzard S, Millet JK, Licitra BN, Whittaker GR. Mechanisms of coronavirus cell entry mediated by the viral spike protein. *Viruses* 2012; **4**: 1011–1033.
102 Chang A, Dutch RE. Paramyxovirus fusion and entry: multiple paths to a common end. *Viruses* 2012; **4**: 613–636.
103 Garg H, Viard M, Jacobs A, Blumenthal R. Targeting HIV-1 gp41-induced fusion and pathogenesis for anti-viral therapy. *Curr. Top. Med. Chem.* 2011; **11**: 2947–2958.
104 Falanga A, Vitiello MT, Cantisani M, Tarallo R, Guarnieri D, Mignogna E, Netti P, Pedone C, Galdiero M, Galdiero S. A peptide derived from herpes simplex virus type 1 glycoprotein H: membrane translocation and applications to the delivery of quantum dots. *Nanomed.-Nanotechnol.* 2011; **7**: 925–934.
105 Galdiero S, Russo L, Falanga A, Cantisani M, Vitiello M, Fattorusso R, Malgieri G, Galdiero M,Isernia C. Structure and orientation of the gH625-644 membrane interacting region of herpes simplex virus type 1 in a membrane mimetic system. *Biochemistry* 2012; **51**: 3121–3128.
106 Lopper M, Compton T. Coiled-coil domains in glycoproteins B and H are involved in human cytomegalovirus membrane fusion. *J. Virol.* 2004; **78**: 8333–8341.
107 Okazaki K, Kida H. A synthetic peptide from a heptad repeat region of herpesvirus glycoprotein B inhibits virus replication. *J. Gen. Virol.* 2004; **85**: 2131–2137.
108 Matthews T, Salgo M, Greenberg M, Chung J, DeMasi R,Bolognesi D. Enfuvirtide: the first therapy to inhibit the entry of HIV-1 into host CD4 lymphocytes. *Nat. Rev. Drug Discov.* 2004; **3**: 215–225.
109 Wild C, Oas T, McDanal C, Bolognesi D, Matthews T. A synthetic peptide inhibitor of human immunodeficiency virus replication: correlation between solution structure and viral inhibition. *Proc. Natl. Acad. Sci. U.S.A.* 1992; **89**: 10537–10541.
110 Chan DC, Kim PS. HIV entry and its inhibition. *Cell* 1998; **93**: 681–684.
111 Kliger Y, Aharoni A, Rapaport D, Jones P, Blumenthal R, Shai Y. Fusion peptides derived from the HIV type 1 glycoprotein 41 associate within phospholipid membranes and inhibit cell-cell fusion. Structure-function study. *J. Biol. Chem.* 1997; **272**: 13496–13505.
112 Richardson CD, Scheid A,Choppin PW. Specific inhibition of paramyxovirus and myxovirus replication by oligopeptides with amino acid sequences similar to those at the N-termini of the F1 or HA2 viral polypeptides. *Virology* 1980; **105**: 205–222.
113 Silburn KA, McPhee DA, Maerz AL, Poumbourios P, Whittaker RG, Kirkpatrick A, Reilly WG, Manthey MK, Curtain CC. Efficacy of fusion peptide homologs in blocking cell lysis and HIV-induced fusion. *AIDS Res. Hum. Retroviruses* 1998; **14**: 385–392.
114 Jesus T, Rogelio L, Abraham C, Uriel L, J-Daniel G, Alfonso MT, Lilia BB. Prediction of antiviral peptides derived from viral fusion proteins potentially active against herpes simplex and influenza A viruses. *Bioinformation* 2012; **8**: 870–874.
115 Xu Y, Rahman NA, Othman RB, Hu P, Huang M. Computational identification of self-inhibitory peptides from envelope proteins. *Proteins* 2012; **80**: 2154–2168.
116 Saez-Cirion A, Arrondo JL, Gomara MJ, Lorizate M, Iloro I, Melikyan G, Nieva JL. Structural and functional roles of HIV-1 gp41 pretransmembrane sequence segmentation. *Biophys. J.* 2003; **85**: 3769–3780.
117 Wimley WC, White SH. Experimentally determined hydrophobicity scale for proteins at membrane interfaces. *Nat. Struct. Biol.* 1996; **3**: 842–848.
118 Akkarawongsa R, Pocaro NE, Case G, Kolb AW,Brandt CR. Multiple peptides homologous to herpes simplex virus type 1 glycoprotein B inhibit viral infection. *Antimicrob. Agents Chemother.* 2009; **53**: 987–996.
119 Cloninger MJ. Biological applications of dendrimers. *Curr. Opin. Chem. Biol.* 2002; **6**: 742–748.
120 Sebestik J, Niederhafner P, Jezek J. Peptide and glycopeptide dendrimers and analogous dendrimeric structures and their biomedical applications. *Amino Acids* 2011; **40**: 301–370.
121 Carberry TP, Tarallo R, Falanga A, Finamore E, Galdiero M, Weck M, Galdiero S. Dendrimer functionalization with a membrane-interacting domain of herpes simplex virus type 1: towards intracellular delivery. *Chemistry* 2012; **18**: 13678–13685.
122 Lee CC, MacKay JA, Fréchet JMJ,Szoka FC. Designing dendrimers for biological applications. *Nat. Biotech.* 2005; **23**: 1517–1526.
123 Galdiero S, Vitiello M, Falanga A, Cantisani M, Incoronato N, Galdiero M. Intracellular delivery: exploiting viral membranotropic peptides. *Curr. Drug Metab.* 2012; **13**: 93–104.
124 Tarallo R, Accardo A, Falanga A, Guarnieri D, Vitiello G, Netti P, D'Errico G, Morelli G, Galdiero S. Clickable functionalization of liposomes with the gH625 peptide from herpes simplex virus type I for intracellular drug delivery *Chemistry* 2011; **17**: 12659–12668.
125 Heegaard PM, Boas U. Dendrimer based anti-infective and anti-inflammatory drugs. *Recent Pat. Antiinfect. Drug Discov.* 2006; **1**: 331–351.
126 Rosa Borges A, Schengrund CL. Dendrimers and antivirals: a review. *Curr. Drug Targets Infect. Disord.* 2005; **5**: 247–254.
127 Bourne N, Stanberry LR, Kern ER, Holan G, Matthews B, Bernstein DI. Dendrimers, a new class of candidate topical microbicides with activity against herpes simplex virus infection. *Antimicrob. Agents Chemother.* 2000; **44**: 2471–2474.
128 Gong E, Matthews B, McCarthy TD, Chu J, Holan G, Raff J, Sacks S. Evaluation of dendrimer SPL7013, a lead microbicide candidate against herpes simplex viruses. *Antivir. Res.* 2005; **68**: 139–146.
129 McCarthy TD, Karellas P, Henderson SA, Giannis M, O'Keefe DF, Heery G, Paull JR, Matthews BR, Holan G. Dendrimers as drugs: discovery and preclinical and clinical development of dendrimer-based microbicides for HIV and STI prevention. *Mol Pharm* 2005; **2**: 312–318.
130 Rupp R, Rosenthal SL, Stanberry LR. VivaGel (SPL7013 Gel): a candidate dendrimer – microbicide for the prevention of HIV and HSV infection. *Int. J. Nanomedicine* 2007; **2**: 561–566.
131 Tarallo R, Carberry T, Falanga A, Vitiello M, Galdiero S, Galdiero M, Weck M. Dendrimers functionalized with membrane-interacting peptides for viral inhibition. *Int. J. Nanomedicine* 2013; **8**.

CHEMISTRY
A EUROPEAN JOURNAL

ChemPubSoc
Europe

DOI: 10.1002/chem.201202358

Dendrimer Functionalization with a Membrane-Interacting Domain of Herpes Simplex Virus Type 1: Towards Intracellular Delivery

Tom P. Carberry,[a] Rossella Tarallo,[b] Annarita Falanga,[b] Emiliana Finamore,[c] Massimiliano Galdiero,[c] Marcus Weck,*[a] and Stefania Galdiero*[b]

Abstract: A poly(amide)-based dendrimer was synthesized and functionalized with the membrane-interacting peptide gH(625–644) (gH625) derived from the herpes simplex virus type 1 (HSV-1) envelope glycoprotein H, which has previously been shown to assist in delivering large cargoes across the cellular membrane. We demonstrate that the attachment of the gH625 peptide sequence to the termini of a dendrimer allows the conjugate to penetrate into the cellular matrix, whereas the unfunctionalized dendrimer is excluded from translocation. The peptide-functionalized dendrimer is rapidly taken into the cells mainly through a non-active translocation mechanism. Our results suggest that the presented peptidodendrimeric scaffold may be a promising material for efficient drug delivery.

Keywords: click chemistry · delivery · dendrimers · membrane translocation · peptides

Introduction

Crossing of the cellular membranes remains a major obstacle for the delivery of therapeutics.[1] The aqueous extra- and intracellular matrices are separated by a hydrophobic lipid bilayer, which acts as a barrier separating the cellular components from the extracellular milieu. Although small molecules and ions can diffuse across this barrier, large conjugates with molecular weight over 500 amu are generally excluded from simple diffusion into the cell.[2] Larger molecules can be taken up endocytically, which allows them to exist in the cell. However, the molecule is still separated from the cytoplasm by an endosomal lipid bilayer.[3] In addition to size, membrane permeability is dependent on the hydrophilicity or lipophilicity of the molecule in question.[2] Even the delivery of a potent drug can be foiled due to its insolubility in either the aqueous cell environment or the lipid membrane. These problems can be alleviated by complexation to a macromolecular conjugate which assists the cargo's solubility and permeability into desired areas.[4] Indeed, there are several recent reports of successful intracellular delivery of macromolecular conjugates, which release their cargo through biological triggers (e.g., pH changes or enzymatic cleavage).[5]

However, as many macromolecular drug conjugates are internalized via active translocation mechanisms, for example, endocytosis, they can exhibit poor activity due to the cargo being unable to escape the endosome before lysosomal degradation occurs.[1,3,4] Certain peptide sequences have been shown to efficiently cross the cellular membrane.[6] These cell-penetrating peptides (CPPs) are useful for the transport of larger macromolecules across the membrane.[7] Many CPPs act by an endocytic mechanism, trapping the conjugate in an endosome.[8]

Our approach is based on a membrane-interacting peptide that operates through a different internalization mechanism. In particular, we are interested in viral peptides, such as those derived from the herpes simplex virus type 1 (HSV-1). These peptides are capable of internalizing cargo by inducing membrane perturbation.[9] HSV-1 uses four glycoproteins, glycoproteins B (gB), D (gD), H (gH), and L (gL), to mediate the viral–cell fusion and subsequent infection.[10] We have previously reported that HSV-1 gH contains several domains that are mostly hydrophobic, suggesting that these regions are those that interact with cellular membranes.[11] One of these domains, His625–Phe644 (gH625), showed great effectiveness in inducing lipid mixing of large unilamellar vesicles (LUVs), showing its membrane-interacting potential. These results suggest that this sequence could be important in the interaction of viruses with cells.[11–12] Figure 1 shows the sequence of this peptide. When folded into an α helix, nonpolar residues tend to concentrate on one side of the helix giving the peptide an amphiphilic

[a] T. P. Carberry, Prof. Dr. M. Weck
Molecular Design Institute and Department of Chemistry
New York University, New York, NY 10003 (USA)
Fax: (+1) 212-995-4895
E-mail: marcus.weck@nyu.edu

[b] R. Tarallo, Dr. A. Falanga, Prof. Dr. S. Galdiero
Dipartimeno di Scienze Biologiche
Università di Napoli "Federico II"
Via Mezzocannone 16, Napoli 80134 (Italy)
Fax: (+39) 081-253-6642
E-mail: sgaldier@unina.it

[c] Dr. E. Finamore, Prof. Dr. M. Galdiero
Dipartimento di Medicina Sperimentale
Seconda Università degli Studi di Napoli
Via de Creccio 7, Napoli 80138 (Italy)

Supporting information for this article is available on the WWW under http://dx.doi.org/10.1002/chem.201202358.

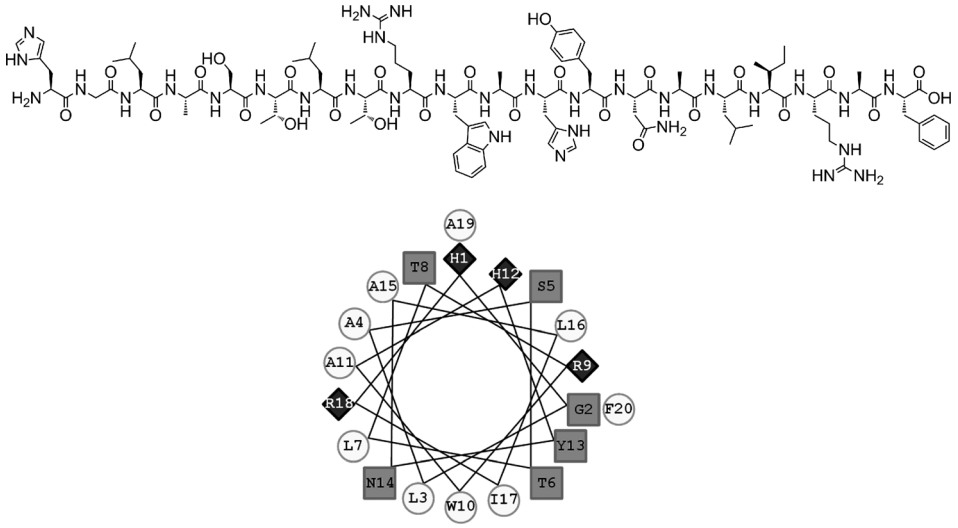

Figure 1. Top: sequence of the gH625 peptide. Bottom: helical wheel projection of gH625. Nonpolar residues are signified by circles, uncharged polar residues by squares, and basic residues by diamonds.

character. We have described the use of this peptide for membrane translocation and delivery of quantum dots into cells.[13] These studies also showed that gH625 is nontoxic to cells up to a concentration of 400 μM. Beyond this concentration, gH625 was less toxic than the commonly used Tat peptide. We further analyzed the properties of this peptide by attaching it to liposomes. The conjugated liposomes could successfully be used to deliver doxorubicin to cells, showing that the peptide is able to deliver larger cargoes inside cells.[14]

Liposomes are just one of the many scaffolds used to deliver drugs to cells.[15] Other widely used scaffolds include micelles,[16] nanoparticles,[17] and dendrimers.[18] The benefits and drawbacks of each have been reviewed previously.[18a,19] Unlike many other scaffolds, however, dendrimers have the benefit of a highly controlled synthesis as well as yielding a single monodisperse compound, giving perfect control over the size, weight, and terminal functionalities of the resulting structure. Moreover, highly branched structures generally exhibit longer blood circulation times due to their inability to reptate through renal pores.[20] Dendrimers have been shown to have extended lifetimes, in vivo,[21] whereas lipid complexes are usually rapidly cleared from circulation by splenic and hepatic phagocytes.[22]

Dendrimers are perfectly branched macromolecules with well-defined structures.[23] They exhibit different properties to linear polymers with the same composition and molecular weight.[18a] The high concentration of terminal functional groups on a dendrimer's surface will generally dictate the solubility of the entire compound; dendrimers have been used as unimolecular micelles, that is, hydrophobic dendrimers, that are water soluble due to peripheral hydrophilic groups or vice versa.[24] Traditional dendrimers are synthesized from monomers with the structure AB_n.[25] Addition of another generation of monomers causes the dendrimer to grow radially with an exponential increase in both mass and number of free termini compared to the previous generation, but only a minimal increase in the physical size of the structure. This causes the termini to become more closely packed.

Dendrimers represent a very promising tool for drug delivery, combining the advantageous features of nanoparticles (ideal size as in vivo carriers, multivalency), polymeric materials (low cost, tunable properties, biocompatibility) and small molecules (monodispersity and detailed control of their properties).[18a,26] Little information is available on the mechanism of dendrimer uptake and intracellular trafficking.[27] Studies performed on PAMAM dendrimers[28] and PAMAM dendrimers functionalized with the CPP, Tat,[29] indicate that endocytosis mechanisms contribute to the internalization and intracellular trafficking. Some reports show that the cellular internalization mechanism of PAMAM dendrimers can be tuned by altering surface charges or hydrophobicity, but these uptake mechanisms are still mainly endocytic.[30] Other reports show that dendrimers can successfully deliver cargoes when terminated by guanidinyl units;[31] however, in one case, it was shown that adding the Tat peptide failed to enhance delivery efficiency over the native PAMAM dendrimer.[29] Studies using cationic PAMAM dendrimers, showed that they tend to insert into the lipid bilayer, which has the potential of weakening or forming holes in the membrane.[32]

Our goal is to combine the benefits of dendrimer chemistry with a cell-internalization unit that can cross the cell membrane mainly via a non-active translocation mechanism. Here we present the synthesis of a dendrimer containing terminal peptide chains, and follow its cell uptake, in vitro. Our dendrimers are poly(amide)-based following the 1→3 connectivity scheme first reported by Newkome and co-workers.[33] We chose these materials since poly(amide)-based dendrimers have been shown to exhibit both high biocompatibility, due to the peptide-like backbone,[34] and low to no toxicity to cells.[35] In order to attach the desired peptides to the dendrimer scaffold, we synthesized a derivative of gH635 containing a propargylglycine (PrA) residue to introduce an alkynyl handle. Our synthetic scheme involves the synthesis of a monofunctional dendrimer with azide termini, to which the peptides could be coupled by copper-catalyzed azide–alkyne cycloaddition (CuAAC). The structure of peptidodendrimer **1**, the poly(amide) dendrimer terminated by gH625 peptides, is shown in Figure 2.

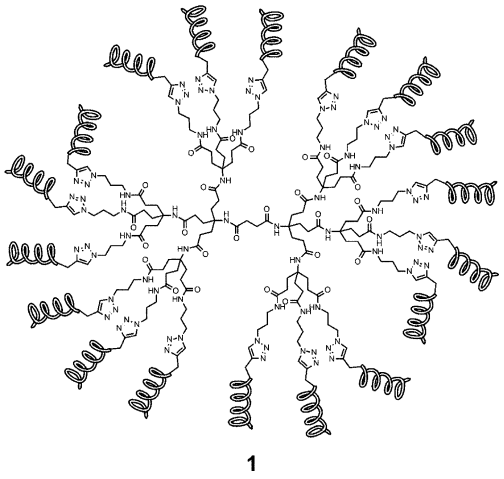

Figure 2. Structure of peptidodendrimer **1**. The helices represent the gH625 peptide sequence.

Results and Discussion

Synthesis of the octadecaazide dendrimer: The second generation Newkome-style dendron **2** was first functionalized at the amine terminus with succinic anhydride to afford the hemisuccinate dendron **3**. Coupling dendrons **2** and **3** by using 2-[7-aza-1*H*-benzotriazol-1-yl]-1,1,3,3-tetramethyluronium hexafluorophosphate (HATU) as coupling agent afforded the symmetrical dendrimer **4**. Acidic deprotection of the terminal *tert*-butyl esters resulted in the formation of the octadecaacid dendrimer **5**. Reaction between the terminal carboxylic acid groups and an azido-terminated amine linker afforded the octadecaazide dendrimer **6** (Scheme 1).

Functionalization of the dendrimer: The gH625 peptide sequence was synthesized with a propargylglycine residue (PrA) at the C terminus to provide a handle for the CuAAC reaction. Functionalization of **6** was performed in a water/methanol solution (1:1 v/v) by using $CuSO_4 \cdot 5H_2O$ as catalyst and sodium ascorbate as reducing agent (Scheme 2). The complete functionalization of peptidodendrimer **1** was confirmed by determining the amount of peptide attached by UV analysis ($\lambda_{gH625} = 7000\,M^{-1}cm^{-1}$ at $\lambda = 280$ nm)[11] and comparing this to the amount of dendrimer initially used for reaction (18 mol peptide per mol dendrimer). IR analysis showed the disappearance of the azide stretch at 2098 cm^{-1} confirming that within the instrumental error range, all azides were consumed, thus suggesting complete functionalization of the dendrimer with peptides was obtained (see the Supporting Information). The functionalization was also performed by using the same peptide containing a nitrobenzofurazan fluorescent tag (**1–NBD**) and an alkynyl fluorophore (**7**). All sequences used for functionalization are shown in Table 1. Functionalization of dendrimer **7** was also confirmed by UV/Vis spectroscopy ($\lambda_{NBD} = 1696\,M^{-1}cm^{-1}$ at $\lambda = 452$ nm; see the Supporting Information).

Structure of the peptidodendrimer: As previously reported,[11] the gH625 peptide adopts a random coil in aqueous

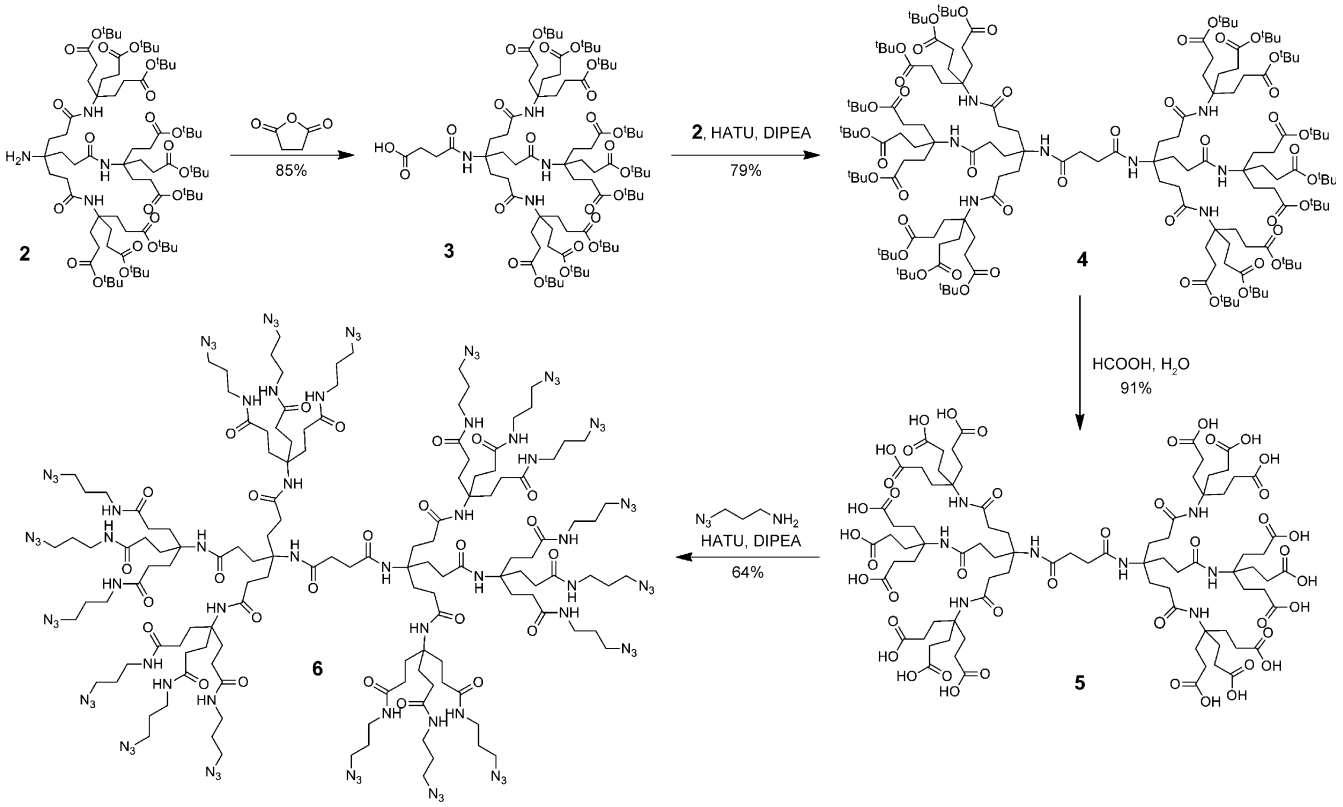

Scheme 1. Synthesis of the azide-terminated dendrimer used in this study.

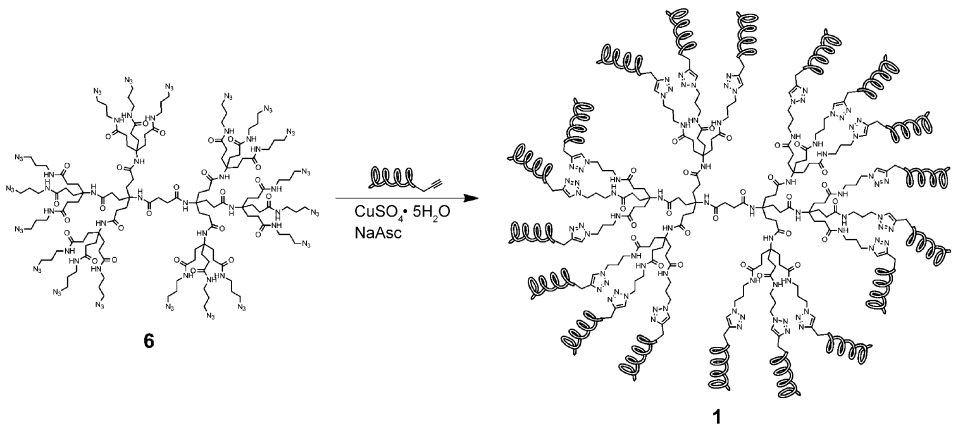

Scheme 2. Functionalization of dendrimer **6** by CuAAC reaction. Shown is the functionalization with gH625 to synthesize **1**.

Table 1. Sequences used to functionalize dendrimer **6**.

Name	Sequence[a]	Compound
gH625	NH_2-HGLASTLTRWAHYNALIRAFX-CONH	**1**
gH625–NBD	NBD-HGLASTLTRWAHYNALIRAFX-$CONH_2$	**1–NBD**
NBD–CCH	NBD-$CH_2C\equiv CH$	**7**

[a] X = propargylglycine, NBD = (7-nitrobenzofurazanyl)amino.

media, but forms an α helix in membrane-mimetic environments. Circular dichroism (CD) spectra in several percentages of trifluoroethanol (TFE, allowing the solution to mimic the environment of the membrane) show that gH625 at a concentration of 8 μM adopts an α helix (Figure 3A). The CD spectra of the peptidodendrimer at a peptide concentration of 8 μM (18 peptides per dendrimer; concentration of dendrimer = 0.4 μM) exhibited a shape indicative of an α helix, suggesting that the secondary structure of the peptide was not disturbed by attachment to a dendrimer (Figure 3B).

The size of peptidodendrimer **1** increased greatly upon the addition of the peptide sequences. Dendrimer **6** is too small to be accurately resolved by most techniques, but the increase in size after the addition of the peptides makes it resolvable by light scattering and non-optical microscopy techniques. Dynamic light scattering (DLS) measurements were complicated by significant aggregation, most likely due to the dendrimer's relatively hydrophobic terminal peptides in aqueous solution. At low concentrations, a signal was observed corresponding to a hydrodynamic radius of 5.6-(±1.5) nm (see the Supporting Information). This was confirmed by scanning transmission electron microscopy (STEM), which gave an average particle diameter of 12.66-(±0.82) nm (see the Supporting Information).

Fusogenic properties of the peptidodendrimer: Peptide gH625 has been previously characterized,[12b,13] indicating its strong interaction with LUVs, although the exact mechanism of interaction awaits complete understanding. We have previously shown that gH625 penetrates into the membrane, but the peptide does not form pores inside the bilayer. Here, in order to understand the membrane interacting behavior of the peptide when linked to the dendrimer, we performed lipid mixing, inner-monolayer fusion, and leakage experiments as indicators of the interaction and perturbation of the lipid membrane caused by the peptidodendrimer (Figure 4).

After establishing the size and degree of functionalization of our peptide dendrimers, we carried out lipid-mixing experiments (Figure 4A). For these studies, a population of 55:45 phosphatidylcholine/cholesterol (PC/Chol) LUVs labeled with nitrobenzoxadiazole- and rhodamine-phosphatidylethanolamine (NBD-PE and Rho-PE) was mixed with a population of unlabeled LUVs, and increasing amounts of gH625, dendrimer **6**, or peptidodendrimer **1** were added. Dilution of the fluorescently labeled vesicles by membrane fusion induced a reduction in the fluorescence energy transfer efficiency, hence dequenching of

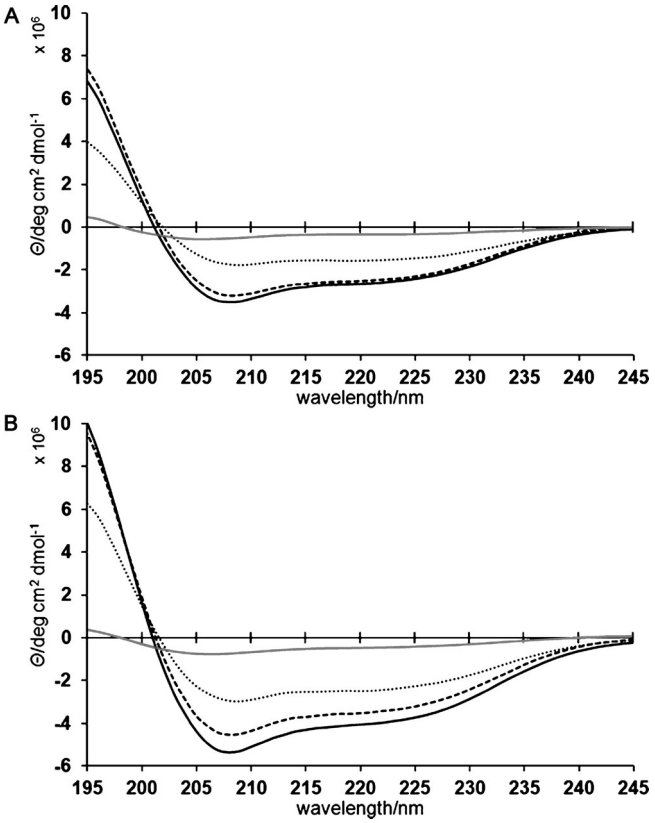

Figure 3. CD spectra of: A) peptide gH625, and B) peptidodendrimer **1** at 8 μM (8 μM peptide corresponds to a dendrimer concentration of 0.4 μM) in aqueous solution with varying amounts of TFE: 0% (——), 20% (••••), 40% (----), 60% (——).

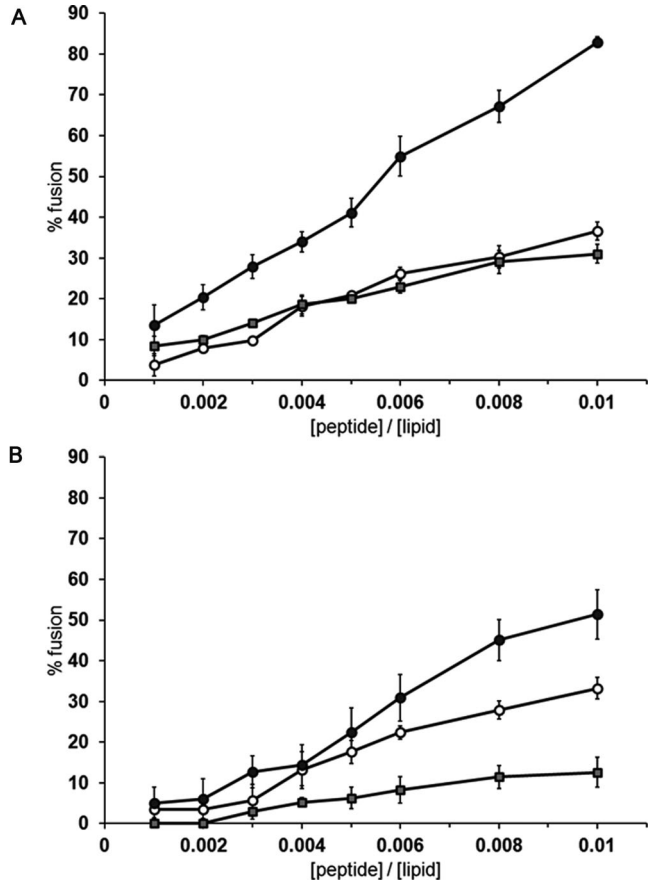

Figure 4. Interaction of peptide gH625 (filled squares), dendrimer **6** (open circles), and peptidodendrimer **1** (filled circles) with PC/Chol LUVs; the dose dependence is reported according to the concentration of the peptides (18 peptides per dendrimer) and each trace represents an average of three independent experiments. A) Lipid-mixing, B) inner-monolayer assays.

the donor fluorescence. In order to compare data, the percentage of lipid mixing as a function of the peptide to lipid molar ratio was calculated. The peptide and **6** induced low levels of fusion at the concentration at which **1** induced high levels of fusion. In particular, we observed a significant increase of activity with the peptidodendrimer system. This shows that the peptidodendrimer is even more effective than the native peptide at interacting with and fusing lipid membranes, showing its efficacy as a membrane-perturbing agent.

In the inner-monolayer fusion assay, the fluorescence from the vesicle membranes' outer monolayer is eliminated by the addition of an aqueous reducing agent, and this experiment reveals the extent of lipid mixing between the inner monolayers of vesicles in solution. Figure 4B shows that gH625, **6**, and **1** show only slightly lower inner-monolayer fusion than the total fusion observed from the lipid-mixing experiment. This indicates that under these experimental conditions, all three compounds were able to induce fusion significantly to both the inner and outer lipid monolayers; ergo, we can confirm that the peptide, dendrimer, and peptidodendrimer are all able to interact strongly with and penetrate inside the lipid bilayer.

A contents-mixing assay was employed to monitor any mixing of internal vesicle components as a result of vesicle exposure to the peptide or the peptidodendrimer **1**. Release of ANTS (1-aminonaphthalene-3,6,8-trisulfonate) and DPX (*p*-xylene-bispyridinium bromide) from the vesicle is commonly used as a measure of bilayer perturbation and is interpreted as "transient pore formation".[36] Contents-mixing is manifested by a decrease in fluorescence intensity if vesicles encapsulating the fluorescent cargo (e.g., ANTS) merge contents with those containing quenchers (e.g., DPX). No contents-mixing occurs under the same conditions and peptide/lipid ratio range at which substantial outer monolayer lipid-mixing was observed (data not shown); this corroborates the presence of vesicle hemifusion within our system not only for the peptide alone but also for the peptide–dendrimer system.

The present results can be used as qualitative indicators of the peptidodendrimer translocation or bilayer perturbation, with relevance for the direct penetration mode of cell entry, or for the steps of endosomal membrane translocation or endosomal escape. Using peptidodendrimer **1**, we have not detected any significant pore formation; vesicle fusion events were not accompanied by leakage of the aqueous contents of the vesicle as was previously reported for gH625 and for other peptides.[13,37]

Flow cytometry measurements: We have determined the fraction of the labeled peptide gH625–NBD and labeled peptidodendrimer **1–NBD** taken up by HeLa cells using flow cytometry based on a method previously introduced by McIntyre and Sleight to measure the transbilayer distribution of NBD–phospholipid analogues.[38] The distribution was determined by comparing the fluorescence intensity before and after addition of sodium dithionite, an essentially membrane impermeant molecule, which suppresses irreversibly the fluorescence of the accessible NBD moiety localized on the external cell surface.

We incubated the peptide and the peptidodendrimer with HeLa cells at 37 °C at different concentrations (1, 5, 10, and 20 μM in peptide). After 1 h incubation, we measured the quenching of the NBD by dithionite treatment. The dithionite reaction was performed at low temperature (4 °C) because the dithionite crossing of biological membranes is strongly reduced compared to high temperatures.[39] Before the addition of dithionite, we observed that approximately 90 % of peptide gH625–NBD or **1–NBD** was not washed away, suggesting they were internalized or bound to the membrane bilayer. After the addition of dithionite, the fluorescence of the internalized peptide and **1–NBD** were slightly reduced (Figure 5A). Increasing the dithionite concentration did not result in a modification of the extent of quenching, indicating that the entire accessible NBD label was quenched by 1 M dithionite (data not shown). To exclude the possibility that the fluorescence signal could have been due to the internalization of the fluorochrome itself, the NBD

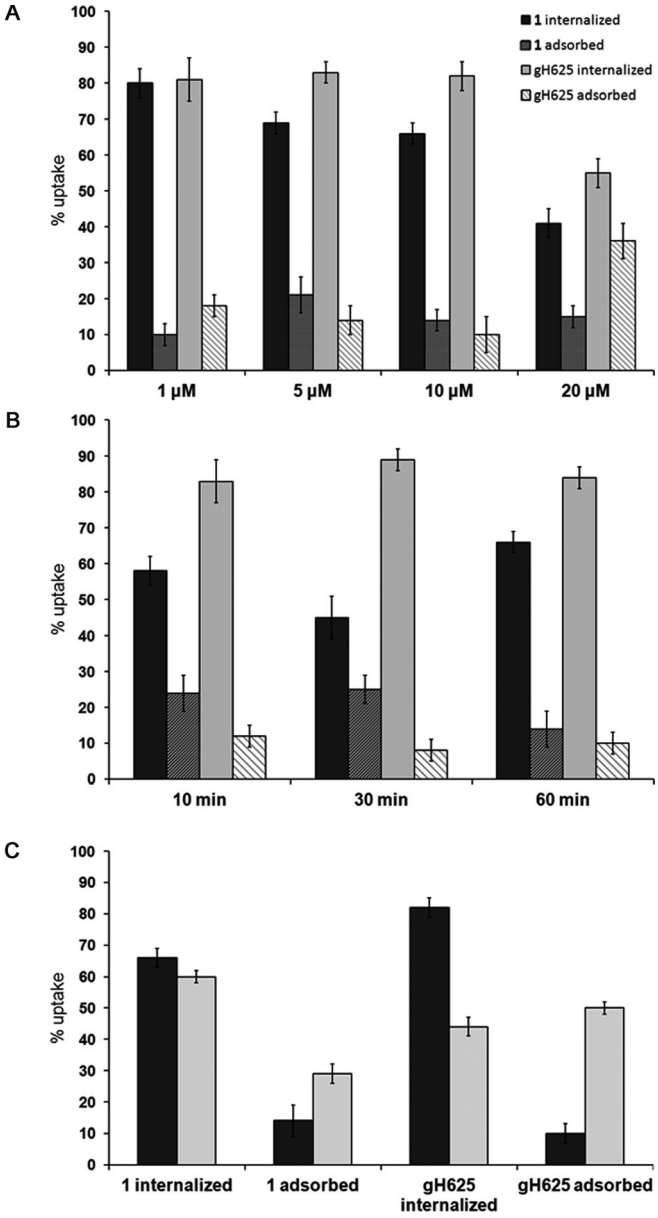

Figure 5. Percentage uptake graphs of peptidodendrimer **1**–**NBD** versus gH625–NBD in HeLa cells under various conditions: A) 1 h incubation with various concentrations of peptide; B) incubation at 10 μM (in peptide) for various times; C) incubation at 10 μM (in peptide) for 15 min at various temperatures; ■: 37 °C, ■: 4 °C.

moiety was used in the same in vitro assay conditions; no cellular fluorescence was observed at concentrations up to 20 μM.

To measure the kinetics of import into cells, we incubated gH625–NBD and **1**–**NBD** with cells at 37 °C for 10, 30, and 60 min, and then determined the remaining fluorescence following treatment with dithionite. Figure 5B shows the fraction of molecules taken up by cells. The uptake is very rapid and seems to reach a plateau after 1 h incubation.

The influence of temperature on the intracellular accumulation was studied to investigate whether the uptake depended on a passive translocation mechanism or an active process. We incubated gH625–NBD and **1**–**NBD** with HeLa cells at both 37 °C and 4 °C; the amounts of internalized peptide and **1** at low temperature (Figure 5C) are reduced for both molecules with an increase in the amount bound to the membrane and a decrease of the internalized quantity. The reduction of internalized or bound molecule was less significant for **1**, indicating a minor involvement of active mechanisms of internalization.

Fluorescence microscopy studies: The cellular uptake ability of **1** was explored by incubating an aqueous solution of **1** with live cells (Figure 6). HeLa cells were incubated for 2 h with a 20 μM solution of the fluorescently labeled **1**–**NBD** (concentration relative to peptides; concentration of dendrimer = 1.1 μM). After incubation, excess fluorophore was washed away and the cells were imaged. The cells exhibited fluorescence even after being washed, suggesting that the NBD-labeled dendrimer was interacting with the cellular membranes. Control experiments against dendrimer **7**, containing the fluorophore but no peptide, showed extremely little fluorescence in the cells, suggesting the peptides were required for efficient membrane interaction.

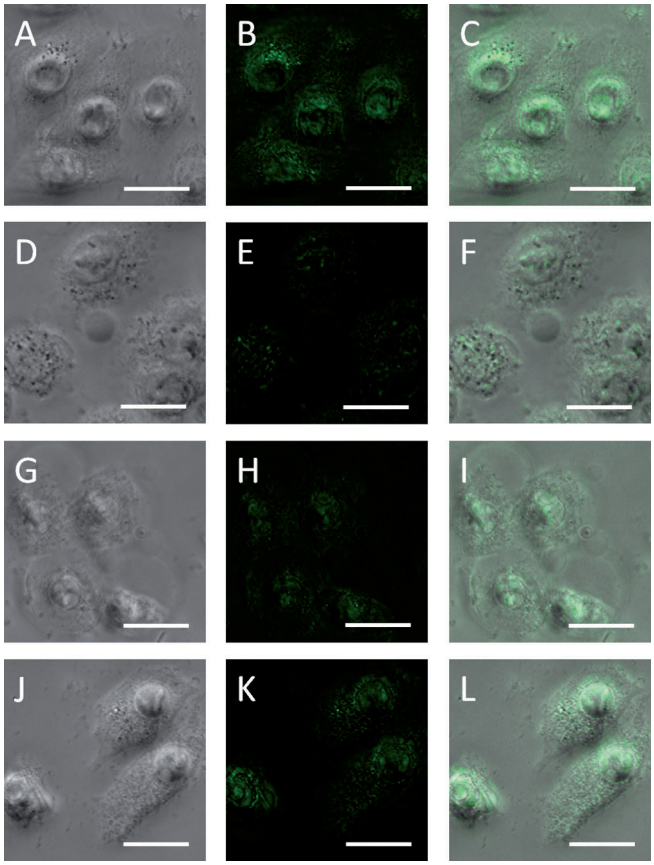

Figure 6. Fluorescence microscopy images from the cellular uptake study. A)–C) Incubation at 37 °C with peptidodendrimer **1** (20 μM) for 2 h; D)–F) incubation at 37 °C with dendrimer **7** (20 μM) for 2 h; G)–I) incubation at 4 °C with peptidodendrimer **1** (20 μM) for 15 min; J)–L) same as (A–C), but after preincubating the cells with NaN_3 (40 μM) for 30 min. A), D), G), J) Transmission images; B), E), H), K) fluorescence images; C), F), I), L) overlay; scale bars: 20 μm.

In order to explore the mechanism of interaction, the cellular uptake studies were also performed under conditions that inhibit active translocation mechanisms. First, incubation was carried out with the 20 μM (in peptide) peptidodendrimer solution for 15 min at 4 °C. At 4 °C, the cells are almost unable to take up the dendrimers endocytically. The fluorescence intensity of the cells was decreased but still observed, suggesting that the compound is able to enter into cells without undergoing an active translocation mechanism (Figure 6 G). The cells were also incubated with **1** after pre-incubation with sodium azide (40 μM), which is a known inhibitor of oxidative phosphorylation.[40] After this pre-incubation, the cells were unable to produce ATP in the membrane and to perform endocytosis. Again, the cells were able to fluoresce after this pre-incubation, suggesting that **1** can enter the cells through a non-active mechanism (Figure 6 J).

We also incubated the cells with the 20 μM (in peptide) solution of **1–NBD** for different lengths of time to observe the uptake kinetics. As we showed with the flow cytometry measurements, the cells exhibited fluorescence as early as 30 min after addition, showing the rapid uptake of the peptidodendrimer (Figure 7).

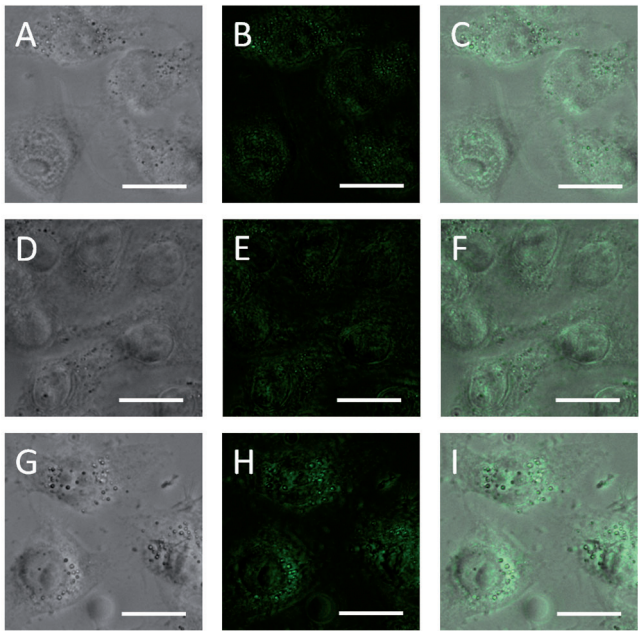

Figure 7. Fluorescence microscopy images from the cellular uptake kinetic study, incubating with dendrimer **1–NBD** (20 μM) at 37 °C for various times: A)–C) 30 min; D)–F) 1 h; G)–I) 2 h; A), D), G) transmission images; B), E), H) fluorescence images; C), F), I) overlay; scale bars: 20 μm.

Conclusion

We have synthesized a peptidodendrimeric scaffold that has the potential to be used as a cellular delivery platform. The dendrimer is able to enter the cells due to the attachment of the gH625 peptide at the termini. The peptide, derived from herpes simplex virus type I, does not rely on heavily positively charged residues (Arg, Lys) for translocation. Previously Kang et al. reported the failure of Tat to enhance the intracellular delivery of PAMAM dendrimers, which they attributed to the highly positive charges of both the dendrimer and the peptide.[29] Our dendrimer is made in a facile and scalable synthesis, and can be functionalized efficiently. We showed that the peptidodendrimer is able to fully fuse liposomes, even more significantly than the peptide alone; moreover, it is able to do so without inducing leakage of vesicles.

These data further support the view that the mechanism of lipid–peptide association plays a key role in the translocation activity. The gH625 cellular uptake is associated with its ability to interact with membrane lipids and to form a transient helical structure that temporarily affects membrane organization, thereby facilitating insertion into the membrane and translocation.

The cellular uptake of the peptidodendrimer was measured by flow cytometry and fluorescence microscopy. After 1 h of incubation with HeLa cells at 37 °C and 4 °C, most of the gH625 functionalized dendrimer **1** was localized intracellularly. The internalization in HeLa cells can occur at 37 °C, and to a lesser extent at 4 °C, supporting the view that the internalization mechanism does not involve entirely endocytosis. The kinetics of internalization is rapid and reaches a plateau after 1 h. We confirmed, by fluorescence microscopy, that indeed the peptidodendrimer is inside the cells. Our studies have shown that not only is a dendrimer functionalized with the gH625 peptide sequence an effective vehicle for intracellular delivery it can do so via a passive translocation mechanism. This allows the cargo to be released directly into the intracellular milieu as opposed to being entrapped in endosomes, from which the cargo might not be able to escape before lysosomal degradation.

Experimental Section

Peptide functionalization of dendrimer: A 1:1 methanol/water solution of peptide gH625–PrA (660 μL, 30.33 equiv), an aqueous solution of $CuSO_4 \cdot 5H_2O$ (10 μL, 1.46 mM, 1 equiv), and an aqueous solution of sodium ascorbate (50 μL, 1.17 mM, 4 equiv) were added to dendrimer **6** (50 μg, 0.0146 μmol) in a 1:1 water/methanol solution (280 μL). The mixture was stirred, overnight. Then, the mixture was concentrated and purified by size-exclusion chromatography. Peptides **1** and **1–NBD** were obtained in quantitative yield. IR (cast on poly(ethylene)): $\tilde{\nu} = 3295, 1658, 1545, 1471, 1203\ cm^{-1}$. No peak at $2098\ cm^{-1}$ was observed. CD: 208 nm; UV/Vis (water): $\lambda_{max} = 193, 273$ nm. Synthesis of dendrimer **7**, due to its poor solubility, was performed in a 1:1 mixture of THF/H_2O as solvent, and purification was carried out by dialysis (1000 MWCO) against 1:1 water/methanol. Yield: approximately 20%; UV/Vis (MeOH): $\lambda_{max} = 452$ nm.

Acknowledgements

We thank the National Science Foundation (CHE-0234863, CHE-0958457, CHE-01162222, DMR-0923251) and New York University for

support of analytical equipment. We also thank Professor Lara K. Mahal, Tomasz Kurcon, and Dr. Francesca Gruppi (NYU) for assistance with the cell uptake studies. This work was supported by Progetto FARO (Prot. 2012-0043756) and New York University.

[1] V. P. Torchilin, *Annu. Rev. Biomed. Eng.* **2006**, *8*, 343–375.
[2] C. A. Lipinski, F. Lombardo, B. W. Dominy, P. J. Feeney, *Adv. Drug Delivery Rev.* **1997**, *23*, 3–25.
[3] L. M. Bareford, P. W. Swaan, *Adv. Drug Delivery Rev.* **2007**, *59*, 748–758.
[4] R. Duncan, *Nat. Rev. Drug Discovery* **2003**, *2*, 347–360.
[5] a) R. J. Amir, L. Albertazzi, J. Willis, A. Khan, T. Kang, C. J. Hawker, *Angew. Chem.* **2011**, *123*, 3487–3491; *Angew. Chem. Int. Ed.* **2011**, *50*, 3425–3429; b) Y. E. Kurtoglu, M. K. Mishra, S. Kannan, R. M. Kannan, *Int. J. Pharm.* **2010**, *384*, 189–194.
[6] a) K. M. Stewart, K. L. Horton, S. O. Kelley, *Org. Biomol. Chem.* **2008**, *6*, 2242–2255; b) C. Foged, H. M. Nielsen, *Expert Opin. Drug Delivery* **2008**, *5*, 105–117.
[7] a) E. Vivès, P. Brodin, B. Lebleu, *J. Biol. Chem.* **1997**, *272*, 16010–16017; b) A. M. Angeles-Boza, A. Erazo-Oliveras, Y.-J. Lee, J.-P. Pellois, *Bioconjugate Chem.* **2010**, *21*, 2164–2167.
[8] H. Brooks, B. Lebleu, E. Vivès, *Adv. Drug Delivery Rev.* **2005**, *57*, 559–577.
[9] S. Galdiero, M. Vitiello, A. Falanga, M. Cantisani, N. Incoronato, M. Galdiero, *Curr. Drug Metab.* **2012**, *13*, 93–104.
[10] P. G. Spear, R. Longnecker, *J. Virol.* **2003**, *77*, 10179–10185.
[11] S. Galdiero, A. Falanga, M. Vitiello, H. Browne, C. Pedone, M. Galdiero, *J. Biol. Chem.* **2005**, *280*, 28632–28643.
[12] a) S. Galdiero, A. Falanga, M. Vitiello, L. Raiola, R. Fattorusso, H. Browne, C. Pedone, C. Isernia, M. Galdiero, *J. Biol. Chem.* **2008**, *283*, 29993–30009; b) S. Galdiero, A. Falanga, M. Vitiello, L. Raiola, L. Russo, C. Pedone, C. Isernia, M. Galdiero, *J. Biol. Chem.* **2010**, *285*, 17123–17136.
[13] A. Falanga, M. Vitiello, M. Cantisani, R. Tarallo, D. Guarnieri, E. Mignogna, P. Netti, C. Pedone, M. Galdiero, S. Galdiero, *Nanomedicine* **2011**, *7*, 925–934.
[14] R. Tarallo, A. Accardo, A. Falanga, D. Guarnieri, G. Vitiello, P. Netti, G. D'Errico, G. Morelli, S. Galdiero, *Chem. Eur. J.* **2011**, *17*, 12659–12668.
[15] K. Maruyama, *Adv. Drug Delivery Rev.* **2011**, *63*, 161–169.
[16] E. Gravel, J. Ogier, T. Arnauld, N. Mackiewicz, F. Ducongé, E. Doris, *Chem. Eur. J.* **2012**, *18*, 400–408.
[17] S. M. Janib, A. S. Moses, J. A. MacKay, *Adv. Drug Delivery Rev.* **2010**, *62*, 1052–1063.
[18] a) C. C. Lee, J. A. MacKay, J. M. J. Fréchet, F. C. Szoka, *Nat. Biotechnol.* **2005**, *23*, 1517–1526; b) R. Esfand, D. A. Tomalia, *Drug Discovery Today* **2001**, *6*, 427–436; c) K. Sadler, J. P. Tam, *Rev. Mol. Biotechnol.* **2002**, *90*, 195–229; d) M. J. Cloninger, *Curr. Opin. Chem. Biol.* **2002**, *6*, 742–748; e) P. Niederhafner, J. Šebestík, J. Ježek, *J. Pept. Sci.* **2005**, *11*, 757–788; f) R. K. Tekade, P. V. Kumar, N. K. Jain, *Chem. Rev.* **2009**, *109*, 49–87.
[19] L. Huynh, C. Neale, R. Pomès, C. Allen, *Nanomedicine* **2012**, *8*, 20–36.
[20] M. E. Fox, F. C. Szoka, J. M. J. Fréchet, *Acc. Chem. Res.* **2009**, *42*, 1141–1151.
[21] H. Kobayashi, M. W. Brechbiel, *Curr. Pharm. Biotechnol.* **2004**, *5*, 539–549.
[22] J.-S. Zhang, F. Liu, L. Huang, *Adv. Drug Delivery Rev.* **2005**, *57*, 689–698.
[23] G. R. Newkome, C. N. Moorefield, F. Vögtle, *Dendrimers and Dendrons: Concepts, Synthesis Applications*, Wiley-VCH, Weinheim, **2001**.
[24] a) S. Stevelmans, J. C. M. van Hest, J. F. G. A. Jansen, D. A. F. J. van Boxtel, E. M. M. de Brabander-van den Berg, E. W. Meijer, *J. Am. Chem. Soc.* **1996**, *118*, 7398–7399; b) M. Liu, K. Kono, J. M. J. Fréchet, *J. Controlled Release* **2000**, *65*, 121–131.
[25] a) C. Hawker, J. M. J. Fréchet, *J. Chem. Soc. Chem. Commun.* **1990**, 1010–1013; b) G. R. Newkome, C. D. Shreiner, *Polymer* **2008**, *49*, 1–173; c) C. Ornelas, M. Weck, *Chem. Commun.* **2009**, 5710–5712.
[26] E. R. Gillies, J. M. J. Fréchet, *Drug Discovery Today* **2005**, *10*, 35–43.
[27] M. Najlah, A. D'Emanuele, *Curr. Opin. Pharmacol.* **2006**, *6*, 522–527.
[28] F. P. Seib, A. T. Jones, R. Duncan, *J. Controlled Release* **2007**, *117*, 291–300.
[29] H. Kang, R. DeLong, M. H. Fisher, R. L. Juliano, *Pharm. Res.* **2005**, *22*, 2099–2106.
[30] a) A. Saovapakhiran, A. D'Emanuele, D. Attwood, J. Penny, *Bioconjugate Chem.* **2009**, *20*, 693–701; b) L. Albertazzi, M. Serresi, A. Albanese, F. Beltram, *Mol. Pharmaceutics* **2010**, *7*, 680–688; c) K. M. Kitchens, A. B. Foraker, R. B. Kolhatkar, P. W. Swaan, H. Ghandehari, *Pharm. Res.* **2007**, *24*, 2138–2145.
[31] a) K. Huang, B. Voss, D. Kumar, H. E. Hamm, E. Harth, *Bioconjugate Chem.* **2007**, *18*, 403–409; b) I. Tsogas, Z. Sideratou, D. Tsiourvas, T. A. Theodossiou, C. M. Paleos, *ChemBioChem* **2007**, *8*, 1865–1876; c) C. V. Bonduelle, E. R. Gillies, *Pharmaceuticals* **2010**, *3*, 636–666.
[32] a) P. E. S. Smith, J. R. Brender, U. H. N. Dürr, J. Xu, D. G. Mullen, M. M. Banaszak Holl, A. Ramamoorthy, *J. Am. Chem. Soc.* **2010**, *132*, 8087–8097; b) I. Tsogas, D. Tsiourvas, G. Nounesis, C. M. Paleos, *Langmuir* **2006**, *22*, 11322–11328.
[33] G. R. Newkome, K. K. Kotta, C. N. Moorefield, *J. Org. Chem.* **2005**, *70*, 4893–4896.
[34] J. C. Roberts, M. K. Bhalgat, R. T. Zera, *J. Biomed. Mater. Res.* **1996**, *30*, 53–65.
[35] C. Ornelas, R. Pennell, L. F. Liebes, M. Weck, *Org. Lett.* **2011**, *13*, 976–979.
[36] a) H. Ellens, J. Bentz, F. C. Szoka, *Biochemistry* **1984**, *23*, 1532–1538; b) R. A. Parente, S. Nir, F. C. Szoka, *Biochemistry* **1990**, *29*, 8720–8728.
[37] P. E. G. Thorén, D. Persson, P. Lincoln, B. Nordén, *Biophys. Chem.* **2005**, *114*, 169–179.
[38] J. C. McIntyre, R. G. Sleight, *Biochemistry* **1991**, *30*, 11819–11827.
[39] C. Angeletti, J. W. Nichols, *Biochemistry* **1998**, *37*, 15114–15119.
[40] G. Drin, S. Cottin, E. Blanc, A. R. Rees, J. Temsamani, *J. Biol. Chem.* **2003**, *278*, 31192–31201.

Received: July 2, 2012
Published online: September 11, 2012

NANO MICRO small

Drug Delivery

Shuttle-Mediated Nanoparticle Delivery to the Blood–Brain Barrier

Daniela Guarnieri, Annarita Falanga, Ornella Muscetti, Rossella Tarallo, Sabato Fusco, Massimiliano Galdiero, Stefania Galdiero, and Paolo A. Netti**

***M**any therapeutic drugs are excluded from entering the brain due to their lack of transport through the blood–brain barrier (BBB). The development of new strategies for enhancing drug delivery to the brain is of great importance in diagnostics and therapeutics of central nervous diseases. To overcome this problem, a viral fusion peptide (gH625) derived from the glycoprotein gH of Herpes simplex virus type 1 is developed, which possesses several advantages including high cell translocation potency, absence of toxicity of the peptide itself, and the feasibility as an efficient carrier for delivering therapeutics. Therefore, it is hypothesized that brain delivery of nanoparticles conjugated with gH625 should be efficiently enhanced. The surface of fluorescent aminated polystyrene nanoparticles (NPs) is functionalized with gH625 via a covalent binding procedure, and the NP uptake mechanism and permeation across in vitro BBB models are studied. At early incubation times, the uptake of NPs with gH625 by brain endothelial cells is greater than that of the NPs without the peptide, and their intracellular motion is mainly characterized by a random walk behavior. Most importantly, gH625 peptide decreases NP intracellular accumulation as large aggregates and enhances the NP BBB crossing. In summary, these results establish that surface functionalization with gH625 may change NP fate by providing a good strategy for the design of promising carriers to deliver drugs across the BBB for the treatment of brain diseases.*

1. Introduction

Neurological disorders contribute significantly to the global burden of disease and are likely to increase in the coming years due to an aging population; thus, significant efforts have been devoted towards the development of improved therapies for central nervous system (CNS) diseases. However, despite these efforts, treatments remain limited due to the inability of therapeutic agents to effectively cross the blood-brain barrier (BBB).[1] The BBB is a dynamic barrier protecting the brain against invading organisms and unwanted substances; thus, the BBB is a formidable obstacle to the effective delivery

Dr. D. Guarnieri, Dr. O. Muscetti, Dr. S. Fusco, Prof. P. A. Netti
Center for Advanced Biomaterials for Health Care@CRIB
Istituto Italiano di Tecnologia, Largo Barsanti e Matteucci 53
80125 Napoli and Interdisciplinary Research Centre on
Biomaterials (CRIB) University of Naples Federico II
Piazzale Tecchio 80, 80125 Napoli, Italy
E-mail: nettipa@unina.it

Dr. A. Falanga, Dr. R. Tarallo, Prof. S. Galdiero
Department of Biological Sciences
Division of Biostructures and Centro Interuniversitario
di Ricerca sui Peptidi Bioattivi - University of
Naples "Federico II"
Via Mezzocannone 16, 80134, Napoli, Italy
E-mail: sgaldier@unina.it

Prof. M. Galdiero
Department of Experimental Medicine - II University of Naples
Via De Crecchio 7, 80138, Napoli, Italy

DOI: 10.1002/smll.201201870

of drugs to the CNS and poses a major challenge to drug development efforts. Therefore, the development of effective strategies to enhance drug delivery to the brain, that is, the availability of a drug at its site of action in the brain for sufficient time to exert its biological effect, is the ultimate aim of any CNS clinical and pharmaceutical program.

Most strategies to transport pharmaceutical compounds inside the CNS causes disruption of the anatomical texture of the BBB, therefore impairing its natural function. Effective delivery approaches should be cautiously assessed considering their impact on the overall protective function of the BBB. It is now well-known that there are several invasive or non-invasive transport routes by which brain drugs cross the BBB.[2] The invasive approaches consist of a temporary disruption of the BBB allowing the entry of a drug into the CNS or the direct drug delivery by means of intraventricular or intracerebral administration[3] while the non-invasive ones involve the systemic application of colloidal drug carriers undergoing a receptor or adsorptive mediated transcytosis mechanism[4] or the passing of the BBB via intranasal delivery.[5] In particular, targeted delivery of a therapeutic cargo to the intended site of action in the brain appears to be one of the most promising noninvasive approach to overcome the BBB, combining the advantages of brain targeting, high incorporation capacity, reduction of side effects and circumvention of the multidrug efflux system.[6]

Nanocarriers (linear and hyperbranched polymers, dendrimers, liposomes, micelles, niosomes and cyclodextrins)[7] are an emerging class of drug delivery systems that can be easily tailored to deliver drugs to various compartments of the body, including the brain. Nanocarriers possess unique features due to their size and the possibility of being functionalized with multiple copies of the drug molecule of interest. In particular, they allow the transport of a range of drugs, therefore modification of nanocarrier surface properties ensues. These properties make nanocarriers an attractive alternative to existing methods for transporting drugs across the BBB. Despite a large variety of nanocarriers developed so far for cellular internalization, it is noteworthy that only amphiphilic molecule-formed liposomes and polymeric nanoparticles have been extensively exploited for brain drug delivery.[8] Several of those systems are now in clinical trials mainly for anticancer drug delivery.

An essential role for nanoparticles is to help drugs gaining increased water stability, better pharmacokinetics, reduced toxicity and improved therapeutic efficacy.[9] Because of nanoparticles versatility, diagnostic and therapeutic drugs can be either physically encapsulated or covalently conjugated to nanoparticles. In this context, the conjugation of therapeutic molecules to shuttles that can cross the BBB and thus carry drugs into the brain emerges as an attractive alternative. A key mechanism to further enhance nanoparticle delivery is to improve their transport by modification of their surface with bioactive peptides such as cell-penetrating peptides (CPPs).

CPPs are a group of relatively short peptides (5–40 amino acids) deriving either from natural sources or from synthetically designed constructs, that are able to penetrate cell membranes and transport a large variety of cargo molecules/materials inside cells.[10] While individual CPPs differ in length and sequence, they all share some common features, which include their amphipathic nature, net positive charge, theoretical hydrophobicity and helical moment, the ability to interact with lipidic membranes, and to adopt a distinct secondary structure upon association with lipids.[11] The general application of CPPs in cellular delivery has been hampered by the controversy regarding the uptake mechanism used by these peptides. The major dogma has been that CPPs enter cells by a receptor and energy-independent process although the exact mechanism is not yet fully understood; but it is now evident that for most CPPs, endocytosis is an almost exclusive mechanism of internalization. By following this pathway, cargos transported by CPPs, such as therapeutic molecules or functionalized nanoparticles, may experience lysosomal pH (around 5), which can strongly accelerate drug degradation, and/or nanoparticle accumulation within late endosomes by making less effective the transport of nanoparticles through the BBB.

Although several studies demonstrate the effectiveness of CPPs, such as TAT,[12] in promoting the transport of nanoparticles across the BBB, the compelling need of enhancing delivery to the brain makes it essential to exploit novel molecules which use different internalization mechanisms. Moreover, the controversy regarding the mechanism of action and the growing number of peptides with cell-penetrating properties has increased the challenge. Recently, great attention has been devoted to the study of hydrophobic peptides that efficiently traverse biological membranes, promoting lipid membrane-reorganizing processes, such as fusion or pore formation and thus involving temporary membrane destabilization and subsequent reorganization.[13]

The nineteen residues peptide gH625, was previously identified as a membrane-perturbing domain in the glycoprotein gH of *Herpes simplex* virus type I;[14] gH625 interacts with biological membranes, contributing to the merging of the viral envelope and the cellular membrane; it is able to traverse the membrane bilayer and to transport a cargo into the cytoplasm.[15] We already reported the ability of the peptide gH625 to transport quantum dots inside the cytoplasm in an efficient way and only partially involving endocytic pathways.[15a]

Here we report the effect of gH625 on the penetration of 100 nm polystyrene nanoparticles (NPs) through an in vitro BBB model based on bEnd3, an immortalized mouse cerebral endothelial cell line.

We demonstrated that, by opportunely modifying surface properties, it is possible to change the fate of nanoparticles. In particular, we verified that gH625 conjugation enhances nanoparticles transport across the BBB, thereby enhancing the CNS bioavailability of an eventual drug. This study holds importance for treatment of brain infections and tracking of nanoparticles in vivo, a step closer to the development of a clinically applicable nanocarrier for treatment as well as monitoring brain related disorders.

2. Results and Discussion

2.1. Characterization of Peptide-Conjugated Nanoparticles

To verify the secondary structure of the peptide bound to the nanoparticles we performed circular dichroism (CD)

small 2012,
DOI: 10.1002/smll.201201870

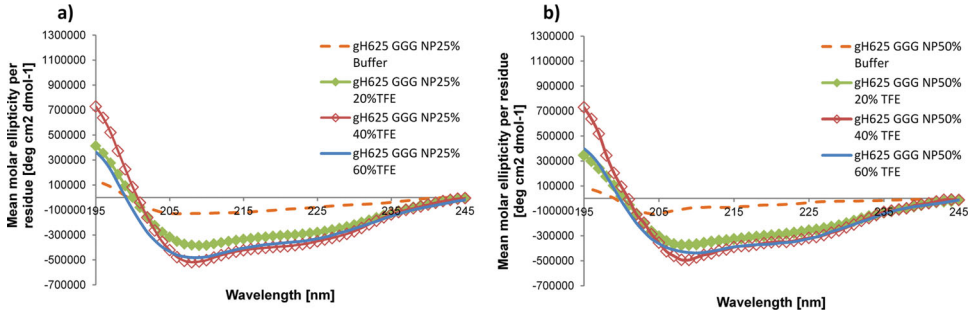

Figure 1. Circular dichroism spectra of polystyrene NPs at 25% (a) and 50% (b) degrees of functionalization with gH625 peptide.

experiments. CD data confirmed that gH625 retains its structure (helical) when bound to the nanoparticle surface as previously reported also for other peptides.[16] The spectra obtained at different percentages of functionalization indicate an helical structure in all conditions (**Figure 1**A,B).

To further investigate the effect of the peptide functionalization (25, 35, and 50%) on the size of nanoparticles, we performed dynamic light scattering (DLS) measurements. After functionalization, the hydrodynamic size of nanoparticles with 25, 35, and 50% of gH625 in aqueous medium at pH 7 was found to be respectively 96.68 ± 0.43 nm, 95.64 ± 0.19 nm and 96.76 ± 0.07 nm, with polydispersity values of ca. 0.08, indicating a narrow distribution of the particle size at the pH used for all the experiments (**Table 1**).

To elucidate the colloidal stability of functionalized nanoparticles at different pH values, which is a crucial parameter correlated to their functionalization, measurements of the zeta potential and of the hydrodynamic radius (D_H) were carried out (Table 1). For NPs alone, the colloidal stability is strongly pH-dependent because it is mainly due to electrostatic repulsion between particles. It is widely accepted that at high values of z-potential (over 30 mV, positive or negative) the electrostatic interactions between particles are strong enough for electrostatic stability, while at intermediate values of z-potential, near their isoelectric point, particles can flocculate. Table 1 shows both z-potential and mean hydrodynamic diameter of blank NPs and NPs at different degrees of functionalization as a function of pH. In presence of peptide, the D_H of the functionalized NPs remained nearly constant over the entire pH range, with no sign of aggregation in spite of the lower values of the zeta potential observed at pH 8. Such a behavior highlights that their stabilization is via steric hindrance rather than electrostatic repulsion. In particular, by increasing the percentage of functionalization NPs zeta potential increases from about +30 mV to +35 mV at pH 7. At these zeta potential values, NPs D_H remains nearly about 100 nm. Only at pH 8, we observed a lower zeta potential for 25% functionalized NPs, indicating that in this condition the functionalized nanoparticles are still partially aggregated and their behavior is similar to non-functionalized NPs.

These data indicate that the peptide bound to the NPs is able to retain its helical structure in all the conditions tested and is able to completely prevent NPs aggregation at 35 and 50% of functionalization.

2.2. Effect of gH625 Peptide Conjugation on NP Intracellular Trafficking

We previously demonstrated that the conjugation of the peptide gH625 enhances cellular uptake of quantum dots[15a]

Table 1. Zeta potential and size measurements of pure NPs and NPs at different degrees of functionalization as a function of pH.

	pH	pH 4	pH 7	pH 8	pH 9
NP	ζ potential [mV][a)]	44.9 ± 5.26	51.6 ± 1.08	−11.1 ± 0.60	−32 ± 1.22
	Size [d.nm][a)]	106.5 ± 2.52	137 ± 1.19	848.4 ± 48.33	473.6 ± 1.81
	PDI	0.18	0.31	0.25	0.30
NP-gH625 25%	ζ potential [mV][a)]	33.13 ± 1.11	30.77 ± 2.40	10.93 ± 0.76	−33.33 ± 1.36
	Size [d.nm][a)]	242.3 ± 1.39	96.58 ± 0.43	103.37 ± 1.14	231.77 ± 6.67
	PDI	0.25	0.08	0.13	0.28
NP-gH625 35%	ζ potential [mV][a)]	34.13 ± 2.42	30.9 ± 0.79	18.43 ± 0.91	−33.17 ± 1.07
	Size [d.nm][a)]	114.93 ± 1.40	95.64 ± 1.09	96.27 ± 0.67	99.92 ± 0.50
	PDI	0.14	0.08	0.08	0.10
NP-gH625 50%	ζ potential [mV][a)]	33.83 ± 1.98	35.1 ± 2.43	17.77 ± 0.76	−28.03 ± 1.82
	Size [d.nm][a)]	102.1 ± 0.36	96.76 ± 0.07	97.53 ± 0.20	99.65 ± 0.70
	PDI	0.12	0.09	0.09	0.10

[a)]Mean value ±SD, n = 3.

DOI: 10.1002/smll.201201870

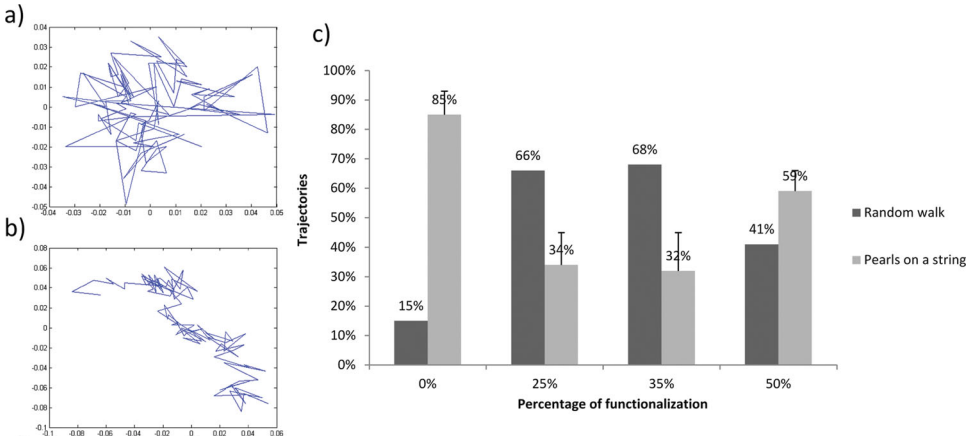

Figure 2. MPT analysis of blank and gH625-NPs. Examples of "random walk" (a) and "pearls on a string" (b) trajectories. c) Percentage of "random walk" and "pearls on a string" trajectories as a function of functionalization degree.

and liposomes[15b] in HeLa cells in vitro. However, no evidences of the effect of gH625 on nanoparticle uptake in brain endothelial cells have been previously reported. Moreover, the exact mechanism used by gH625 to facilitate cargos transport through cell membranes has not yet been understood in details. Therefore, in this work we studied the effect of gH625 on polystyrene NP uptake mechanisms on mouse brain endothelial bEnd3 cells.

We first tested the cytotoxicity of blank NP and gH625-NP on bEnd3 cell line by Alamar Blue Assay and we verified that blank NPs and gH625-NPs at 50% functionalization did not affect cell viability in the experimental condition used for the assay compared to non-treated control cells (data not shown).

Once internalized, NPs can follow different fates: i.e., particle degradation inside lysosomal compartments, accumulation in other organelles, recycling to the plasma membrane or transcytosis to the basal surface of endothelium. Furthermore, the routes of NP intracellular trafficking might give some indications not only about the fate of NP, but also about the mechanisms driving cellular uptake.[17] To address this issue, multiple particle tracking (MPT) gives a strong contribution compared to traditional techniques (spectroscopy, microscopy, etc.).[18] In particular, MPT technique can provide quantitative (diffusivity and velocity) and qualitative (transport mode and directionality) information of internalized NPs, by evaluating the time-resolved trajectories of tens of NPs. Therefore, in order to study the effect of NP surface functionalization with gH625 on NP internalization mechanism, we followed and analyzed their intracellular motion. **Figure 2** shows a snapshot of the detected trajectories generated by MPT routines. By shape, trajectories can already be split in two different types: i) Brownian-like trajectories, suggesting NPs random movement between cytosolic structures, and ii) pearls-on-a-string trajectories, derived by a combination of random and linear walk, indicative of motor protein facilitated transport, mediated by endocytic vesicles and motor proteins.[19] Evaluating the time dependence of mean square displacement (MSD) of each tracked NP we classified the particles transport mechanisms into diffusive and super-diffusive motion. In particular, to perform NPs diffusive mode classification we evaluated the exponent of each fitting MSD curve by the equation described in the Methods section.

Particle trajectories revealed a substantial heterogeneity in particle intracellular dynamics, both for blank NPs and gH625-NPs. However, for blank NPs, most trajectories resulted in a combination of random and linear walk with a pearls-on-a-string trajectory, indicative of motor protein facilitated transport, mediated by endocytic vesicles (Figure 2). Whereas, only a lower percentage of blank NPs appeared to follow a purely diffusive behavior (random walk), suggesting no particular interaction between NPs and cytosolic structures (Figure 2).

Conversely, in presence of peptide functionalization, we observed that most trajectories showed a random walk behavior while a lower percentage resulted in a pearls-on-a-string trajectory. In particular, this behavior is more evident at lower percentages of functionalization with an optimum at 35% peptide functionalization degree.

These data suggest that the effect of the peptide could depend on its concentration/density on the NP surface. In fact, we theoretically estimated the surface density of peptide of about 3, 4, and 6 peptides/nm^2 for 25%, 35% and 50% functionalized NPs, respectively. We hypothesized that a lower peptide surface density (3 and 4 peptides/nm^2) could promote the correct peptide orientation and interaction with membrane lipids. Conversely, a higher peptide surface density (6 peptides/nm^2) hinders the correct orientation of peptide aminoacidic residues and their interaction with cell membrane. Indeed, recently, we structurally characterized gH625 peptide in a membrane-mimicking DPC micellar environment to gain insight into how gH fuses with the cell membrane.[20] We reported a model of gH625 peptide structure and orientation indicating that both electrostatic and hydrophobic interactions work in concert to mediate membrane penetration. In particular, the function of the aromatic residues is to cause the peptide insertion into the membrane interface while the basic residues stabilize this interaction by linking the negatively charged headgroups as shown in other systems using both NMR[21] and EPR.[22]

small 2012,
DOI: 10.1002/smll.201201870

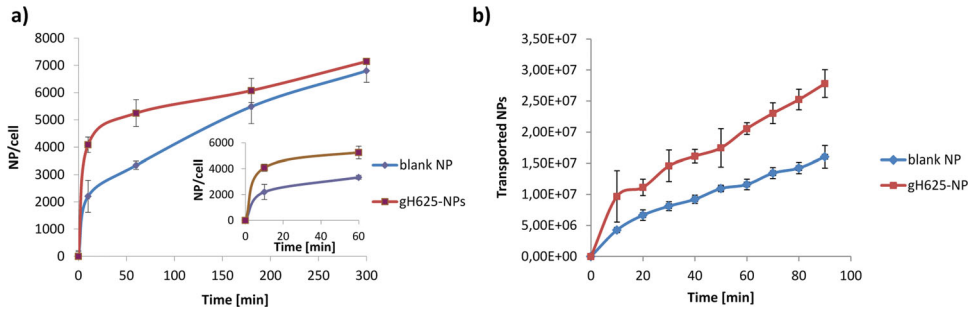

Figure 3. Uptake kinetics of blank and 35% functionalized gH625-NPs in bEnd3 cells (a). Effect of peptide functionalization in NP crossing of a confluent bEnd3 cell monolayer (b).

Since we observed that the 35% functionalized NPs showed a good stability in aqueous suspension and the ability to penetrate cells using a random walk behavior, we performed all the other experiments at this percentage of functionalization.

2.3. Uptake Kinetics and in vitro BBB Crossing of Peptide-Conjugated NPs

To study the effect of surface functionalization with gH625 on NPs internalization, we performed NP uptake experiments. **Figure 3**A shows that after 10 minutes of incubation, both functionalized and blank NPs were internalized by bEnd3 cells and the number of internalized nanoparticles increases as a function of incubation time. However, the amount of internalized gH625-NPs is higher than blank NPs and this effect is more evident at early time of NP uptake kinetic. While after longer incubation time the amount of internalized NPs is quite similar, probably due to the saturation of the uptake mechanism mediated by the gH625 peptide.

bEnd3 cells are able to form a confluent monolayer that mimics permeability properties of primary culture models of early passages.[23] We tested the ability of gH625 peptide to enhance NPs crossing of a bEnd3 confluent monolayer. Data reported in Figure 3B show that gH625-NPs cross more efficiently the endothelial layer than blank NPs. More precisely, the permeability (P) of the monolayer was $(0.43 \pm 0.02) \times 10^{-6}$ cm/s for gH625-NPs, almost two fold higher than P value reported for blank-NPs ($(0.24 \pm 0.02) \times 10^{-6}$ cm/s)(**Table 2**). These data are in agreement with cell uptake kinetic results. In fact, by focusing at early incubation time, also the uptake rate of peptide-conjugated NPs was approximately double compared to blank NPs (see the insert in Figure 3A). Moreover, no changes in BSA-TRITC permeability were observed after exposure to both blank and gH625-NPs, indicating that these NPs did not perturb the integrity of the cell monolayer in the experimental conditions used for the assay (data not shown).

Table 2. Permeability values of BBB in vitro model to blank and gH625-functionalized NP.

	Permeability [$\times 10^{-6}$ cm/s] (±SD, n = 5)
NP	0.24 ± 0.02
gH625-NP	0.43 ± 0.02

2.4. Uptake Mechanisms of Peptide-Conjugated NPs

Nanoparticles usually enter the cells using a cell-mediated mechanism, called endocytosis. After endocytosis, endosomes can fuse with lysosomes or can deliver their cargo across the cell by transcytosis processes. Several works reported that caveolae are involved in the endocytosis and transcytosis processes in brain endothelial cells.[24] Thus, in order to study if the nanoparticle functionalization with gH625 could affect the mechanisms of NP internalization, we performed confocal microscope analyses to investigate the colocalization of NPs with lysosomes and caveolae in absence of peptide and with 35% of peptide functionalization. **Figure 4** shows that both blank and gH625-NPs partially colocalized with lysosomes. However, the percentage of colocalization was about 4.68% for blank NPs and 0.62% for gH625-NPs. On the other hand, concerning caveolin1, a molecular marker for caveolar structures, no colocalization of gH625-NPs was observed, while blank NPs showed 0.74% of colocalization. These data indicate that the peptide could change the mechanism of nanoparticle uptake by inducing an alternative penetration pathway. To further investigate this issue, we treated cells with cytochalasin D that inhibits macropynocytosis by disrupting microfilaments. Results demonstrate that the uptake of blank NPs was drastically reduced after cytochalasin D treatment (**Figure 5**A–F). On the other hand, gH625-NPs uptake was almost not affected by microfilament depolymerization (Figure 5G–L). Indeed, confocal microscope z-sectioning analysis demonstrate that the most part of gH625-NPs were inside the cells and only a small amount (less than 30%) was just adsorbed on cell membrane (Figure 5M). Moreover, quantitative analysis of NP uptake showed a decrease of about 85% and 15% for blank-NP and gH625-NP uptake, respectively, after cytochalasin D treatment (Figure 5N). Taken all together these data indicate that blank NPs might enter the cells mainly by macropinocytosis. Conversely, gH625-NPs could use a different mechanism to cross cell membrane.

Previous works demonstrated that gH625 peptide shows a particular tropism for lipidic membranes, which is

DOI: 10.1002/smll.201201870

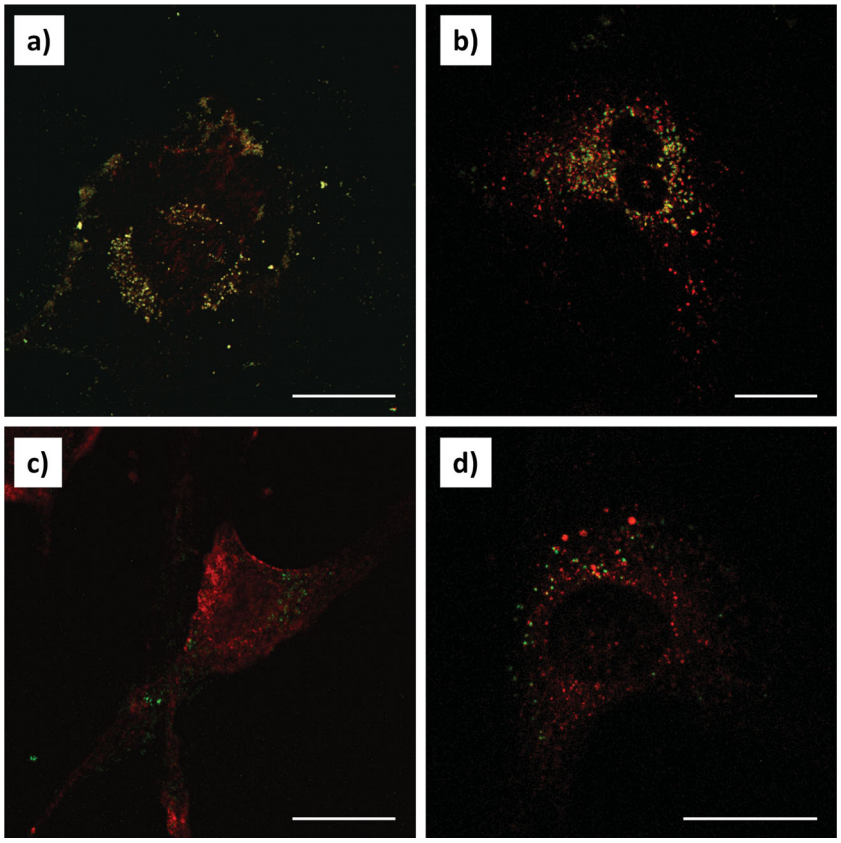

Figure 4. Colocalization of non-functionalized (a,b) and gH625-functionalized (c,d) NPs with caveolae (a,c) and lysosomes (b,d) after 24h incubation in bEnd3 cells. Green: NPs; red: caveolin1 and lysotracker. Magnification bar: 20 µm.

strongly dependent on its amphipathic nature.[14a,14d,14e] Thus, we hypothesized that the presence of the peptide on the NP surface could enhance its interaction with the cell membrane and promote NPs passage through cell membranes. To verify this hypothesis, scanning electron microscopy (SEM) analyses were performed. SEM micrographs showed that, after 5 min of incubation, a high number of gH625-NPs was visible on the cell surface (**Figure 6**A,B). Conversely, very few blank NPs were present on the cell surface and some of these formed small aggregates (Figure 6C,D). SEM results suggest a different interaction of gH625-NPs with cell membrane compared to blank-NPs. Moreover, accordingly to cell uptake kinetics (Figure 3), these observations indicate a better and more rapid adsorption of gH625-NPs on cell membrane, compared to blank-NPs after 10 min incubation, probably due to the membrane tropism of the peptide and, thus, an enhancement of gH625-NP internalization.

In order to understand if the different behavior of gH625-NPs implied a different intracellular fate of NPs, we performed transmission electron microscopy (TEM) analyses. **Figure 7** shows

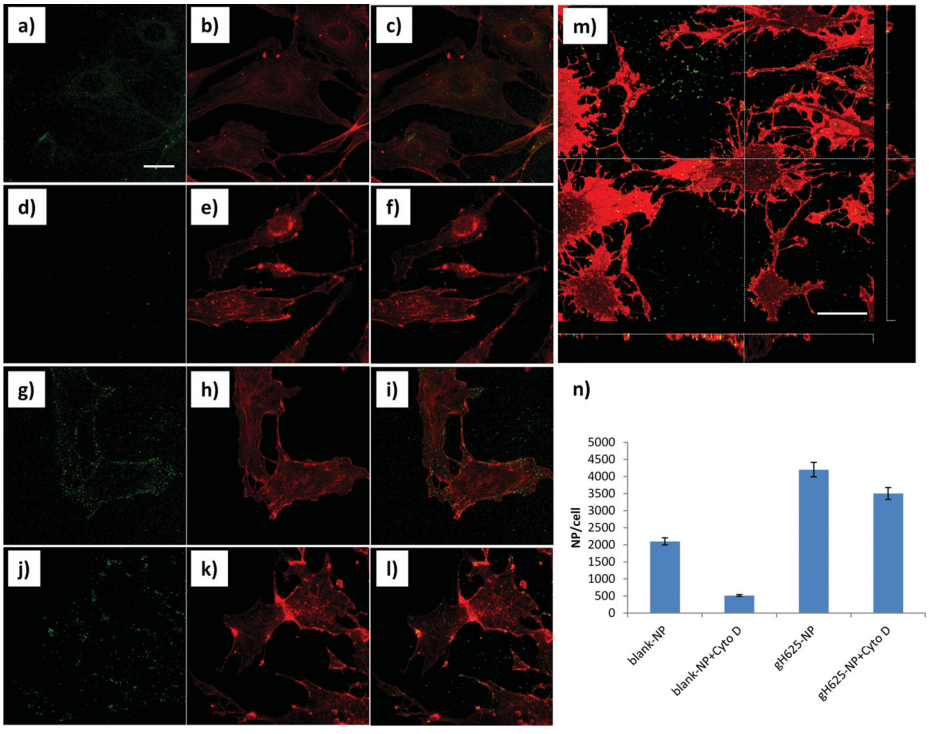

Figure 5. Cytochalasin D treated bEnd3 cells incubated with blank NPs (d–f) and gH625-NPs (j–m) for 10 min at 37°C. Non-treated control cells incubated with blank NPs (a–c) and gH625-NPs (g–i) for 10 min at 37°C. Nanoparticles (a,d,g,j); phalloidin stained microfilaments (b,e,h,k); merge (c,f,i,l). Green fluorescent nanoparticles and red fluorescent WGA stained cell membrane confocal z-sectioning (m). Section thickness: 0.2 µm. Z-stack size: 10 µm. Magnification bar: 20 µm.

small 2012,
DOI: 10.1002/smll.201201870

NANO MICRO small

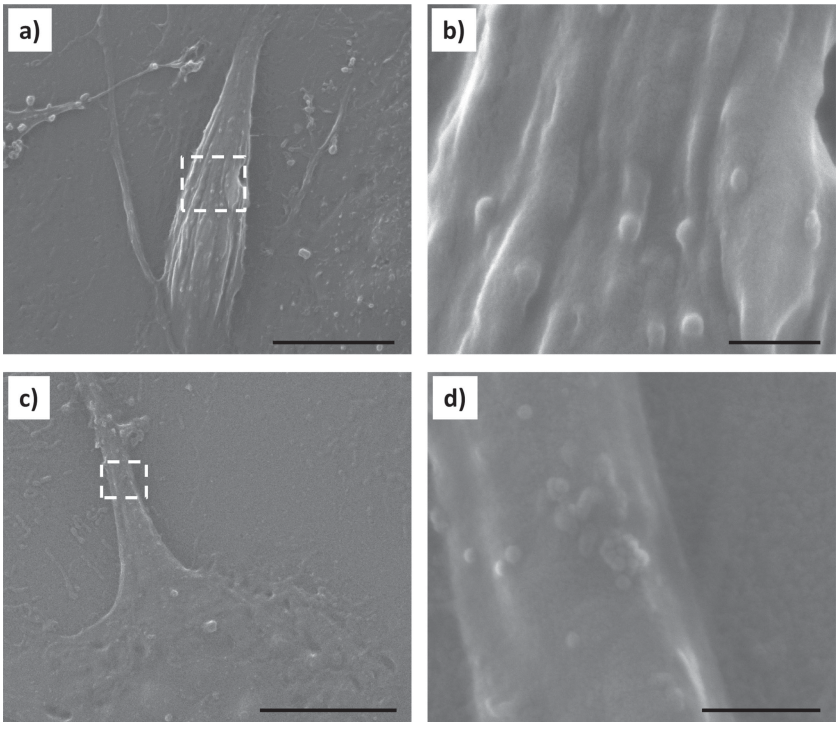

Figure 6. SEM micrographs of bEnd3 cells incubated with gH625-NPs (a,b) and blank NPs (c,d) for 5 min at 37 °C. Dashed squares in panels (a,c) indicate the zoomed areas shown in panels (b,d). Magnification bar: 10 µm (a,c) and 1 µm (b,d).

TEM micrographs of gH625-NPs and blank NPs after 24 h incubation with bEnd3 cells. Inside the cells, gH625-NPs were organized in very small aggregates of 3-4 particles within the cytoplasm, mainly localized in vesicular structures, probably early endosomes (Figure 7A) and multi-vesicular bodies (MVBs) (Figure 7C). On the other hand, for blank-NPs, many and larger aggregates associated to vesicular structures within the cytoplasm were observed (Figure 7B–D). Furthermore, no gH625- or blank-NPs were localized in the nucleus.

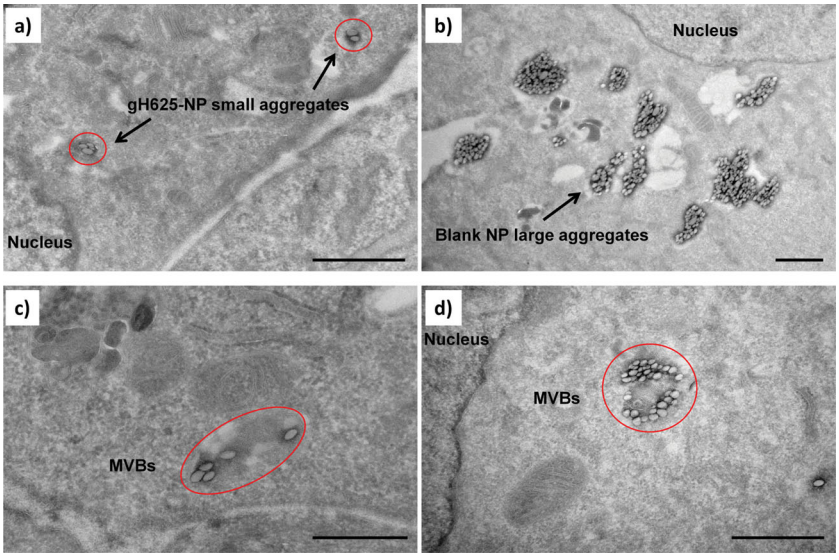

Figure 7. TEM micrographs of bEnd3 cells incubated 24 h with gH625-NPs (a,c) and blank NPs (b,d) at 37 °C. Magnification bar: 1 µm.

For obtaining deeper details on the intracellular distribution of gH625-NPs, we followed the formation and the growth of gH625- or blank-NP aggregates with time by a confocal microscope image analysis. **Figure 8** shows gH625- and blank-NP aggregates within bEnd3 cell cytoplasm after 10 min and 24 h incubation. At early times, gH625-NPs formed a huge number of small aggregates (Figure 8A,E). Moreover, by increasing the incubation time, the average size of the aggregates remained almost unchanged (Figure 8B,E). Conversely, for blank NPs, at early times, the average size of aggregates increased with time indicating that these NPs tend to accumulate in the cell (Figure 8C,D,F).

Taken altogether, these observations demonstrate a different behavior between gH625- and blank-NPs. In particular, NP conjugation with gH625 peptide changes NP destination by reducing their accumulation and promoting NP escape/exit from the cell. However, further investigations are needed to better understand which intracellular compartments gH625-NPs are localized in and what the intracellular pathways are followed by these functionalized NPs that dictate their fate.

3. Conclusion

The aim of the present work was to verify if synthetic peptides derived from viral membranotropic sequences can be used successfully to deliver biologically active substances inside the BBB in order to pose the basis for developing new effective strategies for drug delivery into the brain. The HSV gH-derived-peptide was covalently bonded with polystyrene nanoparticles and investigated for the ability to translocate through the BBB in an in vitro model. The functionalized nanoparticles were thoroughly characterized using a variety of complementary techniques to gain a better understanding of their properties and showed that gH625-NPs only slightly modified the particle sizes with a z-potential indicative of colloidal stability at pH 7. gH625-NPs translocated efficiently across cell membranes and cell internalization does not seem to exclusively involve classical endocytosis mechanisms. In fact, conjugation with the gH625 facilitated the delivery of nanoparticles across the BBB, leading to significant higher cell uptake and crossing. To the best of our knowledge, the gH625 represent a cell translocation motif never reported before in a BBB in vitro analysis and could be applied

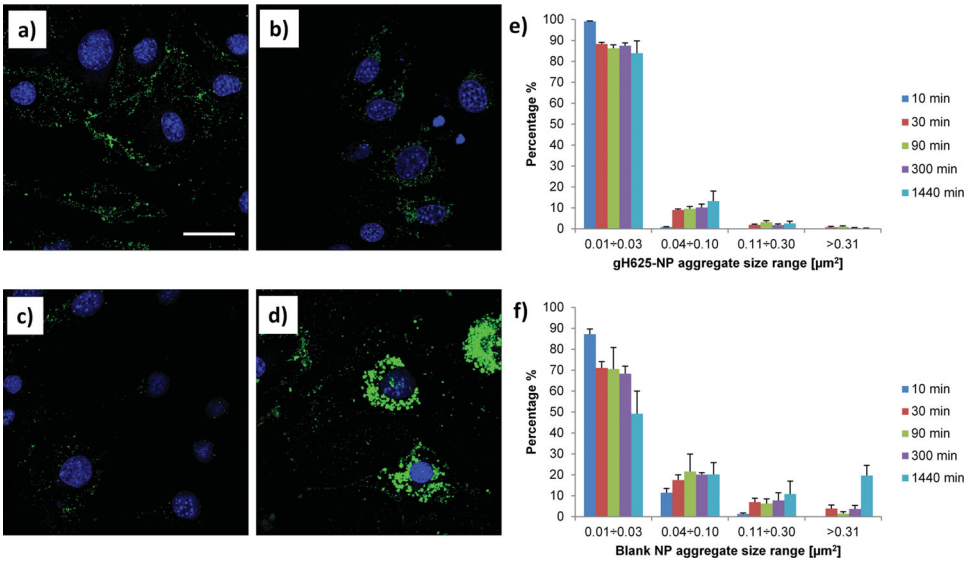

Figure 8. Confocal microscope images of bEnd3 cells incubated with gH625-NPs for 10 min (a) and 1440 min (b) and blank-NPs for 10 min (c) and 1440 min (d). Blue: nuclei; Green: NPs; Magnification bar: 20 μm. gH625- (e) and blank-NP (f) aggregate analysis. Charts show the size distribution of NP aggregates at different observation time (10, 30, 90, 300, and 1440 min). NP aggregate sizes were split in four intervals: 0.01÷ 0.03 μm^2; 0.04÷ 0.10 μm^2; 0.11÷ 0.30 μm^2; >0.31 μm^2.

to the design of a drug delivery system homing to the brain and bypassing the endocytosis entrapment. Therefore, these novel nanocarriers could be regarded as a promising strategy to design delivery systems for administration of therapeutical compounds to the brain, deserving further investigations to more precisely characterize the mechanism by which gH625 crosses the BBB and to address the cell specificity issue by linking to the nanosystem also molecules specifically recognized by the brain endothelium.

4. Experimental Section

Materials: Protected Fmoc-amino acid derivatives, coupling reagents and Wang resin were purchased from Fluka, and the other chemicals were purchased from Sigma-Aldrich, Fluka (Buchs, Switzerland) or LabScan (Stillorgan, Dublin, Ireland) and were used as received, unless otherwise stated. Orange fluorescent amine-modified polystyrene, 100 nm, (NP-NH2) were purchased by Sigma-Aldrich.

Peptide Synthesis: The peptide gH625 (Ac-HGLASTLTRWAHY-NALIRAFGGG-COOH) was synthesized using the standard solid-phase-9-fluorenylmethoxycarbonyl (Fmoc) method as previously reported.[14f] The peptide was obtained with good yields (30–40%).

Peptides Conjugation to NPs: A solution of the peptide, EDC (1-ethyl-3(3-dimethylamino-propyl)-carbodiimide, hydrochloride) and NHS (*N*-Hydroxysuccinimide) in molar ratio of 4:4:1 was prepared in PBS buffer at pH 7.4, at room temperature under stirring for 30 min. NPs were conjugated with the preactivated-peptide, in MES 0.1 M buffer at pH 5.5 for 3 h at room temperature in presence of Tween 20 and the yield of the reaction was higher than 90%. The peptide-NPs were purified from the un-conjugated-NPs by exclusion chromatography on a 1 × 18 cm Sephadex G-50 (Amersham Biosciences) column pre-equilibrated in PBS buffer at pH7.4. The fluorescence spectra of peptide-NPs and un-conjugated NPs were measured in a Cary Eclipse Varian fluorescence spectrophotometer in the same condition. Peptide-NPs were prepared with several degrees of functionalization: 25%, 35% and 50%.

Circular Dichroism: CD spectra were recorded using a Jasco J-715 spectropolarimeter in a 1.0 or 0.1 cm quartz cell at room temperature. The spectra are an average of 3 consecutive scans from 260 to 195 nm, recorded with a band width of 3 nm, a time constant of 16 s, and a scan rate of 10 nm/min. Spectra were recorded and corrected for the blank sample.

Size and Z-potential: Measurements of zeta potential and size of gH625 NPs and blank-NPs were made with a Zetasizer Nano-ZS (Malvern Instruments, Worcestershire, UK). The measurements were conducted at 25 °C using a 3.6×10^{10} NP/ml suspension at pH 4, 7, 8 and 9. All measurements were performed in triplicate for each sample.

Cell Culture: Immortalized mouse cerebral endothelial cells, bEnd3 cells (American Type Culture Collection, Manassas, VA) were grown in DMEM with 4.5 g/L glucose, 10% Fetal Bovine Serum (FBS), 3.7 g/L sodium bicarbonate, and 4 mM glutamine, 100 U/mL penicillin and 0.1 mg/mL streptomycin in 100 mm diameter cell culture dish, in a humidified atmosphere at 37°C and 5% CO_2. Cells used in all experiments were at passage 28–35.

Multiple Particle Tracking: Images of NPs internalized in End3 cells were collected in real time for about 100 s with a time resolution of ~1 s by using Olympus Cell-R system equipped with 60× oil immersion objective. Tracking algorithm has been described in detailed elsewhere.[17b] From the NP trajectories the mean square displacement (MSD) was derived. Indicated with $\langle r^2 \rangle$, MSD was related to the NPs diffusion coefficient D by the Equation (1)

$$\langle r^2 \rangle = nDt^{\alpha} + v^2 t^2 \quad (1)$$

small 2012,
DOI: 10.1002/smll.201201870

NANO MICRO small

where D is the diffusion coefficient, v the NP rate and α represents the time dependence. The first term of the equation is related to the random diffusion of the nanoparticles, whereas the second one reflects the active motion along the filaments due to the action of molecular motors (for NPs that undergo to Brownian motion such term becomes negligible). By fitting the MSD curve of each tracked bead by using equation (1), informations concerning the nature of particle motion into the cells were gained. In particular, nanoparticles, exhibiting MSD curve that undergo a power law with exponent minor or equal to unity, were classified as Brownian ($\alpha = 1$) or sub-diffusive ($\alpha < 1$). Particles presenting MSD, whose dependence on time was well described by the power law with $\alpha > 1$, were indicated as super-diffusive. During the experiments the MSD of 226 (NPs-NH_2), 105 (NPs-gH625 25%), 38 (NPs-gH625 35%) and 574 (NPs-gH625 50%) distinct objects was evaluated. For each degree of peptide functionalization, at least, 3 cells were analyzed.

Quantification of Nanoparticle Uptake Kinetics: To evaluate cell uptake of NPs as a function of NP surface functionalization with gH625 peptide, about 5×10^4 cells were seeded in a 96-well. Blank-NPs and gH625-NPs were dispersed in cell culture medium at the final concentration of 3.6×10^{10} NP/mL. Cells were incubated with NP suspensions for 0, 10, 60, 180, and 300 min. After incubation, cells were rinsed with PBS and lysed with 1% Triton ×100 in PBS. Cell lysates were analyzed by a spectrofluorometer (Wallac 1420 Victor2, Perkin–Elmer, USA) to measure the amount of internalized NPs.

Permeability Experiments: Cells were seeded at a density of 5×10^4 cells/cm^2 on Transwell permeable inserts (6.5 mm in diameter, 3 μm pores size; Corning Incorporated, Corning, NY). Transendothelial electrical resistance (TEER) was measured by using Millicell1-ERS voltohmmeter (Millipore, Billerica, MA) to assess the growth of cells on inserts. Permeability experiments were performed on the monolayer 7 days after cell seeding, allowing sufficient time for the cells to develop the junctions between cells.

On the day of experiment, Transwell insert filter was washed with PBS, and then the media of the donor chamber was filled with 150 μL cell culture medium w/o phenol red containing 0.5 mg/mL rhodaminated BSA and 3.6×10^{10} NPs/mL while the acceptor chamber was filled with 400 μL cell culture medium without phenol red. The samples of 100 μL were drawn every 10 min for 90 min from the acceptor chamber and were then replaced with the same amount of fresh medium. The fluorescence tracer concentration in the samples was determined by a spectrofluorometer (Victor, Wallac, PerkinElmer), and the excitation and emission wavelengths were set to 540 and 615 nm and 485 and 535 nm, respectively, for BSA and NPs. The solute permeability P of the monolayer was calculated according to the following equation,

$$P = \frac{\frac{\Delta C_A}{\Delta t} \times V_A}{C_D \times S}$$

Where $\Delta C_A/\Delta t$ is the increase in fluorescence concentration in the acceptor chamber during the time interval Δt, C_D is fluorescence concentration in the donor chamber (assumed to be constant during the experiment), V_A is the volume of the acceptor chamber, and S is the surface area of the filter. The experiments were performed in triplicate.

Colocalization with Lysosomes and Caveolae: For indirect immunofluorescence, after NPs incubation, cells were firstly rinsed twice with PBS to remove non internalised NPs and fixed with paraformaldehyde 4% for 20 min. Then, cells were incubated with Triton ×100 0.1% in PBS for 10 min and with PBS-BSA 0.5% for 15 min at room temperature (RT). Caveolae were localized by incubating samples first with rabbit anti-caveolin 1 (Abcam) primary antibodies. After primary antibodies incubation, Alexa-fluor 568 goat anti-rabbit secondary antibodies (Molecular Probes, Invitrogen) were used. Afterward, samples were rinsed three times with PBS. For lysosomes localization, LysoTracker Red DND-99 (Molecular Probes, Invitrogen) was used following manufacturer's procedure on non-fixed cells.

Immunofluorescence analyses were performed by means of confocal laser scanning microscope (CLSM)(LSM510, Zeiss), equipped with an argon laser, at a wavelength of 488 nm, and a He–Ne laser, at a wavelength of 543 nm, and 63x objective. Images were acquired with a resolution of 1024×1024 pixels. Colocalization was estimated by an ImageJ software plugin.

Cytochalasin D Treatment: To disassemble actin microfilaments, cells were treated with 30 μM cytochalasin D in cell culture medium for 30 min at 37°C before NP incubation. After cytochalasin D treatment, cells were incubated with a NP suspension for 15 min. Then, cells were rinsed with PBS to remove non-internalized NPs, fixed with paraformaldehyde 4% for 20 min and observed by CLSM. Quantification of NP uptake was performed as described above.

Scanning Electron Microscopy (SEM): After 10 min incubation with blank NPs and gH625-NPs, cells were rinsed with PBS, fixed with 2.5% glutaraldehyde for 2 h at 4 °C and dehydrated in increasing ethanol series (70%, 80%, 95%, and 100%) and by critical point. The samples were gold-sputtered and analyzed by ESEM Quanta 200 (FEI Company) at 25 kV and 6.8 mm working distance.

Transmission Electron Microscopy (TEM): TEM was performed to precisely localise the intracellular nanoparticles. After 24 h incubation with blank NPs and gH625-NPs, cells were rinsed with PBS and fixed with 2% paraformaldehyde+0.2% glutaraldehyde for 2 h at room temperature. Afterwards, cells were scraped, harvested in centrifuge tubes, embedded in 12% gelatine solution in PBS and infused in 2.3 M sucrose at 4 °C. Sections were cut with a Leica Cryo-ultramicrotome and examined with Leica EM FC7.

Quantification of NP Aggregates: To measure the size of NP aggregates within cell cytoplasm, bEnd3 cells were incubated with NP suspension for 30, 90, 1440 minutes at 37 °C. After incubation, cells were rinsed twice with PBS, fixed with paraformaldehyde 4% for 20 min and observed by confocal microscope (Leica). Images were analyzed by an ImageJ software plugin. About 50 cells per each sample were analyzed. The size distribution of NP aggregates was split in four intervals (0.01÷ 0.03 μm^2; 0.04÷ 0.10 μm^2; 0.11÷ 0.30 μm^2; >0.31 μm^2) and data reported as percentage of NP aggregates respect to the total number of NP aggregates per cell.

Statistical Analyses: Quantitative data were reported as mean ± standard deviation (SD). Statistical analyses were performed using a one-way analysis of variance (ANOVA). Results repeats were compared by analysis of variance (ANOVA), and a p value < 0.05 was considered statistically significant.

DOI: 10.1002/smll.201201870

Acknowledgements

The authors thank Roman Polishchuk, Elena Polishchuk and Simona Iacobacci (Telethon Institute of Genetics and Medicine - Tigem, Napoli, Italy) for TEM sample preparation and analysis.

This work was supported by Progetto FARO (Prot.2012/0043756) and PON01_02388 "Verso la medicina personalizzata: nuovi sistemi molecolari per la diagnosi e la terapia di patologie oncologiche ad alto impatto sociale - SALUTE DELL'UOMO E BIOTECNOLOGIE Responsabile Scientifico Prof. Carlo Pedone.

[1] E. Neuwelt, N. J. Abbott, L. Abrey, W. A. Banks, B. Blakley, T. Davis, B. Engelhardt, P. Grammas, M. Nedergaard, J. Nutt, W. Pardridge, G. A. Rosenberg, Q. Smith, L. R. Drewes, *Lancet Neurol.* **2008**, *7*, 84.

[2] N. J. Abbott, L. Ronnback, E. Hansson, *Nat. Rev. Neurosci.* **2006**, *7*, 41.

[3] G. Tosi, L. Costantino, F. Rivasi, B. Ruozi, E. Leo, A. V. Vergoni, R. Tacchi, A. Bertolini, M. A. Vandelli, F. Forni, *J. Control. Release* **2007**, *122*, 1.

[4] J. Kreuter, *Adv. Drug Deliv. Rev.* **2001**, *47*, 65.

[5] S. V. Dhuria, L. R. Hanson, W. H. Frey II, *J. Pharm. Sci.* **2010**, *99*, 1654.

[6] a) S. D. Mahajan, W. C. Law, R. Aalinkeel, J. Reynolds, B. B. Nair, K. T. Yong, I. Roy, P. N. Prasad, S. A. Schwartz, *Methods Enzymol.* **2012**, *509*, 41; b) K. K. Jain, *Nanomedicine* **2012**, *7*, 1225; c) G. Orive, O. A. Ali, E. Anitua, J. L. Pedraz, D. F. Emerich, *Biochim. Biophys. Acta* **2010**, *1806*, 96; d) R. Qiao, Q. Jia, S. Huwel, R. Xia, T. Liu, F. Gao, H. J. Galla, M. Gao, *ACS Nano* **2012**, *6*, 3304.

[7] a) B. DiBlasio, S. Galdiero, M. Saviano, G. DeSimone, E. Benedetti, C. Pedone, W. A. Gibbons, R. Deschenaux, E. Rizzarelli, G. Vecchio, *Supramolecular Chem.* **1996**, *7*, 47; b) D. Paolino, D. Cosco, R. Molinaro, C. Celia, M. Fresta, *Drug Discov. Today* **2011**, *16*, 311; c) H. Yang, *Pharm. Res.* **2010**, *27*, 1759.

[8] E. Garcia-Garcia, K. Andrieux, S. Gil, P. Couvreur, *Int. J. Pharm.* **2005**, *298*, 274.

[9] J. C. Olivier, *NeuroRx* **2005**, *2*, 108.

[10] M. Zorko, U. Langel, *Adv. Drug Deliv. Rev.* **2005**, *57*, 529.

[11] S. Deshayes, M. C. Morris, G. Divita, F. Heitz, *Cell Mol. Life Sci.* **2005**, *62*, 1839.

[12] L. Liu, S. S. Venkatraman, Y. Y. Yang, K. Guo, J. Lu, B. He, S. Moochhala, L. Kan, *Biopolymers* **2008**, *90*, 617.

[13] a) S. Galdiero, M. Vitiello, A. Falanga, M. Cantisani, N. Incoronato, M. Galdiero, *Curr. Drug Metab.* **2012**, *13*, 93; b) A. Falanga, M. Cantisani, C. Pedone, S. Galdiero, *Protein Pept. Lett.* **2009**, *16*, 751; c) S. Galdiero, A. Falanga, M. Vitiello, M. D'Isanto, C. Collins, V. Orrei, H. Browne, C. Pedone, M. Galdiero, *ChemBioChem* **2007**, *8*, 885; d) S. Galdiero, M. Vitiello, M. D'Isanto, A. Falanga, M. Cantisani, H. Browne, C. Pedone, M. Galdiero, *ChemBioChem* **2008**, *9*, 758.

[14] a) G. Vitiello, A. Falanga, M. Galdiero, D. Marsh, S. Galdiero, G. D'Errico, *Biochim. Biophys. Acta* **2011**, *1808*, 2517; b) S. Galdiero, A. Falanga, M. Vitiello, M. D'Isanto, M. Cantisani, A. Kampanaraki, E. Benedetti, H. Browne, M. Galdiero, *Peptides* **2008**, *29*, 1461; c) S. Galdiero, A. Falanga, G. Vitiello, M. Vitiello, C. Pedone, G. D'Errico, M. Galdiero, *Biochim. Biophys. Acta* **2010**, *1798*, 579; d) S. Galdiero, A. Falanga, M. Vitiello, L. Raiola, L. Russo, C. Pedone, C. Isernia, M. Galdiero, *J. Biol. Chem.* **2010**, *285*, 17123; e) S. Galdiero, A. Falanga, M. Vitiello, L. Raiola, R. Fattorusso, H. Browne, C. Pedone, C. Isernia, M. Galdiero, *J. Biol. Chem.* **2008**, *283*, 29993; f) S. Galdiero, A. Falanga, M. Vitiello, H. Browne, C. Pedone, M. Galdiero, *J. Biol. Chem.* **2005**, *280*, 28632.

[15] a) A. Falanga, M. T. Vitiello, M. Cantisani, R. Tarallo, D. Guarnieri, E. Mignogna, P. Netti, C. Pedone, M. Galdiero, S. Galdiero, *Nanomedicine* **2011**, *7*, 925; b) R. Tarallo, A. Accardo, A. Falanga, D. Guarnieri, G. Vitiello, P. Netti, G. D'Errico, G. Morelli, S. Galdiero, *Chemistry* **2011**, *17*, 12659; c) T. P. Carberry, R. Tarallo, A. Falanga, E. Finamore, M. Galdiero, M. Weck, S. Galdiero, *Chemistry* **2012**,

[16] P. Nygren, M. Lundqvist, K. Broo, B. H. Jonsson, *Nano Lett.* **2008**, *8*, 1844.

[17] a) H. Jin, D. A. Heller, M. S. Strano, *Nano Lett.* **2008**, *8*, 1577; b) D. Guarnieri, A. Guaccio, S. Fusco, P. A. Netti, *J. Nanoparticle Res.* **2011**, *13*, 15.

[18] H. Ewers, A. E. Smith, I. F. Sbalzarini, H. Lilie, P. Koumoutsakos, A. Helenius, *Proc. Natl. Acad. Sci. USA* **2005**, *102*, 15110.

[19] a) A. Blocker, F. F. Severin, J. K. Burkhardt, J. B. Bingham, H. Yu, J. C. Olivo, T. A. Schroer, A. A. Hyman, G. Griffiths, *J. Cell Biol.* **1997**, *137*, 113; b) A. Caspi, O. Yeger, I. Grosheva, A. D. Bershadsky, M. Elbaum, *Biophys. J.* **2001**, *81*, 1990.

[20] S. Galdiero, L. Russo, A. Falanga, M. Cantisani, M. Vitiello, R. Fattorusso, G. Malgieri, M. Galdiero, C. Isernia, *Biochemistry* **2012**, *51*, 3121.

[21] a) W. Zhang, E. Crocker, S. McLaughlin, S. O. Smith, *J. Biol. Chem.* **2003**, *278*, 21459; b) W. Jing, H. N. Hunter, J. Hagel, H. J. Vogel, *J. Pept. Res.* **2003**, *61*, 219.

[22] M. E. Rauch, C. G. Ferguson, G. D. Prestwich, D. S. Cafiso, *J. Biol. Chem.* **2002**, *277*, 14068.

[23] a) R. C. Brown, A. P. Morris, R. G. O'Neil, *Brain Res.* **2007**, *1130*, 17; b) Y. Omidi, L. Campbell, J. Barar, D. Connell, S. Akhtar, M. Gumbleton, *Brain Res.* **2003**, *990*, 95.

[24] S. Nag, *Methods Mol. Biol.* **2011**, *686*, 3.

Received: August 2, 2012
Revised: September 12, 2012
Published online:

DOI: 10.1002/smll.201201870

Send Orders of Reprints at bspsaif@emirates.net.ae

Current Protein and Peptide Science, **2012**, *13*, **843-854**

Microbe-Host Interactions: Structure and Role of Gram-Negative Bacterial Porins

Stefania Galdiero[1,*], Annarita Falanga[1], Marco Cantisani[1], Rossella Tarallo[1], Maria Elena Della Pepa[2], Virginia D'Oriano[2] and Massimiliano Galdiero[2,*]

[1]*Department of Biological Sciences, Division of Biostructures, University of Naples "Federico II" and Istituto di Biostrutture e Bioimmagini, CNR, Via Mezzocannone 16, 80134, Naples, Italy;* [2]*Department of Experimental Medicine, Division of Microbiology - II University of Naples, Via De Crecchio 7, 80138, Naples, Italy*

Abstract: Gram negative bacteria have evolved many mechanisms of attaching to and invading host epithelial and immune cells. In particular, many outer membrane proteins (OMPs) are involved in this initial interaction between the pathogen and their host. The outer membrane (OM) of Gram-negative bacteria performs the crucial role of providing an extra layer of protection to the organism without compromising the exchange of material required for sustaining life. The OM, therefore, represents a sophisticated macromolecular assembly, whose complexity has yet to be fully elucidated. This review will summarize the structural information available for porins, a class of OMP, and highlight their role in bacterial pathogenesis and their potential as therapeutic targets.

The functional role of porins in microbe-host interactions during various bacterial infections has emerged only during the last few decades, and their interaction with a variety of host tissues for adhesion to and invasion of the cell and for evasion of host-defense mechanisms have placed bacterial porins at the forefront of research in bacterial pathogenesis. This review will discuss the role that porins play in activating immunological responses, in inducing signaling pathways and their influence on antibiotic resistance mechanisms that involve modifications of the properties of the OM lipid barrier.

Keywords: Porin, bacteria, immunobiology, signaling pathways, structure.

INTRODUCTION

Infectious diseases are major threats to human health worldwide, and tremendous effort is continuously devoted to the understanding of various infectious agents and their mechanisms of virulence. The field of bacterial pathogenesis is a rapidly evolving and expanding one.

The mammalian immune system has in place a line of defense specialized in recognizing and eradicating invading pathogens; however, sometimes the pathogen evades these mechanisms and establishes diseases in its host. The treatment of bacterial infections with antibiotics is one of the key concepts of human medicine. Therapies like antibiotics and vaccination support the immune system in its fight against pathogenic microbes. After several decades of continued success of antibiotic therapy, we are now facing a worrying prospect: the accelerated evolution of antibiotic resistance of important human pathogens, which presents a global health problem with a strong social and economic impact. This bacterial adaptation to antibiotic use is directly involved in the current increase of morbidity and mortality caused by infection diseases. Over time, resistance to antibiotics has developed due to the intense selective pressure the antibiotics place on bacteria. Furthermore, while a number of vaccines have been successful, far too many infectious diseases still do not have efficacious vaccines. An urgent need for new therapeutics exists and understanding the complex relationship among the host and invading pathogens will provide important insight for the rational design of therapeutics.

Gram negative bacteria comprise a major proportion of drug resistant pathogens and display a complex envelope with an outer (OM) and an inner (IM) membrane delimiting a periplasmic space. This cellular organization results in the presence of various protein channels involved in the transport, uptake or efflux, of a large variety of compounds, nutrients or toxic molecules (sugars, drugs, small peptides, chemicals).

The outer membrane is the first line of defense for Gram-negative bacteria against toxic compounds. This barrier is impermeable to large, charged molecules. Influx is largely controlled by porins, which are water-filled open channels that span the outer membrane and allow the passive penetration of hydrophilic molecules. Bacterial pathogenicity is largely dependent on its surface structures. Among the components of the bacterial outer membrane, outer membrane proteins (OMPs), such as the porins, play a fundamental role in pathogenicity and in protection and represent useful targets for therapeutic development [1-3].

*Address correspondence to these author at the Department of Biological Sciences, Division of Biostructures, University of Naples "Federico II" and Istituto di Biostrutture e Bioimmagini, CNR, Via Mezzocannone 16, 80134, Naples, Italy; Department of Experimental Medicine, Division of Microbiology - II University of Naples, Via De Crecchio 7, 80138, Naples, Italy; Tel: +39 081 2534503; Fax: +39 081 5667578;
Emails: sgaldier@unina.it and massimiliano.galdiero@unina2.it

1875-5550/12 $58.00+.00

Porins are involved in the exchange of nutrients over the outer membrane of Gram-negative bacteria but are also involved in pathogenesis. The present review will focus on the description of the structure and the role of Gram-negative bacterial porins in the bacteria-host interactions.

DESCRIPTION OF BACTERIAL ENVELOPES

Bacteria in order to face unpredictable and often hostile environments have evolved a sophisticated and complex cell envelope that protects them while allowing selective passage of nutrients from the outside and waste products from the inside. In particular, Gram-negative bacteria can be divided into several subcellular compartments [4]. There are three principal layers: the outer membrane (OM), the peptidoglycan cell wall, and the inner membrane (IM). The two membrane layers delimit two aqueous compartments called the cytoplasm and the periplasm. Present throughout these compartments are proteins with diverse and important biological functions (Fig. **1**). Some of these proteins are membrane-embedded and allow the transfer of molecules between compartments. Others are soluble enzymes involved in metabolic reactions. Much work has been devoted toward understanding how each of these compartments is formed and maintained. The OM is a characteristic feature of Gram-negative bacteria, and in fact Gram-positive bacteria lack this structure. The OM is a lipid bilayer intercalated with proteins, superficially resembling the plasma membrane; it contains phospholipids confined to its inner leaflet, while the outer leaflet contains glycolipids, mainly lipopolysaccharide (LPS).

The barrier property of the OM can be largely attributed to the presence and asymmetrical distribution of the complex glycolipid LPS. In fact, LPS monomers in the bilayer exhibit a strong lateral interaction with other LPS molecules, these interactions together with the enrichment of fully saturated phospholipids in the inner leaflet of the OM greatly reduce the OM fluidity, which is rigid and gel-like in comparison to the inner membrane. LPS molecules are made of three distinct regions: the lipid A, the core oligosaccharide and the distal O-antigen (Fig. **2**). Lipid A secures LPS in the OM; the core is covalently bound to the lipid A through an acidic sugar, the 3-deoxy-D-manno-oct-2-ulopyranosonic acid (Kdo). The general pattern of the lipid A from diverse Gram-negative bacteria is highly conserved. The core oligosaccharide is very variable among bacterial species; so different species can express uniquely modified types of LPS. The O-antigen, if present, is the most variable part of LPS and shows even a high degree of variability between different strains of the same species.

With few exceptions, the proteins intercalated in the OM can be divided into two classes, proteins that traverse the membrane and assume a β-barrel structure and lipoproteins, anchoring the outer membrane to the underlying peptidoglycan stratum (Fig. **1**). Lipoproteins contain lipid moieties that embed lipoproteins in the inner leaflet of the OM, and are thus not supposed to be transmembrane proteins. The outer membrane proteins (OMPs) of Gram-negative bacteria have been well characterized and many assume a β-barrel conformation. The OMPs serve as a molecular filter for hydrophilic substances, mediate the transport of nutrients and ions across the membrane into the periplasm, some small β-barrels seem to serve primarily as membrane anchors or to promote bacterial adhesion to mammalian cells, or are membrane-bound enzymes such as protease, phospholipase.

The most abundant proteins of the bacterial outer membrane are porins which are essentially trimeric β-barrels forming channels with various grades of selectivity. Porins form passive pores that do not bind their substrates; they generally form water-filled pores, through which relatively small (<600 Da) solutes diffuse, driven by their concentra-

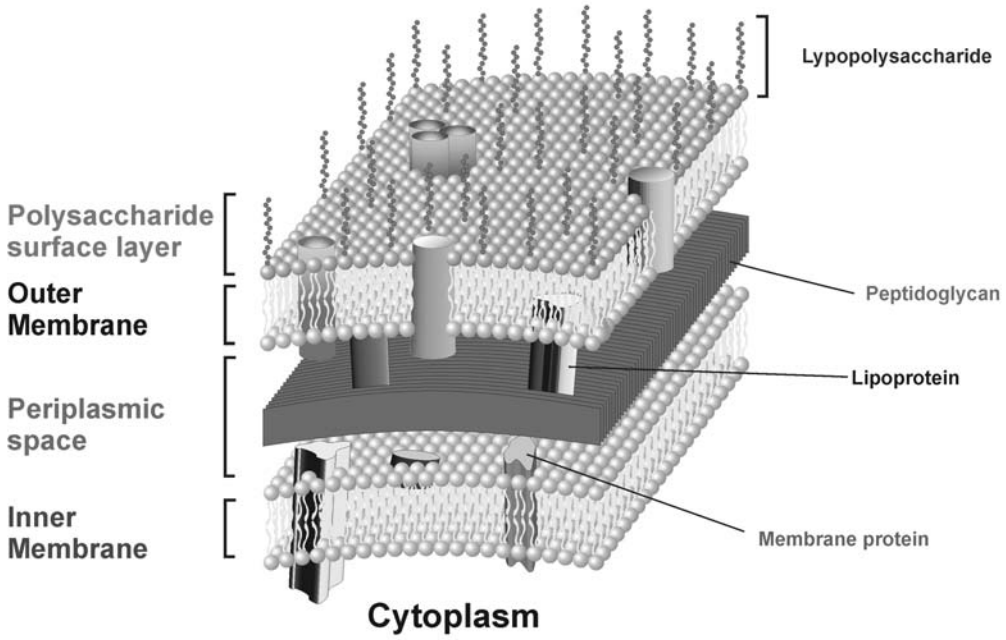

Fig. (1). Schematic representation of the inner and outer bacterial membrane.

tion gradient. For nutrients that are present at low concentrations in the extracellular environment, passive diffusion is no longer efficient and transport occurs via substrate-specific and active transporters [5-9].

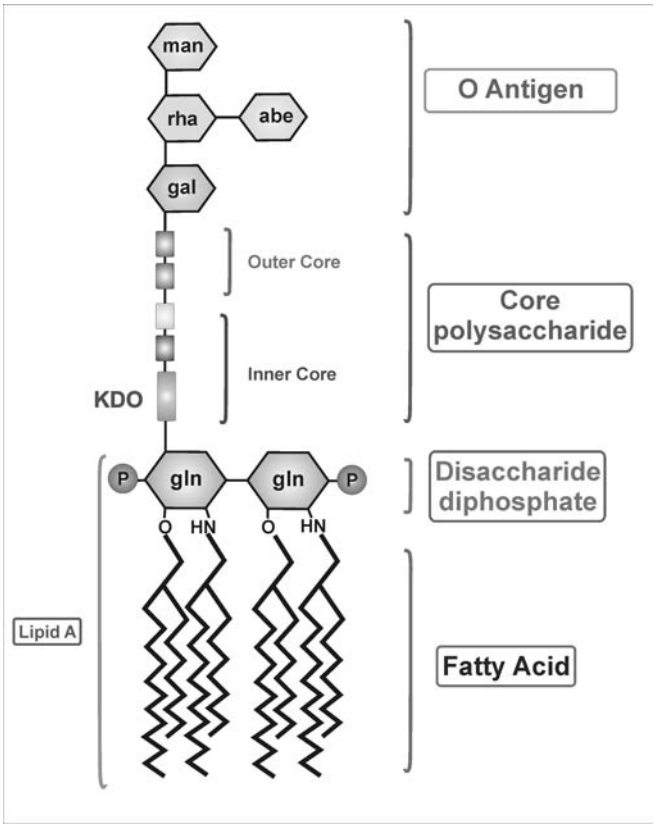

Fig. (2). Schematic representation of the structure of lipopolysaccharide (LPS).

BACTERIAL PORINS: STRUCTURE

Bacterial porins have been studied in great detail since many years; the first high-resolution X-ray structure was published in 1990/1991 and was the major outer membrane protein of *Rhodobacter capsulatus*. The structure of this trimeric porin showed the archetypical fold of 16 tilted β-strands, all of which are connected by extraplasmic loops and periplasmic turns with the particularly long loop L3 folded inside the barrel (Fig. **3A**) [10,11]. Many additional porin structures have been determined since then with a high similarity in architecture and only smaller variations, mainly in loop topology and surface charges [12-15]. Porins made of 16 strands were classified as general or non-specific porins and form pores allowing the diffusion of hydrophilic molecules, showing no particular substrate specificity, despite some selectivity for either cations or anions; while 18 strands porins were classified as substrate specific porins, both of which are trimeric (Fig. **3B**) [6,7]. This concept has been proved useful for many years and provided a clear structure-based classification into e.g. sugar-specific channels, such as ScrY or LamB with 18 β-strands, or unspecific channels with 16 strands involved in the uptake of small and mostly inorganic molecules (e.g. Omp32, OprP and PhoE) [16-18]. However, during recent years and owing to the discovery of new bacterial cell envelopes and outer membrane protein structures, the group of porins became more diverse and a simple classification seems more difficult. Recently OmpG or CymA (14-stranded monomeric proteins) [19,20] showed a different fold and quaternary structure (Fig. **3C**). In addition, a number of porins previously classified as unspecific were later proved to bind small, typically negatively charged (organic acids or phosphates) ligands, thereby providing a structural and functional rationale for the facilitated small metabolite uptake in bacteria and their specific lifestyle conditions [16,17].

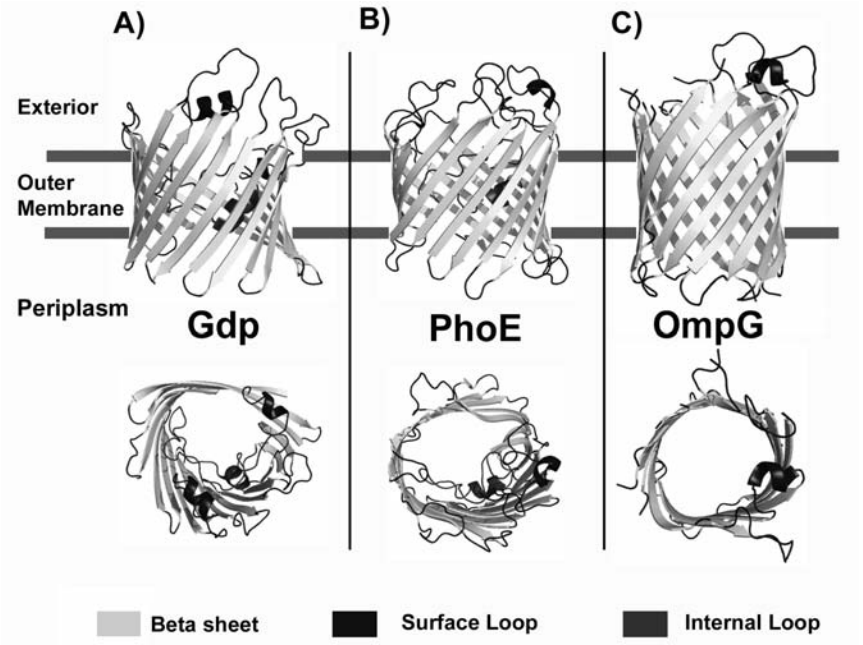

Fig. (3). Three dimensional structures of three different porins: Gdp from *Rhodobacter capsulatus*, PhoE and OmpG from *Escherichia coli*. Surface and internal loops are shown in dark grey. The extracellular space is located at the top of the figure and the periplasmic space is at the bottom.

The majority of porins studied so far is typically of oval shape and have an overall dimension of laterally ~30–35Å and ~50 Å in height for the monomer. All these proteins share similar properties, such as their high abundance in native membranes, an increased thermal stability and the regular content of β- sheet structures (in the range of 60%), as well as their specific conductance profiles in planar membranes [15]. The general characteristic of their structural architecture is the closure of the barrel by pairing of the first and last β-strand in an antiparallel way. All strands are connected by eight or nine long loops, facing the extracellular side, with seven or eight small turns in the periplasmic space. In all porins, the constriction at the barrel center is formed by an inserted long loop L3, which is not exposed to the cell surface but folds back into the barrel, forming a constriction zone at half the height of the channel and contributing significantly to the permeability of the pore. The type of residues outlining the channel determines the specificity of the pore. All porins form homotrimers in the OM; each subunit produces a channel and the trimer therefore contains three channels (Fig. **4**). For most porins, loops L1, L2 and L4 are important for monomer-monomer interactions within the porin trimer; loop L3 is internal; loops L5, L6 and L7 are superficial; loop L8 folds back into the barrel interior, contributing to the formation of the channel opening at the external side (Fig. **4A**). Peptide sequences corresponding to superficial loops are responsible for most of the biological activity of porins. Another feature is the presence of aromatic girdles with tyrosine and phenylalanine residues located at the outer and inner membrane boundaries. Tyrosine residues are more frequent at the extraplasmic sites, whereas phenylalanine residues are located at the periplasmic side of the highly asymmetric membrane [21]. These aromatic girdles are also present in α-helical membrane proteins and presumably adjust secondary structure elements at the borders of natural membranes [22]. Residues located between these girdles and facing the hydrophobic lipid environment mainly have high Kyte–Doolittle values (e.g. leucine, valine and isoleucine). Additional girdles, often charged, such as observed in Omp32, exist in bacterial porins and may have some implications in a tighter interaction with lipid head groups or with LPS molecules [15]. At the very C-terminus almost all porins have a phenylalanine residue, which is an important prerequisite for proper import and folding in the outer membrane [23,24].

The pore diameter ranges from 15 Å for the general porins to 6 Å for the highly selective porins. Larger pores usually contain charged residues at opposite sides that form a local transversal electric field at the pore eyelet. This field constitutes an energy barrier for low-polarity solutes so that the bacterium can exclude unwanted nonpolar molecules such as antibiotics while presenting a spacious eyelet for collecting large polar molecules such as sugars. A systematic study changing the pore properties by point mutations showed a strong correlation between the eyelet cross section and diffusion rate [25]. Charge reversals affect selectivity and voltage gating. Interesting results were obtained with mutations at loop L3, for example the specificity of the sucrose porin was changed toward that of the maltoporin.

The outer membrane contains also porins with specificity for certain substrates. The best known proteins of this class are the sucrose-specific ScrY from *Salmonella typhimurium* [7,26] and the maltooligosaccharide-specific maltoporin LamB from *Escherichia coli* [27]. Both form homotrimers with monomers consisting of 18-stranded antiparallel β-strands, with loop L3 folding back inside the barrel and with hydrophilic surface exposed loops; unlike general porins, their β-barrel contains 18 (rather than 16) strands, and some of the external loops coalesce to form an umbrella that shields the underlying pore and restricts its entrance, transforming it in an elongated pore which may adapt to the shape of maltodextrins.

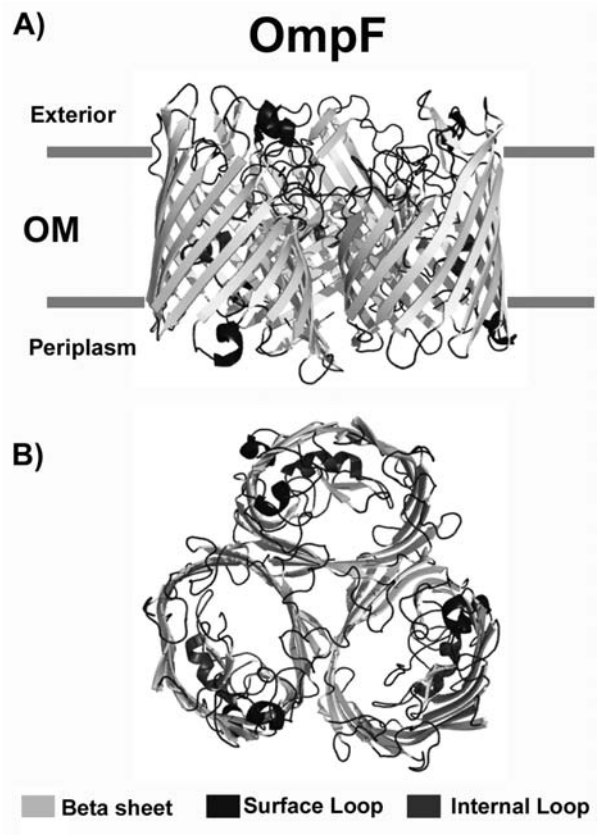

Fig. (4). Three-dimensional structure of the porin OmpF from *Escherichia coli.* Surface and internal loops are shown in dark grey. The extracellular space is located at the top of the figure and the periplasmic space is at the bottom. The trimer is shown.

Although porin structures typically contain 16 or 18 β-sheets depending on the definition of the protein family [28]. Recently several outer membrane proteins have been classified as porin although their structure is characterized by a number of strands lower than 16 (8, 12 and 14 strands) and are also monomeric. Other barrel proteins with fewer strands have been investigated, most of which have a specific function not related to the diffusion of hydrophilic molecules and are not classified as porins. These proteins are instead designed for the exchange of hydrophobic molecules, such as lipids or hydrophobic substances (e.g. toluene) and are typically closed by loop or cork-domain-like structures [29,30,31].

The structure of the 14-stranded porin OmpG from *Escherichia coli* has been determined by X-ray crystallography [20,32]. In E. coli the main porins for sugar uptake are LamB

[33] and ScrY [7]; in mutants where LamB is either nonfunctional or deleted, the uptake of sugars is facilitated by OmpG [32]. OmpG has all features of porins: a signal sequence of 21 amino acids at its N-terminus, which is cleaved during export, absence of long hydrophobic stretches, lack of cysteine residues, and a C-terminal phenylalanine, which is important for membrane insertion. OmpG is a monomer and there is no evidence to suggest a physiological oligomer. Owing to a missing loop L3, present in the archetypical porins, the pore opening is considerably large. A long extracellular loop assumes two distinct, well-defined conformations, apparently in response to the pH of the medium. At neutral pH this loop projects into the extracellular medium, leaving the pore wide open, whereas at low pH it folds across the pore channel and blocks it, suggesting a direct role in pH dependent pore-gating.

NanC belongs to the family of small monomeric related porins [34]. NanC folds into a 28 Å high, 12-stranded β-barrel, resembling the β-domain of autotransporter NalP and defining an open pore with an average radius of 3.3 Å. The channel is lined by two strings of basic residues facing each other across the pore, a feature that appears largely conserved within the substrate specific autotransporter family and is likely to facilitate the diffusion of acidic oligosaccharides. Also AlgE from *Pseudomonas aeruginosa* [35] involved in the secretion of newly synthesized alginate across the outer membrane is a monomeric 18-stranded β-barrel. It is characterized by a highly electropositive pore constriction formed by an arginine rich conduit that likely acts as selectivity filter for the negatively charged alginate polymer. Interestingly, the pore constriction is occluded on both sides by extracellular loop L2 and an unusually long periplasmic loop, T8.

OprP from *Pseudomonas aeruginosa* is involved in the high-affinity acquisition of the concentrations of phosphate that are crucial for *Pseudomonas* growth and proliferation [17]. Each monomer of OprP adopts a 16-stranded antiparallel slightly elliptical β-barrel structure and it forms a prominent trimer in solution, but unlike most of porins, OprP has an extended periplasmic N terminus that is involved in stabilizing the trimer through a 'tricorn'-like strand exchange. Three prominent elongated loop regions are evident in OprP structure, the extracellular loops L3 and L5 and the periplasmic loop T7. The L3 loop contains α-helices that extend deep into the cavity of the barrel and are responsible for the size and constriction of the pore, as seen in other membrane-spanning β-barrel proteins. Uniquely in OprP, the L5 loop runs along the inner surface of the pore toward the center of the channel, creating an electropositive surface to attract anions. In L5, there are five arginine residues that, together with two arginine residues in sheet B2 create a distinct, evenly spaced seven-step arginine ladder, creating an electropositive slide that propels the phosphate down the inner region of the exoplasmic surface toward the constriction zone. On the extracellular surface of the OprP trimer, each monomer contributes to the formation of a giant funnel. The funnel has three separate electropositive arginine ladders that spiral down toward the point of greatest constriction near the periplasmic face of the transporter.

MspA is a channel protein present in the outer membrane of mycobacteria that has been classified as a porin and is involved in the uptake of small hydrophilic nutrients [36]. The atomic structure of this porin shows a β-structure that differs completely from its counterparts in Gram-negative bacteria. The structure is an octamer containing a central channel of 16 β-strands with a diameter of 40Å; the base of the barrel contains a second short 16-stranded β-barrel that forms a channel constriction, also called a pore eyelet with a diameter of 28 Å. This barrel is similar to that of pore forming toxins such as α-hemolysin [37,38].

Among the porin channels are also found proteins such as the P100 protein from *Thermus thermophilus*. Initially this protein was reported to form the S-layer (surface protection layer) of this bacterium [39], later it was shown to form a densely packed structure of porin molecules in native membranes and to be a multi-domain structure made of a N-terminal peptidoglycan binding domain, a long coiled-coil domain and an unusually large porin domain [40,41].

ASSEMBLY AND OLIGOMERIZATION

Studies of bacteriorhodopsin [42] have largely contributed to the comprehension of the assembly and folding processes of α-helical membrane proteins; on the contrary, even though there is a growing understanding of the complex folding process of β-barrel membrane proteins, progress has been much slower. The membrane insertion process is the rate-limiting step, because of the side chain and secondary structure rearrangements required for pore formation.

Proteins that have to reach the OM must be transported from the ribosome to the inner membrane, where they must be discriminated from inner-membrane proteins, then transported across the inner membrane into the periplasm, carried across the periplasm and finally assembled within the outer membrane in their mature conformations [43]. OMPs are synthesized in the cytoplasm with N-terminal cleavable signal peptides that target them for delivery to the periplasm and thanks to their low hydrophobicity they are presumably exported into the periplasm just like any other periplasmic protein; then, they are refolded into their stable β-barrel conformations and are inserted into the outer membrane. It is not clear whether the refolding process precedes insertion or vice versa, but nascent, monomeric porins can be assembled into the final trimer *in vitro*, in the presence of phospholipids. It has been proposed that the central part of the homotrimer including all N and C termini folds in the periplasm like a water soluble protein so that the membrane facing parts of the β-barrels dangle as 200 residue loops into the solvent. On membrane insertion, these loops can easily meander forming the special β-sheet topology. Studies on OmpA [44-47] provided most of the information on the folding process of outer membrane proteins. The insertion and folding reactions of OMP occur spontaneously without the need of accessory proteins *in vitro*; however, the folding kinetics are relatively slow suggesting that folding *in vivo* might be facilitated by folding catalysts;[24] in particular, membrane insertion and folding of OmpA was most efficient at specific molar ratios of OmpA, Skp and LPS [48]. The water-soluble form of OmpA is unstructured and upon membrane interaction, a membrane-bound intermediate is formed, which is localized at the bilayer interface and is composed of single or paired β-strands with dynamic and metastable hydrogen-bonding contacts. A new intermediate is formed with some of the charac-

teristics of β-barrels which only after an extensive amount of rearrangements assumes the mature structure.

Its insertion into the outer membrane is mediated by a protein complex that contains the OMP BamA and four associated lipoproteins (BamBCDE) [49-51]. The mechanism by which the Bam complex catalyzes the assembly of OMPs is not known. Bam is a heteropentamer composed of a very highly conserved OM β-barrel (BamA) and four OM lipoproteins (BamBCDE) that dock with BamA. BamA and BamD are indispensable in *E. coli*, and depletion of either leads to rapid accumulation of unassembled OMPs in the periplasm followed by cell death. The periplasmic domain of BamA is essential for its function; it binds the C-terminal signal sequences of β-barrel OMPs, which contain a C-terminal phenylalanine or tyrosine residue. Binding of an OMP causes a conformational change in the C-terminal domain of BAM, which allows the OMP to insert into the outer membrane. Dissociation of the BAM subunits releases the assembled OMPs into the outer membrane, where final conformational changes in the cell-surface-exposed loops may be induced by interactions with the lipopolysaccharides.

Thus, the Bam complex recognizes the C-terminal motif in β-barrel proteins and before its role became clear, it was already detected in porins and autotrasporters. There is a general mechanism for autotransport, where the different types of autotransporters follow the general route for β-barrel protein insertion into the OM. An extended signal peptide in many cases ensures slow processing by the Sec machinery, to gain time for proper OM insertion before the passenger domain is released. Moreover, premature folding in the periplasm is inhibited by the known periplasmic chaperone systems, and also by sequence intrinsic properties of the passenger polypeptides, such as a reduced folding rate, high solubility of the unfolded passenger domains and little to no propensity to aggregate when in the unfolded state. Most probably already during membrane insertion a hairpin structure is formed, and the sequential folding of the passenger domain on the cell surface drives the process to completion.

ROLE OF BACTERIAL PORINS

During their interaction with the host, porins from several Gram-negative bacteria have diverse biological activities on several eukaryotic cell types, in fact, porins can be considered important inducers of biological activity in host-cell interactions [52]. Several studies have been performed to analyze their immunobiological activities, showing that porins have important effects in several pathogenic mechanisms. Since comprehensive reviews describing the functional behavior of porin channels are available [28], we will mainly focus on three aspects of their role: a) immunological activity of porins, b) porins induced signaling pathways, and c) porins influence on the emergence of antibiotic resistant strains of pathogenic bacteria.

IMMUNOBIOLOGY OF BACTERIAL PORINS

Although the structural features and function of porins have been well studied, their role in the pathogenesis of various bacterial infections has emerged only during the last decade. Bacterial porins interact with a variety of host tissues for adhesion to and invasion of the cell and for evasion of host-defense mechanisms and are able to elicit innate and acquired immune responses.

S. typhimurium porins inhibit phagocytic activity in a dose dependent fashion by activating the adenylate cyclase system [53] and are able to induce the activation of the complement system by acting both on the classic pathway and on the alternative pathway [54]. These porins are clearly endowed with pro-inflammatory activity, in fact, when injected into the paw of male Wistar rats induced dose-dependent edema with long-lasting effects and the induced inflammation is sensitive to both steroid (dexamethasone) and non-steroid (indomethacin) anti-inflammatory drugs. *In vitro* studies carried out on rat resident peritoneal cells showed that porin-induced inflammation may depend on the release of histamine, even though the arachidonic acid metabolites may also participate. In fact, *in vitro* results exclude an increase of 6-keto-prostaglandin and subsequent prostacyclin release, whereas *in vivo* results confirm both the prolonged duration of porin-induced edema and its marked inhibition by indomethacin. Porin-induced inflammation was also observed in decomplemented animals. Further *in vivo* experiments were carried out by intraperitoneal inoculation of 100 μg/ml of porins in guinea pigs [54], therefore, it is unlikely that the activation of the complement system plays a major role in the inflammation induced by porins [54]. Recognition of pathogenic bacteria by host toll-like receptors (TLRs) is the first step in the activation of the inflammatory responses of the innate immune system [55,56].

While CD-14, CD-11/18 and Toll-like receptors 2 and 4 appear to be very important LPS signal transducer, porin-specific receptors are still unknown. Therefore, it is possible that porin stimulation is not due to binding to specific receptors, but the consequence of the perturbation of the cell membrane lipoproteic phase, induced during adsorption or porin penetration. CD-14 is a glycosyl-phosphatidyl inositol linked 55 kDa protein present on the surface of monocytes and polymorphonuclear leucocytes, and it functions as the cell surface receptor for LPS and several surface components of Gram-positive bacteria. CD14 is also found as a soluble protein (sCD14) in human serum. CD14 lacks transmembrane and cytokine-binding domains and is not believed to have intrinsic signaling capabilities. TLRs make up a family of evolutionary conserved pattern recognition molecules that are important signal transducers for the induction of mammalian innate immunity responses, including cytokine responses. TLR2 is involved in the recognition of a wide assay of bacterial products, including peptidoglycan, lipopeptides, zymosan and bacterial lipoproteins, whereas TLR4 is activated by LPS. CD14 acts as a broad specificity coreceptor that can enhance cell activation induced by TLR4 or TLR2 agonists. In many cases, porins interact with host immune cells and can be considered as pathogen associated molecular patterns (PAMPS) due to their ability to signal via TLR molecules and other pattern recognition receptors.

TLR1, TLR2, TLR6, and MD2 have each been suggested to be involved in the recognition of a broad range of OMPs [57-61] . Data from *Haemophilus influenzae* (Hib) porin and from *Neisseria* porin (PorB) indicate that porins from different bacteria may be recognized by TLR-2 [58]. The Hib porin-induced TNF-α and IL-6 production was eliminated in macrophages from TLR2 or MyD88 deficient mice. In con-

trast, macrophages from LPS hyporesponsive C3H/HeJ mice which are defective in TLR4 function, responded normally to Hib porin. Neisserial porin adjuvant activity was mediated by surface expression of B7-2 and class 2 major histocompatibility complexes on B cells by TLR-2-dependent mechanisms; the presence of the adaptor molecule MyD88 was also required. CD11/18 [58] integrin may also participate in LPS signaling. These families of receptors are heterodimer cell surface glycoproteins composed of a CD11 and a CD18 subunit. The release of TNF-α, IL-6 and IL-8 by THP-1 cells stimulated by porins is independent of CD14, but is partially dependent on CD11/18 integrins.

The basis for the recognition of OMPs by TLRs is difficult to envision because OMPs vary in sequence, structure, diameter, and conductance. However, the analysis of the crystal structures of PorB and the TLR1/2 heterodimer [62] allowed the development of a model for the initial recognition of OMPs by TLR1/2. PorB and other Gram-negative porins have been shown to contain a ring of positively charged residues on the extracellular side of the protein that interacts with the negatively charged lipopolysaccharides to stabilize the porin within the bacterial outer membrane [15,63]. An electrostatic analysis of the TLR1/2 heterodimer revealed that both ectodomains, which mediate recognition, are predominantly negatively charged [64]. The negatively charged surface could be attracted to the ring of positive charges from PorB by nonspecific electrostatic attraction.

Several reports have shown that porins are able to induce signal transmission, activation of nuclear factors, activation of gene promoters and finally release of cytokines. Porins by *Salmonella enterica serovar typhimurium* induce the release of TNF-α, IL-1, IL-6, and TGF by macrophages and IL-4 and IFN-γ by lymphocytes. *Salmonella enterica serovar typhimurium* porins enhance the synthesis and release of IL-6 in U937 cells regulating the transcriptional activity of IL-6 gene by nuclear transduction of NF-κB. The characterization of the human IL-6 promoter revealed a highly conserved control region of 300bp upstream of the transcriptional initiation site that contains the elements necessary for its induction by a variety of stimuli commonly associated with acute inflammatory or proliferative states. In particular, electrophoresis mobility shift assay, as well as promoter deletion and point mutation analysis, revealed the presence of an NF-κB binding element. In U937 cells stimulated by *Salmonella* porins, NF-κB is able to enhance IL-6 gene promoter activity. Activation of this nuclear factor may be responsible for porin induced expression and release of IL-6 [65]. OmpA from *Shigella flexneri* 2a induces the release of proinflammatory cytokines through activation of NF-kB via TLR2 , moreover the induction of IFN-γ expression in CD4+ T cells, through the production of IL-12, in macrophages, demonstrated that OmpA plays a critical role in the development of Th1 adaptive skewed immune response [66].

Haemophilus influenza type b (Hib) porin also induces the early release of cytokines in central nervous system cells, amplifying the inflammatory response. Hib porin inserted into the fourth ventricle of the brain elicited the appearance of serum proteins and the development of brain edema. These effects were followed by increase in the number of neutrophils both in cerebrospinal fluid and in the tissue sections around the porin inoculation site. IL-1α, TNF-α and MIP-2 mRNA appeared quickly in the tissue near the inoculation site [67].

As described in this section, porins are deeply involved in inflammation and immune response and several report have shown that mice immunization with porin proteins or DNA immunization with plasmids containing their genes, leads to production of humoral antibodies and also promotes a Th1 cell-mediated immune response. Most functional antibodies raised to non-typable *Haemophilus influenza* (NTHI) are directed to loop L5, which is thought to contain strain-specific and immunodominant epitopes [68], and antibodies to loop L6 of NTHI showed complement-dependent bactericidal activity [69]. Surface exposed loop regions of porins are immunodominant as shown by immunizing mice with whole bacterial cells [70]; synthetic peptides representing epitopes of outer membrane protein F of *Pseudomonas aeruginosa* elicit antibodies reactive with whole cells of heterologous immunotype strains of *Pseudomonas aeruginosa* [71]; major immunogenic epitopes of PorA and FetA of *meningococci* correspond to contiguous peptide sequences located in putative surface-exposed loops of those proteins [72,73].

PORINS INDUCED SIGNALING PATHWAYS

The molecular mechanisms during the interaction of Gram-negative bacteria with macrophages are well understood, but the mechanisms used by porins to activate cells are not well characterized. LPS, porins or other OMPs probably activate cells through similar but not identical mechanisms [2]. The intracellular signaling pathways are complex networks of biochemical events that culminate in specific patterns of nuclear gene expression mediated by transcription factors.

Salmonella enterica serovar typhimurium porins induce signal transduction in mouse macrophages [74]. Porin activation of macrophages results in increased inositol triphosphate and intracellular Ca^{2+} mobilization, translocation of protein kinase C (PKC) to the membrane, NO release within the macrophages and increased binding of infected macrophages resulting in macrophage activation and triggering of specific signaling pathways. *Salmonella enterica* serovar typhimurium, *Mannheimia haemolytica*, and *Haemophilus influenzae* (Hib) porins induce tyrosine phosphorylation in THP-1 cells and in C3H/HeJ mouse macrophages [67], with Hib porin being the most powerful stimulator. The pattern of phosphorylation observed following LPS or porin stimulation is essentially similar, but a difference can be observed in the cytoplasmic fraction bands of 50-60 kDa, which are more evident after treatment with LPS, and in the insoluble fraction band of 80kDa and the cytoplasmic fraction band of 250kDa, which are more evident after porin treatment.

Among the most prominent tyrosine-phosphorylated bands in porin-stimulated cells, a number of proteins with a molecular mass that is similar to that of the family of tyrosine/serine/threonine protein kinases were observed. *Salmonella enterica* serovar typhimurium porins stimulation of U937 cells induces tyrosine phosphorylation of ERK1-2, protein kinase A (PKA), PKC and protein-tyrosine kinase (NT-PTKs). In the cells pretreated with tyrphostin, a specific

PTK inhibitor, or with H-89, a specific PKA inhibitor, or calphostin C, a specific PKC inhibitor, decrease of the relevant activity was observed [75].

Neisserial porins induced protein tyrosine phosphorylation and alter the surface expression of the co-stimulatory molecule B7-2 [76]. Recent evidence suggests that the Raf-1-MEK1/2-MAPK pathways are included among the proteins which are phosphorylated following porin stimulation [77]. The use of some specific inhibitors of phosphorylation pathways such as SB-203580 (p38 inhibitor), PD-098059 (MEK/ERK kinase inhibitor) and forskolin (Raf-1 inhibitor) demonstrated that they modulate in a different way cytokine mRNA expression in cells stimulated with porins. Neisserial porins induce nuclear translocation of the transcription factor NF-κB in B cells and dendritic cells that was maximal by 3 h of stimulation [76]. *Salmonella enterica* serovar typhimurium porins also activated AP-1 and NF-κB in U937 cells involving the Raf-1-MEK1/2-MAPK pathways [77]. Pretreatment with PD-098059 and with SB-203580 markedly affected the activation, indicating that the p38 signaling pathway is mainly involved in AP-1 and NF-κB activation [78]. In fact, PD-098059 is a good and specific inhibitor of MEK-1/2 [79]. In contrast, forskolin pretreatment did not block transcription factor activation by porins, suggesting that a Raf-1-independent pathway may also be involved following porin stimulation. The formation of a different complex represents a further difference between stimulation with LPS and stimulation with porins. This may be added to past observations where mRNA cytokine expression after stimulation with porin begins after 120 min and continues for 5-6 h, while following LPS stimulation begins after 30 min and decreases at 120 min. Forskolin did not block NF-κB translocation after porin stimulation. Raf-1 induces the dissociation of cytoplasmic NF-κB-IκB complexes [80], suggesting that a Raf-1-dependent pathway may be involved in NF-κB activation. In fact, Raf-1 plays a central role in regulating multiple survival pathways in eukaryotic cells and has been also involved in the regulation of the activation of immune effector cells [81]. Moreover, Ras→Raf-1 mediated axis has been also involved in the triggering of a survival response to antiproliferative and immune regulating cytokines such as interferon alpha in human epithelial cells [82]. However, it is known that PKC triggers the activation of several kinases suggesting that MEK/ERK pathways may also participate in NF-κB activation by enhancing an AP-1-NF-κB cross-coupling mechanism. The porin P2 from *Hib*, like porins from *Salmonella enterica* serovar typhimurium, activates mainly but not exclusively the JNK and p38 pathways. Synthetic peptides, corresponding to the amino acid sequences of variable loop regions facing the cell exterior are responsible for most of the biological activity of porins; in contrast, peptides modeled on internal β-strands were ineffective in inducing phosphorylation of such pathways [83,84]. In particular, loop L7 of porin OMPK36 from *Klebsiella pneumoniae* is involved in the interaction with C1q [85]; loops L5, L6 and L7 of porin P2 from *Haemophilus influenzae* activate JNK and p38 mitogen-activated protein kinase (MAPK) pathways [83] and induce the release of TNF-α and IL-6 [84].

A speculative scheme of signal transduction pathways involved in porin-mediated responses is depicted in (Fig. **5**). Accumulating evidence has suggested that the regulation of transcriptional factors and the subunit composition by porin stimulation may affect the adaptive immune mechanism to modulate the production of biologically active proteins or peptides. The engagement of multiple pathways during signal transmission makes the possible use of molecular inhibitors as therapeutic agents very difficult; although recent findings show that peptides complementary to loop regions have a certain ability to block the activity of the porin [86].

Activation of the coagulation and fibrinolytic systems is an important manifestation of the systemic inflammatory response of the host to infection. The *in vivo* effect of a synthetic peptide corresponding to loop L7 from *Haemophilus influenzae* type b (Hib) porin was compared with the effect of the entire protein to evaluate its role on the coagulative/fibrinolytic cascade and the circulating markers of endothelial injury [87]. Plasma was obtained from rats injected intravenously with the peptide and tested for fragment 1+2 (F1+2), tissue-type plasminogen activator (tPA), plasminogen activator inhibitor type I (PAI-1) antigen, von Willebrand factor (vWF) and soluble E-selectin (sE-selectin). The coagulative/fibrinolytic cascade was impaired as determined by the increased level of PAI-1. Concomitantly, E-selectin, a marker of endothelial injury, was also significantly elevated. In addition either loop L7 or Hib porin injection induced hyperglycaemia and inflammatory cytokine production. The data were correlated with hemodynamic functions (significant reduction of blood pressure and increase of heart rate) indicate that loop L7 plays an essential role in the pathophysiologic events observed during gram-negative infections.

PORINS INFLUENCE ON THE EMERGENCE OF ANTIBIOTIC RESISTANT STRAINS OF PATHOGENIC BACTERIA

Multidrug resistance (MDR) is frequently reported in clinical Gram-negative bacteria. This problem poses severe limits to therapeutic options available to clinicians and is a major cause of mortality when acquired as a nosocomial infection [88,89]. MDR is prevalent in key Gram-negative clinical pathogens, such as *Escherichia coli, Salmonella spp., Klebsiella spp., Enterobacter spp., Campylobacter spp., Acinetobacter spp.* and *Pseudomonas spp*. Three major bacterial strategies have emerged for the development of drug resistance: the membrane barrier limits the intracellular access of an antibiotic; the enzymatic barrier produces detoxifying enzymes that degrade or modify the antibiotic; and the target protection barrier impairs target recognition and thus antimicrobial activity [90]. These mechanisms can act simultaneously in clinical isolates, giving rise to a high level of resistance in a single species. The OM of Gram-negative bacteria behaves as a highly selective barrier mainly through the combined effect of a hydrophobic lipid bilayer together with pore-forming proteins of specific size-exclusion properties. The permeability properties of this barrier, therefore, have a major impact on the susceptibility of the microorganism to antibiotics, which are essentially intracellularly targeted. Small hydrophilic drugs, such as β-lactams, as well as tetracycline, chloramphenicol and fluoroquinolones, use the pore-forming porins to gain access to the cell interior, while macrolides and other hydrophobic drugs diffuse across the

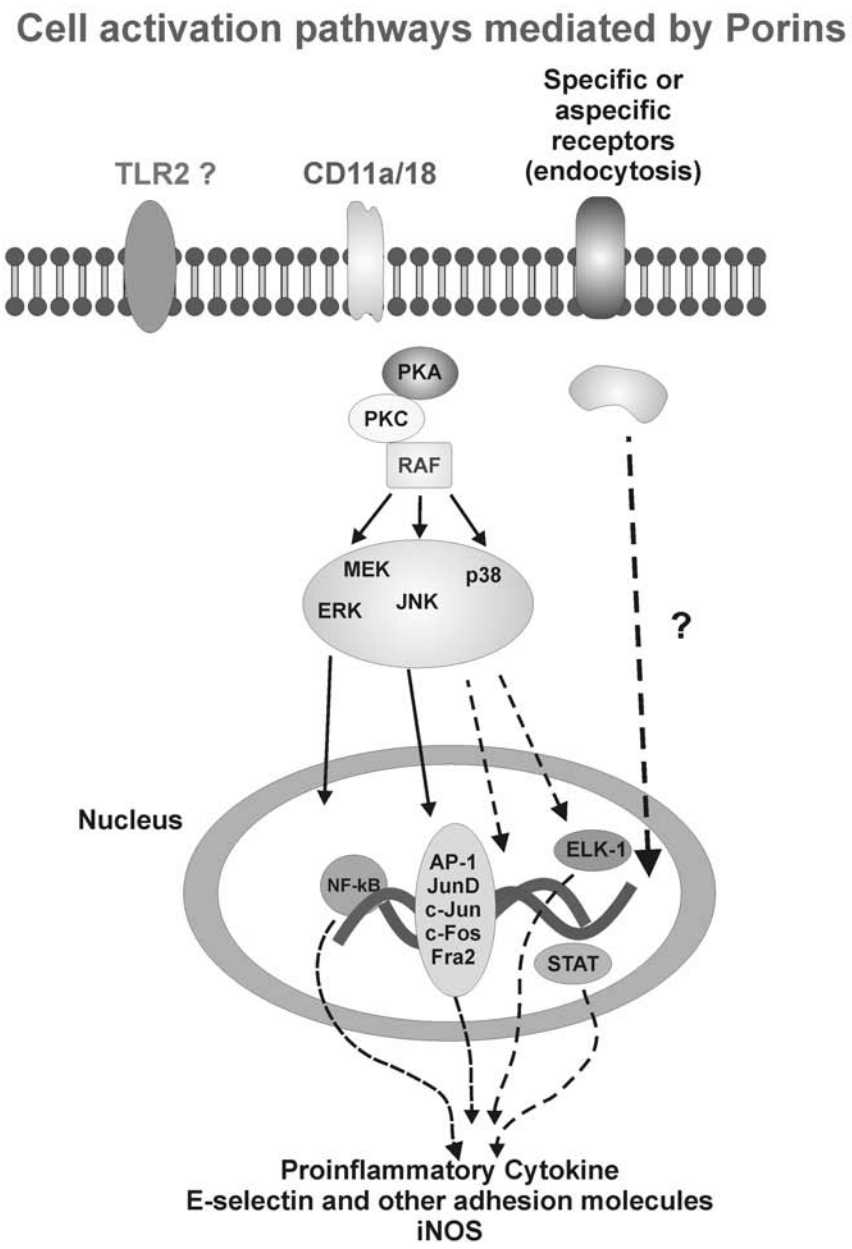

Fig. (5). Speculative scheme of porin signal transduction pathways. Putative porin-specific receptors are shown to be transmembrane. The solid arrows indicate the known association between superficial porin receptors and activation of several transcription factors; dotted arrows indicate hypothetical events.

lipid bilayer. The emergence of drug-resistant strains in a large number of bacterial species due to modifications in the lipid or protein composition of the OM highlights the importance of the OM barrier in antibiotic sensitivity. Resistance generally emerges when a decrease in the rate of entry of these compounds is generated. There are several reports where antibiotic resistance is acquired as a consequence of loss or functional impairment of porins in a large number of organisms, such as *Escherichia coli*, *Pseudomonas aeruginosa*, *Neisseria gonorrhoeae*, *Enterobacter aerogenes* and *Klebsiella pneumonia* [1,91-93]. There are two major porin-based mechanisms for antibiotic resistance that have been reported in clinical isolates: 1) alterations of outer membrane profiles, including either loss/severe reduction of porins or replacement of one or two major porins by another; 2) altered function due to specific mutations reducing permeability. Antibiotic-driven tetracylcine resistance can occur by exposing sensitive *Escherichia coli* cells to increasing concentrations of the antibiotic, leading to a chromosome-mediated multiple antibiotic resistance (Mar phenotype). Multiple proteins including porins and drug efflux pumps are involved, through upregulation of marA which ends up in inhibition of OmpF RNA translation [94]. Decreased OmpF levels can also derive from periplasmic accumulation of other OM proteins, such as TolC and OmpX, which might compete with the same substrate for assembly of porins in the OM [95]. The substitution of a general-diffusion porins normally present on the bacterial surface with a narrower

porin is a further mechanism for acquiring antibiotic resistance. This is the case of substitution of OmpK35 and OmpK36 from K. pneumoniae with OmpK37, known to form smaller pores [96]. Reduced permeation rate as a consequence of altered function of porin represents yet another strategy found in antibiotic resistant bacteria. Several mutations in the L3 loop have been described that induce a constriction of the pore, for example, a clinical isolate of *Enterobacter aerogenes* with a glycine to aspartate substitution [97]. This mutation may cause a modification of the loop with a reduction of the pore lumen [98] and consequently a consistent decrease in porin conductance and reduction in cephalosporin sensitivity. Similar alterations have been demonstrated in the amino acid composition of the *Neisseria gonorrhoeae* porin Por [99]. Resistance to carbapenems in *P. aeruginosa* has been described in mutants lacking the porin-specific OprD and in mutants with deletions in the L2 loop of OprD [100]. These examples illustrate the role of porin channels in the mechanisms of antibiotic resistance emergence and provide molecular insights which could enable identification of new strategies to design more effective antimicrobials.

CONCLUSION

Bacteria have developed sophisticated virulence factors such as the OM to mount their attack against the host. One of the most fascinating aspects of the OM of Gram-negative bacteria is its ability to act as a highly selective barrier mainly through the combined effect of a hydrophobic lipid bilayer together with pore-forming proteins of specific size-exclusion properties. Porins from several Gram-negative bacteria play a fundamental role in the host-pathogen interaction, eliciting diverse biological proinflammatory activities and immune responses. In fact, porins present an intrinsic biological activity when interacting with eukaryotic cells, but also behave as antigens stimulating specific immune responses. While the structure determination of β-barrel membrane proteins has benefited from both an increased interest in the field and by the advancement of new crystallization and sample preparation techniques, the field remains an exciting challenge for future research efforts. The structures of many unidentified bacterial OM proteins with unknown functions are still unsolved, and the mechanism by which β-barrels are properly folded and inserted into the OM is still poorly understood. Mechanisms affecting the barrier properties of the OM through the modification of expression and/or function of the porin channels may have an huge impact on the sensitivity of Gram-negative bacteria to antibiotics, therefore a better understanding at the molecular level of both the structure and the function of bacterial porins will allow improvements of the current drug therapies or the design of new types of antibiotics that target these surface exposed structures.

CONFLICT OF INTEREST

The author(s) confirm that this article content has no conflicts of interest.

ACKNOWLEDGEMENT

Declared none.

REFERENCES

[1] Achouak, W.; Heulin, T.;Pages, J.M. Multiple facets of bacterial porins. *FEMS Microbiol. Lett*., **2001**, *199*, 1-7.

[2] Galdiero, M.; Vitiello, M.;Galdiero, S. Eukaryotic cell signaling and transcriptional activation induced by bacterial porins. *FEMS Microbiol. Lett*., **2003**, *226*, 57-64.

[3] Naumann, M.; Rudel, T.;Meyer, T.F. Host cell interactions and signaling with Neisseria gonorrhoeae. *Curr. Opin. Microbiol*., **1999**, *2*, 62-70.

[4] Silhavy, T.J.; Kahne, D.;Walker, S. The bacterial cell envelope. *Cold Spring Harb. Perspect. Biol*., **2010**, *2*, a000414.

[5] Galdiero, S.; Galdiero, M.;Pedone, C. beta-Barrel membrane bacterial proteins: structure, function, assembly and interaction with lipids. *Curr. Prot. Pept. Sci*., **2007**, *8*, 63-82.

[6] Schirmer, T.; Keller, T.A.; Wang, Y.F.;Rosenbusch, J.P. Structural basis for sugar translocation through maltoporin channels at 3.1 A resolution. *Science*, **1995**, *267*, 512-514.

[7] Forst, D.; Welte, W.; Wacker, T.;Diederichs, K. Structure of the sucrose-specific porin ScrY from Salmonella typhimurium and its complex with sucrose. *Nat. Struct. Biol*., **1998**, *5*, 37-46.

[8] Dutzler, R.; Schirmer, T.; Karplus, M.;Fischer, S. Translocation mechanism of long sugar chains across the maltoporin membrane channel. *Structure*, **2002**, *10*, 1273-1284.

[9] Pages, J.M.; James, C.E.;Winterhalter, M. The porin and the permeating antibiotic: a selective diffusion barrier in Gram-negative bacteria. *Nat. Rev. Microbiol*., **2008**, 6, 893-903.

[10] Weiss, M.S.; Wacker, T.; Weckesser, J.; Welte, W.;Schulz, G.E. The three-dimensional structure of porin from Rhodobacter capsulatus at 3 A resolution. *FEBS Lett*., **1990**, 267, 268-272.

[11] Weiss, M.S.; Abele, U.; Weckesser, J.; Welte, W.; Schiltz, E.;Schulz, G.E. Molecular architecture and electrostatic properties of a bacterial porin. *Science*, **1991**, *254*, 1627-1630.

[12] Cowan, S.W.; Schirmer, T.; Rummel, G.; Steiert, M.; Ghosh, R.; Pauptit, R.A.; Jansonius, J.N.;Rosenbusch, J.P. Crystal structures explain functional properties of two E. coli porins. *Nature*, **1992**, *358*, 727-733.

[13] Hirsch, A.; Breed, J.; Saxena, K.; Richter, O.M.; Ludwig, B.; Diederichs, K.;Welte, W. The structure of porin from Paracoccus denitrificans at 3.1 A resolution. *FEBS Lett*., **1997**, *404*, 208-210.

[14] Kreusch, A.; Neubuser, A.; Schiltz, E.; Weckesser, J.;Schulz, G.E. Structure of the membrane channel porin from Rhodopseudomonas blastica at 2.0 A resolution. *Protein Sci*., **1994**, *3*, 58-63.

[15] Zeth, K.; Diederichs, K.; Welte, W.;Engelhardt, H. Crystal structure of Omp32, the anion-selective porin from Comamonas acidovorans, in complex with a periplasmic peptide at 2.1 A resolution. *Structure*, **2000**, *8*, 981-992.

[16] Zachariae, U.; Kluhspies, T.; De, S.; Engelhardt, H.;Zeth, K. High resolution crystal structures and molecular dynamics studies reveal substrate binding in the porin Omp32. *J. Biol. Chem*., **2006**, *281*, 7413-7420.

[17] Moraes, T.F.; Bains, M.; Hancock, R.E.;Strynadka, N.C. An arginine ladder in OprP mediates phosphate-specific transfer across the outer membrane. *Nat. Struct. Mol. Biol*., **2007**, *14*, 85-87.

[18] Korteland, J.; Tommassen, J.;Lugtenberg, B. PhoE protein pore of the outer membrane of Escherichia coli K12 is a particularly efficient channel for organic and inorganic phosphate. *Biochim. Biophys. Acta*., **1982**, *690*, 282-289.

[19] Pajatsch, M.; Andersen, C.; Mathes, A.; Bock, A.; Benz, R.;Engelhardt, H. Properties of a cyclodextrin-specific, unusual porin from Klebsiella oxytoca. *J. Biol. Chem*., **1999**, *274*, 25159-25166.

[20] Yildiz, O.; Vinothkumar, K.R.; Goswami, P.;Kuhlbrandt, W. Structure of the monomeric outer-membrane porin OmpG in the open and closed conformation. *EMBO J*., **2006**, *25*, 3702-3713.

[21] Schulz, G.E. Bacterial porins: structure and function. *Curr. Opin. Cell Biol*., **1993**, *5*, 701-707.

[22] Elofsson, A.;von Heijne, G. Membrane protein structure: prediction versus reality. *Annu. Rev. Biochem*., **2007**, *76*, 125-140.

[23] Walther, D.M.; Rapaport, D.;Tommassen, J. Biogenesis of beta-barrel membrane proteins in bacteria and eukaryotes: evolutionary conservation and divergence. *Cell Mol. Life Sci*., **2009**, *66*, 2789-2804.

[24] Schleiff, E.;Soll, J. Membrane protein insertion: mixing eukaryotic and prokaryotic concepts. *EMBO Rep*., **2005**, *6*, 1023-1027.

[25] Jeanteur, D.; Schirmer, T.; Fourel, D.; Simonet, V.; Rummel, G.; Widmer, C.; Rosenbusch, J.P.; Pattus, F.;Pages, J.M. Structural and functional alterations of a colicin-resistant mutant of OmpF porin from Escherichia coli. *Proc. Natl. Acad. Sci. USA.*, **1994**, *91*, 10675-10679.

[26] Charbit, A. Maltodextrin transport through lamb. *Front Biosci.*, **2003**, *8*, s265-274.

[27] Meyer, J.E.; Hofnung, M.;Schulz, G.E. Structure of maltoporin from Salmonella typhimurium ligated with a nitrophenyl-maltotrioside. *J. Mol. Biol.*, **1997**, *266*, 761-775.

[28] Nikaido, H. Molecular basis of bacterial outer membrane permeability revisited. *Microbiol. Mol. Biol. Rev.*, **2003**, *67*, 593-656.

[29] Hearn, E.M.; Patel, D.R.; Lepore, B.W.; Indic, M.;van den Berg, B. Transmembrane passage of hydrophobic compounds through a protein channel wall. *Nature*, **2009**, *458*, 367-370.

[30] Hearn, E.M.; Patel, D.R.;van den Berg, B. Outer-membrane transport of aromatic hydrocarbons as a first step in biodegradation. *Proc. Natl. Acad. Sci. USA.*, **2008**, *105*, 8601-8606.

[31] Lepore, B.W.; Indic, M.; Pham, H.; Hearn, E.M.; Patel, D.R.;van den Berg, B. Ligand-gated diffusion across the bacterial outer membrane. *Proc. Natl. Acad. Sci. USA*, **2011**, *108*, 10121-10126.

[32] Subbarao, G.V.;van den Berg, B. Crystal structure of the monomeric porin OmpG. *J. Mol. Biol.*, **2006**, *360*, 750-759.

[33] Dutzler, R.; Wang, Y.F.; Rizkallah, P.; Rosenbusch, J.P.;Schirmer, T. Crystal structures of various maltooligosaccharides bound to maltoporin reveal a specific sugar translocation pathway. *Structure*, **1996**, *4*, 127-134.

[34] Wirth, C.; Condemine, G.; Boiteux, C.; Berneche, S.; Schirmer, T.;Peneff, C.M. NanC crystal structure, a model for outer-membrane channels of the acidic sugar-specific KdgM porin family. *J. Mol. Biol.*, **2009**, *394*, 718-731.

[35] Whitney, J.C.; Hay, I.D.; Li, C.; Eckford, P.D.; Robinson, H.; Amaya, M.F.; Wood, L.F.; Ohman, D.E.; Bear, C.E.; Rehm, B.H.;Howell, P.L. Structural basis for alginate secretion across the bacterial outer membrane. *Proc. Natl. Acad. Sci. USA*, **2011**, *108*, 13083-13088.

[36] Faller, M.; Niederweis, M.;Schulz, G.E. The structure of a mycobacterial outer-membrane channel. *Science*, **2004**, *303*, 1189-1192.

[37] Galdiero, S.;Gouaux, E. High resolution crystallographic studies of alpha-hemolysin-phospholipid complexes define heptamer-lipid head group interactions: Implication for understanding protein-lipid interactions. *Protein Sci.*, **2004**, *13*, 1503-1511.

[38] Song, L.Z.; Hobaugh, M.R.; Shustak, C.; Cheley, S.; Bayley, H.;Gouaux, J.E. Structure of staphylococcal alpha-hemolysin, a heptameric transmembrane pore. *Science*, **1996**, *274*, 1859-1866.

[39] Faraldo, M.L.; de Pedro, M.A.;Berenguer, J. Cloning and expression in Escherichia coli of the structural gene coding for the monomeric protein of the S layer of Thermus thermophilus HB8. *J. Bacteriol.*, **1991**, *173*, 5346-5351.

[40] Caston, J.R.; Berenguer, J.; de Pedro, M.A.;Carrascosa, J.L. S-layer protein from Thermus thermophilus HB8 assembles into porin-like structures. *Mol. Microbiol.*, **1993**, *9*, 65-75.

[41] Maier, E.; Polleichtner, G.; Boeck, B.; Schinzel, R.;Benz, R. Identification of the outer membrane porin of Thermus thermophilus HB8: the channel-forming complex has an unusually high molecular mass and an extremely large single-channel conductance. *J. Bacteriol.*, **2001**, *183*, 800-803.

[42] Booth, P.J.;Curran, A.R. Membrane protein folding. *Curr. Opin. Struct. Biol.*, **1999**, *9*, 115-121.

[43] Reusch, R.N. Insights into the structure and assembly of Escherichia coli outer membrane protein A. *FEBS J.*, **2012**,

[44] Buchanan, S.K. beta-Barrel proteins from bacterial outer membranes: structure, function and refolding. *Current Opinion in Structural Biology*. **1999**, 9, 455-461.

[45] Kleinschmidt, J.H.;Tamm, L.K. Folding intermediates of a beta-barrel membrane protein. Kinetic evidence for a multi-step membrane insertion mechanism. *Biochemistry*, **1996**, *35*, 12993-13000.

[46] Surrey, T.;Jahnig, F. Kinetics of folding and membrane insertion of a beta-barrel membrane-protein. *J. Biol. Chem.*, **1995**, *270*, 28199-28203.

[47] Tamm, L.K.; Arora, A.; Kleinschmidt, J.H. Structure and assembly of beta-barrel membrane proteins. *J. Biol. Chem.*, **2001**, *276*, 32399-32402.

[48] Bulieris, P.V.; Behrens, S.; Holst, O.;Kleinschmidt, J.H. Folding and insertion of the outer membrane protein OmpA is assisted by the chaperone Skp and by lipopolysaccharide. *J. Biol. Chem.*, **2003**, *278*, 9092-9099.

[49] Rigel, N.W.; Schwalm, J.; Ricci, D.P.;Silhavy, T.J. BamE modulates the Escherichia coli beta-barrel assembly machine component BamA. *J. Bacteriol.*, **2012**, *194*, 1002-1008.

[50] Rigel, N.W.;Silhavy, T.J. Making a beta-barrel: assembly of outer membrane proteins in Gram-negative bacteria. *Curr. Opin. Microbiol.*, **2012**, *15*, 189-193.

[51] Ricci, D.P.; Hagan, C.L.; Kahne, D.;Silhavy, T.J. Activation of the Escherichia coli beta-barrel assembly machine (Bam) is required for essential components to interact properly with substrate. *Proc. Natl. Acad. Sci. USA*, **2012**, *109*, 3487-3491.

[52] Galdiero, M., Cantisani, M., Tarallo, R., Falanga, A., Galdiero, S., Septic Shock by Gram-Negative Infections: Role of Outer Membrane Proteins, in: D.R. Fernandez (Ed.), Understanding a serious killer, InTech, **2012**, 27-46.

[53] Di Donato, A.; Draetta, G.F.; Illiano, G.; Tufano, M.A.; Sommese, L.;Galdiero, F. Do porins inhibit the macrophage phagocyting activity by stimulating the adenylate cyclase? *J. Cyclic Nucleotide Prot. Phosphor. Res.*, **1986**, *11*, 87-97.

[54] Galdiero, F.; Tufano, M.A.; Sommese, L.; Folgore, A.;Tedesco, F. Activation of complement system by porins extracted from Salmonella typhimurium. *Infect. Immun.*, **1984**, *46*, 559-563.

[55] Akira, S.; Uematsu, S.;Takeuchi, O. Pathogen recognition and innate immunity. *Cell*, **2006**, *124*, 783-801.

[56] West, A.P.; Koblansky, A.A.;Ghosh, S. Recognition and signaling by toll-like receptors. *Annu Rev Cell Dev. Biol.*, **2006**, *22*, 409-437.

[57] Banerjee, P.; Biswas, A.;Biswas, T. Porin-incorporated liposome induces Toll-like receptors 2- and 6-dependent maturation and type 1 response of dendritic cell. *Int Immunol.*, **2008**, *20*, 1551-1563.

[58] Galdiero, M.; Finamore, E.; Rossano, F.; Gambuzza, M.; Catania, M.R.; Teti, G.; Midiri, A.;Mancuso, G. Haemophilus influenzae porin induces Toll-like receptor 2-mediated cytokine production in human monocytes and mouse macrophages. *Infect. Immun.*, **2004**, *72*, 1204-1209.

[59] Massari, P.; Henneke, P.; Ho, Y.; Latz, E.; Golenbock, D.T.;Wetzler, L.M. Cutting edge: Immune stimulation by neisserial porins is toll-like receptor 2 and MyD88 dependent. *J. Immunol.*, **2002**, *168*, 1533-1537.

[60] Massari, P.; Visintin, A.; Gunawardana, J.; Halmen, K.A.; King, C.A.; Golenbock, D.T.;Wetzler, L.M. Meningococcal porin PorB binds to TLR2 and requires TLR1 for signaling. *J. Immunol.*, **2006**, *176*, 2373-2380.

[61] Ray, A.; Chatterjee, N.S.; Bhattacharya, S.K.;Biswas, T. Porin of Shigella dysenteriae enhances mRNA levels for Toll-like receptor 2 and MyD88, up-regulates CD80 of murine macrophage, and induces the release of interleukin-12. *FEMS Immunol. Med. Microbiol.*, **2003**, *39*, 213-219.

[62] Jin, M.S.; Kim, S.E.; Heo, J.Y.; Lee, M.E.; Kim, H.M.; Paik, S.G.; Lee, H.;Lee, J.O. Crystal structure of the TLR1-TLR2 heterodimer induced by binding of a tri-acylated lipopeptide. *Cell*, **2007**, *130*, 1071-1082.

[63] Ferguson, A.D.; Welte, W.; Hofmann, E.; Lindner, B.; Holst, O.; Coulton, J.W.;Diederichs, K. A conserved structural motif for lipopolysaccharide recognition by procaryotic and eucaryotic proteins. *Structure*, **2000**, *8*, 585-592.

[64] Tanabe, M.; Nimigean, C.M.;Iverson, T.M. Structural basis for solute transport, nucleotide regulation, and immunological recognition of Neisseria meningitidis PorB. *Proc. Natl. Acad. Sci. USA*, **2010**, *107*, 6811-6816.

[65] Finamore, E.; Vitiello, M.; D'Isanto, M.; Galdiero, E.; Falanga, A.; Kampanaraki, A.; Raieta, K.;Galdiero, M. Evidence for IL-6 promoter nuclear activation in U937 cells stimulated with Salmonella enterica serovar Typhimurium porins. *Eur. Cytokine Netw.*, **2009**, *20*, 140-147.

[66] Pore, D.; Mahata, N.;Chakrabarti, M.K. Outer membrane protein A (OmpA) of Shigella flexneri 2a links innate and adaptive immunity in a TLR2-dependent manner and involvement of IL-12 and nitric oxide. *J. Biol. Chem.*, **2012**, *287*, 12589-12601.

[67] Galdiero, M.; D'Amico, M.; Gorga, F.; Di Filippo, C.; D'Isanto, M.; Vitiello, M.; Longanella, A.;Tortora, A. Haemophilus influenzae porin contributes to signaling of the inflammatory cascade in rat brain. *Infect. Immun.*, **2001**, *69*, 221-227.

[68] Yi, K.;Murphy, T.F. Importance of an immunodominant surface-exposed loop on outer membrane protein P2 of nontypeable Haemophilus influenzae. *Infect. Immun*., **1997**, *65*, 150-155.

[69] Haase, E.M.; Yi, K.; Morse, G.D.;Murphy, T.F. Mapping of bactericidal epitopes on the P2 porin protein of nontypeable Haemophilus influenzae. *Infect. Immun*., **1994**, *62*, 3712-3722.

[70] Neary, J.M.; Yi, K.; Karalus, R.J.;Murphy, T.F. Antibodies to loop 6 of the P2 porin protein of nontypeable Haemophilus influenzae are bactericidal against multiple strains. *Infect Immun*., **2001**, *69*, 773-778.

[71] Hughes, E.E.; Gilleland, L.B.;Gilleland, H.E., Jr. Synthetic peptides representing epitopes of outer membrane protein F of Pseudomonas aeruginosa that elicit antibodies reactive with whole cells of heterologous immunotype strains of P. aeruginosa. *Infect Immun*., **1992**, *60*, 3497-3503.

[72] Maiden, M.C.; Suker, J.; McKenna, A.J.; Bygraves, J.A.;Feavers, I.M. Comparison of the class 1 outer membrane proteins of eight serological reference strains of Neisseria meningitidis. *Mol. Microbiol*., **1991**, *5*, 727-736.

[73] Thompson, E.A.; Feavers, I.M.;Maiden, M.C. Antigenic diversity of meningococcal enterobactin receptor FetA, a vaccine component. *Microbiology*, **2003**, *149*, 1849-1858.

[74] Gupta, S.; Kumar, D.; Vohra, H.;Ganguly, N.K. Involvement of signal transduction pathways in Salmonella typhimurium porin activated gut macrophages. *Mol. Cell Biochem*., **1999**, *194*, 235-243.

[75] Galdiero, M.; D'Isanto, M.; Vitiello, M.; Finamore, E.;Peluso, L. Monocytic activation of protein tyrosine kinase, protein kinase A and protein kinase C induced by porins isolated from Salmonella enterica serovar Typhimurium. *J. Infect*., **2003**, *46*, 111-119.

[76] Massari, P.; Ram, S.; Macleod, H.;Wetzler, L.M. The role of porins in neisserial pathogenesis and immunity. *Trends Microbiol*., **2003**, *11*, 87-93.

[77] Galdiero, M.; Vitiello, M.; Sanzari, E.; D'Isanto, M.; Tortora, A.; Longanella, A.;Galdiero, S. Porins from Salmonella enterica serovar Typhimurium activate the transcription factors activating protein 1 and NF-kappaB through the Raf-1-mitogen-activated protein kinase cascade. *Infect Immun*., **2002**, *70*, 558-568.

[78] Vitiello, M.; Galdiero, M.; Finamore, E.;Galdiero, S. NF-kappaB as a potential therapeutic target in microbial diseases. *Mol. Biosyst*., **2012**, *8*, 1108-1120.

[79] Caraglia, M.; Tagliaferri, P.; Marra, M.; Giuberti, G.; Budillon, A.; Gennaro, E.D.; Pepe, S.; Vitale, G.; Improta, S.; Tassone, P.; Venuta, S.; Bianco, A.R.;Abbruzzese, A. EGF activates an inducible survival response via the RAS-> Erk-1/2 pathway to counteract interferon-alpha-mediated apoptosis in epidermoid cancer cells. *Cell Death Differ*., **2003**, *10*, 218-229.

[80] Li, S.;Sedivy, J.M. Raf-1 protein kinase activates the NF-kappa B transcription factor by dissociating the cytoplasmic NF-kappa B-I kappa B complex. *Proc. Natl. Acad. Sci. USA*, **1993**, *90*, 9247-9251.

[81] Caraglia, M.; Tassone, P.; Marra, M.; Budillon, A.; Venuta, S.;Tagliaferri, P. Targeting Raf-kinase: molecular rationales and translational issues. *Ann. Oncol*., **2006**, *17* Suppl 7, vii124-127.

[82] Caraglia, M.; Marra, M.; Tagliaferri, P.; Lamberts, S.W.; Zappavigna, S.; Misso, G.; Cavagnini, F.; Facchini, G.; Abbruzzese, A.; Hofland, L.J.;Vitale, G. Emerging strategies to strengthen the anti-tumour activity of type I interferons: overcoming survival pathways. *Curr. Cancer Drug Targets*., **2009**, *9*, 690-704.

[83] Galdiero, S.; Capasso, D.; Vitiello, M.; D'Isanto, M.; Pedone, C.;Galdiero, M. Role of surface-exposed loops of Haemophilus influenzae protein P2 in the mitogen-activated protein kinase cascade. *Infect Immun*., **2003**, *71*, 2798-2809.

[84] Galdiero, S.; Vitiello, M.; Amodeo, P.; D'Isanto, M.; Cantisani, M.; Pedone, C.;Galdiero, M. Structural requirements for proinflammatory activity of porin P2 Loop 7 from Haemophilus influenzae. *Biochemistry*, **2006**, *45*, 4491-4501.

[85] Alberti, S.; Rodriquez-Quinones, F.; Schirmer, T.; Rummel, G.; Tomas, J.M.; Rosenbusch, J.P.;Benedi, V.J. A porin from Klebsiella pneumoniae: sequence homology, three-dimensional model, and complement binding. *Infect. Immun*., **1995**, 63, 903-910.

[86] Cantisani, M.; Vitiello, M.; Falanga, A.; Finamore, E.; Galdiero, M.;Galdiero, S. Peptides complementary to the active loop of porin P2 from Haemophilus influenzae modulate its activity. *Int. J. Nanomedicine*., **2012**, 7, 2361-2371.

[87] Vitiello, M.; Galdiero, S.; D'Isanto, M.; D'Amico, M.; Di Filippo, C.; Cantisani, M.; Galdiero, M.;Pedone, C. Pathophysiological changes of gram-negative bacterial infection can be reproduced by a synthetic peptide mimicking loop L7 sequence of Haemophilus influenzae porin. *Microb. Infect*., **2008**, *10*, 657-663.

[88] Rice, L.B. Emerging issues in the management of infections caused by multidrug-resistant gram-negative bacteria. *Cleve. Clin. J. Med*., **2007**, *74* Suppl 4, S12-20.

[89] Blot, S.; Depuydt, P.; Vandewoude, K.;De Bacquer, D. Measuring the impact of multidrug resistance in nosocomial infection. *Curr. Opin. Infect. Dis.*, **2007**, *20*, 391-396.

[90] Davin-Regli, A.; Bolla, J.M.; James, C.E.; Lavigne, J.P.; Chevalier, J.; Garnotel, E.; Molitor, A.;Pages, J.M. Membrane permeability and regulation of drug "influx and efflux" in enterobacterial pathogens. *Curr. Drug Targets*, **2008**, *9*, 750-759.

[91] Hancock, R.E.;Bell, A. Antibiotic uptake into gram-negative bacteria. *Eur. J. Clin. Microbiol. Infect. Dis.*, **1988**, *7*, 713-720.

[92] Poole, K. Outer membranes and efflux: the path to multidrug resistance in Gram-negative bacteria. *Curr. Pharm. Biotechnol*., **2002**, *3*, 77-98.

[93] Poole, K. Resistance to beta-lactam antibiotics. *Cell Mol. Life Sci*., **2004**, *61*, 2200-2223.

[94] George, A.M.;Levy, S.B. Gene in the major cotransduction gap of the Escherichia coli K-12 linkage map required for the expression of chromosomal resistance to tetracycline and other antibiotics. *J. Bacteriol*., **1983**, *155*, 541-548.

[95] Viveiros, M.; Dupont, M.; Rodrigues, L.; Couto, I.; Davin-Regli, A.; Martins, M.; Pages, J.M.;Amaral, L. Antibiotic stress, genetic response and altered permeability of E. coli. *PLoS One*, **2007**, *2*, e365.

[96] Domenech-Sanchez, A.; Hernandez-Alles, S.; Martinez-Martinez, L.; Benedi, V.J.;Alberti, S. Identification and characterization of a new porin gene of Klebsiella pneumoniae: its role in beta-lactam antibiotic resistance. *J. Bacteriol*., **1999**, *181*, 2726-2732.

[97] De, E.; Basle, A.; Jaquinod, M.; Saint, N.; Mallea, M.; Molle, G.;Pages, J.M. A new mechanism of antibiotic resistance in Enterobacteriaceae induced by a structural modification of the major porin. *Mol. Microbiol*., **2001**, *41*, 189-198.

[98] Simonet, V.; Mallea, M.;Pages, J.M. Substitutions in the eyelet region disrupt cefepime diffusion through the Escherichia coli OmpF channel. *Antimicrob. Agents Chemother*., **2000**, *44*, 311-315.

[99] Gill, M.J.; Simjee, S.; Al-Hattawi, K.; Robertson, B.D.; Easmon, C.S.;Ison, C.A. Gonococcal resistance to beta-lactams and tetracycline involves mutation in loop 3 of the porin encoded at the penB locus. *Antimicrob. Agents Chemother*., **1998**, *42*, 2799-2803.

[100] Huang, H.;Hancock, R.E. The role of specific surface loop regions in determining the function of the imipenem-specific pore protein OprD of Pseudomonas aeruginosa. *J. Bacteriol*., **1996**, *178*, 3085-3090.

Received: July 05, 2012 **Revised: July 20, 2012** **Accepted: July 25, 2012**

OPEN ACCESS Freely available online

PLoS one

Biophysical Characterization and Membrane Interaction of the Two Fusion Loops of Glycoprotein B from Herpes Simplex Type I Virus

Annarita Falanga[1,2], Rossella Tarallo[1], Giuseppe Vitiello[3], Mariateresa Vitiello[4], Emiliana Perillo[1], Marco Cantisani[1,2], Gerardino D'Errico[3], Massimiliano Galdiero[2,4]*, Stefania Galdiero[1,2,5]*

1 Division of Biostructures, Department of Biological Sciences, University of Naples "Federico II", Napoli, Italy, **2** Centro Interuniversitario di Ricerca sui Peptidi Bioattivi, University of Naples "Federico II", Napoli, Italy, **3** Department of Chemistry, University of Naples "Federico II" and Consorzio per lo Studio dei Sistemi a Grande Interfase, CSGI, Monte Sant'Angelo, Napoli, Italy, **4** Department of Experimental Medicine, II University of Naples, Napoli, Italy, **5** Istituto di Biostrutture e Bioimmagini, CNR, Napoli, Italy

Abstract

The molecular mechanism of entry of herpesviruses requires a multicomponent fusion system. Cell invasion by Herpes simplex virus (HSV) requires four virally encoded glycoproteins: namely gD, gB and gH/gL. The role of gB has remained elusive until recently when the crystal structure of HSV-1 gB became available and the fusion potential of gB was clearly demonstrated. Although much information on gB structure/function relationship has been gathered in recent years, the elucidation of the nature of the fine interactions between gB fusion loops and the membrane bilayer may help to understand the precise molecular mechanism behind herpesvirus-host cell membrane fusion. Here, we report the first biophysical study on the two fusion peptides of gB, with a particular focus on the effects determined by both peptides on lipid bilayers of various compositions. The two fusion loops constitute a structural subdomain wherein key hydrophobic amino acids form a ridge that is supported on both sides by charged residues. When used together the two fusion loops have the ability to significantly destabilize the target membrane bilayer, notwithstanding their low bilayer penetration when used separately. These data support the model of gB fusion loops insertion into cholesterol enriched membranes.

Citation: Falanga A, Tarallo R, Vitiello G, Vitiello M, Perillo E, et al. (2012) Biophysical Characterization and Membrane Interaction of the Two Fusion Loops of Glycoprotein B from Herpes Simplex Type I Virus. PLoS ONE 7(2): e32186. doi:10.1371/journal.pone.0032186

Editor: Robert J. Geraghty, University of Minnesota, United States of America

Received October 24, 2011; **Accepted** January 23, 2012; **Published** February 23, 2012

Funding: This work was supported by MIUR (Ministero dell'Istruzione, dell'Università e della Ricerca) (FIRB Prot. RBRN07BMCT). The funders had no role in study design, data collection and analysis, decision to publish, or preparation of the manuscript.

Competing Interests: The authors have declared that no competing interests exist.

* E-mail: massimiliano.galdiero@unina2.it (MG); sgaldier@unina.it (SG)

Introduction

Enveloped viruses infect host cells by fusion of viral and target membranes. The initial apposition step is followed by fusion of the outer leaflets of membranes (the hemifusion step), leading to the formation of a transient fusion intermediate, which evolves into the fusion of inner leaflets and the formation of a pore, with the mixing of the internal compartments of both fusion partners. Thus, the viral genome is transferred to the cytoplasm of the host cell and viral replication ensues [1–3]. This fusion event is triggered by specific glycoproteins in the viral envelope. Fusion glycoproteins belong to either class I, class II or the newly described class III, depending upon their arrangement at the surface of the virion, their structure and the location within the protein of a short stretch of hydrophobic amino acids called the fusion peptide, which is able to induce the initial lipid destabilization that ends in fusion [4].

Although, viral fusion proteins are divided in three classes and the cellular membrane undergoing fusion might vary (plasma membrane vs. endosomal membrane), these proteins have to act on lipid assemblies. Thus, lipids contribute to fusion through their physical, mechanical and/or chemical properties and play a role in determining the preferential partitioning of some amino acid sequences into membrane microdomains called "rafts", and/or in modulating the curvature of the membranes involved in the fusion process [3].

Considering lipids and fusion proteins the necessary partners involved in the fusion process, it becomes clear that the overall gist of viral-induced membrane fusion is dictated by several features common to different families of viruses [1]. All fusion machineries need to interact with lipids, so they possess hydrophobic segments (fusion peptides) or are able after rearrangements to make hydrophobic interactions with membranes; moreover, need to adopt specific conformations related to the pre and post-fusion states, since fusion is limited in space and time. Therefore, different viruses infect their host cells by very similar mechanisms at the molecular level and fusion peptides represent a key element of the fusion machinery, being the trigger for controlled membrane destabilization.

Recently, the novel concept of "lipid packing sensor" emerged, indicating protein motifs or domains that recognize the curvature of lipid membranes. The most studied sensor is the amphipathic helical motif present both in cellular membrane proteins and in viral proteins [5,6]; but also other structural motifs, such as loops or unfolded peptides, may be involved in the sensing of the membrane curvature and in the initial steps of membrane fusion.

The discovery of sensor motifs opens new perspectives with respect to viral fusion proteins, which may contain such sensors; and may help our understanding of the subtle and complex interplay between protein-induced fusion and lipid modulation and may represent targets for future antiviral therapies.

Herpes simplex virus type 1 (HSV-1) is a member of the α-herpesvirus subfamily and enters cells through fusion of the viral envelope with a cellular membrane in a cascade of molecular interactions involving multiple viral glycoproteins and cellular receptors. The envelope glycoproteins gH/gL, gB and gD are all essential for the entry process [7] and expression of this quartet of glycoproteins induces the fusion of cellular membranes in the absence of virus infection [8]. gH/gL and gB, also play important roles in primary fusion events that occur during egress of the capsid from the nucleus of infected cells [9]. Recently, it was shown that gB and gH/gL interact with each other concomitantly with fusion and that this interaction is triggered by binding of gD to its cellular receptor [10,11]. Thus, gB may function cooperatively with gH/gL, and each may have some fusogenic potential on its own. Although gB and gH/gL constitute the core fusion machinery of all members of the Herpesviridae, their mechanisms of action are still under investigation.

Peptides derived from the ectodomain of gH block virus entry [12], while others have the ability to bind and disrupt model membranes [13–18]. The recently solved crystal structure of the gH-gL complex [19] showed that gH has no structural homology with any known fusion protein supporting the hypothesis that gH may act as a regulator of fusion through interactions with gB, while the crystal structure of the gH-gL complex of EBV presents considerable differences in the structural arrangements of domains supporting the view that the complex can undergo dynamic rearrangements [7,20].

gB is highly conserved within all the members of the Herpesviridae and is involved in virus attachment, penetration and cell-to-cell spread. gB may undergo large conformational changes to bring about fusion and even though evidence for its refolding has yet to be obtained a model for pre-fusion gB has been proposed and it seems that gB undergoes a refolding transition during fusion. The structures of gB from HSV-1 [21] and EBV [22] demonstrated that gB has structural homology with viral fusion proteins belonging to other virus families: the vesicular stomatitis virus (VSV) G protein [23] and the baculovirus protein gp64 [24] and is probably the key fusion protein; moreover, several synthetic gB peptides induced the fusion of large unilamellar vesicles and inhibited herpes virus infection [25,26]. gB belongs to a newly formed group of fusion proteins, class III, which share similar individual domain structures and contain a central three-stranded coiled-coil reminiscent of the class I proteins. Whereas class I proteins have an N-terminal fusion peptide, class III proteins have internal bipartite fusion loops within domain I which are similar to the single fusion loop of class II fusion proteins. The class II fusion loop is composed entirely of hydrophobic amino acids whereas those of gB have both hydrophobic and charged residues [21–24]. In particular, the fusogenic loops correspond to the domains 173–179 and 258–265 of the protein gB.

Hydrophobic amino acids within the gB loops (W174, F175, G176, Y179, A261) are essential for gB function [27]. Similar studies of VSV G, gp64 and EBV gB support the notion that hydrophobic amino acids of both fusion loops are critical for fusion [28,29] and together constitute a fusion domain. Moreover, also charged amino acids play a fundamental role, in fact, mutations of H263 or R264 also negatively affected gB function [27]. These data support the view that the two fusion loops constitute a subdomain where key hydrophobic amino acids form a ridge that is flanked on both sides by charged amino acids that enhance the ability to interact with target membranes, in fact, one of the two gB fusion loops (namely HB168–186) was identified by highly interfacial hydrophobicity analysis without the aid of structural data [25].

Although much information has been gathered in recent years, we do not yet know the precise molecular mechanism behind herpesvirus host cell membrane fusion; thus, elucidating the nature of the fine interactions between gB fusion loops and the membrane may help to districate this interesting matter. In the present study, we report the synthesis and characterization of membrane interactions of the two fusion peptides present in gB. The goals of the experiments reported here were to verify the fusion ability of the two peptides, to assess the dependence of the fusion activity on the composition of the membrane and in particular on the content of cholesterol and to verify the eventual presence of a synergic or cooperative effect when the two isolated peptides are used together.

As far as we know, this is the first biophysical study on the two putative fusion peptides of gB, with a particular focus on the effects determined by both peptides on lipid bilayers of various compositions.

Results

Design of peptides

The proposed post-fusion structure of gB ectodomain is comprised of three protomers, and each protomer coils around the others with a left-handed twist [21]. There are multiple contacts between protomers throughout the molecule contributing to trimer stability. Each protomer of gB can be divided into five distinct domains: I, base; II, middle, III, core; IV crown; and V, arm (Figure 1). Domain I (Ile154 to Val363) is a β sandwich composed of two nearly orthogonal β sheets of four and three strands, with a long loop and short helix covering one opening of the β sandwich. An insertion (Tyr165 to Ile272) between strands β4 and β11 creates a subdomain at the base of the trimer, consisting of a four-stranded β sheet (with three long and one short strand), the convex side of which is covered with an α helix, a β hairpin, and a short two-stranded β sheet; the four-stranded β-sheet presents hydrophobic tips that have been proposed to represent the fusion peptides of gB (Figure 1). Fusion peptides are generally considered as being domains with a high interfacial hydrophobicity calculated with the Wimley-White hydrophobicity scale which was systematically used for searching fusion peptides in other viral glycoproteins. HB168–186, comprising the precise fusion loop HB173–179 [21], is located in the insertion between strands β4 and β11 and we were able to identify this region on the basis of its hydrophobicity, and analyse its role in peptide/lipid fusion assays [25]. The second loop (HB258–265), identified on the basis of structural data [21] contributes to the formation of the bipartite fusion peptide, but does not correspond to a hydrophobicity peak calculated with the interfacial scale and thus was not considered in our previous study [25].

Both fusion loops have been characterized by point-mutations in the protein sequence and showed to be critical for gB function in cell fusion [30]. In the present study, we report on the structural characterization of the two fusion loops by using peptides corresponding to their sequences. We synthesised a short version, corresponding exactly to the sequences of the loops, and a longer version, embracing the flanking β-sheets, in order to understand the contributions of each region that constitutes the gB fusogenic domain (Table 1). Moreover, we tried to understand the

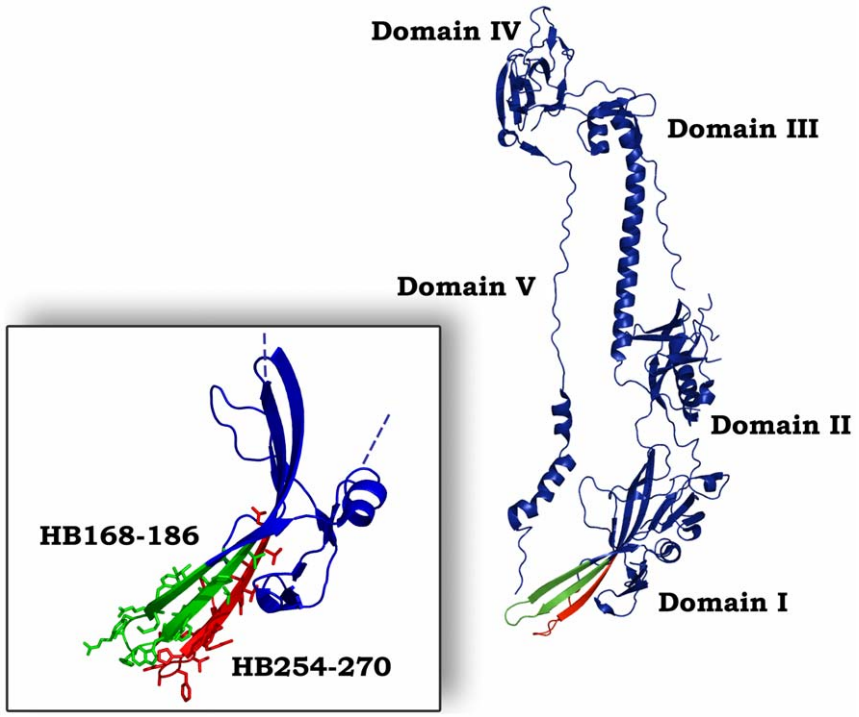

Figure 1. Three dimensional structure of a single gB protomer. The different domains are shown. In the insert are shown molecular details of the two fusion loops: HB168–186 (green) and HB254–270 (red).
doi:10.1371/journal.pone.0032186.g001

contribution of lipids that take part to the interplay between the membrane and fusogenic peptides.

Ability of peptides to induce lipid mixing

To investigate the fusogenicity of gB peptides, NBD and Rho labelled PE were used as the donor and acceptor of fluorescence energy transfer. A population of LUVs labelled with both was mixed with a population of unlabelled LUVs and increasing amounts of peptides were added. Dilution of the fluorescent-labelled vesicles via membrane fusion induced by the peptide results in a reduction of the fluorescence energy transfer efficiency, hence dequenching of the donor fluorescence. The dependence of the extent of lipid mixing on the peptide to lipid molar ratio was analysed. The fusogenic capacity was monitored by measuring their ability to induce lipid mixing of model membranes composed of DOPG, DOPG/Chol (3/2), DOPC, DOPC/Chol (3/2), POPC/Chol (3/2), and POPC/Chol/SM at various ratios (4/1/1, 2/1/1, 1/1/1).

Table 1. Peptides.

	Sequence
HB168–186	NH_2-VTVSQVWFGHRYSQFMGIF-COOH
HB173–179	NH_2-VWFGHRY-COOH
HB254–270	NH_2-YNPSRVEAFHRYGTTVN-COOH
HB258–265	NH_2-RVEAFHRY-COOH
scrambled	NH_2-MRWFSVVSYQVIGTQFGFH-COOH

doi:10.1371/journal.pone.0032186.t001

Interestingly, there was a different behaviour of the peptides depending on the lipid composition of LUVs. Figure 2A and B show the results of lipid mixing assays in LUVs of different compositions for peptides HB168–186 and HB254–270. The graphs show that in all tested conditions HB168–186 has higher fusogenic ability. DOPC/Chol, POPC/Chol and DOPG/Chol all proved to be good fusogenic conditions. Furthermore, it is evident from the results obtained that DOPG in presence or absence of cholesterol represents a less fusogenic condition, indicating that the negatively charged phospholipids are not preferred. This is a rather interesting result as both peptides contain arginine residues and thus we could expect a greater interaction with anionic lipids. Several viruses such as HIV, influenza virus and Semliki Forest virus have been shown to involve lipid microdomains, which are enriched in cholesterol during virus budding as well as virus entry. Also herpesvirus has been shown to require cholesterol [31,32], and such a need for cholesterol has also been highlighted in our experiments using model membranes where a significant increase in fusion is always observed in presence of cholesterol. The lipids allowing the highest level of fusion are DOPC and POPC which are both zwitterionic but present a difference in their unsaturation, with POPC having only one unsaturated acyl chain and DOPC having two. DOPC results in a more flexible bilayer, which appears to be an important feature for the fusion activity of the analyzed peptides. We also tested the peptide fusion ability of liposomes containing sphingomyelin, a component commonly found in lipid rafts. The ternary lipid system POPC/Chol/SM is a good model for lipid rafts and from the ternary phase diagram [33] it is possible to determine the boundaries for lipid rafts which are strongly dependent on the percentage of each lipid in the system. We used three different conditions to probe the activity of our peptides in LUVs mimicking rafts: POPC/Chol/SM 4/1/1, 2/1/1 and 1/1/1, characterized by different percentages of the liquid

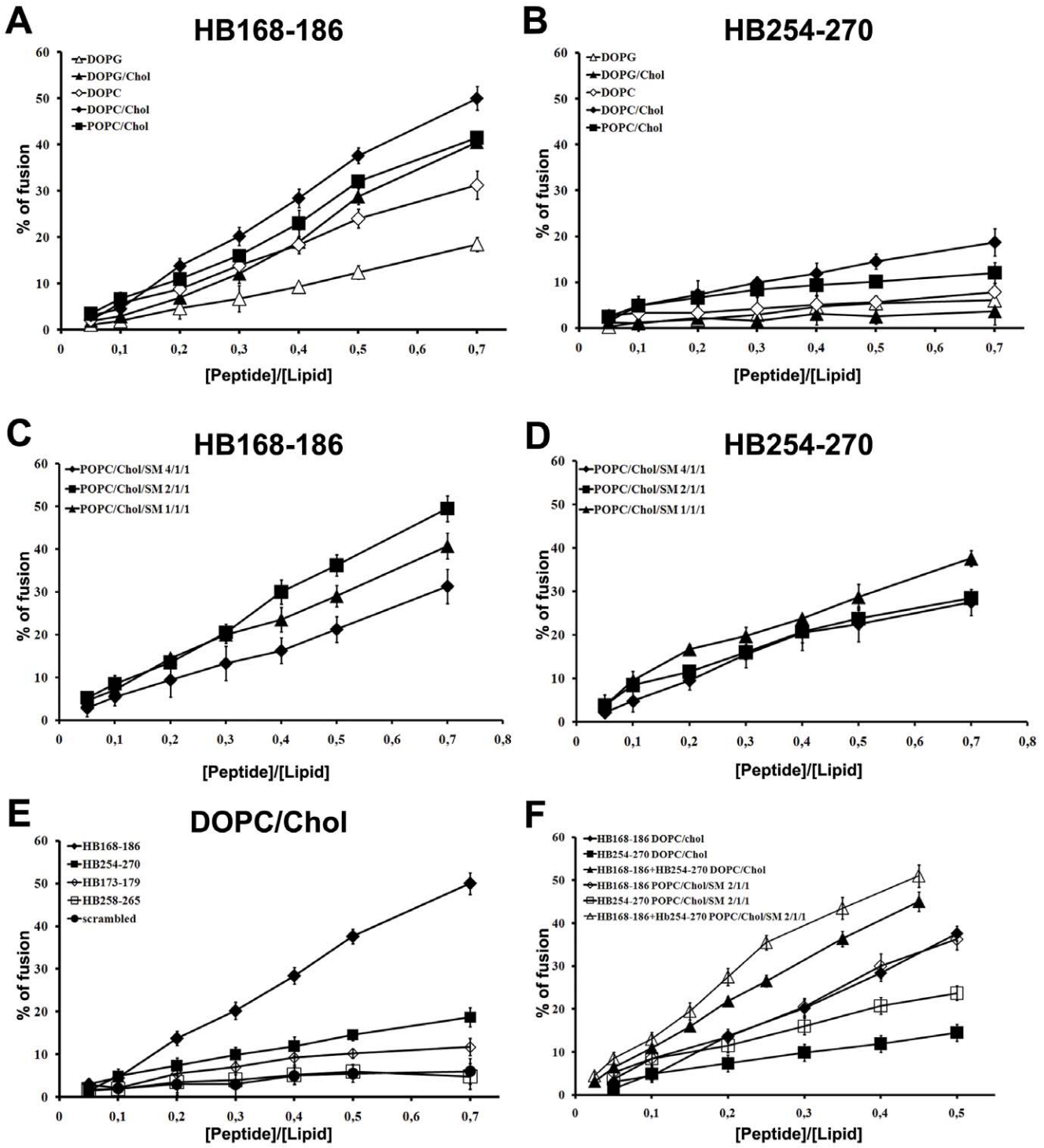

Figure 2. Ability of peptides to induce lipid mixing. Peptide-promoted membrane fusion as determined by lipid mixing; peptide aliquots were added to 0.1 mM LUVs, containing 0.6% NBD and 0.6% Rho. The increase in fluorescence was measured after the addition of peptide aliquots; reduced Triton-X-100 (0.05% v/v) was referred to as 100% of fusion. In figure is reported the dose dependence of lipid mixing at 37°C: panels A and B HB168–186 and HB254–270 in LUVs of different composition; panels C and D HB168–186 and HB254–270 in LUVs mimicking lipid rafts; panel E HB168–186, HB254–270 and shorter versions in DOPC/Chol LUVs; panel F equimolecular mixtures of peptides HB168–186 and HB254–270 in DOPC/Chol (3/2) and POPC/Chol/SM (2/1/1).
doi:10.1371/journal.pone.0032186.g002

ordered and liquid disordered phases. The results obtained (Figure 2 C–D) show that both peptides present a significant percentage of fusion

Figure 2E shows the results obtained in DOPC/Chol for the peptides HB168–186 and HB254–270 as well as their shorter versions corresponding exactly to the loop sequences derived from

the crystallographic structure. The two shorter peptides (HB173–179 and HB258–265) induced lower levels of fusion compared to longer sequences, suggesting that shorter peptides were unable to cross or stably position inside the bilayer. This result further supports the view that fusion loops are structured by the overall organization of the fusion domain of the protein and longer peptides are, therefore, necessary to evidence an appreciable fusion activity.

In the case of the peptide equimolar mixtures (Figure 2F), we can observe that in DOPC/Chol as well as in POPC/Chol/SM (2/1/1) we have a significant fusion activity supporting a cooperative mechanism.

Ability of peptides to induce lipid mixing of inner-monolayer

In the inner monolayer assay, the fluorescence from the vesicle membranes' outer monolayer is eliminated by the addition of an aqueous reducing agent, and this experiment reveals the extent of lipid mixing between the inner monolayers of vesicles in solution. Figure 3A shows a significant fusion of the inner monolayer in DOPC/Chol. This is slightly lower than the fusion level obtained in the lipid mixing experiment, since the latter measures both hemi-fusion and complete fusion. Therefore, this assay clearly indicates that the two peptides are able to induce fusion of both the inner and the outer monolayers.

We also verified the ability of peptide equimolar mixtures to induce lipid mixing of the inner-monolayer. The results obtained indicate that the peptides cooperate in the fusion process.

Ability of peptides to induce membrane leakage

In order to explore the effects of the peptides in the destabilization of membrane vesicles, we studied their effect on the release of encapsulated fluorophores in model membranes made of DOPC/Chol. A content-mixing assay (Figure 3B) was employed to monitor any mixing of internal vesicle components as a result of vesicle exposure to HB168–186 and HB254–270. Release of ANTS and DPX from vesicle is commonly used as a measure of bilayer perturbation and interpreted as ''transient pore formation'' [34,35]. Content-mixing is manifested by a decrease in fluorescence intensity if vesicles encapsulating fluorescent cargo (e.g., ANTS) merge contents with those containing quenchers (e.g., DPX). The leakage experiment shows that the probe did not leak out significantly to the medium after the interaction with any of the peptides used in this study. Figure 3B shows that no content-mixing occurs over the same P/L range where substantial outer and inner monolayer lipid-mixing occurs, confirming that vesicle fusion may happen within our system without concomitant pore formation. The low leakage value observed for both peptides might be due to the fact that they are located at the membrane interface and do not completely traverse the bilayer. We also verified the eventual ability of equimolar mixtures of HB168–186 and HB254–270 to induce membrane leakage, but no significant difference from results obtained for individual peptides was detected.

Peptide aggregation

The peptide's aggregation state in buffer and DOPC/Chol LUVs was assayed using ThT [36], in order to know the possible effects of the peptide aggregation on the membranes. As observed in Figure 4 A–B, the two peptides present a completely different behaviour. The peptide HB168–186 at a concentration of 4 μM (Figure 4A) is already aggregated in an aqueous medium, in fact, the fluorescence change increased dramatically after the addition of the peptide from a stock solution, while in the presence of DOPC/Chol a lower aggregation is reported. The peptide HB254–270 is not aggregated in the aqueous medium nor in the presence of DOPC/Chol at the same concentration. Furthermore, we studied the intrinsic relationship between the concentration of the peptides and the aggregation in buffer and in LUVs and we can interpret the data for HB168–186 reported in Figure 4C as aggregated both in the aqueous medium and in LUVs at high concentrations. Our results are consistent with two hypothesis; the first is an initial aggregation in the aqueous medium, followed by a disaggregation when initially interacting with the membrane and again an aggregation inside the membrane bilayer, indicating that the insertion of the peptide into the membrane could occur in a monomeric form and only afterwards the peptide aggregates again; while the second hypothesis is that the peptide can interact with the membranes already in an oligomerized state.

Tryptophan/tyrosine fluorescence emission analysis

We measured the intrinsic fluorescence of HB168–186 and HB254–270 (due to the presence of a tryptophan residue in the sequence of HB168–186 and two tyrosines for HB254–270) to evaluate the degree of penetration of the peptides into the membrane bilayer. We compared the fluorescence emission spectra in DOPC/Chol vesicles with that in buffer (data not shown). The quantum yield of aromatic residues of a peptide or protein normally changes when the amino acid is located in a more hydrophobic environment such as a phospholipid membrane, normally increasing the intensity of the fluorescence emission and shifting the maximal spectral position toward shorter wavelengths (blue shift). Changes in the spectral properties were observed for both peptides, suggesting that the single tryptophan residue of HB168–186 and the two tyrosines of HB254–270 move to a less polar environment upon interaction with lipids. Emission intensity was enhanced and the maxima shifted to lower wavelength. (Figure S1) Blue shifts of this magnitude are generally observed when amphiphilic aromatic-containing peptides interact with phospholipid bilayers and are consistent with the aromatic moiety becoming partially immersed in the membrane, further suggesting that the analysed peptides are capable of penetrating a lipid bilayer [37].

The increase in fluorescence for tryptophan or tyrosines binding to membrane phospholipids was used for the generation of binding isotherms for HB168–186 and HB254–270, therefore partition coefficients could be calculated. The concentrations of peptides used were low enough to cause minimal aggregation in the aqueous phase and were assumed not to disrupt the bilayer structure. To determine the surface partition coefficient, the fluorescence intensities were converted to moles of bound peptide per moles of lipid and plotted as a function of the free peptide concentration as described in material and methods (Figure 5). As partition coefficients depend on the concentration of lipid accessible to peptide, the curves obtained by plotting X_b* (the molar ratio of bound peptide per 60% of the total lipid) vs C_f (the equilibrium concentration of free peptide in the solution) are referred to as the conventional binding isotherms. The shape of a binding isotherm of a peptide can provide information on the organization of the peptide within the membrane. A straight line indicates a simple adhesion process. The shape of the binding isotherm of all the peptides tested was not linear indicating that peptide accumulation at the surface is not a simple phenomenon without cooperative association. In particular, this behaviour is the hallmark for peptides that self-associate at membrane surfaces upon partitioning. If aggregation occurred only in the water but not in the bilayer phase, the opposite course of the isotherms

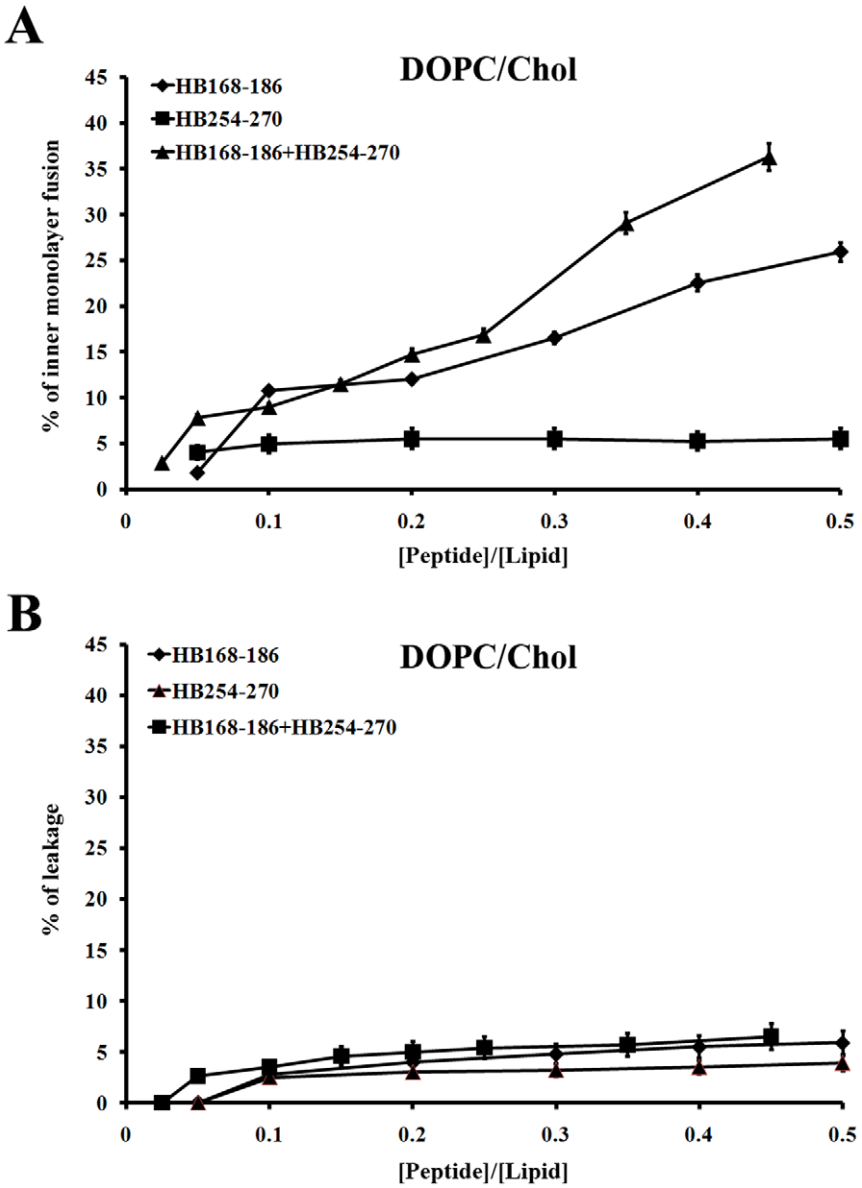

Figure 3. Ability of peptides to induce lipid mixing of inner-monolayer and membrane leakage. Peptide interactions with DOPC/Chol LUVs (A–B), the dose dependence is reported and each trace represents an average of three independent experiments. A) Inner monolayer assay. C) Leakage of ANTS/DPX.
doi:10.1371/journal.pone.0032186.g003

should be expected: a steep rise at the origin, followed by pronounced flattening; thus, the shape of the isotherms obtained could be interpreted as reflecting a process whereby peptides first incorporate into the membrane and then aggregate there within. Moreover, there was no evidence of significant aggregation in water at the concentration used in this experiment (0.1 μM) for HB254–270, although we have an indication of aggregation in water for HB168–186 as shown in Figure 4C. In the isotherms obtained, the total extent of incorporation (X_b^*) slowly increases until a critical concentration is reached, where massive internal aggregation apparently starts to develop.

The surface partition coefficients K_p were estimated by extrapolating the initial slopes of the curves to C_f values of zero. Curves are shown in Figure 5.

The K_p values for the peptides HB168–186 and HB254–270 are shown in Table 2. The K_p value obtained for HB168–186 is 2.5 10^4, indicating that the tryptophan in HB168–186 is able to interact significantly with the bilayer and that most of the peptide HB168–186 is located inside the liposomes. The K_p value for HB254–270 is 3.2 10^4, indicating that the tyrosine residues present in this peptide are located inside the liposomes and are stably inserted.

Quenching of tryptophan/tyrosines by Acrylamide

The observed changes in the characteristics of the tryptophan/tyrosine emission upon binding of peptides HB168–186 and HB254–270 to lipid vesicles indicate their insertion into the hydrophobic region of the bilayers. We also studied the accessibility of the tryptophan/tyrosine residues of membrane-bound peptides towards acrylamide, a neutral, water-soluble, highly efficient quenching molecule, which is unable to penetrate

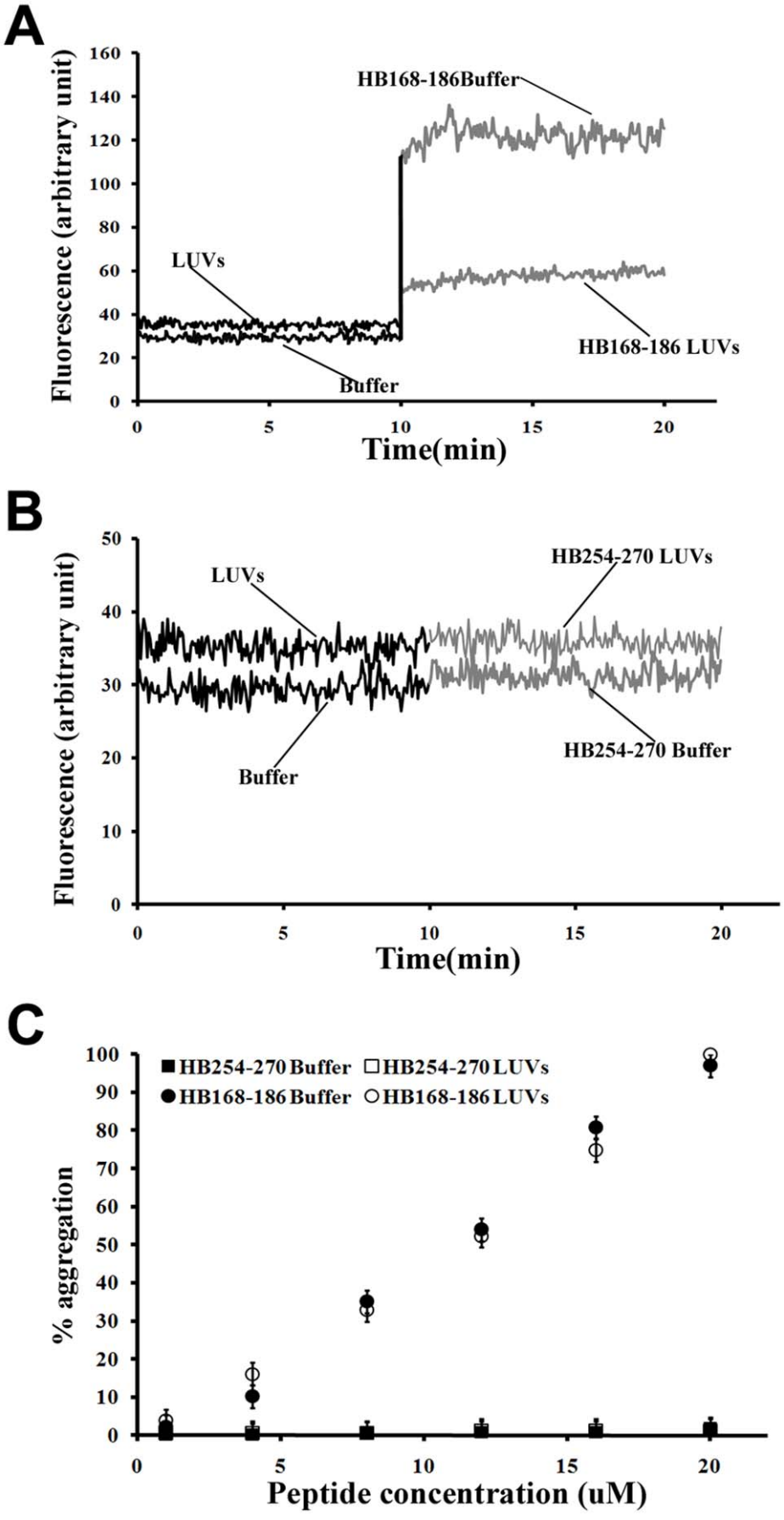
A
Fluorescence (arbitrary unit)
HB168-186Buffer
LUVs
HB168-186 LUVs
Buffer
Time(min)
B
Fluorescence (arbitrary unit)
LUVs
HB254-270 LUVs
HB254-270 Buffer
Buffer
Time(min)
C
HB254-270 Buffer
HB254-270 LUVs
HB168-186 Buffer
HB168-186 LUVs
% aggregation
Peptide concentration (uM)

Figure 4. Peptide aggregation. Fluorescence variation of ThT after addition of HB168–186 (A) and HB254–270 (B) peptides to an aqueous solution and in the presence of LUVs of DOPC/Chol at a peptide concentration of 4 μM. (C) Percentage of aggregation as a function of peptide concentration for HB168–186 and HB254–270 in buffer (closed symbols) and in LUVs (open symbols).
doi:10.1371/journal.pone.0032186.g004

into the hydrophobic core of the lipid bilayer. The more deeply a tryptophan/tyrosine residue is buried, the less strongly it can be quenched by acrylamide. Stern-Volmer plots for the quenching of tryptophan by acrylamide, recorded in the absence and presence of lipid vesicles, are depicted in Figure 6. Fluorescence of tryptophan/tyrosine decreased in a concentration-dependent manner by the addition of acrylamide to the peptide solution both in the absence and presence of liposomes, without other effects on the spectra. However, we can observe a substantial difference between the two peptides. In the presence of liposomes, a great decrease in fluorescence intensity was evident for HB254–270, thus revealing that tyrosine residues are less accessible to the quencher in the presence of LUVs. In fact, the values for K_{sv} were lower (Table 3) in LUVs, suggesting that tyrosines were more buried in the bilayers, becoming more inaccessible for quenching by acrylamide. From Figure 6, it is evident that we can observe for the peptide HB168–186 a low accessibility to the quencher both in absence and presence of liposomes, indicating that the peptide has a significant tendency to aggregate also in an aqueous solution.

ESR Results

The ESR spectroscopy, by using spin-labelled substances (peptides and/or lipids) has been proved to give substantial information on the interaction of peptide deriving from viral fusion glycoproteins with lipid membranes [38–41]. In the present work, the association of the two peptides, HB168–186 and HB254–270, with lipid bilayers was investigated by analysing changes in ESR spectra of spin-labelled phospholipids. The samples investigated were phosphatidylcholine spin-labelled at different positions, *n*, in the *sn*-2 chain (*n*-PCSL, $n = 5, 7, 10, 14$) incorporated in DOPC/Chol membranes (3/2), in the presence of the peptides. Preliminarily, the spectra in the absence of the peptides were registered. Inspection of Figure 7A (solid lines) shows that all the spectra present a clearly defined axially anisotropic lineshape, an evidence that, due to the high cholesterol content, the DOPC/Chol bilayer is in the liquid-ordered state [42]. In an attempt to quantitatively analyse the spectra, the outer hyperfine splitting, $2A_{max}$, was calculated. The $2A_{max}$ variation, shown in Figure 7B, is an evidence of the flexibility gradient in segmental acyl chain mobility [38,43], indicating that the lipid bilayer presents a rigid surface and relatively fluid interior [44–47].

Association of peptides to the lipid bilayer causes a significant variation in the ESR spectra of spin-labelled phospholipids. In Figure 7A, ESR spectra of 5-PCSL and 14-PCSL in DOPC/Chol bilayers, in the presence of HB168–186, HB254–270 and HB168–186:HB254–270 mixture at a lipid/peptide weight ratio of 1/1, are also reported. The presence of two peptides induces significant changes in the spin-label ESR spectra, which are mainly detectable from the low- and high-field component position and lineshape. In an attempt to quantify this evidence, the $2A_{max}$ values were determined. Figure 7B shows the dependence of these parameters on chain position, *n*, for the *n*-PCSL spin-labels in DOPC/Chol membranes, in the absence and in the presence of the peptides. In all cases, the flexibility gradient with the chain position of the lipid bilayer membranes is preserved. However, inspection of the figure reveals a significantly different behaviour of the lipid chain mobility in the co-presence of the two peptides.

In fact, addition of HB168–186 or HB254–270 significantly reduces the $2A_{max}$ value of 5-PCSL. In both cases, no changes in the spectra of the spin-labels bearing the nitroxide group in the more interior positions were observed. Strikingly, addition of the HB168–186:HB254–270 mixture results in a strongly $2A_{max}$ decrease for all the considered spin-labels. These results show a cooperation of the peptides in perturbing the bilayer microstructure in that only in the presence of both of them the increase of segmental mobility propagates along the whole acyl chains. Thus, the contemporary interaction of both peptides with the lipid membrane surface effectively perturbs the local order and dynamics of the lipid leaflet they come in contact with.

Secondary structure in lipid bilayers

The CD spectra of the peptides in buffer and bound to LUVs made of DOPC/Chol are shown in Figure 8. The binding of the peptides to the membrane bilayer did not affect their structure. The spectra are indicative of random conformation for both peptides.

Discussion

Membrane fusion is of fundamental importance in the biological life of a cell and is of particular interest during enveloped virus infections. A common feature of all fusion events is the involvement of the fusion peptide in these phenomena and the key role played by lipids in the conformational changes leading to the interaction of the fusion peptide with target membranes, and in the membrane deformation following the initial peptide-membrane interactions. Extensive research data on viral membrane fusion proteins have disclosed the existence of several protein domains involved in the viral fusion process. It is, thus, an accepted view the presence of different membrane-active regions in viral fusion glycoproteins, although their biological function is still unclear. It has been hypothesised that these regions may have a different role on either pore formation and stabilization, viral budding or both of them.

In the present work we have investigated the role played by the two fusion loops of HSV-1 gB in the mechanism of membrane fusion. In particular, three important issues were addressed: the ability of peptide analogues of the fusion loops to induce fusion of liposomes, their ability to interact with the membrane bilayer when alone and when used in equimolar concentrations and the role of the target membrane composition. For herpesviruses, cholesterol is thought to play a key role, in fact, lipid raft may act as a platform allowing cell entry and potential coreceptors clustering [32] or cholesterol may modulate the HSV entry process regardless of its ability to promote lipids microdomains [48]. In this work evidences have been obtained indicating the ability of the two fusion peptide to induce fusion of liposomes in vitro, their ability to strongly interact with a membrane bilayer containing cholesterol and finally their different mode of interaction with the bilayer indicating that although being both involved in the fusion mechanism they may play a different role.

The two fusion loops constitute a structural subdomain wherein key hydrophobic amino acids form a ridge that is supported on both sides by charged residues. The two charged residues located on both sides of the ridge represent a novel feature of viral fusion peptides and probably enhance the ability of the hydrophobic residues to interact with target membranes and to promote fusion.

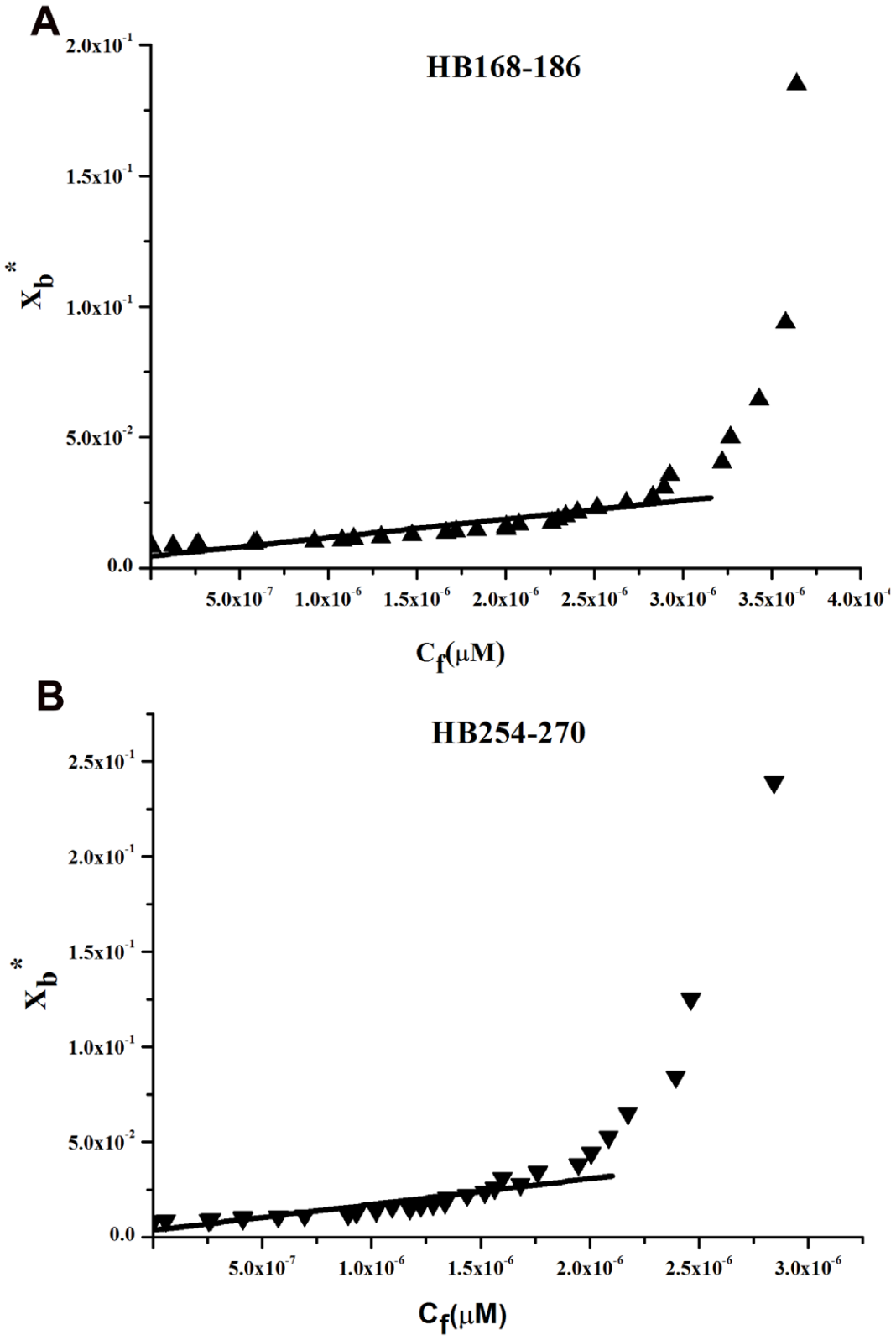

Figure 5. Tryptophan/tyrosine fluorescence emission analyses. Binding isotherms obtained plotting X_b^* versus C_f for HB168–186 and HB254–270.
doi:10.1371/journal.pone.0032186.g005

Table 2. Partition coefficient for the binding of peptides with PC/Chol.

	HB168–186	HB254–270
K_p	$(2.5\pm0.3)10^4$	$(3.2\pm0.2)10^4$

doi:10.1371/journal.pone.0032186.t002

Table 3. Stern-Volmer (Ksv) quenching constant calculated from the equation $F_0/F = 1+Ksv\ [Q]$ for HB168–186 and HB254–270.

	HB168–186	HB254–270
K_{sv} (M^{-1}) in buffer	8.3±0.2	71.1±1.1
K_{sv} (M^{-1}) in LUVs	6.4±0.4	8.5±0.1

doi:10.1371/journal.pone.0032186.t003

The analysis of the location of the fusion loops into the three-dimensional structure of gB points out that the hydrophobic residues do not appear to be able to insert deeply into a target membrane. The hydrophilic residues on either side of the hydrophobic ridge may help to stabilize insertion of gB into cholesterol enriched membranes or more generally membranes mimicking lipid rafts, but both fusion loops seem unable to deeply penetrate into the hydrophobic core of the bilayer.

The fusion ability of the two peptides was analysed using LUVs with different compositions. Membrane components, such as anionic lipids (DOPG), unsaturated phospholipids (DOPC, POPC), sphingolipid (SM) and cholesterol (Chol) were used in this study. Lipid raft formation occurs by spontaneous aggregation of certain naturally occurring lipids that aggregate in the plane of the membrane and are characterized by a higher degree of molecular order and by being thicker than the surrounding liquid-disordered lipids in the membrane. To investigate lipid raft characteristics in model membranes, Chol and SM are commonly combined with phospholipids having unsaturated and therefore kinked fatty acyl chains, such as POPC. Our results are consistent with previous studies showing the specific association of gB with cholesterol-rich rafts [32]. We found that gB peptides associate with lower fusion ability with liposomes in the absence of cholesterol. Our data further suggest that the cholesterol dependence of gB is not necessarily dependent on a protein receptor in rafts, but because cholesterol itself enhances insertion of the fusion loops. In Semliki Forest virus fusion protein E1, a class II fusion protein that inserts preferentially into membranes enriched in cholesterol and sphingolipid [49], a point mutation in the loop adjacent to the fusion loop confers increased cholesterol independence [50,51].

Lipid mixing, inner-monolayer and leakage are three independent experiments which describe different processes during the interaction of peptides with liposomes. In particular, the lipid mixing experiment evidences the fusion of both the inner and outer monolayer, the inner monolayer experiment evidences the eventual presence of fusion of the inner monolayer, while the leakage describes the pore formation. Results were consistent among the three experiments for both peptides, supporting the hypothesis that the two peptides induce fusion of inner and outer monolayers but not formation of pores whenever used alone or in equimolar concentrations. The present results can be used as qualitative indicators of bilayer perturbation due to its interaction with the peptides and their superficially positioning. We have not detected any significant pore formation; in fact, vesicle fusion events were not accompanied by leakage of the aqueous contents of the vesicle as also reported for other peptides in a study published by Thoren et al. [52].

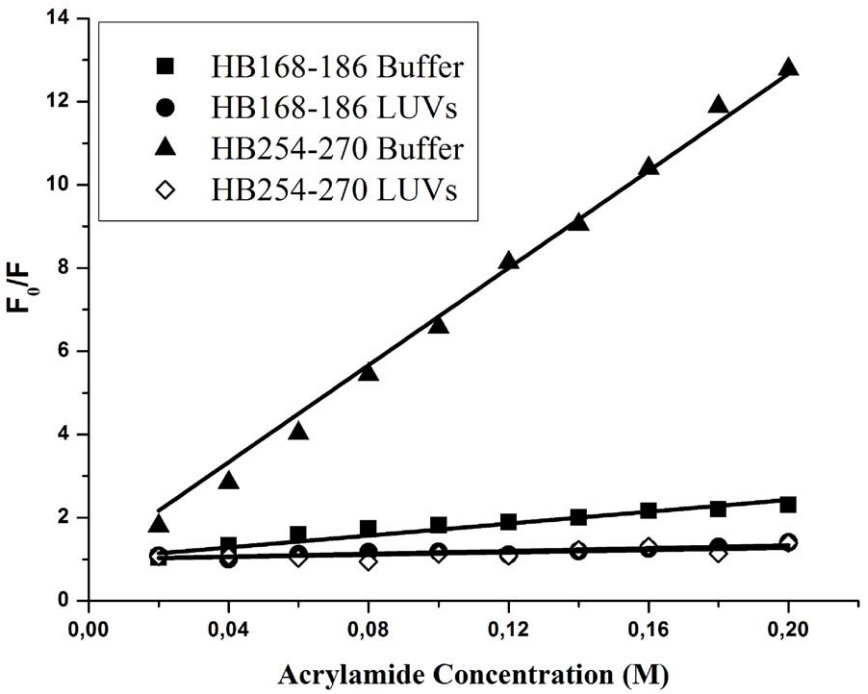

Figure 6. Quenching of tryptophan/tyrosines by Acrylamide. Stern-Volmer plots of acrylamide quenching of HB168–186 and HB254–270 in buffer (closed symbols) and in LUVs (open symbols).
doi:10.1371/journal.pone.0032186.g006

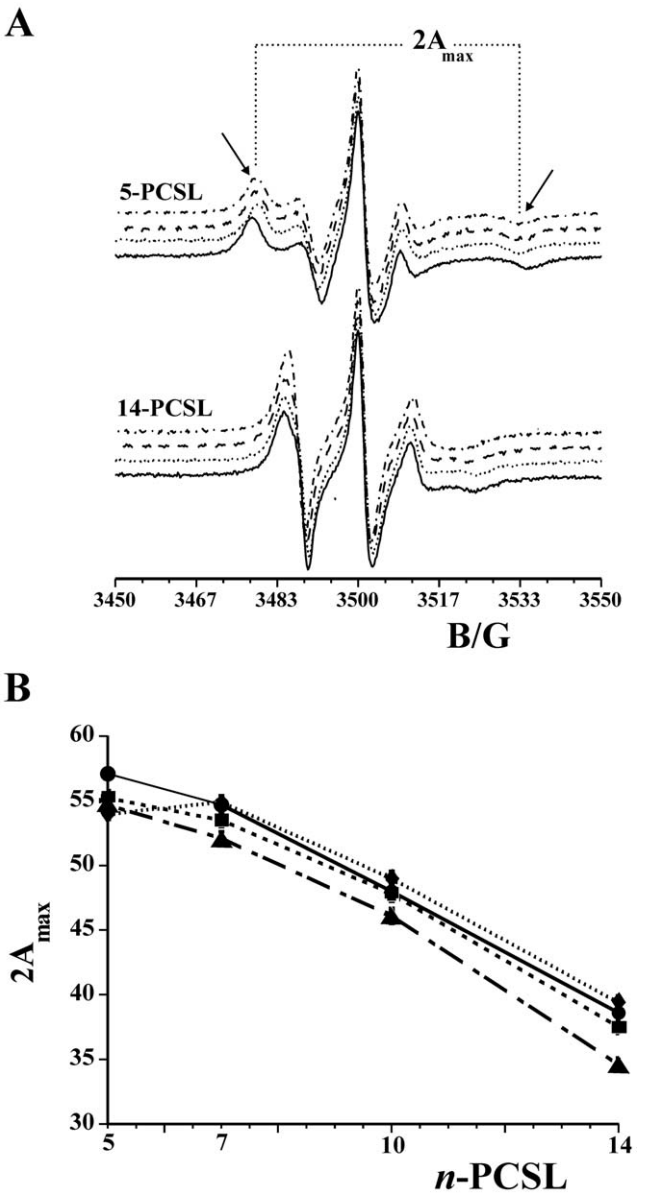

Figure 7. ESR Results. (**A**) ESR spectra of 5-PCSL and 14-PCSL spin-labels in DOPC/Chol membranes in the absence of peptides (solid line) and in the presence of HB168–186 (dotted line), HB254–270 (dashed line) and HB168–186–HB254–270 mixture (dashed-dotted line). (**B**) Dependence on spin-label position, *n*, of the outer hyperfine splittings, $2A_{max}$, of the *n*-PCSL in DOPC/Chol bilayers in the absence (○) and in the presence of HB168–186 (■), HB254–270 (●) or HB168–186: HB254–270 (▲) at T = 25°C.
doi:10.1371/journal.pone.0032186.g007

Another novel feature revealed in the present work is the demonstration of oligomerization concomitant to fusion taking place. Although a correlation between penetration and fusion awaits further experimental support, our results suggest that oligomerization is another parameter related to the nature of the interaction of the peptide with the target membrane and plays a key role in governing fusion activity. The peptide HB168–186 presents a high tendency to oligomerize both in aqueous solution and inside the membrane. On the contrary, the peptide HB254–280 is not oligomerized in aqueous solution but it is able to oligomerize when interacting with the membranes.

Tryptophan and tyrosine side chains are often found at the interface between charged phospholipids and hydrophobic fatty acid chains of lipid membranes. The K_p values for the two peptides are reported in Table 2. Since K_p values are all of the same order (10^4), we concluded that the peptides have similar membrane-binding affinities. The values of K_p obtained are within the range of those obtained for membrane-permeating bioactive peptides such as mellitin and its derivatives [53], the Staphylococcus δ-toxin [54], the antibiotic dermaseptin [55], pardaxin analogues [56]. All the results obtained support a shallow insertion of the two peptides that may expand the head-group region of one of the monolayers and generate elastic stresses that are released by bilayer deformation. Our results demonstrate that these two gB peptides bind and interact with membranes and could thus be directly involved in merging of the viral and cellular membranes and might work cooperatively with other membrane active regions present on herpesvirus glycoproteins to boost the fusion process. These results improve the current understanding of the critical features required for viral fusogenic peptides to cross the membrane bilayer and seem promising for the development of new carrier peptides that could exploit viral membranotropic peptides for intracellular delivery [57–59].

HSV-1 might have several domains involved in the fusion process which either directly or indirectly, might interact with biological membranes, contributing to the viral envelope and cell membrane merging. Although the detailed mechanism of herpesvirus entry remains unclear, some important insights into the interplay of the proteins involved in membrane fusion have been gained recently, but there are still many unsolved questions such as if the two fusion loops are the only HSV fusion peptide; what triggers them to be inserted into the target membrane, what is the role of gH in fusion and if fusion domains present in gH are directly involved in fusion.

Materials and Methods

Materials

The Phospholipids: 1-palmitoyl-2-oleoyl-*sn*-glycero-3-phosphocholine (POPC), dioleoyl phosphatidylcholine (DOPC), dioleoyl phosphatidylglycerol (DOPG), N-octadecanoyl-D-*erythro*-sphingosylphosphorylcholine (SM), the fluorescent probes N-(7-nitrobenz-2-oxa-1,3-diazol-4-yl)phosphatidylethanolamine (NBD-PE) and N-(Lissamine-rhodamine-B-sulfonyl) phosphatidylethanolamine (Rho-PE) were purchased from Avanti Polar Lipids (Birmingham, AL, USA), while cholesterol (Chol) and Triton-×100 were from Sigma (St. Louis, MO, USA). All other reagents were of analytical grade. Spin-labelled phosphatidylcholines (n-PCSL) with the nitroxide group at different positions, n, in the sn-2 acyl chain were synthesized as described by Marsh [60]. The spin-labels were stored at −20°C in ethanol solutions at a concentration of 1 mg/mL.

Peptide synthesis

Peptides were synthesised using standard solid-phase-9-fluorenylmethoxycarbonyl (Fmoc) method as previously reported [25]. All purified peptides (purity higher than 98%) were obtained with good yields (30–40%). Table 1 shows the sequences of all the synthesized peptides. Peptide stock solutions were prepared in buffer with 2% dimethyl sulfoxide (DMSO).

Liposome preparation

Large unilamellar vesicles (LUVs) consisting of DOPG, DOPG/Chol (3/2), DOPC, DOPC/Chol (3/2), POPC/Chol (3/2),

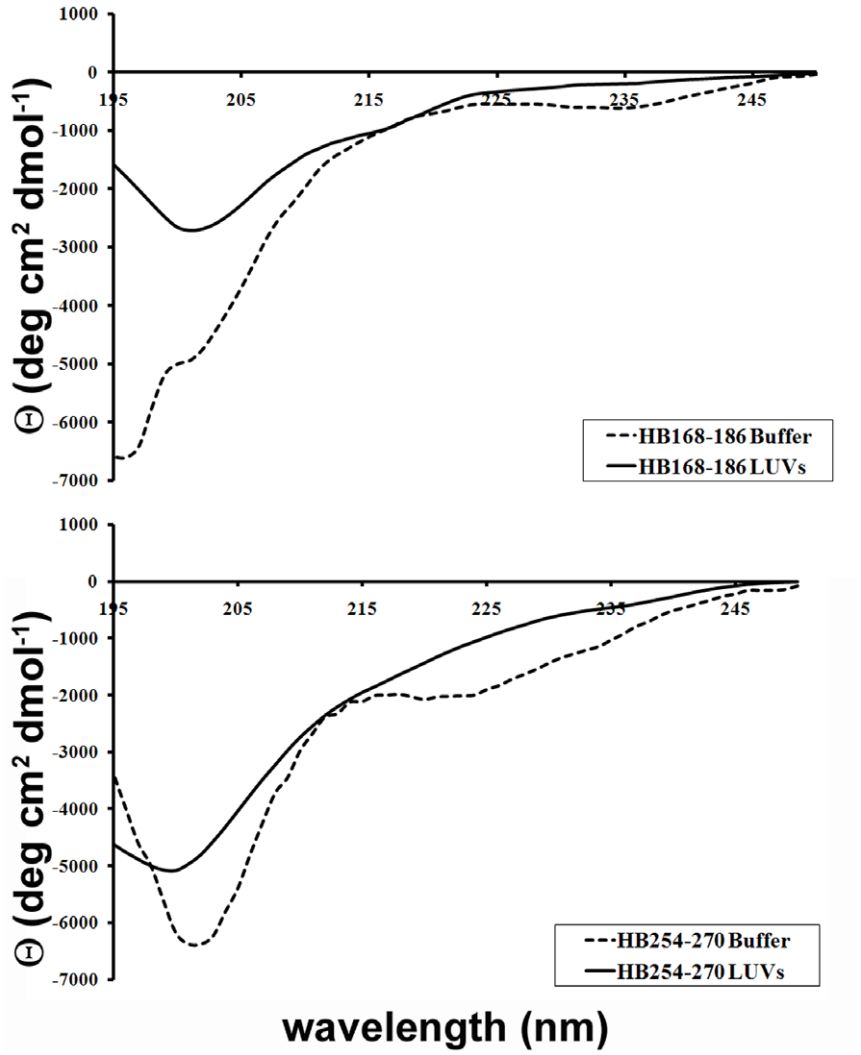

Figure 8. Secondary structure in lipid bilayers. CD spectra of HB168–186 and HB254–270 in buffer and in DOPC/Chol LUVs.
doi:10.1371/journal.pone.0032186.g008

POPC/Chol/SM (4/1/1), POPC/Chol/SM (2/1/1) and POPC/Chol/SM (1/1/1), and when necessary containing Rho-PE and NBD-PE, were prepared according to the extrusion method of Hope et al. [61] in 5 mM HEPES, 100 mM NaCl, pH 7.4. Lipids were dried from a chloroform solution with a nitrogen gas stream and lyophilized overnight. For fluorescence and circular dichroism experiments, dry lipid films were suspended in buffer by vortexing for 1 h; then the lipid suspension was freeze-thawed 6 times and extruded 20 times through polycarbonate membranes with 0.1 μm diameter pores to produce LUVs. Lipid concentrations of liposome suspensions were determined by phosphate analysis [62]. For ESR spectroscopy, multi-lamellar vesicles (MLVs) were prepared. In these samples, 1% (wt/wt) of the spin-label, dissolved in ethanol, was added to the lipid mixture in organic solvent before drying. MLVs suspensions were obtained by the same procedure described above, excluding the extrusion step.

Lipid mixing assays

Membrane lipid mixing was monitored using the resonance energy transfer assay (RET) reported by Struck et al. [63]. The assay is based on the dilution of the NBD-PE (donor) and Rho-PE (acceptor). Dilution due to membrane mixing results in an increase in NBD-PE fluorescence. The change in donor emission was monitored as aliquots of peptides were added to vesicles. Vesicles containing 0.6 mol % of each probe were mixed with unlabelled vesicles at a 1:4 ratio (final lipid concentration 0.1 mM). Small volumes of peptides in dimethylsulfoxide (DMSO) were added; the final concentration of DMSO in the peptide solution was no higher than 2%. The NBD emission at 530 nm was followed with the excitation wavelength set at 465 nm. A cut off filter at 515 nm was used between the sample and the emission monochromator to avoid scattering interferences. The fluorescence scale was calibrated such that the zero level corresponded to the initial residual fluorescence of the labelled vesicles and the 100% value corresponding to complete mixing of all lipids in the system was set by the fluorescence intensity of vesicles upon the addition of Triton X-100 (0.05% v/v) at the same total lipid concentrations of the fusion assay. Lipid mixing experiments were repeated at least three times and results were averaged. Control experiments were performed using a scrambled peptide and DMSO. All the experiments were performed at 37°C.

Inner-monolayer phospholipid-mixing (fusion) measurement

Peptide-induced phospholipid-mixing of the inner monolayer was measured by a modification of the phospholipid-mixing measurement reported elsewhere [64]. The concentration of each of the fluorescent probes within the liposome membrane was 0.6% mol. LUVs were treated with sodium dithionite 100 mM (from a stock solution of 1 M dithionite in 1 M TRIS, pH 10.0) to completely reduce the NBD-labelled phospholipid located at the outer monolayer of the membrane, for approximately 1 h on ice in the dark. Sodium dithionite was then removed by size exclusion chromatography through a Sephadex G-75 50 DNA Grade filtration column (GE Healthcare) eluted with a buffer containing 10 mM TRIS, 100 mM NaCl, and 1 mM EDTA, pH 7.4.

Measurements of ANTS/DPX leakage

The ANTS/DPX assay [34] was used to measure the ability of the peptide to induce leakage of ANTS/DPX pre-encapsulated in liposomes. Details of this assay can be found elsewhere [35]. To initiate a leakage experiment, the peptide, in a stock solution at pH 7.4 containing 5 mM Hepes and 100 mM NaCl, was added to the stirred vesicle suspension (0.1 mM lipid) at 37°C.

Thioflavin T assays for peptide aggregation

Peptide aggregation was assayed using Thioflavin T (ThT). ThT associates rapidly with aggregated peptides giving rise to a new excitation maximum at 450 nm and an enhanced emission at 482 nm [36]. LUVs in 100 mM NaCl, 10 mM Tris–HCl, 25 μM ThT, pH 7.4 (final phospholipid concentration of 0.1 mM) were titrated with a peptide concentration of 1, 4, 8, 12, 16, 20 μM. Fluorescence was measured before and after the desired amount of peptide was added into the cuvette using a Varian Cary Eclipse fluorescence spectrometer at 37°C. Samples were excited at 450 nm (slit width, 5 nm) and fluorescence emission was recorded at 482 nm (slit width, 5 nm). Aggregation was quantified according to the equation, $\%A = (F_f - F_0)/(F_{max} - F_0) \times 100$, where F_f is the value of fluorescence after peptide addition, F_0 the initial fluorescence in the absence of peptide and F_{max} is the fluorescence maximum obtained immediately after peptide addition. Kinetic data were obtained at a concentration of 4 μM.

Tryptophan and Tyrosine fluorescence measurements

Emission spectra of the peptides (1 μM) containing the tryptophan and tyrosine residue in the absence or presence of target vesicles (DOPC/Chol 1/1) were recorded: between 300 and 400 nm with an excitation wavelength of 295 nm for the peptide HB168–186 and 290 and 350 with an excitation wavelength of 274 nm for the peptide HB254–270.The degree of peptide association with lipid vesicles was measured by adding lipid vesicles to 1 μM peptides and the fluorescence intensity was measured as a function of the lipid/peptide molar ratio, in three to four separate experiments. The fluorescence values were corrected by taking into account the dilution factor corresponding to the addition of microliter amounts of liposomes and by subtracting the corresponding blank. The lipid/peptide molar ratio was 200:1.

The binding of hydrophobic peptides to membranes can be described as a partition equilibrium: $X_b = K_p C_f$ where K_p is the apparent partition coefficient in units of M^{-1}, X_b is the molar ratio of bound peptide per total lipid and C_f is the equilibrium concentration of the free peptide in solution, as previously suggested by Schwarz et al. [65]. F_∞ was obtained by extrapolation of a double reciprocal plot of the total peptide fluorescence vs the total lipid concentration in the outer leaflet, i.e. $1/F$ vs $1/0.6C_L$. The fraction of membrane-bound peptide, f_b, was determined by the formula $f_b = (F - F_0)/(F_\infty - F_0)$, where F represents the fluorescence of peptide after the addition of the vesicles and F_0 represents the fluorescence of the unbound peptide. f_b allowed us to calculate the equilibrium concentration of free peptide in the solution, C_f, and the extent of peptide binding X_b. Assuming that the peptides were initially partitioned only over the outer leaflet of the SUV (60% the total lipid) [66], values of X_b were corrected as follows: $X_b^* = X_b/0.6$.

The curve resulting from plotting X_b^* versus the concentration of the free peptide, C_f, is the binding isotherm.

Tryptophan and Tyrosine quenching by Acrylamide

Aliquots of a 4 M solution of the water-soluble quencher were added to the solution containing the peptide (1 μM) in the absence or presence of liposomes at a peptide/lipid molar ratio of 1/200. The maximal concentration of acrylamide is 0.2 mmol/ml. Tryptophan fluorescence was measured with an excitation wavelength of 295 nm, to reduce acrylamide absorbance (and the resulting inner filter effect), and emission at a wavelength of 340 nm, to eliminate interference from the Raman band of water [67] and tyrosine fluorescence was measured with an excitation wavelength of 274 nm, and emission at a wavelength of 305. The data were analyzed according to the Stern-Volmer equation [68], $F_0/F = 1 + K_{sv}[Q]$, where F_0 and F represent the fluorescence intensities in the absence and the presence of the quencher (Q), respectively, and K_{sv} is the Stern-Volmer quenching constant, which is a measure of the accessibility of tryptophan to acrylamide. Acrylamide does not significantly partition into the membrane bilayer [67], and the value for K_{sv} is a reliable reflection of the bimolecular rate constant for collisional quenching of the aromatic residues present in the aqueous phase. Accordingly, K_{sv} is determined by the amount of non-vesicle-associated free peptide as well as the fraction of the peptide residing at the surface of the bilayer.

Electron Spin Resonance Spectroscopy

ESR spectra were recorded with a 9 GHz Bruker Elexys E-500 spectrometer (Bruker, Rheinstetten, Germany). The lipid suspensions to be investigated were transferred into 25 μL glass capillaries and flame sealed. The capillaries were placed in a standard 4 mm quartz sample tube containing light silicone oil for thermal stability. All the measurements were performed at 25°C. Spectra were recorded using the following instrumental settings: sweep width, 100 G; resolution, 1024 points; time constant, 20.48 ms; modulation frequency, 100 kHz; modulation amplitude, 1.0 G; incident power, 6.37 mW. Samples containing the peptides were prepared by hydrating the lipid film directly with the peptide solution in buffer. In all samples, the peptide to lipid ratio was set to 1:1 wt/wt. In samples containing both HB168–186 and HB254–270, the total peptide to lipid ratio was maintained to 1:1 wt/wt, while the HB168–186:HB254–270 ratio was 1:1 wt/wt.

Several scans, typically 16, were accumulated to improve the signal-to-noise ratio. Values of the outer hyperfine splitting, $2A_{max}$, were determined by measuring the difference between the low-field maximum and the high-field minimum, through a home-made, MATLAB-based, software routine. This parameter is a useful empirical measure of the lipid chain dynamics and order in both gel and fluid phases of lipid bilayers [44–46]. The main source of error on the $2A_{max}$ value is the uncertainty in composition of samples prepared by mixing few microliters of mother solutions. For this reason, reproducibility of $2A_{max}$ determinations was estimated by evaluating its value for selected independently

prepared samples with the same nominal composition. It was found to be ±0.2–0.3 G.

Circular dichroism spectroscopy

CD spectra were recorded using a Jasco J-715 spectropolarimeter in a 1.0 cm quartz cell at room temperature. The spectra are an average of 3 consecutive scans from 260 to 195 nm, recorded with a band width of 3 nm, a time constant of 16 s, and a scan rate of 10 nm/min. Spectra were recorded and corrected for the blank sample. Mean residue ellipticities (MRE) were calculated using the expression MRE = $Obsd/(lcn)$, where $Obsd$ is the ellipticity measured in millidegrees, l is the path length of the cell in cm, c is the peptide concentration in mol/l, and n is the number of amino acid residues in the peptide. Solutions of 4 μM of HB168–186 and 10 μM of HB254–270 with LUVs were prepared as described previously [31]. The measurements were performed at peptide/lipid ratios of 0.5 mol/mol.

Supporting Information

Figure S1 Fluorescence spectra of tryptophan and tyrosine. Fluorescence spectra of HB168–186 and HB254–270 in buffer and in LUVs.
(TIF)

Acknowledgments

The authors thank Mr. Leopoldo Zona for technical assistance.

Author Contributions

Conceived and designed the experiments: MG SG. Performed the experiments: AF RT GV MV EP MC. Analyzed the data: AF GD MG SG. Contributed reagents/materials/analysis tools: MG SG. Wrote the paper: AF GD MG SG.

References

1. Falanga A, Cantisani M, Pedone C, Galdiero S (2009) Membrane fusion and fission: enveloped viruses. Prot Pept Lett 16: 751–759.
2. Galdiero S (2009) Developments in membrane fusion. Prot Pept Lett 16: 711.
3. Chernomordik LV, Kozlov MM (2003) Protein-lipid interplay in fusion and fission of biological membranes. Annu Rev Biochem 72: 175–207.
4. Harrison SC (2008) Viral membrane fusion. Nature Structural Molecular Biology 15: 690–698.
5. Drin G, Casella JF, Gautier R, Boehmer T, Schwartz TU, et al. (2007) A general amphipathic alpha-helical motif for sensing membrane curvature. Nat Struct Mol Biol 14: 138–146.
6. Antonny B (2011) Mechanisms of membrane curvature sensing. Annu Rev Biochem 80: 101–123.
7. Connolly SA, Jackson JO, Jardetzky TS, Longnecker R (2011) Fusing structure and function: a structural view of the herpesvirus entry machinery. Nat Rev Microbiol 9: 369–381.
8. Turner A, Bruun B, Minson T, Browne H (1998) Glycoproteins gB, gD, and gHgL of herpes simplex virus type 1 are necessary and sufficient to mediate membrane fusion in a Cos cell transfection system. J Virol 72: 873–875.
9. Farnsworth A, Wisner TW, Webb M, Roller R, Cohen G, et al. (2007) Herpes simplex virus glycoproteins gB and gH function in fusion between the virion envelope and the outer nuclear membrane. Proc Natl Acad Sci U S A 104: 10187–10192.
10. Atanasiu D, Whitbeck JC, Cairns TM, Reilly B, Cohen GH, et al. (2007) Bimolecular complementation reveals that glycoproteins gB and gH/gL of herpes simplex virus interact with each other during cell fusion. Proc Natl Acad Sci U S A 104: 18718–18723.
11. Avitabile E, Forghieri C, Campadelli-Fiume G (2007) Complexes between herpes simplex virus glycoproteins gD, gB, and gH detected in cells by complementation of split enhanced green fluorescent protein. J Virol 81: 11532–11537.
12. Galdiero S, Vitiello M, D'Isanto M, Falanga A, Collins C, et al. (2006) Analysis of synthetic peptides from heptad-repeat domains of herpes simplex virus type 1 glycoproteins H and B. J Gen Virol 87: 1085–1097.
13. Galdiero S, Falanga A, Vitiello M, Browne H, Pedone C, et al. (2005) Fusogenic domains in herpes simplex virus type 1 glycoprotein H. J Biol Chem 280: 28632–28643.
14. Galdiero S, Falanga A, Vitiello M, D'Isanto M, Collins C, et al. (2007) Evidence for a role of the membrane-proximal region of herpes simplex virus Type 1 glycoprotein H in membrane fusion and virus inhibition. Chembiochem 8: 885–895.
15. Galdiero S, Falanga A, Vitiello M, D'Isanto M, Cantisani M, et al. (2008) Peptides containing membrane-interacting motifs inhibit herpes simplex virus type 1 infectivity. Peptides 29: 1461–1471.
16. Galdiero S, Falanga A, Vitiello M, Raiola L, Fattorusso R, et al. (2008) Analysis of a membrane interacting region of herpes simplex virus type 1 glycoprotein H. J Biol Chem 283: 29993–30009.
17. Galdiero S, Falanga A, Vitiello G, Vitiello M, Pedone C, et al. (2010) Role of membranotropic sequences from herpes simplex virus type I glycoproteins B and H in the fusion process. Biochim Biophys Acta 1798: 579–591.
18. Galdiero S, Falanga A, Vitiello M, Raiola L, Russo L, et al. (2010) The presence of a single N-terminal histidine residue enhances the fusogenic properties of a Membranotropic peptide derived from herpes simplex virus type 1 glycoprotein H. J Biol Chem 285: 17123–17136.
19. Chowdary TK, Cairns TM, Atanasiu D, Cohen GH, Eisenberg RJ, et al. (2010) Crystal structure of the conserved herpesvirus fusion regulator complex gH-gL. Nat Struct Mol Biol 17: 882–888.
20. Matsuura H, Kirschner AN, Longnecker R, Jardetzky TS (2010) Crystal structure of the Epstein-Barr virus (EBV) glycoprotein H/glycoprotein L (gH/gL) complex. Proc Natl Acad Sci U S A 107: 22641–22646.
21. Heldwein EE, Lou H, Bender FC, Cohen GH, Eisenberg RJ, et al. (2006) Crystal structure of glycoprotein B from herpes simplex virus 1. Science 313: 217–220.
22. Backovic M, Longnecker R, Jardetzky TS (2009) Structure of a trimeric variant of the Epstein-Barr virus glycoprotein B. Proc Natl Acad Sci U S A 106: 2880–2885.
23. Roche S, Bressanelli S, Rey FA, Gaudin Y (2006) Crystal structure of the low-pH form of the vesicular stomatitis virus glycoprotein G. Science 313: 187–191.
24. Kadlec J, Loureiro S, Abrescia NG, Stuart DI, Jones IM (2008) The postfusion structure of baculovirus gp64 supports a unified view of viral fusion machines. Nat Struct Mol Biol 15: 1024–1030.
25. Galdiero S, Vitiello M, D'Isanto M, Falanga A, Cantisani M, et al. (2008) The identification and characterization of fusogenic domains in herpes virus glycoprotein B molecules. Chembiochem 9: 758–767.
26. Akkarawongsa R, Pocaro NE, Case G, Kolb AW, Brandt CR (2009) Multiple peptides homologous to herpes simplex virus type 1 glycoprotein B inhibit viral infection. Antimicrob Agents Chem 53: 987–996.
27. Hannah BP, Heldwein EE, Bender FC, Cohen GH, Eisenberg RJ (2007) Mutational evidence of internal fusion loops in herpes simplex virus glycoprotein B. J Virol 81: 4858–4865.
28. Roche S, Albertini AA, Lepault J, Bressanelli S, Gaudin Y (2008) Structures of vesicular stomatitis virus glycoprotein: membrane fusion revisited. Cell Mol Life Sci 65: 1716–1728.
29. Sun X, Belouzard S, Whittaker GR (2008) Molecular architecture of the bipartite fusion loops of vesicular stomatitis virus glycoprotein G, a class III viral fusion protein. J Biol Chem 283: 6418–6427.
30. Hannah BP, Heldwein EE, Bender FC, Cohen GH, Eisenberg RJ (2007) Mutational evidence of internal fusion loops in herpes simplex virus glycoprotein B. J Virol 81: 4858–4865.
31. Vitiello G, Falanga A, Galdiero M, Marsh D, Galdiero S, et al. (2011) Lipid composition modulates the interaction of peptides deriving from herpes simplex virus type I glycoproteins B and H with biomembranes. Biochim Biophys Acta 1808: 2517–1526.
32. Bender FC, Whitbeck JC, Ponce de Leon M, Lou H, Eisenberg RJ, et al. (2003) Specific association of glycoprotein B with lipid rafts during herpes simplex virus entry. J Virol 77: 9542–9552.
33. de Almeida RFM, Fedorov A, Prieto M (2003) Sphingomyelin/Phosphatidylcholine/cholesterol phase diagram: boundaries and composition of lipid rafts. Biophys J 85: 2406–2416.
34. Ellens H, Bentz J, Szoka JrFC (1984) pH-induced destabilization of phosphatidylethanolamine-containing liposomes: role of bilayer contact. Biochemistry 23: 1532–1538.
35. Parente RA, Nir S, Szoka JrFC (1990) Mechanism of leakage of phospholipid vesicle contents induced by the peptide GALA. Biochemistry 29: 8713–8719.
36. Levine III H (1993) Thioflavine T interaction with synthetic Alzheimer's disease β-amyloid peptides: Detection of amyloid aggregation in solution. Prot Sci 2: 404–410.
37. Yau WM, Wimley WC, Gawrisch K, White SH (1998) The preference of tryptophan for membrane interfaces. Biochemistry 37: 14713–14718.
38. Gordon LM, Curtain CC, Zhong YC, Kirkpatrick A, Mobley PW, et al. (1992) The amino-terminal peptide of HIV-1 glycoprotein 41 interacts with human erythrocyte membranes: peptide conformation, orientation and aggregation. Biochim Biophys Acta 1139: 257–274.

39. Curtain C, Separovic F, Nielsen K, Craik D, Zhong Y, et al. (1999) The interactions of the N-terminal fusogenic peptide of HIV-1 gp41 with neutral phospholipids. European Biophysical Journal 28: 427–436.
40. D'Errico G, D'Ursi AM, Marsh D (2008) Interaction of a peptide derived from glycoprotein gp36 of feline immunodeficiency virus and its lipoylated analogue with phospholipid membranes. Biochemistry 47: 5317–5327.
41. Spadaccini R, D'Errico G, D'Alessio V, Notomista E, Bianchi A, et al. (2010) Structural characterization of the transmembrane proximal region of the hepatitis C virus E1 glycoprotein. Biochim Biophys Acta 1798: 344–353.
42. Marsh D (2010) Liquid-ordered phases induced by cholesterol: a compendium of binary phase diagrams. Biochim Biophys Acta 1798: 688–699.
43. Swamy MJ, Marsh D (1994) Spin-label electron spin resonance studies on the dynamics of the different phases of N-biotinylphosphatidylethanolamines. Biochemistry 33: 11656–11663.
44. Moser M, Marsh D, Meier P, Wassmer KH, Kothe G (1989) Chain configuration and flexibility gradient in phospholipid membranes. Comparison between spin-label electron spin resonance and deuteron nuclear magnetic resonance, and identification of new conformations. Biophys J 55: 111–123.
45. Rama Krishna YVS, Marsh D (1990) Spin label ESR and 31P-NMR studies of the cubic and inverted hexagonal phases of dimyristoylphosphatidylcholine/myristic acid (1:2, mol/mol) mixtures. Biochim Biophys Acta 1024: 89–94.
46. Lange A, Marsh D, Wassmer KH, Meier P, Kothe G (1985) Electron spin resonance study of phospholipid membranes employing a comprehensive line-shape model. Biochemistry 24: 4383–4392.
47. D'Errico G, Vitiello G, Ortona O, Tedeschi A, Ramunno A, et al. (2008) Interaction between Alzheimer's Abeta(25–35) peptide and phospholipid bilayers: the role of cholesterol. Biochim Biophys Acta 1778: 2710–2716.
48. Hannah BP, Cairns TM, Bender FC, Whitbeck JC, Lou H, et al. (2009) Herpes simplex virus glycoprotein B associates with target membranes via its fusion loops. J Virol 83: 6825–6836.
49. Ahn A, Gibbons DL, Kielian M (2002) The fusion peptide of Semliki Forest virus associates with sterol-rich membrane domains. J Virol 76: 3267–3275.
50. Chatterjee PK, Eng CH, Kielian M (2002) Novel mutations that control the sphingolipid and cholesterol dependence of the Semliki Forest virus fusion protein. J Virol 76: 12712–12722.
51. Vashishtha M, Phalen T, Marquardt MT, Ryu JS, Ng AC, et al. (1998) A single point mutation controls the cholesterol dependence of Semliki Forest virus entry and exit. J Cell Biol 14: 91–99.
52. Thorén PE, Persson D, Lincoln P, Nordén B (2005) Membrane destabilizing properties of cell-penetrating peptides. Biophys Chem 114: 169–179.
53. Stankowski S, Schwarz G (1990) Electrostatics of a peptide at a membrane/water interface. The pH dependence of melittin association with lipid vesicles. Biochim Biophys Acta 1025: 164–72.
54. Thiaudière E, Siffert O, Talbot JC, Bolard J, Alouf JE, et al. (1991) The amphiphilic alpha-helix concept. Consequences on the structure of staphylococcal delta-toxin in solution and bound to lipids. Eur J Biochem 195: 203–13.
55. Pouny Y, Rapaport D, Mor A, Nicolas P, Shai Y (1992) Interaction of antimicrobial dermaseptin and its fluorescently labeled analogues with phospholipid membranes. Biochemistry 31: 12416–23.
56. Rapaport D, Shai Y (1991) Interaction of fluorescently labeled pardaxin and its analogues with lipid bilayers. J Biol Chem 266: 23769–23775.
57. Falanga A, Vitiello MT, Cantisani M, Tarallo R, Guarnieri D, et al. (2011) A peptide derived from herpes simplex virus type 1 glycoprotein H: membrane translocation and applications to the delivery of quantum dots. Nanomedicine NBM 7: 925–934.
58. Tarallo R, Accardo A, Falanga A, Guarnieri D, Vitiello G, et al. (2011) Clickable Functionalization of Liposomes with the gH625 Peptide from Herpes simplex Virus Type I for Intracellular Drug Delivery. Chem Eur J 17: 12659–12668.
59. Galdiero S, Vitiello M, Falanga A, Cantisani M, Incoronato N, et al. (2012) Intracellular Delivery: Exploiting Viral Membranotropic Peptides. Curr Drug Met 12: 93–104.
60. Marsh D (2008) Electron spin resonance in membrane research: Protein–lipid interactions. Methods 46: 83–96.
61. Hope MJ, Bally MB, Webb G, Cullis PR (1985) Vesicles of variable sizes produced by a rapid extrusion procedure. Biochim Biophys Acta 812: 55–65.
62. Fiske CH, Subbarow Y (1925) The colorimetric determination of phosphorus. J Biol Chem 66: 375–400.
63. Struck DK, Hoekstra D, Pagano RE (1981) Use of resonance energy transfer to monitor membrane fusion. Biochemistry 20: 4093–4099.
64. Cummings JE, Vanderlock TK (2007) Aggregation and hemi-fusion of anionic vesicles induced by the antimicrobial peptide cryptdin-4. Biochim Biophys Acta 1768: 1796–1804.
65. Schwarz G, Stankowsky S, Rizzo V (1986) Thermodynamic analysis of incorporation and aggregation in a membrane: application to the pore-forming peptide alamethicin. Biochim Biophys Acta 861: 141–151.
66. Beschiaschvili G, Seelig J (1990) Melittin binding to mixed phosphatidylglycerol/phosphatidylcholine membranes. Biochemistry 29: 52–58.
67. De Kroon AIPM, Soekarjo MW, De Gier J, De Kruijff B (1990) The role of charge and hydrophobicity in peptide-lipid interaction: a comparative study based on tryptophan fluorescence measurements combined with the use of aqueous and hydrophobic quenchers. Biochemistry 29: 8229–8240.
68. Eftink MR, Ghiron CA (1976) Fluorescence quenching of indole and model micelle systems. J Phys Chem 80: 486–493.

International Journal of Nanomedicine

Dovepress
open access to scientific and medical research

Open Access Full Text Article

ORIGINAL RESEARCH

Dendrimers functionalized with membrane-interacting peptides for viral inhibition

Rossella Tarallo[1]
Tom P Carberry[2]
Annarita Falanga[1]
Mariateresa Vitiello[3]
Stefania Galdiero[1]
Massimiliano Galdiero[3]
Marcus Weck[2]

[1]Dipartimento di Farmacia, Università di Napoli "Federico II," and DFM Scarl, Napoli, Italia; [2]Molecular Design Institute and Department of Chemistry, New York University, New York, NY, USA; [3]Dipartimento di Medicina Sperimentale, Seconda Università degli Studi di Napoli, Napoli, Italia

Correspondence: Massimiliano Galdiero
Dipartimento di Medicina Sperimentale, Seconda Università degli Studi di Napoli, Via de Crecchio 7, Napoli 80138, Italia
Tel +39 0815667646
Fax +39 0815667578
Email massimiliano.galdiero@unina2.it

Marcus Weck
Molecular Design Institute and Department of Chemistry, New York University, New York, NY 10003, USA
Tel +1 212 992 7968
Fax +1 212 995 4895
Email marcus.weck@nyu.edu

Abstract: This contribution reports the synthesis of a poly(amide)-based dendrimer functionalized at the termini with a membrane-interacting peptide derived from the herpes simplex virus (HSV) type 1 glycoprotein H, namely gH625-644. This peptide has been shown to interact with model membranes and to inhibit viral infectivity. The peptidodendrimer inhibits both HSV-1 and HSV-2 at a very early stage of the entry process, most likely through an interaction with the viral envelope glycoproteins; thus, preventing the virus from coming into close contact with cellular membranes, a prerequisite of viral internalization. The 50% inhibitory concentration was 100 and 300 nM against HSV-1 and HSV-2 respectively, with no evidence of cell toxicity at these concentrations. These results show that the functionalization of a dendrimer with the peptide sequence derived from an HSV glycoprotein shows promising inhibitory activity towards viruses of the *Herpesviridae* family.

Keywords: peptidodendrimer, antiviral activity, membranotropic peptides

Introduction

Herpes simplex viruses (HSVs) are responsible for a wide variety of clinical manifestations and represent a significant worldwide disease and economic burden. There are two serotypes of HSV, HSV-1 and HSV-2, which can infect either oral or genital sites respectively. For some populations, between 60% and 95% are infected with HSV-1 and between 6% and 50% with HSV-2.[1] Even if HSV infections are often subclinical, their incidence and severity have increased over the past decades due to the increasing number of immunocompromised patients. In particular, the impact of genital herpes as a public health threat is amplified because of its epidemiological synergy with the human immunodeficiency virus (HIV). Synthetic nucleoside analogs targeting viral DNA polymerase (eg, acyclovir) are routinely used as standard treatment of symptomatic HSV infections;[2] however, their clinical use in immunocompromised patients receiving long-term treatments may lead to treatment failures due to the emergence of antiviral-resistant strains.[3] Thus, it is imperative to develop new anti-HSV agents with antiviral activity based on alternative mechanisms of action. Inhibition of HSV attachment and/or entry represents a particularly attractive antiviral strategy since it may prevent the establishment of infection. Target compounds with this mode of action could provide a starting point for the development of topical microbicides that block transmission at the mucosal surface, thereby providing a method of prophylactic intervention.[4]

Dendrimers have been extensively studied as vehicles for the delivery of therapeutics or as carriers for in vivo imaging.[5–10] Dendrimers are highly branched macromolecules

submit your manuscript | www.dovepress.com
Dovepress
http://dx.doi.org/10.2147/IJN.S37739

with well defined three-dimensional architectures.[11] The appeal of dendrimers lies in their unique perfectly branched architectures which affords them different properties than corresponding linear polymers of the same composition and molecular weights.[5] As dendrimers increase in generation, they exponentially increase the number of termini, while only linearly increasing in radius; thus, the termini become more densely packed giving the entire structure a globular shape, where the termini radiate outwards from a central core. The globular structure of a dendrimer has a significant effect on its rheological properties with important biological implications; for example, a linear analog of a dendrimer will generally see much reduced blood circulation times.[12]

"Click reactions," such as the copper catalyzed 1,3-dipolar alkyne/azide cycloaddition (CuAAC),[13] have been used extensively for polymer functionalizations due to their high yielding character.[14,15] Using CuAAC, dendrimers have been functionalized with amines, peptides, and polysaccharides and investigated as antiviral agents.[16–19] While the mechanisms of action of the antiviral activity is not fully understood, it is thought that the interactions used by viruses to infect cells can be inhibited due to the dendrimer physically blocking or interfering with the fusion mechanism between the virus and the cell.[20] Notable is the poly(lysine)-based dendrimer SPL7013,[21] which is a sulfonate terminated dendrimer gel that has been shown to act as a topical virucide against HIV-1,[22–24] and is now undergoing Phase II clinical trials as VivaGel® (Starpharma, Melbourne, Australia). Peptide-functionalized dendrimers have also been investigated as antiviral agents. Both Luganini et al and Donalisio et al have synthesized dendritic structures based on a poly(lysine) core containing four short (~10 mer) peptide sequences.[20,25,26] These dendrons were shown to have antiviral activity. Using a linear analog greatly diminishes antiviral activity, suggesting the dendritic structure is necessary for the antiviral effect. The peptides used by Hunter are lysine-rich, giving the outer surface of the dendron a positive charge to interact with biological membranes. However, poly(cationic) structures generally show cytotoxic effects, which limits their usefulness.[27]

Herein, the functionalization of a dendrimer terminated with a membranotropic peptide sequence, the gH(625–644) domain derived from viral fusion proteins that has been shown to exhibit antiviral properties is reported.[28] The current authors have previously identified several regions of the herpes simplex virus type I glycoprotein H that have membrane-interacting capabilities.[29–33] Of these, the gH(625-644) domain proved to be a good candidate for the purposes of this study: it is mainly hydrophobic in nature and displays an amphiphilic character when in an α-helical form. Furthermore, it folds easily into a helix in a membrane-mimetic environment.[29–31] Finally, the authors of this present paper previously reported the ability of gH625 to inhibit HSV entry.[31] The gH625 peptide was therefore used to functionalize dendrimers and their properties as antiviral agents were investigated.

Experimental section

Materials

Fmoc-protected amino acids, coupling reagents, and Rink-amide *p*-methylbenzhydrylamine (MBHA) resin were purchased from Calbiochem-Novabiochem (San Diego, CA, USA). Fmoc-L-propargylglycine (Fmoc-PrA-OH) was purchased from NeoSystem (Tysons Corner, VA, USA). All other chemicals were purchased from Sigma-Aldrich (St Louis, MO, USA), Alfa Aesar (Ward Hill, MA, USA), or TCI International (Portland, Oregon, USA). Dialysis membranes (SpectraPor 6) were purchased from Spectrum Laboratories (Rancho Dominguez, CA, USA) and used after rinsing the membrane in water for 30 minutes. Size-exclusion chromatography was performed using a 1 cm × 18 cm Sephadex G-50 column. The octadecaazidedendrimer (**1**) was synthesized as described in the literature.[34]

Solid-phase peptide synthesis

Peptides were synthesized on a Syro I Multisynthec GmbH (Witten, Germany) automatic synthesizer. Syntheses were performed using standard Fmoc solid-phase techniques on a 20 μmol scale as previously reported.[30] Peptide purification was performed on LC8 Shimadzu (Kyoto, Japan) high-performance liquid chromatography with a Phenomonex (Torrance, CA, USA) C18 column (300Å, 250 mm × 21.20 mm, 5 μ) and a Waters (Milford, MA, USA) ultraviolet (UV) Lambda-Max model 481 detector. Peptide purity was analyzed by a Thermo Electron (San Jose, CA, USA) Finnigan Surveyor MSQ single quadrupole ESI LC-MS with a Phenomenex C18 column and the same eluent system (NH_2-HGLASTLTRWAHYNALIRAFX-$CONH_2$, X = PrA, Rt = 9.41 minutes, molecular weight = 2392.7 [M + 2H]+/2 = 1197 amu).

Peptide functionalization of 1

To obtain compound **2**, to a solution of **1** (50 μg, 0.0146 μmol) in 208 μL of water/methanol (1:1) was added 660 μL of a 1:1 methanol water solution of the peptide gH625-PrA (30.33 eq), 10 μL of a water solution of $CuSO_4 \cdot 5H_2O$ (1.46 mM, 1 eq), and 50 μL of a water solution of sodium ascorbate

(1.17 mM, 4 eq). The mixture was stirred for 12 hours. The reaction mixture was then concentrated and peptide functionalized dendrimer **2** was purified by size-exclusion chromatography. The amount of peptide functionalization on **2** was confirmed by UV analysis ($\varepsilon = 7000\ M^{-1}\ cm^{-1}$ at $\lambda = 280$ nm).

Cells and viruses

African green monkey kidney cells (Vero) (ATCC CCL-81) were grown in Dulbecco's modified Eagle's medium (DMEM) supplemented with 10% fetal calf serum. HSV-1 (strain SC16) and HSV-2 (strain 333), both carrying a *lacZ* gene driven by the CMV IE-1 promoter to express β-galactosidase, were propagated on Vero cells monolayers.

Virus entry assays

For all experiments below, compounds **1**, **2**, and peptide gH625 were dissolved in DMEM without serum and used at concentrations of 0, 5.5, 55, 280, and 550 nM. The concentrations used for the peptide correspond to the quantity present on each dendrimer molecule, ie, 18 times the concentrations of the dendrimer. All experiments were conducted in triplicate. The percentage of infectivity inhibition was calculated by setting the number of plaques obtained in positive controls where no antiviral compounds were added to the cell monolayers to 0% inhibition. To assess the effect of peptides on inhibition of HSV infectivity, cell monolayers were treated in different ways:

a. Virus yield reduction assay
   Confluent Vero cell monolayers (12-well plates) were washed with phosphate-buffered saline (PBS) and infected with either HSV-1 or HSV-2 at multiplicity of infection (MOI) of 1 plaque-forming unit (pfu)/cell for 1 hour at 37°C. The virus inocula were mixed with the antiviral compound to be tested in each experiment as stated above. Non-penetrated viruses were inactivated by citrate buffer at pH 3.0. The infected cells were washed with PBS, covered with fresh culture medium, and incubated for 48 hours. The infected cells were then scraped into culture medium and disrupted by sonication. The total virus yield in each well was titrated by plaque assay. Plaques were stained with X-gal (5-bromo-4-chloro-3-indolyl-β-D-galactopyranoside) and microscopically counted. The mean plaque counts for each drug concentration were expressed as a percentage of the mean plaque count for the control virus. The number of plaques was plotted as a function of drug concentration; concentrations producing 50% reductions in plaque formation were determined as the IC_{50}.
b. Posttreatment assay
   Vero cell monolayers (12-well plates) were incubated with HSV-1 or HSV-2 for 45 minutes at 37°C. The above compounds were then added to the inoculum followed by an additional incubation period of 30 minutes at 37°C. For all treatments, non-penetrated viruses were inactivated by citrate buffer at pH 3.0 after the 45 minute incubation with cells at 37°C. The cells were then incubated for 24 hours at 37°C in DMEM supplemented with carboxymethyl cellulose (CMC). Monolayers were fixed, stained with X-gal, and plaque numbers were scored.
c. Cytopathic effect inhibition assay
   Confluent Vero cell monolayers in a 96-well plate were infected with HSV-1 and HSV-2 at an MOI of 0.01 pfu/cell at 37°C for 1 hour. Following removal of virus inocula, the infected cells were washed with citrate buffer at pH 3.0 followed by a PBS wash and covered with medium containing the above compounds for 3 days at 37°C. The cytopathic effect was monitored daily, and an arbitrary score was assigned at the end of the incubation period in consideration of the protection from the cytopathic effect observed.
d. Attachment
   To assess the effect of the dendrimer and the peptidodendrimer on viral attachment, two experimental procedures were carried out. Briefly, prechilled Vero cell monolayers (12-well plates) were infected with precooled HSV-1 or HSV-2 at an MOI of 0.1 pfu/cell for 2 hours at 4°C to allow viral attachment. Cells were then washed three times with cold MEM to remove unattached virus and treated with various concentrations of the above compounds or heparin for 3 hours at 37°C prior to inactivation of extracellular virus with citrate buffer for 2 minutes at room temperature. Subsequently, the cells were washed three times with warm medium to return the pH to neutral and overlaid with CMC and incubated for 2 days at 37°C. Plates were then fixed, stained with X-gal, and plaques were counted. The second attachment experiment was performed as the former, except the prechilled Vero cell monolayers were treated with inocula containing both the viruses and the antiviral compounds precooled to 4°C. Following a 2 hour incubation at 4°C to allow viral attachment, the plates were treated as before and shifted at 37°C.
e. Cell pretreatment
   Prechilled Vero cell monolayers were treated as above with the above compounds or heparin for 30 minutes at 4°C and infected with precooled HSV-1 or HSV-2 at an MOI of 0.1 pfu/cell for 2 hours at 4°C. Cells were then washed three times with cold MEM to remove unattached

virus and compounds, overlaid with CMC, and incubated for 2 days at 37°C. Plates were then fixed, stained with X-gal, and the number of plaques was scored.

f. Virucidal assay
The aforementioned compounds were added to aliquots of HSV-1 or HSV-2 (10^4 pfu) and incubated at either 4°C or 37°C for 2 hours. After incubation, the samples were diluted with medium to reduce the concentration of the antiviral compound to one that was not active in an antiviral assay. The MOI of HSV-1 and HSV-2 after dilution was of 0.01 pfu/cell. The viruses were then titrated on Vero cell monolayers. Plates were then fixed, stained with X-gal, and the number of plaques was scored.

Cytoxicity

Vero cells were exposed to increasing concentrations of compounds, and the number of viable cells was determined using the 3-(4,5-dimethylthiazol-2-yl)-2,5-diphenyltetrazolium bromide (MTT) assay that is based on the reduction of the yellowish MTT to the insoluble and dark blue formazan by viable and metabolically active cells.[35] Vero cells were subcultured in 96-well plates at a seeding density of 2×10^4 cells/well and treated with compounds **1** or **2** at 0.28, 0.55, 1.1, 2.8, or 5.5 μM for 3 and 24 hours. The medium was then gently aspirated, MTT solution (5 mg/mL) was added to each well, and cells were incubated for a further 3 hours at 37°C. The medium with MTT solution was removed, and the formazan crystals were dissolved with dimethyl sulfoxide. The absorption values were measured at 570 nm using a Bio-Rad Microplate Reader (Bio-Rad Laboratories, Hercules, CA, USA). The viability of Vero cells in each well was presented as a percentage of control cells.

Flow cytometry analysis of apoptosis

Vero cells were exposed to compounds **1** and **2** at the concentration of 0.55 μM for 24 hours. Annexin V-FITC (MedSystems Diagnostics, Vienna, Austria) (fluorescein isothiocyanate) was used in conjunction with a vital dye, propidium iodide (PI) (Sigma-Aldrich), to distinguish apoptotic (Annexin V-FITC positive, PI negative; or Annexin V-FITC positive, PI positive) from necrotic (Annexin V-FITC negative, PI positive) cells. Briefly, cells were incubated with Annexin-V-FITC and in a binding buffer (10 mM Hepes, pH 7.4, 150 mM NaCl, 5 mM KCl, 1 mM $MgCl_2$, 2.5 mM $CaCl_2$) for 10 minutes at room temperature, washed, and resuspended in the same buffer. Analysis of apoptotic cells was performed by flow cytometry (FACScan; BD, Franklin Lakes, NJ, USA). For each sample, 2×10^4 events were acquired. Analysis was carried out by triplicate determination on at least three separate experiments.

Results

Peptide analysis

The literature describes the potential of fusion peptides and/or membranotropic peptides of orthomyxoviruses, paramyxoviruses, and HIV as virus entry inhibitors.[28,29,31,36–38] The accepted view is that the inhibition of infectivity may be due to the formation of inactive aggregates between the fusogenic stretches present in both the viral protein and the synthetic peptides.[28,30,31] These aggregates are formed as a consequence of their nature for intrinsic oligomerization or their ability to mimic the modes of binding of their original domains in their partner protein; they are thus predicted to stabilize a pre-fusion intermediate and prevent merging of the bilayers. The Wimley–White interfacial hydrophobicity scale was used to identify the sequence gH625 that proved to effectively interact with the membrane bilayer and possess some antiviral activity;[30,31] therefore, gH625 has the potential of being developed into an inhibitor to prevent viral entry and viral infectivity. This sequence was selected for coupling to the dendrimer to investigate whether a dendrimer-gH625 conjugate can yield an HSV-1 inhibitor. The sequence alignment of HSV-1 and HSV-2 gH(625-644) (Table 1) shows that the two segments have a high degree of sequence identity with the substitution of the histidine with the arginine at the N-terminus and two other substitutions in the rest of the molecule (L627V and T630V). While His625 (HSV-1) was proven to be fundamental for the interaction with the membrane bilayer and for translocation across the membrane,[31,33,39–41] the absence of this residue induced similar levels of viral inhibition when compared with the full peptide. This indicates a direct correlation between the α-helical potential and the inhibitory activity and suggests that the substitution of His625 with an arginine residue, as in HSV-2, may not exhibit a significant difference in viral inhibitory activity. The substitution of Leu627 with a valine residue does not alter the hydrophobicity of the peptide, and thus should not influence its infectivity inhibition properties. The authors of this present paper have demonstrated previously

Table 1 Peptide amino acid sequence of gH625-644 in HSV-1 and HSV-2

Virus	Peptide sequence
HSV-1	HGLASTLTRWAHYNALIRAF
HSV-2	RGVASVLTRWAHYNALIRAF

Abbreviation: HSV, herpes simplex virus.

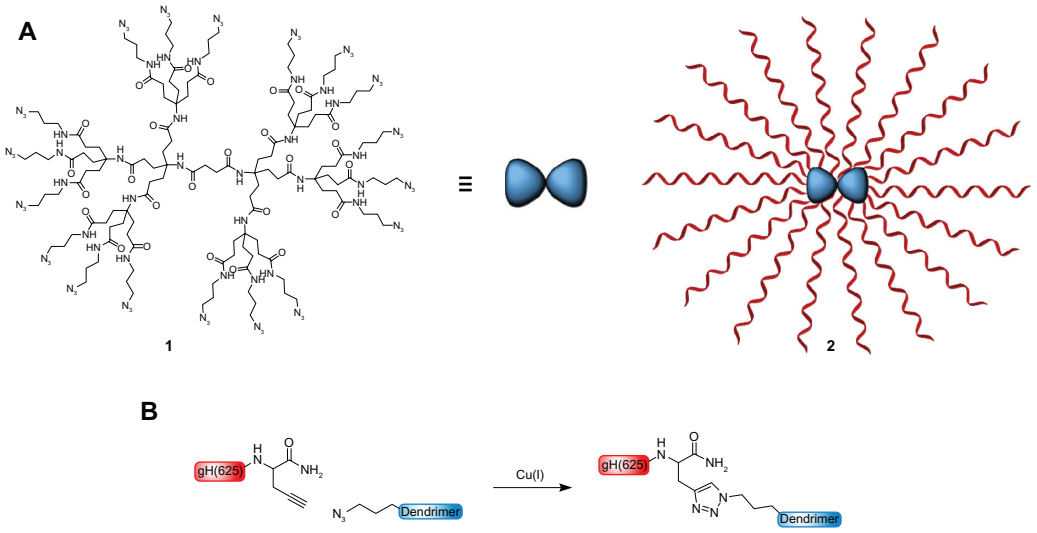

Figure 1 (**A**) Structures of the poly(amide)-based azidodendrimer **1** and cartoon of the peptidodendrimer **2**. The helices on the structure represent the gH625 peptide sequence. (**B**) Schematic representation of the CuAAC reaction to functionalize **1** with peptides. Shown is the C-terminal PrA residue.
Abbreviations: CuAAC, copper catalyzed 1,3-dipolar alkyne/azide cycloaddition; PrA, propargylglycine.

that the substitution of leucine with a polar residue (serine) substantially reduces the peptide's inhibitory activity.[29] There is no evidence from previous works on the substitution of Thr630 with a hydrophobic residue, but the current authors hypothesize this substitution does not alter the aggregation properties of gH625, as the valine is a small hydrophobic residue.

Synthesis of peptidodendrimers

The starting point was the poly(amide)-based dendrimer **1** (Figure 1A) that is based on the 1→3 connectivity scheme first reported by Newkome et al.[42] Poly(amide)-based dendrimers have been reported to exhibit high biocompatibility due to the peptide-like backbone,[43] and thus have been shown to be suitable delivery vehicles.[44] The synthesis of **1** was performed according to a previous report.[34]

To obtain compound **2**, compound **1** was functionalized via the CuAAC using a modified gH625 peptide containing a PrA residue at the C-terminus (NH_2-HGLASTL-TRWAHYNALIRAFX-$CONH_2$, X = PrA) (Figure 1B). The reaction was run in a water/methanol solution using $CuSO_4$/sodium ascorbate as catalyst. After purification,

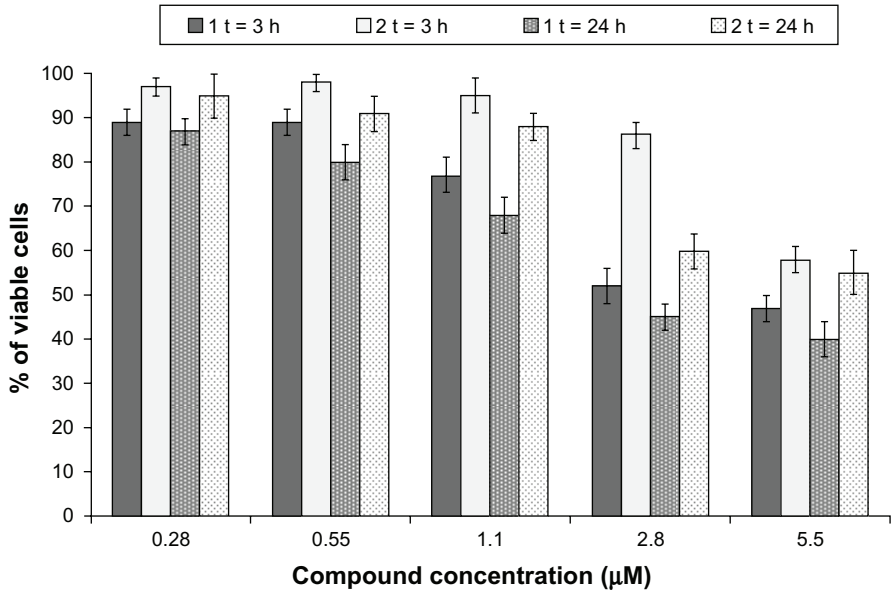

Figure 2 Cell viability measured by the MTT assay for 3 and 24 hours for the dendrimer (**1**) and peptidodendrimer (**2**).
Abbreviation: MTT, 3-(4,5-dimethylthiazol-2-yl)-2,5-diphenyltetrazolium bromide.

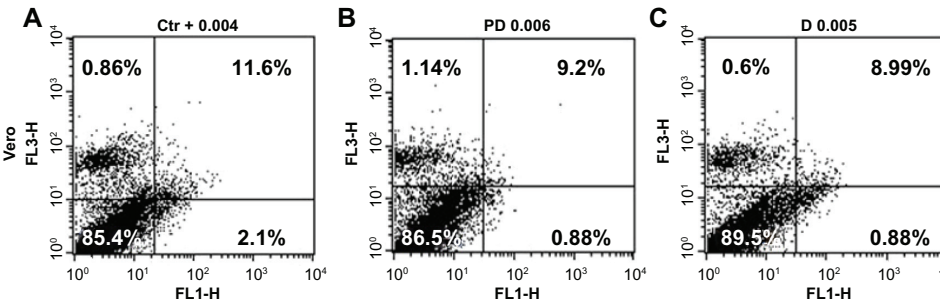

Figure 3 Apoptotic effects of **1** and **2** on Vero cells. FACS analysis after double labeling with propidium iodide and FITC-Annexin V of Vero cells: (**A**) untreated cells, (**B**) treated with **1**, and (**C**) treated with **2** for 24 hours at 0.55 μM. The experiments were performed three times, and the results were always similar.
Note: Insets, percentage of positive cells.
Abbreviations: FACS, fluorescence activated cell sorting; FITC, fluorescein isothiocyanate.

quantitative functionalization was determined by UV ($\varepsilon_{peptide}$ = 7000 M^{-1} cm^{-1} at λ = 280 nm) and infrared (disappearance of signal at 2100 cm^{-1}) analyses.[34] See also Supplementary materials.

Cytotoxicity studies

To confirm that dendrimer **1** and peptidodendrimer **2** do not exert toxic effects on cells, monolayers of Vero cells were exposed to different concentrations (0.28, 0.55, 1.1, 2.8, 5.5 μM) of each compound for 3 and 24 hours, and cell viability was quantified by the MTT assay. No statistical difference was observed between the viability of control (untreated) cells and that of cells exposed to the peptidodendrimer (Figure 2) up to the concentration used in antiviral testing. Minimal toxicity was observed for the dendrimer without the peptides linked to its termini, but only at concentrations that were considerably higher than those required for antiviral activity.

Thereafter, the effects of treatments with **1** and **2** in inducing apoptosis, assessed by FACS analysis after double labeling with FITC-Annexin V and PI, were evaluated. It was found that neither of the treatments induced apoptosis of Vero cell populations (Figure 3 and Table 2). Over 86% of cells treated with **1** and over 89% of cells treated with **2** were alive with only 3% of cells treated with **1** showing markers for early apoptosis.

Antiviral studies

To test whether the peptidodendrimer can affect HSV infectivity in vitro, a virus yield reduction assay in which the peptidodendrimer of interest was present in the cell culture during and after viral adsorption was used. The extent of HSV-1 and HSV-2 replication, assessed by titration of harvested viruses, showed a consistent decrease in replication efficiency for both viruses with more than 80% inhibition at a peptidodendrimer concentration of 280 nM; inhibition of HSV-1 replication was able to reach 90% under these conditions. Dendrimer **1**, without any peptide functionalization, was able to produce an inhibition close to 35% at a concentration of 280 nM, suggesting that the dendrimer structure itself confers an antiviral activity which is enhanced by the specific amino acid sequence added to its termini. The IC_{50} of the peptidodendrimer was 100 and 300 nM against HSV-1 and HSV-2 respectively, while the IC_{50} of **1** was over 550 nM for both viruses (Figure 4).

To elucidate the mechanism of inhibition, the compounds were tested under different conditions to identify the step in the entry process that was being inhibited by the dendrimer. Since inhibition of HSV infectivity could be due to either an interference during the early penetration phase or as a consequence of a peptidodendrimer action inside the cell at a post-entry event, a "posttreatment" test was performed by adding the compounds at different concentrations 2 hours after virus infection (Figure 5). None of the concentrations used significantly reduced HSV-1 and HSV-2 replication. Similarly, a cytopathic effect inhibition assay proved that both the dendrimer and the peptidodendrimer were ineffective once the viruses had already gained their access inside the cell. These results strongly suggest that both the dendrimer and the peptidodendrimer target an early step of the HSV infection cycle.

To investigate whether the inhibitory activities of **1** and the peptidodendrimer **2** are due to the inhibition of HSV entry into cells, prechilled Vero monolayers were infected with HSV-1 and HSV-2 for 2 hours at 4°C. The incubation at 4°C

Table 2 Study of apoptosis in Vero cells after treatment with **1** and **2**

24 hour Vero	Necrosis	Late apoptosis	Alive	Early apoptosis
Untreated	11.6%	0.86%	85.4%	2.1%
1	9.2%	1.14%	86.5%	3.1%
2	8.99%	0.6%	89.5%	0.88%

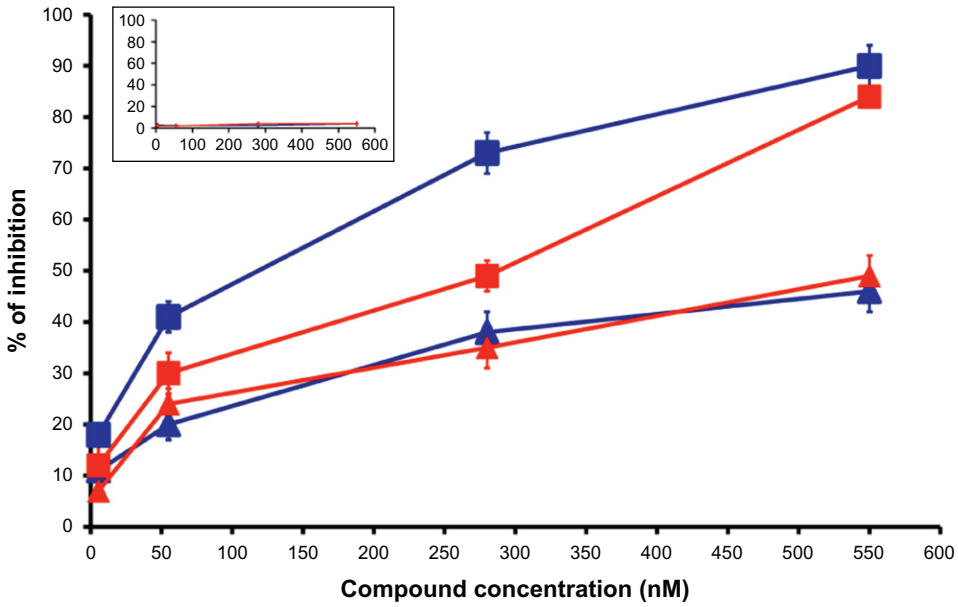

Figure 4 Virus yield reduction assay. Vero cells were infected with either HSV-1 (blue lines) or HSV-2 (red lines) in the presence of increasing concentrations of the dendrimer **1** (triangles) or the peptidodendrimer **2** (squares).
Notes: The percentage of inhibition was calculated with respect to no-compound control experiments. Data points represent an average of three experiments, and error bars represent standard deviations.
Abbreviation: HSV, herpes simplex virus.

blocks the virus' penetration but allows its attachment to the cell surface via its cellular receptors, thereby synchronizing cell penetration. Dendrimer **1** and **2** were then added to the infected cells which were shifted to 37°C. After 45 minutes at 37°C, unpenetrated viruses were inactivated by an acid wash and overlaid with CMC to measure infectivity of penetrated viruses. As shown in Figure 6A, none of the concentrations of **1** or **2** investigated was able to affect HSV-1 or HSV-2 entry and replication. When prechilled Vero monolayers were infected with HSV-1 and HSV-2 in the presence of **1** or **2** for 1 hour at 4°C, however, an inhibitory effect was observed (Figure 6B). For this experiment, a modification of the procedure was introduced, in fact, the same attachment test was also performed adding heparin as a control, and as expected,

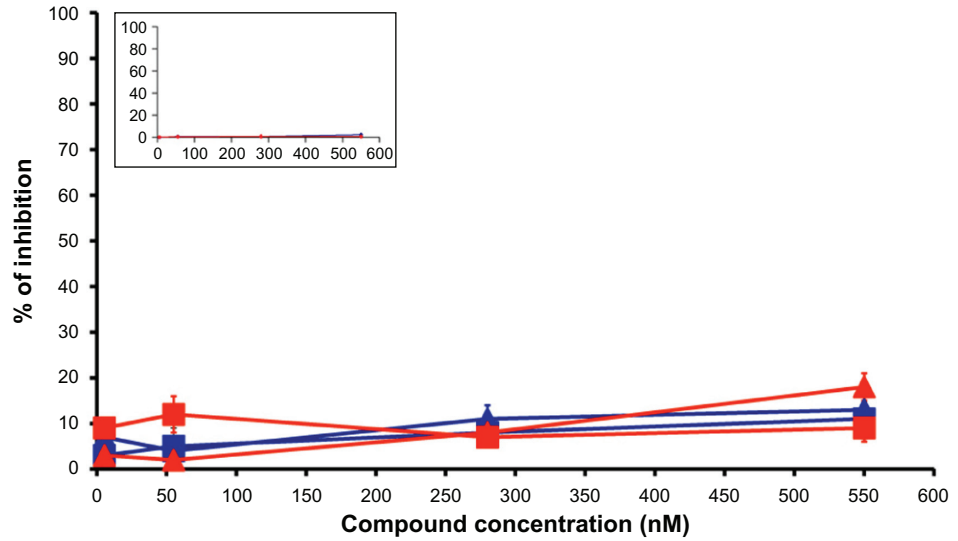

Figure 5 Posttreatment assay. HSV-1 (blue lines) and HSV-2 (red lines) infected Vero cells were treated with increasing concentrations of the dendrimer **1** (triangles) or the peptidodendrimer **2** (squares), then overlaid with CMC and incubated for 24 hours at 37°C.
Notes: Plaque numbers were scored, and the percentage of inhibition was calculated with respect to no-compound control experiments. Data points represent an average of three experiments, and error bars represent standard deviations.
Abbreviations: HSV, herpes simplex virus; CMC, carboxymethyl cellulose.

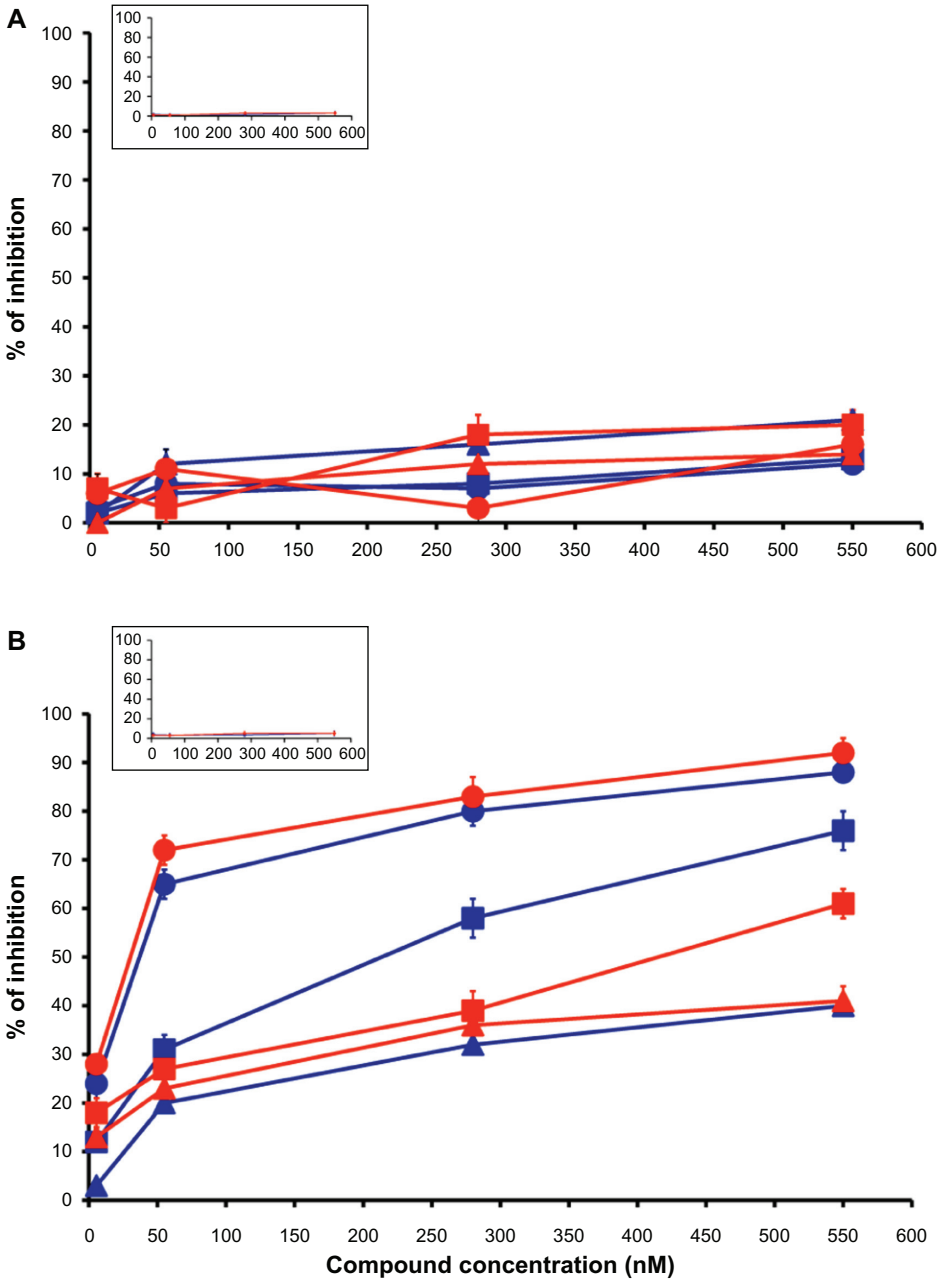

Figure 6 Effect of **1** and **2** on viral attachment. (**A**) Vero cell monolayers were infected with HSV-1 (blue lines) or HSV-2 (red lines) at an MOI of 0.1 pfu/cell for 2 hours at 4°C. After unattached virus removal, plates were treated with various concentrations of **1** (triangles), **2** (squares), or heparin (circles) for 3 hours at 37°C. Finally, cells were overlaid with CMC and incubated for 2 days at 37°C. (**B**) Vero cell monolayers were treated with inocula containing both the viruses and the antiviral compounds precooled at 4°C.
Notes: Plaque numbers were scored, and the percentage of inhibition was calculated with respect to "no-compound" control experiments. Data are reported in triplicate, and error bars represent standard deviations.
Abbreviations: HSV, herpes simplex virus; MOI, multiplicity of infection; pfu, plaque-forming unit; CMC, carboxymethyl cellulose.

heparin was completely able to block the ability of HSV-1 and HSV-2 to attach to Vero cells, preventing the interaction of the virions with cell surface heparin sulfate.

The possibility of **2** to interfere with an early penetration step was further explored. Vero cells were pretreated with **1** or **2** for 1 hour before infection. No significant reduction of infectivity with **2** was observed (Figure 7). In contrast, a clear activity of the dendrimer itself was observed. Since the toxicity of the dendrimer is marginal, it is assumed that it may exert an antiviral activity by blocking the cell surface. The lack of activity of the peptidodendrimer is probably due to the fact that this molecule is able to penetrate inside the cell efficiently in virtue of its functionalization with the membranotropic HSV-1 gH derived sequence,[34,45] therefore, during the 1 hour of cell pretreatment, the majority of **2** may have already translocated inside the cell where it is

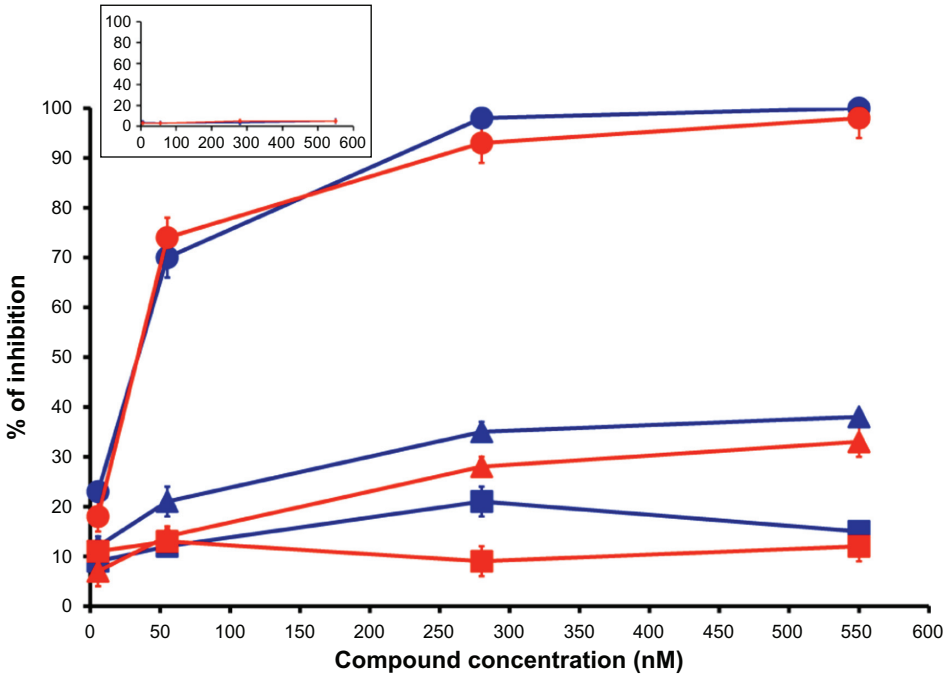

Figure 7 Cell pretreatment assay. Vero cell monolayers were treated with various concentrations of **1** (triangles), **2** (squares), or heparin (circles) for 30 minutes at 4°C before being infected with precooled HSV-1 (blue lines) or HSV-2 (red lines) at 0.1 pfu/cell in the presence of the compounds for 2 hours at 4°C. After the removal of excess compounds, cells were overlaid with CMC, and incubated for 2 days at 37°C.

Notes: Plaque numbers were scored, and the percentage of inhibition was calculated with respect to "no-compound" control experiments. Data points represent an average of three experiments, and error bars represent standard deviations.

Abbreviations: HSV, herpes simplex virus; pfu, plaque-forming unit; CMC, carboxymethyl cellulose.

probably inactive accordingly with the posttreatment assay. The amount of peptidodendrimer left on the cell surface may be below the concentration needed to maintain an antiviral activity.

Since inhibition of HSV penetration might result from an irreversible peptidodendrimer-induced inactivation of the virions, the possibility that the compounds could interfere with HSV particles and inactivate viral infectivity was explored. To do this, HSV-1 and HSV-2 aliquots were incubated with different concentrations of **1** and **2** at 4°C and 37°C for 2 hours. After incubation, the samples were diluted to reduce the antiviral agents' concentrations well below the threshold for HSV replication inhibition (0.001 to 0.1), and the infectivity of preincubated virions was measured by titration on Vero cells. As shown in Figure 8, the incubation of virions with the peptidodendrimer reduced the infectivity in both HSV-1 and HSV-2. The pre-incubation of virions with **1** also produced a decrease of infectivity, albeit of lower intensity.

Discussion

The goal of the research reported herein is to investigate the antiviral properties of a dendrimer whose termini have been functionalized with the HSV-1 derived peptide gH625 that has been shown previously to possess antiviral activity.[28,29,31] The key characteristics of gH625 are: (1) the ability to interact with model membranes, (2) penetration of the bilayer with its N-terminus, (3) high efficiency of inducing lipid mixing of model membranes, and (4) the ability to adopt a helical conformation with its hydrophobic residues on one face of the helix and polar or charged residues on the opposite face.[29,31,33] The inhibitory effect of gH625 appeared conditioned by its ability to partition into membranes and aggregate within them. Since gH625 peptides self-associate in aqueous and lipidic solutions, it is possible that they bind to their counterparts in the HSV-1 gH fusion protein, suggesting that the inhibition of viral entry may occur via peptide association with their counterpart on wild-type gH. In this contribution, a peptidodendrimer carrying the gH625 peptide at its termini was constructed. The functionalization of the dendrimer with the gH625 peptide was quantitative as evidenced by UV and infrared analyses. Dynamic light-scattering and scanning electron microscopy showed the average particle size to be 12 nm. Circular dichroism showed that the terminal peptides fold into an α-helix in a membrame-mimetic environment.[34]

To analyze the antiviral activity of the peptidodendrimer, a virus yield assay on both HSV-1 and HSV-2 was first

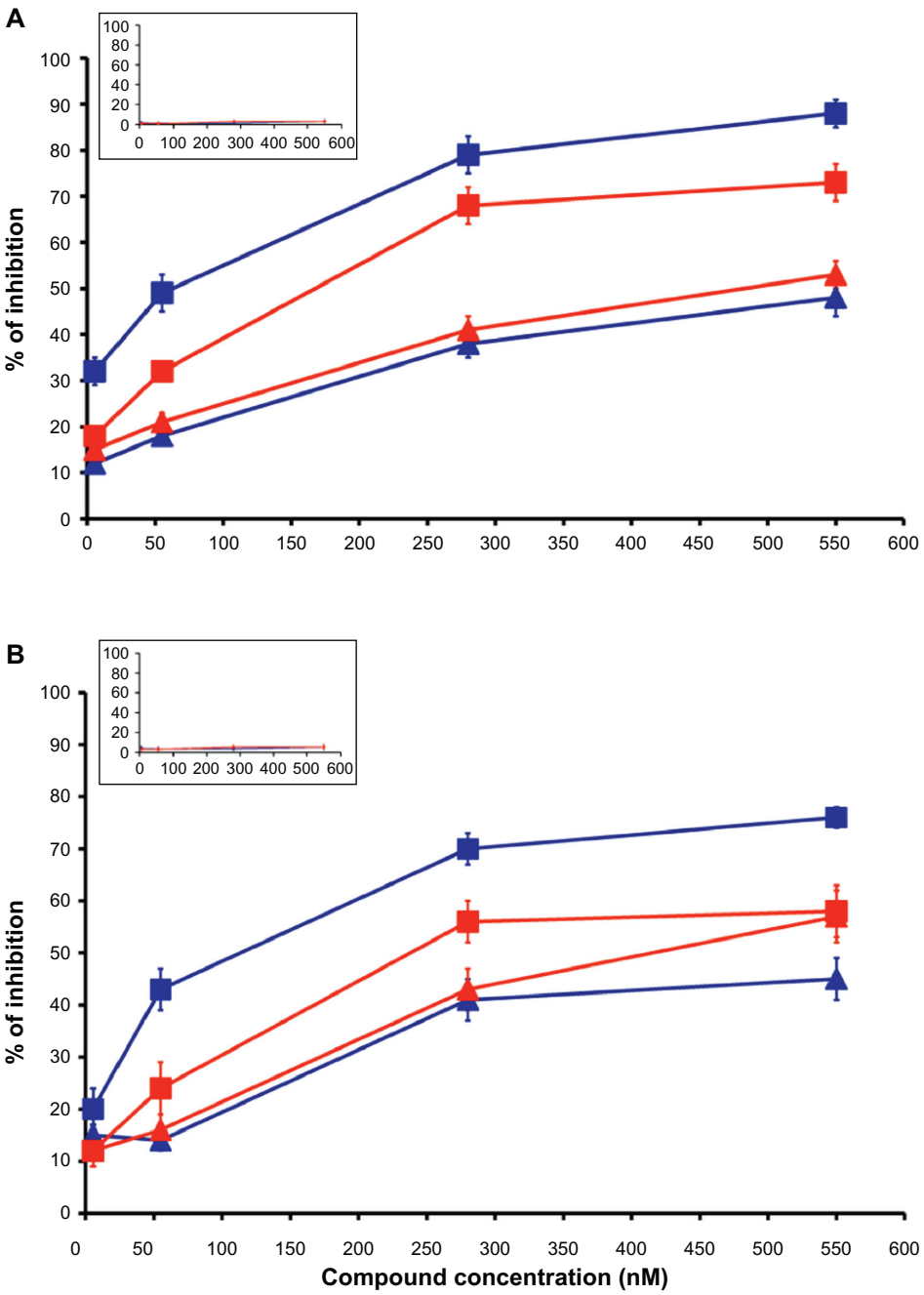

Figure 8 Virucidal assay. Different concentrations of **1** (triangles) and **2** (squares) were added to aliquots (10^4 pfu) of HSV-1 (blue lines) or HSV-2 (red lines), and incubated at either 4°C (**A**) or 37°C (**B**) for 2 hours. After incubation, the samples were diluted to reduce the compound concentrations below the threshold for inhibition of viral replication, and the virus was titrated on Vero cells.

Notes: Plaque numbers were scored and the percentage of inhibition was calculated with respect to "no-compound" control experiments. Data points represent an average of three experiments, and error bars represent standard deviations.

Abbreviations: HSV, herpes simplex virus; pfu, plaque-forming unit.

performed, and a consistent decrease in replication efficiency for both viruses was obtained. Interestingly, the dendrimer itself was able to inhibit virus replication, albeit to a lesser extent compared with the peptidodendrimer, while the peptide on its own was unable to show any inhibition when tested at a concentration corresponding to the peptide present on the peptidodendrimer. The multivalent display of gH625 on the dendrimer scaffold results in an almost sixfold increase of antiviral activity for HSV-1 and twofold for HSV-2 in comparison to the activity of the dendrimer itself, and a more than 100-fold increase in the activity of the unsupported peptide. The IC_{50} of the peptidodendrimer was 100 and 300 nM against HSV-1 and HSV-2, respectively, while the IC_{50} of the unfunctionalized dendrimer was over 550 nM

for both viruses. The cytotoxicity profile measured by the MTT assay showed that the peptidodendrimer was not toxic to Vero cells up to the highest concentration investigated in antiviral testing, while some toxicity was observed for the unfunctionalized dendrimer, especially at higher concentrations, demonstrating another advantage of the peptide functionalization. To further analyze intact cell activity, a FACS analysis was performed after double labeling with FITC-Annexin V and PI to evaluate the effects of **1** and **2** on induction of apoptosis and concluded that the majority of cells are still alive and functional after 24 hours at the active antiviral concentration.

Further experiments were carried out to identify which step in the entry process could be responsible for the observed infectivity inhibition. Any inhibitory activity can be excluded when the compounds were added at a post-entry step and also when cells were pretreated with the dendrimer derivatives. Both the peptidodendrimer and the dendrimer are not able to interfere with viral replication once the virus has gained access to the cellular milieu. When cells were pretreated with **1** or **2** for 1 hour before infection, the peptidodendrimer was unable to yield a significant reduction of infectivity, while a clear inhibition was obtained by the dendrimer itself. The lack of activity of the peptidodenrimer is probably due to the fact that this molecule is able to penetrate inside the cell efficiently in virtue of its functionalization with the membranotropic HSV-1 gH derived sequence.[34] Therefore, during the 1 hour of cell pretreatment, the majority of the peptidodendrimer may have already translocated inside the cell where it was probably inactive according to the posttreatment assay. On the other hand, **1** enters much more slowly and, more importantly, it partially remains on the cell surface. This allows the dendrimer to reduce membrane mobility and inhibit viral entry or to produce a consistent delay in viral entrance.[34] After excluding also the attachment step (Figures 6 and 7) as being responsible for the antiviral activity, the possibility that the peptidodendrimer could directly inactivate the virions was explored. The results of virus-pretreatment assay showed a strong and consistent inhibition of viral infectivity for HSV-1 and a slightly lower inhibition of HSV-2. The pre-incubation of virions with the unfunctionalized dendrimer also produced a decrease of infectivity, albeit of lower intensity. The authors hypothesize that the peptidodendrimer might sterically hinder the gH relative domain, either in a pre-fusogenic or in an intermediate conformation, preventing a complete and functional interaction between gH and the membrane to fuse. Due to the high degree of complexity of the interaction of HSV surface glycoproteins during the fusion process, it was not able to unequivocally identify the path of antiviral action of the peptidodendrimer. It may act by binding to gH itself through oligomerization of the gH625-644 domain present on the glycoprotein, in a probable rearrangement of its structural domains. Alternatively, the gH sequence present on the peptidodendrimer may interact with other glycoproteins present on the virion envelope, such as gB or gD.

The results of this study indicate that the modification of a dendrimer scaffold with antiviral peptides represent an attractive strategy for the design of a new class of antiviral drugs that exert their effect, coupling the intrinsic antiviral properties of the dendrimer with the activity of antiviral peptides. These antiviral drugs possess several advantageous features, such as target specificity, low toxicity, and the possibility to modify surface characteristics easily. Moreover, peptidodendrimers have the potential of being developed as multifunctionalized scaffolds to provide a therapeutic molecule that could be directly delivered to its target.

Acknowledgments

We thank the National Science Foundation (CHE-0234863, CHE-0958457, CHE-01162222) and New York University for support of the analytical equipment. SG and AF thank MIUR for financial support by PON01_02388 "Verso la medicina personalizzata: nuovi sistemi molecolari per la diagnosi e la terapia di patologie oncologiche ad alto impatto sociale - SALUTE DELL'UOMO E BIOTECNOLOGIE Responsabile Scientifico Prof. Carlo Pedone. Viral strains were kindly donated by Dr. Helena Browne, Department of Pathology of the University of Cambridge, UK.

Disclosure

The authors report no conflicts of interest in this work.

References

1. van Benthem BH, Spaargaren J, van Den Hoek JA, Merks J, Coutinho RA, Prins M. Prevalence and risk factors of HSV-1 and HSV-2 antibodies in European HIV infected women. *Sex Transm Infect*. 2001;77(2):120–124.
2. Superti F, Ammendolia MG, Marchetti M. New advances in Anti-HSV chemotherapy. *Curr Med Chem*. 2008;15(9):900–911.
3. Greco A, Diaz JJ, Thouvenot D, Morfin F. Novel targets for the development of anti-herpes compounds. *Infect Disord Drug Targets*. 2007;7(1):11–18.
4. Keller MJ, Tuyama A, Carlucci MJ, Herold BC. Topical microbicides for the prevention of genital herpes infection. *J Antimicrob Chemother*. 2005;55(4):420–423.
5. Lee CC, MacKay JA, Fréchet JMJ, Szoka FC. Designing dendrimers for biological applications. *Nat Biotech*. 2005;23(12):1517–1526.
6. Esfand R, Tomalia DA. Poly(amidoamine) (PAMAM) dendrimers: from biomimicry to drug delivery and biomedical applications. *Drug Discov Today*. 2001;6(8):427–436.

7. Sadler K, Tam JP. Peptide dendrimers: applications and synthesis. *Rev Mol Biotechnol*. 2002;90:195–229.
8. Cloninger MJ. Biological applications of dendrimers. *Curr Opin Chem Biol*. 2002;6:742–748.
9. Niederhafner P, Šebestík J, Ježek J. Peptide dendrimers. *J Peptide Sci*. 2005;11:757–788.
10. Tekade RK, Kumar PV, Jain NK. Dendrimers in oncology: an expanding horizon. *Chem Rev*. 2009;109(1):49–87.
11. Newkome GR, Moorefield CN, Vögtle F. *Dendrimers and Dendrons: Concepts, Synthesis, Applications*. Weinheim: Wiley-VCH; 2001.
12. Fox ME, Szoka FC, Fréchet JMJ. Soluble polymer carriers of the treatment of cancer: the importance of molecular architecture. *Acc Chem Res*. 2009;42(8):1141–1151.
13. Kolb HC, Finn MG, Sharpless KB. Click chemistry: diverse chemical function from a few good reactions. *Angew Chem Int Ed*. 2001; 40(11):2004–2021.
14. Franc G, Kakkar A. Dendrimer design using Cu-catalyzed alkyne-azide "click chemistry". *Chem Commun*. 2008;44(42):5267–5276.
15. Astruc D, Liang L, Rapakousiou A, Ruiz J. Click dendrimers and triazole-related aspects: catalysts, mechanism, synthesis, and functions. A bridge between dendritic architectures and nanomaterials. *Acc Chem Res*. 2012;45(4):630–640.
16. Bourne N, Stanberry LR, Kern ER, Holan G, Matthews B, Bernstein DI. Dendrimers, a new class of candidate topical microbicides with activity against herpes simplex virus infection. *Antimicrob Agents Chemother*. 2000;44(9):2471–2474.
17. Gao H, Louche G, Sumerlin BS, Jahed N, Golas P, Matyjaszewski K. Gradient polymer elution chromatographic analysis of α,ω-dihydroxypolystyrene synthesized via ATRP and click chemistry. *Macromolecules*. 2005;38(22):8979–8982.
18. Vogt AP, Sumerlin BS. An efficient route to macromonomers via ATRP and click chemistry. *Macromolecules*. 2006;39(16): 5286–5292.
19. Li H, Cheng F, Duft AM, Adronov A. Functionalization of single-walled carbon nanotubes with well-defined polystyrene by "click" coupling. *J Am Chem Soc*. 2005;127(41):14518–14524.
20. Luganini A, Nicoletto SF, Pizzuto L, et al. Inhibition of herpes simplex virus type i and type ii infections by peptide-derivatized dendrimers. *Antimicrob Agents Chemother*. 2011;55(7):3231–3239.
21. Jiang Y-H, Emau P, Cairns JS, et al. SPL7013 gel as a topical microbicide for prevention of vaginal transmission of SHIV in macaques. *AIDS Res Hum Retrovir*. 2005;21(3):207–213.
22. Gong E, Matthews B, McCarthy TD, et al. Evaluation of dendrimer SPL7013, a lead microbicide candidate against herpes simplex viruses. *Antivir Res*. 2005;68(3):139–146.
23. O'Loughlin J, Millwood I, McDonald HM, Price CF, Kaldor JM, Paull JRA. Safety, tolerability, and pharmacokinetics of SPL7013 gel (VivaGel). *Sex Transm Dis*. 2010;37(2):100–104.
24. Telwatte S, Moore K, Johnson A, et al. Virucidal activity of the dendrimer microbicide SPL7013 against HIV-1. *Antivir Res*. 2011;90(3): 195–199.
25. Luganini A, Giuliani A, Pirri G, Pizzuto L, Landolfo S, Gribaudo G. Peptide-derivatized dendrimers inhibit human cytomegalovirus infection by blocking virus binding to cell surface heparan sulfate. *Antivir Res*. 2010;85(3):532–540.
26. Donalisio M, Rusnati M, Civra A, et al. Identification of a dendrimeric heparan sulfate-binding peptide that inhibits infectivity of genital types of human papillomaviruses. *Antimicrob Agents Chemother*. 2010; 54(10):4290–4299.
27. Hunter AC. Molecular hurdles in polyfectin design and mechanistic background to polycation induced cytotoxicity. *Adv Drug Deliv Rev*. 2006;58(14):1523–1531.
28. Galdiero S, Falanga A, Vitiello M, et al. Peptides containing membrane-interacting motifs inhibit herpes simplex virus type I infectivity. *Peptides*. 2008;29:1461–1471.
29. Galdiero S, Falanga A, Vitiello M, et al. Analysis of a membrane interacting region of herpes simplex virus type i glycoprotein H. *J Biol Chem*. 2008;283(44):29993–30009.
30. Galdiero S, Falanga A, Vitiello M, Browne H, Pedone C, Galdiero M. Fusogenic domains in herpes simplex virus type i glycoprotein H. *J Biol Chem*. 2005;280(31):28632–28643.
31. Galdiero S, Falanga A, Vitiello M, et al. The presence of a single N-terminal histidine residue enhances the fusogenic properties of a membranotropic peptide derived from herpes simplex virus type I glycoprotein H. *J Biol Chem*. 2010;285(22):17123–17136.
32. Galdiero S, Falanga A, Vitiello G, et al. Role of membranotropic sequences from herpes simplex virus type i glycoproteins B and H in the fusion process. *Biochim Biophys Acta*. 2010;1798(3):579–591.
33. Galdiero S, Russo L, Falanga A, et al. Structure and orientation of the gH625-644 membrane interacting region of herpes simplex virus type 1 in a membrane mimetic system. *Biochemistry*. 2012;51(14): 3121–3128.
34. Carberry TP, Tarallo R, Falanga A, et al. Dendrimer functionalization with a membrane-interacting domain of herpes simplex virus type 1: towards intracellular delivery. *Chem Eur J.* 2012;18(43):13678–13685.
35. Mosmann T. Rapid Colorimetric assay for cellular growth and survival: application to proliferation and cytotoxicity assays. *J Immunol Methods*. 1983;65(1–2):55–63.
36. Vitiello M, Galdiero M. Inhibition of viral-induced membrane fusion by peptides. *Protein Pept Lett*. 2009;16(7):786–793.
37. Xu Y, Rahman NA, Othman RB, Hu P, Huang M. Computational identification of self-inhibitory peptides from envelope proteins. *Proteins*. 2012;80(9):2154–2168.
38. Galdiero S, Falanga A, Vitiello M, et al. Evidence for a role of the membrane-proximal region of herpes simplex virus type 1 glycoprotein H in membrane fusion and virus inhibition. *Chembiochem*. 2007;8(8): 885–895.
39. Tarallo R, Accardo A, Falanga A, et al. Clickable functionalization of liposomes with the gH625 peptide from herpes simplex virus type i for intracellular drug delivery. *Chem Eur J*. 2011;17(45):12659–12668.
40. Falanga A, Vitiello MT, Cantisani M, et al. A peptide derived from herpes simplex virus type 1 glycoprotein H: membrane translocation and applications to the delivery of quantum dots. *Nanomed Nanotechnol*. 2011;7(6):925–934.
41. Galdiero S, Vitiello M, Falanga A, Cantisani M, Incoronato N, Galdiero M. Intracellular delivery: exploiting viral membranotropic peptides. *Curr Drug Metab*. 2012;13(1):93–104.
42. Newkome GR, Kotta KK, Moorefield CN. Convenient synthesis of 1 → 3 C-branched dendrons. *J Org Chem*. 2005;70(12):4893–4896.
43. Roberts JC, Bhalgat MK, Zera RT. Preliminary biological evaluation of polyamidoamine (PAMAM) Starburst™ dendrimers. *Biomed Mater Res*. 1996;30(1):53–65.
44. Majoros IJ, Myc A, Thomas T, Mehta CB, Baker JR Jr. PAMAM dendrimer-based multifunctional conjugate for cancer therapy: synthesis, characterization, and functionality. *Biomacromolecules*. 2006; 7(2):572–579.
45. Guarnieri D, Falanga A, Muscetti O, et al. Shuttle-mediated nanoparticle delivery to the blood-brain barrier. *Small*. Epub November 7, 2012. doi: 10.1002/smll.201201870

Supplementary materials

Materials and methods

The analysis of the three molecules: crude peptidodendrimer, peptide and dendrimer was carried out on an analytical Agilent Technologies (Santa Clara, CA, USA) 1200 Series HPLC system with a Phenomenex (Torrance, CA, USA) analytical C_5 column (Jupiter 5 µ 300Å, 150 mm × 4.60 mm, 5 micron). The mobile phase used was: H_2O 0.1% trifluoroacetic acid as eluent A and CH_3CN 0.1% TFA as eluent B from 30% to 95% over 20 minutes at 1 mL min^{-1} flow. The compounds were dissolved in a 30% CH_3CN 0.1% TFA and 70% H_2O 0.1% TFA solution before being loaded onto the column: the coupling was performed using one equivalent of dendrimer and two equivalents of peptide.

Discussion

The peptidodendrimer presents a different retention time from both the peptide and dendrimer alone. As we can see from the crude peptidodendrimer chromatogram, the peak relative to the dendrimer disappears, confirming that all the dendrimer is bound to peptide.

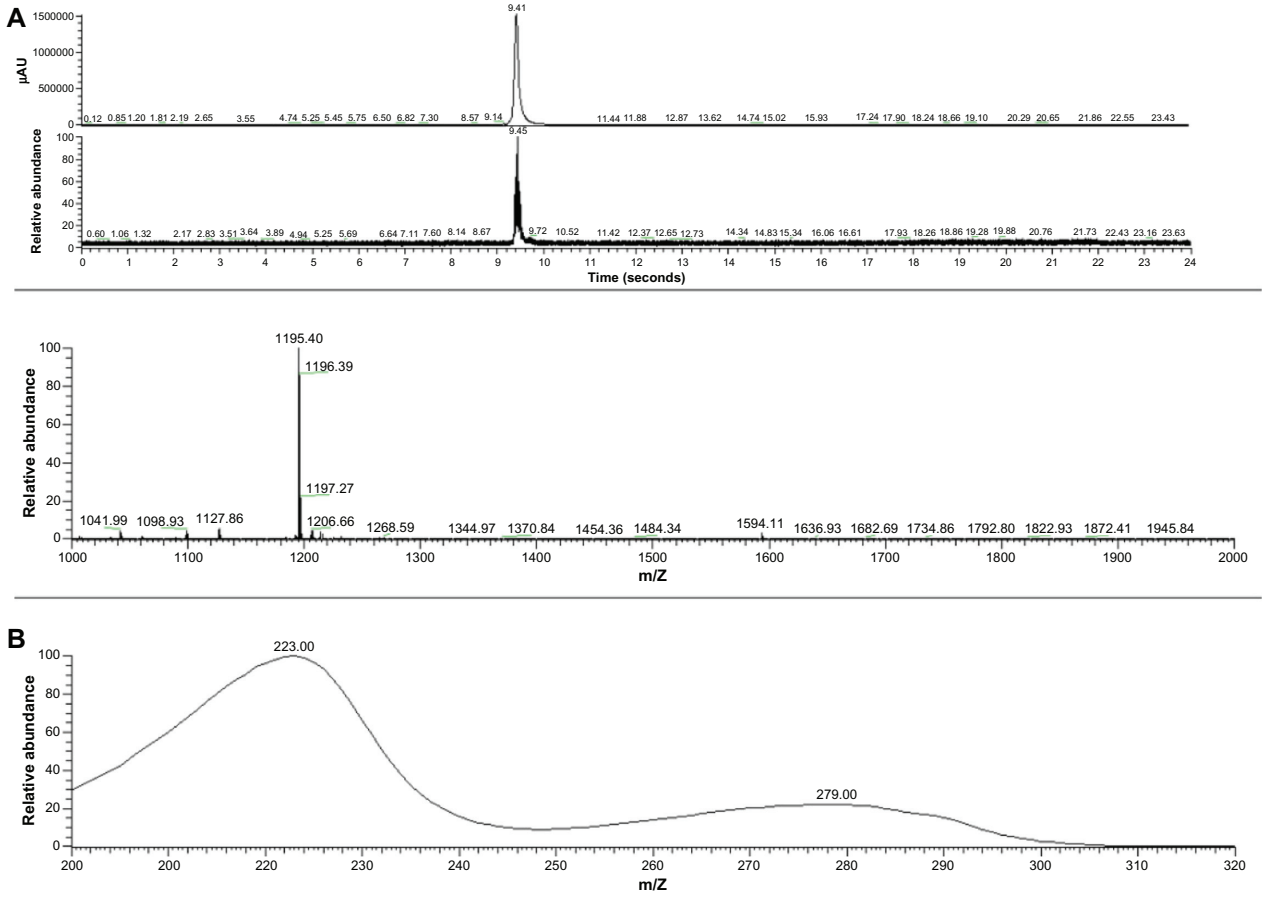

Figure S1 LC-MSQ spectra of gH625-PRA peptide. gH625-PRA (MW: 2392.7) purity and identity was assessed by analytical LC-MS analyses using Finnigan Surveyor MSQ single quadrupole electrospray ionization (Thermo Electron, San Jose, CA, USA), column: C_{18}-Phenomenex eluted with H_2O/0.1% TFA (**A**) and CH_3CN/0.1% TFA (**B**) from 20% to 80% over 10 minutes at a flow rate of 0.8 mL min^{-1}.

Notes: The final yield of purified peptide was approximately 40%. NH_2-HGLASTLTRWAHYNALIRAFX-$CONH_2$, X = PrA, Rt = 9.4 minutes; (MW = 2392.7) [M + 2H]+/2 = 1197 amu.

Abbreviations: LC-MS, liquid chromatography-mass spectrometry; LC-MSQ, liquid chromatography-mass spectrometry quadrupole; MW, molecular weight; TFA, trifluoroacetic acid.

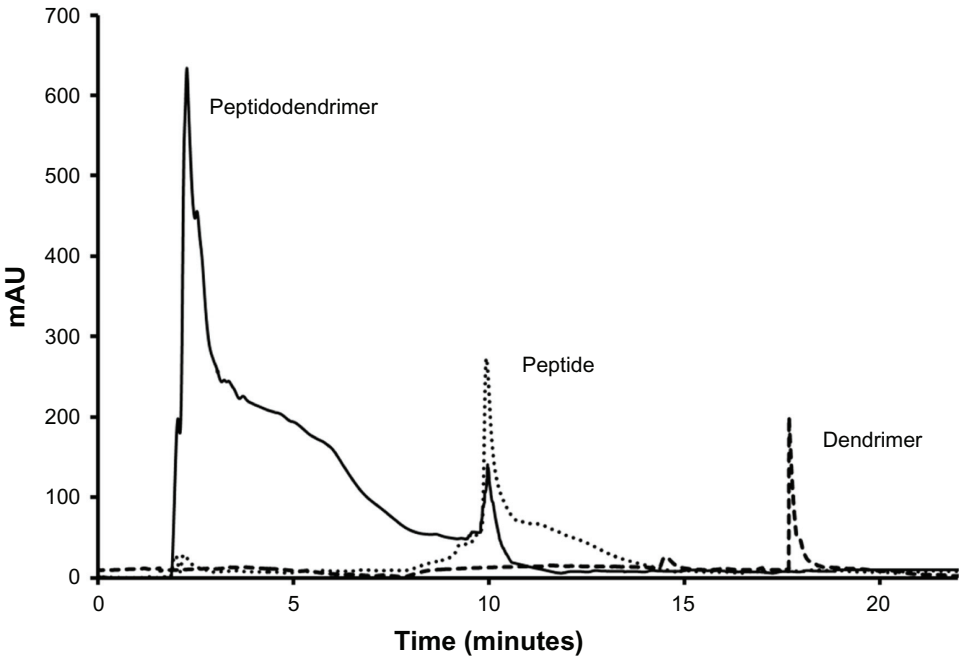

Figure S2 LC-MSQ spectra of the crude peptidodendrimer.

DOI: 10.1002/chem.201101425

Clickable Functionalization of Liposomes with the gH625 Peptide from *Herpes simplex* Virus Type I for Intracellular Drug Delivery

Rossella Tarallo,[a] Antonella Accardo,[a] Annarita Falanga,[a] Daniela Guarnieri,[b] Giuseppe Vitiello,[c] Paolo Netti,[b] Gerardino D'Errico,[c] Giancarlo Morelli,*[a] and Stefania Galdiero*[a]

Abstract: Liposomes externally modified with the nineteen residues gH625 peptide, previously identified as a membrane-perturbing domain in the gH glycoprotein of *Herpes simplex* virus type I, have been prepared in order to improve the intracellular uptake of an encapsulated drug. An easy and versatile synthetic strategy, based on click chemistry, has been used to bind, in a controlled way, several copies of the hydrophobic gH625 peptide on the external surface of 1,2-dioleoyl-*sn*-glycero-3-phosphocholine (DOPG)-based liposomes. Electron paramagnetic resonance studies, on liposomes derivatized with gH625 peptides, which are modified with the 2,2,6,6-tetramethylpiperidine-1-oxyl-4-amino-4-carboxylic acid (TOAC) spin label in several peptide positions, confirm the positioning of the coupled peptides on the liposome external surface, whereas dynamic light scattering measurements indicate an increase of the diameter of the liposomes of approximately 30% after peptide introduction. Liposomes have been loaded with the cytotoxic drug doxorubicin and their ability to penetrate inside cells has been evaluated by confocal microscopy experiments. Results suggest that liposomes functionalized with gH625 may act as promising intracellular targeting carriers for efficient delivery of drugs, such as chemotherapeutic agents, into tumor cells.

Keywords: click chemistry · drug delivery · liposomes · peptides · viruses

Introduction

Intracellular delivery of therapeutic molecules is one of the key problems in drug development: many drugs are poorly internalized by cells because they cross the membrane rather inefficiently.[1] Cell-penetrating peptides (CPP) are short and usually basic amino acid rich peptides originating from proteins that are able to cross biological barriers, such as the viral Tat protein. CPPs are considered as the most promising tools for the intracellular delivery of therapeutics, both in vitro and in vivo.[2] Although the mechanism of their cellular uptake is still under debate, CPPs are able to translocate various entities into cells, including small molecules, peptides, proteins, DNA/RNA, liposomes, and other supramolecular aggregates. Endosomal entrapment may limit their utility, though some peptides and other biologically active molecules can escape this environment to achieve a specific desired biological action. Therefore, it is fundamental to exploit novel molecules, which use different internalization mechanisms. Recently, great attention has been devoted to the study of hydrophobic peptides that efficiently traverse biological membranes, promoting lipid-membrane-reorganizing processes, such as fusion or pore formation and thus, involving temporary membrane destabilization and subsequent reorganization.[3]

The nineteen residues peptide gH625, was previously identified as a membrane-perturbing domain in the gH protein of *Herpes simplex* virus type I;[4] gH625 interacts with biological membranes, contributing to the merging of the viral envelope and the cellular membrane; it is able to traverse the membrane bilayer and to transport a cargo into the cytoplasm.[5] We already reported the ability of gH625 to transport quantum dots inside the cytoplasm in an efficient way and only partially involving endocytic pathways.[5] We are now studying gH625 as a potential transporter of liposomes loaded with anticancer drugs, such as doxorubicin.

Liposomal aggregates have attracted great attention due to their success as in vivo carriers of active principles.[6] Liposomes display some unique pharmacokinetic properties and can be adapted to a wide range of therapeutic agents; in particular, they are non-toxic, biodegradable, and non-immunogenic, thanks to their size ranging in mean diameter from 50 to 300 nm. Benefits associated with liposomal drugs

[a] R. Tarallo, Dr. A. Accardo, Dr. A. Falanga, Prof. G. Morelli, Dr. S. Galdiero
Department of Biological Sciences, CIRPeB & IBB CNR
University of Naples "Federico II"
Via Mezzocannone 16 80134 Naples (Italy)
Fax: (+39) 0812536642
E-mail: gmorelli@unina.it
sgaldier@unina.it

[b] Dr. D. Guarnieri, Prof. P. Netti
IIT@CRIB, Center for Advanced Biomaterials in Health Care
Piazzale Tecchio 80, 80125 Naples (Italy)

[c] Dr. G. Vitiello, Dr. G. D'Errico
Department of Chemistry, University of Naples "Federico II"
and Consorzio per lo Studio dei Sistemi a Grande Interfase
CSGI, Monte Sant'Angelo, 80126, Naples (Italy)

can arise from protection of encapsulated drugs from chemical or metabolic degradation after injection, reduced toxicity through decreased exposure of antineoplastics to susceptible healthy tissues, and increased antitumor activity resulting from a relatively long systemic circulation time, an extended exposure and tumor selective accumulation in sites of tumor growth. Moreover, liposomes exhibit preferential extravasation and accumulation at the site of solid tumors due to increased endothelial permeability and reduced lymphatic drainage in these tissues, which has been defined as enhanced permeability and retention effect, respectively.[7] Thus, associating a drug with liposomes markedly changes its pharmacokinetic and pharmacodynamic properties and lowers systemic toxicity; furthermore, the drug is prevented from early degradation and/or inactivation.[8]

To enhance the antitumor efficacy of liposomal drugs, many research groups are working to improve the cellular internalization of liposomes through the addition of surface ligands. Recently, several peptides, such as penetratin[9] and Tat,[10] have been successfully used for the intracellular delivery of liposomes.

CPPs, by interacting with charged phospholipids on the outer surface of the cell membrane and destabilizing the bilayer, are capable of carrying hydrophilic compounds across the plasma membrane, which may be useful in facilitating the intracellular delivery of liposomal drugs.[11] Here, we report the synthesis and the structural characterization of liposomes decorated with the novel viral peptide gH625 loaded with doxorubicin. Different synthetic procedures can be used to introduce a bioactive molecule on the external surface of liposomes.[12] The different strategies involve the coupling of the peptide to the lipid moiety before or after the assembly of the liposome.

The strategy is strongly dependent on the peptide that has to be linked to the liposomes; in fact the coupling of charged peptides can be performed before the formation of the liposome, although this strategy has the disadvantage that a fraction of the conjugated peptide remains entrapped in the interior region of the liposome. The coupling of a hydrophobic peptide is complicated by the low solubility of the compound and by the higher tendency of the peptide to locate in the hydrophobic region of the bilayer rather than the external surface. Thus, the preferable way to obtain liposomes functionalized on the surface with a hydrophobic peptide consists in the coupling of peptide derivatives on pre-assembled liposome.

The conjugation of a ligand on the surface of pre-assembled liposomes can be performed by using a variety of techniques, including physical adsorption, electrostatic binding, specific recognition, and covalent coupling, each of which has its own advantages and disadvantages. Chemically controlled conjugation on pre-assembled liposomes that carry functionalized lipid anchors should ideally combine several features, such as mild reaction conditions in aqueous media, high yields, and chemoselectivity. The application of click chemistry is particularly appealing because of its regiospecificity, chemoselectivity, and mainly tolerance to a wide variety of other functional groups.

In the present study the gH625-modified liposomes are prepared by using a post-aggregation strategy based on click chemistry (see Scheme 1).[13] This procedure consists in the preparation of liposomes containing accessible azido functions on their external surface and subsequently in the coupling of the azido functions with alkyne moieties present in the peptide derivative, according to click-chemistry procedures.[14] The positioning of the coupled peptide relative to the liposome surface is investigated by electron paramagnetic resonance (EPR) spectroscopy, by using peptides modified according to a site-directed spin-labeling approach. The ability of gH625-functionalized liposomes, loaded with doxorubicin, to penetrate inside cells is evaluated by confocal microscopy experiments.

Results and Discussion

Peptide synthesis and conjugation of gH625 peptides to the surface of preformed liposomes: The coupling of a bioactive ligand on the surface of liposomes can be obtained according to several synthetic approaches. The choice of the strategy depends on whether it is necessary to perform the coupling before or after the liposome assembly. The coupling before the assembly of liposomes is, in principle, chemically less complicate, but has the disadvantage that a fraction of the ligand remains entrapped in the liposome inner region and is not available to play its biological function. This strategy is the preferred choice for amphiphilic peptides, but it remains unsuitable for poorly hydrophilic or mainly hydrophobic peptides. In these cases the coupling of the ligand can be performed after the assembly of the liposomes by using activated functional groups introduced onto the external side of unilamellar liposomes. Activated functional groups must be compatible with liposome preparation and they should remain available on the surface for an efficient chemical ligation of the ligand.

gH625 is a hydrophobic peptide (see Table 1 for the amino acid sequence of gH625 and of the gH625 derivatives

Table 1. Peptide sequences and their molecular weight.

Peptide	Sequence	M_w
gH625	NH_2-HGLASTLTRWAHYNALIRAF-$CONH_2$	2297.1
gH625-Pra	NH_2-HGLASTLTRWAHYNALIRAF-Pra-$CONH_2$	2391.3
A643K(TOAC)-gH625-Pra[a]	NH_2-HGLASTLTRWAHYNALIRK(TOAC)F-Pra-$CONH_2$	2644.6
A639K(TOAC)-gH625-Pra	NH_2-HGLASTLTRWAHYNK(TOAC)LIRAF-Pra-$CONH_2$	2644.6
A635K(TOAC)-gH625-Pra	NH_2-HGLASTLTRWK(TOAC)HYNALIRAF-Pra-$CONH_2$	2644.6
A628K(TOAC)-gH625-Pra	NH_2-HGLK(TOAC)STLTRWAHYNALIRAF-Pra-$CONH_2$	2644.6
NBD-gH625-Pra	NBD-HGLASTLTRWAHYNALIRAF-Pra-$CONH_2$	2537.9
NBD-Pra	NBD-Pra-$CONH_2$	258.9

[a] TOAC = 2,2,6,6-tetramethylpiperidine-1-oxyl-4-amino-4-carboxylic acid.

used in this study) with high tendency to locate in the hydrophobic portion of liposomes; thus, for the preparation of liposomes decorated by gH625 a post-aggregation pathway based on click chemistry methods was chosen (Scheme 1).

This procedure involves a copper(I)-catalyzed Huisgen 1,3-dipolar cycloaddition reaction of azides and alkynes yielding 1,4-disubstituted 1,2,3-triazole-linked conjugates.[7a,8c] The unreactive nature of both azides and alkynes towards any other functional group present in the biomolecules, as well as the thermal and hydrolytical stability of their cycloaddition product make this reaction particularly appealing for the functionalization of liposomes with peptides.

The click reaction was performed between 1,2-dioleoyl-*sn*-glycero-3-phosphocholine (DOPG)/$(C18)_2$L-N_3 liposomes (90:10 molar ratio), obtained according to classical proce-

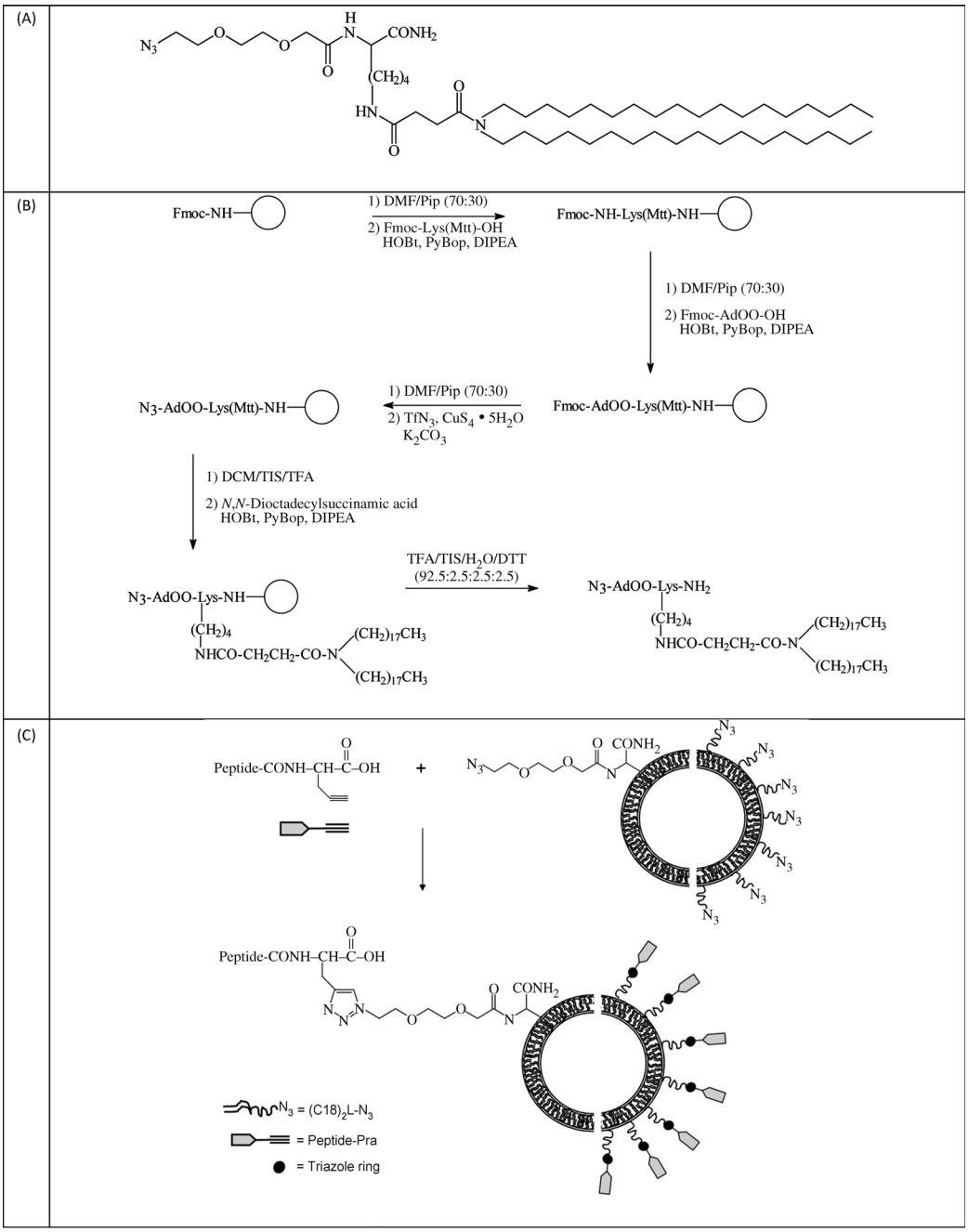

Scheme 1. A) Schematic representation of the synthetic monomer $(C18)_2$L-N_3. B) Scheme for the solid-phase synthesis of the (C18)2L-N_3 monomer. The Rink-amide resin is schematically represented as an empty circle. C) Coupling of the gH625-Pra peptide to azide-functionalized liposomes by a click-chemistry reaction. Fmoc = 9-fluorenylmethoxycarbonyl, Pip = piperidine, Mtt = 4-methyltrityl, Fmoc-AdOO-OH = Fmoc-8-amino-3,6-dioxaoctanoic acid, HOBt = 1-hydroxybenzotriazole, PyBOP = benzotriazole-1-yl-oxy trispyrrolidinophosphonium hexafluorophosphonate, DIPEA = *N*,*N*-diisopropylethylamine, Tf = trifluoromethanesulfonyl, TIS = triisopropylsilane, TFA = trifluoroacetic acid, DTT = dithiothreitol, Pra = propargylglycine.

dures for the preparation of mixed liposomes, and the peptide gH625 bearing a propargylglycine moiety (gH625-Pra). The click reaction, performed in an aqueous solvent system, was catalyzed by Cu^{I} generated, in situ, by reduction of $CuSO_4$ with ascorbic acid[7a] (Scheme 1C).

The click-chemistry reactants, that is, the gH625-Pra peptide and the liposome component $(C18)_2$L-N_3, were synthesized by solid-phase methods according to standard solid-phase peptide synthesis (SPPS) protocols with Fmoc/*t*Bu (*t*Bu = *tert*-butyl) chemistry. In the case of gH625-Pra (see Table 1), the alkyne moiety was introduced in the peptide sequence at the C-terminal position as L-propargylglycine. $(C18)_2$L-N_3 (Scheme 1A) was synthesized on solid phase following a modified protocol of the classical Fmoc/*t*Bu strategy, as indicated in Scheme 1B. Fmoc-Lys(Mtt)-OH was anchored to the Rink amide resin. After removal of the Fmoc protecting group, an ethoxylic linker was introduced, and its NH_2 function was converted into an azide function by diazo transfer by using a sulfonyl azide, as previously reported in the literature.[15] After removal of the Mtt group from the N_ε amino function of the lysine, the lipid chains were added. As expected, no reductive side reaction of the azide-functionalized derivative was observed during the cleavage step of the lysine derivative from the resin (data not shown).[16] Both gH625-Pra and $(C18)_2$L-N_3 were collected in good yields (20–40% and 85%, respectively) after HPLC-RP purification, and analyzed by mass spectrometry (MALDI-TOF), ^{1}H and ^{13}C NMR spectroscopy (for $(C18)_2$L-N_3), and HPLC to confirm the compound identity and the purity.

In order to determine the number of functional groups present on the external surface of the liposomes and the number of molecules of gH625 that were effectively linked to the liposome, the 7-nitrobenzofurazan (NBD)-labeled Pra and NBD-labeled gH625-Pra fluorescent derivatives were used. NBD fluorescence emission at $\lambda = 530$ nm was measured after the click reaction, on both the liposome and the NBD-Pra-containing fractions, and the percentage of functionalization was calculated as the ratio of bound NBD-Pra to its total amount. The results confirm that about 50% of the azido functions are located on the external leaflet of the liposome. When starting with an equimolar mixture of NBD-gH625-Pra and azido functions on the liposome surface, the expected gH625-functionalized liposomes were obtained with a yield higher than 90% after 12 h at room temperature.

In the absence of the copper catalyst no reaction was observed. gH625-Pra analogues, labeled with the TOAC radical group through a site-directed spin-labeling approach, were synthesized for EPR studies. Because the spin label is relatively hydrophobic,[17] it was introduced in the peptide sequence at the Ala positions. As the four Ala are almost equally spaced along the peptide sequence (in position 628, 635, 639, and 643, the numbering being that of the entire gH protein), we obtained four labeled peptides (A628K-(TOAC)-gH625-Pra, A635K(TOAC)-gH625-Pra, A639K-(TOAC)-gH625-Pra, and A643K(TOAC)-gH625-Pra) bearing the reporter moiety in positions regularly distributed from the N to the C terminus. For the synthesis of the four TOAC-labeled peptide derivatives, the four alanine residues were replaced one by one by Lys(Mtt). After removal of the Mtt moiety from the side chain of the lysine, the coupling of the TOAC residue was performed by using (7-azabenzotriazole-1-yl)tetramthyluronium hexafluorophosphate (HATU) as activating agent.[18] The TOAC-containing Pra peptides have been purified by HPLC by using standard TFA-containing eluents and gradients; treatment of the peptide in aqueous ammonia (pH 9.0) for 6 h at room temperature is required in order to restore the chemical integrity of the nitroxide moiety after HPLC elution.[18] Liposomes derivatized with TOAC-containing Pra peptides were obtained by using the click chemistry procedures, as above reported in the case of gH625-Pra peptide derivative.

Structural characterization of peptide–liposomes: Dynamic light scattering (DLS) measurements were performed at $\theta = 90°$ on liposomes composed of DOPG/$(C18)_2$l-N_3 at a molar ratio of 90:10 and on liposomes functionalized with gH625 as well as liposomes functionalized with TOAC peptide derivatives. Inspection of Figure 1 shows that all liposome solutions present a monomodal distribution due to a translational diffusion process, which could be attributed to liposome aggregates. The Stokes–Einstein equation [Eq. (1)] is used to evaluate the hydrodynamic radius (R_H), at infinite dilution.

$$R_H = \frac{K_B T}{6\pi\eta D_0} \quad (1)$$

D_0 is the translational diffusion coefficient at infinite dilution, K_B is the Boltzmann constant, T is the absolute temperature, and η is the solvent viscosity.[19] Due to the high solution dilution ($c = 1\times10^{-4}$ M) of the studied systems, we have approximately $D \approx D_0$, and Equation (1) can be reasonably used to estimate the hydrodynamic radius of the aggregates. Diffusion coefficients, together with hydrodynamic radius values obtained through Equation (2) (see the Experimental Section), are reported in Table 2. The hydrodynamic radius of DOPG/$(C18)_2$L-N_3 liposome (90:10 molar ratio) is (69.43 ± 23.36) nm. As expected, the introduction of a small amount of the synthetic monomer $(C18)_2$L-N_3 does not influence the size of the DOPG liposomes.[20] Figures 1B and C display the structural evolution of liposomes obtained after click reaction of gH625-Pra and four TOAC-labeled Pra-peptides. In all cases, liposomes decorated by peptides show an increase of about 30% in diameter (see Table 2). From a structural point of view, this increase in size is in good agreement with the other targeted liposomal systems reported in literature;[14] moreover, the TOAC moieties do not cause additional significant structural variations in the size of the aggregates.

Secondary structure of gH625: The secondary structures of gH625 and of all the analogues with Lys(TOAC) in substitution for alanine residues were determined by CD spectros-

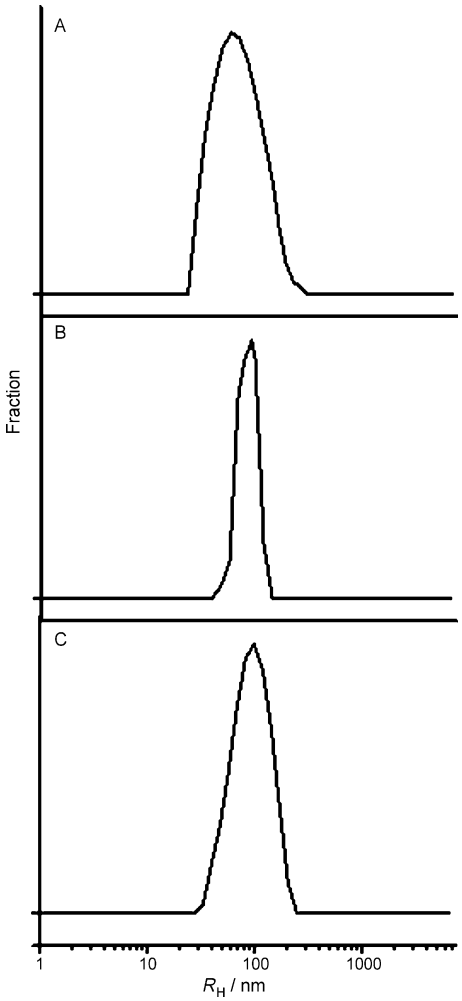

Figure 1. DLS spectra at 25 °C with a liposome concentration of 1×10^{-4} M. A) DOPG/(C18)2L-N3 (90:10 molar ratio) liposomes; B) DOPG/(C18)2L-gH625 liposomes obtained after click reaction; C) DOPG/(C18)2L-A635K(TOAC)-gH625 liposomes.

Table 2. Diffusion coefficients and hydrodynamic radii obtained from dynamic light scattering measurements for the studied systems.

System	D [$\times10^{-12}$ m^2 s^{-1}]	R_H [nm]
DOPG/$(C18)_2$L-N_3	(2.9±0.7)	(69.43±23.36)
DOPG/$(C18)_2$L-gH625	(2.2±0.3)	(90.38±13.50)
DOPG/$(C18)_2$L-A643K(TOAC)-gH625	(2.1±0.5)	(95.40±23.80)
DOPG/$(C18)_2$L-A639K(TOAC)-gH625	(2.1±0.5)	(92.32±25.22)
DOPG/$(C18)_2$L-A635K(TOAC)-gH625	(2.0±0.5)	(97.60±25.01)
DOPG/$(C18)_2$L-A628K(TOAC)-gH625	(2.2±0.5)	(91.32±24.45)

copy (Figure 2). As previously reported,[4a,b,c] gH625 assumes a random conformation in aqueous buffer solution, whereas it assumes an α-helical structure in membrane mimetic environments. gH625 and the Lys(TOAC) derivatives in water solution containing 20% TFE, show a helical structure with a slightly increase in ellipticity for the peptides where the modification are localized in the center of the peptide, as clearly evident from the spectra of the gH625 native peptide

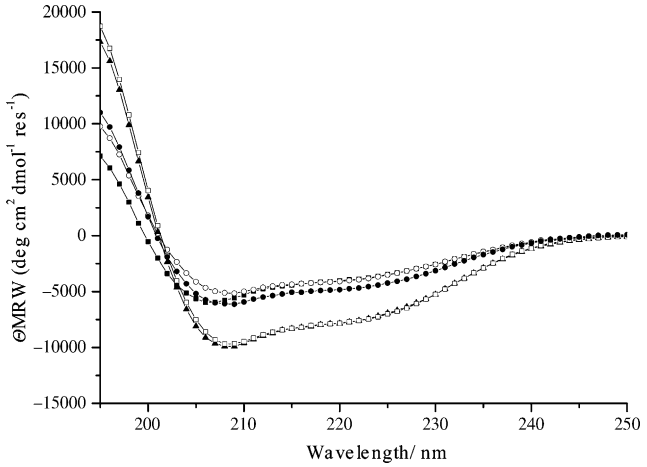

Figure 2. Circular dichroism spectra of gH625 (■) and its analogues with Lys(TOAC) in substitution for alanine residues (○ = A643K(TOAC)-gH625, ▲ = A639K(TOAC)-gH625, □ = A635K(TOAC)-gH625, ● = A628K(TOAC)-gH625), obtained in 2-(4-(2-hydroxyethyl)-1-piperazinyl)-
ethanesulfonic acid (HEPES) buffer containing 20% trifluoroethanol (TFE).

and of the Lys(TOAC) peptide derivatives. These data clearly show that the introduction of the TOAC moiety does not modify the gH625 peptide conformation, and Lys(TOAC) gH625 derivatives could be used in EPR studies to define peptide positioning.

Determination of the position of gH625 by EPR spectroscopy: The peptide positioning relative to the liposome surface was investigated by EPR spectroscopy. To this aim gH625-Pra analogues, labeled with the TOAC radical group through a site-directed spin-labeling approach, were used. The EPR spectra of the free, labeled peptides dissolved in HEPES buffer (10 mM) consist of three narrow lines (see Figure 3A for an example), typical of an unstructured peptide with few constraints on the motion of the reporter group and consistent with the observed random coil CD spectrum. Subsequently, the labeled peptides were chemically linked to the DOPG/$(C18)_2$L-N_3 liposomes by following the same procedure used for the parent unlabelled peptide, yielding four suspensions of functionalized liposomes. The analysis of their EPR spectra (see Figure 3A) gives information on the positioning of the gH625 relative to the surface of the liposome to which it is linked. In all cases a clearly defined axially anisotropic line shape is observed, indicating that the reporter group, wherever positioned along the peptide sequence, assumes a well-defined orientation relative to the bilayer. This behavior indicates that the peptide does not protrude in the aqueous medium surrounding the liposome, in which the label would have assumed a much higher mobility freedom, but rather interacts with the surface of the lipid bilayer.

Analysis of Figure 3 shows that the spectrum anisotropy increases in going from A628K(TOAK)-gH625 to A643K-(TOAC)-gH625, indicating that the peptide segments closer to the C terminus, which is chemically linked to the lipid,

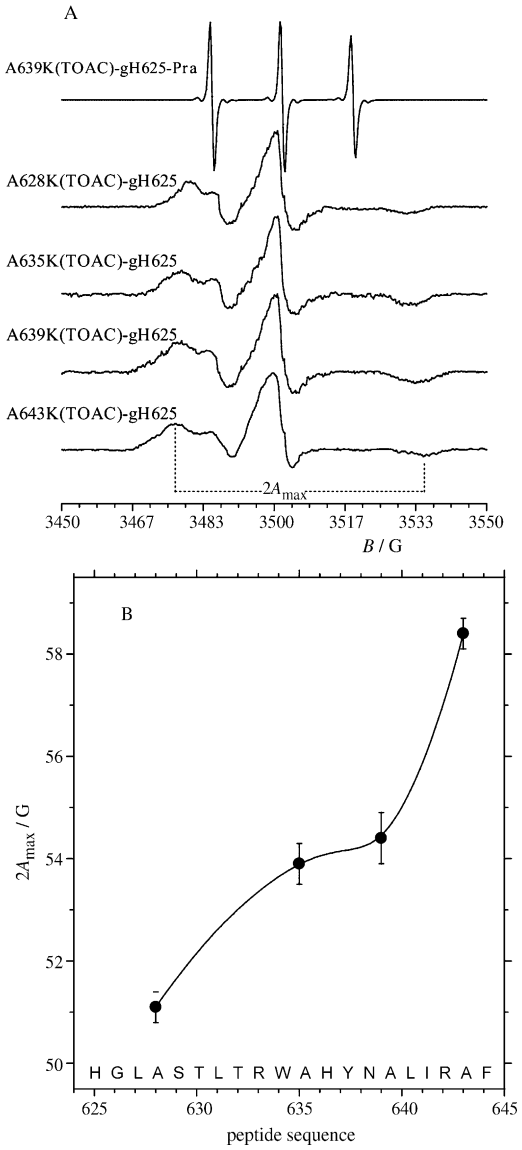

Figure 3. A) EPR spectra of TOAC-labeled peptides linked to DOPG/$(C18)_2$L-N_3 liposomes. An EPR spectrum of the free peptide A639K-(TOAC)-gH625-Pra in aqueous buffer is also shown. B) Dependence of the outer hyperfine splitting, $2A_{max}$ on the spin-label position along the peptide sequence the of TOAC-labeled peptides linked to DOPG/$(C18)_2$L-N_3 liposomes.

are more strictly oriented relative to the bilayer. This evidence can be easily quantified by measuring the outer hyperfine splitting, $2A_{max}$, which is a reliable and easy to perform estimate of the segmental chain mobility. $2A_{max}$ is defined as separation, expressed in Gauss, between the low-field maximum and the high-field minimum of the spectrum, and tends to increase with increasing the restriction in the label mobility. Figure 3B shows that, as the label position is moved from position 628 to 643, $2A_{max}$ increases. This evidence suggests that the peptide does not insert in the bilayer hydrophobic core, but rather remains adsorbed on its surface, remaining exposed to the aqueous environment. This result confirms the possibility of using our synthetic strategy to bind an hydrophobic peptide on the liposome external surface; the use of a short linker may also provide steric restrictions for the peptide insertion inside the liposome.

Doxorubicin loading: Cytotoxic doxorubicin (Dox) was loaded into DOPG/$(C18)_2$L-N_3 liposomes by using the well-assessed procedures based on an ammonium sulfate gradient;[21] in particular, solution containing doxorubicin was incubated under stirring for 30 min at 60 °C. Subsequently, unloaded doxorubicin was removed on a Sephadex G50 column pre-equilibrated with HEPES buffer (10 mM) at pH 7.4. The drug/lipid weight ratio chosen for the loading experiments was 0.1. The doxorubicin loading content (DLC) was calculated by UV/Vis measurements at $\lambda =$ 480 nm and was above 95 % of the total. The resulting Dox-loaded liposomes were then efficiently modified with the gH625-Pra peptide according to the click-chemistry procedure used in the case of empty liposomes.

Determination of the cellular uptake by confocal microscopy: To study the cellular internalization of doxorubicin-loaded liposomes functionalized with gH625, we examined their uptake and intracellular localization in living HeLa cells by confocal microscopy. Cells were incubated with a 1 μM solution of free Dox or of Dox-loaded, gH625-functionalized liposomes for 1, 5, 17 h at 37 °C. The results obtained after 5 h of incubation are reported in Figure 4. As expected, after 5 h free Dox is able to enter the cell and translocate into the nucleus as indicated by the green fluorescence in the center of the cell body (Figure 4A–C). Also in the case of DOPG/$(C18)_2$L-N_3/Dox liposomes, cell nuclei appear fluorescent due to Dox accumulation in DNA and a slight diffuse fluorescence in the cytoplasm is observed, suggesting a Dox release from the liposomes (Figure 4D–F). Conversely, gH625-functionalized liposomes encapsulating Dox accumulate in the cytoplasm, without entering into the nucleus (Figure 4G–I). Indeed, cell nuclei are dark and only green fluorescent spots, distributed in the cytoplasm, are visible. These results suggest that the functionalization of liposomes with gH625 could affect the uptake mechanism of liposomes and, thus, their intracellular distribution and Dox release. This evidence could be useful in the design of carriers for a controlled delivery and release of Dox in order to avoid side effects associated to Dox itself.

Conclusion

Liposomes composed of a phospholipid bilayer, which entirely surrounds an internal aqueous core, used for drug encapsulation have been shown to be optimal for the delivery of chemotherapeutic agents to tumor cells.[22] Being larger than micelles they have the ability to deliver greater amounts of the chemotherapeutic agent to the tumor site, while minimizing the risk associated with premature leakage. In addition, liposomes also have the ability to accom-

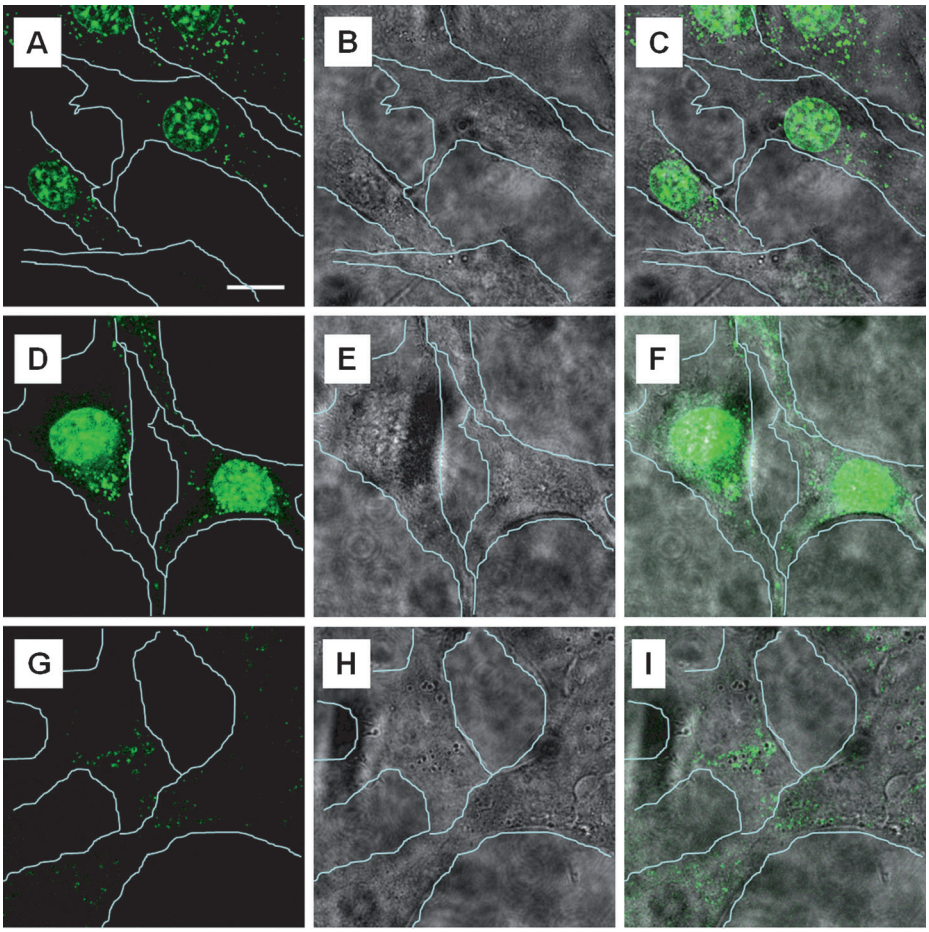

Figure 4. Confocal microscopy images of HeLa cells after 5 h incubation with a 1 μM solution of free Dox (A–C), a 1 μM solution of DOPG/$(C18)_2$L-N_3/Dox (D–F), or a 1 μM solution of DOPG/$(C18)_2$L-gH625/Dox (G–I). A,D,G) Fluorescence images of Dox accumulation within the cells. B,E,H) Transmission images of HeLa cells. C,F,I) Merge of fluorescence and transmitted light images. The white line indicates the cell boundaries; scale bar = 20 μm.

modate both hydrophilic as well as hydrophobic drugs either in the internal aqueous core or in the lipid bilayer. When compared with conventional drugs, liposomal treatment has been shown to dramatically reduce some of the traditional side effects associated with chemotherapy, such as nausea and vomiting.[23]

Current research is aimed at actively targeting liposomes to tumor cells. In this view the development of chemical procedures for the attachment of bioactive ligands to the liposome external surface is particularly important.

Here, we have demonstrated the utility of the click chemistry for modification of the external surface of DOPG-based liposomes with the hydrophobic peptide gH625, previously identified as a membrane-perturbing domain in the gH protein of *Herpes simplex* virus type I. According to this synthetic procedure, azide-modified, DOPG-based liposomes react, under mild conditions, with Pra-modified gH625, giving stable and well-defined peptide-modified liposomes. The click-chemistry procedure described here, appears of a general utility for liposome functionalization; in fact azide-modified liposomes could constitute a stable and ready-to-use suspension of reactive liposomes that could be functionalized with different Pra-modified peptides. In our case, an increase of the liposome diameter of approximately 30% after peptide introduction is observed by DLS measurement. Moreover, the peptide positioning relative to the liposome surface has been investigated by EPR spectroscopy; the data obtained indicated that the peptide does not insert in the bilayer hydrophobic core, but rather remains exposed to the aqueous environment adsorbed on the liposomal surface and, thus, able to achieve its biological function.

To be effective as a chemotherapeutic agent, it has to be active against cancer cells, while having minimal toxic effects on healthy cells, tissues, and organs. Thus, once carriers loaded with chemotherapeutic agents are systemically introduced, their uptake by the reticuloendothelial system (RES) must be minimized, allowing prolonged circulation of the carriers in the blood.[24] The longer the drug circulates in the blood, the more likely it encounters the tumor as a result of the enhanced permeability of leaky tumor blood vessels. The enhanced permeability and retention effect is considered the primary mechanism of preferential accumulation of long-circulating nanoparticles in solid tumors. Polymeric drug carrier systems that use various approaches to address these challenges have been intensively developed,[25] and adding a targeting moiety, such as a peptide or an antibody was shown to help the cellular uptake and to reduce systemic clearance of anticancer drug. Here, we verified the drug carrier ability of gH625-functionalized, DOPG-based liposomes encapsulating Dox, which is an intrinsically fluorescent anticancer drug. The exact mechanism of doxorubicin antitumor activity still remains unclear; it is known that it intercalates into DNA, which results in the blocking of topoisomerase II activity, preventing DNA replication and cell division. In general, the use of liposome-encapsulated Dox reduces toxicity. The presence of the carrier hinders the intercalation of Dox into DNA; in fact, confocal microscopy reveals differences between the uptake mechanism of free and encapsulated Dox.[8] The nuclear accumulation of free Dox can be attributed to diffu-

sion. In contrast, encapsulated Dox remains mostly in the cytoplasm with negligible nuclear accumulation.[8]

Our experiments provide proof of principle for efficient gH625-mediated delivery of DOPG-based liposomes into cells. gH625 attached to the liposome surface needs to be non-shielded and accessible for cell membrane experiments and we showed that coupling the peptide on the pre-assembles liposomes allows the obtainment of liposomes decorated on their surface with the peptide. Although the mechanism still remains to be established, our results seem to support the hypothesis that the peptide allows a better penetration of liposomes. The approach described may have important application for drug and DNA delivery into the cell cytoplasm in different protocols for drug administration or ex vivo treatments.

Experimental Section

Materials: Fmoc-protected amino acid derivatives, coupling reagents, and Rink amide *p*-methylbenzhydrylamine (MBHA) resin were purchased from Calbiochem-Novabiochem (Laufelfingen, Switzerland). Fmoc-8-amino-3,6-dioxaoctanoic acid (Fmoc-AdOO-OH) and Fmoc-L-propargylglycine (Fmoc-Pra-OH) were purchased from Neosystem (Strasbourg, France). 4-Chloro-7-nitrobenzofurazan (NBD-Cl), doxorubicin hydrochloride, and the other chemicals were purchased from Sigma–Aldrich, Fluka (Buchs, Switzerland), or LabScan (Stillorgan, Ireland) and were used as received, unless otherwise stated. 1,2-Dioleoyl-*sn*-glycero-3-phosphocholine (DOPG) was purchased from Avanti Polar Lipids (Alabaster, AL). Fmoc-TOAC-OH ((2,2,6,6-tetramethylpiperidine-*N*-oxide-4-(9-fluorenylmethyloxycarbonyl-amino)-4-carboxylic acid) spin label was kindly provided by Prof. C. Toniolo of the University of Padua (Italy).

Solid-phase peptide synthesis: Peptides (for amino acid sequences and peptide modifications see Table 1) were synthesized by using standard solid-phase 9-fluorenylmethoxycarbonyl (Fmoc) procedures by using a Syro I MultiSynThec GmbH (Wullener, Germany) automatic synthesizer. The Rink amide MBHA resin (substitution 0.51 mmol g^{-1}) was used as the solid-phase support, and syntheses were performed on a scale of 20 μmol. Fmoc-protected amino acids (4 equiv relative to resin loading), were coupled according to the PyBop/HOBt/DIPEA method: Fmoc-amino acid (1 equiv), PyBOP (1 equiv), HOBt (0.5 M in DMF, 1 equiv), and DIPEA (1.0 M in DMF, 2 equiv). The Fmoc protecting group was removed with 30% piperidine in DMF (v/v). All couplings were performed twice for 1 h. Fmoc-Pra-OH was coupled once for 45 min with 2 equivalents of PyBop/HOBt and 2 equivalents of DIPEA. Peptides were fully deprotected and cleaved from the resin with TFA with 2.5% (v/v) water, 2.0% (v/v) anisole, and 2.0% (v/v) thioanisole as scavengers, at room temperature, and then precipitated with ice-cold ethyl ether, filtered, dissolved in water, and lyophilized. The crude peptides were purified by RP-HPLC on a LC8 Shimadzu HPLC system (Shimadzu Corporation, Kyoto, Japan) equipped with a UV lambda-Max Model 481 detector using a Phenomenex (Torrance, CA) C18 (300 Å, 250×21.20 mm, 5 μ) column eluted with H_2O/0.1% TFA (A) and CH_3CN/0.1% TFA (B) from 20–80% over 20 min at a flow rate of 20 mL min^{-1}. Purity and identity were assessed by analytical LC-MS analyses by using Finnigan Surveyor MSQ single quadrupole electrospray ionization (Finnigan/Thermo Electron Corporation San Jose, CA), column: C18-Phenomenex eluted with H_2O/0.1% TFA (A) and CH_3CN/0.1% TFA (B) from 20–80% over 10 min at a flow rate of 0.8 mL min^{-1}. The final yields of purified peptides ranged between 20 and 40%.

Peptides labeled with TOAC (A628K(TOAC)-gH625-Pra, A635K-(TOAC)-gH625-Pra, A639K(TOAC)-gH625-Pra, and A643K(TOAC)-gH625-Pra) were synthesized by introducing the spin label directly on the solid phase. For the incorporation of the TOAC moiety, peptides containing Lys(Mtt) in substitution for the Ala residues were first synthesized: A628K(Mtt)-gH625-Pra, A635K(Mtt)-gH625-Pra, A639K(Mtt)-gH625-Pra, and A643K(Mtt)-gH625-Pra. The Mtt protecting group from the side chain of the lysine residue was cleaved by treatment with 1% TFA, 5% TIS, 94% CH_2Cl_2 (10 times for 1 min). The TOAC residue was doubly coupled for 3 h by using 2-fold molar excess of Fmoc-TOAC-OH (40 μmol) and HATU (40 μmol) as activating agent in presence of DIPEA (1:1:2). The Fmoc protecting group was removed with 30% piperidine in DMF (v/v). After TFA cleavage and HPLC purification, TOAC-containing peptides were submitted to alkaline treatment with aqueous ammonia (pH 9.5) for 6 h at room temperature to regenerate the chemical integrity of the nitroxide moiety.[18,26] The identities of the TOAC peptides were confirmed by LC-MS.

When necessary, NBD-labeling was performed on resin-bound peptides as previously reported by Rapaport and Shai.[27] Briefly, after removal of the Fmoc protecting group of the N-terminal amino-acid, the resin-bound peptide was treated with NBD-Cl in DIPEA (2 M in DMF, 3–4 equiv). After 24 h, the resin-bound peptides were washed thoroughly with CH_2Cl_2 and the peptides were cleaved and purified as previously described. The identity of the NBD peptides was confirmed by LC-MS.

Preparation of trifluoromethanesulfonyl azide (TfN_3): Sodium azide (650 mg, 10 mmol) was dissolved in distilled water (1.5 mL) and then dichloromethane (2.4 mL) was added. The mixture was cooled in an ice bath for 20 min. Trifluoromethanesulfonyl anhydride (336 μL, 2 mmol) was added slowly over 5 min and the mixture was stirred for 2 h. The mixture was extracted with CH_2Cl_2 two times. The organic portions, containing the trifluoromethanesulfonyl azide, were pooled, washed once with saturated aqueous Na_2CO_3 solution, and evaporated to dryness.

Synthesis of azide-AdOO-Lys(C(O)CH_2CH_2C(O)N-($C_{18}H_{37}$)$_2$)-amide ((C_{18})$_2$L-N_3): (C_{18})$_2$L-N_3 monomer was synthesized on the solid phase under standard conditions by using the Fmoc/*t*Bu strategy. Rink-amide MBHA resin (0.51 mmol g^{-1}, 0.1 mmol, 0.196 g) was used as polymeric support. The Fmoc protecting group on the resin was removed by a DMF/piperidine (70:30) mixture. Fmoc-Lys(Mtt)-OH (0.125 g, 0.2 mmol) was activated with PyBop (1 equiv) and HOBt (1 equiv) and DIPEA (2 equiv) in DMF and coupled on the resin, while stirring the suspension for 1 h. The N_α amine function of the lysine residue was deprotected, and Fmoc-AdOO-OH (2 equiv) was coupled under standard condition in DMF for 1 h. After Fmoc removal the peptidyl-resin was washed three times with DMF and three times with MeOH, and treated with a solution containing K_2CO_3 (0.04 mmol), $CuSO_4{\cdot}5H_2O$ (0.01 mol), and TfN_3 (2 mmol) in water (1 mL). The reaction mixture was stirred at room temperature overnight. The solution was filtered and the resin was washed four times with CH_2Cl_2; the Mtt protecting group on the N_ε amino function of lysine was removed by treatment with CH_2Cl_2/TIS/TFA (94:5:1, 5.0 mL) for 2 min. This procedure was repeated several times until the solution became colorless. The resin was washed three times with CH_2Cl_2 and three times with DMF. Then, *N*,*N*-dioctadecylsuccinamic acid (0.249 g, 0.4 mmol) was coupled twice for 1 h in NMP (*N*-methylpyrrolidone)/DCM (1:1). *N*,*N*-Dioctadecylsuccinamic acid was synthesized according to a published procedure.[28] The lipophilic moiety was activated in situ by the standard HOBt/PyBop/DIPEA procedure. The coupling was monitored by the qualitative Kaiser test. The resin was washed three times with DMF, three times with CH_2Cl_2, and three times with ethyl ether. (C_{18})$_2$L-N_3 was removed from the resin by treatment with TFA containing TIS (2.5%), dithiothreitol (DTT, 2.5%), and water (2.5%) under vortexing for 2 h. The crude product was slowly precipitated at 0 °C by adding water dropwise. The precipitate was washed several time with small portions of water and lyophilized in order to remove the solvent. The white solid was recrystallized from MeOH/H_2O and recovered with high yields (>85%). The product was identified by MS (ESI+) and NMR spectroscopy. ^1H NMR and ^{13}C NMR spectra were recorded on a Varian 400 MHz spectrometer (Palo Alto, CA). **(C18)$_2$L-N_3**: ^1H NMR (400 MHz, $CDCl_3$/CD_3OD 50:50): $\delta = 4.3$ (m, 1H; C*H*Lysα), 4.04 (m, 2H; OCH_2CONH), 3.70 (s, 4H; OCH_2CH_2O), 3.42 (t, $J = 7.61$ Hz, 2H; $N_3CH_2CH_2$O), 3.25–3.20 (m, 4H; N-CH_2), 3.23 (t, $J = 8.01$ Hz, 2H; CH_2Lysε), 3.20 (t, $J = 8.01$ Hz, 2H; $N_3CH_2CH_2$O), 2.64–2.49 (m, 4H; NHCOCH_2CH_2CO), 1.74 (m, 2H; CH_2Lysβ), 1.55 (m, 2H; CH_2Lysδ),

1.45 (m, 2H; CH_2Lysγ), 1.40 (m, 4H; RCH_2CH$_3$), 1.25 (m, 60H; CH_2 aliphatic), 0.88 ppm (t, $J=6.86$ Hz, 6H; CH_3); ^{13}C NMR (100.512 MHz, $CDCl_3/CD_3OD$ 50:50): $\delta=173.98$ (*C*ONH$_2$), 173.27 (*C*ONH), 171.94 (CH$_3$(*C*H$_2$)$_{17}$N*C*O), 170.55 (*C*ONH), 72.3 (CO*C*H$_2$O), 70.0 (*C*H$_2$N$_3$), 69.4(O*C*H$_2$*C*H$_2$O), 52.4 (NH(CH$_2$)$_4$*C*H), 51.05 (NH*C*H$_2$(CH$_2$)$_3$*C*H), 48.6 (CH$_3$(CH$_2$)$_{16}$*C*H$_2$N), 46.8 (CH$_3$(CH$_2$)$_{15}$*C*H$_2$CH$_2$N), 39.3 (NH-(CH$_2$)$_3$*C*H$_2$CH), 32.4–32.0 (NHCH$_2$(*C*H$_2$)$_2$CH$_2$CH), 29.2 (NCO*C*H$_2$*C*H$_2$CONH), 30.2–27.5 (CH$_3$CH$_2$(*C*H$_2$)$_{14}$CH$_2$CH$_2$N), 23.17 (CH$_3$*C*H$_2$(CH$_2$)$_{16}$), 14.60 ppm (*C*H$_3$CH$_2$(CH$_2$)$_{16}$): MS (ESI+): *m/z* (%) calcd for $H_{101}C_{52}N_7O_6$ [$M-H^+$]:916.64; found: 915 (100).

Preparation of liposomes: Mixed aggregates of DOPG and (C18)$_2$L-N$_3$ (90:10 molar ratio) were prepared by dissolving the two amphiphiles in a small amount of chloroform, and subsequently evaporating the solvent by slowly rotating the tube containing the solution under a stream of nitrogen. In this way a thin film of amphiphiles was obtained. A dry lipid film was suspended in HEPES buffer (10 mM) at pH 7.4 by vortexing; then the lipid suspension was freeze–thawed ten times and extruded twenty times thought a polycarbonate membrane with 100 nm pore size by using a mini-extruder purchased from Avanti Polar Lipids (Usa, Canada).

Procedure for the "click" reaction: The Click reaction was carried out on DOPG/(C18)$_2$L-N$_3$ liposomes at 1×10^{-3} M concentration in HEPES buffer (10 mM) at pH 7.4. The reaction was carried out by adding $CuSO_4\cdot5H_2O$ (4.4 equiv), ascorbic acid (6.7 equiv), and the peptide derivative (1 equiv) with respect to the azido moiety. In particular, solutions containing $CuSO_4\cdot5H_2O$ (40 mM, solution A), ascorbic acid (57 mM, solution B), and the alkyn-modified peptide (0.8 mM, solution C) were freshly prepared in water. Solution A (43.6 μL), solution B (48 μL), and solution C (408.4 μL) were added to a suspension of azido-functionalized liposomes in HEPES buffer (500 μL). The concentration of solution C was determined by measuring the absorbance on a UV/Vis Jasco V-5505 spectrophotometer. The reaction mixture was stirred at 40°C for 30 min and successively left overnight at room temperature. After the conjugation step the liposomes were purified by exclusion chromatography on a 1× 18 cm Sephadex G-50 (Amersham Biosciences) column pre-equilibrated with HEPES buffer.

Functionalization of liposomes: The number of functional groups present on the external surface of the liposomes and the number of molecules of gH625 that were effectively linked to the liposome were determined by using NBD-labeled Pra and NBD-labeled gH625-Pra. The amount of NBD-Pra or NBD-gH625-Pra grafted to the liposome surface were estimated by fluorescence spectroscopy by using calibration curves obtained by measuring the fluorescence emission at $\lambda=530$ nm. Fluorescence spectra were recorded at room temperature on a Jasco Model FP-750 spectrofluorophotometer in a 1.0 cm path length quartz cell. Equal excitation and emission bandwidths were used throughout the experiments, with a recording speed of 125 nm min^{-1} and automatic selection of the time constant. The percentage of functionalization was calculated as the ratio of bound NBD-Pra or NBD-gH625-Pra to their total amount.

DLS characterization: For DLS measurements self-assembled liposomes in isotonic HEPES buffer were prepared with a final concentration of 1×10^{-4} M. Samples were centrifuged at room temperature at 13000 rpm for 5 min. Dynamic light scattering measurements were performed with a setup composed of a Photocor compact goniometer, a SMD 6000 Laser Quantum 50 mW light source operating at 5325 Å, and a PMT and correlator obtained from Correlator.com. All the measurements were performed at (25.00±0.05)°C with the use of a thermostat bath. In the DLS experiments, the intensity autocorrelation function $g(2)(t)$ is measured and related to the electric field autocorrelation $g(1)(t)$ by the Siegert relation;[29] $g(1)(t)$ can in turn be related through a Laplace transform to the distribution function of the relaxation rates G from which the z average of the diffusion coefficient D may be obtained [Eq. (2)]:[30]

$$D=\lim_{q\to0}\frac{\Gamma}{q^2} \qquad (2)$$

in which $q=4\pi n_0/\lambda\sin(\theta/2)$ is the modulus of the scattering vector, n_0 is the refractive index of the solution, λ is the incident wavelength, and θ represents the scattering angle. D is thus obtained from the limit slope of Γ as a function of q^2, in which Γ is measured at different scattering angles.

Circular dichroism measurements: Far-UV CD spectra were recorded from $\lambda=260$–195 nm on a Jasco J-810 spectropolarimeter equipped with a NesLab RTE111 thermal controller unit by using a 0.1 mm quartz cell at 25°C. CD spectra of gH625-Pra and of its analogues in which each Ala residue was replaced by a Lys(TOAC) residue were recorded at a concentration of 8×10^{-4} M in HEPES buffer in presence and in absence of 20% TFE. Other experimental settings were: scan speed: 10 nm min^{-1}, sensitivity: 50 mdeg, time constant: 16 s, bandwidth: 1 nm. Each spectrum was obtained through averaging three scans, subtracting the contributions from other species in solution, and converting the signal to mean residue ellipticity.

EPR measurements: EPR spectra of spin-labeled peptides chemically linked to the liposome surface were recorded on a Elexys E-500 EPR spectrometer from Bruker (Rheinstetten, Germany) operating in the X band. As references, spectra of the "free" spin-labeled peptides in aqueous buffer and in the presence of liposomes were also registered. Flame-sealed capillaries containing the samples were placed in a standard 4 mm quartz sample tube. The temperature of the sample was regulated and maintained constant during the measurement by blowing thermo-stated nitrogen gas through a quartz Dewar. The samples were investigated at 25°C. The instrumental settings were as follows: sweep width: 120 G, resolution: 1024 points, modulation frequency: 100 kHz, modulation amplitude: 1.0 G, time constant: 20.5 ms, sweep time: 42 s, incident power: 5.0 mW. For samples subjected to the click-chemistry reaction up to 128 scans were accumulated to improve the signal-to-noise ratio.[31] For all the other samples, eight scans were accumulated.

Doxorubicin loading: Doxorubicin was remote-loaded in DOPG/(C18)$_2$L-N$_3$ liposomes through an ammonium sulfate gradient method and the free Dox was removed by gel filtration. Briefly, a liposomal solution (1 mM) was prepared as reported above in an ammonium sulfate solution (250 mM) at pH 5.5. Next, liposomes were passed on a Sephadex G-50 column pre-equilibrated with HEPES buffer (10 mM) at pH 7.4, and a Dox solution in water (27 μL, 2.54×10^{-3} M) was added to an aliquot of the liposomal solution (500 μL). This suspension was stirred for 30 min at 60°C and subsequently unloaded doxorubicin was removed by using a Sephadex G50 column. The Dox concentration was determined by spectroscopic measurements (UV and fluorescence) by using calibration curves obtained by measuring the absorbance at $\lambda=480$ nm or the fluorescence emission at $\lambda=590$ nm. Emission spectra were recorded at room temperature. The Dox loading content (DLC, defined as the weight ratio of encapsulated Dox vs. the amphiphilic moieties) was quantified by subtraction of the amount of Dox removed from the total amount of Dox loaded. Finally, Dox pre-loaded liposomes were modified with gH625 by using the click-chemistry reaction procedure, as reported above for empty liposomes.

Cellular uptake by confocal microscopy: Uptake kinetic experiments were performed on non-fixed living cells. HeLa cells were incubated with liposomes functionalized with gH625 and pre-loaded with Dox with a concentration of Dox of 1 μM at 37°C for 1, 5, and 17 h. After incubation, the cells were rinsed twice with phosphate-buffered saline (PBS) and fresh cell culture medium without phenol red was added. All the samples were observed by a confocal laser scanning microscope (CLSM)(LSM510, Zeiss) equipped with an argon laser line at $\lambda=488$ nm, with a 63× objective.

Acknowledgements

This work was supported by MIUR (FIRB Prot. RBRN07BMCT). The authors thank Prof. Claudio Toniolo for providing the TOAC moiety, Leopoldo Zona for help with the NMR measurements, and Prof. Luigi Paduano for discussion on DLS data.

[1] L. M. Bareford, P. W. Swaan, *Adv. Drug Delivery Rev.* **2007**, *59*, 748.
[2] F. Heitz, M. C. Morris, G. Divita, *Br. J. Pharmacol.* **2009**, *157*, 195.
[3] S. Galdiero, M. Vitiello, A. Falanga, M. Cantisani, N. Incoronato, M. Galdiero, *Curr. Drug Metab.* **2011**, DOI: BSP/CDM/E-PUB/00197.
[4] a) S. Galdiero, A. Falanga, M. Vitiello, H. Browne, C. Pedone, M. Galdiero, *J. Biol. Chem.* **2005**, *280*, 28632; b) S. Galdiero, A. Falanga, M. Vitiello, L. Raiola, R. Fattorusso, H. Browne, C. Pedone, C. Isernia, M. Galdiero, *J. Biol. Chem.* **2008**, *283*, 29993; c) S. Galdiero, A. Falanga, M. Vitiello, L. Raiola, L. Russo, C. Pedone, C. Isernia, M. Galdiero, *J. Biol. Chem.* **2010**, *285*, 17123; d) S. Galdiero, A. Falanga, G. Vitiello, M. Vitiello, C. Pedone, G. D'Errico, M. Galdiero, *Biochim. Biophys. Acta Biomembr.* **2010**, *1798*, 579.
[5] A. Falanga, M. Vitiello, M. Cantisani, R. Tarallo, D. Guarnieri, E. Mignogna, P. Netti, C. Pedone, M. Galdiero, S. Galdiero, *Nanomedicine* **2011**, DOI: 10.1016/j.nano.2011.04.009.
[6] a) G. Gregoriadis, B. E. Ryman, *Biochem. J.* **1972**, *129*, 123; b) E. Cukierman, D. R. Khan, *Biochem. Pharmacol.* **2010**, *80*, 762.
[7] a) A. Sharma, U. S. Sharma, *Int. J. Pharm.* **1997**, *154*, 123; b) M. I. Papisov, *Adv. Drug Delivery Rev.* **1998**, *32*, 119; c) C. R. Miller, B. Bondurant, S. D. McLean, K. A. McGovern, D. F. OBrien, *Biochemistry* **1998**, *37*, 12875; d) H. Maeda, J. Wu, T. Sawa, Y. Matsumura, K. Hori, *J. Controlled Release* **2000**, *65*, 271.
[8] a) M. B. Bally, R. Nayar, D. Masin, M. J. Hope, P. R. Cullis, L. D. Mayer, *Biochim. Biophys. Acta Biomembr.* **1990**, *1023*, 133; b) T. M. Allen, E. H. Moase, *Adv. Drug Delivery Rev.* **1996**, *21*, 117; c) T. M. Allen, *Drugs* **1997**, *54*, 8; d) A. J. Coukell, C. M. Spencer, *Drugs* **1997**, *53*, 520.
[9] S. Albrizio, L. Giusti, G. D'Errico, C. Esposito, F. Porchia, G. Caliendo, E. Novellino, M. R. Mazzoni, P. Rovero, A. M. D'Ursi, *J. Med. Chem.* **2007**, *50*, 1458.
[10] E. Vives, P. Brodin, B. Lebleu, *J. Biol. Chem.* **1997**, *272*, 16010.
[11] Y. L. Tseng, J. J. Liu, R. L. Hong, *Mol. Pharmacol.* **2002**, *62*, 864.
[12] D. C. Drummond, O. Meyer, K. Hong, D. B. Kirpotin, D. Papahadjopoulos, *Pharmacol. Rev.* **1999**, *51*, 691.
[13] a) H. C. Kolb, M. G. Finn, K. B. Sharpless, *Angew. Chem.* **2001**, *113*, 2056; *Angew. Chem. Int. Ed.* **2001**, *40*, 2004; b) H. C. Kolb, K. B. Sharpless, *Drug Discovery Today* **2003**, *8*, 1128.
[14] a) F. Said Hassane, B. Frish, F. Schuber, *Bioconjugate Chem.* **2006**, *17*, 849; b) S. Cavalli, A. R. Tipton, M. Overhand, A. Kros, *Chem. Commun.* **2006**, 3193.
[15] Y. Liu, L. Zhang, J. Wan, Y. Li, Y. Xu, Y. Pan, *Tetrahedron* **2008**, *64*, 10728.
[16] P. E. Schneggenburger, B. Worbs, U. Diederichsen, *J. Pept. Sci.* **2010**, *16*, 10.
[17] Y. G. Yu, T. Thorgeirsson, Y. K. Shin, *Biochemistry* **1994**, *33*, 14221.
[18] P. Hanson, G. Millhauser, F. Formaggio, M. Crisma, C. Toniolo, *J. Am. Chem. Soc.* **1996**, *118*, 7618.
[19] A. Vergara, L. Paduano, R. Sartorio, *J. Phys. Chem. B* **2001**, *105*, 328.
[20] A. Ertel, A. G. Marangoni, J. Marsh, F. R. Hallett, J. M. Woodt, *Biophys. J.* **1993**, *64*, 426.
[21] a) P. G. Tardi, N. L. Boman, P. R. Cullis, *J. Drug Targeting* **1996**, *4*, 129; b) A. Fritze, F. Hens, A. Kimpfler, R. Schubert, R. Peschka-Süss, *Biochim. Biophys. Acta Biomembr.* **2006**, *1758*, 1633.
[22] D. R. Siwak, A. M. Tari, G. Lopez-Berestein, *Clin. Cancer Res.* **2002**, *8*, 1172.
[23] a) D. D. Lasic, *Trends Biotechnol.* **1998**, *16*, 307; b) *Liposomes: A Practical Approach*, 2nd ed. (Eds.: V. P. Torchilin, V. Weissing), Oxford University, Oxford, **2003**.
[24] a) A. A. Gabizon, *Cancer Res.* **1992**, *52*, 891; b) S. M. Moghimi, A. C. Hunter, J. C. Murray, *Pharmacol. Rev.* **2001**, *53*, 283.
[25] a) C. Mot, D. C. Drummond, K. Hong, D. B. Kirpotin, J. W. Park, *Drug Resist. Updates* **2003**, *6*, 271; b) E. S. Lee, K. Na, Y. H. Bae, *J. Controlled Release* **2005**, *103*, 405.
[26] a) C. R. Nakaie, S. Schreier, A. C. M. Paiva, *Biochim. Biophys. Acta Protein Struct. Mol. Enzymol.* **1983**, *742*, 63; b) S. R. Barbosa, E. M. Cilli, M. T. Lamy-Freund, A. M. L. Castrucci, C. R. Nakaie, *FEBS Lett.* **1999**, *446*, 45.
[27] D. Rapaport, Y. Shai, *J. Biol. Chem.* **1991**, *266*, 23769.
[28] L. Schmitt, C. Dietrich, *J. Am. Chem. Soc.* **1994**, *116*, 8485.
[29] B. J. Berne, R. Pecora, *Dynamic Light Scattering with Applications to Chemistry, Biology, and Physics*, Dover, New York, **1975** .
[30] G. A. Brehm, V. A. Bloomfield, *Macromolecules* **1975**, *8*, 663.
[31] M. Kveder, G. Pifat, S. Pecar, M. Schara, P. Ramos, H. Esterbauer, *Chem. Phys. Lipids* **1997**, *85*, 1.

Received: May 10, 2011
Published online: September 28, 2011

BASIC SCIENCE

Nanomedicine: Nanotechnology, Biology, and Medicine
7 (2011) 925–934

Research Article

nanomedjournal.com

A peptide derived from herpes simplex virus type 1 glycoprotein H: membrane translocation and applications to the delivery of quantum dots

Annarita Falanga, PhD[a,b,c], Maria Teresa Vitiello, PhD[d], Marco Cantisani, PhD[a,b,c], Rossella Tarallo, MS[a], Daniela Guarnieri, PhD[e], Eleonora Mignogna, MS[d], Paolo Netti, PhD[e], Carlo Pedone, PhD[a,b,c], Massimiliano Galdiero, MD[b,d], Stefania Galdiero, PhD[a,b,c,*]

[a]*Department of Biological Sciences, Division of Biostructures - University of Naples "Federico II," Napoli, Italy*
[b]*Centro Interuniversitario di Ricerca sui Peptidi Bioattivi - University of Naples "Federico II," Napoli, Italy*
[c]*Istituto di Biostrutture e Bioimmagini, CNR, Napoli, Italy*
[d]*Department of Experimental Medicine - II University of Naples, Napoli, Italy*
[e]*IIT@CRIB, Center for Advanced Biomaterials in Health Care, Napoli, Italy*

Received 26 October 2010; accepted 15 April 2011

Abstract

Cell membranes are impermeable to most molecules that are not actively imported by living cells, including all macromolecules and even small molecules whose physiochemical properties prevent passive membrane diffusion. However, recently, we have seen the development of increasingly sophisticated methodology for intracellular drug delivery. Cell-penetrating peptides (CPPs), short peptides believed to enter cells by penetrating cell membranes, have attracted great interest in the hope of enhancing gene therapy, vaccine development and drug delivery. Nevertheless, to achieve an efficient intracellular delivery, further strategies to bypass the endocytotic pathway must be investigated. We report on a novel peptide molecule derived from glycoprotein gH of herpes simplex type I virus that is able to traverse the membrane bilayer and to transport a cargo into the cytoplasm with novel properties in comparison with existing CPPs. We use as cargo molecule quantum dots that do not significantly traverse the membrane bilayer on their own.

From the Clinical Editor: Cell-penetrating peptides have recently attracted great interest in optimizing gene therapy, vaccine development and drug delivery. In this study, a peptide derived from glycoprotein gH of herpes simplex I is investigated from this standpoint.

Key words: Peptide; Quantum dots; Delivery; Virus

The efficacy of a molecule that is to be used as a therapeutic agent in biomedical research and in the pharmaceutical industry is subject to its pharmacodistribution properties. In particular many pharmaceutical agents should be delivered intracellularly to exert their therapeutic action inside the cytoplasm or onto individual organelles, such as nuclei (targets for gene and antisense therapy), lysosomes (target for the delivery of deficient lysosomal enzymes) and mitochondria (targets for pro-apoptotic anticancer drugs). Most drugs are poorly internalized by cells because the drugs cross the membrane rather inefficiently. Thus, intracellular delivery of therapeutic molecules is one of the key problems in drug delivery.

To date, multiple but only partially successful attempts have been made to bring various drugs and drug-loaded pharmaceutical carriers directly into the cell cytoplasm, bypassing the endocytic pathway to protect them from the lysosomal degradation. In fact, any molecule entering the cell via the endocytic pathway becomes entrapped into the endosome and eventually ends in the lysosome, where active degradation processes take place. Thus, even if an efficient cellular uptake via endocytosis were observed, the delivery of intact peptides and proteins is compromised by an insufficient endosomal escape and subsequent lysosomal degradation. Other methods, such as microinjection or electroporation, used for the delivery of membrane-impermeable molecules are generally invasive and could damage cellular membrane.[1,2] Certain peptides efficiently traverse biological membranes, promoting lipid membrane-reorganizing processes, such as fusion or pore formation involving temporary membrane destabilization and subsequent reorganization.

No conflict of interest was reported by the authors of this article.

*Corresponding author: Department of Biological Sciences, Division of Biostructures University of Naples "Federico II," Via Mezzocannone 16, 80134, Napoli, Italy.
E-mail address: sgaldier@unina.it (S. Galdiero).

1549-9634/$ – see front matter © 2011 Elsevier Inc. All rights reserved.
doi:10.1016/j.nano.2011.04.009

Cell-penetrating peptides (CPPs) can enter cells and have been used for intracellular delivery of various cargoes with molecular weights significantly greater than their own.[3,4] They are now considered to be the most promising tool for the intracellular delivery of therapeutics both in vitro and in vivo.[5-7] Examples of CPP are penetratin,[8] VP22,[9] transportan,[10] model amphipathic peptide (MAP),[11] signal sequence-based peptides,[12] synthetic polyarginines,[13] and TAT peptide.[3,4] Such proteins or peptides contain domains of fewer than 20 amino acids that are highly rich in basic residues. The peptide TAT is one of the most studied and efficient CPP known to date. TAT is a small basic peptide based on the arginine-rich region of the human immunodeficiency virus type 1 transcription transactivating protein and has been proved to have little cytotoxicity. Although its mechanism of cellular uptake is still debated, it has been shown to translocate various entities into cells, including small molecules, peptides, proteins, DNA/RNA, liposomes and particles. CPPs can either require chemical linkage or involve formation of stable noncovalent complexes.[14] The noncovalent strategy has been used for short amphipathic peptides, proteins, oligonucleotides and siRNAs to improve their delivery into mammalian cells.[14]

Early attempts to define a mechanism for the cellular import of CPPs, including TAT, indicated that the direct transport of peptides across the lipid bilayer was independent of both receptor recognition and energy-requiring processes, such as endocytosis in its various forms.[4] Although such mechanisms may still be valid in part and are perhaps more likely at very high peptide concentrations, more recent observations, using a fluorescently labeled TAT-derived CPP, indicate a fundamental role of endocytosis.[15,16] Other authors[17] have confirmed further that an energy-dependent route may be a common internalization mechanism for the cellular entry of polycationic CPPs. They have stressed the involvement of cell-surface polysaccharides, including heparan sulphate, as a binding site for cationic peptides. In particular, Brooks[18] proposed that TAT, because of its adherence to negatively charged membrane constituents, is internalized by any pinocytic process occurring at cell membranes. Endosomal entrapment may thus limit their utility, though some peptides and/or biologically active cargoes can escape this environment to achieve a specific desired biological action.

Therefore, it is essential to identify novel molecules that use different internalization mechanisms. We previously reported the identification of a membrane-perturbing domain in the protein gH of herpes simplex virus type 1.[19-22] The peptide gH625 is a mainly hydrophobic peptide that interacts with biological membranes, contributing to the merging of the viral envelope and the cellular membrane. When gH625 is in helical conformation, the polar residues concentrate on one face of the helix, giving an amphiphilic character common to fusion peptides of most fusion glycoproteins of enveloped viruses; moreover, gH625 is very effective in inducing lipid mixing of model membranes.

To evaluate the possibility of using this peptide as a more effective transport vector, we determined the relationships among several physicochemical properties such as cell association, cellular uptake, lipid membrane binding and conformation. Flow cytometry was used to measure cellular uptake of gH625 in HeLa cells. For peptides that strongly bind to the cell plasma membranes and remain associated with cells even after repeated washings, FACS analysis cannot be used to evaluate cellular uptake with validity unless a protease digestion step of the adsorbed CPP is included in the protocol. In our study to measure the fraction of internalized peptide accurately, we used a method based on the selective chemical extinction by dithionite of the 4-chloro-7-nitrobenz-2-oxa-1,3-diazole (NBD) moiety attached to the peptide. This membrane-impermeable reagent was used previously to measure cellular uptake of penetratin.[23] We also report confocal microscopy experiments showing the cellular uptake of gH625.

To assess the ability of the peptide gH625 to deliver drugs inside the cell, we used quantum dots (QDs) as a model cargo. QDs have been demonstrated as a new type of fluorescence probe[24] with high luminescence efficiency and with their emission peak tunable depending on their size. In addition, the excellent photostability of QDs gives them great potential in cellular labeling and bioimaging, and a number of works have shown these characteristics in different kinds of biological systems. QDs are advantageous due to their nanometer size, broad excitation, narrow emission, bright photoluminescence and high photostability. However, wide application of QDs to intracellular and molecular imaging has been hampered by their insufficient ability to traverse cell membranes. Thus, to use QDs as biological probes for intracellular applications, their delivery has to be improved significantly. Several authors recently reported on the functionalization of QDs with the TAT peptide or other positively charged CPPs as enhancer of cell penetration and reported on the endosomal uptake of QDs and escape from the endosomal system.[25-29] Here we describe a novel and mainly hydrophobic peptide derived from a viral protein involved in membrane fusion and its application to QD delivery. Similar delivery methods may enable the implementation of the next generation of QDs capable of long-term intracellular monitoring.

Methods

Peptide synthesis

Peptides (gH625: Ac-HGLASTLTRWAHYNALIRAFGGG-COOH; TAT: Ac-GRKKRRQRRRGGG-COOH) were synthesized using the standard solid-phase-9-fluorenylmethoxycarbonyl (Fmoc) method as previously reported.[19] All purified peptides were obtained with good yields (30–40%).

NBD labeling of peptides

Labeling was performed on resin-bound peptides as previously reported by Rapaport and Shai.[30] Briefly, 30–70 mg of resin-bound peptide (10–25 μmol) was treated with piperidine in DMF to remove the Fmoc-protecting group of the N-terminal amino acid of the linked peptide. The resin-bound peptide was then reacted with 4-chloro-7-nitrobenz-2-oxa-1,3-diazole (NBD-Cl) in DIPEA 2 M (3–4 equivalent) in DMF. After 24 hours the resin-bound peptides were washed thoroughly with methylene chloride, and the peptides were cleaved from the resin and purified. The identity of the NBD-peptides was confirmed by liquid chromatography–mass spectrometry (LC/MS).

Peptides conjugation to QDs

Solution of peptides, EDC (1-Ethyl-3(3-dimethylaminopropyl)-carbodiimide, hydrochloride) and NHS (N-Hydroxysuccinimide) were prepared in PBS buffer at pH 7.2 in molar ratio of 4:4:1. QDs were conjugated with the preactivated peptides in a molar ratio of 1:200, in MES buffer at pH 5.5 for 3 hours. The fluorescence spectra of peptide QDs and un-conjugated QDs were measured in a Cary Eclipse Varian fluorescence spectrophotometer in the same condition. In all the reported confocal experiments we used the same peptide concentration and thus the QDs' concentration was 200 times lower.

MTT assay for cell viability

Methylthiazolyldiphenyl-tetrazolium (MTT) bromide reduction was used to examine the metabolic activity of the cells. The MTT assay is based on the reduction of the yellowish MTT to the insoluble and dark blue formazan by viable and metabolically active cells.[31] HeLa cells were subcultured in 96-well plates at a seeding density of 2×10^4 cells per well. For assessing the cytotoxic effect of gH625 and TAT peptides, HeLa cells were incubated with different concentration of peptides (10, 50, 100, 200, 400 μM) for 24 hours. Then, the medium was gently aspirated, MTT solution (5 mg/mL) was added to each well and cells were incubated for a further 3 hours at 37°C. The medium with MTT solution was removed, and the formazan crystals were dissolved with DMSO. The absorption values were measured at 570 nm using a Bio-Rad Microplate Reader (Bio-Rad Laboratories, Inc., Hercules, California). The viability of HeLa cells in each well was presented as a percentage of control cells.

LDH assay

Lactate dehydrogenase (LDH) released into the culture medium was measured by monitoring fluorometrically the production of nicotinamide adenine dinucleotide (NAD^+) from NADH during the conversion of pyruvate to lactate.[32] For assessing the plasma membrane integration upon the exposure to gH625 and TAT peptides, HeLa cells were subcultured in 96-well plates at a seeding density of 2×10^4 cells per well. Twenty-four hours later, cells were incubated with different concentration of peptides (10, 50, 100, 200, 400 μM) for 24 hours. The cell supernatant (100 μL) was incubated with 0.18 mM NADPH and 0.60 mM pyruvate in 50 mM phosphate buffer (pH 7.4). The rate of NAD^+ formation was monitored for 1 minute by reading the fluorescence in a fluorescence reader with the excitation filter set at 360 nm and the emission filter set at 460 nm. LDH leakage was expressed as a percentage of untreated or control cells, which was designated as 100%.

Liposome preparation

Large unilamellar vesicles (LUVs) consisting of PC/Chol (1:1), and when necessary containing Rho-PE and NBD-PE, were prepared according to the extrusion method of Hope et al[33] in 5 mM Hepes, 100 mM NaCl, pH 7.4. Lipids were dried from a chloroform solution with a nitrogen-gas stream and lysophilized overnight. For fluorescence experiments, dry lipid films were suspended in buffer by vortexing; the lipid suspension was freeze-thawed 6 times and extruded 20 times through polycarbonate membranes with 0.1 μm diameter pores to produce large unilamellar vesicles. Lipid concentrations were determined by phosphate analysis.[34]

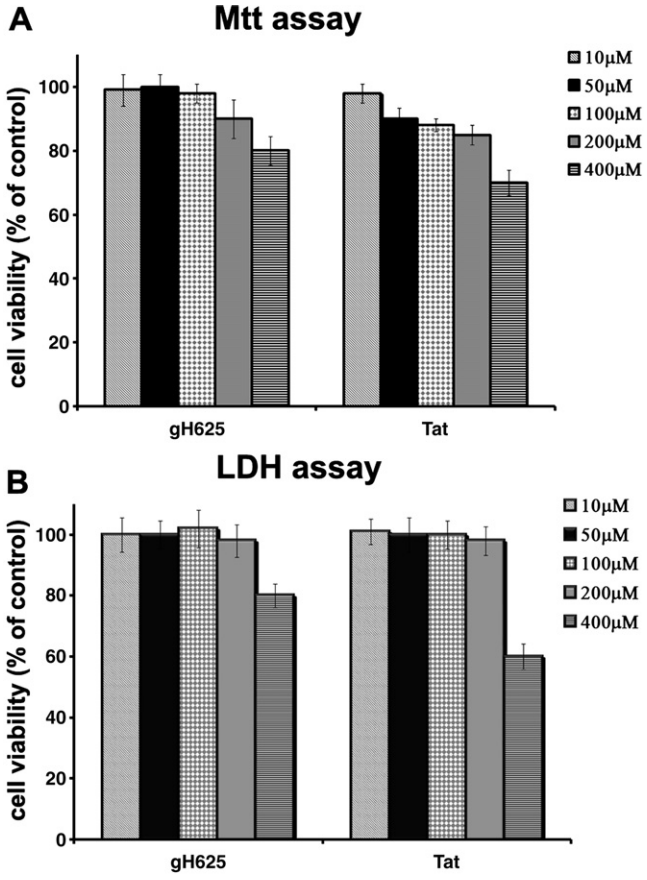

Figure 1. Effect of peptides on the viability of HeLa cells. Cytotoxic effect of gH625 and TAT peptides determined by the MTT (panel **A**) assay and by measuring the efflux of lactate dehydrogenase (LDH) into the culture medium (panel **B**). HeLa cells were treated with the indicated concentrations of peptides for 24 h. The values shown are the percentages of viable cells and LDH release relative to control cells.

Inner-monolayer phospholipid-mixing measurement

Peptide-induced phospholipid mixing of the inner monolayer was measured by a modification of the phospholipid-mixing measurement as reported elsewhere.[35] The concentration of each of the fluorescent probes within the liposome membrane was 0.6% mol. LUVs were treated with sodium dithionite to completely reduce the NBD-labeled phospholipid located at the outer monolayer of the membrane. The final concentration of sodium dithionite was 100 mM (from a stock solution of 1 M dithionite in 1 M TRIS, pH 10.0) and it was incubated for approximately 1 hour on ice in the dark. Sodium dithionite was then removed by size exclusion chromatography through a Sephadex G-75 filtration column (Pharmacia, Uppsala, Sweden) eluted with buffer containing 10 mM TRIS, 100 mM NaCl, and 1 mM EDTA, pH 7.4. The NBD emission at 530 nm was followed

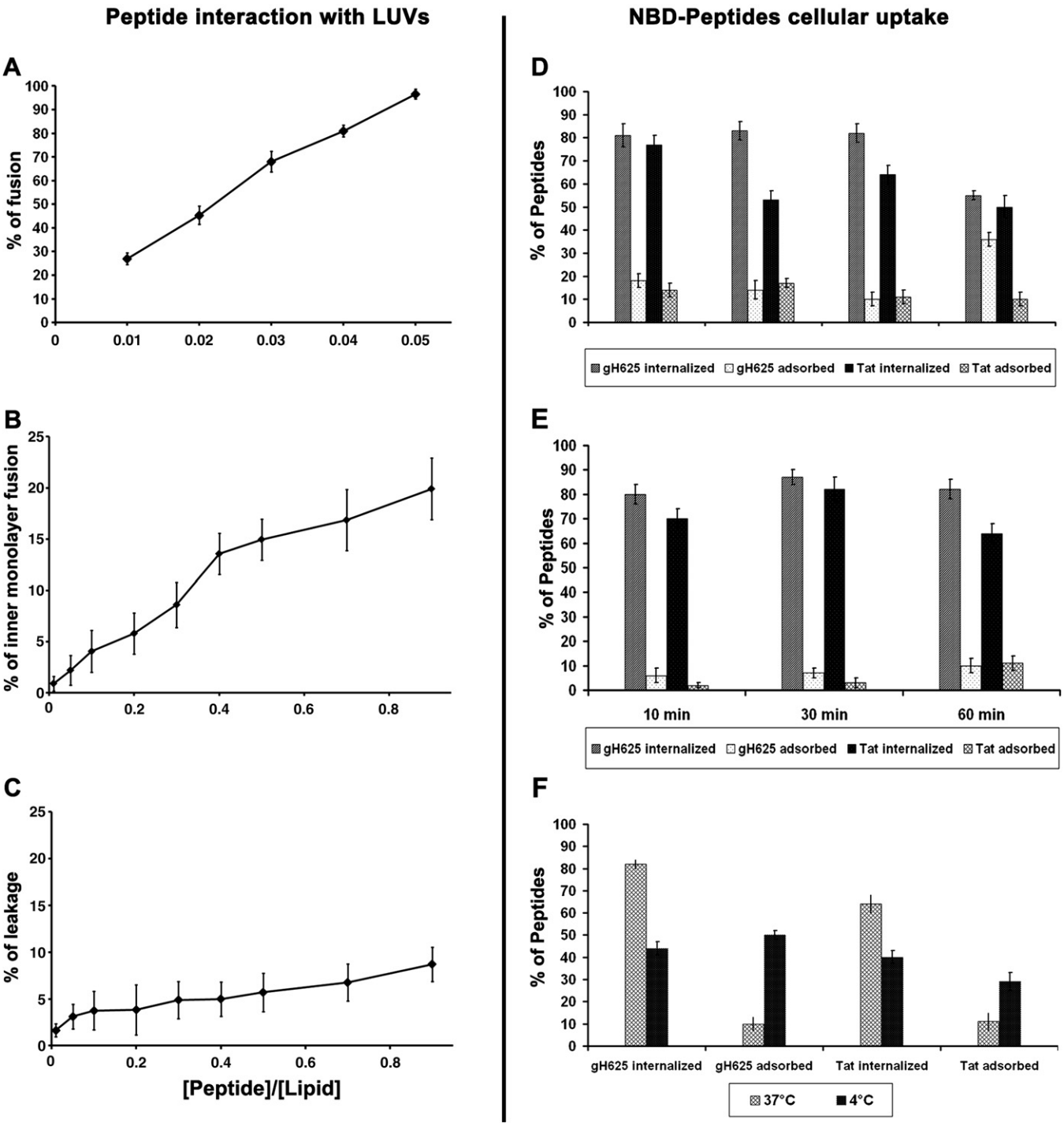

Figure 2. Peptide interaction with PC/Chol LUVs **(A**,**B**,**C)**, the dose dependence is reported and each trace represents an average of 3 independent experiments. **(A)** Lipid mixing; **(B)** Inner monolayer assay. **(C)** Leakage of ANTS/DPX. NBD-peptide cellular uptake **(D-E-F)**, the percentage of internalized and bound peptides are reported. HeLa cells were incubated with **(D)** increasing concentrations of NBD-peptides (1, 5, 10, 20 μM) for 60 min. **(E)** 10 μM NBD-peptides for 10, 30 and 60 min. **(F)** NBD-peptides at 37° and 4°C.

with the excitation wavelength set at 465 nm. A cut-off filter at 515 nm was used between the sample and the emission monochromator to avoid scattering interferences. The fluorescence scale was calibrated such that the zero level corresponded to the initial residual fluorescence of the labeled vesicles and the 100% value corresponding to complete mixing of all lipids upon the addition of Triton X-100 (0.05% v/v). All fluorescence measurements were conducted in PC/Chol (1:1) LUVs, were repeated at least 3 times and results were averaged. All the experiments were performed at 37°C.

Measurements of ANTS/DPX leakage

The ANTS/DPX assay[36] was used to measure the ability of the peptide to induce leakage of ANTS/DPX pre-encapsulated in liposomes. Details of this assay can be found elsewhere.[37] To initiate a leakage experiment, the peptide, in a stock solution at pH 7.4 containing 5 mM Hepes and 100 mM NaCl, was added to the stirred vesicle suspension (0.1 mM lipid) at 37°C.

Flow cytometry of cell association of peptide

HeLa cells were cultured in RPMI medium supplemented with 10% fetal bovine serum. Cells were diluted at 3×10^5 cells mL^{-1} 1 day before the experiment. Cell association was measured by flow cytometry using a FACScan (Becton Dickinson, Franklin Lakes, New Jersey). NBD-labeled peptides (1, 5, 10, 20 μM) were incubated with HeLa cells (5×10^5 cells mL^{-1}) in Opti-MEM medium at 37°C for various periods of time (10, 30, and 60 minutes) in a final volume of 0.5 mL. Thereafter, the cells were washed twice and then resuspended in 0.5 mL of ice-cold NaCl/Pi for flow cytometric analysis. Cell-associated fluorophores were excited at 465 nm and fluorescence was measured at 530 nm. A histogram of fluorescence intensity per cell (1×10^4) was obtained and the calculated mean of this distribution was considered as representative of the amount of cell-associated peptide. A stock solution of dithionite (1 M) was freshly prepared in 1 M Tris solution (pH 10). Following flow cytometric analysis, 5 μL of dithionite stock solution was added to cells maintained at 4°C and the fluorescence of internalized peptides was measured after 5 minutes.

To further study the mechanism of internalization, experiments were performed at 4°C until the end of the cell fixation procedure. Cells were preincubated for 30 minutes at 4°C before being incubated with the peptide solution.

Cellular uptake of peptides by confocal microscopy

For cellular uptake experiments, peptides were diluted in cell culture medium; the final concentration of NBD conjugated to the peptides is 1, 10 and 20 μM; the final concentration of QDs conjugated to the peptide is 5, 50 and 100 nm. In addition, 70% confluent HeLa cells, seeded on 12-mm diameter glass coverslips, were incubated with 200 μl of peptide conjugated to the NBD or to QDs at 37°C for 1 hour and at 4°C for 10 minutes. For localization of peptides in lysosome organelles, LysoTracker reagent (Molecular Probes, Invitrogen, Carlsbad, California) was added to cell culture medium containing peptides and incubated with cells for 1 hour at 37°C according to manufacturer's procedure. After incubation, cells were rinsed twice with PBS to remove noninternalized peptides and fixed with 4% paraformaldehyde for 20 minutes.

For peptide uptake-kinetics experiments on nonfixed living cells, HeLa cells were incubated with 10 μM of NBD-peptide solutions and with 50 nm QD-peptide solutions at 37°C for 1, 5 and 17 hours. After incubation, cells were rinsed twice with PBS and fresh cell culture medium without phenol red was added. To inhibit the endocytosis pathway, 40 μM sodium azide were added to the cell culture medium for 30 minutes followed by 1 hour of incubation with peptides.

All the samples were observed by a confocal laser scanning microscope (CLSM) (LSM510, Zeiss, Thornwood, New York) equipped with a He-Ne and an Argon laser lines at the wavelengths of 543 nm and 488 nm, respectively, with a 63× objective.

Results

Toxicity of peptides

The cell viability was measured using MTT and LDH assays. LDH is of great value as an in vitro marker for cellular toxicity. Figure 1, *A* shows the results obtained with the MTT assay, and Figure 1, *B* shows the results of the LDH assay. To evaluate the cell toxicity of both gH625 and TAT peptides, escalating doses of the peptides were applied to HeLa cells. The addition of TAT or gH625 did not affect HeLa cell viability up to 200 μM. A low level of toxicity was observed when the peptides' concentration reached 400 μM. In the conditions used, different sensitivity was observed for the 2 assays, with the MTT assay being slightly more sensitive in detecting cytotoxic events in comparison with the LDH leakage assay. In conclusion, both peptides were not toxic at concentrations lower than 400 μM, and at this concentration, TAT was slightly more toxic than gH625.

Peptide interaction with LUVs

The peptide gH625 has been previously characterized.[19-22] indicating its strong interaction with LUVs, although the exact mechanism of interaction awaits complete understanding. We previously showed that gH625 penetrates into the membrane by studying the tryptophan or NBD fluorescence emissions, which are environmentally sensitive. The depth of insertion was also determined by means of differential quenching using brominated lipids at different positions, which indicated that the peptide was not adsorbed on the top of the membrane but had a deep interfacial partitioning. Membrane disturbance upon peptide insertion was previously evaluated by vesicle fusion[21] in several liposomes composed of different lipids showing the best fusogenic activity in PC/Chol as shown in Figure 2, *A*. As transmembrane-pore formation has been suggested to explain the uptake of other translocating peptide[38-40] we previously tested this possibility for gH625 using surface plasmon resonance[41]; the values of the ratio of the binding affinity to bilayers in comparison with to monolayers demonstrates that the peptide is not influenced by the membrane inner layer.

Here, to further support the hypothesis that the peptide is able to diffuse inside lipidic vesicles without involving pore formation, we performed the inner monolayer fusion and leakage experiments as indicators of the interaction and perturbation of the lipid membrane caused by the peptide.

In the inner monolayer, the fluorescence from the vesicle membranes' outer monolayer is eliminated by the addition of an aqueous reducing agent, and this experiment reveals the extent of lipid mixing between the inner monolayers of vesicles in solution. Figure 2, *B* shows that a small fusion of the inner monolayer is observed only at a peptide lipid ratio of approximately 0.8, and the occurrence of the same level of membrane fusion by the lipid mixing experiment, whether it is hemifusion or complete fusion,

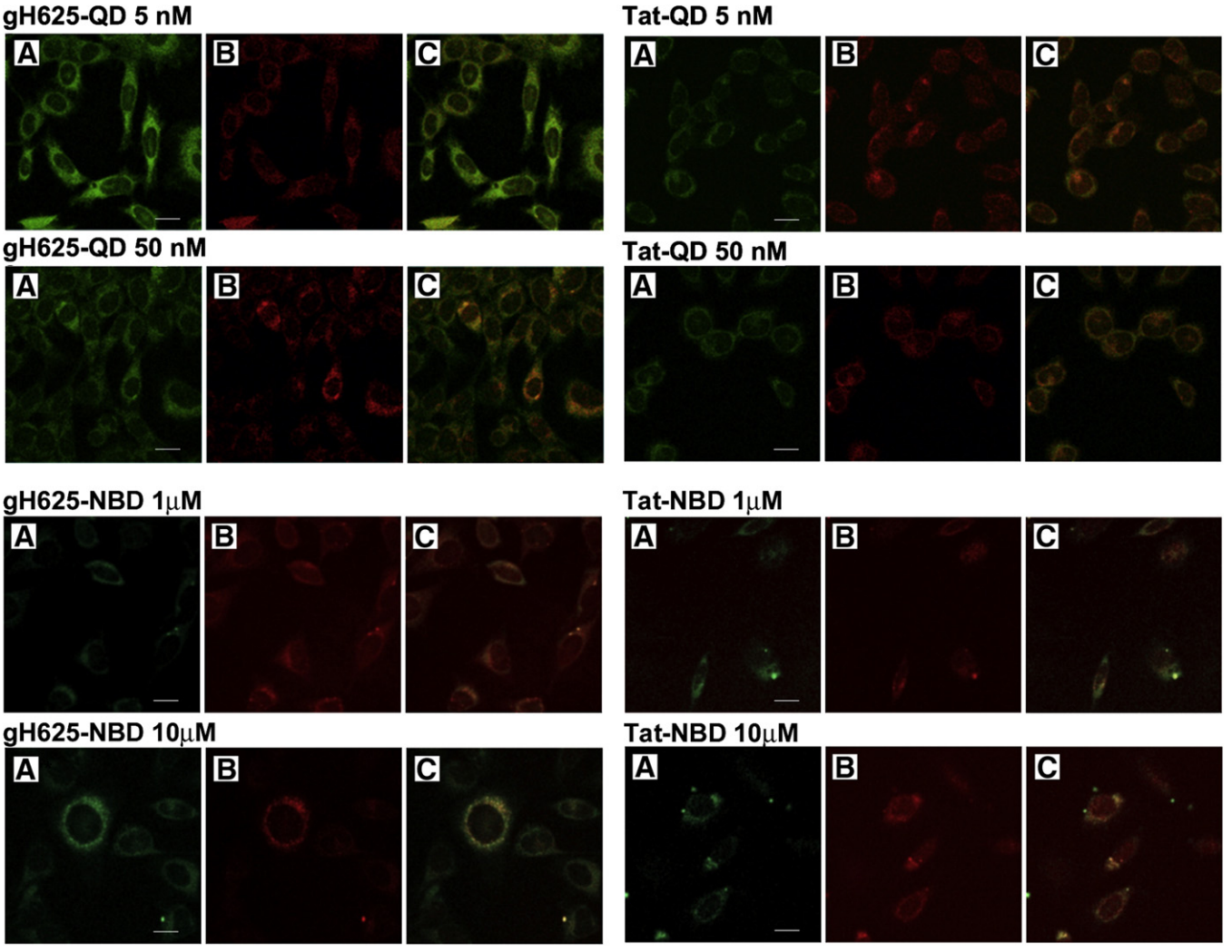

Figure 3. Fluorescence images of QD-peptides at 5 and 50 nM and NBD-peptides, at 1 and 10 μM. Panel A shows the peptide in green; Panel B shows the LysoTracker in red and Panel C shows the merge of the two images. Bar = 10 μm.

was observed at a peptide lipid ratio of 0.01. This assay clearly indicates that the peptide gH625 induces only hemifusion at peptide-to-lipid ratios between 0 and 0.1.

A contents-mixing assay was employed to monitor any mixing of internal vesicle components because of vesicle exposure to gH625. Release of ANTS and DPX from vesicles is commonly used as a measure of bilayer perturbation and interpreted as "transient pore formation."[36, 37] Contents mixing is manifested by a decrease in fluorescence intensity if vesicles encapsulating fluorescent cargo (e.g., ANTS) merge contents with those containing quenchers (e.g., DPX). Figure 2, *C* shows that no contents mixing occurs over the same P/L range where substantial outer monolayer lipid mixing occurs, corroborating the presence of vesicle hemifusion in our system. The agreement of contents-mixing assays and inner monolayer lipid-mixing assays gives full confidence in the finding of peptide-induced hemifusion for gH625.

These results can be used as qualitative indicators of peptide translocation or bilayer perturbation with relevance for the direct-penetration mode of cell entry, or for the steps of endosomal membrane translocation or endosomal escape. We have not detected any significant pore formation; vesicle fusion events not accompanied by leakage of the aqueous contents of the vesicle were also reported for other peptides in a study published by Thoren et al.[42]

Determination of NBD-peptide cellular uptake

We have determined the fraction of NBD-labeled peptide taken up into HeLa cells by flow cytometry. The experiment is based on a method previously introduced by McIntyre and Sleight[43] to measure the transbilayer distribution of NBD-phospholipid analogues. The distribution is determined by comparing the fluorescence intensity before and after addition of sodium dithionite, an essentially membrane-impermeant molecule, which suppresses irreversibly the fluorescence of the accessible NBD-moiety localized on the external cell surface.

We incubated gH625-NBD with HeLa cells at 37°C at different concentrations (1, 5, 10, 20 μM). After 1 hour of

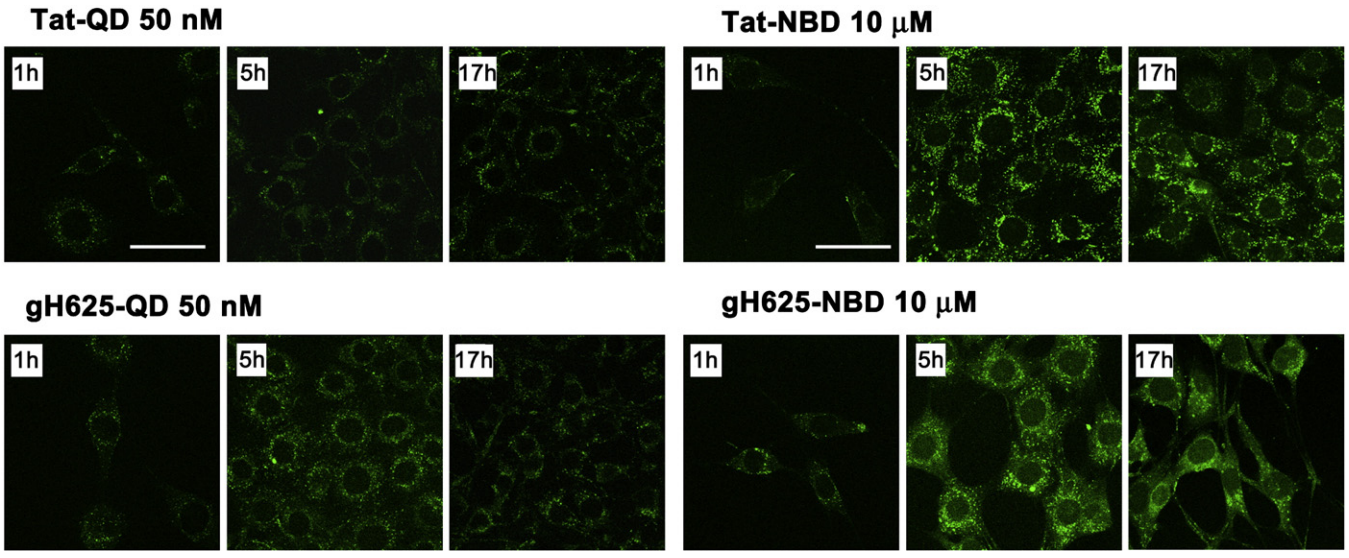

Figure 4. Uptake kinetics of QD-peptides (50 nm) and NBD-peptides (10 μM) in HeLa cells after 1, 5 and 17 h of incubation at 37°C. Bar = 50 μm.

incubation, we measured the quenching of the peptide by dithionite treatment. The dithionite reaction was performed at low temperature (4°C) because the dithionite crossing of biological membranes is strongly reduced[44] in comparison with high temperatures. Upon stabilization of the initial fluorescence, dithionite was added to initiate quenching. Before the addition of dithionite we observed that approximately 90% of gH625-NBD was not washed away and thus was internalized or bound to the membrane bilayer; after the addition of dithionite the internalized peptide was 80% (Figure 2, *D*). We performed the same experiment on TAT-NBD as a reference; and before the addition of dithionite we observed that approximately 70% of the peptide was internalized or bound to the membrane bilayer; after the addition of dithionite, the internalized peptide was approximately 60% (Figure 2, *D*). Increasing dithionite concentration did not result in a modification of the extent of quenching, indicating that the entire accessible NBD label was quenched by 1 M dithionite (data not shown). These results show that the use of dithionite permits efficient measurement of the fraction of internalized peptide inside the cells. To exclude the possibility that the fluorescence signal could have been due to the internalization of the fluorochrome itself, the NBD moiety was used in the same in vitro assay conditions, and no cellular fluorescence was observed at concentrations up to 20 μM (data not shown).

To measure the kinetics of import of gH625-NBD into cells, we incubated the peptide with cells at 37°C for various times (10, 30, and 60 minutes) and then determined the remaining fluorescence following treatment with dithionite. Figure 2, *E* shows the fraction of peptide taken up by cells. The uptake is very rapid and seems to reach a plateau after 1 hour of incubation.

The influence of temperature on the intracellular accumulation was studied to see whether the uptake depended on a translocation mechanism or a cellular process. We incubated the peptide with HeLa cells at both 37°C and 4°C; the amount of internalized gH625-NBD at low temperature (Figure 2, *F*) is reduced for both peptides, with an increase in the quantity bound to the membrane and a substantial decrease of the quantity of internalized peptide. The reduction of internalized or bound peptide was more significant for TAT peptide.

NBD-peptide localization

To confirm the peptide internalization, we examined its uptake and intracellular localization by confocal microscopy. We used concentrations of 1 and 10 μM and a time of 60 minutes as selected by the flow cytometry experiments. Both peptides are efficiently internalized and we observe a significant colocalization with the LysoTracker, indicating a partial confinement within the endosomal compartments (Figure 3).

Recently, it has been reported that cell-fixation protocols induce the apparent translocation and nuclear localization of positively charged peptides and this has been previously proved for the TAT peptide.[15] We have examined the possibility that the translocation observed for gH625 could be the result of such an effect. As shown in Figure 4, although the penetration of the TAT-NBD in living cells is lower than with fixed cells, indicating that a large portion of surface-bound peptide diffuses into the cytoplasm during the fixation step, the penetration of gH625-NBD is not affected by fixing protocols. The NBD alone at a concentration of 10 μM is almost unable to penetrate inside cells as shown in Figure 5.

Delivery of QDs

Delivery of QDs to living cells should consist of 2 phases: QDs are initially bound to plasma membrane of cells, and then are gradually internalized by cells. QDs alone have a poor affinity for the plasma membrane of HeLa cells at the concentration of 50 nm used in these experiments (Figure 5). The peptide conjugation to QDs enhanced their membrane-bound ability providing a favorable condition for the cellular internalization. Figure 4 clearly shows their intracellular distribution in HeLa cells at concentrations of 5 and 50 nm.

The images indicate a more efficient internalization of QDs linked to the peptide gH625 in comparison with TAT, with a more significant colocalization with the LysoTracker for the TAT. Experiments performed in living cells show a marked difference at 5 hours in the penetration of QDs conjugated to the TAT and to gH625, with a clearly detectable major increase of penetration when linked to gH625. Additionally, with QDs conjugated with gH625 we can deduce that the translocation observed is not the result of such fixing protocols.

Metabolic inhibitors

The influence of temperature and metabolic inhibitors on the intracellular penetration of NBD-peptides or QD-peptides was studied to see whether the uptake depended on a translocation mechanism or a cellular process. We compared the images obtained at 4°C to determine the degree of endocytosis in the cellular uptake (Figure 6, *C*). The analysis of the results indicates that the endocytosis is more significant for TAT than for gH625. Sodium azide is an oxidative phosphorylation inhibitor commonly used to abolish ATP production within the cell membrane.[45] As shown in Figure 6, *A*, *B*, and *C*, a marked decrease of TAT internalization was observed both when conjugated to NBD and when conjugated to QDs, indicating that endocytosis is the main process involved in TAT penetration. On the contrary, gH625 penetration is not influenced significantly by the treatment with sodium azide, indicating that endocytosis does not affect gH625 transduction.

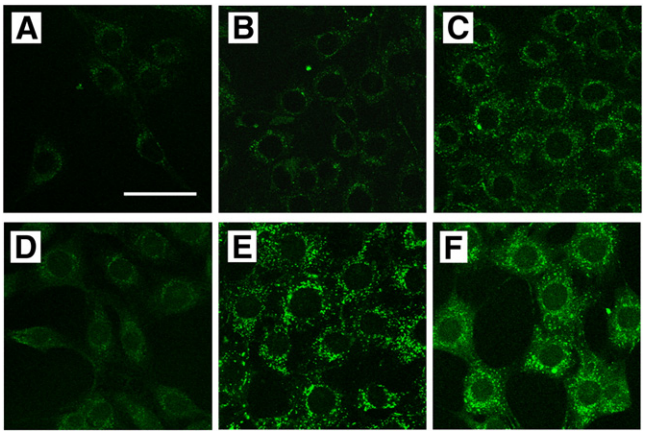

Figure 5. Uptake of QD **(A)**, Tat-QD **(B)** and gH625-QD **(C)** at 50 nm and NBD **(D)**, Tat-NBD **(E)** and gH625-NBD **(F)** at 10 μM in HeLa cells after 5 h of incubation at 37°C. Bar = 50 μm

Discussion

Our objective was to describe a new molecule that could be used for the intracellular delivery. We sought to achieve this by combining flow cytometry, a quantitative method that allows accurate measurement of peptide internalization, with confocal microscopy. Labeling the peptide with the NBD group allowed the comparison of cellular uptake with phospholipid binding and analysis of the physicochemical properties required for translocation. To measure cellular uptake of NBD-labeled peptide we have used the dithionite method, which allows the estimation of the peptide fraction localized inside the cell. We determined by flow cytometry that after 1 hour of incubation with HeLa cells at 37°C and 4°C, most of gH625-NBD was localized intracellularly; our results show that the peptide internalization in HeLa cells can occur at 37°C and to a lesser extent at 4°C, supporting the view that the internalization mechanism does not involve only endocytosis. The kinetic of internalization of gH625-NBD is rapid and reaches a plateau after 1 hour. We confirmed by confocal microscopy that indeed the NBD-peptide is inside the cell and its penetration is not induced by cell-fixation protocols as previously found for the TAT peptide.[15]

The amount of cell-associated peptide represents the sum of internalized peptide and of peptide remaining on the cell surface after cells wash. We previously reported results from surface plasmon-resonance[21,41] assays on peptide gH625, which allowed us to examine the contribution of the inner leaflet of the membrane with regard to the binding properties of viral membranotropic peptides. This approach was used to discriminate between transmembrane pore formation and membrane perturbation. We showed that the peptide stably inserts into the PC/Chol membrane but is unable to form pores; here, we confirm this result showing that it is unable to fuse the inner monolayer as well as inducing leakage of vesicles. The ANTS and DPX assay indicates that no permeabilization occurs upon binding of peptide to a lipid bilayer; this suggests that the peptide interacts with the lipid membrane but does not form pores inside the membrane, further supporting the view that the mechanism of lipid/peptide association plays a key role in the translocation activity. Additionally, gH625 cellular uptake is associated with its ability to interact with membrane lipids and to form a transient helical structure that temporarily affects membrane organization, thereby facilitating insertion into the membrane and translocation.

The main objective of this study was to analyze the internalization of the peptide gH625 in the absence of an attached cargo for a better understanding of the behavior of this membranotropic domain and to test the hypothesis regarding its use for delivering macromolecules. We therefore report an example of the application of gH625 to the delivery of QDs into the cells.

QDs are a new class of fluorescent probes under intense research and development for broad applications in molecular, cellular and in vivo imaging. QDs have unique functional and structural properties, such as size and composition-tunable fluorescence emission, large absorption cross sections and exceptional brightness and photostability when compared with organic dyes and fluorescent proteins. Although considerable success has been achieved in using QDs for labeling fixed cells and for imaging cell membrane proteins, only limited progress has been made for molecular imaging inside living cells. A major problem is the lack of efficient methods for delivering single QDs into the cytoplasm of living cells. Our results clearly indicate that the gH625-QDs are internalized more effectively than TAT-QDs and their internalization only partially involves the endocytic pathway. Further assays have been undertaken to understand the exact mechanism of internalization of gH625-QDs conjugates better.

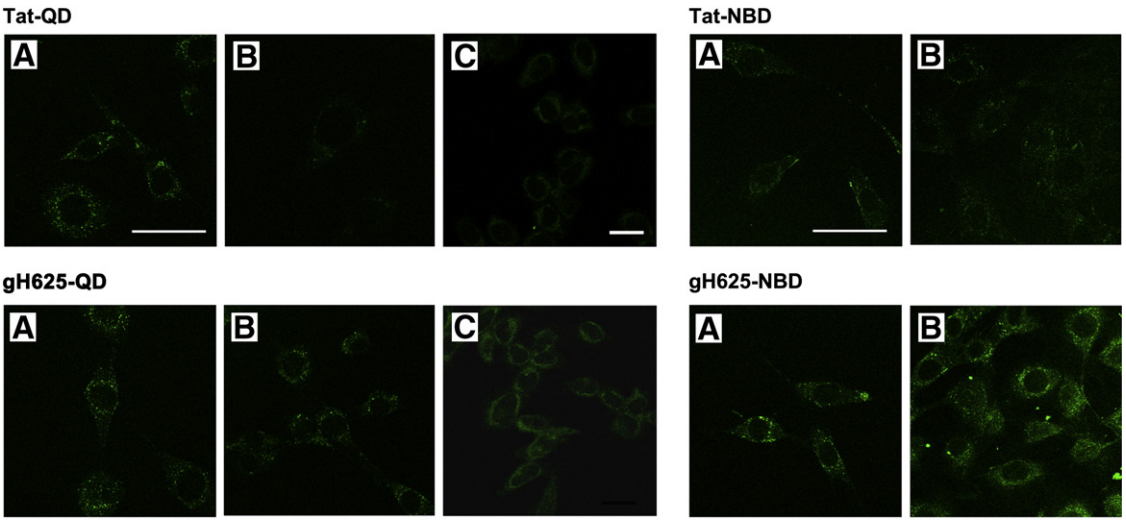

Figure 6. Endocytosis inhibition experiments of HeLa cells incubated for 1 h with 50 nm QD peptides and with 10 μM NBD peptides. **(A)** Nontreated cells and **(B)** 40 μM NaN_3 treated cells; bar = 50 μm. Panel C reports the fluorescence images of gH625-QD and TAT-QD at 100 nm incubated with HeLa cells at 4°C; bar = 10 μm.

Furthermore, gH625 has showed very low toxicity during in vitro studies when used at concentrations up to 400 μM; therefore, it seems suitable for being used as a delivery system. Of importance is that when conjugated with QDs, gH625 exerts an action of translocation through cellular plasma membranes, which seems to be only relatively dependent on the endocytic route of entry. It has been previously reported that TAT peptide conjugated with small molecules enters cytoplasm and eventually the cell nuclei and that TAT-QDs remain trapped in vesicles. This difference in the intracellular fate of TAT peptide-conjugated molecules and TAT-QDs is likely caused by differences in the sizes of the cargoes. QDs are much larger than standard molecules and are thus less able to escape from vesicles. On the contrary, gH625-QDs are present in the cytoplasm in a more punctuated form in comparison with TAT-QDs. Therefore, we can hypothesize a different mechanism of entry between TAT-QDs and gH625-QDs, and this is of particular interest because peptides with different biophysical characteristics are able to condition the entry pathway of the same macromolecular cargo. These results make gH625-QDs an interesting compound for recognizing specific targets in the cytoplasm.

Our results provide new insights into the mechanism of gH625-mediated delivery and for the development of nanoparticle probes for intracellular targeting and imaging, and for biology and medicine.

References

1. Chakrabarti R, Wylie DE, Schuster SM. Transfer of monoclonal antibodies into mammalian cells by electroporation. J Biol Chem 1989;264:15494-500.
2. Arnheiter H, Haller O. Antiviral state against influenza virus neutralized by microinjection of antibodies to interferon-induced Mx proteins. EMBO J 1988;7:1315-20.
3. Schwarze SR, Dowdy SF. In vivo protein transduction: intracellular delivery of biologically active proteins, compounds and DNA. Trends Pharmacol Sci 2000;21:45-8.
4. Vives E, Brodin P, Lebleu B. A truncated HIV-1 TAT protein basic domain rapidly translocates through the plasma membrane and accumulates in the cell nucleus. J Biol Chem 1997;272:16010-7.
5. Dietz GP, Bahr M. Delivery of bioactive molecules into the cell: the Trojan horse approach. Mol Cell Neurosci 2004;27:85-131.
6. Mae M, Langel U. Cell-penetrating peptides as vectors for peptide, protein and oligonucleotide delivery. Curr Opin Pharmacol 2006;6: 509-14.
7. Stewart KM, Horton KL, Kelley SO. Cell-penetrating peptides as delivery vehicles for biology and medicine. Org Biomol Chem 2008;6: 2242-55.
8. Derossi D, Calvet S, Trembleau A, Brunissen A, Chassaing G, Prochiantz A. Cell internalization of the third helix of the antennapedia homeodomain is receptor-independent. J Biol Chem 1996;271:18188-93.
9. Elliott G, O'Hare P. Intercellular trafficking and protein delivery by a herpes virus structural protein. Cell 1997;88:223-33.
10. Pooga M, Hallbrink M, Zorko M, Langel U. Cell penetration by transportan. FASEB J 1998;12:67-77.
11. Oehlke J, Scheller A, Wiesner B, Krause E, Beyermann M, Klauschenz E, et al. Cellular uptake of an alpha-helical amphipathic model peptide with the potential to deliver polar compounds into the cell interior non-endocytically. Biochim Biophys Acta 1998;1414:127-39.
12. Rojas M, Donahue JP, Tan Z, Lin YZ. Genetic engineering of proteins with cell membrane permeability. Nat Biotechnol 1998;16:370-5.
13. Futaki S, Suzuki T, Ohashi W, Yagami T, Tanaka S, Ueda K, et al. Arginine-rich peptides. An abundant source of membrane-permeable peptides having potential as carriers for intracellular protein delivery. J Biol Chem 2001;276:5836-40.
14. Heitz F, Morris MC, Divita G. Twenty years of cell-penetrating peptides: from molecular mechanisms to therapeutics. Brit J Pharm 2009;157: 195-206.
15. Richard JP, Melikov K, Vives E, Ramos C, Verbeure B, Gait MJ, et al. Cell-penetrating peptides: a re-evaluation of the mechanism of cellular uptake. J Biol Chem 2003;278:585-90.
16. Suzuki T, Futaki S, Niwa M, Tanaka S, Ueda K, Sugiura Y. Possible existence of common internalization mechanisms among arginine-rich peptides. J Biol Chem 2002;277:2437-43.

17. Duchardt F, Fotin-Mleczek M, Schwarz H, Fischer R, Brock R. A comprehensive model for the cellular uptake of cationic cell-penetrating peptides. Traffic 2007;8:848-66.
18. Brooks H, Lebleu B, Vives E. TAT peptide-mediated cellular delivery: back to basics. Adv Drug Deliv Rev 2005;57:559-77.
19. Galdiero S, Falanga A, Vitiello M, Browne H, Pedone C, Galdiero M. Fusogenic domains in herpes simplex virus type 1 glycoprotein H. J Biol Chem 2005;280:28632-43.
20. Galdiero S, Falanga A, Vitiello M, Raiola L, Fattorusso R, Browne H, et al. Analysis of a membrane interacting region of Herpes Simplex virus type 1 glycoprotein H. J Biol Chem 2008;283:29993-30009.
21. Galdiero S, Falanga A, Vitiello M, Raiola L, Russo L, Pedone C, et al. A single amino acid addition enhances the fusion promotion activity of a membranotropic region of HSV-1 glycoprotein H. J Biol Chem 2010; 285:17123-36.
22. Galdiero S, Galdiero M, Pedone C, Falanga A, Vitiello M. Method For Delivery Of Molecules Into Intracellular Targets – Provisional. n°US61/ 285,619. 12/11/2009.
23. Drin G, Mazel M, Clair P, Mathieu D, Kaczorek M, Temsamani J. Physico-chemical requirements for cellular uptake of pAntp peptide: role of lipid-binding affinity. Eur J Biochem 2001;268:1304-14.
24. Pinaud F, Clarke S, Sittner A, Dahan M. Probing cellular events, one quantum dot at a time. Nat Methods 2010;7:275-85.
25. Medintz IL, Pons T, Delehanty JB, Susumu K, Brunel FM, Dawson PE, et al. Intracellular delivery of quantum dot-protein cargos mediated by cell penetrating peptides. Bioconjug Chem 2008;19:1785-95.
26. Lee H, Kim I-K, Park TG. Intracellular trafficking and unpacking of siRNA/quantum dot-PEI complexes modified with and without cell penetrating peptide: confocal and flow cytometric FRET analysis. Bioconjug Chem 2010;21:289-95.
27. Delehanty JB, Bradburne CE, Boeneman K, Susumu K, Farrell D, Mei BC, et al. Delivering quantum dot-peptide bioconjugates to the cellular cytosol: escaping from the endolysosomal system. Integr Biol 2010;2:265-77.
28. Yeh H-Y, Yates MV, Mulchandani A, Chen W. Molecular beacon-quantum dot-Au nanoparticle hybrid nanoprobes for visualizing virus replication in living cells. Chem Commun 2010;46:3914-6.
29. Jung J, Solanki A, Memoli KA, Kamei K, Kim H, Drahl MA, et al. Selective inhibition of human brain tumor cells through multifunctional quantum-dot-based siRNA delivery. Angew Chem Int Ed 2010;49: 103-7.
30. Rapaport D, Shai Y. Interaction of fluorescently labeled pardaxin and its analogues with lipid bilayers. J Biol Chem 1991;266:23769-75.
31. Mosmann T. Rapid colorimetric assay for cellular growth and survival: application to proliferation and cytotoxicity assays. J Immunol Methods 1983;65:55-63.
32. Imahashi D. Quantitation of LDH isoenzymes by the fluorimetric and colorimetric methods. Can J Med Technol 1968;30:235-48.
33. Hope MJ, Bally MB, Webb G, Cullis PR. Production of large unilamellar vesicles by a rapid extrusion procedure. Characterization of size distribution, trapped volume and ability to maintain a membrane potential. Biochim Biophys Acta 1985;812:55-65.
34. Fiske CH, SubbaRow Y. The colorimetric determination of phosphorus. J Biol Chem 1925;66:374-89.
35. Cummings JE, Vanderlock TK. Aggregation and hemi-fusion of anionic vesicles induced by the antimicrobial peptide cryptdin-4. Biochim Biophys Acta 2007;1768:1796-804.
36. Ellens H, Bentz J, Szoka Jr FC. pH-induced destabilization of phosphatidylethanolamine-containing liposomes: role of bilayer contact. Biochemistry 1984;23:1532-8.
37. Parente RA, Nir S, Szoka Jr FC. Mechanism of leakage of phospholipid vesicle contents induced by the peptide GALA. Biochemistry 1990;29: 8713-9.
38. Matsuzaki K, Murase O, Fujii N, Miyajima K. Translocation of a channel-forming antimicrobial peptide, magainin 2, across lipid bilayers by forming a pore. Biochemistry 1995;34:6521-6.
39. Deshayes S, Gerbal-Chaloin S, Morris MC, Aldrian-Herrada G, Charnet P, Divita G, et al. On the mechanism of non-endosomial peptide-mediated cellular delivery of nucleic acids. Biochim Biophys Acta 2004;1667:141-7.
40. Deshayes S, Heitz A, Morris MC, Charnet P, Divita G, Heitz F. Insight into the mechanism of internalization of the cell-penetrating carrier peptide Pep-1 through conformational analysis. Biochemistry 2004;43:1449-57.
41. Galdiero S, Falanga A, Vitiello G, Vitiello M, Pedone C, D'Errico G, et al. Role of membranotropic sequences from herpes simplex virus type I glycoproteins B and H in the fusion process. Biochim Biophys Acta 2010;1798:579-91.
42. Thorén PE, Persson D, Lincoln P, Nordén B. Membrane destabilizing properties of cell-penetrating peptides. Biophys Chem 2005;114:169-79.
43. McIntyre J, Sleight R. Fluorescence assay for phospholipids membrane asymmetry. Biochemistry 1991;30:11819-27.
44. Angeletti C, Nichols JW. Dithionite quenching rate measurement of the inside-outside membrane bilayer distribution of 7-nitrobenz-2-oxa-1,3-diazol-4-yl-labeled phospholipids. Biochemistry 1998;37:15114-9.
45. Drin G, Cottin S, Blanc E, Rees AR, Temsamani J. Studies on the internalization mechanism of cationic cell-penetrating peptides. J Bio Chem 2003;278:31192-201.

2

Septic Shock by Gram-Negative Infections: Role of Outer Membrane Proteins

Marilena Galdiero[1], Marco Cantisani[2], Rossella Tarallo[2], Annarita Falanga[2] and Stefania Galdiero[2]
[1]*Second University of Naples, Naples*
[2]*University of Naples "Federico II", Naples*
Italy

1. Introduction

The magnitude of septic shock as a clinical problem is often understated. Despite advances in our ability to diagnose and treat infectious diseases, severe sepsis leading to shock due to gram-negative infections remains one of the leading causes of mortality worldwide. Septic shock develops because of a disregulation in the host response, and the mechanisms initially recruited to fight infection produce life-threatening tissue damage and death. Recent research has witnessed a significant increase in our understanding of host-pathogen interactions, particularly in the area of innate immunity and the molecular recognition of gram-positive and gram-negative bacteria. Important new mediators of sepsis and novel mechanisms of host-cell toxicity have been identified and, together with clinical trials targeting pathways considered central to sepsis pathogenesis, provide new insight into the molecular and cellular basis of sepsis for the formulation of new strategies of intervention.
Research on septic shock pathogenesis by gram-negative bacteria is mainly focused on the understanding of the molecular and cellular role played by lipopolysaccharide (LPS). Strong experimental evidence and clinical observations suggest that the release of proinflammatory cytokine mediators by LPS-responsive cells (mainly macrophages, endothelial cells and neutrophils) in response to toxic products sets in motion the genetic and physiologic program that manifests as shock. The best characterized of these toxic components is LPS, which is considered as a paradigm for other less well-characterized toxic microbial molecules. The immune protection stimulated by highly purified LPS in animals does not resolve the symptomatology of septic shock, while LPS mixed to outer membrane proteins shows a better protective activity. Several studies evidence the major role played by outer membrane proteins in the molecular interaction between the host cell and the gram-negative bacteria. Endotoxin-associated proteins consist of a complex of several major proteins that are intimately associated with the LPS. Very little is known about release of non-LPS gram-negative outer membrane components such as OMPs in sepsis. Among the OMPs, porins have been shown to play an important role in pathogenesis of bacterial infections. Porins were pyrogenic in rabbits and elicited a localized reaction when used as the sensiting and eliciting agent. Porins were also shown to kill D-galactosamine sensitized LPS-responsive and LPS-unresponsive mice. Treatment of Human Umbilical Vein Endothelial Cells: (HUVEC) with porins increased the transmigration of different leukocyte populations, in

particular of neutrophils. Porins by several gram-negative bacteria induce cytokine release by human leukocytes as well as enhancement of cytokine gene expression. Also, other components of the bacterial envelope are important in the induction and pathogenesis of septic shock such as bacterial lipoproteins (LP). As anti-LPS therapies does not seem to improve by the addition of proteins from the outer membrane or small fragments of these proteins, a great alternative to existing strategies will involve the blockage of signal transduction pathways, cytokine and inflammatory mechanisms.

2. The outer membrane of gram-negative bacteria

Bacteria in order to face unpredictable and often hostile environment have evolved a sophisticated and complex cell envelope that protects them while allowing selective passage of nutrients from the outside and waste products from the inside. There are three principal layers in the envelope: the outer membrane (OM), the peptidoglycan cell wall, and the inner membrane (IM). The two membrane layers delimit an aqueous cellular compartment called periplasm. The OM is a characteristic feature of Gram-negative bacteria, and in fact Gram-positive bacteria lack this structure. The OM is a lipid bilayer intercalated with proteins, superficially resembling the plasma membrane. The OM does contain phospholipids but they are confined to the inner leaflet of this membrane. The outer leaflet is composed of glycolipids, mainly lipopolysaccharide (LPS).

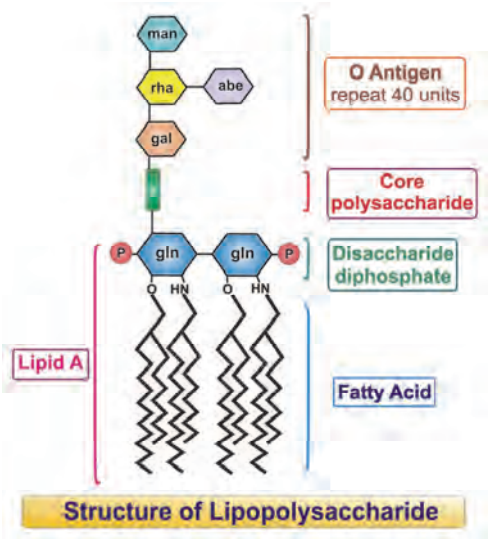

Fig. 1. Schematic representation of the structure of lipopolysaccharide (LPS).

LPS is a complex glycolipid exclusively present in the outer leaflet of the OM of gram-negative bacteria. LPS is one of the molecules responsible for the endotoxic shock associated with the septicemia, and is a sure indicator of infection as the human innate system is sensitized to this molecule. LPS molecules consist of a bisphosphorylated lipid (lipid A) forming the hydrophilic region of the outermost membrane leaflet which is stabilized by divalent cations and a hydrophilic polysaccharide (PS), extending outward from the

bacterium. A schematic structure for LPS from *Escherichia coli* together with the chemical structure of lipid A (Figure 1) reveals its key features. The LPS consists generally of two distinct regions, a core oligosaccharide chain of repeating units, the O-specific chain, which constitutes the major anti-LPS immune response. The core is covalently bound to the lipid A through an acidic sugar, the 3-deoxy-D-manno-oct-2-ulopyranosonic acid (Kdo). The outer core region consists of neutral or amino hexoses such as D-glucose, D-galactose, D-glucosamine, D-galactosamine or N-acetyl derivatives, while the inner core also contains heptose residues which are often substituted by phosphate, pyrophosphate or diphosphoethanolamine. Kdo represent a covalent bridge between lipid A and heptose units joined by diester phosphate linkages. The general pattern of the lipid A from diverse gram-negative bacteria is highly conserved. The lipid A from *E. coli* has a β-1,6-linked D-glucosamine disaccharide phosphorylated in positions 1 and 4′. Lipid A often contains up to four moles of (R)-3-hydroxytetradecanoic acids symmetrically distributed on the two glucosamine residues of the backbone. The hydroxyl in position 6′ is linked to Kdo (Figure 1). The core oligosaccharide is very variable among bacterial species; so different species can express uniquely modified types of LPS. The O-antigen, if present, is the most variable part of LPS and shows even a high degree of variability between different strains of the same species.

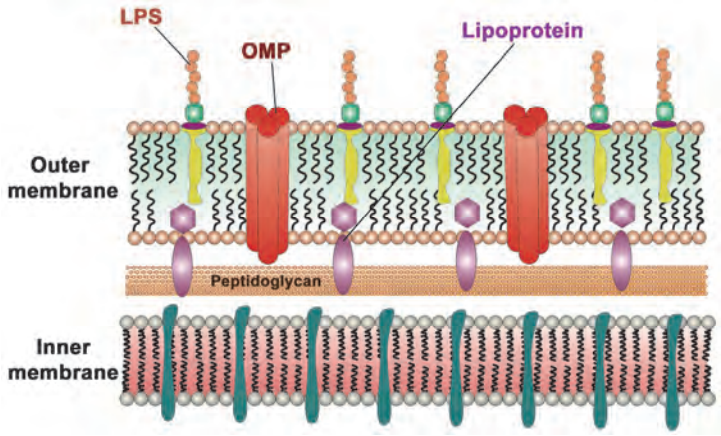

Fig. 2. Schematic representation of the inner and outer bacterial membrane.

With few exceptions, the proteins intercalated in the OM can be divided into two classes, proteins that traverse the membrane and assume a β-barrel structure and lipoproteins, anchoring the outer membrane to the underlying peptidoglycan stratum (Figure 2). Lipoproteins contain lipid moieties that are attached to an amino-terminal cysteine residue. It is generally thought that these lipid moieties embed lipoproteins in the inner leaflet of the OM, and are thus not supposed to be transmembrane proteins. Lipoproteins are low molecular weight proteins and are considered to be the most abundant proteins in the *E. coli* cell on the basis of molecular members. Lipoproteins are generally covalently linked to the peptidoglycan, but may also be present without covalent bonds.

The outer membrane proteins (OMPs) of gram-negative bacteria have been well characterized; they assume a β-barrel conformation. The OMPs serve as a molecular filter for

hydrophilic substances, and mediate the transport of nutrients and ions across the membrane into the periplasm. The OMPs can be divided into three classes (Nikaido, 2003): porins, substrate specific transporters and active transporters. Porins are a group of trimeric proteins that form pores of a fixed diameter through the lipid bilayer of the membrane. They constitute the major component of the OM and are thus indicated as "major outer membrane proteins" of high molecular weight.

Porins form passive pores that do not bind their substrates; they form trimeric, water-filled pores, through which relatively small (<600 Da) solutes diffuse, driven by their concentration gradient. For nutrients that are present at low concentrations in the extracellular environment, passive diffusion is no longer efficient and transport occurs via substrate-specific (substrate specific porins and transporters) and active transporters (Galdiero, 2007). The active transporters (FepA and FhuA) bind their substrates with high affinity and transport them against a concentration gradient. This process requires energy, which is provided by the inner membrane protein Ton B. The substrate-specific porins and transporters contain low affinity substrate saturable binding sites that allow efficient diffusion of substrates at very low concentration gradients. Among the substrate specific porins are LamB (maltose and maltodextrins) and SerY (sucrose); among the substrate specific transporters are Tsx and FadL, while among auto-transporters are NaLP and Hia. Whereas the composition, structure and function of the OM are well known, its assembly in the absence of energy sources has remained largely enigmatic. All the components of the OM are synthesized in the cytoplasm or at the cytoplasmic face of the IM, and they have to be transported across the IM and through the periplasm to reach their destination and to assemble into the OM.

3. The porins

The most abundant proteins of the bacterial outer membrane are porins which form channels with various degrees of selectivity (Schulz, 2002). Porins form β-barrels and their structures typically contain 14, 16 or 18 β-sheets. The majority of porins studied so far belong to the 16 or 18 stranded bacterial porins; and the general motif of their structural architecture is the closure of the barrel by pairing of the first and last β-strand in an antiparallel way. All strands are connected by eight or nine long loops, facing the extracellular side, with seven or eight small turns in the periplasmic space. In all porins, the constriction at the barrel center is formed by an inserted long loop L3, which is not exposed to the cell surface but folds back into the barrel, forming a constriction zone at half the height of the channel and contributing significantly to the permeability of the pore. Another feature is the presence of aromatic girdles with tyrosine and phenylalanine residues located at the outer and inner membrane boundaries. Residues located between these girdles and facing the hydrophobic lipid environment are mainly leucine, valine and isoleucine residues. At the very C-terminus almost all porins have a phenylalanine residue that is fundamental for proper import and folding in the outer membrane.

Porins made of 16 strands are called general or non-specific porins and form pores allowing the diffusion of hydrophilic molecules, showing no particular substrate specificity, despite some selectivity for either cations or anions; while 18 strands porins are substrate specific porins. Porins are passive diffusion channels with a pore diameter ranging from 15 Å for the general porins to 6 Å for the highly selective porins. Larger pores usually contain charged residues at opposite sides that form a local transversal electric field at the pore eyelet. This

field constitutes an energy barrier for low-polarity solutes so that the bacterium can exclude unwanted nonpolar molecules such as antibiotics while presenting a spacious eyelet for collecting large polar molecules such as sugars. A systematic study changing the pore properties by point mutations showed a strong correlation between the eyelet cross section and diffusion rate. Charge reversals affect selectivity and voltage gating. Interesting results were obtained with mutations at loop L3, for example the specificity of the sucrose porin was changed toward that of the maltoporin.

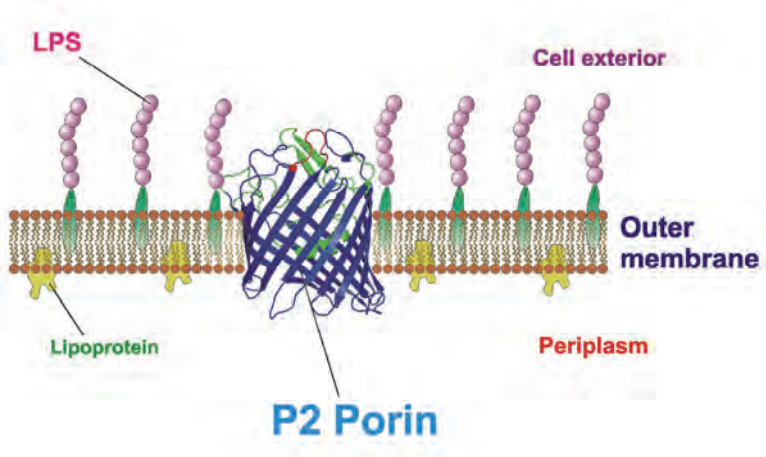

Fig. 3. Three dimensional model of the P2 monomer from *Haemophilus influenzae* type b. Surface loops are shown in green except L7 that is red. The extracellular space is located at the top of the figure and the periplasmic space is at the bottom. The position of the membrane bilayer is shown.

All porins form homotrimers in the OM; each subunit produces a channel and the trimer therefore contains three channels. For most porins, loops L1, L2 and L4 are important for monomer-monomer interactions within the porin trimer; loop L3 is internal; loops L5, L6 and L7 are superficial; loop L8 folds back into the barrel interior, contributing to the formation of the channel opening at the external side (Figure 3). Data from the literature indicate that peptide sequences corresponding to superficial loops are responsible for most of the biological activity of porins. In particular, loop L7 of porin OMPK36 from *Klebsiella pneumoniae* is involved in the interaction with C1q (Alberti, 1995); loops L5, L6 and L7 of porin P2 from *Haemophilus influenzae* activate JNK and p38 mitogen-activated protein kinase (MAPK) pathways (Galdiero, 2003) and induce the release of TNF-α and IL-6 (Galdiero, 2006); most functional antibodies raised to NTHI are directed to loop L5, which is thought to contain strain-specific and immunodominant epitopes (Yi, 1997); antibodies to loop L6 of NTHI showed complement-dependent bactericidal activity (Haase, 1994); the surface exposed loop regions are immunodominant as shown by immunizing mice with whole bacterial cells (Neary, 2001); synthetic peptides representing epitopes of outer membrane protein F of *Pseudomonas aeruginosa* elicit antibodies reactive with whole cells of heterologous immunotype strains of *Pseudomonas aeruginosa* (Hughes, 1992); major immunogenic epitopes of PorA and FetA of *meningococci* correspond to contiguous peptide

sequences located in putative surface-exposed loops of those proteins (Maiden, 1991; Thompson, 2003).

4. Lipoproteins

Lipoproteins are a major component of the outer membrane of bacteria, with low molecular weights (about 7000 Da). Lipid modification of bacterial proteins enables the anchoring of hydrophilic proteins to hydrophobic surfaces through the hydrophobic interaction of the attached acyl groups to the cell wall phospholipids, allowing the protein to function effectively in the aqueous environment (Kamalakkannan, 2004). Lipoproteins can localize in various places of the cell. *E. coli* has more than 90 lipoproteins, the majority of which is located at the periplasmic face of the OM, with some present at the periplasmic face of the IM (Narita, 2004). Although all the known lipoproteins in *E. coli* face the periplasm, in some gram-negative bacteria, lipoproteins are also present on the outer leaflet of the OM. However, little is known about the exact mechanism of how they translocate across the OM whether they are exposed or not to the outside surface of the outer membrane. Moreover, in those *E. coli* strains that have defects in LPS structure, the lipoproteins seem to react with antilipoprotein serum.

Lipoproteins are low molecular weight proteins lacking histidine, tryptophan, glycine, proline and phenylalanine. They are linked by the ε-amino group of their C-terminal lysine to the carboxyl group of every tenth to twelfth meso-diaminopimelic acid residue of the peptidoglycan. The N-terminal portion of the lipoprotein consists of glycerylcysteine to which two fatty acids are linked by two ether linkages and one fatty acid by an amide linkage. The amide-linked fatty acid consists of 65% palmitate, with the rest being mainly monosaturated fatty acids. The fatty acid bound as esters are similar to the fatty acids found in the phospholipids of the inner layer of the membrane. Lipoproteins exist in the membrane also as free form without covalent bonds to the peptidoglycan. There are about 2.4×10^5 molecules of the bound form per cell, and about twice as much of the free form. The total free and bound lipoprotein molecules 7.2×10^5 make lipoproteins the numerically most abundant protein in the membrane. Lipoproteins are required for virulence and play a variety of roles in host-pathogen interactions, from surface adhesion to initiation of inflammatory processes (Kovacs-Simon, 2011).

5. Outer membrane blebbing

Extracellular secretion is the major mechanism by which gram-negative pathogens communicate with and damage host cells. Vesicles released from the envelope of the growing bacteria serve as secretory vehicles for protein and lipids of gram-negative bacteria. Vesicles production occurs in infected tissues and is influenced by environmental factors. Vesicles play an important role in colonization, carrying and transmitting virulence factors into host cells and modulating host defense and immune response. Gram-negative bacteria release membrane vesicles of average diameter 10-300 nm into the environment during all stages of normal growth as well as in a variety of growth environments such as infected tissues. The amount of released vesicles is increased several folds during periods of bacterial stress such as exposure of microorganisms to antibiotics or human serum. The vesicles are formed by protrusions of the bacterial outer membrane that are released into the environment (Ellis, 2010). Outer membrane vesicles (OMVs) are formed by blebbing and

pinching off segments of the bacterial outer membrane (Kulp, 2010). These vesicles contain the main components of the outer membrane such as LPS, OMPs and fractions of the underlying bacterial periplasm. Importantly, OMVs are not a product of cell death since they are produced without concomitant bacterial lysis and newly synthesized proteins are present. Active concentrations of both LPS and porins are often accumulated at infection sites from either gram-negative bacteria outer membrane blebbing or bacterial lysis. Gram-negative bacteria contain about 10^5 molecules of porin per cell (molecular mass, about 36kDa) and about 3.4 x 10^6 molecules of LPS (molecular mass, about 4,5KDa), therefore, 10^6 to 10^9 bacterial cells are enough to reach a concentration of 500 ng/ml to 20 μg/ml (about 0.02 to 0.8 μM) for porin or a concentration of 100 ng/ml to 10 μg/ml (about 0.05 to 5 μM) for LPS.

OMVs from pathogenic bacteria contribute to the pathogenicity in vivo (Ellis, 2010). Thus, OMVs are likely a key factor in effecting an inflammatory response to pathogens, being immunogenic and capable of eliciting proinflammatory responses. Immunization with *Vibrio cholera* OMVs induces protection in mice (Schild, 2008); the OMVs immunized mice were protected against *Salmonella* infections (Alaniz, 2007). Furthermore, OMVs influence inflammation and disease in vivo; it was shown that, in response to *Helicobacter pylori* and *Pseudomonas aeruginosa* OMVs (Bauman, 2006), epithelial cells produce interleukin-8, a cytokine that plays a fundamental role in neutrophil and monocyte recruitment.

Septic shock has been associated with an early excessive inflammatory response to LPS and other bacterial components, among which OMPs and lipoproteins. During sepsis and septic shock large quantities of OMVs are released into serum and tissues. In particular, fragments containing LPS, OMPA and a protein of 17kDa, were affinity purified from filtrate of human serum incubated with *Salmonella enterica* serovar *Abortus equi* using O-chain-specific anti-LPS IgG (Freudenberg, 1992); similarly, complexes containing LPS and at least three OMPs, with molecular masses of 35, 18 and 5-9 kDa were affinity purified from filtrates of normal human serum incubated with *Escherichia coli* cells, using O-chain-specific anti-LPS IgG (Hellman, 2000). These molecules or macromolecular complexes have been shown to derive from the OMVs formed by the blebbing of bacterial cells.

6. OMPs and endothelial cells

Bacteria or bacterial products may constitute important inducers of surface molecule expression on endothelial cells (Rawadi, 1996). The microvascular endothelium plays an important role in regulating the exchange of fluids, macromolecules and cells between the blood and the extravascular tissues. The endothelium is a pervasive organ covering a surface area of 4000-7000 m^2. Endothelial cells are highly active, constantly responding to alteration in the local extracellular environment, as might occur in the setting of transient bacteremia or other important stress such as septic invasion. Endothelial cell activation occurs as a normal adaptative response, the nature and duration of which depends on the type of stimulus. Endothelial cell injury contributes significantly to the pathophysiology of bacterial sepsis and endotoxic shock. Components of the bacterial surface activate pattern recognition receptors on the surface of the endothelium. Gram-negative bacteria contain several surface molecules interacting with endothelial cells. The role of LPS is well known while the roles of other surface molecules of gram-negative bacteria are less understood. Several studies have recently shown the activity of major outer membrane proteins on endothelial cells. The bacterial surface contains a wide assortment of molecules that interfere

with the complex network regulating the leucocyte traffic. The initial adhesion of circulating leukocyte to vascular endothelium is induced by interaction of constitutively functional leukocyte homing receptors with regulated endothelial cell ligands or counter receptors. Leukocyte-endothelial cell interactions both in vivo and in vitro are active multistep processes, as clearly demonstrated in studies of neutrophil interactions with inflamed sites (Von Andrian, 1991). During sepsis a dramatic increase of endothelial cell surface molecules expression occurs that facilitate adhesion of blood leukocytes. These kinds of interactions have been mainly studied in brain microvascular endothelial cells (BMEC).

The crossing of the blood-barrier by circulating bacteria is a complex process, requiring several bacterial and host factors and their interactions, such as a high degree of bacteremia, binding to and invasion of BMEC, BMEC actin cytoskeleton rearrangements and related signaling pathways. Among *E. coli* structures necessary for crossing of the blood-brain barrier in vitro and in vivo, outer membrane protein A (OmpA) contributes to *E. coli* K1 invasion of BMEC (Kim, 2002). OmpA has been implicated as an important virulence factor in several gram-negative bacterial infections such as *E. coli* K1, a leading cause of neonatal meningitis associated with significant mortality and morbidity (Mittal, 2011). *E. coli* K1 OMPA interacts with a gp96 protein on human BMEC. Purified OMPA as well as gp96 and gp96 antibody inhibited *E. coli* K1 invasion of human BMEC in a dose dependent fashion. OMPA is a major outer membrane protein of *E. coli*; it is present as an 8-stranded and anti-parallel β-barrel structure in the membrane, connected by large hydrophilic surface exposed loops and short periplasmic turns (Smith, 2007). Although OMPA's role in pathogenesis has been demonstrated, the exact role of individual loops is still to be determined (Maruvada, 2011). In particular, the synthetic peptides representing a part of the first loop and the tip of the second loop of OMPA have been shown to inhibit *E. coli* adhesion to BMEC (Prasadarao, 1996). The first and second loops are shown to be the sites for the interaction with the carbohydrate epitope of the BMEC receptor glycoprotein. OmpA extracellular loops play a fundamental role in the pathogenesis of meningitis and may help in designing effective preventive strategies against this deadly disease (Mittal, 2011). Loop regions 1 and 2 play an important role in the survival of *E. coli* K1 inside neutrophils and dendritic cells, and loop regions 1 and 3 are needed for survival in macrophages. Mutations in loop 4 of OmpA enhance the severity of the pathogenesis by allowing the pathogen to survive better in circulation and to produce high bacteremia levels. Loop 2 appears to be involved in the majority of the interactions and represents an interesting target for immunization.

Among the major surface proteins, the 34K and 36K porins from *Salmonella typhimurium* modulate leukocyte migration by acting on endothelial cells and leukocytes. The transmigration increase was dose-dependent and optimal endothelial activation occurred after 4-6 hours using porin as stimulus, after 2-4 hours using LPS. Stimulation of leukocytes with either porins or LPS slightly increased their transmigration through porin-non-activated endothelial cells. The simultaneous stimulation in vitro of HUVEC with IL-1β and either porins or LPS causes overlapping effects leading to a very high migration index (Galdiero, 1999). In natural inflammatory process the combination of several stimuli induces high endothelial permeability of vessels to migrating cells. The main adhesion molecules of endothelial cells are activated by porins. Neutrophil transmigration through HUVEC cells treated with porins was partially inhibited by MoAbs binding to E-selectin; the transmigration of lymphocytes and monocytes was partially inhibited by MoAb anti-VCAM-1; the transmigration of neutrophils, lymphocytes and monocytes was partially inhibited by MoAb anti ICAM-1. Soluble E-selectin and ICAM-1 were found in the

supernatants from IL-1 and TNF-α activated endothelial cells. Also porins were able to stimulate the release of soluble E-selectin and soluble ICAM-1. Protein H from *Pasteurella multocida* in vitro induces neutrophil adhesion and transmigration through bovine endothelial cells (Galdiero, 2000). An increase of the expression of the vascular cell adhesion molecule 1 on the aortic endothelium has been reported in rabbit experimentally infected with *Pasteurella multocida* (Galdiero, 2000). These results evidence a local and systemic microcirculatory dysfunction that is considered central in the development of multiple organ dysfunction syndromes in septic shock.

7. OMPs and host-cells

Among surface components, porins and LPS may be important inducers of biological activity in host-interactions. Several studies have been carried out to dissect the immunobiological activities of *Salmonella enterica* or *typhimurium* porins, showing that these proteins have important effects on macrophage viability and functions; in particular, porins inhibit their phagocytic activity in a dose dependent fashion by activating the adenylate cyclase system (Di Donato, 1986). Porins induce the activation of the complement system by acting both on the classic pathway and on the alternative pathway (Galdiero, 1984), acting as mitogens for B lymphocytes. Furthermore, in rats they increase the toxicity of cardio-toxic molecules (Galdiero, 1986) and damage renal tubules (Tufano, 1987). Porins are clearly endowed with pro-inflammatory activity; when injected into the rat paw induce dose-dependent edema with long-lasting effects. The inflammation induced by porins is sensitive to both steroid (dexamethasone) and non-steroid (indomethacin) anti-inflammatory drugs. The in vitro studies carried out on peritoneal cells of the rat show that porins are able to induce the release of histamine and also of prostacyclin. Porin-induced inflammation may depend on the release of histamine, even though the arachidonic acid metabolites may also participate. In fact, in vitro results exclude an increase of 6-keto-prostaglandin and subsequent prostacyclin release, whereas in vivo results confirm both the prolonged duration of porin-induced edema and its marked inhibition by indomethacin. Porin-induced inflammation was also observed in decomplemented animals; therefore, it is unlikely that the activation of the complement system plays a major role in the inflammation induced by porins (Galdiero, 1984). Porins isolated from *S. typhimurium* are lethal at the dose of 100 ng to both LPS-responder (BALB/cByS) and non responder (C3H/HeJ) mice sensitized with D-galactosamine. The lethal action could be prevented by anti-TNF-α serum. Porins were also pyrogenic to rabbits and elicited a Shwartzman reaction when used as the sensitizing and eliciting agent (Galdiero, 1994). *Haemophilus influenza* type b (Hib) porin also induces the early release of cytokines in central nervous system cells, amplifying the inflammatory response. Hib porin inserted into the fourth ventricle of the brain elicited the appearance of serum proteins and the development of brain edema. These modifications were followed by increase in the number of neutrophils both in cerebrospinal fluid and in the tissue sections around the porin inoculation site. IL-1α, TNF-α and MIP-2 mRNA appeared quickly in the tissue near the inoculation site (Galdiero, 2001a).

Activation of the coagulation and fibrinolytic systems is an important manifestation of the systemic inflammatory response of the host to infection. The in vivo effect of a synthetic peptide corresponding to loop L7 from *Haemophilus influenzae* type b (Hib) porin was compared with the effect of the entire protein to evaluate its role on the coagulative/fibrinolytic cascade and the circulating markers of endothelial injury (Vitiello,

2008). Plasma was obtained from rats injected intravenously with the peptide and tested for fragment 1+2 (F1+2), tissue-type plasminogen activator (tPA), plasminogen activator inhibitor type I (PAI-1) antigen, von Willebrand factor (vWF) and soluble E-selectin (sE-selectin). The coagulative/fibrinolytic cascade was impaired as determined by the increased level of PAI-1. Concomitantly, E-selectin, a marker of endothelial injury, was also significantly elevated. In addition either loop L7 or Hib porin injection induced hyperglycaemia and inflammatory cytokine production. The data were correlated with hemodynamic functions (significant reduction of blood pressure and increase of heart rate). The results indicated that, in that experimental model, the loop L7 plays an essential role in the pathophysiologic events observed during gram-negative infection.

OMPA from *E. coli* K1 plays a fundamental role in pathogenesis and great importance are correlated with the host signaling events underlying its entry into host cells. OMPA contributes to endothelial cells activation through a ligand- receptor interaction. OMPA activates PI3K but exhibited no effect on RhoA activation. The RhoA and PI3K host cell signaling pathways involvement in *E. coli* K1 invasion of human BMEC was further supported by the treatment of human BMEC with Rho kinase inhibitor (Y27632) and PI3K inhibitor (LY294002) which resulted in significant greater inhibition of *E. coli* K1 invasion compared to individual inhibitors alone.

The properties of Lipid-A associated proteins (LAP) have been extensively reviewed by Hitchcock and Morris (Hitchcock, 1984). Preparations of LAP from *S. typhimurium* have IL-1 like properties. LAP from *Actinobacillus actinomycetemcomitans*, an aquaporin associated with various forms of inflammatory periodontal disease, stimulate the release of IL-1β and IL-6 from human monocytes or human gingival fibroblast. LAP from *Porphyromonas gingivalis*, one of the causative organisms of peridontitis, are potent stimulators of IL-6 release from human gingivalis fibroblasts (Reddi, 1995).

8. Activation of eukaryotic cell signaling and transcriptional activation induced by OMPs

The molecular mechanisms during the interaction of gram-negative bacteria with macrophages are well understood, but the mechanisms used by porins to activate cells is not well characterized. LPS, porins or other OMPs probably activate cells through similar but not identical mechanisms (Galdiero, 2003b). A variety of extracellular factors, such as growth factors or bacterial surface components, induce a complex cellular signaling by binding specific transmembrane receptors on the host cell membrane. The intracellular signaling pathways are complex networks of biochemical events that culminate in specific patterns of nuclear gene expression mediated by transcription factors. Signal transduction pathways and transcriptional activation known to occur during immune cell activation have been investigated by numerous authors and protein tyrosine phosphorylation plays a central role in transduction mediated by bacteria or LPS or toxins (Evans, 1998; Rosenshine, 1992; Weinstein, 1992). Cytoplasmic signal transduction is regulated by several enzymatic pathways among which the mitogen-activated protein kinase (MAPK) pathway is especially activated during the adhesion and penetration of bacteria into the host cell (Evans, 1998; Rosenshine, 1992) and when stimulating the cell with products of bacterial origin (Weinstein, 1992).

MAPK/extracellular signal-regulated kinases are serine/threonine protein kinase members of sequential protein phosphorylation pathways involving c-Jun N-terminal kinases (JNKs)

and ERKs (Davis, 2000). The MAPK pathway activates a number of transcription factors such as activating protein-1 (AP-1) and nuclear factor-kappa B (NFκB). The contribution of AP-1 family members to transcriptional regulation is controlled by a number of well characterized mechanisms (Karin, 1997). AP-1 is a ubiquitous class of gene regulatory factors and AP-1 proteins form either Jun-Jun homodimers comprised of members of the Jun family (c-Jun, JunD, and JunB) or Fos-Jun heterodimers derived from the various Fos family members. The AP-1 family members differ in their abilities to transactivate or repress transcription (Karin, 1997). NF-κB is a dimeric transcription factor and has multiple functions in immunity and is also critical for development and cellular survival. Mammalian cells contain five NF-κB subunits (p65, c-Rel, RelB, p50and p52) which form various hetero- and homodimers. NF-κB is present in the cytoplasm of resting cells bound to its inhibitor IκBα. The activation of NF-κB requires sequential phosphorylation, ubiquitination, and degradation of IκB. Multiple kinases have been shown to phosphorylate IκB at specific amino-terminal serine residues. In response to a large spectrum of chemically diverse agents and cellular stress conditions including LPS and porins, microbial and viral pathogens, cytokines and growth factors, NF-κB translocates in the nucleus, activating expression of target genes mainly involved in inflammatory and immunological responses (Caamano, 2002).

Several studies have addressed the mechanism by which porins stimulate cells. *S. enterica* serovar typhimurium porins induce signal transduction in mouse macrophages (Gupta, 1999). Porin activation of macrophages results in increased inositol triphosphate and intracellular Ca^{2+} mobilization, translocation of protein kinase C (PKC) to the membrane, NO release within the macrophages and increased binding of infected macrophages resulting in macrophage activation and triggering of specific signaling pathways. *S. enterica* serovar typhimurium, *Mannheimia haemolytica*, and *Haemophilus influenzae* (Hib) porins induce tyrosine phosphorylation in THP-1 cells and in C3H/HeJ mouse macrophages (Galdiero, 2001), with Hib porin being the most powerful stimulator. Incubation of porins with either THP-1 or macrophages from C3H/HeJ mice resulted in tyrosine phosphorylation of specific host cell proteins with the appearance of tyrosine-phosphorylated proteins in the soluble cytoplasmic fraction, in the membrane fraction and in the insoluble protein fraction. The pattern of phosphorylation observed following LPS or porin stimulation is essentially similar, but a difference can be observed in the cytoplasmic fraction bands of 50-60 kDa, which are more evident after treatment with LPS, and in the insoluble fraction band of 80kDa and the cytoplasmic fraction band of 250kDa, which are more evident after porin treatment.

Among the most prominent tyrosine-phosphorylated bands in porin-stimulated cells, a number of proteins with a molecular mass that is similar to that of the family of tyrosine/serine/threonine protein kinases were observed. *S. enterica* serovar typhimurium porins induce tyrosine phosphorylation of ERK1-2. Porins of *S. enterica* serovar typhimurium were also able to stimulate protein kinase A (PKA), PKC and protein-tyrosine kinase (NT-PTKs) in U937 cells. In the cells pretreated with tyrphostin, a specific PTK inhibitor, or with H-89, a specific PKA inhibitor, or calphostin C, a specific PKC inhibitor, decrease of the relevant activity was observed (Galdiero, 2003a).

Neisserial porins induce protein tyrosine phosphorylation and alter the surface expression of the co-stimulatory molecule B7-2 (Massari, 2003). Recent evidence suggests that the Raf-1-MEK1/2-MAPK pathways are included among the proteins which are phosphorylated following porin stimulation (Galdiero, 2002). The use of some specific inhibitors of phosphorylation pathways such as SB-203580 (p38 inhibitor), PD-098059 (MEK/ERK kinase

inhibitor) and forskolin (Raf-1 inhibitor) demonstrated that they modulate in a different way cytokine mRNA expression in cells stimulated with porins. Neisserial porins induce nuclear translocation of the transcription factor NF-κB in B cells and dendritic cells that was maximal by 3 h of stimulation (Massari, 2003). *S. enterica* serovar typhimurium porins also activate AP-1 and NF-κB in U937 cells involving the Raf-1-MEK1/2-MAPK pathways (Galdiero, 2002); pretreatment with PD-098059 and with SB-203580 markedly affected the activation, indicating that the p38 signaling pathway is mainly involved in AP-1 and NF-κB activation. In contrast, forskolin pretreatment did not block transcription factor activation by porins, suggesting that a Raf-1-independent pathway may also be involved following porin stimulation. Electrophoresis mobility shift assays, using antibodies to specific transcription factor protein subunits, showed that in U937 cells the AP-1 complex contains Jun-D and c-Fos heterodimers and probably no other homodimers or heterodimers. In U937 cells treated with LPS, AP-1 complexes containing Jun-D, c-Fos and c-Jun appeared, while stimulation by porins induces AP-1 complexes containing fra-2 in addition to the other subunits. The formation of a different complex represents a further difference between stimulation with LPS and stimulation with porins. This may be added to past observations where mRNA

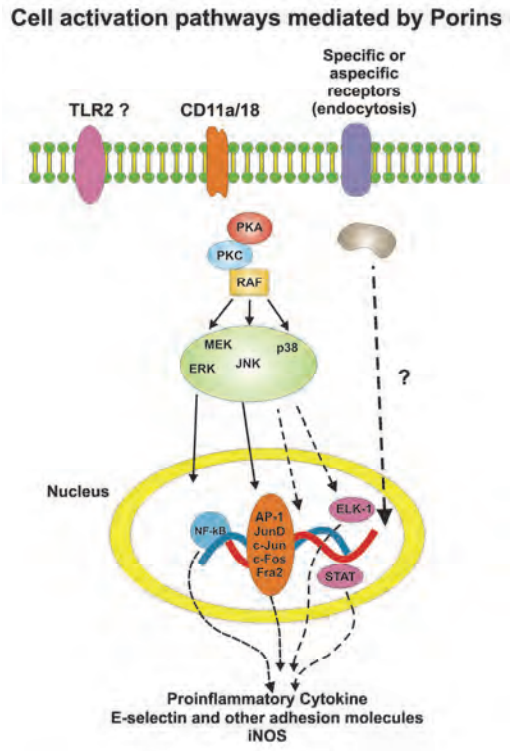

Fig. 4. Speculative scheme of porin signal transduction pathways. Putative porin-specific receptors are shown to be transmembrane. The solid arrows indicate the known association between superficial porin receptors and activation of several transcription factors; dotted arrows indicate hypothetical events.

cytokine expression after stimulation with porin begins after 120 min and continues for 5-6 h, while following LPS stimulation begins after 30 min and decreases at 120 min. Forskolin did not block NF-κB translocation after porin stimulation. Raf-1 induces the dissociation of cytoplasmic NF-κB-IκB complexes (Li, 1993), suggesting that a Raf-1-dependent pathway may be involved in NF-κB activation. However, it is known that PKC triggers the activation of several kinases suggesting that MEK/ERK pathways may also participate in NF-κB activation by enhancing an AP-1-NF-κB cross-coupling mechanism. The porin P2 from *Hib*, like porins from *S. enterica* serovar typhimurium, activates mainly but not exclusively the JNK and p38 pathways. Synthetic peptides, corresponding to the amino acid sequences of variable loop regions facing the cell exterior and thus more probably involved in the initial interaction with the host cell, proved to be able to activate the MEK1-MEK2/MAPK pathways similarly to the entire protein. In contrast, peptides modelled on internal β-strands were ineffective in inducing phosphorylation of such pathways (Galdiero, 2003c).
A speculative scheme of signal transduction pathways involved in porin-mediated responses is depicted in Figure 4. Accumulating evidence has suggested that the regulation of transcriptional factors and the subunit composition by porin stimulation may affect the adaptive immune mechanism to modulate the production of biologically active proteins or peptides. The engagement of multiple pathways during signal transmission makes the possible use of molecular inhibitors as therapeutic agents very difficult; although recent findings show that peptides complementary to loop regions have a certain ability to block the activity of the porin (Cantisani, 2011).

9. OMPs and septic shock

Septic shock is a major cause of death in the world. Gram-negative infection frequently results in systemic manifestations of sepsis and septic shock. The systemic syndrome is caused by the host response to gram-negative surface components. This response may set in motion a cascade of pathophysiologic consequences that result in multiple organ systemic failure and death. The host response to gram-negative bacterial infection is complex and multifaceted. Strong experimental evidence and clinical observations suggest that the release of proinflammatory cytokine mediators in response to toxic bacterial products set in motion an uncontrolled pathophysiologic program that manifests as sepsis or septic shock. The best characterized and most important of these toxic products is gram-negative endotoxin. For the general scientific public, the terms endotoxin and LPS are interchangeable. The term lipopolysaccharide (LPS) obtained by using the Westphal extraction procedure (Westphal, 1952), should be reserved for purified bacterial LPS extracts which are free of detectable contaminants, particularly proteins. In contrast, the term endotoxin should be used to refer to macromolecular complexes of LPS, protein and phospholipid normally obtained by extraction of bacteria with trichloroacetic acid, butanol and EDTA. Endotoxin associated protein consist of complex of four or five major proteins that range in size from 10 to 35 kDa. Originally considered to be a superfluous carrier of LPS, endotoxin associated proteins are now recognized to have potent biological activities (Mangan, 1992). Endotoxin associated proteins are powerful mitogen for C3H/HeJ mice, which are hyporesponsive to LPS. Techniques previously used in the extraction of stable LPS from the endotoxin had greatly favored the study of this portion of the molecule, ignoring the denaturable protein fraction, allowing the identification of most of the effects of endotoxin with those of LPS. Subsequent extraction techniques for membrane proteins (in

their native form) then allowed the study of the protein fraction, which was extracted globally in the endotoxin (Hindennach, 1975). Although much is known about the role of LPS in septic shock, little is known about the role of the proteic components. Approximately 50% of the dry mass of the outer membrane of the gram-negative bacteria consists of proteins and more than 20 immunochemically distinct proteins (OMPs) have been identified in *E. coli*. Several OMPs have been shown to be potent inducers of cytokine synthesis. The most abundant of OMPs are porins. Porins isolated from *Salmonella enterica* serovar typhimurium, *Yersimia enterocolitica*, and *Mannheimia haemolytica* have been shown to stimulate the release of a range of proinflammatory and immunomodulating cytokines including IL-1, IL-4, Il-6, IL-8, TNF-α and INN-γ by monocytes and lymphocytes. Porins stimulate also the release of granulocyte-monocyte colony stimulating factor (GM-CSF), soluble intercellular adhesion molecule-1 (ICAM-1) and soluble E-selectin (SE-selectin) in a dose-dependent fashion by HUVEC cells (Donnarumma, 1996).

In vitro and in vivo experiments supported the involvement of porins in the septic shock pathogenesis. The administration of porin to animals affects their hemodynamics, body temperature, blood clotting, cellular and humoral immunities proliferation of B lymphocytes and macrophages, and release of various endogenous mediators. The role played by porins and in general by OMPs in sepsis has been further supported by conflicting results obtained with the immunotherapy. The notion that the core regions of most strains of gram-negative bacterial LPS were quite similar, supported the development of a broadly effective immunotherapy for gram-negative sepsis using antibodies raised against LPS, through the use of a bacterial strain with an outer membrane that features no side chains, while bearing only the conserved core elements of LPS. The strain selected was the J5 mutant of *E. coli* O111:B4, whose LPS contains only the core determinants, primarily lipid A. Although it has generally been assumed that immunoglobulins to rough mutant *E. coli* J5 protect by binding to LPS, it has been demonstrated that IgG in those antisera bind only weakly to LPS from heterologous gram-negative strains. Also anti-lipid A monoclonal antibodies did not induce the expected results (Siber, 1985). Recently, it has been demonstrated that IgG in polyclonal antiserum raised to heat-killed *E. coli* J5 binds to three conserved gram-negative bacterial outer-membrane proteins. (5-9, 18, and 35 kDa). These OMPs are exposed on the surface of bacterial cells and are released into human serum in complexes that also contain LPS (Binkley, 1945). The role of porins in pathogenesis is also confirmed by studies on the development of an effective vaccine against serogroup B *Neisseria meningitides*. The nonimmunogenicity of serogroup B capsular polysaccharide has led to the development of outer membrane vesicle (OMV) vaccines, based on the presence of PorB (Jolley, 2001; Wright, 2002). The porin proteins adopt a β-sheet structure within the outer membrane with surface exposed loops (Van der Ley, 1991). OMPs epitopes mainly involved in the interaction with the host cells are those on the surface. The wide antigenic variability of gram-negative bacteria is due also to the great sequence amino acid variability of surface exposed loops. Although, cross-reactivity of the major OMPs of *Enterobacteriacae* has been reported by several investigators (Hofstra 1979, Hofstra, 1980), their role in the pathogenesis of sepsis and shock has not been fully dissected.

Bacterial lipoproteins are important in the induction and pathogenesis of septic shock; in fact, they induce proinflammatory cytokine production in macrophages and lethal shock in LPS-responsive and nonresponsive mice. Lipoproteins are released from growing bacteria and released lipoproteins may play an important role in the induction of cytokine production and pathologic changes associated with gram-negative bacterial infections; treatment of bacteria with antibiotics significantly enhances lipoprotein release.

Lipoproteins activate macrophages; induce lethal shock in mice, and act synergistically with LPS to induce these responses (Zhang, 1997). Some gram-negative microorganisms have the ability to secrete lipoproteins to the extracellular environment; among those peptidoglycan-associated lipoproteins, Pal is released into the bloodstream during infection, and this process contributes to the development of septic shock (Hellman, 2002; Liang, 2005). Lipoproteins play an important role in septic shock induced by bacteria; moreover, they act synergistically with LPS to induce lethal shock which suggest that they activate cells through different mechanisms. Bacterial lipoproteins have been shown to affect both the innate and acquired immune system via TLR2 signaling and generation of cytotoxic T lymphocytes and bactericidal antibodies (Masignani, 2003).

10. Novel perspectives for therapies

Gram-negative sepsis remains a significant cause of morbidity and mortality in site of the ongoing development of new antimicrobial agents (Lazaron, 1999); the reason may be attributed to the failure of antimicrobial therapy to address the described pathogenetic mechanism involved in the systemic inflammatory response due to gram-negative bacteria. The systemic syndrome is caused by the host response to gram-negative infection; which sets in motion a cascade of pathophysiologic consequences that result in dysregulation of hemodynamics, oxygen use, and intermediate metabolism, and often results in multiple organ failure with further increased morbidity and mortality; these may happen also after apparent eradication of the original infection. The immunotherapy in the treatment of sepsis and shock did not produce the expected results. In fact, polyclonal *E. coli* J5 antiserum is not suitable for commercial development, especially for the viability of antiserum activity. The mass production of IgM monoclonal antibodies allowed the obtainment of an antibody E5 binding more specifically to Lipid A. E5 monoclonal antiserum, tested in two randomized placebo-controlled clinical trials demonstrated no clinical benefit to patients with gram-negative sepsis (Greenman, 1991). Also a human hybrid monoclonal antibody, HA-1A has been problematic. Anti-LPS core directed antibodies have not shown a survival benefit in clinical trials. The sometimes protective results observed using polyclonal *E. coli* J5 antiserum, may be attributed to the presence of antibodies against surface epitopes of OMPs. The great variability of surface loops of OMPs makes it rather difficult the preparation of specific antiserum that could be used for all gram-negative infections. As death by septic shock has been derived by an early excessive inflammatory response, therapeutic strategies have been designed to block the cytokines and other mediators involved into pathogenesis. However, the sepsis and septic shock are not restricted only to the activation of the inflammatory response, but also to compensatory anti-inflammatory mechanism usually leading to immunosuppression. Patients in this state have a poor prognosis; in fact, the majority of deaths occur in patients with sepsis who are immunosuppressed (Adib-Conquy, 2009).

11. Acknowledgment

This work was supported by MIUR (FIRB Prot. RBRN07BMCT)

12. References

Adib-Conquy, M. & Cavaillon, J.M. (2009). Compensatory anti-inflammatory response syndrome. *Journal of Thrombosis and Haemostasis*, Vol.101, No.1, pp.36-47.

Alaniz, R.C., Deatherage, B.L., Lara, J.C. & Cookson, B.T. (2007). Membrane vesicles are immunogenic facsimiles of Salmonella typhimurium that potently activate dendritic cells, prime B and T cell responses, and stimulate protective immunity in vivo. *Journal of Immunology*, Vol.179, No.11, pp.7692-701.

Alberti, S., Rodriquez-Quinones, F., Schirmer, T., Rummel, G., Tomas, J. M., Rosenbusch, J. P. & Benedi, V. J. (1995). A porin from Klebsiella pneumoniae: sequence homology, three-dimensional model, and complement binding. *Infection and Immunity*, Vol.63, No.3, pp.903-910.

Bauman, S.J. & Kuehn, M.J. (2006). Purification of outer membrane vesicles from Pseudomonas aeruginosa and their activation of an IL-8 response. *Microbes and Infection*, Vol.8, No.9-10, pp. 2400-2408.

Binkley, F., Goebel, W.F., & Perlman, E. (1945). Studies in the Flexner group of dysentery bacilli. II. The chemical degradation of the specific antigen of type Z Shigella paradysenteiae (Flexner). *Journal Experimental Medicine*, Vol.81, No.4, pp.331–341.

Caamano, J. & Hunter, C.A. (2002) NF-UB family of transcription factors: central regulators of innate and adaptive immune functions. *Clinical Microbiology Reviews*, Vol.15, No.3, pp.419-429.

Cantisani, M., Vitiello, M., Falanga, A., Finamore, E., Pedone, C., Galdiero, M. & Galdiero, S. (2011) Peptides complementary to the active loop of porin P2 from Haemophilus influenzae modulate its activity, unpublished data

Davis, R.J. (2000) Signal transduction by the JNK group of MAP kinases. *Cell*, Vol.103, No.2, pp.239-252.

Di Donato, A., Draetta, G.F., Illiano, G., Tufano, M.A., Sommese, L. & Galdiero, F. (1986) Do porins inhibit the macrophage phagocyting activity? *Journal of Cyclic Nucleotide and Protein Phosphorylation Research* Vol.11, No.2, pp.87-97.

Donnarumma, G., Brancaccio, F., Cipollaro de l'Ero, G., Folgore, A., Marcatili, A. & Galdiero, M. (1996) Release of GM-CSF, sE-Selectin, and sICAM-1 by human vascular endothelium stimulated with gram-negative and gram-positive bacterial components. *Endothelium* Vol.4, pp.11-22.

Ellis, T.N. & Kuehn, M.J. (2010) Virulence and immunomodulatory roles of bacterial outer membrane vesicles. *Microbiology Molecular Biology Review* Vol.74, No.1, pp.81-94.

Evans, D.J., Frank, D.W., Finck-Barbancon, V., Wu, C. & Fleiszig, S.M. (1998) Pseudomonas aeruginosa invasion and cytotoxicity are independent events, both of which involve protein tyrosine kinase activity. *Infection and Immunity*, Vol.66, No.4, pp.1453-1459.

Freudenberg, M. A., Meier-Dieter, U., Staehelin, T. & Galanos, C. (1991) Analysis of LPS released from Salmonella abortus equi in human serum. *Microbial Pathogenesis*, Vol.10, No.2, pp.93–104.

Galdiero, F., Tufano, M.A., Sommese, L., Folgore, A. & Tedesco, F. (1984) Activation of complement system by porins extracted from Salmonella typhimurium. *Infection and Immunity* Vol.46, No.2, pp.559–563.

Galdiero, F., Tufano, M.A., Rossi, F., Filippelli, W., De Santis, D., Matera, C., Berrino, L. & Marmo, E. (1986) Effect of Salmonella typhimurium porins on the cardiovascular and renal apparatus. *Journal of Medicine*. Vol.17, No.5-6, pp.285–297.

Galdiero, F., Sommese, L., Scarfogliero, P. & Galdiero, M. (1994) Biological activities-lethality, Shwartzman reaction and pyrogenicity- of salmonella typhimurium porins. *Microbial Pathogenesis* Vol.16, No.2, pp.111-119.

Galdiero, M., Folgore, A., Molitierno, M. & Greco, R. (1999) Porins and lipopolysaccharide (LPS) from Salmonella typhimurium induce leucocyte transmigration through human endothelial cells in vitro. *Clinical and Experimental Immunology*, Vol. 116, No.3, pp.453-461.

Galdiero, M., Folgore, A., Nuzzo, I. & Galdiero, E. (2000) Neutrophil adhesion and transmigration through Bovine endothelial cells in vitro by protein H and LPS of Pasteurella multocida. *Immunobiology*, Vol.202, No.3, pp. 226-238.

Galdiero, M., D'Amico, M., Gorga, F., Di Filippo, C., D'Isanto, M., Vitiello, M., Longanella, A. & Tortora, A. (2001a) Haemophilus influenzae porin contributes to signaling of the inflammatory cascade in rat brain. *Infection and Immunity*, Vol.69, No.1, pp.221-227.

Galdiero, M., Vitiello, M., D'Isanto, M., Peluso, L. & Galdiero, M. (2001b) Induction of tyrosine phosphorylated proteins in THP-1 cells by Salmonella typhimurium, Pasteurella haemolytica and Haemophilus influenzae porins. *FEMS Immunology and Medical Microbiology*, Vol.31, No.2, pp.121-130.

Galdiero, M., Vitiello, M., Sanzari, E., D'Isanto, M., Tortora, A., Longanella, A. & Galdiero, S. (2002) Porins from Salmonella enterica serovar Typhimurium activate the transcription factors activating protein 1 and NF-kappaB through the Raf-1-mitogen-activated protein kinase cascade. *Infection and Immunity*, Vol.70, No.2, pp.558-568.

Galdiero, M., D'Isanto, M., Vitiello, M., Finamore, E., Peluso, L. & Galdiero, M. (2003a) Monocyte activation of protein-tyrosine-kinase, protein kinase A and protein kinase C induced by porins isolated from Salmonella enterica serovar Typhimurium. *Journal of Infection*, Vol.46, pp.111-119.

Galdiero, M., Vitiello, M. & Galdiero S. (2003b) Eukaryotic cell signaling and transcriptional activation induced by bacterial porins. *FEMS Microbiology Letters*, Vol.226, No.1, pp.57-64.

Galdiero, S., Capasso, D., Vitiello, M., D'Isanto, M., Pedone, C. & Galdiero, M. (2003c) Role of surface-exposed loops of Haemophilus influenzae protein P2 in the mitogen-activated protein kinase cascade. *Infection and Immunity*, Vol.71, No.5, pp.2798-2809.

Galdiero, S., Vitello, M., Amodeo, P., D'Isanto, M., Cantisani, M., Pedone, C. & Galdiero, M. (2006) Structural requirements for proinflammatory activity of porin P2 Loop 7 from Haemophilus influenzae. *Biochemistry,* Vol.45, No.14, pp.4491– 4501.

Galdiero, S., Galdiero, M. & Pedone C. (2007). β-barrel membrane bacterial proteins: structure, function, assembly and interaction with lipids. *Current Protein & Peptide Science*, Vol.8, (No.1) pp.63-82.

Greenman, R.L., Schein, R.M., Martin, M.A., Wenzel, R.P., MacIntyre, N.R., Emmanuel, G., Chmel, H., Kohler, R.B., McCarthy, M., Plouffe, J., et al. (1991) A controlled clinical trial of E5 murine monoclonal IgM antibody to endotoxin in the treatment of gram-negative sepsis. The XOMA Sepsis Study Group. *JAMA*, Vol.266, No.8, pp.1097-1102.

Gupta, S., Kumar, D., Vohra, H. & Ganguly, N.K. (1999) Involvement of signal transduction pathways in Salmonella typhimurium porin activated gut macrophages. *Molecular and Cellular Biochemistry*, Vol.194, No.1-2, pp.235-243.

Haase, E. M., Yi, K., Morse, G. D. & Murphy, T. F. (1994) Mapping of bactericidal epitopes on the P2 porin protein of nontypeable Haemophilus influenzae. *Infection and Immunity*, Vol.62, No.9, pp.3712–3722.

Hellman, J., Loiselle, P.M., Tehan, M.M., Allaire, J.E., Boyle, L.A., Kurnick, J.T., Andrews, Sik, D.M., Kim, K. & Warren, H.S. (2000) Outer membrane protein A, peptidoglycan-associated lipoprotein, and murein lipoprotein are released by Escherichia coli bacteria into serum. *Infection and Immunity*, Vol.68, No.5, pp.2566-2572.

Hellman, J., Roberts, J.D., Tehan, M.M. Allaire, J.E. & Warren, H.S. (2002) Bacterial peptidoglycan-associated lipoprotein is released into the bloodstream in gram-negative sepsis and causes inflammation and death in mice. *The Journal of Biological Chemistry*, Vol. 277, No.16, pp. 14274-14280.

Hindennach, I. & Henning, U. (1975) The major proteins of Escherichia coli outer cell envelope membrane preparative isolation of all major membrane proteins. *European Journal of Biochemistry,* Vol.59, No.1, pp.207-213.

Hitchcock, P. J., & Morrison, D. C. (1984) The protein component of bacterial endotoxins, pp. 339–374. In E. T. Rietschel (ed.), Handbook of endotoxin, vol. 1. Chemistry of endotoxin. Elsevier/North-Holland Publishing Co., Amsterdam.

Hofstra, H. & Dankert, J. (1979) Antigenic cross-reactivity of major outer membrane proteins in Enterobacteriaceae species. *Journal General Microbiology,* Vol.111, No.2, pp.293-302.

Hofstra, H., Van Tol, M.J.D. & Dankert, J. (1980) Cross-reactivity of major outer membrane proteins of Enterobacteriaceae, studied by crossed immunoelectrophoresis. *Journal of Bacteriology,* Vol.143, No.1, pp.328-337.

Hughes, E.E., Gilleland, L.B. & Gilleland, H.E.jr (1992) Synthetic peptides representing epitopes of outer membrane protein F of Pseudomonas aeruginosa that elicit antibodies reactive with whole cells of heterologous immunotype strains of P. aeruginosa. *Infection and Immunity*, Vol. 60, No.9, pp.3497-3503.

Jolley, K.A., Appleby, L., Wright, J.C., Christodoulides, M. & Heckels, J.E. (2001) Immunization with recombinant Opc outer membrane protein from Neisseria meningitides: influence of sequence variation and levels of expression on the bactericidal immune response against meningococci. *Infection and Immunity,* Vol.69, No.6, pp.3809-3916.

Kamalakkannan, S., Murugan, V., Jagannadham, M.V., Nagaraj, R. & Sankaran, K. (2004) Bacterial lipid modification of proteins for novel protein engineering applications. *Protein Engineering Design Selection*, Vol.17, No.10, pp.721-729.

Karin, M., Liu, Z. & Zandi, E. (1997) AP-1 function and regulation. *Current Opinion Cell Biology*, Vol.9, No.2, pp.240-246.

Kim, K.S. (2002) Strategy of Escherichia coli for crossing the blood-brain barrier. *The Journal of Infection Disease*, Vol.186, Suppl 2, pp.S220-224.

Kovacs-Simon, A., Titball, R.W., Michell, S.L. (2011) Lipoproteins of bacterial pathogens. *Infection and Immunity*, Vol79, No.2, pp548-561.

Kulp, A. & Kuehn, M.J. (2010) Biological functions and biogenesis of secreted bacterial outer membrane vesicles. *Annual Review Microbiology*, Vol.64, pp.163-84.

Lazaron, V. & Barke, R.A. (1999) Gram-negative bacterial sepsis and the sepsis syndrome. *Urologic Clinics of North America*, Vol.26, No.4, pp.687-699.

Li, S., & Sedivy, J.M. (1993) Raf-1 protein kinase activates the NFkappa B transcription factor by dissociating the cytoplasmic NFkappa B-I kappa B complex. *Proceedings of the National Academy of Sciences USA,* Vol.90, pp.9247-9251.

Liang, M.D., Bagchi, A., Warren, H. S. Tehan M.M., Trigilio J.A., Beasley-Topliffe L.K., Tesini B.L., Lazzaroni J.C., Fenton M.J. & Hellman J. (2005) Bacterial peptidoglycan-associated lipoprotein: a naturally occurring toll-like receptor 2 agonist that is shed into serum and has synergy with lipolysacchardide. The *Journal of Infectious Disease*, Vol.191, No.6, pp.939-948.

Maiden, M.C.S., Suker, J., Mekema, A.S., Buggraves, J.A. & Feavers, I.M. (1991) Comparison of the class 1 outer membrane proteins of eight serological reference strains of Neisseria meningitidis *Molecular Microbiology* Vol.5 , No.3, pp.727-736.

Mangan, D.F., Wahl, S.M., Sultzer, B.M. & Mergenhagen, S.E. (1992) Stimulation of Human monocytes by endotoxin-associated protein: inhibition of programmed cell death (apoptosis) and potential significance in adjuvanticity. *Infection and Immunity* Vol.60, No.4, pp.1684-1686.

Maruvada, R. & Kim, K. S. (2011) Extracellular loops of the Escherichia coli outer membrane protein A contribute to the pathogenesis of meningitis. *The Journal of Infectious Diseases*, Vol. 203, No.1, pp.131-140.

Masignani, V., Comanducci, M., Giuliani, M.M., Bambini, S., Adu-Bobie, J., Arico, B., Brunelli, A., Pieri, A., Santini, L., Savino, S., Serruto, D., Litt, D., Kroll, S., Welsch, J.A., Granoff, D.M., Rappuoli, R. & Pizza, M. (2003) Vaccination against Neisseria meningitidis using three variants of the lipoprotein GNA1870. *Journal Experimental Medicine*, Vol. 197, No.6, pp.789-799.

Massari, P., Ram, S., Macleod, H., & Wetzler, L.M. (2003) The role of porins in neisserial pathogenesis and immunity. *Trends Microbiology*, Vol.11, No.2, pp.87-93.

Mittal, R., Krishnan, S., Gonzalez-Gomez, I. & Prasadarao, N.V. (2011) Deciphering the roles of outer membrane protein A extracellular loops in the pathogenesis of Escherichia coli K1 meningitis. *Journal of Biological Chemistry*, Vol.286, No.3, pp.2183-2193.

Narita, S., Matsuyama, S. & Tokuda, H. 2004. Lipoprotein trafficking in Escherichia coli. *Archives Microbiology*, Vol.182, No.1, pp.1-6.

Neary, J. M., Yi, K., Karalus, R. J. & Murphy, T. F. (2001) Antibodies to loop 6 of the P2 porin protein of nontypeable Haemophilus influenzae are bactericidal against multiple strains. *Infection and Immunity*, Vol.69, No.2, pp.773-778.

Nikaido H. (2003) Molecular basis of bacterial outer membrane permeability revisited. *Microbiology and Molecular Biology Reviews*, Vol.67, No.4, pp.593-656.

Prasadarao, N.V., Wass, C.A., Weiser, J.N., Stins, M.F., Huang, S.H. & Kim, K.S. (1996) Outer membrane protein A of Escherichia coli contributes to invasion of brain microvascular endothelial cells. *Infection and Immunity,* Vol.64, No.1, pp.146-153.

Rawadi, G. & Roman-Roman, S. (1996) Mycoplasma membrane lipoproteins induced proinflammatory cytokines by a mechanism distinct from that of lipopolysaccharide. *Infection and Immunity*, Vol.64, No.2, pp.637-643.

Reddi, K., Poole, S., Nair, S., Meghji, S., Henderson, B. & Wilson, M. (1995) Lipid A-associated proteins from periodontopathogenic bacteria induce interleukin-6 production by human gingival fibroblasts and monocytes. *FEMS Microbiology Immunology*, Vol.11, No.2, pp.137–144.

Rosenshine, I., Donnenberg, M.S., Kaper, J.B. & Finlay, B.B. (1992) Signal transduction between enteropathogenic Escherichia coli (EPEC) and epithelial cells: EPEC induces tyrosine phosphorylation of host cell proteins to initiate cytoskeletal rearrangement and bacterial uptake. *EMBO Journal*, Vol.11, No.10, pp.3551-3560.

Schild, S., Nelson, E.J. & Camilli, A. (2008) Immunization with Vibrio cholerae outer membrane vesicles induces protective immunity in mice. *Infection and Immunity*, Vol.76, No.10, pp.4554-63.

Schulz, G.E. (2002) The structure of bacterial outer membrane proteins. *Biochimica Biophysica Acta*, Vol.1565, No.2, pp.308-17.

Siber, G.R., Kania, S.A. & Warren, H.S. (1985) Cross-reactivity of rabbit antibodies to lipopolysaccharides of Escherichia coli J5 and other gram-negative bacteria. *Journal of Infectious Disease*, Vol.152, No.5, pp.954-64.

Smith, S.G.J., Mahon, V., Lambert, M.A. & Fagan, R.P. (2007) A molecular Swiss army knife: OmpA structure, function and expression. *FEMS Microbiology Letters*, Vol.273, No.1, pp.1–11.

Thompson, E.A., Feavers, I.M. & Maiden, M.C. (2003) Antigenic diversity of meningococcal enterobactin receptor FetA, a vaccine component. *Microbiology*, Vol.149, No.7, pp.1849-1858.

Tufano, M.A., Capasso, G., Anastasio, P., Giordano, D.R., Giordano, D., Galdiero, E., Sommese, L. & De Santo, N.G. (1987) Clearance studies on the renal action of porins extracted from Salmonella typhimurium. *International Journal Pediatric Nephrology*, Vol.8, No.4, pp.193–198.

Van der Ley, P., Heckels, J.E., Virji, M., Hoogerhout, P. & Poolman, J.T. (1991) Topology of outer membrane porins in pathogenic Neisseria spp. *Infection and Immunity*, Vol.59, No.9, pp.2963-2971.

Vitiello, M., Galdiero, S., D'Isanto, M., D'Amico, M., Di Filippo, C., Cantisani, M., Galdiero, M. & Pedone, C. (2008) Pathophysiological changes of gram-negative bacterial infection can be reproduced by a synthetic peptide mimicking loop L7 sequence of Haemophilus influenzae porin. *Microbes and Infections*, Vol.10, No.6, pp.657-663.

Von Andrian, U.H., Chambers, J.D., McEvoy, L., Bargatze, R.F., arfors, K.E. & Butcher, E. C. (1991) A two step model of leukocyte-endothelial cell interaction in inflammation: distinct roles for LECAM-1 and the leukocyte b2 integrins in vivo. *Proceedings of the National Academy of Sciences USA*, Vol.88, No.17, pp.7538-7542.

Weinstein, S.L., Sanghera, J.S., Lemke, K., DeFranco, A.L. & Pelech, S.L. (1992) Bacterial lipopolysaccharide induces tyrosine phosphorylation and activation of mitogen-activated protein kinases in macrophages. *Journal Biological Chemistry*, Vol.267, No.21, pp.14955-14962.

Westphal, O., Luderitz, O. & Bister, F. (1952) Uber die extraktion von bacterien mit phenol/wasser. *Naturforsch,* Vol.7, pp.148–156.

Wright, J.C., Williams, J.N., Christodoulides, M. & Heckels, J.E. (2002) Immunization with recombinant PorB outer membrane protein induces a bactericidal immune response against Neisseria meningitides. *Infection and Immunity,* Vol.70, No.8, pp.4028-4034.

Yi, K. & Murphy, T. F. (1997) Importance of an immunodominant surface-exposed loop on outer membrane protein P2 of nontypeable Haemophilus influenzae. *Infection and Immunity*, Vol.65, No.1, pp.150-155.

Zhang, H., Peterson, J.W., Niesel, D.W. &Klimpel, G.R. (1997) Bacterial lipoprotein and lipopolysaccharide act synergistically to induce lethal shock and proinflammatory cytokine production. *Journal of Immunology*, Vol.159, No.10, pp.4868-78.